Thermoset Nanocomposites for Engineering Applications

Editor: Rumiana Kotsilkova

SMITHERS rapra TECHNOLOGY

Thermoset Nanocomposites for Engineering Applications

Editor: Rumiana Kotsilkova

With contributions from:

Polycarpos Pissis
Clara Silvestre
Sossio Cimmino
Donatella Duraccio

Smithers Rapra Technology Limited
A wholly owned subsidiary of The Smithers Group

Shawbury, Shrewsbury, Shropshire, SY4 4NR, United Kingdom
Telephone: +44 (0)1939 250383 Fax: +44 (0)1939 251118
http://www.rapra.net

First Published in 2007 by

Smithers Rapra Technology Limited

Shawbury, Shrewsbury, Shropshire, SY4 4NR, UK

A catalogue record for this book is available from the British Library.

Soft-backed ISBN: 978-1-84735-062-6
Hard-backed ISBN: 978-1-84735-063-3

Typeset, printed and bound by Smithers Rapra Technology Limited
Cover printed by Livesey, Shropshire, UK

Contents

Preface

Nanocomposites hold the promise of advances that exceed those achieved in recent decades in composite materials. The nanostructure created by a nanophase in polymer matrix represents a radical alternative to the structure of conventional polymer composites. These complex hybrid materials integrate the predominant surfaces of nanoparticles and the polymeric structure into a novel nanostructure, which produces critical fabrication and interface implementations leading to extraordinary properties. Organic/inorganic hybrids represent the most challenging nanostructures investigated to date. What differentiates nanocomposite materials from classical composites is the degree of control of fabrication, processing and performance, that can be achieved nearly down to the atomic scale.

Thermoset polymer nanocomposites have received less interest in their scientific development and engineering applications than thermoplastic nanocomposites. However, some of these materials may be relatively easy to bring into production. The understanding of characteristics of the interphase region and the estimation of technology-structure-property relationships are the current research frontier in nanocomposite materials.

The present book summarises the developments in science and technology of thermoset nanocomposites, prepared by various nanofiller particles dispersed in resin matrices. The central goal was to make a link between the rheology of nanocomposites, their structure and molecular dynamics, with their related mechanical and physical properties. The scientists must conduct substantial fundamental research to provide a basic understanding of how to exploit the nano-engineering potential of these materials. The aim of this book is to summarise the experimental results on thermoset nanocomposites obtained from the collaboration of three research groups from Bulgaria, Greece and Italy, and to analyse some of results reported in the literature. The engineering resin nanocomposites are restricted to the most commonly used thermosets, such as epoxy resins, unsaturated polyester, acrylic resin, and so on. Various nanoparticles prove to be useful for nanocomposite preparation with thermosetting polymers, along with smectite clay, diamond, graphite, alumina and ferroxides.

The book is organised into seven chapters, providing condensed information on technology, structure, molecular dynamics and properties of thermoset nanocomposites, suitable for various engineering applications.

Chapter 1 Introduction - focuses on the advantages of nanocomposites over the conventionally filled polymers; compares the structure of filled polymers with that generated in nanocomposites, and presents an overview on the problems of thermoset nanocomposite technology.

Chapter 2 Rheological Approach to Nanocomposite Design - presents a general review on the rheology of polymer nanocomposites related to the nanocomposite structure. An original rheological approach is proposed as a tool for control of nanocomposite technology. Three rheological methods are developed for the control and the characterisation of nanocomposites at an early stage of their preparation, as follows:

(i) Rheology Method I, controlling the degree of nanofiller dispersion in matrix polymer;

(ii) Rheology Method II, characterising the superstructure of nanocomposites; and

(iii) Rheology Method III, determining the effects of nanofiller on polymer relaxation.

Many examples are presented to prove the application of rheological methods for providing rapid control of dispersions prepared by various nanofillers and resins. Moreover, an approach to prognostic design of nanocomposite properties is proposed, based on rheological characteristics and percolation concept.

Chapter 3 Formation of Thermoset Nanocomposites - outlines fundamental principles and kinetics of thermoset nanocomposite formation, related to the role of curing agents, organoclay, solvent, and preparation technology. Diverse effects of clay nanofillers on the glass transition temperature are discussed from the standpoint of epoxy crosslinking density and interfacial interactions.

Chapter 4 Structure and Morphology of Epoxy Nanocomposites with Clay, Carbon and Diamond - provides a brief overview of the recent progress on polymer/clay nanocomposites. An innovative study on morphology and structure of polymer systems with binary nanofillers is discussed. The epoxy-clay systems are incorporated with graphite/diamond particles to form hybrid nanocomposites and finally mixed with isotactic polypropylene (iPP). The addition of combined fillers of smectite clay and carbon nanoparticles to iPP causes drastic modifications in the structure, morphology, tensile and thermal properties of iPP.

Chapter 5 Molecular Dynamics of Thermoset Nanocomposites - presents the results obtained by three dielectric techniques for molecular dynamic studies. The chapter discusses the overall behaviour, the secondary and primary relaxations, glass transition, and conductivity effects in variety of nanocomposite formulations of thermoset resins and nanofillers. The results are related to the investigation of structure-property relationships, distribution of nanoparticles and degree of agglomeration.

Chapter 6 Performance of Thermoset Nanocomposites - considers specific properties of thermoset nanocomposites of interests for engineering applications. Experimental results for mechanical properties, viscoelasticity (DMTA), tensile, flexural and impact strength are presented. The reinforcement effects of clay, diamond, graphite and alumina nanoparticles are related with percolation mechanism and polymer-filler interactions. Thermal properties are discussed with examples of enhanced thermal stability and flammability resistance of epoxy/smectites. Unique thermal conductivity results of a range of epoxy nanocomposites containing different nanofillers are presented. Original data for wear resistance and water absorption of epoxy and polyester nanocomposites illustrated the high protective and barrier properties of these materials.

Chapter 7 Design of Physical Properties of Thermoset Nanocomposites - highlights the electrical conductivity and microwave absorption properties of thermoset nanocomposites incorporating both magnetic and conducting nanofiller particles. A rheological approach is proposed for optimising formulations of the binary fillers in the resin matrix. A synergistic effect is observed between conducting and magnetic nanoparticles resulting in wide-band wave absorption of nanocomposite films. Rheological investigations demonstrate that the synergy effects might be reached only at optimal packaging of the binary fillers in the matrix polymer.

Closing remarks - summarises most suitable results for engineering applications of technology-structure-molecular dynamics-properties relationships of thermoset nanocomposites.

Each chapter contains a list of references related to the topics.

Thermoset polymer nanocomposite technology has come a long way to reach this understanding and control on the fabrication, nanostructure and properties. Hopefully, this book will help with answers for some questions related to design of nanocomposites by controlling the processing technology and structure. The book is addressed not only to researchers and engineers who actively work in the broad field of nanocomposite technology, but also to newcomers and students who have just started investigations in this multidisciplinary field of material science.

There are many people to whom authors must express their sincere thanks, but first they thank their colleagues for providing data, for experimentation and/or for valuable discussions. Rumiana Kotsilkova wishes to thank Professor Tadao Kotaka, Professor Kiyohito Koyama and Dr. Tatsuhiro Takahashi for collaboration in the nanocomposite research, and Academician Ya. Ivanov, Dr. Wolfgang Gleissle and Professor Hans Buggish for the supervision of the PhD and post-doctoral research on rheology.

R. Kotsilkova
August 2007

Contributors

Professor Rumiana Kotsilkova
Bulgarian Academy of Sciences
Central Laboratory of Physico-Chemical Mechanics
Academician G Bonchev Street, Block 1
1113 Sofia
Bulgaria

Professor Polycarpos Pissis
National Technical University of Athens
Department of Physics
Zografou Campus
15780 Athens
Greece

Dr Clara Silvestre
Istituto di Chimica e Tecnologia dei Polimeri
ICTP-CNR
Via Campi Flegrei, 34
80078 Pozzuoli (Napoli)
Italy

Dr Sossio Cimmino
Istituto di Chimica e Tecnologia dei Polimeri
ICTP-CNR
Via Campi Flegrei, 34
80078 Pozzuoli (Napoli)
Italy

Dr Donatella Duraccio
Istituto di Chimica e Tecnologia dei Polimeri
ICTP-CNR
Via Campi Flegrei, 34
80078 Pozzuoli (Napoli)
Italy

About the Authors

Rumiana Kotsilkova

Professor of Materials Science in the Central Laboratory of Physico-Chemical Mechanics of the Bulgarian Academy of Sciences. Leader of the Thematic Group "Clusters, Nanoparticles, Composites" and member of the Expert Council of the National Centre on Nanotechnology.

Career History: Doctor of Sciences (2005) on technology, structure and properties of thermoset nanocomposites and Ph.D (1983) on applied and theoretical rheology. Joined the Bulgarian Academy of Sciences in 1973. Alexander von Humboldt Fellow (post doc) in Karlsruhe University, Germany (1988-1990). Visiting professor in Japan at the Toyota Technological Institute, Nagoya (JSPS Fellowship, 1997), and the Yamagata University, Yonezawa (2001).

Her *current research interests* focus on polymer nanocomposites – thechnology of preparation, rheology for the design, structure-property relationships, and application of nanocomposites as structural and functional materials. Publication activities include more then 100 papers and a number of conference presentations. She leads projects and advises researchers, students and technology companies on material sciences, nanotechnology and strategic partnerships. Member of the Organizing Committees of national conferences and workshops. Expert in international and national Programs and Adviser Groups at the European Commission and the National Science Fund of Bulgaria.

Research collaborations established with the Institute of Chemistry and Technology of Polymers, CNR, Naples, Italy and the National Technical University of Athens, Greece are basis for the edition of this book.

Polycarpos Pissis

Professor of Materials Science in the Department of Physics of the National Technical University of Athens (NTUA).

Career History: He studied Physics at the University of Goettingen in Germany, where he received his diploma (1973) and Ph.D (1977). He joined NTUA in 1978. He teaches several topics of Physics and Materials Science at undergraduate and postgraduate levels.

Prof. Pissis has published more than 170 papers in scientific journals, 6 chapters in books and more than 60 papers in conference proceedings, in various fields of polymer and composite science and technology. His *current research interests* focus on the investigation of the structure-property relationships in polymer nanocomposites and

nanostructured materials by a variety of experimental techniques, in collaboration with several research groups worldwide. He has made valuable contributions in various fields, including: the development of methodologies for using dielectric techniques for structural and morphological characterization; the investigation of effects on structure and local dynamics of glass-forming liquids induced by confinement in small volumes of nanometer size; the investigation of the hydration properties of polymers (including hydrogels) and biopolymers, with emphasis on the organization of water and the effects of water on structure and local dynamics of the matrix material.

Dr. Clara Silvestre

Senior Research Scientist at Institute of Chemistry and Polymer Technology of Consiglio Nazionale delle Ricerche (Italy). ICTP-CNR.

Career History: Visiting Researcher at University of Bristol England and Associate Researcher at University of Massachusetts, Coordinator head office Mediterranean Network on Science and Technology of Polymer Based Material. Supervisor optical microscopy laboratory. Member of the scientific committee of the ICTP. Lecturer in several schools, meetings, conferences and seminars. Supervisor of PhD thesis. Responsible of several Italian and International Projects. Referee of prestigious journals on polymer science. EU expert evaluator for 5 and 6 FP programs. MIUR consultant for EU project preparation.

Author of over 100 papers published on international journals and books.

Current research interests: Design of innovative polymer based materials (homopolymers, copolymers, polymer blends, nanocomposites) through new mixing techniques, new formulations and control of morphology to be used in the packaging, agriculture, membrane and textiles fields.

Dr. Sossio Cimmino

Director of Research at Institute of Chemistry and Polymer Technology of Consiglio Nazionale delle Ricerche (Italy).

Career History: Associate Researcher at University of Massachusetts, Amherst (USA). Visiting researcher at DSM- Geleen (The Netherlands). Lecturer in several international schools, meetings, conferences and seminars. Referee of several journals of polymer science. Coordinator of Italian and European programs. Author of: 95 papers published on international journals and books; 96 congress communications; 3 patents.

Main research activities: morphology and properties of polymers, polymer blends and composites; miscibility and compatibility of polymer systems; polymer systems for packaging and agricultural applications; polymer recycling.

Main collaborations: Basell SpA (Italy), Eastman SpA (The Netherlands); Repsol YPF (Spain); University A.Mira of Bejaia (Algeria), University "Federico II" of Naples (Italy); Bulgarian Academy of Science (Sofia, Bulgaria); Romanian Academy, "Petru Poni" Institute of Macromolecular Chemistry (Iasi, Romania).

Dr. Donatella Duraccio

Dr. Duraccio has a Post Doc position at Institute of Chemistry and Polymer Technology of Consiglio Nazionale delle Ricerche (Italy).

Career History: Degree in Chemistry at Faculty of Chemistry, Napoli. Mark: 110/110 cum laude. Diploma Title: "Stucture and Mechanical Properties relationship of sindiotactic Ethylene-Propylene copolymers ". Visit researcher at University of Phisics in Rostock (Germany) on March 2006. Visiting researcher at Central Laboratori of Physico-Chemical Mechanics (CLPhChM-BAS) in Sofia (Bulgaria). Author of: 5 papers published on international journals and books; 7 congress communications.

Main research activities: morphology and properties of polymers, polymer blends and composites; polymer systems for packaging.

1 Introduction

R. Kotsilkova

1.1 Why Nanocomposites?

During the past decade, nanocomposites have become a new class of materials that circumvent classic composite material performance by accessing new properties and exploiting unique synergism between materials. This only occurs when the length scale of morphology and the fundamental effects associated with a property coincide on the nanoscale. Indeed, the nanoscale can lead to new phenomena, providing opportunities for novel multifunctional materials applications. The rapidly growing area of nano-engineered materials will develop many perspectives for plastics and composites dictated by the final application of the polymer nanocomposites.

Polymer nanocomposites were developed in the late 1980s in both commercial research organisations and academic laboratories. The term 'nanocomposites' was used first in 1984 by Roy and Komarneni [1, 2] to emphasise the fact that the polymeric product consisted of two or more phases each in the nanometre size range. Since then, the term 'nanocomposite' has been universally accepted as describing a very large family of materials involving structures in the nanometre size range (e.g., 1–100 nm), where the properties are of interest due to the size of the structures, and are typically different from those of the bulk matrix [1–5]. The first company to commercialise polymer/layered silicate nanocomposites was Toyota [6, 7], which used nanocomposite parts in the production of their novel car models. Later, a number of other companies also began investigating nanocomposites, which resulted in a dramatic expansion of the research and commercial interests in this novel class of materials in broad fields of applications. However, most commercial interests in nanocomposites have been focused on thermoplastic polymers, and thermoset nanocomposites are investigated still less.

Polymer nanocomposites are defined as an interacting mixture of two phases – a polymer matrix and a solid phase – which is in the nanometre size range in at least one dimension [5]. Different approaches for the creation of polymer nanocomposites producing different strengths of interface interaction can be found in the literature. One successful approach is *in situ* polymerisation of metal alkoxides in organic materials via the sol–gel process [5, 8-10]. Another approach involving inorganic materials that can be broken down into their nanoscale building blocks is proposed as a superior alternative for the

preparation of nanostructured hybrid organic–inorganic composites [11]. Recently, this approach was widely used for the preparation of intercalated and exfoliated polymer/clay nanocomposites, which have been synthesised by direct intercalation of polymer melt or solution, as well as by *in situ* intercalative polymerisation of monomers in the clay galleries [12–14].

There are references in the literature to the enormous potential of polymer nanocomposites for improved mechanical, thermal and optical properties, etc., compared to conventionally filled polymers [5, 11, 15–20]. The properties of polymer nanocomposites are greatly influenced by the length scale of the component phases [21–24]. However, being much smaller than the wavelength of visible light but much larger than the size of simple molecules, it is difficult to characterise the structure and to control the processes and properties of polymers incorporating nanofillers. Thus, the synthesis of true nanocomposites recently became an important scientific and technological challenge in materials science.

The reinforcement of polymers using fillers, whether inorganic or organic, is common in the production of modern plastics. Conventional composites, filled with micrometre size particles, fibres or platelets, have been studied for many years for use in a large number of industrial applications [25]. For example, composites based on thermosetting resins are widely used for structural materials applications, such as fibre-reinforced plastics, polymer concretes, construction details, adhesives, etc. Very often, the micro- or macrofiller particles are inactive and their major function is to lower the cost of the final products. In polymer composites containing *inactive fillers*, the most important factors governing the properties are the shape, size and distribution of the filler, whereas the chemistry and surface morphology play a minor role. In contrast, polymer composites containing *active fillers* display a reinforcing effect of the filler on mechanical properties, depending mostly on the polymer–filler interactions and the morphology of the matrix polymer [26]. In general, polymers with active fillers of micrometre size demonstrate improved hardness but their elastic and impact properties become worse due to stress concentration resulting from the presence of filler particles.

Moreover, conventional micrometre size fillers have a relatively high density (~2–4 g/cm^3) compared to the low density of the matrix polymer (~0.8–1.2 g/cm^3). In order to gain a reinforcing effect of engineering polymers, a large amount (30–60%) of fillers is traditionally used in composites, leading to about 20–30% increase in the weight of the final material, which to a great extent has limited the advantages of polymer composites over unfilled polymers [27].

Polymer nanocomposites have been developed recently as a radical alternative to the conventional polymer composites, incorporating a small amount of *nanofiller* dispersed at a molecular level in the matrix polymer [6, 7, 28–29]. Uniform dispersion of the nanoscale filler particles produces ultra-large interfacial area per unit volume between the nano-element and the matrix polymer. This immense internal interfacial area and

the nanoscopic dimensions between the particles lead to the formation of a hybrid structure, which fundamentally differentiates polymer nanocomposites from traditionally filled plastics [30–32]. A unique feature of polymer nanocomposites is that a dramatic improvement in properties is reached at low filler content, which results in lightweight materials having optical properties similar to those of the matrix polymer [33, 34].

Despite the large number of combinations of reinforcing nanofillers and matrices, polymer nanocomposites share common features with regard to preparation methodologies, morphology characterisation and fundamental physics [35]. The key to nanocomposite fabrication processes is the engineering of the polymer–nanoparticle interface. In most cases, this is achieved by organic modifiers, ionically associated with or chemically bonded to the nanoparticle surface. The surface modifiers commonly have complex functions, such as lowering the interfacial free energy, catalysing interfacial interactions or initiating polymerisation, which result in improved strength of polymer–filler interactions. However, to date the optimal modifier is mostly chosen empirically.

The main challenges of nanocomposite research and manufacturing to date are the synthesis of materials by design, the development and general understanding of structure–property relationships, and the development of cost-effective and programmable production techniques [36-38]. New combinations of properties that ensue from the nanoscale structure of polymer nanocomposites provide opportunities to outperform conventional reinforced plastics, thus enhancing the promise of nano-engineered materials applications.

1.2 Structure Formation in Filled Polymers

In filled polymers structure formation plays an important role in the reinforcement effects. This process depends on various factors, such as the type of matrix polymer, surface chemistry, and the size and shape of the filler particles. Moreover, two effects, i.e., particle–particle and polymer–filler interactions, are commonly the determining factors for the strength of the filler structure in such polymers.

The mechanism of structure formation in dispersions of micrometre size fillers was determined by Rebinder in 1966 [39]. The author proposed that the major properties of the disperse systems and the interactions between the two phases depend strongly on the interface phenomena. Thus, the role of interfaces increases on increasing the filler content, or decreasing the filler size, due to the absorption of polymer molecules as a bound polymer layer at the inorganic surface. The mechanism of structure formation in polymer-based disperse systems was explained by the presence of lyophilic and lyophobic sections (centres) at the inorganic surface [26, 40]. As a result of electrostatic particle–particle and polymer–filler interactions, two types of structures are usually formed in filled polymers, namely: (i) *coagulated network*, formed by particle–particle

aggregation; and (ii) *structural network*, constructed by the absorbed polymer layers and the filler particles present, due to polymer–particle interactions.

A coagulated network is generated by colloidal particles or anisotropic particles by increasing the filler content. Classical colloidal dispersions form structures if the mean interparticle spacing is of the order of 10–100 nm [40]. This structure is formed much more easily by particles with non-uniform inorganic surface, e.g., the presence of lyophilic and lyophobic centres (sectors) at the surface. For example, the presence of lyophobic centres leads to strong particle–particle aggregation; whereas lyophilic centres at the inorganic surfaces allow polymer–filler interactions. Therefore, an appropriate mosaic chemistry of the inorganic surface is required in order to form a coagulated network of particles through a bound polymer layer [40].

Rebinder [39] related the reinforcing effect of the filler in colloidal dispersions with the formation of a coagulated network. Later, Lipatov [26] applied this approach for the case of filled polymers, proposing that, at low filler content, weak coagulated structures of particle aggregates are formed through a bound polymer layer leading to a reinforcement of the matrix polymer. At sufficiently high filler content, the entire amount of polymer from the bulk is absorbed at the inorganic interfaces, resulting in the formation of a structural network, which consists of a coagulated network of particles and absorbed polymer layer. Such a structure was proposed to dominate the properties of highly filled polymers.

The process of structure formation in filled polymers is commonly controlled by chemical modification of the filler, thus changing the non-uniformity of the inorganic surface. The aim of successful surface modification is to produce a mosaic surface chemistry by creating lyophilic and lyophobic centres [40]. Some authors [41] considered the interfacial interactions dependent on the acid–base properties of the polymers and fillers. In the case of using modified fillers in polymers, the choice of optimal modifier is very important in order to ensure the best compatibility between ingredients [26]. An absorbed polymer layer is formed in filled polymers only if chemical reactions (covalent bonding) between reactive groups of the polymer and the surface modifier, or van der Waals interactions, take place at the interfaces.

1.3 Generation of Nanocomposite by Nanophase Dispersed in Polymer

The nanostructure created by nanophase elements in a polymer matrix represents a radical alternative to the structure of conventionally filled polymers. Because of the thermodynamic instability of systems with large surface area, nanoparticles have very short lifetime due to their high reactivity. They are stabilised by covering their surface with ligands, or by embedding them in suitable protecting matrices. In all these cases, electronic interactions take place at the interfaces, which range from van der Waals interactions to covalent bonding. If such interactions involve charge transfer processes,

they are called *chemical interactions* [42–44]. Importantly, the cluster chemical interface reactions may be precisely controlled by adding selected reactants, and this is the main difference from planar or colloidal particles surface reactivity [42-45]. Such chemical processes at the nanoparticle–matrix interface may cause drastic changes in the atomic and electronic structures of the clusters compared to the free ones.

The technology of polymeric nanocomposites is concerned with nanoparticles dispersed in a polymer matrix, and thus nanocomposites combine two concepts, i.e., composites and nanometre size materials. The aim is to gain control of structures at the atomic, molecular and supramolecular levels and to maintain the stability of interfaces in order to manufacture these materials efficiently. Because of the small nanoscale size of the filler and the chemical processes that occur at the nanoparticle–matrix interface, nanocomposites exhibit novel and significantly improved properties. As is known, when the dimensions of a material structure are below the critical length scale of about 100 nm, then models and theories are not able to describe the novel phenomena. Therefore, the new behaviour at the nanoscale is not necessarily predictable from that observed at larger size scales.

As polymer nanocomposites combine the concept of filled polymers with that of nanostructured materials, some similarities may be observed in the structure formation of nanocomposites and traditional composites. Similar to micrometre scale composites, the polymer–particle and particle–particle interactions are key to the structure and properties of polymer nanocomposites. For example, researchers have pointed to the important role of swelling of the nanofiller surface by polymer in order to gain enhanced mechanical, physical or chemical properties of the final materials [46–48]. Based on thermodynamic considerations, the swelling of nanofiller surface by polymer is strongly dependent on the ability to form an absorbed layer. Important for nanocomposites is the fact that, at very low filler contents, the predominant interfaces produce the absorption of the entire amount of polymer on the inorganic surface [2, 5, 49, 50]. However, complex interfacial interactions reduce the molecular dynamics in nanocomposites much more strongly than in conventionally filled polymers [50]. Witten and co-workers [51] proposed that chemical interactions at the nanofiller–polymer interface are expected to produce a strong energetic barrier for the mobility of the absorbed polymer segments. Therefore, the structure, properties and relaxation processes of the absorbed polymer layer created in nanocomposites differ significantly from those in macrocomposites [52, 53].

In contrast to macrocomposites, a hybrid structure of interpenetrating nanofiller/polymer network is formed at the molecular level in polymer nanocomposites by increasing the filler content. Kim and co-workers [54] proposed a nanostructured network model for polymer/layered silicate nanocomposites that accounts for the polymer junctions at the silicate surfaces. According to this model, the polymer segments are located perpendicular to the exfoliated and parallel ordered silicate nanolayers, and in addition the segments are chemically bonded at the silicate surfaces. Such structural perfection of true nanocomposites is proposed to result in desired super-functional characteristics.

Besides the nanostructured polymer/nanofiller network and the single nanoparticle characteristics, the particle–particle interactions cannot be neglected as a factor dominating the structure in nanocomposites [3, 43, 55]. Pelster and Simon [43] reported that dispersions of nanoparticles differ from colloidal dispersions by having a much smaller interparticle distance, which is very difficult to control. Hence, a small displacement of the particle sizes or filler contents would dramatically change the degree of order, ranging from ordered to random and to disordered structures. The degree of order in nanodispersions is important and it determines the final material applications. Some applications require materials with well-separated particles, for example, for low-loss capacitive devices. Other applications, such as electromagnetic, conducting and also improvement of mechanical properties, need paths of agglomerating particles for energy dissipation. Therefore, the preparation of well-defined systems requires good control of particle aggregation and dispersion processes.

Most of the studies reported in the literature deal with polymer/layered silicate nanocomposites, which gain particular interests from scientific and technological points of view. The concept of polymer nano-reinforcement with layered silicate is attracting a great deal of attention owing to its potential in the preparation of materials that exhibit better physical and mechanical properties than their micro-counterparts. The dispersion of organoclay particles in a polymer matrix can result in the formation of three general types of composite materials: (i) conventional composite, (ii) intercalated nanocomposite, and (iii) exfoliated nanocomposite [11, 18, 22–24]. Nanoscale dispersion of the inorganic layers typically optimises the mechanical, thermal, physical and chemical properties of the matrix polymer. The intercalated polymer/clay nanocomposites can exhibit impressive conductivity, barrier and thermal properties [6, 7, 28]. The exfoliation of smectite clays provides about 1 nm thick layers of smectite clay platelets with high aspect ratios (~1000) and bound polymer molecules at the inorganic surface, which result in dramatic improvement in elongation, tensile strength and modulus [22, 32–34, 49, 52].

In order to obtain materials with the desired properties, a strong control of the structure of nanocomposites is required [56, 57]. Research has reported that such idealised polymer/clay nanostructures are difficult to obtain in real systems. Commonly, a mixed structure of intercalated and exfoliated clay layers is reached in polymer/clay nanocomposites. For example, a variety of nanostructures – intercalated, exfoliated and mixed – are obtained for clay containing nanocomposites with epoxy resin, depending on the chemistry of the resin, the organic modifier and the preparation procedures [32, 58, 59]. Researchers have claimed that the resulting nanostructure is responsible for and a determining factor in nanocomposite properties.

Researchers are just beginning to understand some of the principles to fabricate by design nanostructures with precisely controlled size and composition, based on nanocomposite strategy. The studies in this field are the starting point, but the reported results confirm the benefits that nanostructuring can bring in producing lighter, stronger and programmable materials.

1.4 Thermoset Nanocomposite Technology

Thermosetting polymers are finding an increasing use in a wide range of engineering applications because of their easy processing, good affinity to heterogeneous materials, considerable solvent and creep resistance, and higher operating temperature. Thermoset nanocomposites offer some significant advantages over thermoset resins, and these materials may be relatively easy to bring into production. At this point in time, however, there has been much less commercial interest in thermoset nanocomposites compared to thermoplastics. This neglect may not continue much longer since thermoset nanocomposites demonstrate distinct improvement in properties over conventional thermoset composites [35, 36, 59, 60].

Particulate nanofillers are used in thermosetting resins primarily to reduce thermal shrinkage and brittleness, or to increase hardness and abrasion resistance. Additionally, the introduction of adhesion between the inorganic and organic phases enhances compatibility, thus effectively improving the tensile properties and toughness of the nanocomposites. Recently, a number of publications [61, 62] reported on the use of nanoparticles, such as silica, TiO_2 and AlO_2, as nanofillers in network polymers. This was found to be a more effective way of improving the mechanical and thermal properties of thermoset polymers over the traditionally used micrometre size fillers or direct modification of their molecular compositions.

Over the last few years, most of the research work on nanocomposites has focused on the use of organically modified silicate layers as nanoparticles. A literature search provides many examples demonstrating that a uniform dispersion of organoclay in thermoset resins produces superior mechanical and barrier properties, better thermal stability, lower flammability, and higher resistance to water and aggressive solvents, compared to that observed in macrocomposites [11, 32, 37, 38, 48, 49].

Generally, the properties of nanocomposites are comparable to those of unfilled and conventionally filled polymers, but are not on the same level as those of continuous fibre-reinforced composites. Although nanocomposites may provide enhanced mechanical properties, they should not be considered as an alternative for fibre-reinforced composites [58]. Therefore, an ongoing trend is to combine the advantages of polymer nanocomposites and fibre-reinforced polymers to produce new reinforced plastics with value-added properties, based on epoxy, phenolic and unsaturated polyester resins. Brown and co-workers [63] reported on the possibility of using thermoset nanocomposites as a matrix in conventional fibre-reinforced nanocomposites. The investigations in this field to date are merely the starting point. The dispersion of nanoparticles in hybrid composites and the adhesion between long fibres and the nanocomposite matrix may be the most important problems for manufacturing such reinforced plastics. Scientists must still conduct substantial fundamental research to provide a basic understanding of these materials to enable full exploitation of their nano-engineering potential.

1.4.1 In Situ Polymerisation

The technology of thermoset nanocomposites is concerned with the *in situ* polymerisation method. The first step of the *in situ* polymerisation technology is related to the preparation of the nanofiller dispersion in the thermoset resin precursor (monomer or oligomer). This requires certain preparation conditions, such as mixing procedure, assistance of solvent and organic modifiers, and appropriate swelling temperature. The fundamental principle for such nanocomposite preparation is that monomers and oligomers are able to swell the single nanoparticle and react with the active lyophilic centres at the nanofiller surfaces. For example, a relatively good swelling and intercalation of organically modified clay by the resin is reached due to the low viscosity and the polarity of the thermoset matrix. The second step is related to the initiation of the polymerisation reaction by addition of hardener or other agents. Substantial research efforts are currently under way addressing the fundamental challenge of providing general guidelines for morphology control by *in situ* fabrication processes, including thermodynamic, kinetic and rheological considerations [35, 36, 59].

If we consider the most investigated polymer/layered silicate nanocomposites, the majority of research has been focused on epoxy/layered silicate chemistries [32, 64, 65]. The fundamental principle for nanocomposite preparation is that the monomers and oligomers are able to move within and to react with the intra-gallery ions. The natural or synthetic layered silicates are first modified with appropriate organic intercalant by the ion exchange approach. Contacting clay with the polar molecules of the organic modifier that are absorbed between the platelets forms the intercalate (organoclay), increasing the interlamellar gallery spacing to more than 1 nm. The dispersion of organoclay in the monomer or oligomer produces further intercalation and exfoliation of the clay platelets by the resin molecules. Two alternative processes of organoclay dispersion exist. First, uniform dispersion and exfoliation may be achieved before network formation during curing of the thermoset resin. However, this results in a very high viscosity of dispersions, leading to various processing difficulties. Secondly, the exfoliation may occur coincidently with polymer network formation. In this case, however, a critical balance must be maintained between the rate of silicate layer separation and resin network formation in the fabrication of exfoliated nanocomposites [37, 38, 65]. At the gel point of thermoset polymerisation, the separation of the inorganic layers will be frozen. Therefore, layer separation must occur before the gel (network) formation of the polymer. This process may be controlled by organic surface modifiers, which need to combine miscibility and catalytic functionality [63].

In this book, we discuss nanocomposites with clay and particulate nanofillers, based on epoxy resins, unsaturated polyester, polyimides, and some other most commonly used thermoset polymers for engineering applications.

1.4.2 Epoxy Resin Nanocomposites

Epoxies are used by the plastics industry in several ways. One is in combination with glass fibres to produce high-strength composites or reinforced plastics that provide improved mechanical, electrical and chemical properties, and heat resistance. Epoxies are also used in the encapsulation or casting of various electrical and electronic components and in the powder coating of metal substrates. Major outlets for epoxies also include adhesives, protective coatings in appliances, industrial equipment, etc. Recently, epoxy nanocomposites have been considered as potential replacements of the micrometre size filler composites.

In the field of epoxy/clay nanocomposites the focus to date has been on more flexible resin systems with moderate glass transition temperatures using bifunctional diglycidyl ether of bisphenol-A (DGEBA) resin [11, 32, 63, 64]. However, most of the high-performance applications, such as aircraft components, filaments, pipes, tanks, pressure vessels and tools, require resin systems with improved mechanical properties and higher glass transition temperatures such as those based on the trifunctional triglycidyl *p*-aminophenol (TGAP) and the tetrafunctional tetraglycidyl diaminodiphenylmethane (TGDDM). The addition of organoclay can simultaneously improve the toughness and stiffness of these rigid epoxy resins of higher functionalities [66] and hence provide an attractive alternative to higher concentrations of more commonly used fillers, as well as to fibre-reinforced plastics.

Epoxy/clay nanocomposites are the most extensively studied thermoset hybrids. Scientists vary the type of resin, organic modifiers, curing agents and processing conditions in order to gain fundamental understanding of materials and to optimise the fabrication and processing techniques. The exfoliation processes and morphology, as well as the performance, of epoxy-based nanocomposites with various organoclays have been widely reported by Pinnavaia and co-workers [11, 58, 60, 65], Messersmith and Giannelis [67], Kornmann and co-workers [36, 37, 68], Becker and co-workers [66] and others. Park and Jana [69] studied in detail the catalytic and plasticising effects of quaternary ammonium ions of organoclay in epoxy resins, confirming the mechanism of clay exfoliation in epoxies. Wang and Pinnavaia [64] first reported on the self-polymerisation of epoxy resin in organophilic smectite clays due to the presence of the alkyl-ammonium ion, which is one of the most important phenomena in epoxy nanocomposites.

Researchers agree that the improvement in properties observed with conventionally prepared composites is modest when compared (at equal filler content) to those that have been established for epoxy/clay nanocomposites. The resulting nanocomposites exhibit molecular dispersion of the silicate layers in the epoxy matrix, good optical clarity, and significantly improved mechanical, thermal and barrier properties compared to the unfilled resin. However, a great need still exists for the development of programmable nanocomposite materials with desired structures, which can be mixed, applied in various forms and cured by conventional means.

1.4.3 Nanocomposites Based on Unsaturated Polyester

Unsaturated polyester resins are two-component systems where polar unsaturated prepolymers are dissolved in styrene monomer (usually around 30 wt%). The resin is cured by free-radical polymerisation, using initiators to start the polymerisation, such as peroxides or azo compounds, which produce free radicals during their dissociation. A catalyst is also used in order to speed up the dissociation of the initiator. The characteristics of these materials have proved to be extremely appealing to such markets as automotive, marine, building, electrical applications, corrosion-resistant structures and consumer goods.

Kornmann and co-workers [48, 68] successfully provided the concept of nanoscale reinforcement as a novel opportunity for the synthesis of exfoliated nanocomposites based on clay and unsaturated polyester. These authors noticed that in the synthesis of such nanocomposites the chain polymerisation is partially inhibited by the presence of the clay, as the clay consumed free radicals. The mechanical properties of the nanocomposite are substantially improved as compared with those of the pristine polymer and this happens even at low clay content (less than 5 vol%). The transparency of the material (less than 10 vol%) subjected to red light (700 nm wavelength) is found to be very good; however, purple light (400 nm wavelength) showed poor transmittance. This confirmed the size of the phase domains in such relatively highly concentrated hybrids.

Bharadwaj and co-workers [70] established the structure–property relationships in polyester/clay nanocomposites crosslinked at room temperature. Although firm evidence showed the formation of a nanocomposite structure of mixed type, containing intercalated and exfoliated regions, the tensile modulus and the loss and storage moduli are found to exhibit a progressively decreasing trend with increasing clay concentration of 1–10 wt%. These trends are explained on the basis of a progressive decrease in the degree of crosslinking, due to the presence of organoclay. The authors claimed that the establishment of a morphological hierarchy in polymer/clay nanocomposites is the key factor in understanding the structure–property relationships in these nanocomposites.

1.4.4 Thermoset Polyimide/Clay Nanocomposites

Thermoset polyimides were introduced in the 1960s, followed in the early 1970s by thermoplastic polyimides. They are used in laminates, adhesives, wire enamels, gears, covers, piston rings and valve seats, and in solution form as a laminating varnish. Because of their high glass transition temperature, high thermal stability in various environments and good thermomechanical properties, these materials are attractive for use in aerospace components where durability and reliability are critical concerns.

The nanocomposite approach seems to be a promising way to enhance the properties of the high-performance thermoset polyimide polymers, and particularly the thermal oxidative

stability [71, 72]. It is suggested that a more homogeneous, exfoliated morphology exhibited better properties then intercalated morphologies [73], leading to a novel class of high-temperature nanocomposites. The improved morphology of clay/polyimide mixtures due to intensive chemical bonding between the swelling agent (the clay intercalant) and the polymer molecules resulted in dramatically enhanced thermal and mechanical properties.

One of the main obstacles to the preparation of clay-containing nanocomposites with high-temperature polymers, such as polyimides, is the thermal stability of the organoclay. The ammonium intercalants of the clay, which are commonly used in the preparation of organoclay, are known to exhibit degradation onsets well below the PMR-15 crosslinking temperature of 316 °C, for example. (PMR-15, an oligomer of molecular weight 1500, is the best-known precursor of thermosetting polyimides.) Abdalla and co-workers [72] synthesised thermoset PMR-15 nanocomposites of intercalated morphologies using unmodified clay. They reported significant improvement in the flexural modulus and strength with no reduction in elongation of 2.5% clay-containing systems. However, a slight degradation is possible for the organically modified silicates during the crosslinking step of thermoset polyimide.

In summary, the preparation of nanostructures with a desired perfection in thermoset polyimide/clay based systems is difficult to obtain and requires the development of appropriate methods for design.

1.4.5 Others

In the literature, nanocomposites based on polyurethanes [74, 75] are not as well described as, for example, the epoxy/clay nanocomposites. Wang and Pinnavaia [74] synthesised thermoset polyurethane/clay nanocomposites using a more traditional route for preparation and curing. The organoclay was swollen by polyols, commonly used in polyurethane synthesis. The incorporation of clay was observed to improve simultaneously the tensile strength, stiffness and toughness in these thermoset polyurethane nanocomposites.

According to related reviews, little attention has been paid to elastomers [76, 77] and thermoset rubber [78] until now. Nevertheless, these polymers have been successfully implemented in the synthesis of nanocomposites.

1.4.6 Real Formulations and Problems

The application of nanoscale fillers in polymer matrices has become a topic of growing interest in composite materials science across the world. Nanocomposites exhibit a number of advantages related to their hybrid structure and unique mechanical, physical

and chemical behaviour, based on the specific filler properties and superior polymer–filler interactions. A range of clays and thermosetting polymers have been successfully used in the synthesis of thermoset nanocomposites, but until now only a few commercial successes have been achieved with these new materials. The development and fabrication of nanostructured materials are still at the early stage; however, the research and market interests in these materials are great [79]. The results to date for nanocomposites created by a nanophase dispersed in a polymer matrix are promising, and these materials are expected to act as the next generation for the composite materials technology.

Besides the superior properties reported, many difficulties appear when manufacturing nanocomposite materials. The most critical obstacles to successful commercialisation are access to nanocomposite formulation and process technology. It is known that not all polymers are equally well suited for nanocomposite development. Compatibilisation between the nanofiller and the matrix polymer is an underlying critical success factor that must be highlighted. Dispersion of nanoparticles in polymer is a problem investigated very actively recently, but only a few studies reported the formation of a true nanocomposite structure by using organic modification or grafting of nanoparticles. Many issues concerning the control of nanocomposite structure and the understanding of structure–property relationships in order to ensure the desired property enhancement are unsolved, which strongly limit the industrial applications. All these problems necessitate major research in the field of nanocomposite synthesis, characterisation and application.

The following main problems may be derived, based on a detailed review of the literature on thermoset nanocomposites:

- Technological difficulties exist related to the programmable choice of the surface organic modifier in order to optimise the compatibility between the nanofiller and the matrix resin.
- Fast and easy methods are in great demand for control of the nanofiller/resin dispersions at an early stage of nanocomposite preparation. The macroscopic rheological methods need to be proved in nanodispersions for characterisation of the degree of dispersivity, and the polymer–particle and particle–particle interactions.
- A weak point is the establishment of a technology–structure relationship as an approach to design the desired nanocomposite structure by appropriate control of the preparation technology.
- Improved knowledge of structure–property relationships is required to understand the fundamentals of the improvement of nanocomposite properties.
- The synergistic effect of nanofiller and polymer seems to be a promising novel concept in composite technology, and such phenomena need further investigation.

In summary, the problems above related to the preparation technology, the attainment of the desired structure of the material and how this structure gives rise to nanocomposite properties will be discussed in the present book. The aim of this book is to develop

links between nanocomposite technology, structure and molecular dynamics in order to obtain controlled properties (mechanical and physical) of thermoset nanocomposites incorporating different nanofillers.

References

1. R. Roy in *Nanophase and Nanocomposite Materials*, Ed., S. Komarneni, Materials Research Society, Pittsburgh, PA, USA, 1993, p.241.

2. S. Komarneni, *Journal of Materials Chemistry*, 1992, **22**, 11, 1219.

3. H. Gleiter, *Nanostructured Materials*, 1995, **6**, 1, 3.

4. D.H. Lowndes, *Advanced Materials and Processes*, 2000, **157**, 5, 48.

5. J.E. Mark and J. Wen, *Macromolecular Symposia*, 1995, **93**, 89.

6. A. Okada, Y. Fukushima, M. Kawasumi, S. Inagaki, A. Usuki, S. Sugiyama, T. Kurauchi and O. Kamigaito, inventors; Kabushiki Kaisha Toyota Chuo Kenkyusho, assignee; US 4,739,007, 1988.

7. A. Usuki, T. Mizutami, Y. Fukushima, M. Fujimoto, K. Fukumori, Y. Kojima, N. Sato, T. Kurauchi and O. Kamigaito, inventors; Kabushiki Kaisha Toyota Chuo Kenkyusho, assignee; US 4,889,885, 1988.

8. J. Burdon and P. Calvert, *Materials Research Society Symposium Proceedings*, 1993, **286**, 315.

9. C.L. Beaudry and I.C. Klein in *Nanotechnology – Molecularly Designed Materials*, Eds., G-M. Chow and K.E. Gonsalves, ACS Symposium Series, No.622, American Chemical Society, Washington, DC, USA, 1996, Chapter 26, p.383.

10. J.S. Koehler, *Physical Review B*, 1970, **2**, 2, 547.

11. J. Pinnavaia, T. Lan, Z. Wang, H. Shi and P.D. Kaviratna in *Nanotechnology – Molecularly Designed Materials*, Eds., G-M. Chow and K.E. Gonsalves, ACS Symposium Series, No.622, American Chemical Society, Washington, DC, USA, 1996, Chapter 17, p.251.

12. J.P. Lemmon, J. Wu and M.M. Lerner in *Molecularly Designed Ultrafine/ Nanostructured Materials*, Eds., K. Gonsalves, G-M. Chow, T. Xiao and R. Cammarata, Materials Research Society, Pittsburgh, PA, USA, 1994, p.83.

13. D. Vollath and D.V. Szabo, *Journal of Nanoparticle Research*, 1999, **1**, 2, 235.

14. T. Cagin, J. Che, Y. Qi, Y. Zhou, E. Demiralp, G. Gao and W.A. Goddard, *Journal of Nanoparticle Research*, 1999, **1**, 1, 51.

15. R.E. Newnham and S. Troler-McKinstry, *Ceramics Transactions*, 1990, **8**, 235.

16. Z. Pu, J.E. Mark, J.M. Jethmalani and W.T. Ford, *Polymer Bulletin*, 1996, **37**, 4, 545.

17. W. Helbert, J.Y. Cavaillé and A. Dufresne, *Polymer Composites*, 1996, **17**, 4, 604.

18. E.P. Giannelis, *Advanced Materials*, 1996, **8**, 1, 29.

19. H. Frisch and J.E. Mark, *Chemistry of Materials*, 1996, **8**, 8, 1735.

20. Y.K. Godovski, in *Thermal and Electrical Conductivity of Polymer Materials*, Springer, Heidelberg, 1995, p.79.

21. P.M. Ajayan, L.S. Schadler and P.V. Braun, *Nanocomposite Science and Technology*, Wiley-VCH, Weinheim, 2003.

22. M. Alexandre and P. Dubois, *Material Science and Engineering*, 2000, **28**, 2, 1.

23. L.A. Utracki, *Clay-Containing Polymeric Nanocomposites*, Rapra Technology, Shawbury, Shrewsbury, UK, 2004.

24. M. Okamoto, *Polymer/Layered Silicate Nanocomposites*, Rapra Review Reports, **14**, 7, Report No. 163, Rapra Technology, Shawbury, Shrewsbury, UK, 2003.

25. *Handbook of Composites*, Volumes 1 and 2, Ed., G. Lubin, Van Nostrand Reinhold, New York, NY, USA, 1982.

26. J.S. Lipatov, *Physical Chemistry of Filled Polymers*, Rapra Technology, Shawbury, Shrewsbury, UK, 1979.

27. E. Ruckenstein and Y. Yuan, *Polymer*, 1997, **38**, 15, 3855.

28. A. Usuki, M. Kawasumi, Y. Kojima, A. Okada, T. Kurauchi and O. Kamigaito, *Journal of Materials Research*, 1993, **8**, 5, 1174.

29. A. Usuki, Y. Kojima, M. Kawasumi, A. Okada, Y. Fukushima, T. Kurauchi and O. Kamigaito, *Journal of Materials Research*, 1993, **8**, 5, 1185.

30. K.A. Carrado, *Applied Clay Science*, 2000, **17**, 1–2, 1.

31. B.M. Novak, *Advanced Materials*, 1993, **5**, 6, 422.

32. P.B. Messersmith and E.P. Giannelis, *Chemistry of Materials*, 1994, **6**, 10, 1719.

33. G. Galgali, C. Ramesh and A. Lele, *Macromolecules*, 2001, **34**, 4, 852.

34. G. Lagly, *Applied Clay Science*, 1999, **15**, 1–2, 1.

35. R.A. Vaia and E.P. Giannelis, *Macromolecules*, 1997, **30**, 25, 7990.

36. R.A. Vaia, G. Price, P.N. Ruth, H.T. Nguyen and J. Lichtenhan, *Applied Clay Science*, 1990, **15**, 1–2, 67.

37. X. Kornmann, H. Lindberg and L.A. Berglund, *Polymer*, 2001, **42**, 4, 1303.

38. X. Kornmann, H. Lindberg and L.A. Berglund, *Polymer*, 2001, **42**, 10, 4493.

39. P.A. Rebinder, *Physicochemical Mechanics of Disperse Structures*, Nauka, Moscow, Russia, 1966 [in Russian].

40. S.N. Tolstaja, S.S. Mihailova and A.V. Uvarov, *Macromolecules at the Interphase*, Naukova Dumka, Kiev, Russia, 1971, p.78 [in Russian].

41. Y. Ivanov, V. Cheshkov and M. Natova, *Polymer Composite Materials – Interface Phenomena and Processes*, Kluwer Academic, Dordrecht, 2001, p.1.

42. *Clusters and Colloids: From Theory to Applications*, Ed., G. Schmid, VCH, Weinheim, Germany, 1994.

43. R. Pelster and U. Simon, *Colloid and Polymer Science*, 1999, **277**, 1, 2.

44. A.D. Pomogailo and V.N. Kestelman, *Metallopolymer Nanocomposites*, Springer, Darmstadt, Germany, 2005.

45. T.F. Tardos, *Langmuir*, 1990, **6**, 1, 28.

46. E.P. Giannelis, *Journal of the Minerals, Metals and Materials Society*, 1992, **44**, 28.

47. *Polymer Nanocomposites: Synthesis, Characterization and Modelling*, Eds., R. Krishnamoorti and R.A. Vaia, ACS Symposium Series, No.804, American Chemical Society, Washington, DC, USA, 2001.

48. X. Kornmann, L.A. Berglund, J. Sterte and E.P. Giannelis, *Polymer Engineering and Science*, 1998, **38**, 8, 1351.

49. R. Krishnamoorti and A.S. Silva, in *Polymer–Clay Nanocomposites*, Eds., T.J. Pinnavaia and G.W. Beall, John Wiley & Sons, New York, NY, USA, 2000, p.315–343.

50. G. Philipp and H. Schmidt, *Journal of Non-Crystalline Solids*, 1984, **63**, 1–2, 283.

51. T.A. Witten, L. Liebler and P.A. Pincus, *Macromolecules*, 1990, **23**, 3, 824.

52. R. Krishnamoorti and E. Giannelis, *Macromolecules*, 1997, **30**, 14, 4097.

53. G. Tsagaropoulos and A. Eisenberg, *Macromolecules*, 1995, **28**, 18, 6067.

54. G.G-M. Kim, D.-H. Lee, B. Hoffmann, J. Kressler and G. Stöppelmann, *Polymer*, 2001, **42**, 3, 1095.

55. M. Xiong, S. Zhou, B. You, G. Gu and L. Wu, *Journal of Polymer Science: Polymer Physics Edition*, 2004, **42**, 20, 3682.

56. E. Ruiz-Hitzky, P. Aranda, B. Casal and C. Galvan, *Advanced Materials*, 1995, **7**, 2, 180.

57. R.A. Vaia, H. Ishii and E.P. Giannelis, *Chemistry of Materials*, 1993, **5**, 12, 1694.

58. *Polymer–Clay Nanocomposites*, Eds., T.J. Pinnavaia and G.W. Beall, John Wiley & Sons, New York, NY, USA, 2001.

59. R.A. Vaia and E.P. Giannelis, *Macromolecules*, 1997, **30**, 25, 8000.

60. Z-G. Wang, T. Lan and T. Pinnavaia, *Chemistry of Materials*, 1996, **8**, 9, 2200.

61. G. Ragosta, M. Abbate, P. Musto, G. Scarinzi and L. Mascia, *Polymer*, 2005, **46**, 23, 10506.

62. C.B. Ng, L.S. Schadler and R.W. Siegel, *Nanostructured Materials*, 1999, **12**, 1–4, 507.

63. J.M. Brown, D. Curliss and R.A. Vaia, *Chemistry of Materials*, 2000, **12**, 11, 3376.

64. M.S. Wang and T.J. Pinnavaia, *Chemistry of Materials*, 1994, **6**, 4, 468.

65. Z. Wang and T. Pinnavaia, *Chemistry of Materials*, 1998, **10**, 7, 1820.

66. O. Becker, R.J. Varley and G.P. Simon, *Polymer*, 2002, **43**, 16, 4365.

67. P.B. Messersmith and E.P. Giannelis, *Chemistry of Materials*, 1994, **6**, 10, 1719.

68. X. Kornmann, *Synthesis and Characterization of Thermoset Layered Silicate Nanocomposites*, Luleå University of Technology, 2001 [Ph.D. Thesis].

69. J. Park and S. Jana, *Macromolecules*, 2003, **36**, 22, 8391.

70 R.K. Bharadwaj, A.R. Mehrabi, C. Hamilton, C. Trujillo, M. Murga, R. Fan, A. Chavira and A. K. Thompson, *Polymer*, 2002, **43**, 13, 3699.

71. M. Islam, D. Dean and S. Campbell, *Polymer Science Engineering*, American Chemical Society, Washington, DC, USA, 2001, p.84.

72. M.O. Abdalla, D. Dean and S. Campbell, *Polymer*, 2002, **43**, 22, 5887.

73. P.C. LeBaron, Z. Wang and T. Pinnavaia, *Applied Clay Science*, 1999, **15**, 1–2, 11.

74. Z. Wang and T.J. Pinnavaia, *Chemistry of Materials*, 1998, **10**, 12, 3769.

75. C. Zilg, R. Thomann, R. Mulhaüpt and J. Finter, *Advanced Materials*, 1999, **11**, 1, 49.

76. P.C. LeBaron and T.J. Pinnavaia, *Chemistry of Materials*, 2001, **13**, 10, 3760.

77. S. Wang, C. Long, X. Wang, Q. Li and Z. Qi, *Journal of Applied Polymer Science*, 1998, **69**, 8, 1557.

78. J. Karger-Kocsis and C-M. Wu, *Polymer Engineering and Science*, 2004, **44**, 6, 1083.

79. L.E. Foster, *Nanotechnology: Science, Innovation and Opportunity*, Prentice-Hall, Upper Saddle River, NJ, USA, 2005.

2 Rheological Approach to Nanocomposite Design

R. Kotsilkova

2.1 Rheology of Polymer Nanocomposites – An Overview

The rheological characterisations of polymer nanocomposites are mostly orientated to better understanding the dynamics of nanoscopically confined polymers [1, 2]. Systematic rheological studies of polymer nanocomposites are vital for their process technology, but recent studies on the rheology of nanocomposites reported in the literature have been focused mostly on thermoplastic polymer/layered silicate hybrids [1–20]. The rheology of thermoset nanocomposite precursors is still less investigated.

Important factors for the synthesis of polymer/layered silicate nanocomposites are the dispersion of organoclay (intercalation and/or exfoliation) and the interactions between the matrix polymer and the clay surface. In an early publication Krishnamoorti and co-workers [1] reported on the steady shear flow of systems of organo-montmorillonite dispersed in siloxane polymers. Characteristically, the interaction between the organoclay particles and the polymer matrices was found to be weak and the nanoparticles, exfoliated or not, behaved as solid fillers. Furthermore, Krishnamoorti and co-workers [2, 4] studied the flow of 1–10 wt% organoclay nanocomposites based on poly(ε-caprolactone) and polyamide-6, prepared by an *in situ* polymerisation method. The synthesis process ensured direct bonding between the clay surface and the macromolecules, labelled as an 'end-tethered' structure. Here, the power-law dependence of G' and G'' moduli in the terminal zone decreases with the increase of silicate loading, and such non-terminal behaviour is an indication of a pseudo-solid-like response, similar to that of liquid-crystal systems. The non-terminal rheological behaviour is related mainly to the active interaction between the polymer and the nanofiller surface.

Depending on the preparation method, nanocomposites are either end-tethered or non-tethered. The end-tethered nanocomposites are characterised with a thousand macromolecules attached to the clay surface through the initial intercalant. In contrast, non-tethered systems resemble polymer composites reinforced with platelet solids [2–4]. Sometimes, end tethering is replaced by strong interactions between the polar groups of the polymer and clay surface [5]. In this case, a mechanical coupling between the clay platelets and the polymer was found. The flow at low shear rates was dominated by

clay platelets, but at high shear rates it was dominated by polymer chain orientation. Similar rheological results have been obtained for layered silicate nanocomposites with various polymer matrices, like polyolefins [6–8], polystyrene-*b*-isoprene block copolymer [9, 10], polystyrene (PS) [8–13], polymethylmethacrylate (PMMA) [8, 20], and so on. Therefore, factors such as the degree of dispersion (intercalation and/or exfoliation), the polymer–clay interaction and the clay content are expected to be determining factors for the rheological response of nanocomposites [2, 4, 8].

Diverse rheological methods for the characterisation of polymeric nanocomposites are examined in a few books on polymer/clay nanocomposites [4, 9, 18], as well as several papers [17, 20–26]. Dynamic shear flow, described as non-terminal viscoelastic behaviour, was typically observed for thermoplastic nanocomposite melts. Moreover, the values of the initial slopes of the G' and G'' moduli are completely independent of the nanocomposite structure, i.e., whether it is end-tethered or intercalated, but it depends primarily upon the amount of clay loading [4, 8, 17–26]. The dynamic moduli increase significantly with increasing nanofiller loading, particularly in the low-frequency region. On the other hand, the slopes of $G'(\omega)$ and $G''(\omega)$ are considerably lower for nanocomposites compared to those of conventional microcomposites and unfilled polymer. The viscosity of nanocomposites at low frequency is larger than those of neat polymers, but at high deformation rate the data for nanocomposites are comparable to those obtained for the matrix polymer. Messersmith and Giannelis [24] have attributed the increase of viscosity to the formation of a so-called 'house-of-cards' structure in which edge-to-edge and edge-to-face interactions between dispersed layers form percolation structures. Additionally, time-dependent rheological properties are reported for clay-filled functionalised polyolefins, assuming polymer–clay interactions that result in an entirely new network structure in nanocomposite materials [23].

The steady shear response of layered silicate nanocomposites has also been studied and the results are attributed to the ability of silicate layers to orient during the flow. Krishnamoorti and co-workers [2, 4, 22] reported the significant orientation and alignment of clay platelets even at the lowest shear rates accessed in the steady shear measurements. The unique combination of enhanced shear thinning at low shear rates, viscosities comparable to that of the matrix polymer at high shear rates and unchanged elasticity are observed for intercalated polymer nanocomposites as a result of orientation of anisotropic silicate layers by the application of flow. The orientation of clay platelets in nanocomposites seems to depend on whether they are end-tethered or not.

The time–temperature (t–T) superposition principle is found to hold for end-tethered nanocomposites over a limited range of conditions (e.g., by the glass transition temperature) [2, 7, 9, 17, 18, 27, 28]. Several authors [2, 7, 9, 27, 28] reported results for the horizontal shift factor (a_T) decreasing with T, but almost independent of the matrix polymer and organoclay content. Tanoue and co-workers [17] found that, if t–T superposition is carried out at temperatures below the melting point, an additional vertical shift factor is usually needed to account for the temperature-dependent

variations of the crystalline structure and content. In the molten state, as long as the organoclay/polymer system is miscible, and hence well dispersed, superposition is to be expected. In general, the lack of *t–T* superposition should be taken as an indication of phase separation. It is expected that the changes in miscibility between the matrix polymer and the organic substances used as intercalants and/or compatibilisers will affect the *t–T* superposition. In general, *t–T* superposition breaks down in mixtures with more than one type of relaxation time distribution (e.g., in polymer/filler systems, polymer blends or liquid-crystal polymers).

Extensional flow has also been studied by several authors for polypropylene (PP), PS and PMMA-based nanocomposites with 2–10 wt% clay [8, 17, 20]. Strong strain hardening for maleated polypropylene nanocomposites was found to originate from perpendicular alignment of the clay platelets to the stretching direction [8]. A correlation between strain hardening and birefringence for PMMA nanocomposites has been reported [20]. In contrast, the extensional flow of PS-based nanocomposites demonstrates that the clay particles have small structure-forming ability in PS [17]. The unique combination of enhanced shear thinning and unchanged elasticity, as measured by the first normal stress difference, is attributed to orientation of anisotropic layers by the application of shear flow [22].

Recently, the effects of nanofiller volume fraction on rheological behaviour have been discussed with respect to a relationship with the nanocomposite properties [9, 11, 29–32]. The change from a liquid-like to a pseudo-solid-like flow behaviour was observed above a critical volume fraction of clay, thus presumably related with the mesoscale structure formed by the percolation of nanoclays [29–31]. It is also reported that the formation of a percolated network appears beyond 2–5 wt% clay, and thus is dependent on the length of the exfoliated platelets [9, 17, 29–31], but not predicated on the block architecture of the polymer studied [9]. However, for dilute linear viscoelastic systems, the relative viscosity for nanocomposites follows the standard η_r *versus* ϕ dependence [17, 29].

Although experience has shown that nanofillers provide rheology control across a range of monomers [33] and prepolymers, or polymer solutions [34–36], only a few monomer-based systems have been studied rheologically [37–46]. The majority of thermoset/layered silicate research is focused on epoxy-based chemistries [24, 27, 28, 47, 48], related to the role of organic modifier as the key factor to control the organoclay exfoliation. The rheology of thermoset hybrids prior to curing has not been sufficiently studied. For example, epoxy nanocomposites with Nanomer nanoclays [35, 36] have been found not to require additional rheology control additives. The formulations can be simplified by removal of rheology control agents such as fumed silica. The yield value is found to provide a good indication of anti-settling and coating spreadability of epoxy nanocomposites. Further, due to their extremely small dispersed particle size and active surfaces, nanofiller particles interact with polymer molecules and such interaction creates a thixotropic system with shear thinning behaviour. Rheological

characterisation of the heterogeneous, liquid thermoset nanocomposites prior to curing has recently been applied in our study to gain a fundamental understanding of the structure–property relationship and also to control the processing of these materials [39–46]. From the mechanical and barrier property standpoints, the development of exfoliated systems is preferred [49, 50].

From another perspective, nanocomposites based on nanoscale metal clusters, nanotubes and particles dispersed in, or chemically bonded with, polymers have been of great interest recently with regard to their mechanical, electrophysical, optical, magnetic and biological applications [32, 51–53]. The role of the surface in mediating polymer response is under debate. The presence of an interfacial layer between the bulk polymer and the filler surface, with altered structure and chain mobility, has been established by various techniques [54, 55]. Many of the properties of the material are strongly dependent on the properties of the interfacial layer. Because of the large surface area presented to the polymer by the nanoparticles, this interfacial layer can represent a significant volume of the polymer. However, rheology is still not properly used to gain a fundamental understanding of the interactions of polymer chains with nanofiller surfaces.

Besides the accomplishments mentioned previously, many issues associated with the generality of synthetic approaches of nanocomposites are still unsolved. The most critical obstacles for successful commercialisation of these novel materials are access to nanocomposite formulation and processing technology. Substantially different materials may result by controlling the composition and processing, but a general understanding has yet to emerge. Few studies have reported on the role of processing techniques, which are necessary in ultimately fabricating thermosetting resin-based nanocomposites [24, 47, 56, 57]. The investigation of the clay exfoliation effects on the rheology and molecular dynamics made possible the control of nanocomposite structure [20, 39, 45]. So far, there has been no detailed report about the relationship between composition, processing, rheology and structure of thermoset-based nanocomposites.

In short, rheological measurements at low deformation rates (to prevent destruction of structures) provide the most sensitive method for nanocomposite characterisation, and they are very important when processing. The rheological properties of polymer nanocomposites are primarily determined by the liquid structure of these materials (in melts or dispersions), and thus are dependent on various factors, such as the degree of nanofiller dispersal in the polymer matrix, particle concentration, shape and size distribution, interparticle affinity and interfacial effects. Immense varieties of microstructures are possible depending on the aggregation tendencies and concentration. Characterising the microstructure in detail is exceedingly difficult, but fortunately all the variables mentioned previously are reflected in several simple rheological parameters. These concepts have emphasised that rheology could be a promising and practical method to gain some control over nanocomposite technology.

2.2 Effects of Polymer/Nanofiller Structures

Nanostructures are intermediate in size between molecular and micrometre size systems, such as polymer blends and composites. In fact, polymer nanocomposites consist of a nanometre-scale phase in combination with a molecular phase. The development of nanostructures by dispersing inorganic nanofillers in a polymer matrix and achieving extraordinary properties is an area of active interest in nanocomposite technology. Polymer nanocomposite materials are defined as an interacting mixture of two phases, i.e., a polymer matrix and a solid phase, which is in the nanometre size range in at least one dimension. Following the general scheme of composite nomenclature by Newnham [37], the connectivity of the phases in polymer nanocomposites is described as follows: *zero-dimensional* nanocomposites refers to isolated 0D nanoparticles in a continuous polymer matrix; *one-dimensional* nanocomposites refers to 1D nanotubes in a polymer matrix; *two-dimensional* nanocomposites refers to 2D sheets exfoliated in a polymer matrix (e.g., polymer/layered silicate hybrids); and *three-dimensional* nanocomposites refers to interpenetrating polymer networks [34]. The influence of the nature and strength of polymer–filler interactions, filler–filler interactions and the state of dispersion of the nanocomposite are of importance for the design of tailored properties [22]. The strength of the interaction between the phases divides the organic–inorganic hybrid materials into two classes [27, 28]. *Class I* hybrid materials correspond to weak phase interactions such as van der Waals interactions, hydrogen bonding or simple mechanical blending of the inorganic and organic phases. *Class II* hybrid materials possess strong covalent or ionic-covalent bonds between the inorganic and organic phases. Both of these groups contain some subdivisions, usually differing by way of preparation or specific functions.

Nanocomposite structures are highly susceptible to change upon application of deformation. It has been suggested that the formation of a superstructure of the dispersed layers in the polymer matrix dominates the linear viscoelastic properties of nanocomposites [4, 9, 10]. Some of the resultant rheological characteristics of nanocomposites are similar to those observed in colloidal dispersions, liquid crystals and other mesostructured materials [2, 34].

In general, a distinguishing feature of nanocomposites is the enormously large inorganic surface, which has the potential for strong interfacial polymer–filler interactions. The amount of nanofiller also plays a vital role in controlling the structure and properties of nanocomposites [1, 25–29]. For example, nanofillers of layered silicates have a plate thickness of the order of 1 nm and very high aspect ratios (10–2000) [29], while particles of a few nanometres in size have a very high and active surface area [13]. Thus, a few weight per cent of organically modified clay [26] or nanoparticles that are properly dispersed throughout the matrix create a much higher surface area for polymer–filler interfacial interactions than do conventional composites.

For two-dimensional nanocomposites, such as polymer/layered silicate hybrids, structurally, three broad classes of materials are achievable by direct intercalation

of the polymer into the organically modified clay galleries: *immiscible composites* (conventional); *intercalated nanocomposites* where the interlayer galleries of the silicate stacks are expanded and swollen by the resin; and *exfoliated nanocomposites* where the clay tactoids are fully delaminated and the individual silicate layers are dispersed in the resin matrix [12, 18, 24, 25, 27, 28, 47–49].

The following are the three most popular techniques for the synthesis of polymer/clay nanocomposites:

(i) *in situ polymerisation*, where the organoclay is initially dispersed in the monomer, followed by polymerisation of the monomer within the clay galleries;

(ii) *melt intercalation*, where the polymer molecules intercalate the clay layers during the melt processing; and

(iii) *intercalation in polymer solution*, where the organoclay is dispersed in a polymer solution, following by evaporation of the solvent.

For zero-dimensional (nanoparticle) or one-dimensional (nanofibre/nanotube) composites, besides the single-particle characteristics, the structure of nanodispersions is also of importance. Composites based on nanoscale metal clusters, nanotubes and particles dispersed in, or chemically bonded with, polymers have been of interest recently with regard to their mechanical, electrophysical, optical, magnetic and biological applications [32, 51–53]. Some applications require structures of well-separated particles. Other applications, such as conductivity and mechanical engineering, require well-controlled structures of agglomerated particles. Dispersions of nanoparticles differ from classical colloidal dispersions by having a much smaller mean interparticle spacing, which is therefore much more difficult to control. Pelster and Simon [58] reported different degrees of order – ordered, random and disordered non-random – which are possible by increasing the volume fraction of nanoparticles. The interactions between contacting nanoparticles are very strong, and a small displacement, of either particle size or volume fraction, would change the degree of order. Therefore, the preparation of well-defined systems of nanofiller particles in polymers requires good control of dispersion processes and structure.

In general, the formation of a 3D structure (a network) of nanofiller in a polymer matrix is possible by two mechanisms – either *crowding* (as in classical particle-filled composites), or *chain entanglement*. In the case of entanglements, the strongest effects may be expected when chains of macromolecules are tethered at the clay surfaces, or directly 'bonded' to the nanofiller surfaces by active groups [18]. The role of the surface in mediating polymer response is under debate. It may be that the mobility of the chains within a few nanometres of the surface is reduced while leaving the bulk relatively unaffected, and this has been termed a 'bond polymer layer'. On the other hand, the surface may act to trap entanglements, thus restricting the overall chain mobility of the polymer molecules both near to and far from the filler surface. The presence of an

interfacial layer between the bulk polymer and the filler surface, with altered structure and chain mobility, has been established by various techniques [54, 62]. The association or covalent bonding of the active groups of macromolecules with the nanofiller surfaces plays a dominant role in nanocomposite performance. This is usually related to the structure of the interfacial polymer layer, which is different from the structure and morphology of the matrix polymer.

2.3 Rheological Methods for Nanocomposite Characterisation

The main distinction between the rheology of matrix polymer (single-phase system) and of nanocomposites (multiphase systems) is the effect of the flow field on the rheological response. Flow field affects the structure of the whole deformed volume of the sample, as well as the structure of the dispersed nanoparticles (e.g., dispersion, orientation of platelets, flocculation/deflocculation, and so on). The structure of the liquid samples tested is modified in a different way in flow at high and low strains. Because of sensitivity of the structure to the flow conditions, the selected test method should reflect the final use of the data. For example, low-strain testing should be used for material characterisation, but high-strain flow data are useful for simulation and modelling of the flow [18].

Most rheological studies are carried out with polymer/clay nanocomposites in shear and elongation. These investigations have shown that, even at low clay content, the flow is very complex. The rheological responses vary in a wide range of performance that starts with the traditional behaviour of composites or colloidal systems and ends with end-tethered nanocomposites showing quite distinct and unique flow characteristics [2].

2.3.1 Rheology as a Tool for Control of Nanocomposites

Rheology was recently used for characterisation of nanocomposites, but general concepts for the practical application of rheology as a tool for the control of nanocomposites at the stage of their preparation have still not been reported. Researchers agree that rheological measurements provide potentially the most sensitive methods for nanocomposite characterisation, which are more useful for the processing of nanocomposites than the most commonly used transmission electron microscopy (TEM) and X-ray diffraction (XRD) [18]. However, to our knowledge there are as yet no publications that disclose a complex rheological approach to optimise nanocomposite technology by rapid control of the three most important effects: nanofiller dispersion, formation of 3D structure of nanoparticles, and polymer–filler interactions. Here, we communicate such a rheological approach developed in our laboratory [39, 41, 43–45]. This approach is based on routine rheological experiments and modelling, and it aims at complex control of both technology and formulation of nanocomposites with either thermoset or thermoplastic polymers incorporating nanofillers.

The proposed rheological approach comprises three methods for the characterisation of nanocomposites, which are shown in **Figure 2.1**.

- Rheology method I: compares the degree of dispersion.
- Rheology method II: quantifies the filler superstructure of nanocomposites.
- Rheology method III: estimates the polymer–filler interactions.

Several simple rheological parameters are determined by these methods in order to quantify the effects of nanofiller on polymer matrix. The rheological methods include the following main steps of experiment and modelling:

(i) Routine rheological measurements in dynamic, oscillatory flow and steady-state shear flow.

(ii) Determining basic rheological parameters by fitting models to the experimental data.

(iii) Application of rheological parameters to quantify the degree of nanofiller dispersal, nanofiller superstructure and polymer–filler interactions of liquid-state nanocomposites.

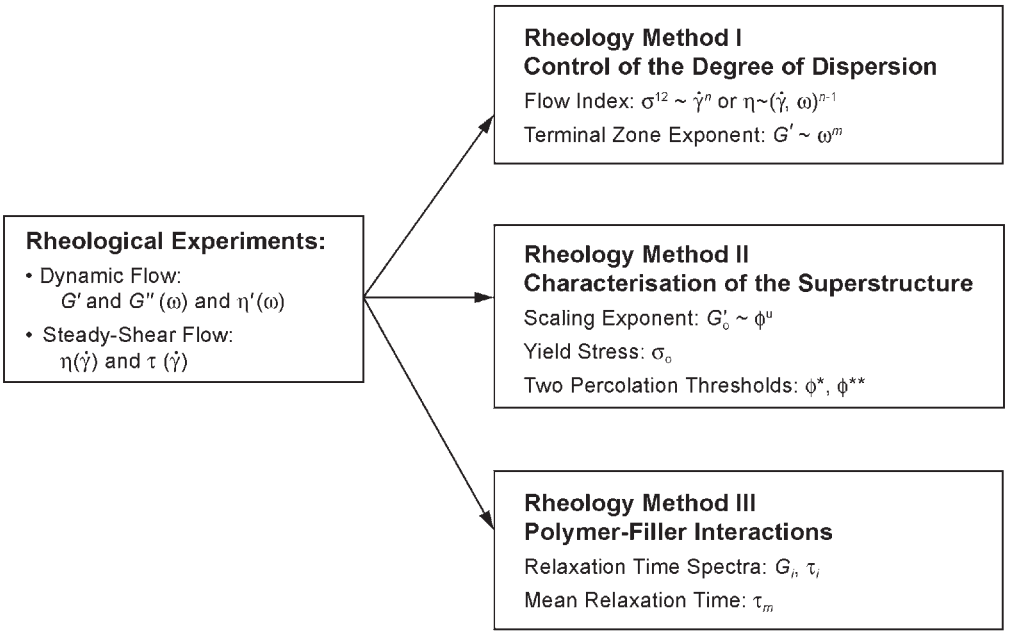

Figure 2.1 Scheme of the three rheological methods for nanocomposite characterisation.

Data from [43]

The three methods rely on standard rheological test equipment, as well as being based on rheological characterisation and modelling, which are routine for polymers and colloidal dispersions. The rheological behaviour of nanodispersions is expected to be much more influenced by particle size and volume fraction than is typical for colloidal dispersions. Such a quantitative distinction appears as a result of the small particle size and very small interparticle distance at low volume fraction of nanofiller, leading to strong particle–particle and polymer–particle interactions.

The proposed rheological approach is expected to become a highly useful analytical tool in the development and optimisation of nanocomposites of thermoset and thermoplastic polymers with virtually all kinds of nanofillers. It might be used for routine and inexpensive control of the nanocomposite preparation technology, in order to identify interesting samples at an early stage of their preparation, and to verify the nanocomposite structure.

2.3.2 Control of the Degree of Nanofiller Dispersion

2.3.2.1 General Approach

Rheology method I proposes an approach that allows control of the degree of nanofiller dispersion in polymer matrices by using experimental data from low-amplitude oscillatory shear and steady-state shear flow. It is assumed that, if the nanofiller content and other variables are kept constant, the primary factor determining the rheological response of nanocomposites at low deformation rates will be silicate delamination and/or nanoparticle dispersion. The method determines two rheological parameters, which are useful to quantify the dispersion quality of nanocomposites [39, 40, 43, 44]:

- terminal zone slopes of the dynamic storage and loss moduli (*m* and *n*);
- shear thinning exponent (*n*, flow index).

However, in order to obtain meaningful data, the comparison samples need to comprise a constant filler concentration, because both shear thinning and terminal regime behaviour are functions of the volume fraction of filler. Moreover, the flow behaviour of the matrix polymer has to be studied as a reference.

This method comprises the following consistent steps of measurement and calculation:

(i) Rheological experiments are carried out in steady shear to obtain flow curves: shear stress *versus* shear rate, $\sigma_{12}(\dot{\gamma})$; viscosity *versus* shear rate/frequency, $\eta(\dot{\gamma})$ or $\eta'(\omega)$; and dynamic storage and loss moduli *versus* angular frequency, $G'(\omega)$ and $G''(\omega)$.

(ii) The experimental data for viscosity and shear stress are fitted to the power-law expressions (2.1)–(2.3) below; data for dynamic storage moduli are fitted to the expression (2.4) [63]. The function $G'(\omega)$ is usually more sensitive to the dispersion of nanofiller in the polymer matrix than is $G''(\omega)$.

$$\sigma_{12} = A\dot{\gamma}^n \tag{2.1}$$

$$\eta = A\dot{\gamma}^{(n-1)} \tag{2.2}$$

$$\eta' = A\omega^{(n-1)} \tag{2.3}$$

$$G' \sim \omega^m \quad \text{and} \quad G'' \sim \omega^n \tag{2.4}$$

where σ_{12} is the shear stress, $\dot{\gamma}$ is the shear rate, η is the apparent steady-state viscosity, η' is the dynamic viscosity, ω is the angular frequency, G' and G'' are the dynamic storage and loss moduli, A is a specific pre-exponential factor, n is the shear thinning exponent (flow index), and m is the terminal zone exponent for the storage modulus.

(iii) The *shear thinning exponent* (flow index, n) of nanocomposites is determined at a given volume fraction, as follows. A double logarithmic plot of the flow curves (from Equations (2.1)–(2.3)) is made and a straight line is fitted to the data at the lowest shear rates, wherein the rheological response is most representative for the nanofiller structure in the composite. At high shear rates the flow is mostly controlled by the polymer matrix. Thus, the shear thinning exponent (n) is determined by the slope of the straight line at the lowest shear rates, thus taking values of $n \leq 1$.

(iv) The *terminal zone exponents* (m and n) of the storage and loss moduli of nanocomposites are quantified at a given volume fraction from the initial slopes of the low-frequency dynamic flow curves. The slopes of the curves of log G' and log G'' *versus* log ω in the terminal zone are expressed by power-law exponents m and n (Equation (2.4)), which have the theoretical values of $m = 2$ and $n = 1$, predicted for the fully relaxed polymer chains. The values of $m < 2$ and $n < 1$ quantify the non-terminal regime behaviour of the storage and loss moduli of measured systems, caused by the presence of nanofiller.

Both the shear thinning exponent (n) and the terminal regime exponent of the storage modulus (m) can be used to compare the degree of nanofiller dispersion in different nanocomposite samples at fixed filler concentration. In general, $n = 1$ is indicative of a Newtonian flow system (typical for monomers and low-viscosity polymer samples), and $m = 2$ is the value of the terminal flow behaviour of fully relaxed polymers. If the filled samples behave as the matrix polymer, essentially Newtonian ($n \approx 1$) or presenting terminal behaviour ($m \approx 2$), they are usually not nanocomposites, and such behaviour indicates the presence of micrometre size aggregates. In contrast, nanocomposite samples demonstrate a considerable shear thinning ($n \sim 0$) and a solid-like behaviour ($m \sim 0$) at a relatively small filler volume fraction, and thus usually comprise the morphology of smooth, finely dispersed nanoscale filler. Additionally, samples with moderate values of $n \leq 0.5$ and $m \leq 1$ are not perfectly dispersed nanocomposites.

Rheology method I, introduced here, might be used for the control of the dispersion quality of every type of composite, e.g., nanolayers, nanoparticles or nanotubes dispersed in thermoset resins, thermoplastic polymers or polymer solutions. This method is expected to be widely used as a practical tool for the rapid control of the processing technology (e.g., composition, compounding or mixing, and so on) when optimising the extent of delamination of platelet stacks or the dispersion of nanoparticle aggregates.

2.3.2.2 Non-Terminal Behaviour of Dynamic Moduli

Low-amplitude dynamic measurements are usually used to evaluate the linear viscoelastic behaviour of polymer systems in oscillatory shear flow, determined by the storage G' and loss G'' moduli, as a function of angular frequency, ω. In the case of polymer samples, at the temperatures and frequencies at which the rheological measurements were carried out, it is expected that they should exhibit characteristic terminal flow behaviour, expressed by the power laws $G' \sim \omega^2$ and $G'' \sim \omega$. In contrast, polymer nanocomposites demonstrate linear viscoelastic behaviour, which is completely different from the behaviour of the homopolymer or conventional polymer–filler composites [2, 3]. Non-terminal zone behaviour of the storage and loss moduli is observed, which was found to be dependent on both the clay content and the interfacial interactions. At low frequencies, the dynamic moduli $G'(\omega)$ and $G''(\omega)$ increase with clay loading, but their power-law initial slopes were found to decrease [2-4, 8]. The values of the power-law exponents, m and n, determined by Equation (2.4) are usually compared to the expectations: for neat polymer $m = 2$ and $n = 1$; for the liquid-crystal polymer (LCP) domain flow, $n = 0.5$; and for systems with yield flow; $n = 0$.

Generally, an LCP-type non-terminal behaviour is reported for nanocomposite melts [17–20]. As an example, the PMMA hybrid melts of 10% and 15% organo-smectite (= 3.3 and 5 vol% inorganic clay), synthesised by an *in situ* polymerisation technique, show that both exponents decrease with increasing SPN smectite loading (the various organo-smectites are listed in **Table 2.4**), and this effect is stronger for the storage modulus G' than for the loss modulus G''. However, the values of the exponents, determined by Equation (2.4), do not exceed $m = 0.65$ and $n = 0.5$ for the concentration range studied; thus the nanocomposite melt behaved like a solution of LCP rather than as a filled melt with yield stress. **Table 2.1** presents the composition and rheological characteristics of SPN smectite hybrids with PMMA at 180 °C [20, 43].

Several authors have reported that end tethering via ionic polymer–filler interactions has very strong effects on the terminal zone behaviour of the dynamic moduli of nanocomposites [2, 13–17, 38, 62]. For example, a range of end-tethered thermoplastic nanocomposites at relatively low organoclay loading of 2–5 wt% behaved like a solution of LCP. In contrast, deviations from homopolymer-like behaviour in non-tethered (either exfoliated or intercalated hybrids) have been observed at relatively high filler loading

Table 2.1 Composition and rheological characteristics of SPN smectite hybrids with polymethylmethacrylate at 180 °C

Sample	Organoclay content* (wt%)	Inorganic clay content (vol%)	Terminal exponent m for $G'(\omega)$	Terminal exponent n for $G''(\omega)$	Limit of linearity γ_0 of damping function $h(\gamma)$ (%)
PMMA	–	0	2	1	5
10% SPN	10	3.3	1.1	0.7	0.3
15% SPN	15	5	0.65	0.5	0.15

**The SPN smectite organoclay contains 33 wt% of inorganic clay and 67 wt% of organic modifier SPN: oligo(oxypropylene)-diethyl-methyl-ammonium chloride*
Data from [43]

(e.g., 20 wt% clay) [2, 17]. Witten and co-workers [38] have suggested that tethering of the polymer molecules is expected to create an energetic barrier to segmental motion at the interfaces, which leads to a dramatic increase in the relaxation time and hence a shift of the terminal relaxation to very low frequencies. Hoffmann and co-workers [14] studied the effects of interfacial interactions in exfoliated polyamide-12 nanocomposites with 4 wt% organoclay. Two types of exfoliated nanocomposites were prepared, end-tethered and non-tethered. They observed that flow of exfoliated but non-tethered nanocomposites is dominated by the matrix behaviour, with only a minor contribution of clay. In contrast, tethering dramatically enhanced the G' and G'' moduli of the exfoliated nanocomposites. It is proposed that the end tethering has a stronger influence on flow than does the exfoliation. Lim and Park [15, 16] also reported dynamic flow rheological data for polymer nanocomposite systems, which demonstrate a sharp distinction between the classical filler-like influence of the exfoliated clays and unique effects assigned to the end-tethered nanocomposites.

The ability of clay platelets to interact and form a 3D network structure depends on the degree of dispersion, aspect ratio, concentration and orientation. Therefore, low values of the initial slopes of the dynamic moduli may be considered as one of the indicators of a higher degree of clay dispersion in polymer nanocomposites, if other factors are kept constant. Tanoue and co-workers [17] have used the values of the initial slopes of the dynamic moduli in the terminal region to compare the degree of clay exfoliation in polystyrene/clay nanocomposites. They observed that, when the clay platelets are exfoliated, the effective aspect ratio reaches its maximum and the possibility of contact is high, even at low organoclay content. By contrast, when clay platelets are dispersed in the matrix as stacks, the interactions are small and the systems behave like a suspension of solid particles with a low intrinsic viscosity, $[\eta]$. The storage modulus G' is found to

be more sensitive than the loss modulus G'' to the dispersion of nanoclay sheets because the interfacial energy between polymer and clays is much more sensitive to the elastic than the viscous characteristics [2, 21, 22, 24, 25, 29].

Further, the values of the terminal zone exponent of the storage modulus, m, are used to compare the extent of smectite delamination in thermoset systems, on varying the type of organic modifier. In several publications [39, 43, 44], the preparation of epoxy-based nanocomposites is reported with the following types of alkaline cations, used as organic intercalant of the smectite (the various organo-smectites are listed in **Table 2.4**): hexadecyl-octadecyl-ammonium chloride (SAN); trioctyl-methyl-ammonium chloride (STN); and oligo(oxypropylene)-diethyl-methyl-ammonium chloride (SPN). An appropriate amount of organo-smectite is dispersed first into anhydride hardener HY917, then DGEBA epoxy resin Araldite LY556 (CIBA) is added in the proportion 90:100. The systems are studied as precursors of the smectite/epoxy nanocomposites prior to thermal curing. The inter-gallery ions of the organic modifiers of smectites are found to assist in a different way in the intercalation of epoxy/anhydride molecules into the smectite galleries.

Figure 2.2 presents the storage modulus G' *versus* angular frequency ω of dispersions with 3 vol% of SAN, STN and SPN smectites in the epoxy/anhydride matrix. The terminal zone exponent m is determined by the slope of the curves (Equation (2.4)) [44].

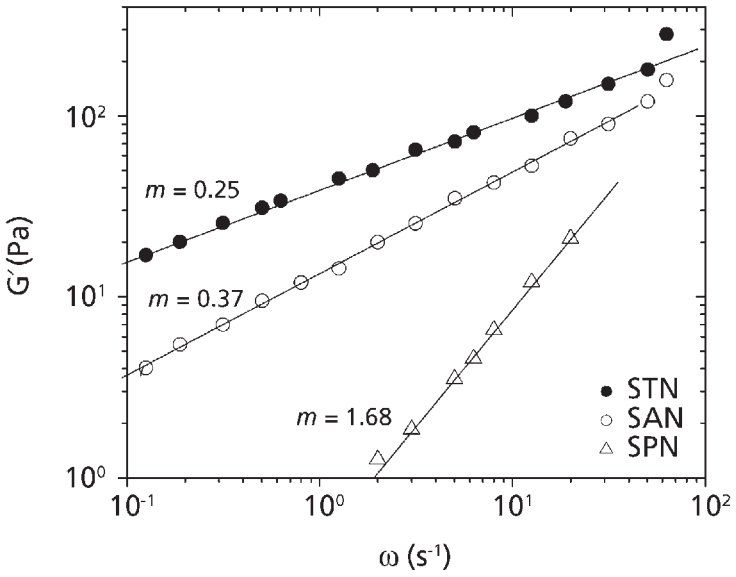

Figure 2.2 Low-amplitude storage modulus G' *versus* angular frequency ω of 3 vol% SAN, STN and SPN smectites in epoxy/anhydride matrix (100/90) at 20 °C. The slope of the curves represents the terminal zone exponent m (Equation (2.4)).

Reproduced with permission from [44]. ©Heron Press, Bulgaria, 2005

In spite of fixed volume content, the slope of the G' modulus is very different for the three types of organo-smectites. The value of m varies in a wide range of m = 1.68, 0.37 and 0.25 for SPN, SAN and STN smectite, respectively. The results account for the different miscibilities of organo-smectites in the epoxy/anhydride matrix. As seen from the low values of m, the best delamination of organo-smectites is reached for STN, followed by SAN dispersions, thus leading to the formation of epoxy/smectite hybrids. In contrast, the value of m = 1.68 indicates a poor quality of delamination for SPN smectite, so this system behaved like a conventional dispersion of clay stacks.

As the epoxy/smectite hybrids are used as the precursor of nanocomposites prior to curing, the extent of delamination of organoclays in the dispersions is the determining factor for the final structure of nanocomposites after curing. Therefore, from the technological point of view, it is important to control the precursor dispersions (i.e., hybrids) in order to design nanocomposites with the desired structure and properties.

2.3.2.3 Shear Thinning Effect

At low shear rates the steady shear viscosity of polymer/layered silicate nanocomposites exhibits enhanced shear thinning, whereas at high shear rates it is almost independent of silicate loading and comparable to that of unfilled polymer. This unique combination of rheological properties is attributed to the ability of the highly anisotropic layered silicates to orient in the flow direction. Several publications [1–4, 9, 16, 22, 59] have reported a qualitative relationship between the extent of shear thinning and the concentration of organoclay platelets. Krishnamoorti and co-workers [22] studied the melt steady shear response of polystyrene/polyisoprene hybrids with various organoclay contents. At high silicate loading (6.7% and 9.5%), the viscosity diverges significantly from that of the homopolymer. The authors related this viscosity effect to the presence of pseudo-solid-like behaviour for the more highly filled nanocomposites, indicative of a percolated filler network and strong filler–filler interactions.

The divergence of viscosity at low shear rates is observed in many other filled systems and is related to the filler network superstructure. However, in conventional composites, such divergence occurs at much higher filler concentration: thus, for example, for glass-fibre-filled PP composites at 30 wt%, and for graphite/diamond-filled elastomers at 12 vol% [11].

In a few publications [20, 22], the shear thinning effect is demonstrated by the concentration dependence of the damping function $h(\gamma)$. The shear stress relaxation of 10 and 15 wt% SPN/PMMA hybrids, $G(t,\gamma)$, has been studied [20] at various strain amplitudes to determine experimentally the shear damping function, $h(\gamma)$. It is observed that the limit of linearity, γ_0, of the damping function, $h(\gamma)$, for nanocomposites displays a decrease in order of magnitude, when compared with that of pure PMMA (see **Table 2.1**). The values of γ_0 determine the deformation limit of the linear viscoelasticity, which is

0.3% to 0.15% for the hybrids and 5% for PMMA. Therefore, the hybrids are very sensitive to the strain amplitude, and this is related to the orientation of anisotropic smectite layers in the shear flow direction.

Wagener and Reisinger [61] proposed shear thinning characterisation as a method to quantify the degree of exfoliation of nanocomposites. The authors calculated the 'shear thinning exponent' n from the initial slope of the complex viscosity as a function of frequency, $\eta^* \sim \omega^{-n}$. It is assumed that, when other factors are constant, the shear thinning exponent n may reflect the exfoliation quality of nanocomposite samples, prepared under intentionally varied conditions (e.g., type of organoclay, processing, and so on). Therefore, n is proposed as another semi-quantitative measure of the degree of exfoliation and delamination of nanocomposites. Interestingly, a relationship between the melt-state shear thinning exponent n and the solid-state tensile modulus of the nanocomposites is observed. The better the silicate platelets are exfoliated, the stronger the reinforcement effect is on the resulting nanocomposite at a given filler content. Similar structure–property relationships are reported for polycarbonate/carbon nanotube composites [32], where the extent of shear thinning has been directly linked to the percolation threshold for electroconductivity.

In [44], the shear thinning exponent n was correlated with the terminal zone exponent of the storage modulus m, in order to quantify the extent of delamination of organo-smectites in an epoxy matrix, on varying the type of organic modifiers. **Figure 2.3** compares the steady-state master flow curves in reduced coordinates, σ *versus* $\dot{\gamma} a_T$ for the same 3 vol% dispersions of SPN, SAN and STN in epoxy/anhydride as in **Figure 2.2**.

For constructing the master curve, the time–temperature superposition is applied to data at 20 °C and 30 °C, with reference temperature T_{ref} = 20 °C and shift factor a_T. The shear thinning exponent n is determined from the slope of the straight line fitted to the experimental data at low shear rates, using Equation (2.1). The values of n decrease significantly from n = 1 for the epoxy resin, to 0.76, 0.40 and 0.26 for the 3% SPN, SAN, and STN dispersions, respectively. Obviously, the rheological response of the dispersions ranges from LCP type (for SPN) to systems with yield stress (for SAN and STN).

As is shown in **Figure 2.3**, time–temperature (t–T) superposition is valid for the investigated systems within the weak temperature region. This unique shear rheological response indicates that the filled systems behave as a single-phase polymer. The temperature shift factor a_T is found to be similar to that of the pure polymer ($a_T \approx 3$) for SPN and SAN dispersions, but is much higher ($a_T \approx 4.5$) for STN dispersions. As shown previously, the STN dispersions could be accepted as well-intercalated hybrids. The higher value of the shift factor suggests that the temperature-dependent relaxation of the STN smectite dispersions is not the same as that of the bulk polymer, thus indicating end tethering.

Figures 2.2 and **2.3** demonstrate a good correlation between the shear thinning exponent, n, and the non-terminal zone exponent of the storage modulus, m, when comparing the miscibility of various organo-smectites within the matrix polymer. This

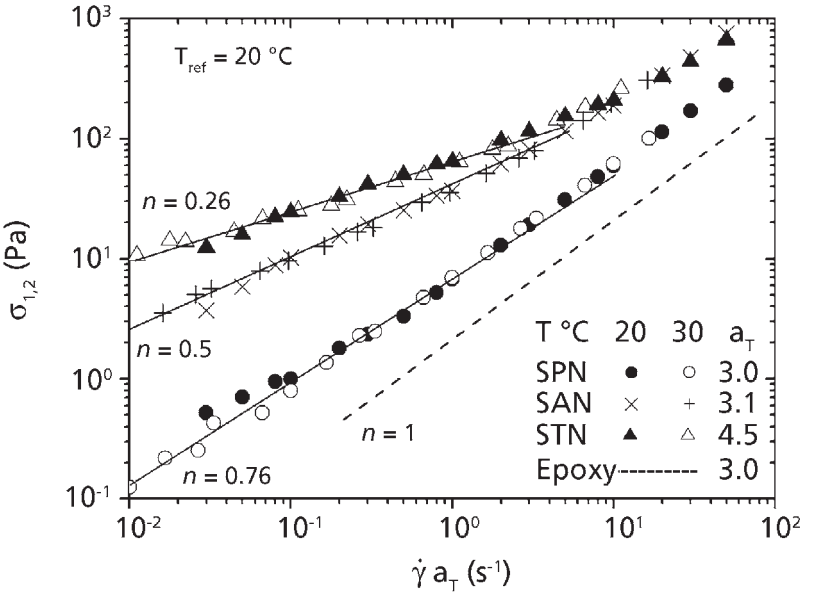

Figure 2.3 Master flow curves in reduced coordinates, σ_{12} *versus* $\dot{\gamma}a_T$, of the systems from **Figure 2.2**, plotted from the experimental data at 20 °C and 30 °C, with T_{ref} = 20°C and shift factor a_T. The slope of the flow curves represents the shear thinning exponent n (Equation (2.1)).

Reproduced with permission from [44]. ©Heron Press, Bulgaria, 2005

result confirms the applicability of the rheological parameters, m and n, to quantify the extent of smectite delamination and to control the structure of nanocomposites. Based on the rheological estimation, we suggest that the STN organo-smectite demonstrates a very good dispersion in an epoxy resin/anhydride matrix, resulting in intercalated hybrids before curing. The other two organo-smectites studied have lower dispersion ability than STN, thus probably forming either mixed intercalated/unintercalated structures (SAN) or conventional dispersions (SPN) with the anhydride/epoxy matrix.

2.3.3 Characterisation of the Superstructure of Nanocomposites

Rheology method II quantifies the development of the particulate superstructure of nanocomposites by increasing the volume fraction of the filler. Our contention is that the filler superstructure, under given conditions, will primarily determine the rheological response of the system, and thus the viscous and viscoelastic characteristics of nanocomposites should be a function of the volume fraction ϕ. The polymer–filler interactions are also

very important for the rheological response, but the emphasis of rheology method II is on the concentration dependence of the rheological characteristics.

This rheological method characterises the complex flow behaviour of nanocomposite materials, on varying the nanofiller content. Nanocomposites are investigated at low rates and at high rates of deformation in order to evaluate how the filler superstructure in the polymer matrix is modified by the application of flow and with increasing filler loading. The most informative is the low-deformation-rate test method, which estimates the strength and the sensitivity of the structure to the flow conditions, as well as the flocculation processes.

The *low-shear-rate test method* determines the following main rheological parameters, which may be used as a practical tool to quantify the filler superstructure of nanocomposites [39–43]:

- scaling characteristic of the storage modulus (scaling exponent μ);
- pseudo-solid-like response (yield stress σ_0, and values of $G' > G''$);
- critical concentrations for structural transition (first and second percolation thresholds, ϕ^* and ϕ^{**}).

The *high-shear-rate test method* might be used for modelling the flow behaviour of nanocomposites (e.g., deflocculation, alignment) by increasing both the shear rate and the filler content. The most applicable for theoretical and practical use are models describing the concentration dependence of viscosity.

2.3.3.1 Low-Shear-Rate Flow Behaviour

2.3.3.1.1 Scaling of Viscoelasticity

The rheological behaviour of nanocomposites is complicated by the fact that, even at small filler volume fractions, a large surface area exists and most polymer chains are at or close to a filler surface. In order to clarify the structural issue in nanocomposites, the theoretical considerations for colloidal dispersions are proved for application in nanocomposites.

Colloidal dispersions exhibit complex rheological behaviour that depends on particle volume fraction and aggregation processes [63, 65]. The cluster–cluster aggregation (CCA) model has been elaborated for the understanding of colloidal aggregation by increasing the filler content [66–71]. According to the CCA model, kinetic aggregation of fine filler particles in polymers is based upon the assumption that the particles are allowed to fluctuate around their main position in the matrix. Upon contact of neighbouring particles or clusters, they stick together and form cluster–cluster aggregates (flocs). Several experimental studies reported on the fractal and temporary nature of the flocs [71, 72].

It is considered that the polymer matrix occluded within the flocs does not participate in the flow [65]. As a result, there is an effective increase of the solid phase presence and a corresponding decrease of system fluidity. The degree of flocculation increases with the concentration of nanofiller and decreases with the intensity of the flow field, thus accounting for the macroscopically observed shear thinning behaviour.

There have been studies on the scaling behaviour of rheological characteristics of colloidal aggregates (flocs) above a critical concentration [71-72]. Colloidal gels are very similar to polymer gels in that both are viscoelastic. In view of this similarity, the scaling of the elastic properties with respect to the particle concentration is proposed, which is dictated by the fractal nature of the flocs. The gel network is considered to be a collection of fractal flocs that are closely packed within the sample. The rheological studies showed that both storage modulus G' and shear modulus G, as well as the limit of linearity γ_0, exhibit a power-law behaviour as a function of particle concentration ϕ [69, 71, 73]. From this, the elastic characteristics of the compound can be described as a function of volume fraction of filler by involving the fractal dimensions characteristic of the floccules, which is consistent with the scaling. An example model is presented by the equation:

$$G'_0 \sim \phi^{\mu} \tag{2.5}$$

where G'_0 is the storage modulus at low frequencies ($\omega < 0.5\ s^{-1}$), ϕ is the volume fraction of filler, and μ is the scaling exponent, expressing the strength of the filler structure.

Equation (2.5) describes the change of floc size as the particle concentration is varied. This is related to the rapid flocculation, which can be characterised by the scaling exponent μ. The theory predicts two types of scaling behaviour when the particle concentration is increased: (i) the strong link regime with $\mu = 3.5 \pm 0.2$ (dominated by individual flocs); and (ii) the weak link regime $\mu = 4.5 \pm 0.2$ (dominated by the 3D network of flocs) [69, 73].

On the basis of the similarity of the flow curves at different filler concentrations for a given material, Lin and Chen [74] elaborated a fractal scaling model, while Trappe and Weitz [75] argued in terms of a percolation concept. Buscall and co-workers [73] showed that a cluster of submicrometre spheres formed by rapid aggregation become space filling and form a network at a critical volume fraction of $\phi \sim 0.05$.

The application of scaling concepts to nanoparticle-filled polymer systems is discussed insufficiently in the literature. It is expected that the scaling of the rheological characteristics in nanocomposites will become somewhat more complicated, since the nature of the solid-like network structure may depend on whether the interparticle attractions or the interactions between particles and polymer chains are stronger. Trappe and Weitz [75] and Jäger and Eggen [76] successfully applied percolation and fractal theories to carbon black/resin compounds. Accordingly, the network strength results theoretically from the number of links per unit surface area, which correlates with the contact probability of carbon black aggregates. As a result, the network is formed at a

critical volume fraction of carbon black. The authors proposed that the ability of carbon black aggregates to form corresponding bonds may account for differences in network strength between various carbon black types. Liu and co-workers [77] analysed the scaling of rheology data of carbon nanotube/polycarbonate composites and described the network structure in terms of two factors: the entanglement of the nanotubes themselves and the polymer–filler interaction.

Evidently, the nature of the network structure in nanocomposites remains controversial and depends largely on the systems investigated. Rheological investigations based on the scaling concept may assist in a better understanding of how the filler and the polymer contribute to the network structure and the viscoelastic properties of nanocomposite systems. For example, determining the values of the *scaling exponent* μ (Equation (2.5)), it might be possible to quantify the evolving superstructure with increasing volume fraction of filler. The scaling exponent μ is very sensitive to the strength of the superstructure of nanofiller in liquid polymer; thus the values of μ and a sudden change of slope above a critical concentration might be used as a quantitative characteristic of flocculation. Moreover, using the exponent μ, one may study the effects of different processing conditions and formulations on the development of the filler superstructure, in order thus to control the nanocomposite technology.

2.3.3.1.2 Pseudo-Solid-Like Response

There is a continuous spectrum of rheological behaviour, associated with the ability of dispersed particles or aggregates to interact with each other [2, 3, 18]. At low nanofiller contents, a liquid-like behaviour is observed, and thus the terminal zone slopes of the storage and loss moduli are lower than the theoretical values (e.g., $m < 2$ and $n < 1$), but the values of the storage modulus remain lower than those of the loss modulus, $G' < G''$. At higher filler contents, a pseudo-solid-like rheological response (e.g., $G' > G''$ and $m, n \sim 0$) is observed in polymer nanocomposites (pseudo-solid-like because G' does not exceed G'' by orders of magnitude as expected for a true solid) [2]. The presence of interacting clay layers and the lack of complete relaxation of polymer chains are proposed to contribute to this rheological response at low frequencies. The pseudo-solid-like behaviour was found to arise from the formation of physical connectivity or a percolated network between the nanoclay sheets dispersed in the polymer matrix, but is not due to the immobilisation of confined polymer chains between the silicate layers [6, 21, 29, 62].

The transition limit from liquid to pseudo-solid-like state is dependent on the morphology spectrum, determined by the degree of dispersion and interfacial interactions [78, 79]. In general, systems with high affinity between the matrix polymer and the organoclay demonstrate better exfoliation, and a lower value of the transition limit to pseudo-solid-like behaviour (percolation limit) is observed [21, 26, 80–84]. Moreover, several authors have reported that the pseudo-solid-like behaviour may occur without total exfoliation, mainly due to the high aspect ratio of the clay [9, 31].

The effect of organo-smectite content on the liquid to solid-like response of the storage and loss moduli of an epoxy resin has been reported [40, 45]. **Figure 2.4** shows the plots of G' and G'' as functions of frequency ω, for three volume fractions (2, 5 and 10 vol%) of STN organo-smectite, modified with trioctyl-methyl-ammonium chloride, dispersed in DGEBA epoxy resin Araldite LY556.

In contrast to the Newtonian behaviour of the basic epoxy matrix, non-terminal flow behaviour is found for the smectite/epoxy dispersions. By increasing the smectite concentration, the material's behaviour gradually changes from liquid-like to pseudo-solid-like. Thus, at 10 vol% smectite a second plateau of the dynamic moduli and values of G' higher than G'' are observed, which are attributed to the high volume fraction of the smectite and the high anisotropy of the exfoliated clay layers.

The transition from liquid-like to solid-like behaviour occurs at different contents of nanofiller depending on the composition and processing. Wooster and co-workers [31] studied the structural transition in a thermosetting nanocomposite, based on an organoclay with cyanate esters. At a low clay concentration, $G' < G''$, indicating that the viscoelastic behaviour of composites is dominated by the viscous matrix. However, on increasing the clay content the difference between G' and G'' decreases dramatically, and at 4 wt% clay $G' > G''$ is observed; therefore the mixture switched from viscous liquid to elastic solid behaviour. Similar results are observed for multiwalled carbon nanotube/

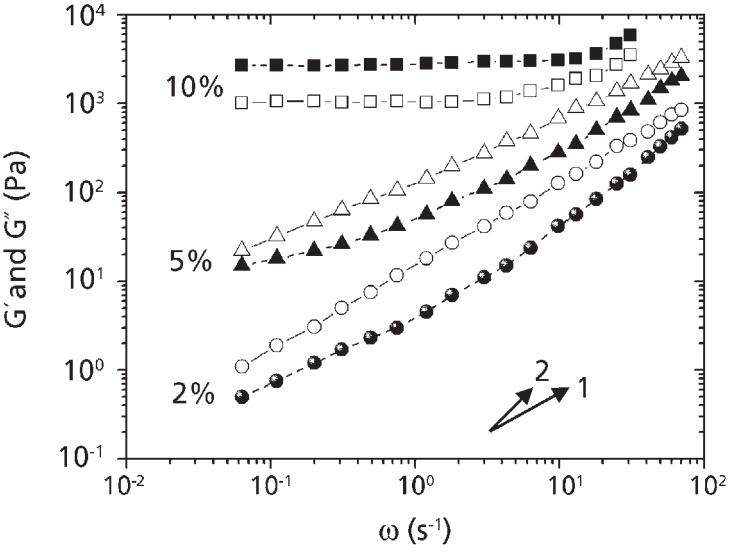

Figure 2.4 Low-amplitude dynamic moduli G' (full symbols) and G'' (open symbols) *versus* frequency ω for 2, 5 and 10 vol% STN smectite in Araldite epoxy resin, at 20 °C.

Reproduced with permission from [40]. ©Heron Press, Bulgaria, 2001

polycarbonate composites [32]. Above the rheological threshold of 2 wt% nanotube content, the viscosity increase is accompanied by an increase in elastic melt properties, represented by the storage modulus, G', which is much higher than the increase of the loss modulus, G''. The viscosity increase is accompanied by an increase in the elastic melt properties, represented by the storage modulus, G', which is much higher than the increase of the loss modulus, G''. The microstructure and properties of these composites also change significantly with the addition of nanotubes above the threshold.

2.3.3.1.3 Apparent Yield Stress

The pseudo-solid-like response of dynamic moduli at low deformation rates of concentrated nanocomposite systems indicates that there exists an infinite yield stress σ_0 in shear flow. The yield stress behaviour is related to the formation of a 3D structure in nanocomposites. Using steady shear flow data, the yield stress is usually determined by fitting Casson's equation (Equation (2.6)) [85] to the initial linear portion of the flow curve, $\sigma_{12}^{1/2} \sim \dot{\gamma}^{1/2}$, where σ_0 is extrapolated (to $\dot{\gamma}^{1/2} = 0$) yield stress:

$$\sigma_{12}^{1/2} = \sigma_0^{1/2} + \eta^{1/2}\ \dot{\gamma} \tag{2.6}$$

where σ_{12} is the shear stress, σ_0 is the yield stress, η is the Casson viscosity, and $\dot{\gamma}$ is the shear rate.

Ren and Krishnamoorti [11] observed that the hybrids of intercalated nanocomposites with styrene–isoprene copolymer display finite non-zero values of the yield stress for the nanocomposites with 6.7 and 9.5 wt% silicate. The steady shear flow yield stress σ_0 is calculated using Equation (2.6). The yield stress values combined with other rheological characteristics, such as solid-like dynamic moduli, diverging viscosities at low shear rates and dramatically enhanced shear thinning, lead to the proposal for the formation of a percolated superstructure in nanocomposites at these silicate contents.

Utracki [19] proposed a theory for the dynamic yield stress of polymer blends, which assumed the formation of dynamic aggregates of dispersed drops. Thus, the yield stress is defined as the strength of the drop–drop interactions, according to:

$$\sigma_y(\omega) = \sigma_y^0[1 - \exp(-\tau_y\omega)]^u \tag{2.7}$$

where $\sigma_y(\omega)$ is the dynamic yield stress function, σ_y^0 defines the interacting entity, τ_y is the relaxation time of the dynamic aggregates, and the exponent u accounts for the aggregate polydispersity.

The same model is used by the author to calculate the dynamic yield stress of clay-containing polyamide nanocomposites [18]. For the nanocomposites, solid-like structure formation with yield stress is reported to take place at a clay concentration about 2.5 times lower than that calculated for the platelet maximum packing fraction. This is related to the presence of end-tethered macromolecules of the chain entanglement type.

The effect of the shape of nanofiller particles on the yield stress values of epoxy-based organo-smectite dispersions has been reported, using rheological data of the steady shear flow [41, 43]. **Figure 2.5** compares the Casson plots, $\sigma^{1/2}$ *versus* $\dot{\gamma}^{1/2}$, of two dispersions in epoxy resin, containing (a) platelet STN smectites, and (b) nanoscale graphite/diamond (e.g., a mixture of finely dispersed graphite and diamond). The volume fraction of nanofillers is varied in the range of 1–10 vol%. The yield stress σ_0 is calculated by extrapolation of data to $\dot{\gamma}^{1/2} = 0$, using Equation (2.6).

As seen from the data shown, at low nanofiller contents, liquid-like shear flow behaviour is observed for both types of nanofiller dispersions. The transition to plastic behaviour with non-zero values of the yield stress appears at a nanofiller content above 2 vol%. The yield values increase dramatically with increasing volume fraction of nanofiller within the range 4–10 vol%, associated with percolation. In the region of high filler contents, the yield values depend strongly on the particle shape. For example, if one compares the systems with a filler content of 10 vol%, the STN smectite/epoxy dispersions demonstrate a yield stress value of $\sigma_0 = 1005$ Pa, which is about eight times higher than that of the nanoscale carbon dispersions, $\sigma_0 = 125$ Pa. This significant difference in the plastic behaviour is obviously due to the high aspect ratio of the exfoliated smectite layers.

In summary, the yield value is very sensitive to the strength of the filler superstructure of nanocomposites and it is an important technological parameter, determinant for the processing.

2.3.3.1.4 Rheological Percolation Transitions

Polymer nanocomposites show a range of performance that starts with the traditional behaviour of conventional composites and ends with end-tethered nanocomposites [9, 18, 29–31]. Generally, two types of filler superstructures are observed in nanocomposite systems on varying the filler content, which are associated with filler–filler and polymer–filler interactions [39, 41, 43].

(i) *Fractal floccules* occur at relatively low nanofiller contents, as a result of the ability of nanofiller particles to diffuse and stick together, thus forming clusters and individual flocs incorporating inside the polymer matrix. We relate such a structure formation with the first rheological threshold, ϕ^* (*flocculation*). The flocculated systems behave like viscous liquids with non-terminal zone behaviour of viscoelasticity ($2 > m > 0.5$), but with $G' < G''$.

(ii) *Network superstructure* occurs at higher nanofiller contents, as a result of the ability of flocs to form a continuous structural network. This structure occurs above the second rheological theshold, ϕ^{**} (*percolation*). The network systems show pseudo-solid-like rheological response with $G' > G''$ and non-zero values of the yield stress.

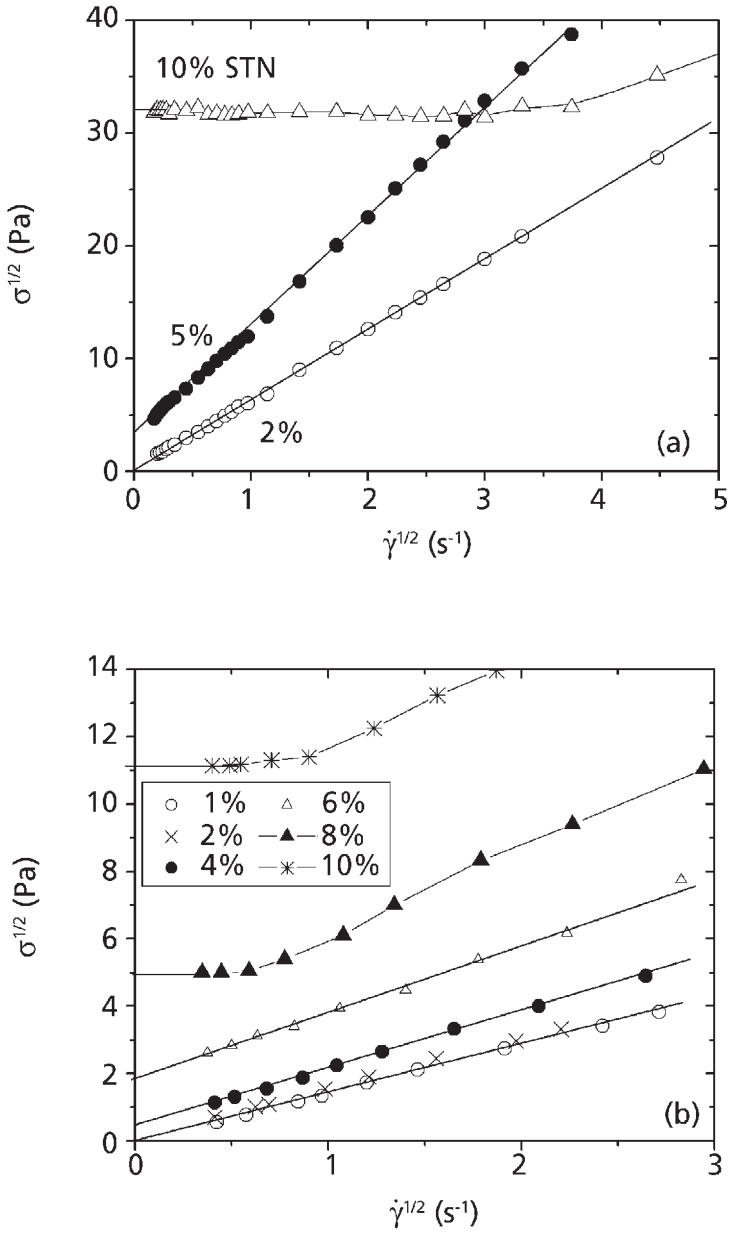

Figure 2.5 Casson plots, $\sigma^{1/2}$ *versus* $\dot{\gamma}^{1/2}$, of dispersions in Araldite LY556 epoxy resin with (a) STN smectite and (b) nanoscale graphite/diamond, on varying the volume fraction of nanofillers in the range 1–10 vol%. The yield stress σ_0 is calculated by extrapolating the data to $\dot{\gamma}^{1/2} = 0$.

Data from [41, 43]. Reproduced with permission from [41]. ©John Wiley Periodicals, 2005

In fact, rheological characteristics are very sensitive to the structural transition of nanocomposites. Moreover, because of the structural transition, it is expected that all the properties of polymer nanocomposites suddenly change beyond the critical value of the filler concentration. Therefore, it is of great theoretical and practical importance to determine the critical filler concentrations, which display the structural transitions. Most of the publications on the rheology of nanocomposites reported on the percolation superstructure of nanofiller and related the sudden changes of the properties of the liquid- and solid-state nanocomposites to the percolation transition [31, 32].

In rheology method II, we propose two critical concentrations, ϕ^* and ϕ^{**}, called the *first* and *second percolation thresholds*. These rheological parameters determine the qualitative structural transitions of nanocomposites with increasing filler content, these are related to local and global percolation. The first percolation threshold, ϕ^* (*flocculation*), expresses the critical concentration of local percolation and formation of fractal flocs. The second rheological threshold, ϕ^{**} (*percolation*) represents the formation of a continuous structural network of fractal flocs [39–43].

The rheological properties change significantly with respect to both critical concentration thresholds. Below the first percolation threshold, ϕ^* (i.e., $\phi < \phi^*$), dispersions show little or no viscoelasticity, and they are typically weakly shear thinning in shear flow. In this low concentration region, the rheological behaviour is similar to that of the homopolymer. Further, in the concentration range between the two percolation thresholds (i.e., $\phi^* < \phi < \phi^{**}$), the rheological behaviour becomes viscoelastic, but still keeps a liquid-like response, with $G'' > G'$, with values of non-terminal zone exponent $m > 0.5$. In contrast, above the second percolation threshold, ϕ^{**} (i.e., $\phi > \phi^{**}$), the rheological response of nanocomposites changes dramatically, which is displayed by the following characteristics: a secondary plateau of the storage modulus G' (i.e., $m \sim 0$); a pseudo-solid-like behaviour of the dynamic moduli ($G' > G''$); sudden increase of the viscosity; and a significant yield stress.

Rheology method II proposes an approach to determine the two percolation thresholds using rheological data from the low-amplitude oscillatory shear flow [43]. As shown in **Figure 2.6**, log–log plots of the low-frequency values of G' and G'' *versus* volume filler content ϕ demonstrate this approach for the example of an STN smectite/epoxy dispersion. The low-frequency storage modulus G'_0 (at $\omega = 0.1\ s^{-1}$) scales with the filler content, $G'_0 \sim \phi^{\mu}$, and a sudden change in the slope of the curve is observed at the critical concentration, ϕ^*. Hence, two values of the scaling exponent μ (3.6 and 7.5) are calculated from this slope as a function of the filler content, by using Equation (2.5). The *first percolation threshold* of $\phi^* \sim 2.5\%$ is determined by the crossover of the two slopes of $G'_0(\phi)$, with $\mu = 3.6$ and $\mu = 7.5$. The change of μ at the percolation threshold ϕ^* represents the transition of the structure from clusters to fractal flocs, produced by cluster–cluster aggregation and rapid flocculation.

In order to determine the *second percolation threshold*, ϕ^{**}, the curves of low-frequency storage and loss moduli, $G'_0(\phi)$ and $G''_0(\phi)$ at $\omega = 0.1\ s^{-1}$, are plotted and compared.

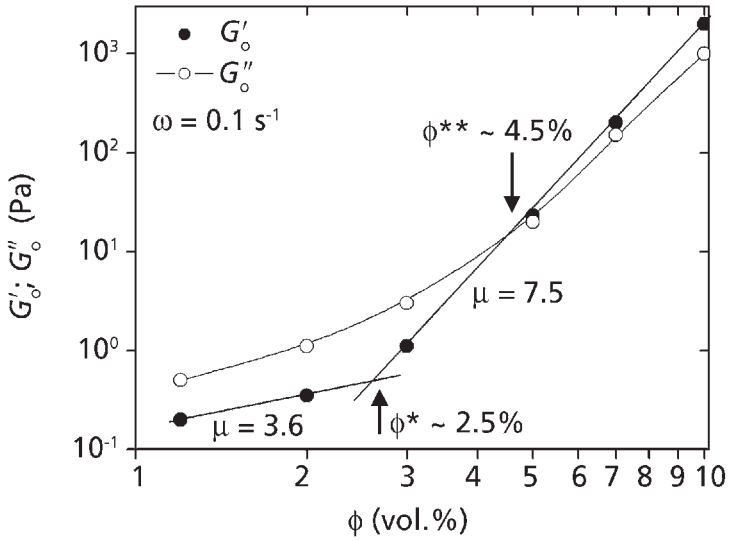

Figure 2.6 Plots of G'_0 and G''_0 at a low frequency ($\omega = 1\ s^{-1}$) *versus* volume filler content ϕ of STN smectite/epoxy dispersions at 20 °C. The first percolation threshold $\phi^* \sim 2.5\%$ is determined by the crossover of the two slopes of 3.6 and 7.5 of the scaling exponent μ. The crossover $\phi^{**} \sim 4.5\%$ of the storage and loss moduli, $G'_0 = G''_0$, determines the second percolation threshold.

Data from [43]

The crossover of the curves, i.e., $G'_0 = G''_0$, is used as an indicator that the mixture has switched from viscous liquid to elastic solid behaviour [31]. Thus, $\phi^{**} \sim 4.5\%$ is determined as the second percolation threshold of the exampled STN smectite/epoxy dispersions (see **Figure 2.6**). Another possibility for determining the second percolation threshold has been reported [39, 42], using the steady shear viscosity data. The ϕ^{**} value is calculated from the relative viscosity curve, $\eta_r(\phi)$, as the point that indicates the sharp increase of the relative viscosity with increasing filler content.

Most of the reported rheological results for polymer nanocomposites deal with the characterisation of the structural transition related to global percolation (i.e., ϕ^{**}). Moreover, there is not good agreement in the literature of how to determine the percolation thresholds rheologically. Wooster and co-workers [31] studied the structural transition of thermosetting nanocomposites with cyanate esters and determined the percolation at 4 wt% organoclay from data of $G' > G''$ indicating the viscoelastic behaviour of composites dominated by the nanofiller structure. Jeon and co-workers [29] determined two critical concentrations of exfoliated polyisoprene/clay nanocomposites, prepared by solution blending, namely the percolation threshold and the effective

maximum packing volume fraction. The percolation threshold of $\phi \approx 0.019$ (1.9%) is determined from the concentration dependence of the terminal zone slope of the storage modulus, *m versus* ϕ, at the point reaching plateau values of $m \sim 0$. The effective maximum packing limit, $\phi_{m,e} \approx 0.032$, is determined from the concentration dependence of the relative dynamic shear viscosity, η'_r *versus* ϕ, at η'_r reaching the plateau values. The value of $\phi_{m,e}$ is found to be much lower than the true maximum random packing limit, $\phi_m \sim 0.06$–0.23, calculated for anisotropic clay layers. The possible implication of the relatively small values of $\phi_{m,e}$ compared to the theoretically predicted ϕ_m is associated with the high aspect ratio of the nanoclay sheets and the strong edge-to-edge and edge-to-face interactions between exfoliated layers [24].

The importance of rheologically determined percolation thresholds is not in doubt. A strong correlation between viscosity, conductivity and microwave characteristics based on two rheologically determined percolation thresholds, ϕ^* and ϕ^{**}, was observed in our study [42], for nanocomposite systems with carbon nanofillers in various thermosets. Usually researchers related the structural transition of the global percolation (i.e., ϕ^{**}) with important physical and mechanical properties of the final nanocomposites. Pötschke and co-workers [32] reported that the rheological theshold occurs in nearly the same concentration range as the conductivity percolation threshold for carbon nanotube composites. This was explained by the fact that the rheological response is sensitive to the interconnectivity of the nanotubes, which is also directly related to electrical conductivity. Wooster and co-workers [30] related the percolation limit with the maximum increase of crack resistance and flexural modulus. A decrease of both mechanical characteristics was found after the percolation limit. Hsieh and co-workers [31] also observed a relation between the mechanical response and the rheological properties of polycarbonate/layered silicate nanocomposites above and near the percolation threshold.

In summary, we assume that a relationship between rheological response, structure and properties of polymer nanocomposites might be proposed based on the two critical percolation concentrations, ϕ^* and ϕ^{**}, displaying structural transitions of the flocculation and the network formation, respectively.

2.3.3.2 High-Shear-Rate Flow Behaviour

2.3.3.2.1 Deflocculation and Alignment

In the case of polymer/layered silicate nanocomposites, the application of a large-amplitude oscillatory shear produces a mesoscopic arrangement of the filler structure, resulting in a global alignment of the silicate layers in the flow direction [2, 11]. The ability of the oscillatory shear to orient these highly anisotropic silicate layers is confirmed using scattering measurements, electron microscopy and linear viscoelastic measurements [2, 8, 21, 33].

Krishnamoorti and Giannelis [2] studied rheologically poly(ε-caprolactone)/clay nanocomposites, and observed significant changes in the viscoelastic response of melts after shear alignment. Thus, the $G'(\omega)$ and $G''(\omega)$ curves of the unaligned sample, measured only under small strain dynamic shear, show high values of both moduli and a pseudo-solid-like behaviour at low frequencies, $G' > G''$, at $\omega < 0.1$ rad/s. However, after long-time shear alignment at a large strain amplitude, the values of both moduli decrease significantly, resulting in a liquid-like behaviour, $G' < G''$, and in addition the initial slope of the G'' modulus increases. Therefore, the application of a large-amplitude oscillatory shear results in shear-aligned materials. Further, the transition from linear to nonlinear viscoelastic behaviour, as manifested by the strain amplitude dependence of the storage modulus [22], decreases with increase of the silicate loading. This is because, by increasing the filler loading, the filler structure is more easily affected by the flow, which is associated with increased filler–filler interaction. The orientation of the clay layers in nanocomposites is considered analogous to that observed in liquid crystals and block copolymers.

The ability of high strains to alter the mesoscale structure and orient the silicate layers results in the failure of the empirical Cox–Merz rule, as demonstrated for polystyrene–polyisoprene/clay nanocomposites [11, 22]. The Cox–Merz rule requires that

$$\eta^*(\omega) = \eta(\dot{\gamma}) \quad \text{for} \quad \omega = \dot{\gamma} \tag{2.8}$$

and is found to be applicable for homopolymers. Generally for nanocomposites, $\eta^*(\omega)$ exceeds $\eta(\dot{\gamma})$ and the magnitude of the difference increases with increase in the silicate loading. Similar data for a failure of the Cox–Merz rule have been observed for conventional polymer composites and other mesostructured materials [78]. However, the dynamic viscosity after prolonged large-amplitude oscillatory shear alignment is less than the steady shear viscosity, $\eta^*_{\text{aligned}}(\omega) < \eta(\dot{\gamma})$, according to data from Krishnamoorti and Giannelis [2]. Therefore, low shear rates result in some orientation of the silicate layers, but high shear rates produce substantial alignment of the silicate layers or tactoids of layers.

Rheological characterisation of polymer/layered silicate nanocomposites at steady-state shear flow confirms the deflocculation and alignment effects of the applied strain. Non-Newtonian behaviour and strong shear thinning at low and intermediate shear rates are observed for steady shear measurements, which are attributed to the ability of steady shear to orient in the flow direction of highly anisotropic silicate layers or tactoids. However, at high shear rates (e.g., $\dot{\gamma} > 1\ s^{-1}$), the viscosity of nanocomposites is found to be nearly independent of the filler loading and comparable to that of unfilled polymer [2, 4, 11, 22]. These observations suggest that, because of the alignment of the clay layers in the flow field, both the viscosity and the shear thinning are dominated by the matrix polymer at high shear rates.

Additionally, polymer/layered silicate nanocomposites demonstrate relatively small effects on the elasticity when compared at an equivalent shear stress. Krishnamoorti

and co-workers [22] reported, for a polystyrene–polyisoprene block copolymer melt and four clay hybrids, that the first normal stress difference N_{12} plotted *versus* the shear stress σ_{12} is independent of the silicate loading and similar to that of the unfilled polymer. Obviously, the silicate layers in nanocomposites do not affect the elasticity of the hybrids. The first normal stress behaviour for polymer/clay nanocomposites contradicted the most often reported results for conventional isotropic particulate composites and anisotropic fibre-filled polymer systems. In traditional filled polymer systems with spherical particle fillers, the elasticity, as measured by the first normal stress difference, decreases at constant shear stress on increasing the filler content, whereas for fibre-filled composites the normal stress difference increases with fibre loading at constant shear stress, even in a Newtonian matrix fluid [86]. Therefore, the results for the elasticity reported for layered silicate nanocomposites are unique and demonstrate unconventional steady shear properties of these materials.

In summary, the independence of the elasticity and the near-independence of the viscosity at high shear rates are associated with a deflocculation and alignment of layered silicates in the flow field.

2.3.3.2.2 Concentration Dependence of Viscosity

The availability of models predicting the concentration dependence of the viscosity of nanocomposite systems is an important issue for theoretical and engineering applications [87]. The relative viscosity of nanocomposites appears to be strongly dependent on the amount of nanofiller, and thus it is valuable to prove the applicability of the well-known theoretical predictions in order to describe the viscosity function, $\eta_r \sim \phi$. A large number of models have been reported for the viscosity of dispersions as a function of the volume fraction and particle shape, but a model for the viscosity of nanodispersions with highly anisotropic filler particles is not available so far.

The simplest rheological dependence for Newtonian suspensions is given by the Einstein relationship for the relative viscosity of hard-sphere suspensions:

$$\eta_r = \eta/\eta_0 = 1 + [\eta]\phi + O(\phi^2) \tag{2.9}$$

where the intrinsic viscosity $[\eta]$ depends on the rigidity and shape of the suspending particles; ϕ is the particle volume fraction. Einstein predicted $[\eta] = 2.5$ for monodisperse and non-interacting hard spheres. For discs with an aspect ratio of $p \leq 300$, the following relationship was found by Utracki [18]:

$$[\eta] = 2.5 + a(pb - 1) \tag{2.10}$$

where $a = 0.025 \pm 0.04$ and $b = 1.47 \pm 0.03$. According to Equation (2.10), when the aspect ratio of the clay platelets varies in the range $p \sim 1$–300, the values of $[\eta]$ could vary from 2.5 to 132, respectively. Therefore, the larger the exfoliated clay layers, the stronger is the effect of $[\eta]$ on the viscosity.

For a concentrated suspension of spherical particles, the Frankel–Acrivos [88] equation predicted well the rapid rise of the viscosity, which is observed at high concentrations, and this can be accounted for by hydrodynamic interactions of neighbouring spheres:

$$\frac{\eta}{\eta_0} \approx \frac{9}{8}\left\{\frac{(\phi/\phi_{max})^{1/3}}{1-(\phi/\phi_{max})^{1/3}}\right\} \tag{2.11}$$

For the description of the concentration dependence of the relative shear viscosity for concentrated suspensions, the Krieger–Dougherty [89] equation is widely used, but it must be taken at constant stress for the multiphase systems:

$$\eta_r = [1 - \phi/\phi_{max}]^{-[\eta]\phi_{max}} \tag{2.12}$$

where ϕ_{max} is the maximum packing volume fraction, which has a unique, theoretically predicted value. For monodisperse hard spheres and oblate ellipsoids, the (experimental) maximum packing volume fraction is $\phi_{max} \approx 0.62$ and $\phi_{max} \approx 0.62/p$, where p is the effective length of the ellipsoids. From geometrical considerations for hard spheres, ϕ_{max} ranged from ~0.52 for simple cubic packing to ~0.74 for rhombohedral packing.

Jeon and co-workers [29] described how the viscoelastic properties are affected with the dispersion or aspect ratio of nanoclays, using the modified Krieger–Dougherty equation:

$$\eta_r = [1 - \phi/\phi_{m,e}]^{-[\eta]\phi_{m,e}} \tag{2.13}$$

In this equation, $\phi_{m,e}$ is the effective maximum packing volume fraction, which accounts for the immobile layer at the nanofiller surface. The value of $\phi_{m,e}$ is lower than the true maximum random packing volume fraction. The authors reported a best fit between the experimental results for the relative viscosity and the values predicted theoretically with Equation (2.13) at $[\eta] = 193$ and $\phi_{m,e} = 0.032$, as well as good agreement between the calculated average aspect ratio and that obtained from TEM observed for the exfoliated polyisoprene/clay nanocomposites studied.

The applicability of the Frankel–Acrivos equation is proved for modelling the concentration dependence of relative viscosity for epoxy dispersions with either smectite clay or nanoscale carbon filler in [39, 42]. **Figure 2.7** presents the results for STN smectite/epoxy dispersions, according to [39]. The effective maximal packing $\phi_{m,e}$ is determined first by plotting $(\eta_r - 1)^{-1}$ *versus* ϕ, and extrapolating to zero ordinate. For the example of STN smectite/epoxy dispersions, values of $\phi_{m,e} = 0.14$ and 0.15 (14–15 vol%) have been determined as the effective maximal packing of dispersions prepared with and without solvent, i.e., 'solvent' and 'direct' processing, respectively. The values of $\phi_{m,e}$ are lower than those usually predicted theoretically, which could be explained by the high anisotropy of the delaminated clay layers, as well as by the polymer layer attracted to the large silicate surface. Note that the values of $\phi_{m,e}$ are shear-dependent; thus, the calculations are carried out using the viscosity at a high shear rate of $\dot{\gamma} = 100\ s^{-1}$, where this dependence is insufficient.

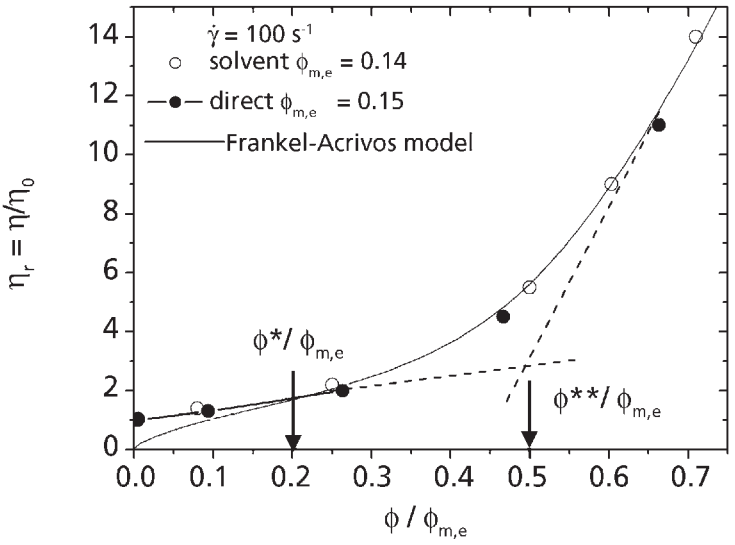

Figure 2.7 Relative viscosity $\eta_r = \eta/\eta_0$ ($\dot{\gamma}$ = 100 s^{-1}) of STN smectite/epoxy dispersions *versus* reduced volume fraction, $\phi/\phi_{m,e}$. Data for 'solvent' (open symbols) and 'direct' (full symbols) processing systems are plotted in reduced coordinates. The full line represents the theoretical prediction of the Frankel–Acrivos model (Equation (2.11)). Arrows show the universal first and second percolation thresholds $\phi^*/\phi_{m,e} \sim 0.2$ and $\phi^{**}/\phi_{m,e} \sim 0.5$, respectively.

Reproduced with permission from [39]. ©Wiley Periodicals, 2005

Based on the above calculations of $\phi_{m,e}$, **Figure 2.7** plots the concentration dependence of the relative viscosity in reduced coordinates, η_r *versus* $\phi/\phi_{m,e}$, which seems to be a universal function.

As shown for STN smectite/epoxy systems, the experimental data of η_r are independent of the different degrees of clay dispersion, produced by 'solvent' and 'direct' processing, if plotted in reduced coordinates. The Frankel–Acrivos model (Equation (2.11), full line) is found to predict the experimental data (points) well at reduced filler concentrations above ~0.2. Thus, the *universal first percolation threshold*, $\phi^*/\phi_{m,e} \sim 0.2$, as well as the *universal second percolation threshold*, $\phi^{**}/\phi_{m,e} \sim 0.5$ are determined from the viscosity curve in reduced coordinates, which are independent of the filler type and processing. Thus, the first percolation limit, $\phi^*/\phi_{m,e} \sim 0.2$, is determined as the crossover of the model curve and the experimental one at very low concentrations (non-interacting particles), wherein the Frankel–Acrivos model generally fails to fit the experimental data. Further, the second percolation limit is determined by examination of the curvature K for the Frankel–Acrivos model (Equation (2.11)) by finding its first and second derivatives. An inflection point is determined at $\phi/\phi_{m,e} \sim 0.5$, where the first derivative of the curvature

function has a minimum at this point [39, 42]. The reduced concentration value of $\phi^{**}/\phi_{m,e} \sim 0.5$ is assumed as the approximate limiting value, after which the rate of viscosity rise becomes much stronger.

2.3.4 Effects of Nanofiller on Relaxation Behaviour

2.3.4.1 Retardation of Polymer Relaxation

It is well known that the rheological and relaxation behaviour of dispersions with micrometre size particles are usually dominated by the rheological properties of the polymer matrix even for high filler concentrations [77, 90, 91]. In the case of dispersions with fine particles, additional relaxation behaviour has been proposed which is attributed to particle clusters at low concentrations or to a particle network for higher concentrations [70]. The relaxation processes are found to be strongly affected by the chemical nature of the nanoparticles' surface and polymer–filler interactions [62, 92–94].

For example, the non-terminal low-frequency behaviour observed in end-tethered polymer/layered silicate nanocomposites is attributed to the retardation of molecular relaxation processes, produced by the tethering of polymer chains to the silicate surface. Krishnamoorti and Giannelis [2] observed that the delaminated hybrids with no end tethering demonstrate classical homopolymer-like terminal behaviour; thus, delamination alone is not sufficient to produce non-terminal flow behaviour. The presence of silicate layers and the lack of relaxation of the polymer chains contribute to the pseudo-solid-like response at low frequencies.

The relaxation processes in polymer systems could be estimated by calculation of the relaxation-time spectra using linear viscoelastic data from experimental rheology and constitutive equation models. The Maxwell model provides the following relationship between the discrete relaxation spectrum and the linear rheological characteristics, wherein (G_i, τ_i) are a discrete set of relaxation spectrum lines [95, 96]:

$$G(t) = \sum_{i=1}^{n} G_i \exp(-t / \tau_i) \tag{2.14}$$

$$G'(\omega) = \sum_{i=1}^{n} G_i \omega^2 \tau_i^2 / (1 + \omega^2 \tau_i^2) \tag{2.15}$$

$$G''(\omega) = \sum_{i=1}^{n} G_i \omega \tau_i / (1 + \omega^2 \tau_i^2) \tag{2.16}$$

$$\eta_E(t) = 3\sum_{i=1}^{n} G_i \tau_i [1 - \exp(-t / \tau_i)] \tag{2.17}$$

Ren and Krishnamoorti [9, 11] provide an analytical description of the linear stress relaxation spectrum for layered silicate-based polystyrene–polyisoprene nanocomposites by fitting to a sum of exponential decays, as in Equation (2.14). The best fit of the spectrum parameters, G_i and τ_i, was found to be the measured data for both the unfilled polymer and the nanocomposites. A significant increase of the longest relaxation time is observed by increasing the silicate loading. The authors reported, for example, that silicate loading of $\phi = 0$, 2.1, 3.5, 6.7 and 9.5 wt% resulted in the following longest relaxation times: $\tau = 0.386$, 1.27, 1.64, 5.1 and 134 s, respectively [11]. Modelling of data by the K-BKZ (Kaye – Bernstein, Kearsley, Zapas) constitutive equation along with the experimentally determined linear stress relaxation and nonlinear damping behaviour was found to be able to capture the viscosity at low shear rates but was inadequate to predict the experimental data at intermediate shear rates.

A spatially linked structure of the dispersed clay particles in the polymer matrix is suggested. Thus, the individual stacked silicate layers are incapable of freely rotating, and hence the relaxation of the structure by imposing small strain is prevented almost completely with high clay content [6, 7, 9, 59, 60]. This type of prevented relaxation led to the presence of pseudo-solid-like behaviour due to the highly geometric constraints or physical jamming of the stacked silicate layers, as well as the lower slope values and the higher absolute values of the dynamic moduli [90, 91].

We have studied the retardation of polymer relaxation processes in PMMA/smectite hybrids, synthesised by *in situ* polymerisation [20]. To prove the reasons for the non-terminal behaviour of the nanocomposite melts, the relaxation-time spectrum $H(\tau)$ ($= G_i\tau_i$) has been calculated by fitting the generalised Maxwell-type model (Equations (2.15) and (2.16)) to the data of the experimental dynamic moduli $G'(\omega)$ and $G''(\omega)$. **Figure 2.8** compares the calculated relaxation-time spectra for unfilled PMMA and hybrids of 10% and 15% SPN smectite, which are 3.3 and 5 vol%, inorganic clay, respectively. As can be seen, the smectite loading produces a shift of the spectra towards longer relaxation times. The longer relaxation time of hybrids in comparison with the homopolymer indicates that the structure of nanocomposites creates a significant energetic barrier to molecular motion during shear flow. This is probably due to the presence of multilayered clay domains, dispersed on a molecular level in the matrix polymer, as well as to interfacial interactions (preferable tethering of the polymer molecules at the silicate surfaces).

Further, modelling the linear viscoelastic relaxation modulus $G(t)$ and the nonlinear elongation viscosity $\eta_E(t)$ are verified by comparing the experimental data to numerically predicted functions (Equations (2.14) and (2.17)). The theoretical prediction showed a sufficiently good fitting with the experimental data in the linear shear and elongation region for both the unfilled polymer and hybrids [20].

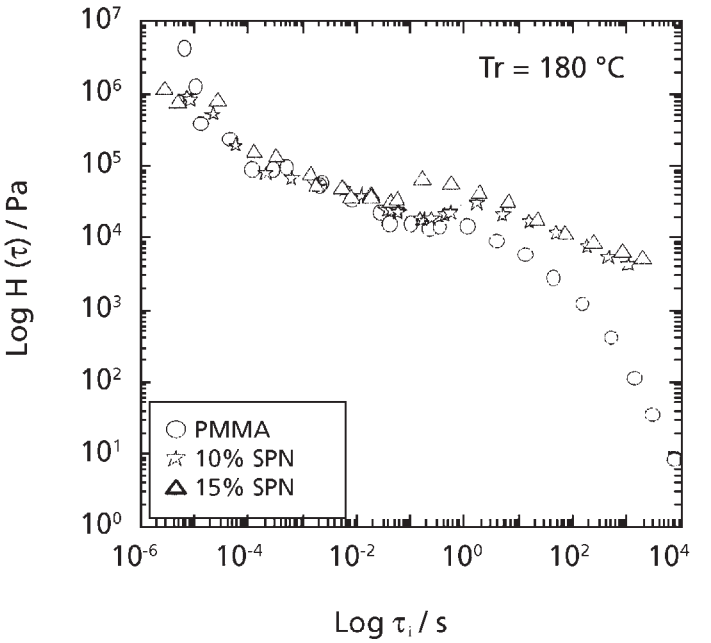

Figure 2.8 Relaxation-time spectrum $H(\tau)$ (= $G_i\tau_i$) of various compositions, i.e., PMMA, and 10% and 15% SPN/PMMA hybrids (3.3 and 5 vol%, inorganic clay), at a reference temperature T_r = 180 °C. The spectra are calculated by fitting the experimental data for linear dynamic moduli G' and G'' to Equations (2.15) and (2.16).

Reproduced with permission from [20]. ©Springer Netherlands, 2002

2.3.4.2 Rheological Characterisation of Polymer–Filler Interactions

Rheology method III proposes an approach to estimate the polymer–nanofiller interactions based on the relaxation-time spectra. The mean relaxation time, τ_m, is calculated from the relaxation spectrum coefficients (G_i, τ_i) by using Equation (2.18). The relative mean relaxation time, $\tau_{m,r}$, is determined as a relationship between the mean relaxation time of the nanocomposite and that of the matrix polymer (Equation (2.19)). Here, $\tau_{m,r}$ is proposed as the *characteristic rheological parameter for polymer–filler interactions*, which presents the 'additional relaxation' of nanocomposites associated with the presence of nanofiller:

$$\tau_m = \sum_{i=1}^{n} G_i \tau_i^2 \Big/ \sum_{i=1}^{n} G_i \tau_i \tag{2.18}$$

$$\tau_{m,r} = \tau_m / \tau_{m,0} \tag{2.19}$$

where G_i and τ_i are relaxation spectrum coefficients, τ_m is the mean relaxation time of the composite system, $\tau_{m,0}$ is the mean relaxation time of the matrix polymer, and $\tau_{m,r}$ is the relative mean relaxation time (characteristic rheological parameter for polymer–filler interactions).

An example of the use of the relative mean relaxation time $\tau_{m,r}$ as a characteristic parameter for quantifying the polymer–filler interactions is presented through the rheological study of the dispersions of graphite/diamond nanoparticles in epoxy resin [41, 43]. The relaxation-time spectrum is calculated from the linear theory of viscoelasticity, by fitting the experimental dynamic moduli $G'(\omega)$ and $G''(\omega)$ to the generalised Maxwell model (Equations (2.15) and (2.16)). **Figure 2.9** compares the relaxation-time spectra, in terms of the spectrum coefficients (G_i, τ_i), of unfilled epoxy resin and dispersions of nanoscale graphite/diamond on varying the filler content in the range 2–10 vol%. **Table 2.2** shows the values of the relaxation characteristics τ_m and $\tau_{m,r}$ (by Equations (2.18) and (2.19)) calculated from the spectra for the unfilled resin and the systems filled with epoxy.

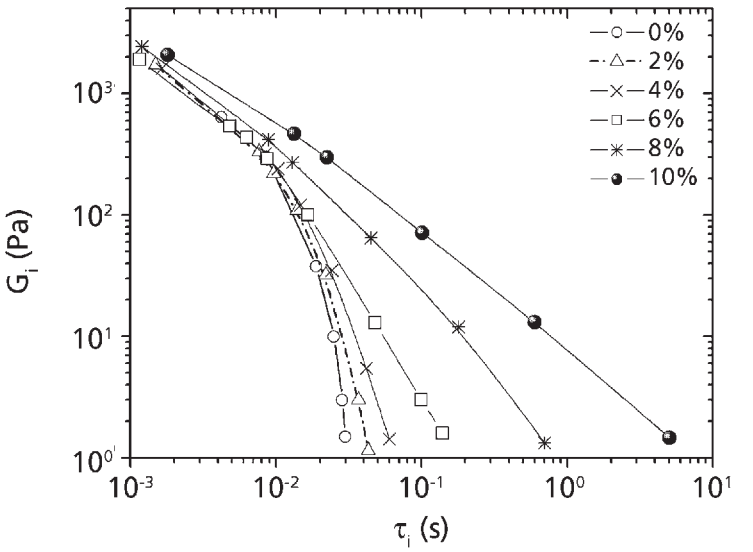

Figure 2.9 Relaxation-time spectra in terms of the relaxation spectrum coefficients, G_i and τ_i, of dispersions with nanoscale graphite/diamond in epoxy resin at 20 °C. The volume fraction of nanofiller varies within the range 2–10 vol%.

Reproduced with permission from [41]. ©Wiley Periodicals, 2005

Table 2.2 Composition and characteristic parameters of relaxation of dispersions with nanoscale graphite/diamond mixture in epoxy resin

Sample	Carbon content (wt%)	Carbon content (vol%)	Mean relaxation time	
			τ_m (s)	$\tau_{m,r}$
Epoxy resin	0	0	0.12	1
1% GD*	1.68	1	0.12	1
2% GD	3.34	2	0.14	1.17
4% GD	6.58	4	0.16	1.33
6% GD	9.74	6	0.33	2.75
8% GD	12.82	8	1.03	8.58
10% GD	15.82	10	5.82	48.5

GD: Graphite/diamond is a mixture of 67 wt% disordered graphite and 33 wt% nanoscale diamond
Data from [43]

Increasing the filler content shifts the spectrum towards longer relaxation times. This is interpreted as an effect of nanofiller–polymer interactions resulting in an 'additional relaxation'. A sharp increase of the relative mean relaxation time $\tau_{m,r}$ is observed above the first percolation threshold accounting for a significantly restricted overall mobility of polymer chains in dispersions with respect to the pure epoxy matrix [41]. For example, the mean relaxation time of 10% GD/epoxy dispersions is about 48 times higher in magnitude than that for the unfilled epoxy resin.

Such a strong increase in $\tau_{m,r}$ beyond the first percolation threshold is related to the flocculation of nanoparticle dispersions, which is considered as formation of individual closely packed fractal flocs. As the fractal flocs occlude the polymer matrix surrounding clusters or nanoparticles by an interface 'bond' layer, they behave as an elastic barrier during shear flow and relax for a longer time than the matrix in the bulk. The degree of flocculation increases with the concentration of nanofiller, and thus the relaxation of the dispersions will be dominated either by interactions within flocs or by interlinking between flocs [65]. Obviously, these interactions produce additional relaxation processes, which are clearly observed both in the non-terminal flow behaviour as well as in the values of the relative mean relaxation time, $\tau_{m,r}$.

Altering the relaxation processes in nanoparticle dispersions is similar to that reported for end-tethered polymer/layered silicate nanocomposites [2, 9]. In general, understanding the relaxation phenomena in nanocomposites based on various nanofillers could be used to elucidate the dynamics of polymer molecules located near to or at the filler surfaces.

2.3.5 Summary

In summary, measurements of the rheological properties of thermoset nanocomposite precursors before curing are found to be crucial to gain a fundamental understanding of the processing and structure–property relationship of these materials.

Thermoset nanocomposites with layered silicates and particulate nanofillers show a range of precursor performance that starts with the traditional rheological behaviour of composites and ends with yield flow behaviour, thus at relatively low filler contents. Important factors dominating the rheological properties are the state of nanofiller dispersion, flocculation processes and polymer–filler interactions. Dispersion structures are highly susceptible to change upon application of deformation. A unique combination of large values of rheological characteristics at low deformation rates and characteristics comparable to those of the matrix polymer at high deformation rates is observed in shear flow. At low deformation rates, small amounts of nanofillers produced strong effects on the linear and nonlinear rheological characteristics of nanocomposites. At high deformation rates the highly anisotropic layered silicates and other anisotropic nanofillers are able to orient in the flow direction. As a result of the shear alignment, the flow behaviour of nanocomposites becomes comparable to that of the matrix polymer.

Three rheological methods for the characterisation of polymeric nanocomposite systems are proposed here, which can be used to examine the shear flow behaviour at low and high deformation rates. The methods were developed as a complex rheological approach to optimise nanocomposite technology by a rapid control of the extent of dispersion, the formation of 3D superstructure of nanofiller, and the polymer–filler interactions. The methods are based on routine rheological experiments and modelling, and aim to control the technology and formulations of nanocomposites of either thermoset or thermoplastic polymers incorporating nanofillers. Each of the three rheology methods might be used for fast and inexpensive control of the nanocomposite preparation technology, in order to identify interesting samples at an early stage of their preparation.

Rheology method I controls the degree of nanofiller dispersion in polymer matrices by using experimental data from low-amplitude oscillatory shear and steady-state shear flow. The method determines two rheological parameters, the terminal slopes (m and n) of the storage and loss moduli, and the shear thinning exponent (n), which are useful to quantify the dispersion quality of nanocomposites. It is assumed that if the nanofiller content and other variables are kept constant, the primary factor determining the rheological response of nanocomposites at low deformation rates will be the degree of dispersion of nanofiller aggregates.

Rheology method II characterises the viscous and the viscoelastic properties as a function of the volume fraction of nanofiller; this is primarily associated with the development of a 3D superstructure in nanocomposites. Nanocomposite systems were investigated at low and high rates of deformation in order to evaluate how the filler superstructure in the polymer

matrix is modified by the application of flow. The most informative is the test method at low deformation rate, which estimates the systems by few rheological parameters, which may be used as a practical tool to quantify the filler superstructure of nanocomposites. The following main parameters are determined by using this method: the scaling exponent of the storage modulus (μ); the pseudo-solid-like response, displayed by the yield stress (σ_0) and values of the storage modulus that exceed the loss modulus ($G' > G''$); as well as the two percolation thresholds (ϕ^* and ϕ^{**}). In the future, the high-shear-rate test method might be used for modelling the concentration dependence of viscosity.

Rheology method III estimates the interfacial interactions in nanofiller-based polymer composites by means of the relaxation-time spectra. The relative mean relaxation time ($\tau_{m,r}$) is proposed as the characteristic rheological parameter for polymer–filler interactions, which presents mainly the 'additional relaxation' of nanocomposites associated with the presence of nanofiller and polymer–filler interactions.

Besides the accomplishments mentioned previously, much research still remains in order to understand the complex rheology–structure–property relationships in polymer nanocomposites. In contrast to the research reported on the rheology of thermoplastic nanocomposite melts, the thermoset nanocomposite systems have been less well investigated. It is necessary to conduct detailed rheological measurements of the liquid nanofiller/resin hybrids prior to curing in order to further our knowledge of thermoset nanocomposite materials. Owing to their extremely small dispersed particle size, nanofiller particles interact with the resin molecules prior to curing. Therefore, in order to understand the processability of these systems and to gain some control over the structure and morphology of the final material, producers may use the proposed three rheology methods as tools for the rapid control of nanocomposite technology.

2.4 Advantages of Rheological Methods for Thermoset Nanocomposite Technology

2.4.1 Preparation and Characterisation of Nanofiller/Resin Hybrids

The rheological approach discussed previously is applied to quantify the degree of nanofiller dispersivity in thermoset matrices and to characterise the structure of the resulting liquid hybrids prior to curing. Various nanofillers are investigated and reported here; these are layered silicates (organo-smectites) and particulate nanoscale fillers (graphite/diamond mixture, and diamond and alumina powders). Thermoset resins, such as epoxy, polyester, acrylic (polymethylacrylate) and polyurethane (polyol isocyanate) are used as matrix polymers. **Table 2.3** shows the characteristics of the thermoset resins; **Tables 2.4** and **2.5** present the characteristics of organo-smectites and particulate nanoscale fillers, respectively. The dispersions of the nanofiller in the thermoset resin are denoted as 'hybrids'.

Table 2.3 Characteristics of thermoset resins

Sample	Tradename and producer	Characteristics	Density, ρ (g/cm^3)	Viscosity at 20 °C, η (Pa-s)
Epoxy resin (ER)	Araldite LY556, CIBA	Bisphenol A type resin	1.17	25.0
Epoxy resin (AP1)	Lackprom	Bisphenol A type resin with dibutylphthalate	1.18	42
Acrylic resin (AR)	BASF	Polymethylacrylate	1.13	2.1
Polyurethane (PU)	BASF	Polyol isocyanate	1.10	1.3
Polyester resin (Viapal)	Viapal VUP4627, Vianova	Vinyl ester resin with styrene	1.10	0.67

Table 2.4 Characteristics of organo-smectites

Sample code	Name and formula of organic modifiers of smectites	Density, ρ (g/cm^3)	Inorganic content* (wt%)	d_{001}† (nm)
SAN	$[C_{16}H_{33})_{0.5}(C_{18}H_{37})_{1.5}N^+(CH_3)_2]Cl^-$ hexadecyl-octadecyl-ammonium chloride	1.56	45.5	2.03
STN	$[(C_8H_{17})_3(CH_3)N^+]Cl^-$ trioctyl-methyl-ammonium chloride	1.58	69.0	2.27
SPN	$[(C_2H_5)_2(CH_3)N^+(O\text{-}iPr)_{25}]Cl^-$ oligo(oxypropylene)-diethyl-methyl-ammonium chloride	1.37	35.5	4.20

**The fraction (wt%) of organoclay that remains after burning the material at 800 °C*
†From XRD data of organo-smectites (data from producer)

Three types of processing techniques are used for the preparation of nanofiller/resin hybrids:

1. *direct processing*, where an appropriate amount of nanofiller is added to the thermoset resin and mixed at a definite temperature (70–80 °C) under certain mixing conditions (e.g., mechanical and ultrasonic dispersing);
2. *solvent processing*, where the organically modified nanofiller is first dispersed in an appropriate solvent and then the resin is added; and
3. *hardener processing*, where the nanofiller is first dispersed in the appropriate amount of the resin hardener (e.g., anhydride) and then the resin is added.

Table 2.5 Characteristics of particulate nanofillers

Sample code	Characteristics	Density, ρ (g/cm^3)	Surface area (m^2/g)	Average size of nanoparticles (aggregate)
Graphite/ diamond (GD)*	67% disordered graphite 33% diamond	1.18	590	6 nm (1–20 nm)
Diamond (D)*	purified from GD	3.36	360	10 nm (6–20 nm)
Disperal D40†	$Al_2O(OH)$ – untreated	2.90	105	50 μm§
Disperal OS1†	Al_2O (OH) – treated with *p*-toluenesulfonic acid	2.70	265	45 μm§
Disperal OS2†	$Al_2O(OH)$ – treated with benzenesulfonic acid	2.70	272	45 μm§

**Produced by shock-wave technology and supplied by Space Research Institute, Bulgarian Academy of Sciences*
†Produced and supplied by SASOL, Germany
§Size of aggregates in dry powder (μm)

The mixing conditions for the ingredients include high-speed mechanical mixing of the dispersions followed by either magnetic stirring, or sonication treatment by a high-power ultrasonic disintegrator. The prepared dispersions are further degassed under vacuum.

For the nanocomposite preparation, *in situ* polymerisation of the nanofiller/resin hybrids is followed under the standard curing conditions used for the basic resin matrix. **Figure 2.10** presents schematically the preparation procedures used in the three types of processing techniques: *direct*, *solvent* and *hardener processing*.

Experimental rheological measurements of the matrix polymers and the dispersions are performed using cone-and-plate type viscometers. Oscillatory shear mode in the frequency range 0.01–100 s^{-1} at a low strain amplitude of 0.01% is used to measure the dynamic moduli within the linear viscoelastic range. Steady-state shear tests are carried out in the shear rate range from 0.01 to 100 s^{-1}.

The nanofiller/resin hybrids are characterised and compared by the rheological methods described previously, in order to optimise the processing conditions and formulations of thermoset nanocomposite systems prior to curing. This is based on the assumption that the rheological parameters determined by the three rheological methods are available for the direct comparison of the dispersion quality of nanocomposites prepared under various conditions. Thus, the rheological methods are proved as a tool for rapid control of the dispersions, and as a useful step in the development of

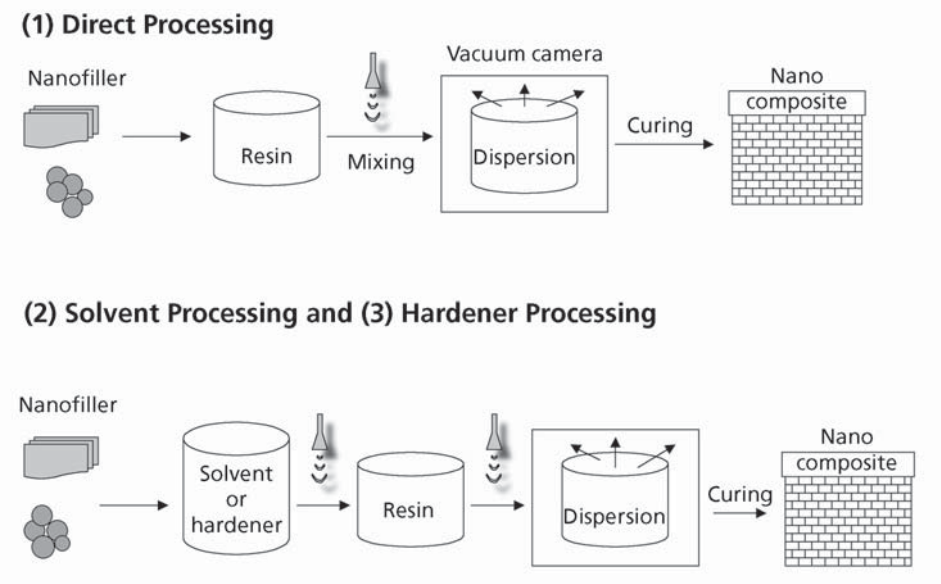

Figure 2.10 Schematic representation of the three types of processing techniques of hybrids used prior to *in situ* polymerisation and synthesis of thermoset nanocomposites: (1) direct processing; (2) solvent processing and (3) hardener processing

nanocomposites. The following rheological parameters and constants are determined in order to control the dispersions:

(i) Shear thinning exponent n and terminal exponent m are calculated and used to compare the degree of dispersion of nanofillers in the matrix polymer.

(ii) Scaling behaviour and the scaling exponent μ are used to provide information about the evolution of the superstructure of the nanoscale dispersions.

(iii) Two critical concentrations of filler dispersion, namely the first and second percolation thresholds (ϕ^* and ϕ^{**}) are determined.

(iv) Based on the concept of the two percolation thresholds, a structure–property relationship is proposed for a prognostic design of thermoset nanocomposites.

2.4.2 Rheological Control of Smectite/Epoxy Hybrids

Dispersions of organo-smectites in epoxy resin were investigated as precursor hybrids of thermoset nanocomposites prior to curing [39, 40, 43–45]. In general, the delamination of smectites and the flocculation of the silicate layers in the matrix resin are the determining factors for the structure and properties of the final nanocomposites.

Therefore, various factors are proved for improving the delamination of clay platelets in the liquid epoxy matrix, as well as for control of the structure of dispersions. Here we discuss the following factors: the processing conditions controlled by solvent and anhydride, and the miscibility of components controlled by organic modifier.

The rheological approach and the three rheology methods discussed previously are used as a tool for controlling the extent of smectite delamination, and the strength of flocculation of the dispersed silicate layers in the epoxy resin matrix. Rheology method I is applied to compare the degree of delamination of organo-smectites in the matrix resin under various processing conditions. The rheological parameters, *shear thinning exponent* (*n*) and *terminal regime exponent* (*m*), are used for the direct comparison of the dispersion quality of systems at a given volume fraction. Rheology method II is used for characterisation of the structure of dispersions and for determination of the two percolation thresholds. Examples of the systems investigated consist of organo-smectites (SAN, STN and SPN) dispersed in a low-viscosity epoxy resin, Araldite [39, 45]. **Tables 2.3** and **2.4** show the characteristics of the ingredients, the epoxy resin and the organo-smectites.

2.4.2.1 Optimisation of Processing Technique

Three types of processing techniques are compared for the epoxy/smectite dispersions, as follows: (1) *direct processing*, where an appropriate amount of organo-smectites are added to the Araldite epoxy resin and mixed; (2) *solvent processing*, where the organo-smectites are first dispersed in toluene (1:3) and then mixed with the epoxy resin; and (3) *anhydride (hardener) processing*, where the organo-smectites are first dispersed in anhydride hardener HY917 (CIBA) and then mixed with the appropriate amount of epoxy resin (epoxy/anhydride = 100/90). The mixing and degassing conditions have been described previously. The smectite volume fraction varies in the range of 0.07–11 vol% and the resulting dispersions are semi-transparent or transparent depending on processing and composition [39].

Figure 2.11 compares the direct and solvent processing techniques. **Figure 2.11(a)** shows the low-amplitude dynamic storage modulus G' *versus* angular frequency ω, and **Figure 2.11(b)** presents the steady-state relative viscosity ($\eta_r = \eta/\eta_0$) *versus* shear rate $\dot{\gamma}$, of STN smectite/epoxy dispersions at various volume fractions of smectite, in the range 0.07–11 vol%. The experimental flow curves $G'(\omega)$ and $\eta_r(\dot{\gamma})$ are fitted with the power-law expressions (2.2) and (2.4), respectively. The terminal zone exponent (*m*) and the shear thinning exponent (*n*) are determined by the slopes of the flow curves from the straight line fitted to the data in the low-shear-rate region $0.05 < (\omega, \dot{\gamma}) < 1\ s^{-1}$. **Table 2.6** summarises the values of (*m*, *n*) of the STN smectite/epoxy systems, presenting data from direct, solvent and anhydride processing techniques.

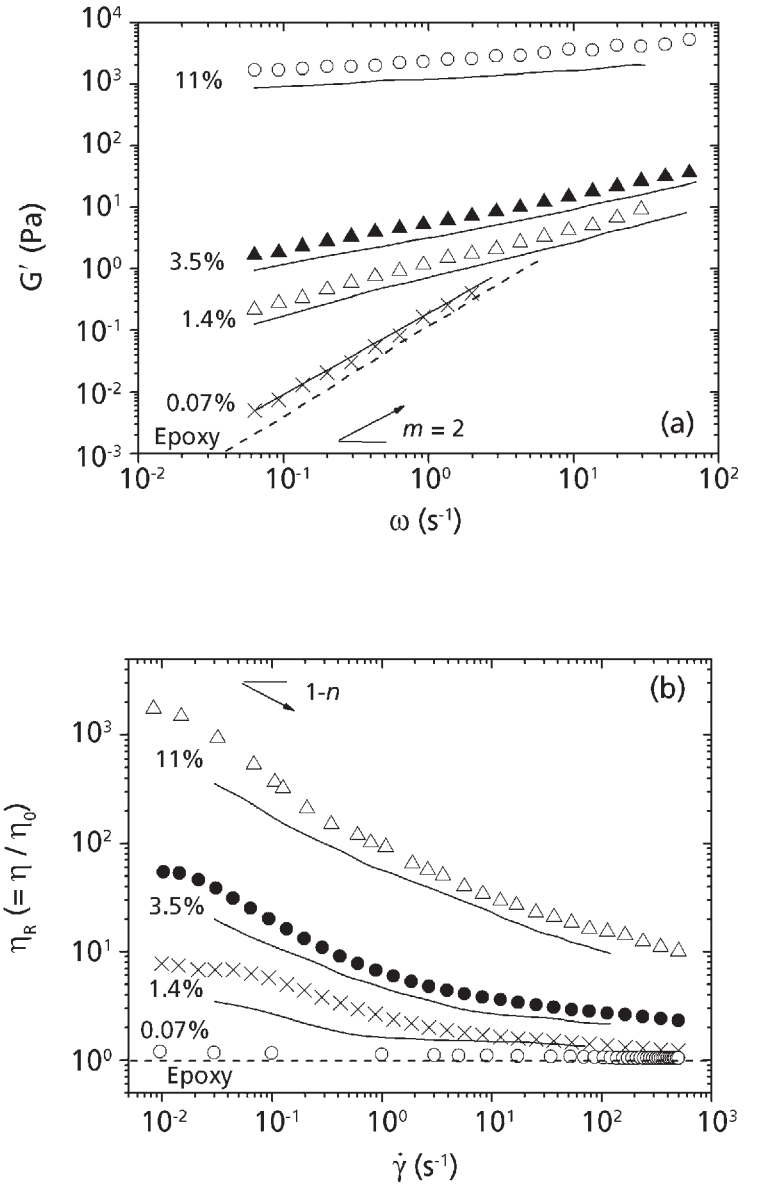

Figure 2.11 (a) Low-amplitude storage modulus *G′ versus* angular frequency ω and (b) relative viscosity $\eta_r = \eta/\eta_0$ *versus* shear rate $\dot{\gamma}$, of STN smectite/epoxy dispersions at various smectite contents (0.07–11 vol%). Solvent processing (symbols) and direct processing (lines) are compared at 25 °C.

Reproduced with permission from [39]. ©Wiley Periodicals, 2005

As seen before, the processing conditions significantly affect the extent of delamination of the smectite platelet stacks in epoxy resin. The storage modulus of the dispersions shows non-terminal zone behaviour, with m varying in the range $2 > m \geq 0$, depending on the filler content and the type of processing. The shear thinning increases significantly on increasing the volume fraction of the smectite, and thus the flow index n varies in the range $1 > n \geq 0$. In general, the solvent processed dispersions demonstrate higher values of G' and η_r, as well as lower values of the exponents m and n, in comparison with those of the direct processed dispersions at a given volume fraction. Taking into account the values of the exponents m and n, it could be concluded that the solvent processing technique produces a better delamination of the smectite stacks if compared to direct processing within the wide range of concentrations studied.

Table 2.6 compares the values of the exponents m and n obtained from the direct, the solvent and the anhydride processing of STN/epoxy dispersions at various filler contents. The lower values of n and m at a fixed volume fraction are taken as a qualitative measure for a better delamination of the smectite in the epoxy matrix. In general, it can be concluded that the three types of processing studied ensure relatively good delamination of the STN smectite, based on the values of m and $n < 0.5$. If the three processing techniques are compared, it could be proposed that the anhydride processing technique, followed by the solvent processing technique, ensures an optimal degree of delamination of smectites leading to intercalated smectite/epoxy hybrids. Obviously, the prior dispersion of smectite, either in anhydride or in toluene, ensured an easy clay delamination. In contrast, the direct mixing of smectite with epoxy resin results in a moderate delamination, leading to a mixture of intercalated/unintercalated hybrids.

In summary, the values of shear thinning exponent n and terminal regime exponent m correlate well in the prediction of the degree of smectite delamination. Rather n and m

Table 2.6 Rheological parameters (n, m) at 25 °C, of STN smectite/epoxy hybrids prepared by direct, solvent and anhydride processing techniques

Sample code	Organo-smectite content (vol%)	Direct processing		Solvent processing		Anhydride processing	
		m (2.4)	n (2.2)	m (2.4)	n (2.2)	m (2.4)	n (2.1)
Epoxy, Araldite	0	2	1	2	1	2	1
0.07% STN	0.07	2	1	1.9	0.78	–	–
1.4% STN	1.4	0.5	0.72	0.4	0.64	0.37	0.40
3.5% STN	3.5	0.32	0.57	0.28	0.35	0.25	0.26
5.0% STN	5	0.30	0.54	0.14	0.20	0.1	0.11
11% STN	10	0.15	0.45	0	0	0	0
Data from [43]							

might be successfully used for comparison of samples, in order to quantify the extent of delamination of smectites in epoxy precursors by varying the processing conditions. Based on the above results, it may be concluded that the solvent and anhydride assisted processing techniques are much more successful for smectite delamination and epoxy intercalation than direct processing.

Additionally, **Figure 2.11** demonstrates that the shear thinning of η_r and the non-terminal behaviour of G' become strongly pronounced above the level of 0.07% smectite, indicating the flocculation of the exfoliated clay layers on increasing the filler content. The terminal zone exponent of the storage modulus decreases significantly from the theoretical value, $m = 2$, with increasing volume fraction and reaches a plateau, $m \sim 0$, at the highest filler content of 11 vol%, accounting for the pseudo-solid-like behaviour. Moreover, the imposition of high deformation rate reduces the viscosity of dispersions near to that of the matrix polymer, accounting for deflocculating and alignment of the stacks or layers within the shear flow field.

Clay dispersions have traditionally been described as plastic flow systems, and they are expected to exhibit intriguing rheology [1, 2, 33, 97, 98]. However, the details are not very well understood in relation to the flow-induced structure of smectites in various media [33, 97, 98]. In order to characterise the nature and the evolution of the structure of dispersions, we study the effect of smectite concentration on the viscoelastic properties. **Figure 2.12** compares the log–log plot of the low-frequency storage modulus G' (at $\omega = 0.1\ s^{-1}$) *versus* volume fraction ϕ of the STN/epoxy dispersions prepared by the direct and solvent processing techniques. Power-law behaviour of this function is represented by Equation (2.5). As seen, the slope μ of the curves suddenly changes its value from $\mu \sim 1.3$ at low filler contents to $\mu \sim 7.15$ at high filler contents, thus at ϕ^*. The crossover point has the values of $\phi^* = 2.5$ vol% and 3 vol% for the solvent and the direct processed systems, respectively.

The value of ϕ^* is interpreted as the first percolation threshold, where a strong flocculation of exfoliated platelets appears. The lower value of the percolation threshold of the solvent processed hybrids, compared to that of the direct processed hybrids, results from a better delamination of smectite with the assistance of solvent. The observed exponent value of $\mu = 7.15$ at $\phi > \phi^*$ is much higher than the theoretical value ($\mu = 4.5$) reported in the literature [73, 98]. The high power is indicative of a strong flocculated structure of the delaminated clay layers at $\phi > \phi^*$. As the clay layers in floccules are presumably ordered in stack-like multilayers and have high aspect ratios of silicates resulting from the 'edge-on-edge' interaction among the unit discs [33, 97], this seems reasonable.

The qualitative change in the structure of dispersions above the percolation threshold ϕ^* and the improvement of smectite delamination by the solvent and anhydride are further compared with the alteration of properties of nanocomposites depending on curing kinetics and morphology.

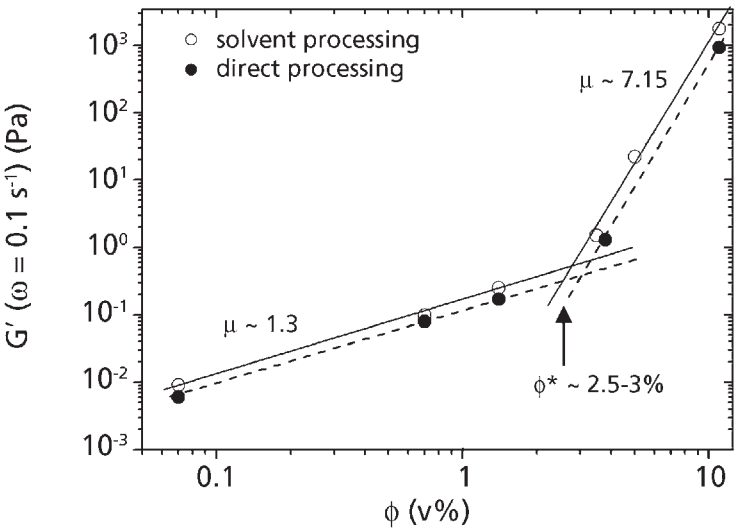

Figure 2.12 Log–log plot of the plateau modulus G'_0 (at $\omega = 0.1\ s^{-1}$) *versus* volume fraction of STN smectite, ϕ, at 25 °C. The theoretical slope μ (Equation (2.5)) suddenly changes from 1.3 to 7.15 and the crossover of the slopes indicates the first percolation threshold, $\phi^* = 2.5\%$ and 3% (arrow) for the solvent and the direct processed hybrids, respectively.

Reproduced with permission from [39]. ©Wiley Periodicals, 2005

2.4.2.2 Long-Time Storage Effects

It is important for practical and theoretical reasons to study the capability of storing liquid epoxy/smectite hybrids for a long time prior to curing. In practice, the storage of liquid epoxy/clay hybrids is a key factor for the technology of nanocomposite preparation. It is important to know the changes of the dispersions during the storage period in order to define their exploitation characteristics. For theoretical reasons, it is important to gain knowledge of the kinetics of nanocomposite formation in epoxy/clay hybrids initiated by the reactive groups of the organo-smectites.

The SAN, STN and SPN organo-smectites studied are modified by quaternised ammonium salts (see **Table 2.4**), which have the potential to affect the curing process of the epoxy resin. Wang and Pinnavaia [49] have prepared clay/polymer nanocomposites by spontaneous self-polymerisation of epoxy resin at elevated temperatures. To study in more detail the possibility of homopolymerisation of epoxy-based smectite hybrids at room temperatures, initiated by the organic modifier of the smectites, the systems prepared by the *direct processing* techniques are left for a long time (120 days). Rheological measurements are performed for control of the hybrids prior to storage

(e.g., just after preparation), as well as step-by-step during storage. The kinetics of nanostructure formation in the smectite/epoxy hybrids during storage is evaluated by comparison of the shear flow behaviour and the viscosity of the dispersions after different storage times [43, 45].

Figure 2.13 compares the relative viscosity, η_r (= η/η_0), *versus* shear rate, $\dot{\gamma}$, curves of 10 vol% SAN, STN and SPN/epoxy hybrids, as affected by the storage (rest) time at 20 °C. The results showed the rheological characteristics of the initial dispersions (right after mixing) and of the dispersions that were left to rest for 70 days.

The viscosity curves of initial dispersions (full symbols) present the best miscibility of STN smectites in epoxy resin, followed by SAN and SPN smectites. The systems show plastic rheological behaviour. For example, the values of the viscosity at a low shear rate of $\dot{\gamma}$ = 0.03 s^{-1} vary from 23 (SPN) to 260 Pa-s (STN), and the viscosity of the unfilled epoxy resin is 2.5 Pa-s (see **Table 2.3**). In contrast, after resting for 70 days the viscosity of the systems dramatically increases by about three decades, the values at $\dot{\gamma}$ = 0.03 s^{-1} varying between 5 × 10^3 (SPN), 1 × 10^5 (SAN) and 4 × 10^5 Pa-s (STN). Such

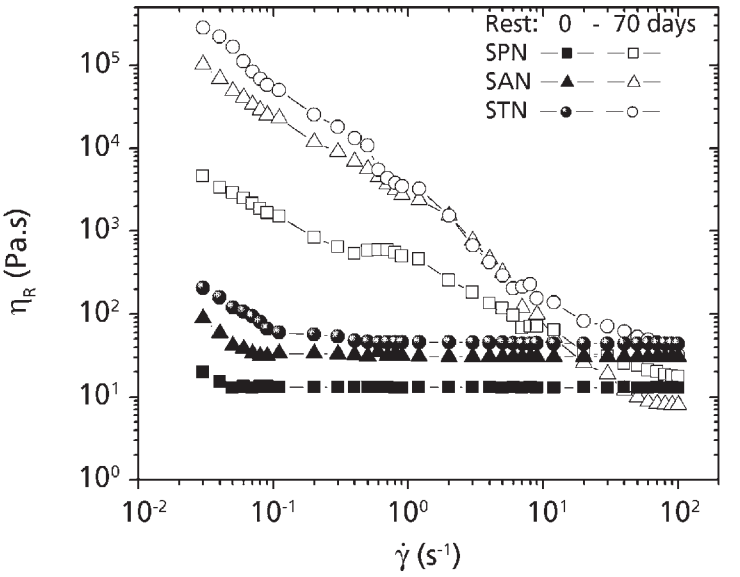

Figure 2.13 Relative viscosity, $\eta_r = \eta/\eta_0$, *versus* shear rate, $\dot{\gamma}$, of 10 vol% SAN, STN and SPN smectite/epoxy hybrids prepared by direct processing. Data for the initial dispersions (full symbols) and for those left to rest for 70 days (open symbols) at 20 °C are compared.

Data from [43]

behaviour might be associated with a self-curing process initiated by the reactive groups of the alkyl-ammonium type modifiers, SAN, STN and SPN. Our observations on the dispersions after a longer resting time of about 3–4 months show that the STN and SAN smectite/epoxy systems turn to a bulk solid material. In contrast, SPN smectite/epoxy systems keep the high-viscosity, pseudo-solid-like behaviour.

Interestingly, during the steady shear flow, the hybrids after 70 days rest show a very strong shear thinning effect. The viscosity decreases by about 4–5 decades by applying shear flow deformation within the range $0.03 < \dot{\gamma} \leq 100\ s^{-1}$. At the highest shear rates, $\dot{\gamma} > 10\ s^{-1}$, the viscosities of the hybrids subjected to storage become even lower than those of the initial dispersions. Moreover, the viscosity curves show three characteristic liquid-crystalline-like regions, corresponding to different arrangements and orientations of the smectite layers in the shear field. The viscosity initially decreases with increasing shear rate, and then a plateau is reached, followed by a second shear thinning region. The viscosity plateau shows evidence of a shear-induced ordering of nanolayers in hybrids at shear flow. The third region of a super-anomalous viscosity, following the plateau region, shows that the steady shear flow becomes metastable because of rapid alignment of the anisotropic smectite layers and tactoids [43, 45].

Evidently, a dramatic increase of the viscosity of the liquid epoxy/smectite hybrids might occur after long-time storage prior to curing. This effect is associated with the evolution of the structure of the dispersions by a self-curing process. Importantly, our observations show that, if the hybrids are prepared by the solvent processing techniques, a short period of rest of the solvent dramatically reduces the self-polymerisation kinetics. The results on the long-term storage ability of epoxy/smectite hybrids provide important information for the processability of the dispersions, as well as for the expected quality of the final nanocomposites, if the precursor hybrids are left in storage.

2.4.3 Rheological Control of Hybrids with Carbon Nanofillers

Nanoscale graphite/diamond and diamond particles are used as fillers in thermoset resins to gain the advantage of novel physical and mechanical properties. For example, the inclusion of conductive nanoscale carbon particles in insulating thermoset matrices leads to electrical conductivity and wave absorption properties being obtained [42, 43]. Recently, a few publications [56, 57] reported on the use of ultrafine diamond as a very hard filler in polymers, resulting in improved strength and wear resistance. A significant reinforcement effect is observed for thermoset composites with nanoscale carbon fillers [41]. Besides single-particle characteristics, the dispersivity of nanofiller particles and the structure formed by nanofiller in polymer are important for the final properties of nanocomposite systems. Conclusions are drawn that the preparation of well-defined systems for specific applications requires control of the dispersion processes and the structure [58, 72, 98].

The aforementioned applications require materials with paths of agglomerating particles for energy dissipation. Such structures to a large extent depend on the particle–particle and polymer–particle interactions, and are also directly related to the rheological response and the specific properties of composites. However, the impact of these interactions on the rheological properties of dispersions and, consequently, on the control of the composite properties have not been examined extensively. Here, we report details of the rheological behaviour of dispersions with carbon nanofillers in thermoset resins because the measurement of the rheological properties of these hybrids before curing is crucial to gain a fundamental understanding of the structure–property relationship for the final nanocomposite materials. The results obtained are applied to assess the optimal compounding conditions of carbon nanoparticles in a given polymeric system in order to maintain certain physical and mechanical properties.

Carbon nanofillers, such as graphite/diamond and diamond, are produced by a shock-wave technology [99] and were supplied by the Space Research Institute, Bulgarian Academy of Sciences. The nanoscale graphite/diamond is a mixture of disordered graphite and nanoscale diamond. Moreover, the nanoscale diamond is produced from the graphite/diamond mixture by chemical purification, which allows the separation of the diamond. The characteristics of carbon nanofillers are presented in **Table 2.5**.

Three types of thermosets are investigated as matrix polymer – Araldite epoxy resin (ER), acrylic resin (AR) and polyurethane resin (PU) – and are presented in detail in **Table 2.3**.

Semidilute and concentrated nanoscale dispersions (hybrids) of graphite/diamond and diamond in resin matrix are prepared at volume fractions ranging from 1 to 10 vol%. The desired amount of nanofiller particles is dispersed in the thermoset resin matrix by using two steps of intensive shearing: high-speed mixing at 7000 rpm for 15 min, followed by sonication for 5 min. The aggregates of carbon nanoparticles are well dispersed in the resin matrices, which leads to stable but non-transparent dispersions. Thus, the carbon/resin hybrids studied have a broad size distribution of particles ranging from nanosized single particles to clusters of micrometre size.

2.4.3.1 Dispersivity of Graphite and Diamond in Epoxy Resin

Rheology method I is applied to the study of the dispersion quality of graphite/diamond (GD) and diamond (D) nanofillers in an epoxy resin/anhydride (100/90) matrix. The hybrids studied are used as a precursor for the nanocomposites prepared further upon anhydride/accelerator-assisted thermal curing. The degree of dispersion is quantified by comparing the rheological parameters, such as shear thinning exponent n and terminal zone exponent m.

Figure 2.14 compares the steady shear and dynamic flow behaviour of 3 vol% graphite/diamond and diamond hybrids in epoxy/anhydride by plots of (a) shear stress σ *versus* shear rate $\dot{\gamma}$, and (b) storage modulus *G′ versus* frequency ω [44].

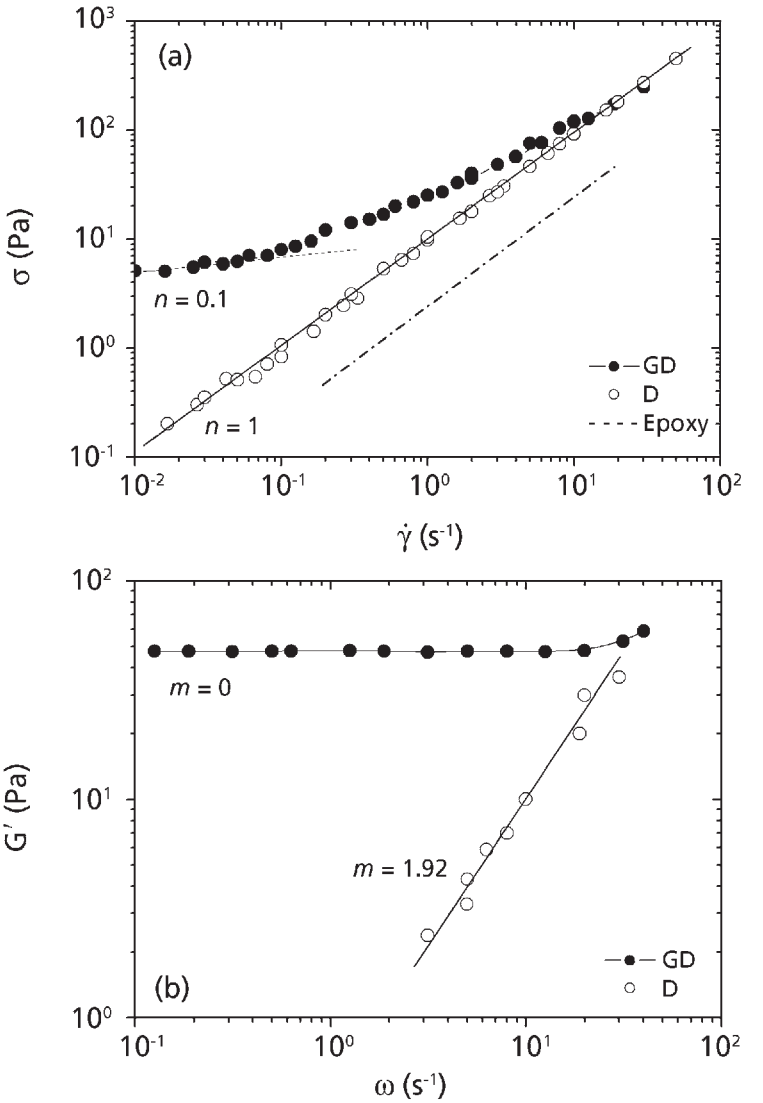

Figure 2.14 Flow curves of (a) shear stress σ *versus* shear rate $\dot{\gamma}$ and (b) storage modulus *G′ versus* ω for 3 vol% graphite/diamond (GD) and diamond (D) in epoxy/anhydride (100/90) matrix, at *T* = 20 °C. The values of the shear thinning exponent *n* and terminal zone exponent *m* indicate a pseudo-solid-like behaviour of epoxy-based graphite/diamond hybrids and a Newtonian behaviour of diamond hybrids.

Reproduced with permission from [44]. ©Heron Press, Bulgaria, 2005

In spite of the fixed volume concentration of 3 vol%, the rheological behaviours of the dispersions seem to be very different. A pseudo-solid-like rheological behaviour (n = 0.1 and m = 0) is found for epoxy-based graphite/diamond hybrids, while a behaviour near to Newtonian is shown for the diamond hybrids (m = 1.92 and n = 1). It can be assumed that at fixed filler content the exponents n and m can be truly dependent on both the degree of dispersion and the different surface areas of the nanoscale fillers. Moreover, the lower surface area of the diamond (~360 m^2/g) in comparison with the graphite/diamond (590 m^2/g) has also to be considered in qualifying the dispersion structure formed by nanofillers.

At a closer look, the diamond/epoxy hybrids show rheological behaviour near to that of the pure matrix, thus representing a low extent of dispersion of diamond aggregates. In contrast, the graphite/diamond/epoxy hybrids demonstrate plateau values of the exponents n and m, indicating that the well-dispersed graphite/diamond nanofiller forms a superstructure of percolated nanoparticles and absorbed polymer layers at the surface, thus at relatively low filler content.

2.4.3.2 Characterisation of the Structure of Hybrids

Experimental and theoretical studies of colloidal dispersions predict that an aggregation of colloidal particles takes place with increase of the inorganic content, which leads to the formation of cluster–cluster aggregates (fractal flocs) at moderate filler content, and to an infinite cluster (network) at high filler content [71, 72, 100]. As pointed out in a few communications [58, 78], dispersions of nanoparticles are characterised by very strong interparticle interactions, so small changes in filler content might change the particle order. Therefore, interactions between carbon nanoparticles cannot be neglected and the preparation of well-defined systems requires a strong control over the dispersion structure. Here, we control the dispersion state and the agglomeration process of carbon nanoparticles in the thermoset systems by varying the volume fraction of nanofiller.

Rheology method II and appropriate rheological measurements are performed, which are informative for analysing the structure of the hybrids and the interaction between particles. We apply an oscillatory flow rheological technique under small strain amplitude, so that the structure of the dispersion is not disturbed from its equilibrium conditions. Example dispersions of nanoscale graphite/diamond in acrylic resin (polymethylacrylate) were studied. **Figure 2.15** plots the low-amplitude dynamic moduli G' and G'' *versus* angular frequency ω of the graphite/diamond/acrylic hybrids with various volume contents of 1–10 vol% [42].

It is seen that a small amount of nanoscale graphite/diamond decreases the terminal slope of the low-amplitude storage modulus from the theoretical value of $G' \sim \omega^2$ for pure resin to $G' \sim \omega^{1.5}$ and $G' \sim \omega^{0.9}$ for 1% and 2% GD/acrylic systems, respectively.

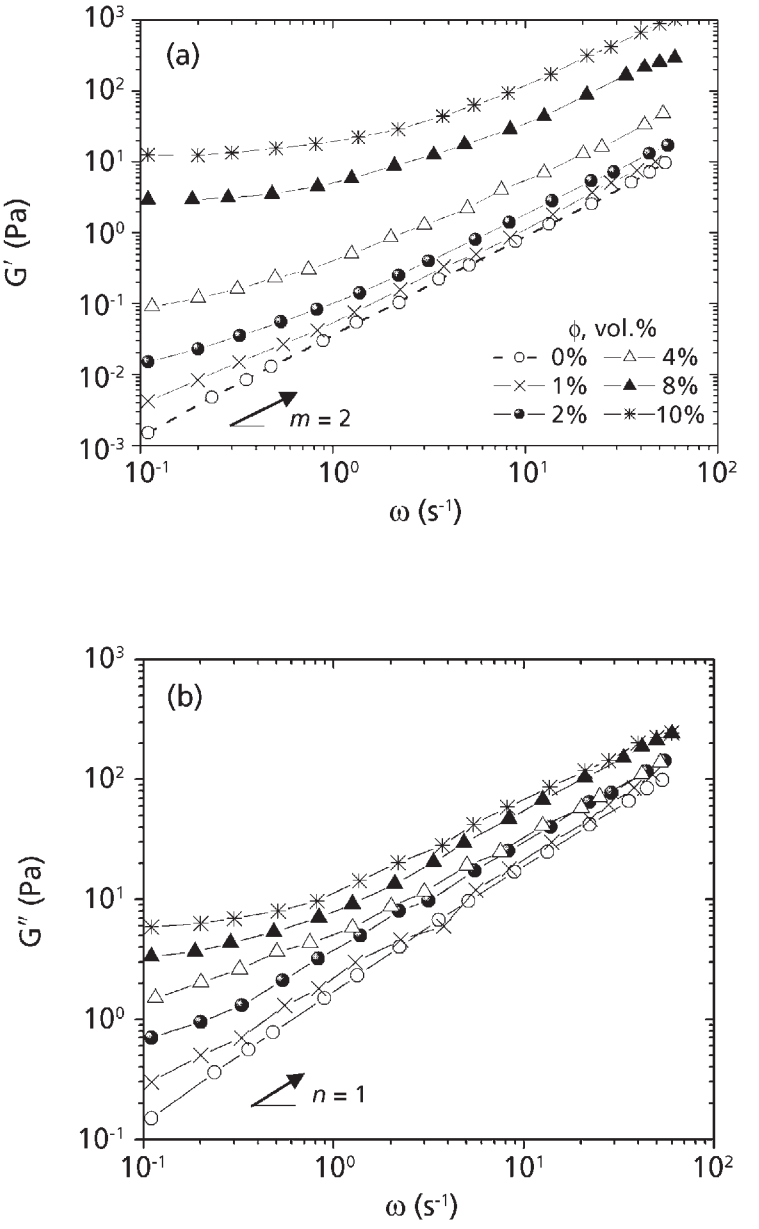

Figure 2.15 Low-amplitude dynamic moduli (a) G' and (b) G'' *versus* angular frequency ω of graphite/diamond/acrylic hybrids with various volume contents, 1–10 vol%; $m = 2$ and $n = 1$ indicate theoretical slopes of G' and G'' of the unfilled polymer.

Reproduced with permission from [42]. ©Wiley Periodicals, 2004

Moreover, within the volume range of 4–10%, both moduli $G'(\omega)$ and $G''(\omega)$ show a trend towards an equilibrium plateau in the terminal region, which could be related to the formation of a percolation structure. The effect of carbon concentration on the non-terminal behaviour of the storage modulus is much more pronounced than that of the loss modulus (Equation (2.4)).

In order to characterise the nature of the superstructure of nanofiller and the structural changes of dispersions in shear flow, we adopt the concept of cluster–cluster aggregation in colloidal dispersions that yields self-similar structures known as fractals [64, 73]. Hence, the percolation threshold is interpreted as a structural transition from a dispersed to an agglomerated state. Above the percolation threshold, the presence of carbon nanoparticles produces a strong increase of the dynamic moduli, particularly at low frequencies, where the dispersion behaviour is dominated by the filler structure.

If the network structure of the dispersion is considered as closely packed fractal flocs, according to Shih and co-workers [71], the elasticity of the dispersion above the percolation threshold will be dominated by either the interactions within flocs or the interlinking between flocs. Such structural interactions in nanodispersions obviously produce an additional relaxation process, which is clearly observed in the terminal flow region (**Figure 2.15**). A quantitative description of the additional relaxation processes of graphite/diamond dispersions in epoxy resin was already presented in **Figure 2.9**, using calculations of the relaxation-time spectrum. By increasing the filler content, the spectrum is shifted towards longer relaxation times, associated with the formation of the superstructure of fractal flocs. The effect is strongly pronounced above the percolation threshold, accounting for a restricted overall mobility of polymer chains in the dispersions with respect to the pure epoxy matrix. As the fractal flocs consist of clusters of nanoparticles surrounded by an interfacial polymer layer, they behave as an elastic barrier during shear flow and relax for a longer time than the matrix in the bulk.

Further, the low-frequency dependence of the storage and loss moduli with filler concentration is discussed in order to determine the first and second percolation thresholds. **Figure 2.16** plots G'_0 and G''_0 at a low frequency ($\omega = 0.1$ s^{-1}) *versus* volume filler content, ϕ, of graphite/diamond/acrylic dispersions, at 20 °C. Evidently, the values of G'' remain higher than those of G' in the concentration range below 8%, so the fluidity dominates the elasticity at these filler contents. In contrast, at higher carbon content above 8%, a pseudo-solid-like behaviour is observed with $G' > G''$. The crossover of the storage and loss moduli ($G'_0 \cong G''_0$) at $\phi^{**} \sim 8\%$ determines the second percolation threshold [43]. The storage modulus at low frequencies is more sensitive to the changes in the superstructure. Hence, the first percolation threshold $\phi^* \sim 4\%$ is determined from the crossover of the scaling slopes $\mu = 3.5$ and $\mu = 6.4$ of the G'_0 storage modulus (Equation (2.5)).

Figure 2.16 shows that the observed scaling exponent $\mu = 6.4$ of hybrids at $\phi > \phi^*$ is higher than the theoretical values of $\mu = 4.5 \pm 0.2$, predicted for the fractal-type

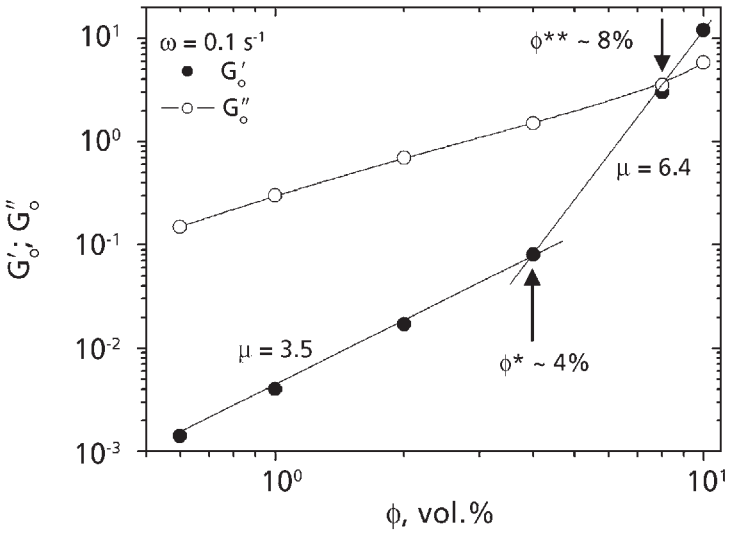

Figure 2.16 Plots of G' and G'' at a low frequency ($\omega = 0.1\ s^{-1}$) *versus* volume filler content, ϕ, of graphite/diamond/acrylic hybrids, at 20 °C. The first percolation threshold $\phi^* \sim 4\%$ is determined by the crossover of the slopes of 3.5 and 6.4 of the scaling exponent μ. The crossover at $\phi^{**} \sim 8\%$ of the storage and loss moduli ($G' \cong G''$) determines the second percolation threshold.

Data from [43]

structure of colloidal dispersions. High values of μ are reported for strongly flocculated dispersions [101]. The high power in ϕ for graphite/diamond/acrylic hybrids could be related to both the strong interparticle interactions produced by the small particle size, and the interfacial interactions. Because of the extended surface area of the nanofiller (590 m^2/g), at volume concentrations above the first percolation, $\phi > \phi^*$, most of the matrix polymer is incorporated in the fractal flocs in the state of an interfacial layer surrounding nanoparticles. This 'bound' polymer layer, having different elasticity from that of the bulk polymer, obviously dominates the overall elasticity of the individual fractal flocs and increases the scaling exponent. In the case of high carbon content above the second percolation threshold, $\phi > \phi^{**}$, it is expected that the full amount of the matrix polymer is associated with nanofiller surfaces and the fractal flocs fill all the volume. The rheological characteristics saturate in the plateau values. Hybrid dispersions of graphite/diamond in polyurethane (PU) and epoxy resin show qualitatively similar rheological behaviour.

These observations on the structure of hybrids at the two percolation transitions are further related to the properties of the cured nanocomposite systems, based on the assumption

for the structure–property relationship. The structural transitions at ϕ^* and ϕ^{**} of the dispersions are indicative for corresponding transitions of the physical properties of the solid composites. Thus, novel properties (electrical conductivity and microwave absorption) appear at ϕ, ϕ^*, and saturate at $\phi > \phi^{**}$ [42]. Importantly, our study has shown that the factors influencing agglomeration processes in hybrid dispersions play an important role for improving the physical and mechanical properties of solid composites [41–43]. These results allow us to propose the rheological characterisation of hybrids as a very useful method for controlling the properties of solid composites.

2.4.3.3 Effects of Polar Additives

This study is focused on improving certain physical properties of nanocomposites (e.g., electrical conductivity and wave absorption) by controlling the superstructure of carbon nanoparticles in the polymeric matrix using polar additives [43]. Generally, it is expected that, for a given volume fraction of carbon, finer agglomerates enable one to achieve smaller interparticle distances and, consequently, electrons can be transferred from particle to particle throughout the matrix. However, the impact of preparation conditions on the particle dispersivity, and consequently on the composite conductivity, has not been extensively examined.

The rheological study of the cluster–cluster aggregation processes in hybrid dispersions provides information about the structural organisation of the nanofiller, which is found to be determinant for various practical applications. It is expected that finer particles cause smaller interparticle distances, and consequently network formation could be monitored by control of interparticle interactions. In general, additives are successfully used to decrease the potential barrier between conducting particles. For example, control of carbon particle aggregation by additives is found to be important for improving the conductivity of composites [102–105].

Electrostatic particle–particle interaction is taken into account when describing aggregation processes of graphite/diamond nanoparticles in resins [43]. Various polar additives, such as $CuCl_2$, oleic acid (OA) and Aldrich polyol Brij 35 (POE) added in a small amount (~0.005–0.01%) to the dispersions, are used for controlling the dispersivity and the agglomeration processes of nanofiller particles in acrylic (polymethylacrylate) and PU (polyol isocyanate) resins. In order to obtain information about the agglomeration processes of carbon nanoparticles controlled by the additives, the rheological behaviour of hybrid dispersions in steady shear flow was investigated.

Figure 2.17 compares the viscosity *versus* shear rate dependence of two hybrid dispersions, (a) 8% graphite/diamond/acrylic and (b) 8% graphite/diamond/PU, on varying the polar additives. It can be seen that the effect of polar additives is significant for the systems based on both acrylic and PU resins. **Table 2.7** compares the viscosity at low and high shear rates, $\eta(\dot{\gamma} = 0.5\ s^{-1})$ and $\eta(\dot{\gamma} = 50\ s^{-1})$, respectively, as well as the

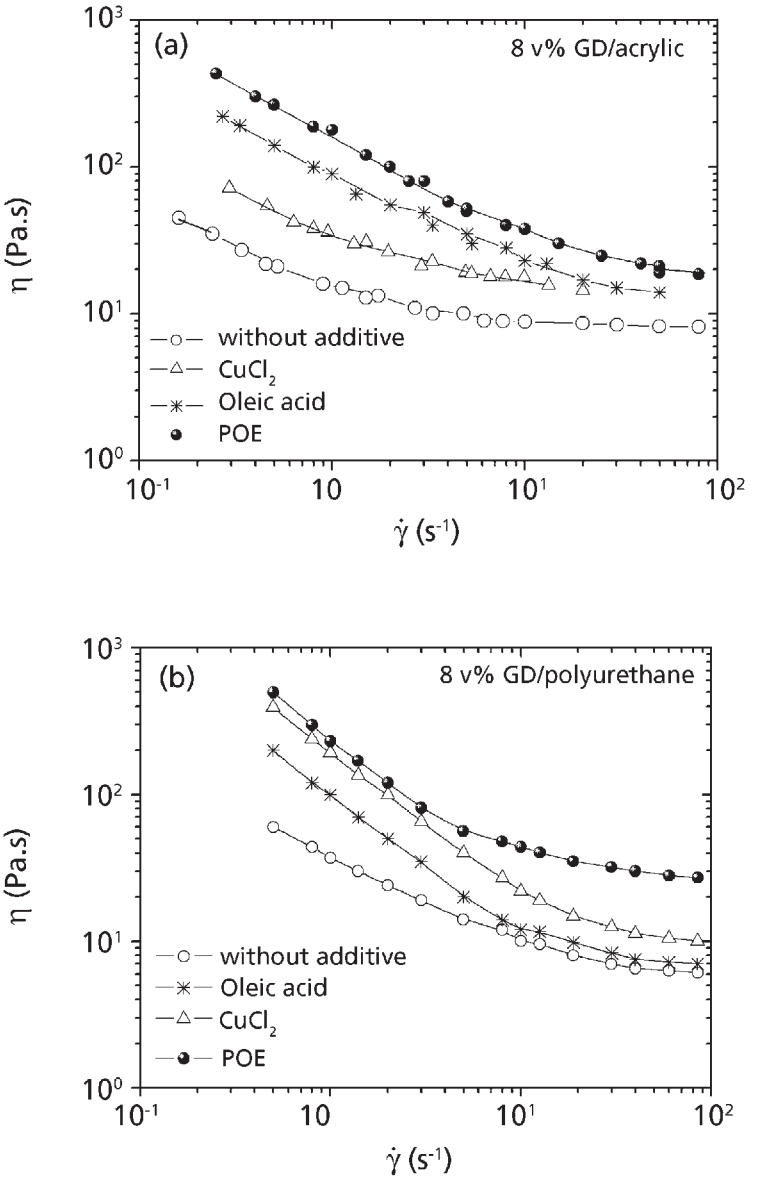

Figure 2.17 Apparent viscosity η *versus* shear rate $\dot{\gamma}$ of (a) 8 vol% GD/acrylic hybrids and (b) 8 vol% GD/polyurethane hybrids, on varying the polar additives: $CuCl_2$, oleic acid and polyol.

Data from [43]

Table 2.7 Viscosity and shear thinning exponent n of 8 vol% GD dispersions in acrylic and polyurethane matrices on varying the polar additives

Sample code	Resin type	Polar additive	η (Pa-s)		
			$\dot{\gamma}$ = 0.5 s^{-1}	$\dot{\gamma}$ = 50 s^{-1}	*n* (2.2)
8% GD/AR	Acrylic resin (AR) polymethylacrylate	Without additive	22	8	0.69
8% GD/AR/$CuCl_2$	–	$CuCl_2$	54	14	0.6
8% GD/AR/OA	–	Oleic acid	191	14	0.52
8% GD/AR/POE	–	Brij 35	264	21	0.4
8% GD/PU	Polyurethane (PU) polyol isocyanate	Without additive	60	6.3	0.54
8% GD/PU/OA	–	Oleic acid	200	7.2	0
8% GD/PU/$CuCl_2$	–	$CuCl_2$	391	10.5	0
8% GD/PU/POE	–	Brij 35	498	28	0
Data from [43]					

shear thinning exponent *n*, determined in the range $\dot{\gamma} < 1\ s^{-1}$.

As seen previously, the viscosity at low shear rate, $\eta(\dot{\gamma} = 0.5\ s^{-1})$ for PU systems is much higher than that for acrylic systems. Obviously, graphite/diamond demonstrates a better miscibility with PU than with acrylic resin. Moreover, data for the low-shear-rate viscosity and the shear thinning exponent *n* show that polar additives have a much stronger effect in the PU matrix systems compared to the acrylic systems. This may be related to the compatibility between the ingredients, but the low-viscosity PU matrix may also assist in the process. Thus, particle diffusion is easier within the PU (η = 1.3 Pa-s) than within the higher-viscosity acrylic resin (η = 2.1 Pa-s) (**Table 2.3**).

In general, a small amount of polar additives significantly increases the viscosity of dispersions, particularly at low shear rates. The plasticity of nanodispersions is increased by the additives, which could be interpreted as either a better dispersion or a stronger interaction of the graphite/diamond nanoparticles within the matrices. Comparison of dispersions by the shear thinning exponent *n* shows that additives significantly increase the degree of dispersion for the PU systems ($n = 0$), but the dispersivity of graphite/diamond in acrylic resin is not sufficiently influenced by additives ($n = 0.4$–0.69) (**Table 2.7**). Additionally, for all systems the viscosity at high shear rates, $\eta(\dot{\gamma} = 50\ s^{-1})$, is also increased by additives, by about a factor of 2, indicating stronger polymer–filler interactions due to the polar groups of the additives.

In summary, the various types of polar additives have different effects on the viscosity of dispersions, so additives can be used to design carbon nanofiller structures of different strengths in thermoset matrices. A small amount of polar additives can control the particle–particle and polymer–particle interactions of graphite/diamond dispersions in acrylic and PU resins by increasing the ionic strength of the dispersions. Therefore, polar additives are suitable to create particle networks with the desired perfection. The mechanism of the process is related to the reduction of the potential barrier among the graphite/diamond nanoparticles, thus allowing the filler to easily form agglomerates with the support of Brownian motion. As a result, a well-defined three-dimensional network, and accordingly a higher conductivity, are created at very low filler content. Subsequently, the effect of additives on the viscosity of dispersions is found to correspond with the conductivity of solid systems [42, 43].

2.4.4 Rheological Control of Hybrids with Nanoscale Alumina

Hybrid dispersions are prepared from a variety of alumina-based (Al_2O_3) nanofiller and resin formulations. The nanoscale alumina fillers Disperal D40 (untreated) and Disperal OS1 and Disperal OS2 (treated by organic modifiers) are supplied by SASOL, Germany (**Table 2.5**). Epoxy resin (AP1) and unsaturated polyester resin (Viapal) were used as matrix polymers (**Table 2.3**). The dispersions with 3 wt% (1.3 vol%) of alumina nanofillers in epoxy and polyester resin were prepared by using two steps of intensive shearing: high-speed mixing at 7000 rpm for 30 min followed by 10 min mixing with an ultrasonic disintegrator. The aggregates of alumina nanoparticles are well dispersed in the polymer matrices, which leads to stable and transparent dispersions. Low-amplitude dynamic measurements in oscillatory shear mode are performed to collect experimental rheological data.

2.4.4.1 Dispersability of Alumina in Epoxy and Polyester Resins

Preliminary results indicate that the properties of thermoset resins are enhanced by nanofiller if the processing technology is optimised [46]. Rheology method I has been proved to optimise the formulations by studying the flow dynamics of both characteristics of viscosity and viscoelasticity in a shear flow field. The degree of nanofiller dispersal is controlled by rheological constants: shear thinning exponent n, and terminal zone exponent m, determined by the models from Equations (2.3) and (2.4). **Table 2.8** presents the calculated values of both exponents.

The flow exponents (n, m) are used as a tool to compare the degree of nanofiller dispersion. **Figure 2.18** presents (a) low-amplitude storage modulus G' and (b) dynamic viscosity η' *versus* angular frequency ω of dispersions with 3 wt% (~1.3 vol%) alumina

Table 2.8 Shear thinning exponent *n*, and terminal zone exponent *m*, of 3 wt% (1.3 vol%) Disperal (untreated and treated) in AP1 epoxy resin and Viapal polyester resin

Sample code	Filler type	*m* (2.4)	*n* (2.3)
Epoxy resin AP1	–	2	1
AP1/D40	Al_2O_3 untreated – D40	1.3	0.84
AP1/OS1	Al_2O_3 treated – OS1	0.7	0.5
AP1/OS2	Al_2O_3 treated – OS2	0.8	0.65
Polyester resin Viapal	–	2	1
Viapal/D40	Al_2O_3 untreated – D40	0.15	0.2
Viapal/OS1	Al_2O_3 treated – OS1	0.5	0.7
Viapal/OS2	Al_2O_3 treated – OS2	0.1	0

Data from [43, 46]. Reproduced with permission from [46]. ©Heron Press, Bulgaria, 2006

(untreated – D40, and treated – OS1 and OS2) in epoxy resin AP1.

Evidently, the treated OS1 and OS2 alumina fillers show good dispersability in the epoxy matrix. The values of the flow exponents (*n*, *m*) for the OS1/epoxy hybrids are in the range of *m*, $n < 1$, which are typical for this low filler content; thus the dispersion behaved like a pseudoplastic system. The untreated D40 alumina showed rheological behaviour similar to the Newtonian behaviour of the matrix polymer, and obviously this alumina has a lower dispersability in the epoxy resin, compared to the organically treated one.

Figure 2.19 shows (a) low-amplitude storage modulus G' and (b) dynamic viscosity η' *versus* angular frequency ω of the dispersions with the same 3 wt% alumina D40, OS1 and OS2 in polyester resin Viapal. It seems that the alumina nanofillers have a much higher degree of dispersivity in the low-viscosity polyester resin matrix than in the epoxy resin. Both OS2 and D40 alumina fillers are well dispersed in polyester resin, resulting in a pseudo-solid-like behaviour at this very low filler concentration, ~1.3 vol%, which could be associated with nanoscale effects. In contrast, higher values of $n = 0.7$ and $m = 0.5$ show that OS1 alumina has a lower degree of dispersivity in polyester resin; this indicates a lower swelling of OS1 modified alumina by polyester resin.

In spite of the very low filler content, the non-terminal zone behaviour of viscoelasticity observed for the systems indicates a lack of complete thermal relaxation. The non-terminal rheological behaviour is related mainly to the active interaction between the polymer and the nanofiller surface.

However, if we compare the viscosity at high shear rates beyond 10 s^{-1}, we see that the

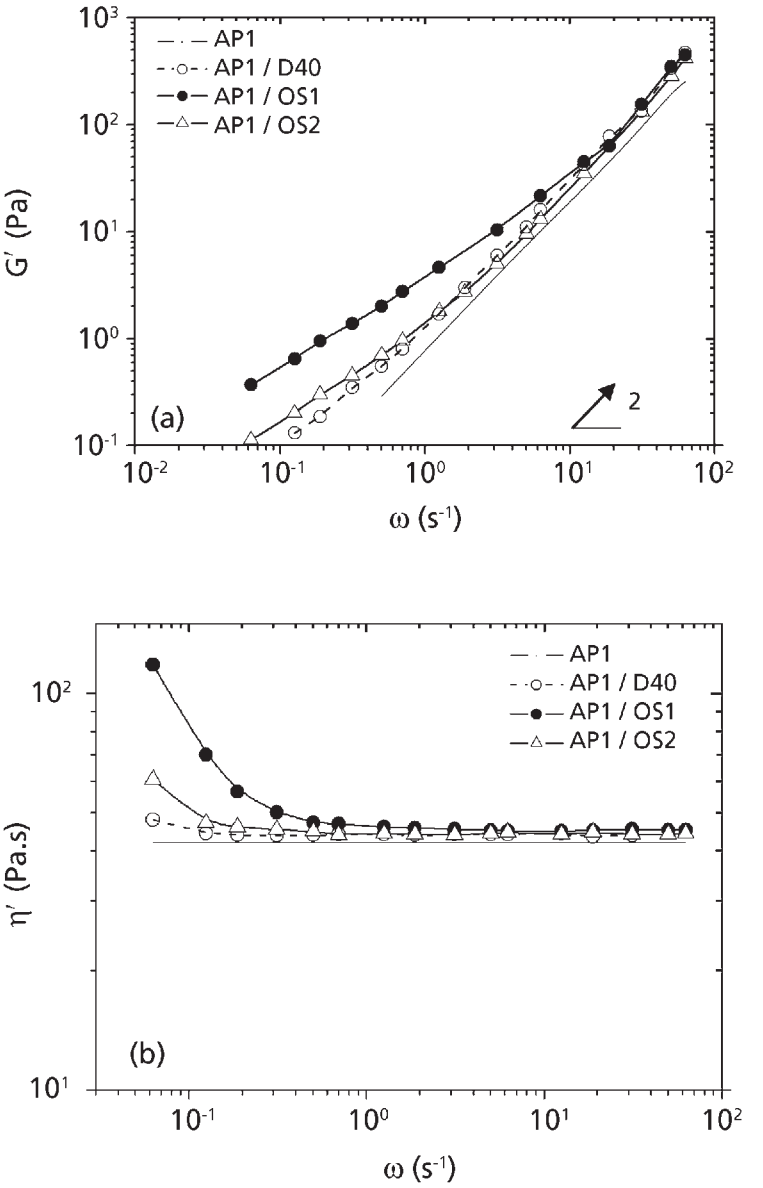

Figure 2.18 (a) Low-amplitude storage modulus G' of hybrids of AP1 epoxy resin with 3 wt% alumina (untreated – D40, and treated – OS1 and OS2) and(b) dynamic viscosity η' *versus* angular frequency ω of hybrids of AP1 epoxy resin with 3 wt% alumina (untreated – D40, and treated – OS1 and OS2).

Reproduced with permission from [46]. ©Heron Press, Bulgaria, 2006

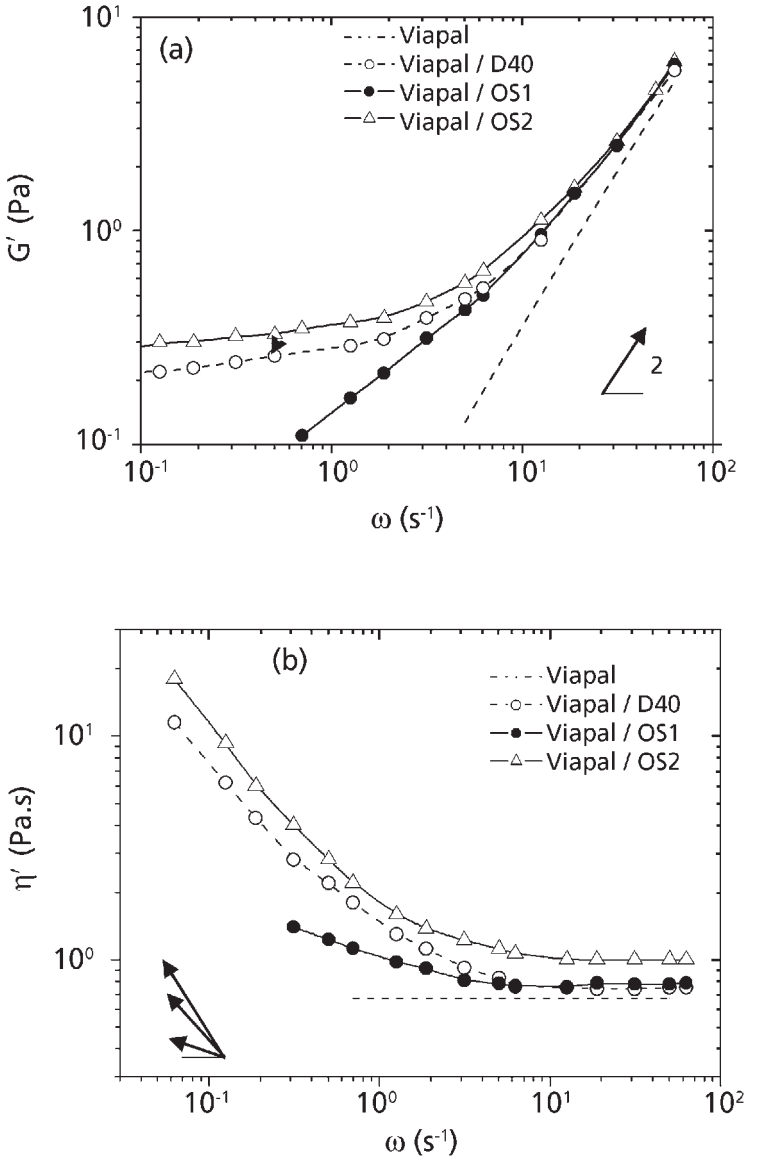

Figure 2.19 (a) Low-amplitude storage modulus G' and (b) dynamic viscosity η' *versus* angular frequency ω of hybrids of Viapal polyester resin with 3 wt% alumina (untreated – D40, and treated – OS1 and OS2).

Reproduced with permission from [46]. ©Heron Press, Bulgaria, 2006

values of hybrids of OS1 and D40 in Viapal are near to that of the unfilled polymer matrix, comparable to the theoretical predictions of the relative viscosity of non-interacting dispersions [18, 63, 87]. The near independence of the viscosity at high shear rates on the filler content in 3 wt% systems could be associated with deflocculation of cluster–cluster aggregates in the flow field. Therefore, at low shear rates the flow is dominated by particle–particle interactions, but at high shear rates it is dominated by the polymer matrix. In contrast, the OS2/Viapal system is the exception, as it shows the strong effect of nanofiller not only at low shear rates but also at high shear rates, where the viscosity at high shear rates remains much higher than that of the other alumina dispersions and the homopolymer. Thus, in the case of the OS2/Viapal hybrid dispersion, not only particle–particle interactions but also polymer–filler interactions play an important role. A 'bonding' of the polymer layer at the alumina surfaces is proposed, leading to much stronger effects on the rheology.

In summary, rheological analysis can be a very useful tool to control the degree of dispersion of treated and untreated alumina nanofillers in epoxy and polyester resins. Moreover, rheological results allow interpretation of the structure–property relationship. Thus, the higher degree of dispersivity and the polymer–filler interactions of liquid hybrids prior to curing are further related to the significant improvement of mechanical properties of cured nanocomposites.

2.5 Rheological Approach to Prognostic Design of Nanocomposites

2.5.1 Structure–Property Relationships

In the last few years, the emphasis of nanocomposite research has been on the understanding of the structure–property relationships of these new materials. Morphological representations such as intercalation and exfoliation are commonly used to describe the state of aggregation of the individual sheets of clay in the polymer/layered silicate nanocomposites. Most notably, the property improvements resulting from the formation of a nanocomposite occur at very low concentrations of the layered silicates (1–5 vol%) compared to conventional phase-separated composites with 20–30 vol% filler in a polymer. The extremely large surface area available for interactions with a polymeric matrix coupled with high aspect ratio (between 10 and 2000) are largely responsible for the observed enhancement [4, 62, 81, 82].

In general, the best properties of polymer/clay nanocomposites are obtained when the clay particles are in the fully exfoliated state and are well dispersed in the polymer matrix [106]. A relationship between the melt-state shear thinning exponent and the solid-state tensile modulus of the nanocomposites is observed [61]. The better the silicate platelets are exfoliated, the stronger is the reinforcement effect on the resulting nanocomposite at given

filler content. The amount of clay content also plays a vital role in controlling the structure of the nanocomposites and hence various material properties. Several authors have related the structural transition of percolation with important mechanical properties of the final nanocomposites [8, 30, 31, 80]. The percolation threshold value has been related to strong flocculation of the stacked, dispersed clay particles, and for this reason all the properties of polymer/layered silicate nanocomposites suddenly changed beyond the percolation value [8, 80]. Hsieh and co-workers [30] observed a relationship between rheological propertes and mechanical response of polycarbonate/layered silicate nanocomposites above and near the percolation threshold. So we can control the flocculation of dispersed silicate layers and, therefore, various materials properties.

Structure–property relationships have also been studied in various thermosetting polymer nanocomposites. Kornmann and co-workers [12, 47] and Suh and co-workers [107] demonstrated that the resulting properties of polyester/clay nanocomposites are greatly dependent on the preparation procedure with regard to the order of mixing of the ingredients, as well as the curing conditions. Wooster and co-workers [31] concluded that the study of the rheology of cyanate ester/montmorillonite mixtures gave an indication of the success of layer separation and allows correct choice of filler to achieve optimal enhancement of the mechanical properties of the thermosetting nanocomposites. The authors found that the dispersion state of clay is a critical factor that determined the change in rheology and mechanical properties. Hence, the most dramatic increase (~80%) in the crack resistance of this thermoset nanocomposite appears around the percolation limit of 4–5 wt%. However, there is a decrease after the percolation limit, which is associated with difficulties in clay dispersion.

Establishing the morphological hierarchy in thermosetting polymer/clay nanocomposites seems to be the key factor in developing and understanding the structure–property relationships in these systems. Bharadwaj and co-workers [81] proposed that two structural arrangements may be envisaged, where the clay sheets are completely delaminated and homogeneously dispersed through the matrix, or there may be localised regions of exfoliated sheets dispersed through the matrix. These two structural situations presumably result in nanocomposites that are completely different in terms of properties. Moreover, the authors found that the clay–modifier–polymer interface plays an important role. Hence, although there is firm evidence that shows the formation of nanocomposite structure, the mechanical properties (e.g., tensile modulus, loss and storage moduli, and so on) of the crosslinked polyester/clay nanocomposites exhibit a progressively decreasing trend with increasing clay concentration [81]. These property reductions account for the chemical effect of organic modifier on the polymer matrix and have been explained on the basis of a progressive decrease in the degree of crosslinking with increasing clay concentration.

In the case of particulate nanofillers, the unique surface and electronic properties of metal and semiconductor nanoparticles and carbon nanotubes combined with the properties of the polymer matrix lead to a variety of chemical and physical applications. Besides

single-particle characteristics, the microstructure of nanodispersions is also of importance. Some applications require materials with well-separated particles, but others need paths of agglomerating particles for energy dissipation. Therefore, the preparation of well-defined systems with desired properties requires good control of the dispersion processes [58].

The results described previously allow us to propose rheological characterisation as a very useful method for prognosis of the structure and properties of nanocomposites. The nanofiller superstructure is expected to be responsible for the alteration of the properties of nanocomposites to such an extent that the solid nanocomposite properties depend on the structure formation and morphology.

2.5.2 Prognostic Design in Relation to Percolation Mechanism

The proposed rheological approach for designing nanocomposites is intended to broaden and integrate the knowledge of the behaviour of nanocomposites through the development of the processing–structure–properties relations for nanocomposite materials.

The importance of the previously discussed percolation thresholds, ϕ^* and ϕ^{**}, is undoubted. For example, the rheologically determined first and second percolation thresholds of carbon/resin hybrids are found to correlate with a corresponding remarkable improvement in the physical and mechanical properties of the cured thermosetting nanocomposite systems [41–43]. The three-dimensional structure of fractal flocs formed at filler concentrations above the first percolation threshold, wherein a large amount of polymer is adsorbed at the particle surface, is thought to play a determining role for the reinforcement of epoxy nanocomposites incorporating either smectite clay or graphite/diamond [39, 41, 43, 46]. Such hybrid structures easily undergo the deformation process and improve both the stiffness and toughness of the nanocomposites.

Moreover, rheologically determined percolation thresholds are found to be critical for the physical properties of thermosetting nanocomposites with graphite/diamond [40, 42]. Novel physical properties appear above the first rheological percolation threshold, ϕ^*, such as electrical conductivity and microwave absorption. Further increasing the carbon content above the second rheological percolation threshold, ϕ^{**}, leads to a saturation plateau of both physical properties. This indicates that the rheological response is sensitive to the interconnectivity of the nanofillers, which is also directly related to electrical conductivity.

The correlation of the two rheologically determined critical concentration transitions, ϕ^* and ϕ^{**}, with the property improvement of solid nanocomposites may be explained by several theoretical approaches [53, 108, 109]. When bonding between fillers and matrix is strong enough, Wu [108, 109] predicted that a connection of shear-yielded zones throughout the whole polymer matrix would result in a brittle–tough transition.

A critical matrix interface layer thickness, τ_c, at which the matrix ductility is improved remarkably, was found to represent a key parameter for the toughening effect. A drastic increase in toughness of a composite is perceivable only when the interparticle distance, τ, determined by Equation (2.20), is smaller than τ_c (i.e., $\tau < \tau_c$)

$$\tau = d[(\pi/6\phi_f)^{1/3} - 1] \tag{2.20}$$

where τ is the interparticle distance, d is the particle diameter and ϕ_f is the particle volume fraction.

Based on this criterion, the smaller the particles, the less filler is needed to realise a brittle–tough transition for sufficient interfacial adhesion. Our example calculations show that, in the case of nanoscale graphite/diamond/acrylic hybrids, at particle diameter of d = 6 nm and filler content of $\phi_f = 0.04$, i.e., $\phi_f = \phi^*$ (equal to the first rheological percolation threshold), the critical interparticle distance of τ_c is calculated to be ~8 nm (by using Equation (2.20)). Such small interparticle distance is indicative of strong electrostatic interactions between particles.

In another approach, a double percolation is assumed [53]. This means: (1) a percolation of shear-yielded zones inside the dispersed phases (e.g., inside the floccules) due to the superposition of stress volumes around the nanoparticles; and (2) a percolation of shear-yielded zones throughout the matrix resin due to the superposition of stress volumes around the dispersed floccules (agglomerates). Based on the filler content dependence of the fraction of stress volume ϕ_s [53, 109]:

$$\phi_s = [(d + \tau_c)/d]^{1/3}\phi_f \tag{2.21}$$

Thus, if we take the above determined values of τ_c = 8 nm and $\phi_f = \phi^* = 0.04$, then using Equation (2.21) we can calculate $\phi_s = 0.053$ as a second critical concentration. This value is lower than the experimentally determined value of the second rheological percolation threshold, $\phi^{**} = 0.08$ (8 vol%), which can be associated with the formation of fractal flocs with a broad size distribution at filler concentrations above the percolation limit.

As reported in [53, 63], the concept of so-called double percolation or multiple percolation has been successfully used in designing very low filler loaded conductive polymer composites [110], as well as a significant improvement of the mechanical performance at rather low filler content [53].

The rheologically determined first percolation threshold ϕ^* has been observed in our studies [39–43, 46] to correlate well with the remarkable rise in nanocomposite mechanical properties [39, 41, 43, 46] and physical properties (electrical conductivity and microwave absorption) [40, 42]. However, at a filler concentration near to the second rheological percolation threshold, ϕ^{**}, the properties tend to plateau or decrease drastically. Hence, it is proposed that the previously mentioned double percolation mechanism might play the leading role here also. Basic assumptions about the relationship between double

rheological percolation, structure and properties of polymer nanocomposites are used to propose a prognostic design of polymer nanocomposites.

Figure 2.20 presents schematically the proposed rheological approach to a prognostic design of nanocomposite structure and properties [43], which consists of the following main steps:

(i) Determination of rheological percolation thresholds, ϕ^* and ϕ^{**}, of nanocomposite systems;

(ii) Correlation of the first and second percolation thresholds with the morphological hierarchy in polymer/filler nanocomposites (using optical microscopy, SEM, TEM, or AFM); and

(iii) Using the two rheological thresholds, ϕ^* and ϕ^{**}, as a *prognostic window* of filler concentrations, wherein the maximum enhanced nanocomposite properties are expected.

Figure 2.20 demonstrates the application of the rheological approach to the prognostic design of example graphite/diamond /epoxy nanocomposite, as follows:

- Rheology methods I and III are used for control of the nanocomposite preparation technology, in order to identify the processing conditions for the best dispersion of nanofiller in the polymer, and to verify the polymer–filler interactions.
- Rheology method II is used to determine the two percolation thresholds, which are for example $\phi^* \sim 5$ vol% and $\phi^{**} \sim 8$ vol% for the graphite/diamond/epoxy systems.
- The rheologically optimised carbon/epoxy hybrid precursors with different filler contents in the range 0–10 vol% are cured and characterised in terms of nanocomposite structure and properties. The morphological arrangements observed by optical microscopy (in this case) localise regions of carbon floccules dispersed through the matrix, which form paths of agglomerating particles at 5%, while at 8% the agglomerates (flocs) fill the volume as a single cluster (3D network). Further, mechanical properties (bending strength, bending dynamic modulus, and impact strength) and physical properties (dc conductivity and wave absorption at 1–20 GHz) of the unfilled resin and nanocomposites are studied.
- The rheological thresholds, ϕ^* and ϕ^{**}, are further used as a *prognostic window* of the filler concentrations where remarkable enhancement of the physical and mechanical properties of the nanocomposite might be expected. The 'prognostic window' is compared with the enhancement of the experimentally determined mechanical and physical properties.

Figure 2.20 compares the measured values of the graphite/diamond/epoxy nanocomposite properties *versus* filler concentration, such as d.c. conductivity, bending strength, bending dynamic modulus, and impact strength. The *prognostic window*, $\phi^* < \phi < \phi^{**}$, is represented by the hatched region of the plot. As may be seen, the prognostic

window includes the optimal filler concentrations wherein the highest improvement of nanocomposite properties appears. This corresponds with relatively low values of the viscosity of the liquid-state hybrids, which is suitable for the processing application.

A good fit of the optimal improvement of the nanocomposite properties with the prognostic window was observed in our study also for other nanocomposite systems [39, 42, 43]. For example, the rheologically determined prognostic window of the smectite/epoxy systems is between $\phi^* = 2.5$ vol% and $\phi^{**} = 4.5$ vol%, which was found to correspond with the optimal mechanical properties [39]. In contrast, the graphite/diamond/acrylic nanocomposites show $\phi^* = 4$ vol% and $\phi^{**} = 8$ vol%, which were found to correlate well with the conductivity percolation and saturation limits [42].

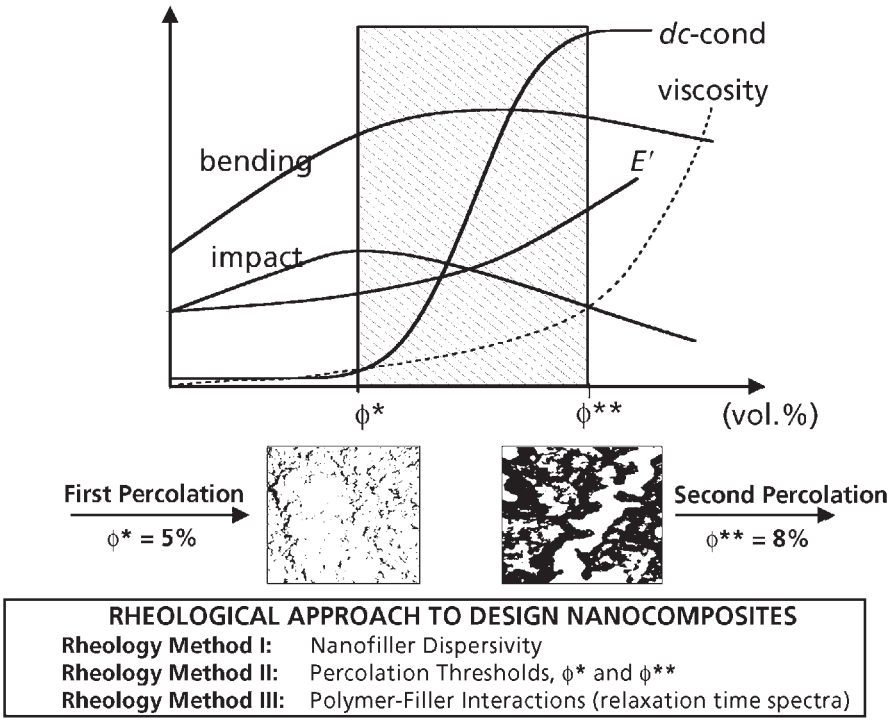

Figure 2.20 Schematic representation of the rheological approach to the design of nanocomposite structure and properties. By using rheology methods I and II, the prognostic window of filler concentrations (hatched region) is determined in the range $\phi^* < \phi < \phi^{**}$. Optical micrographs of the structure of epoxy nanocomposite films with $\phi^* \sim 5\%$ and $\phi^{**} \sim 8\%$ GD are presented. Experimentally determined properties *versus* filler concentration for the example of crosslinked carbon/diamond/epoxy nanocomposites are plotted *versus* filler content of 0–10 vol%.

Data from [43]

These results indicate that the rheological response at the critical concentartions, the first and the second percolation transitions, is sensitive to the interconnectivity of the nanofiller particles, as well as to the polymer–filler interactions, which are also directly related to the improvement of the physical and mechanical properties.

All these results confirm the applicability of the rheological thresholds, ϕ^* and ϕ^{**}, for the prognostic design of both the nanofiller superstructure and the filler concentration region, where an optimal enhancement of properties (physical, thermal and mechanical) might be expected. A prior identification of the rheological prognostic window (i.e., nanofiller concentrations wherein maximum improvements of nanocomposite properties are expected) might be a very useful practical tool for a short-duration consuming synthesis of novel materials having optimal structure and properties. The rheological approach for a prognostic design can be applied to such an extent that the solid nanocomposite properties depend on the structure formation and morphology.

Acknowledgements

The author would like to thank the German company SASOL for supplying alumina fillers and S. Stavrev (BAS) for fruitful collaboration and providing nanoscale graphite/diamond.

References

1. R. Krishnamoorti, R.A. Vaia and E.P. Giannelis, *Chemistry of Materials*, 1996, **8**, 8, 1728.

2. R. Krishnamoorti and E.P. Giannelis, *Macromolecules*, 1997, **30**, 14, 4097.

3. *Filled and Nanocomposite Polymer Materials*, Eds., A.I. Nakatani, R.P. Hjelm, M. Gerspacher and R. Krishnamoorti, MRS Symposium, Vol. 661, Materials Research Society, Pittsburgh, PA, USA, 2001.

4. R. Krishnamoorti and A.S. Silva in *Polymer–Clay Nanocomposites*, Eds., T.J. Pinnavaia and G.W. Beall, John Wiley & Sons, New York, 2001, p.315.

5. G. Schmidt, A.I. Nakatani, P.D. Butler, A. Karim and C.C. Han, *Macromolecules*, 2000, **33**, 20, 7219.

6. G. Galgali, C. Ramesh and A. Lele, *Macromolecules*, 2001, **34**, 4, 852.

7. M.J. Solomon, A.S. Almusallam, K.F. Seefeldt, A. Somwangthanaroj and P. Varadan, *Macromolecules*, 2001, **34**, 6, 1864.

8. M. Okamoto, *Polymer/Layered Silicate Nanocomposites*, Rapra Review Reports, **14**, 7, Report No. 163, Rapra Technology, Shawbury, Shrewsbury, UK, 2003.

9. J. Ren, A.S. Silva and R. Krishnamoorti, *Macromolecules*, 2000, **33**, 10, 3739.

10. C.A. Mitchell and R. Krishnamoorti, *Journal of Polymer Science: Polymer Physics Edition*, 2002, **40**, 14, 1434.

11. J. Ren and R. Krishnamoorti, *Macromolecules*, 2003, **36**, 2, 443.

12. X. Kornmann, L.A. Berglund, J. Sterte and E.P. Giannelis, *Polymer Engineering Science*, 1998, **38**, 8, 1351.

13. B. Hoffmann, C. Dietrich, R. Thomann, C. Friedrich, C. Zilg and R. Mülhaupt, *Macromolecular Rapid Communications*, 2000, **21**, 1, 57.

14. B. Hoffmann, J. Kressler, G. Stöppelmann, C. Friedrich and G-M. Kim, *Colloid and Polymer Science*, 2000, **278**, 7, 629.

15. Y.T. Lim and O.O. Park, *Macromolecular Rapid Communications*, 2000, **21**, 5, 231.

16. Y.T. Lim and O.O. Park, *Rheologica Acta*, 2001, **40**, 3, 220.

17. S. Tanoue, L.A. Utracki, A. Garcia-Rejon, P. Sammut, M-T. Ton-That, I. Pesneau, M.R. Kamal and J. Lyngaae-Jorgensen, *Polymer Engineering and Science*, 2004, **44**, 6, 1061.

18. L.A. Utracki, *Clay-Containing Polymer Nanocomposites*, Rapra Technology, Shawbury, Shrewsbury, UK, 2004.

19. L.A. Utracki in *Rheological Fundamentals of Polymer Processing*, Eds., J.A. Covas, J.F. Agassant, A.C. Diogo, J. Vlachopoulos and K. Walters, Kluwer Academic, Dordrecht, The Netherlands, 1995, p.113.

20. R. Kotsilkova, *Mechanics of Time-Dependent Materials*, 2002, **6**, 3, 283.

21. E.P. Giannelis, R. Krishnamoorti and E. Manias, *Advances in Polymer Science*, 1999, **138**, 107.

22. R. Krishnamoorti, J. Ren and A.S. Silva, *Journal of Chemical Physics*, 2001, **114**, 11, 4968.

23. J. Lee, M. Kontopoulou and J.S. Parent, *Polymer*, 2004, **45**, 19, 6595.

24. P.B. Messersmith and E.P. Giannelis, *Chemistry of Materials*, 1994, **6**, 10, 1719.

25. R.A. Vaia, K.D. Jandt, E.J. Kramer and E.P. Giannelis, *Macromolecules*, 1995, **28**, 24, 8080.

26. P.C. LeBaron, Z. Wang and T.J. Pinnavaia, *Applied Clay Science*, 1999, **15**, 1–2, 11.

27. T.J. Pinnavaia, T. Lan, Z. Wang, H. Shi and P.D. Kaviratna in *Nanotechnology – Molecularly Designed Materials*, Eds., G-M. Chow and K.E. Gonsalves, ACS Symposium Series, No.622, American Chemical Society, Washington, DC, 1996, Chapter 17, p.250.

28. C.I. Beaudry and L.C. Klein, in *Nanotechnology – Molecularly Designed Materials*, Eds., G-M. Chow and K.E. Gonsalves, ACS Symposium Series, No.622, American Chemical Society, Washington, DC, 1996, Chapter 26, p. 382.

29. H.S. Jeon, J.K. Rameshwaram, G. Kim and D.H. Weinkauf, *Polymer*, 2003, **44**, 19, 5749.

30. A.J. Hsieh, P. Moy, F.L. Beyer, P. Madison, E. Napadensky, J. Ren and R. Krishnamoorti, *Polymer Engineering and Science*, 2004, **44**, 5, 825.

31. T. Wooster, S. Abrol and D.R. MacFarlane, *Polymer*, 2005, **46**, 19, 8011.

32. P. Pötschke, T.D. Fornes and D.R. Paul, *Polymer*, 2002, **43**, 11, 3247.

33. M. Okamoto, H. Taguchi, H. Sato, T. Kotaka and H. Tateyama, *Langmuir Letters*, 2000, **16**, 9, 4055.

34. D. Schmidt, D. Shah and E.P. Giannelis, *Current Opinions in Solid State and Materials Science*, 2002, **6**, 3, 205.

35. S.M. Fielding, P. Sollich and M.E. Cates, *Journal of Rheology*, 2000, **44**, 2, 323.

36. *Rheology Control for Epoxy Formulations*, Technical Data for Epoxy Nanocomposites, T17, Nanocor, Arlington Heights, IL, USA, 2005.

37. R.E. Newnham, D.P. Skinner and L.E. Cross, *Material Research Bulletin*, 1978, **13**, 5, 525.

38. T.A. Witten, L. Leibler, and P.A. Pincus, *Macromolecules*, 1990, **23**, 3, 824.

39. R. Kotsilkova, *Journal of Applied Polymer Science*, 2005, **97**, 6, 2499.

40. R. Kotsilkova, P. Pissis and A. Kanapitsas in *Nanoscience and Nanotechnology*, Volume 1, Eds., E. Balabanova and I. Dragieva, Heron Press, Sofia, Bulgaria, 2001, p.77.

41. R. Kotsilkova, D. Fragiadakis and P. Pissis, *Journal of Polymer Science: Polymer*

Physics Edition, 2005, **43**, 5, 522.

42. R. Kotsilkova, D. Nesheva, I. Nedkov, E. Krusteva and S. Stavrev, *Journal of Applied Polymer Science*, 2004, **92**, 4, 2220.

43. R. Kotsilkova, *Relationship Between Technology, Structure and Properties of Thermoset Nanocomposites*, Sofia, Bulgaria, 2005 [D.Sc. Thesis, in Bulgarian].

44. R. Kotsilkova, E. Krusteva, C. Silvestre, S. Cimmino and M. Raimo in *Nanoscience and Nanotechnology*, Volume 5, Eds., E. Balabanova and I. Dragieva, Heron Press, Sofia, Bulgaria, 2005, p.219.

45. R. Kotsilkova in *Proceedings of the 13th International Congress on Rheology*, Cambridge, UK, 2000, Volume 4, p.145.

46. R. Kotsilkova, E.H. Ivanov, B. Milosheva, E. Krusteva, A. Topliyska, C. Silvestre, S. Cimmino and M. Raimo in *Nanoscience and Nanotechnology*, Volume 6, Eds., E. Balabanova and I. Dragieva, Heron Press, Sofia, Bulgaria, 2006, p. 141.

47. X. Kornmann, H. Linberg and L.A. Berglund, *Polymer*, 2001, **42**, 4, 1304.

48. O. Becker, R. Varley and G. Simon, *Polymer*, 2002, **43**, 16, 4365.

49. M.S. Wang and T.J. Pinnavaia, *Chemistry of Materials*, 1994, **6**, 4, 468;

50. T. Lan, P.D. Kaviratna and T.J. Pinnavaia, *Journal of Physics and Chemistry of Solids*, 1996, **57**, 6–8, 1005.

51. A.D. Pomogailo and V.N. Kestelman, *Metallopolymer Nanocomposites*, Springer, Darmstadt, Germany, 2005.

52. H. Miyagawa and L. Drzal, *Polymer*, 2004, **45**, 15, 5163.

53. M.Z. Rong, M.Q. Zhang, Y.X. Zheng, H.M. Zeng and K. Friedrich, *Polymer*, 2001, **42**, 7, 3301.

54. G. Tsagaropoulos and A. Eisenberg, *Macromolecules*, 1995, **28**, 18, 6067.

55. G. Georgoussis, A. Kanapitsas, P. Pissis, Yu.V. Savelyev, V.Ya. Veselov and E.G. Privalko, *European Polymer Journal*, 2000, **36**, 6, 1113.

56. S. Stavrev, R. Kotsilkova, J. Karadjov and Z. Karagyosova in *Nanoscience and Nanotechnology*, Volume 1, Eds., E. Balabanova and I. Dragieva, Heron Press, Sofia, Bulgaria, 2001, p. 154.

57. C. Silvestre, S. Cimmino, M. Raimo, C. Carfagna, V. Capuano and R. Kotsilkova, *Macromolecular Symposia*, 2005, **228**, 99.

58. R. Pelster and U. Simon, *Colloid and Polymer Science*, 1999, **277**, 1, 2.

59. Y.H. Hyun, S.T. Lim, H.J. Choi and M.S. Jhon, *Macromolecules*, 2001, **34**, 23, 8084.

60. H.J. Choi, M.S. Cho, J.W. Kim, C.A. Kim and M.S. Jhon, *Macromolecular Rapid Communications*, 2001, **22**, 5, 320.

61. R. Wagener and T. Reisinger, *Polymer*, 2003, **44**, 24, 7513.

62. *Polymer Nanocomposites – Synthesis, Characterisation and Modeling, Chemistry*, Eds., R. Krishnamoorthi and R.A. Vaia, American Chemical Society, Washington, DC, USA, 2002.

63. H.A. Barnes, J.F. Hutton and K. Walters, *An Introduction to Rheology*, Rheology Series, No. 3, Elsevier, Amsterdam, The Netherlands, 1993.

64. P.C. Hiemenz, *Principles of Colloid and Surface Chemistry*, 2nd Edition, Marcel Dekker, New York, NY, USA, 1986, Chapter 4.

65. C. Tsenoglou, *Journal of Rheology*, 1990, **34**, 1, 15.

66. P. Meakin, *Physical Review Letters*, 1983, **51**, 13, 1119.

67. M. Kolb, R. Botet and R. Jullien, *Physical Review Letters*, 1983, **51**, 13, 1123.

68. P-G. de Gennes, *Scaling Concepts in Polymer Physics*, Cornell University Press, Ithaca, NY, USA, 1979.

69. W.D. Brown and R.C. Ball, *Journal of Physics: Part A*, 1985, **18**, 9, L517.

70. M. Bousmina and R. Müller, *Journal of Rheology*, 1993, **37**, 4, 663.

71. W-H. Shih, W.Y. Shih, S-I. Kim, J. Liu and I.A. Aksay, *Physical Review A*, 1990, **42**, 8, 4772.

72. J. Liu, W.H. Shih, W.Y. Shih and I.A. Aksay in *Fractal Aspects of Materials: Disordered Systems*, Eds., D.A. Weitz, L.M. Sander and B.B. Mandelbrot, Materials Research Society, Pittsburgh, PA, USA, 1988, p. 239.

73. R. Buscall, P.D.A. Mills, J.W. Goodwin and D.W. Lawson, *Journal of the Chemical Society, Faraday Transactions I*, 1988, **84**, 12, 4249.

74. C-R. Lin and W-J. Chen, *Colloid and Polymer Science*, 1999, **277**, 11, 1019.

75. V. Trappe and D.A. Weitz, *Physical Review Letters*, 2000, **85**, 2, 449.

76. K-M. Jäger and S. Eggen, *Polymer*, 2004, **45**, 22, 7681.

77. C. Liu, J. Zhang, J. He and G. Hu, *Polymer*, 2003, **44**, 24, 7529.

78. R.G. Larson, *The Structure and Rheology of Complex Fluids*, Oxford University Press, New York, NY, USA, 1999.

79. A.V. Shenoy, *Rheology of Filled Polymer Systems*, Kluwer, Dordrecht, The Netherlands, 1999.

80. S.S. Ray and M. Okamoto, *Progress in Polymer Science*, 2003, **28**, 11, 1539.

81. R.K. Bharadwaj, A.R. Mehrabi, C. Hamilton, G. Trujillo, M. Murga, R. Fan, A. Chavira and A.K. Thompson, *Polymer*, 2002, **43**, 13, 3699.

82. J-S. Chen, M.D. Poliks, C.K. Ober, Y. Zhang, U. Wiesner and E.P. Giannelis, *Polymer*, 2002, **43**, 18, 4895.

83. S.D. Burnside and E.P. Giannelis, *Chemistry of Materials*, 1995, **7**, 9, 1597.

84. S.J. Kemnetz, A.L. Still, C.A. Cody and R.J. Schwindt, *Coating Technology*, 1989, **61**, 47.

85. N. Casson in *Rheology of Dispersed Systems*, Ed., C.C. Hill, Pergamon Press, Oxford, UK, 1959, p. 84.

86. C.D. Han, *Multiphase Flow in Polymer Processing*, Academic Press, New York, NY, USA, 1981.

87. D.W. Sundstrom, *Rheologica Acta*, 1983, **22**, 4, 420.

88. N.A. Frankel and A. Acrivos, *Chemical Engineering Science*, 1967, **22**, 6, 847.

89. I.M. Krieger and T.J. Dougherty, *Transactions of the Society of Rheology*, 1959, **3**, 1, 137.

90. C. Friedrich, W. Scheuchenpflug, S. Neuhäusler and J.J. Rösch, *Applied Polymer Science*, 1995, **57**, 4, 499.

91. Eckstein, C. Friedrich, A. Lobbrecht, R. Spitz and R. Mulhaupt, *Acta Polymerica*, 1997, **48**, 1–2, 41.

92. S. Steinmann, M. Fahrlander, W. Frassdorf and C. Friedrich in *Proceedings of the 13th International Congress on Rheology*, Cambridge, UK, 2000, Volume 1, p. 197.

93. S. Agarwal and R. Salovey, *Polymer Engineering and Science*, 1995, **35**, 15, 1241.

94. A. Bischoff, M. Klüppel and R.H. Schuster, *Polymer Bulletin*, 1998, **40**, 2–3, 283.

95. J.D. Ferry, *Viscoelastic Properties of Polymers*, 3rd Edition, John Wiley & Sons, New York, NY, USA, 1980.

96. N.W. Tschoegl, *The Phenomenological Theory of Linear Viscoelastic Behaviour: an Introduction*, Springer, Heidelberg, Germany, 1989.

97. U. Brandenburg and G. Lagaly, *Applied Clay Science*, 1988, **3**, 3, 263.

98. J.R. Harbourg, M.J. Walzak and P. Veregin, *Journal of Colloid and Interface Science*, 1990, **138**, 2, 380.

99. S.Y. Stavrev, S.B. Lazarov, K.L. Stoev, L.G. Markov and V.I. Ivanov, inventors; no assignee; US 5,353,708, 1994.

100. G. Schmid, Ed., *Clusters and Colloids: From Theory to Applications*, VCH, Weinheim, Germany, 1994.

101. T.F. Tardos, *Langmuir*, 1990, **6**, 1, 28.

102. R. Schueler, J. Petermann, K. Schülte and H.P. Wentzel, *Journal of Applied Polymer Science*, 1997, **63**, 13, 1741.

103. J.S. Bradley in *Clusters and Colloids: From Theory to Applications*, Ed., G. Schmid, VCH, Weinheim, Germany, 1994, p. 549.

104. G. Schön and U. Simon, *Colloid and Polymer Science*, 1995, **273**, 2, 101.

105. G. Schön and U. Simon, *Colloid and Polymer Science*, 1995 **273**, 3, 202.

106. J. Park and S.C. Jana, *Macromolecules*, 2003, **36**, 22, 8391.

107. D.J. Suh, Y.T. Lim and O.O. Park, *Polymer*, 2000, **41**, 24, 8557.

108. S. Wu, *Polymer*, 1985, **26**, 12, 1855.

109. S. Wu, *Journal of Applied Polymer Science*, 1988, **35**, 2, 549.

110. K. Levan, A. Margolina and A.Z. Patashinsky, *Macromolecules*, 1993, **26**, 15, 4061.

3 Formation of Thermoset Nanocomposites

R. Kotsilkova, C. Silvestre and S. Cimmino

3.1 Fundamental Principles of Thermoset Nanocomposite Formation

Thermoset composites are usually prepared in order to modify dimensional stability, conductivity, mechanical, thermal and other properties or simply to reduce the cost due to the incorporation of micrometre size filler particles within the thermoset resin matrix [1, 2]. For example, epoxy resin is one of the most important thermosets that have been widely used as the matrix of polymer composites and other structural materials due to their high modulus and strength, their excellent chemical resistance and their simplicity in processing. Extensive applications have motivated the preparation of organic/inorganic hybrids of thermoset resins and nanofillers in order to gain improved or novel properties. However, little work has been devoted to the formation of nanocomposites based on thermosetting polymers and layered silicates, in comparison with the extensive studies on nanocomposites based on linear thermoplastics.

In situ intercalative polymerisation has been explored to create thermoset nanocomposites with layered silicates [3–9]. Dispersing unmodified layered silicates in a thermoset resin is very difficult and therefore a compatibilising agent is commonly used. This is a molecule consisting of one hydrophilic and one organophilic function. The compatibilising agent (organic intercalant) allows layered silicates to be dispersed in polymers by substitution of the metallic cations between the silicate layers. The vast majority of research on the formation of thermoset nanocomposites has been focused on epoxy-based chemistries using different curing agents and organic intercalants [10–17].

The fundamental principles of nanocomposite formation are the ability of the monomer to move and to react within the interlayer galleries of the layered silicate [10]. A critical balance between inter- and extra-gallery curing reactions, together with resin and hardener diffusion, is the key factor in controlling organoclay exfoliation [17–23]. Two alternative processes for dispersion of organoclay exist. First, uniform dispersion may be achieved before the network-forming reaction. However, this results in unwanted viscosity increases and processing difficulties of the precursor – the unreacted system [12, 13]. Alternatively, dispersion may occur concurrently with network formation. In this case, layer separation must occur at a sufficiently rapid rate before complete network formation. The ability to enhance the intra-gallery polymerisation rate catalytically to be

comparable with or greater than the extra-gallery polymerisation rate is critical. Hence, the organic surface modifiers need to combine both catalytic functionality to increase the intra-gallery reaction rate and enhanced miscibility towards both components to ensure stoichiometric ratio of reactants between the layers.

Kornmann and co-workers [19] described the exfoliation mechanism of silicate platelets in epoxy resins, proposing that the molecules will intercalate into the gallery only if the nature and polarity of the inter-gallery ions match with those of the monomer and the increase in entropy of the organic ions on gallery separation is sufficient. Before any curing reaction, thermodynamic considerations would determine the amount of diffusion between clay platelets, so the clay layers in the dispersions could only be intercalated by resin molecules. Once the interlayer reaction occurs, the polarity of the resin is reduced and further molecules diffuse into the galleries, pushing the silicate layers apart and finally exfoliating the clay platelets. At the same time, curing outside the clay galleries occurs, inhibiting the migration of more epoxy resin and amines into the galleries until further distribution of the silicate is fixed at the gel point.

Park and Jana [20] considered that nanocomposite preparation by *in situ* polymerisation is composed of two steps: intercalation and exfoliation. In the intercalation step, monomer molecules are allowed to diffuse into clay galleries, leading to an increase of *d*-spacing. The intercalated clay layers remain parallel to each other with strong interlayer interactions. In the exfoliation step, the large polymer molecules formed by polymerisation of the monomer exert an entropic force on the clay layers. If the magnitude of this entropic force is larger than the sum of the forces opposing separation of the clay layers, adjacent clay layers move away from each other to reach an equilibrium separation distance with no apparent interlayer interactions.

Jiankun and co-workers [22] found that organoclays can be easily intercalated by epoxy resin through mild mixing at 70–80 °C to form a stable epoxy/clay intercalated hybrid. Under appropriate conditions, the clays were able to be further exfoliated during the curing process of the epoxy/clay hybrid mixtures. If the organoclays can be exfoliated at all, the exfoliation will be finished at the stage before the gel point of the epoxy resin. Thus, a nanocomposite is obtained. The exfoliating ability of the organoclays is determined by their nature, including the catalytic effect on the curing reaction of the resin, and their miscibility with the curing agent. The curing speed of intra-gallery epoxy relative to that of extra-gallery epoxy is an important factor influencing the exfoliation of clay. It could be concluded that factors promoting the curing reaction of intra-gallery epoxy resin will facilitate the exfoliation of the clay.

3.1.1 The Role of Curing Agent and Organic Modifier

Next to the aforementioned mechanism of nanocomposite formation, the exfoliating ability of the organoclays is basically determined by the nature of the clays and the curing agent used [12, 13, 24–29].

The influence of the curing agent in the polymerisation process appeared to be determinant for the resulting structure and properties of thermoset nanocomposites. Messersmith and Giannelis [12, 13] prepared epoxy/silicate nanocomposite based on the diglycidyl ether of bisphenol A and organo-montmorillonite cured by various hardeners. X-ray diffraction (XRD) patterns indicate that at room temperature a mix of intercalated and unintercalated clay species coexist in the epoxy matrix. Thus the addition of curing agent induced an increase of the interlayer spacing of silicates, which results in partial intercalation. Further curing upon heating results in the disappearance of the interlayer spacing reflection, indicating that delamination of the clay tactoids has occurred. This process depends significantly on the type of curing agent used. For example, when diamines were used, only intercalated epoxy–clay structures could be obtained. However, when other types of curing agents such as nadic methyl anhydride, monomethylamine or benzyldimethylamine were added, delamination during heating of the reaction mixture occurred, resulting in exfoliated epoxy/clay nanocomposites.

Kornmann and co-workers [19] synthesised epoxy/organoclay nanocomposites in which the epoxy was cured with different curing agents. The authors concluded that the choice of the curing agent and the curing conditions controlled the extent of exfoliation of the clay. The largest extent of exfoliation was observed in the aliphatic diamine-cured epoxy systems. Zerda and Lesser [28] examined the synthesis of intercalated nanocomposites prepared by organo-montmorillonite and glassy epoxy, which was cured with aliphatic diamine curing agent.

The curing process appears to involve the modified silicate, which participates in the crosslinking reaction and results in direct attachment of the polymer network to the molecular dispersed silicate layers. Hence, the nature of organoclays determined by the organic ions within the galleries could play an active role. Pinnavaia and co-workers [23] observed that the extent of silicate layer separation is governed by the chain length and the activity of the gallery cations. Thus, montmorillonites intercalated by alkyl-ammonium cations with chain lengths longer than eight carbon atoms yield exfoliated nanocomposites. In contrast, clay intercalated by shorter alkyl-ammonium cations and simple inorganic cations tend to afford an intercalated nanocomposite architecture or lead to conventional composites. The dependence of nanocomposite formation on -onium ion length is explained in terms of different swelling abilities of organoclays by the epoxy monomer, which is proposed to control the initial accessibility of the galleries for polymer formation. Upon solvation of the organoclay by the epoxide monomers, the gallery cations reorient perpendicular to the epoxy molecules inserted between the -onium ions. This may be a general prerequisite for pre-loading the clay galleries with sufficient monomer to achieve layer exfoliation upon intra-gallery polymerisation. Further, it is important to select curing conditions that balance the intra- and extra-gallery polymerisation rates, according to the length and the activity of the intra-gallery -onium ions.

An important feature of the presence of the nano-reinforcement is related to its catalytic effect on the polymerisation reaction. For example, the alkyl-ammonium ions that favour clay exfoliation are acidic and can catalyse the epoxy–amine polymerisation reaction. Therefore, the formation mechanism of an exfoliated epoxy/clay nanocomposite could be described as intra-gallery catalytic polymerisation. Wang and Pinnavaia [9] reported on a direct nanoscopic delamination of smectite clays in a polyether matrix, delivered from the self-polymerisation of an epoxy resin upon heating. The exfoliation of clay takes place spontaneously at the delamination polymerisation temperature, which depends on the heating rate and the nature of the clay exchange cations.

Brown and co-workers [11] also reported on the role of various quaternised ammonium pre-intercalated montmorillonites in epoxy/diamine nanocomposite formation. They proposed that the organic modifier serves as a compatibiliser for the monomers, as well as acting as a catalyst for the epoxy–diamine cure. The heat of reaction calculated for the pure resin and for the nanocomposites is constant, indicating that no difference was observed in the final degree of polymerisation. The main difference observed in the thermograms was in the peak temperature, indicating that the presence of the intercalated filler somehow affects the kinetics of the crosslinking reaction. Park and Jana [20, 21] investigated the plasticisation of crosslinked epoxy networks by hydrocarbon chains of quaternary ammonium ions and its effect on the exfoliation behaviour of nanoclay particles in mixtures of aromatic and aliphatic epoxies. They found that the quaternary ammonium ions, apart from catalysing epoxy curing reactions, are capable of plasticising crosslinked epoxy chains. The effect of such plasticisation is observed in terms of a large reduction of T_g and lowering of the storage modulus of cured epoxy networks. This effect is found to be small for aromatic epoxies and large for aliphatic epoxies [20].

Park and Jana [20] attributed the degree of exfoliation of the clay–epoxy system to be a strong function of the ratio of the storage modulus of intra-gallery crosslinking epoxy molecules and the viscosity of extra-gallery crosslinked epoxy molecules, G'/η^*. For example, exfoliated structures result in higher values of G'/η^* (e.g., ~2–4 s^{-1}), while lower values (e.g., <1 s^{-1}) indicate intercalation, even though the intra-gallery polymerisation rate is faster than the extra-gallery rate in all cases. Moreover, competition between faster curing of epoxy due to plasticisation by the hydrocarbon chains of quaternary ammonium ions affected the G'/η^* ratio and therefore improved the exfoliation behaviour [20].

Additionally, thermal dissociation of alkyl-ammonium ions during the curing process may have adverse effects on nanoclay exfoliation in epoxy–clay systems [21]. For example, at cure temperatures higher than the dissociation temperature of the alkyl-ammonium ions, primary amines were generated from the thermal dissociation of the alkyl-ammonium ions and the excess chloride salt, which reacted readily with the epoxy molecules and formed linear chains. In addition such reactions resulted in an excess of diamine curing agents, which in turn caused additional plasticisation of epoxy networks and lowered the values of intra-gallery storage modulus. In such cases, only intercalated epoxy compounds were produced. Thus, for example, the epoxy curing temperature must be lower than the thermal dissociation temperature of the alkyl-ammonium ions to avoid

prior nanoclay exfoliation behaviour due to reduced intra-gallery storage modulus and possible plasticisation effects.

Several authors have reported on the possibility of synthesising materials with a nanocomposite structure based on organoclays and unsaturated polyester resins [3, 30–32]. Kornmann and co-workers [30] prepared nanocomposites of montmorillonite clay, pre-intercalated with two different silane coupling agents, dispersed in unsaturated polyester resin (with 42% of styrene monomer). The curing is initiated with co-octanoate and peroxide, which leads to partial delamination of the aluminosilicates and synthesis of exfoliated nanocomposites. Suh and co-workers [31] studied the formation mechanism of unsaturated polyester/layered silicate nanocomposites depending on the fabrication method. During the free-radical polymerisation initiated by benzoyl peroxide, the styrene component of the resin solution acts as a curing agent, which bridges the unsaturated polyester molecules. The sequential mixing resulted in increasing crosslinking density and better dispersion. Crosslinked polyester/clay nanocomposites were also prepared by dispersing organically modified montmorillonite in pre-promoted polyester resin and subsequently crosslinking at room temperature [32].

In general, the dispersion of clay platelets in monomer followed by *in situ* polymerisation can result in the formation of three idealised types of composite structures: conventional composites, intercalated and exfoliated nanocomposites. Conventional composites contain unintercalated clay aggregates. Intercalated nanocomposites have a definite structure formed by the insertion of one or more molecular layers of polymer into the clay host galleries, and the properties usually resemble those of the ceramic host [28, 29]. Exfoliated nanocomposites have separated clay layers and usually a low clay content, as well as a high aspect ratio of the exfoliated clay layers (e.g., 200–2000), which afford reinforcement properties comparable to those of fibres for certain polymers [13, 23]. However, it is found to be relatively difficult to achieve complete exfoliation of smectite clays into a polymer matrix, because of strong electrostatic attraction between the silicate layers and the intra-gallery ions. Therefore, the real nanocomposite structure consists mostly of mixtures of intercalated and exfoliated layers.

3.1.2 Kinetics of Formation of Smectite/Epoxy Nanocomposites

A study on the kinetics of the epoxy–amine reaction in the presence of organoclay by using both isothermal and dynamic differential scanning calorimetry (DSC) analyses reported that the activation energy of the curing process of nanocomposites decreased about 10% in comparison to that of the unfilled epoxy resin [33]. This was interpreted as the effects of the alkyl-ammonium ions of the organic modifier on the intra-gallery polymerisation. The researchers proposed that the kinetics of nanocomposite formation in epoxy–clay systems depends on the following factors: (i) the rate of curing of extra-gallery epoxy resin; (ii) the rate of intercalation of epoxy–amine media; and (iii) the rate of curing of intra-gallery epoxy resin. Increasing the nanofiller content increases the viscosity

of the system and therefore suppresses resin intercalation into the silicate galleries. This may be the reason for the decreased activation energy [22]. The competition between the intra-gallery and the extra-gallery polymerisation rates is found to be the determining factor for the extent of clay exfoliation [34].

The kinetics of nanocomposite formation in smectite/epoxy hybrids prepared by dispersing organo-smectites, pre-intercalated with hexadecyl-octadecyl-ammonium (SAN), trioctyl-methyl-ammonium (STN) and oligo(oxypropylene)-diethyl-methyl-ammonium (SPN) ions, within the epoxy resin Araldite LY556 [35, 36] have been studied. The characteristics of the epoxy matrix and the smectites are presented in **Tables 2.3** and **2.4**, respectively. Hybrid dispersions are prepared using *direct* and *solvent processing* techniques, which are described in Section 2.4.1, as follows: (i) *direct processing*, where the smectites were dispersed in the epoxy resin by sonication; and (ii) *solvent processing*, where the smectites were dispersed first in toluene and then mixed with the epoxy resin. The resulting smectite/epoxy hybrid dispersions were degassed under vacuum to remove the solvent and/or air, and then blended with a stoichiometric amount (100/15) of diethylenetriamine (DETA) as a curing agent. The initiating role of the organic modifier on the epoxy curing process is taken into account when stoichiometric proportions of amine are calculated. Then, the samples were moulded and cured by heating for 4 h at 80 °C (the cured stage), followed by post-curing of 1 hour at 140 °C. The gel point of the curing reaction is reached after heating for about 30 min at 80 °C.

By using XRD analyses, we have observed that the process of structure formation in smectite/epoxy hybrids during curing depends significantly on various factors, such as: the heating conditions, the organic modifier and the use of solvent [35, 36]. XRD spectra of samples were measured at different stages of the curing by using Cu Kα radiation in the Θ range 4–35°. **Figure 3.1** compares the XRD diffraction spectra of the three organo-smectites, SAN, STN and SPN, in the diffraction range, Θ = 4–32°. It can be seen that, in contrast to SAN and STN organoclays, the SPN organoclay displays a plateau in the diffraction spectra, indicating better separation of the silicate layers by the organic intercalant. **Table 2.4** also confirms the larger intra-gallery spacings of the SPN smectite, d_{001} = 4.20, compared to 2.03 for SAN and 2.27 for STN.

The key question regarding the structure of smectite/epoxy nanocomposites is whether a true nanocomposite is formed during the curing process. **Figure 3.2** presents evidence for the kinetics of nanocomposite formation of 2.5% SAN, STN and SPN organo-smectites in epoxy resin/DETA systems prepared by *direct processing* [35, 36]. Here, the diffraction spectra of the epoxy resin and the STN, SAN and SPN nanocomposites are compared under different reaction conditions, relative to the three stages of thermal curing: (a) gel point (30 min at 80 °C); (b) cured stage (4 h at 80 °C); and (c) post-cured stage (1 h at 140 °C). The diffraction range Θ = 4–20° is studied in detail, and XRD scattering patterns of nanocomposites are compared to that of the unfilled epoxy resin.

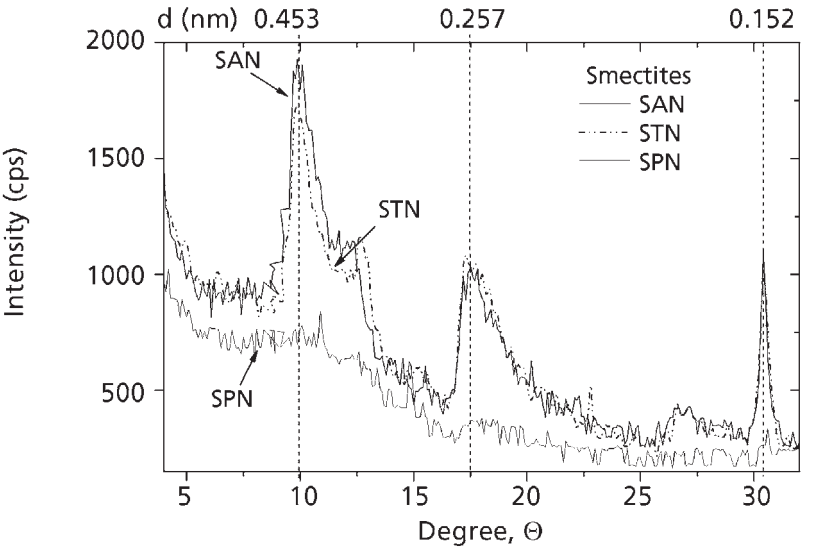

Figure 3.1 XRD scattering patterns of the organo-smectites SAN, STN and SPN. *Data from [36]*

First of all, it is evident that the diffraction spectra of nanocomposites are dominated by the epoxy resin and they do not show the reflection peaks typical of the organo-smectite fillers. This allows one to propose a homogeneous dispersion of smectite aggregates within the resin matrix. As seen in **Figure 3.2(a)**, at the gel point stage the position of the broad basal peak of the epoxy resin ($\Theta \sim 8.5$) is not changed by the presence of smectites SAN, STN and SPN; however, the intensity of the peak decreases in nanocomposites compared to the pure resin. This could be related to the different size of the structure domains of the intra-gallery and extra-gallery epoxy resin affected by the exfoliation of the clay platelets during curing until further distribution of the silicates is fixed at the gel point [17–23]. In contrast, at the cured stage after 4 h heating at 80 °C, not only a decrease of intensity, but also a shift of the position of the reflection towards lower values, from $\Theta \sim 8.5$ (epoxy resin and SAN nanocomposites) to $\Theta \sim 7.4$ (STN and SPN nanocomposites) is observed in **Figure 3.2(b)**. This accounts for the effect of the smectite layers on the epoxy structure formation after the gel point. **Figure 3.2(c)** demonstrates the final structure of the nanocomposites after post-curing of 1 h at 140 °C, which differs from the structure of the samples at the cured stage pointed out in **Figure 3.2(b)**.

It could be proposed that the post-cured stage allows formation of the fully cured structure of both the epoxy resin and the nanocomposites. Here, a broad reflection centred on $\Theta = 8.2$ is observed for pure epoxy resin, corresponding to $d \sim 0.514$ nm. However, the reflection of SAN and STN nanocomposites is found to be broader than that of the pure resin, and the peak is shifted to lower values of $\Theta = 7.8$ and $\Theta = 7.3$, and the values of

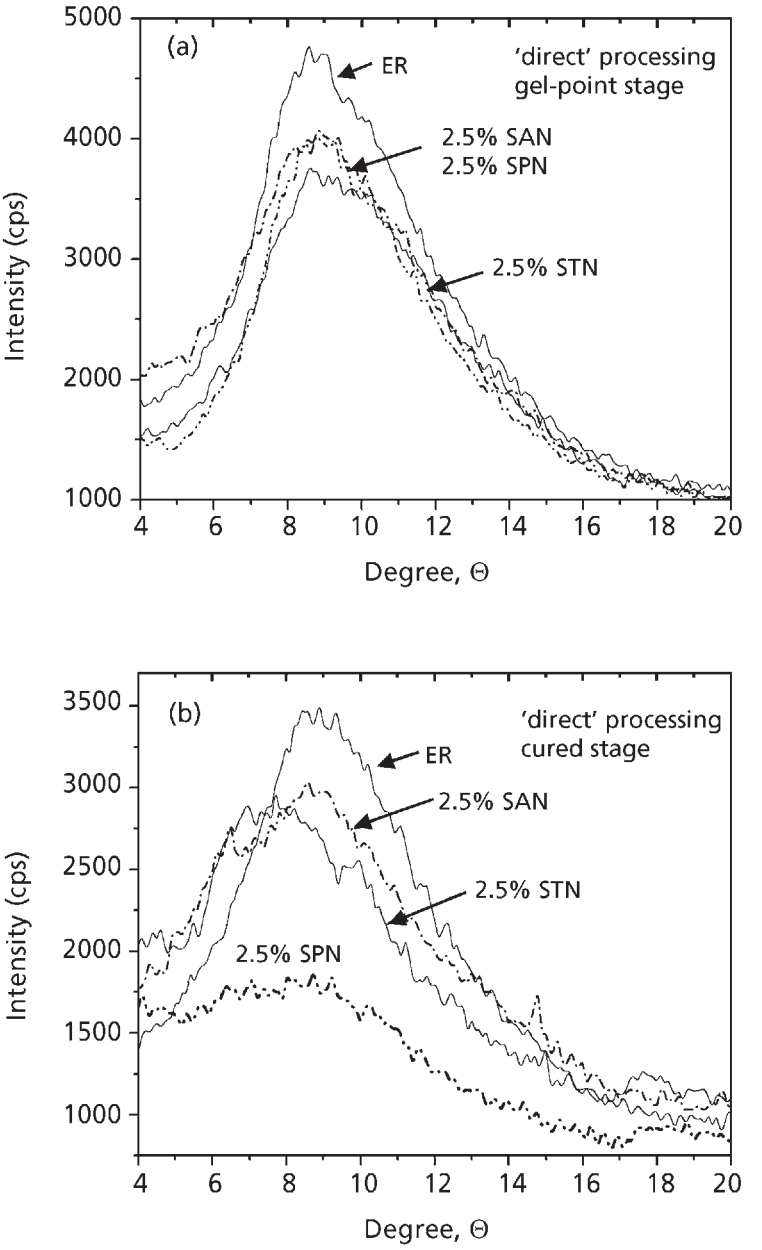

Figure 3.2a,b XRD scattering patterns of epoxy resin and nanocomposites of 2.5 vol% SAN, STN and SPN prepared by the direct processing technique. Curing steps: (a) gel point (30 min at 80 °C); (b) cured state (4 h at 80 °C. Data from [35, 36].

Reproduced with permission from [35]. ©Wiley Periodicals, 2005

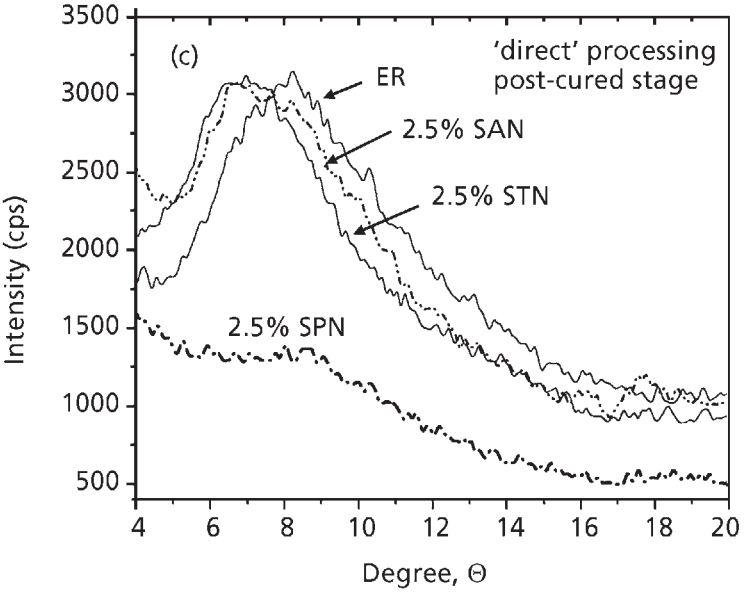

Figure 3.2c XRD scattering patterns of epoxy resin and nanocomposites of 2.5 vol% SAN, STN and SPN prepared by the direct processing technique. Curing steps: (c) post-cured (1 h at 140 °C) states. Data from [35, 36].

Reproduced with permission from [35]. ©Wiley Periodicals, 2005

$d \sim 0.54$ nm and 0.57 nm, respectively, can be calculated. The gradual increase of the values of d for SAN and STN nanocomposites, compared to that of the pure epoxy resin, accounted for the smaller epoxy structure domains formed in the presence of the silicate nanolayers, which is related to the formation of intercalated nanocomposite morphologies. In contrast, the SPN nanocomposite shows no basal reflection in the XRD spectra, which could be related to the formation of an exfoliated nanocomposite.

In general, structure formation in nanocomposites prepared by the direct processing technique is strongly dependent on the organic modifier of the organoclays. The intra-gallery ions SAN, STN and SPN assisted to different extents in exfoliation of smectites during the epoxy–amine thermosetting process. Direct processing leads to the preparation of either intercalated or exfoliated nanocomposites, depending on the swelling ability of the organic modifier of the smectites. The heating conditions are important and the fully cured structure is reached at the post-cured stage.

Based on the XRD results, it could be proposed that the SAN/epoxy and STN/epoxy systems formed intercalated type nanocomposites, while the SPN/epoxy nanocomposite formed presumably exfoliated structure, when direct processing is used.

3.1.3 Effects of Solvent

Solvent is used in some cases of nanocomposite preparation to enhance the miscibility and processability of the initial mixtures. For example, Brown and co-workers [11] produced exfoliated and partially exfoliated epoxy/diamine nanocomposites with organoclay by using a low-boiling solvent. The solvent was found not to alter the structure and properties of the final nanocomposite. Miyagawa and Drzal [37] prepared epoxy nanocomposites reinforced with single-walled carbon nanotubes: the carbon nanotubes are sonicated first in acetone, and then the epoxy resin is added and the solvent removed before blending the mixture with hardener. Abdalla and co-workers [38] synthesised high-temperature thermoset polyimide/clay nanocomposites by blending both unmodified and modified montmorillonites in a methanol solution of monomer (PMR type), the precursor of thermosetting polyimide. They found that the methanol solvent has a propensity to swell the unmodified clay, resulting in nanocomposite formation without the use of modifier.

Smectite/epoxy nanocomposites were prepared by using the solvent processing technique: the organo-smectites are dispersed first in toluene, and then the epoxy resin is added and the solvent removed before blending the mixture with the amine hardener [35]. **Figure 3.3** shows the XRD diffraction spectra of the post-cured samples of the epoxy resin and 2.5% SAN, STN and SPN/epoxy nanocomposites prepared by solvent-assisted processing. Samples are cured at the same heating conditions of 4 h at 80 °C and post-cured at 1 h at 140 °C, as described previously (Section 3.1.2) for the direct processing technique.

The diffraction patterns of nanocomposites in **Figure 3.3** demonstrate a very broad reflection peak with a low intensity for the SAN/epoxy system, as well as the absence of reflection peaks for the STN and SPN/epoxy systems, this accounting for exfoliation.

If one compares the XRD spectra of the post-cured samples prepared by both techniques, solvent processing and direct processing, presented in **Figures 3.3** and **3.2(c)**, respectively, we observe that the three types of organo-smectites SAN, STN and SPN form exfoliated nanocomposites with epoxy resin by using *solvent processing*. Obviously, the prior dispersion of the smectite in toluene enables better swelling and intercalation of the smectites by epoxy resin and amine hardener, which ensures exfoliation of the clay during the thermosetting polymerisation. In contrast, the *direct processing* of smectites (SAN and STN) with epoxy resin enables only intercalation of the epoxy–amine molecules within the clay galleries, but it cannot further exfoliate the smectite tactoids during curing.

Based on the above results, it may be concluded that solvent-assisted processing techniques are more successful for the preparation of exfoliated smectite/epoxy nanocomposites than direct processing. The use of solvent-assisted processing enables exfoliation of the smectites, and here the effect of the organic modifier for the structure formation is

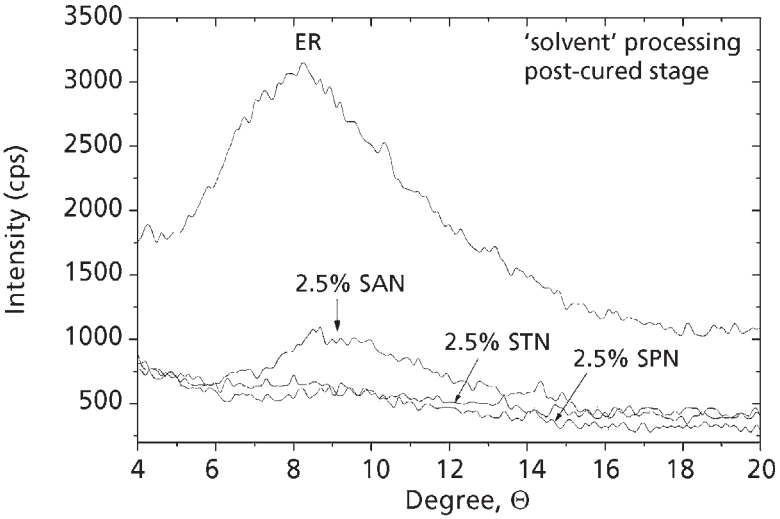

Figure 3.3 XRD scattering profiles of post-cured epoxy resin and nanocomposites of 2.5 vol% SAN, STN and SPN, prepared by the solvent processing technique. Data from [35, 36].

Reproduced with permission from [35]. ©Wiley Periodicals, 2005

insufficient. In contrast, when the direct processing technique is used, the type of organic modifier controls the structure of nanocomposites during curing, resulting mostly in intercalated structures.

It is useful to mention that the enhanced degree of clay dispersion by using the solvent processing technique was predicted by rheological characterisation of the dispersions (Section 2.4.2.1) if compared to those created by the direct processing technique. A better dispersion of the clay ensures a better intercalation of the epoxy resin within the smectite galleries, and this is the basis for further exfoliation during curing.

Recently, interactions of the polymer segments with the reactive groups of the organic modifier at the silicate surface have been reported to be dominant for nanocomposite properties [39, 40]. The researchers reported that the use of a low-boiling solvent during the preparation of systems was not found to alter the structure and properties of the final nanocomposite [11, 37]. In the case of smectite/epoxy nanocomposites, the effects of the organic modifier and the solvent (toluene) on the structure of post-cured systems were investigated by infrared (IR) spectroscopy [35, 36]. **Figure 3.4** compares the IR spectra of the epoxy resin and the 2.5 vol% SAN, STN and SPN nanocomposites, run on a 'Specord 75 IR' spectrometer in the range of 400–2200 cm^{-1}, at a resolution of 4 cm^{-1}. The comparative spectra of nanocomposites prepared by direct processing are

presented in **Figure 3.4(a)**, and the transmission spectra of nanocomposite films are shown in **Figure 3.4(b)**.

The extent of curing of the nanocomposites is roughly equivalent to that of the unfilled epoxy resin, as given by the very low intensity of the epoxy band at 918 cm^{-1}, which indicates completely reacted epoxy groups. Interestingly, **Figure 3.4(a)** shows two new and intense bands that appear in the spectra of the directly processed nanocomposites, at 1600 and 1580 cm^{-1}, which are very slightly indicated in the epoxy spectra and are related to the C–N bands. The increased intensity of these bands in nanocomposites could be related to covalent bonding between the epoxy groups and the reactive groups of the quaternised ammonium salts at the silicate surface. Whatever the mechanism, considerable interaction of the silicate surfaces with the epoxy matrix accounts for an enhanced interlayer reactivity that will not produce true exfoliated nanocomposites if

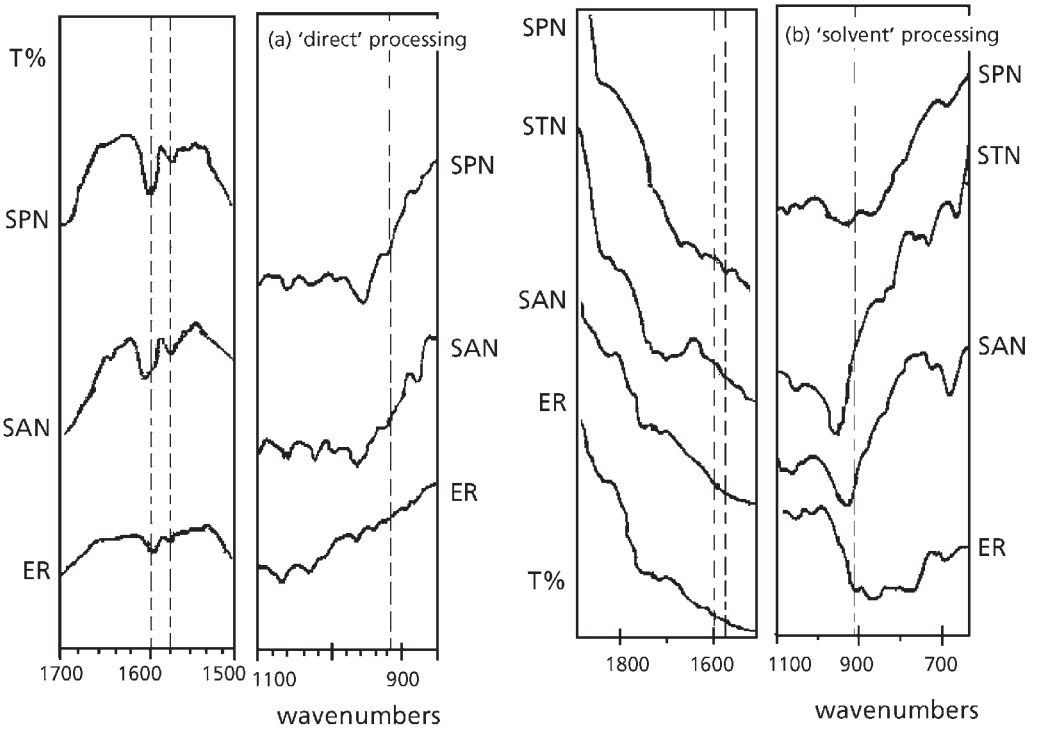

Figure 3.4 IR spectra of 5 vol% smectite/epoxy nanocomposites with SAN, STN and SPN organo-smectites compared to the spectrum of the pure epoxy resin: (a) comparative spectra of nanocomposites prepared by direct processing; and (b) transmission spectra of nanocomposite films prepared by solvent processing.

Data from [35, 36]. Reproduced with permission from [35]. ©Wiley Periodicals, 2005

the miscibility of the components is insufficient. In contrast, in **Figure 3.4(b)** the peaks at 1600 and 1580 cm^{-1} are very slightly indicated in the spectra of both the epoxy resin and the solvent processed nanocomposites.

It could be proposed that the solvent compatibilises the mixture, as well as increasing the mass transport of reagents from the medium into the interlayer by decreasing the viscosity, thus leading to easy separation of smectite aggregates into individual layers. However, the solvent-assisted processing seems to influence the chemical bonding at the interfaces, due to the plasticising effects of the organic modifier and the residual amount of toluene molecules within the intra-gallery spaces.

In summary, it can be concluded that the chemical structure of nanocomposites is controlled by the organic modifier, but the solvent assists in achieving exfoliated morphology of the smectite/epoxy systems. The extent of epoxy curing is found to be equivalent for the pure epoxy resin and the nanocomposites. In order to obtain exfoliated nanocomposites, a balance between the miscibility and the reactivity of the components is required. The organic modifier should ensure a partial miscibility, as well as a surface reactivity of silicates leading to intercalation and the formation of a bonded polymer layer. However, solvent-assisted processing leads to rapid layer separation before gelation and formation of exfoliated nanostructures, but the solvent affects the polymer–surface interactions.

3.2 Cooperative Motion at the Glass Transition Affected by Nanofiller

Recent reports have claimed that the thermal transition associated with the glass transition, T_g, decreased significantly in the case of exfoliated nanocomposites, but it increased in the case of intercalated nanocomposites, if compared with that of the unfilled matrix polymer [33, 34]. The absence of any thermal transition corresponding to T_g is also reported for intercalated hybrids based on polystyrene and polyethylene oxide [39, 40]. Keddie and co-workers [41,42] studied the thermal transition in thin films (below 400 Å) of polystyrene on Si (111) substrate and found a decrease of T_g, which is related to the presence of a liquid-like layer near the surface of the film. In contrast, in the presence of a strongly interacting surface, T_g dramatically increases with increasing film thickness, which was attributed to the presence of a layer close to the surface wherein the mobility is greatly reduced.

The T_g values of epoxy-based nanocomposite systems have been widely investigated and different effects of the organoclay and other nanofillers on the T_g have been reported [7, 11, 13, 15, 20, 43–51]. Several reports on clay/epoxy nanocomposites demonstrated that their T_g values are lower that that of pristine epoxy [7, 10, 20, 44, 46], perhaps because a lack of adhesion between the nanofillers and epoxy molecules causes phase separation or increases the free volume between them. Hence the unrestrained epoxy molecular chains move easily upon heating. Becker and co-workers [10] attributed

such reduction of T_g to a possible lower crosslink density around the clay particles, perhaps due to the perturbing effects of the clay, even though the presence of the clay encourages higher conversion of epoxy. Thus, the clay may change the chemistry of the reaction and indeed the organic ions themselves may catalyse homopolymerisation, although this cannot produce high crosslink density. In contrast, Park and Jana [20] claimed that the reduced values of T_g in the cured epoxy/organoclay systems can be mistakenly attributed to incomplete curing of epoxy molecules. Their experimental data present further evidence that the reduction of T_g of cured epoxy in the presence of quaternary ammonium chloride, as a clay intercalant, was due to plasticisation and not due to reduced degree of curing. In order to confirm this, various amounts of quaternary ammonium chloride was mixed with epoxy resin and the mixtures were cured with stoichiometric amounts of curing agent. The values of T_g gradually decreased with increasing content of quaternary ammonium ions, although complete curing was achieved faster with a higher concentration of quaternary ammonium chloride.

Additionally, a reduction of T_g was found in epoxy nanocomposites reinforced with other nanofillers, such as fluorinated single-walled carbon nanotubes (CNT) [37] and silica-organosol nanoparticles [43]. For example, T_g is found to decrease by approximately 30 °C with the addition of only 0.2 wt% (0.14 vol%) CNT, because of the non-stoichiometry of the epoxy matrix, which was caused by the fluorine modifier on the nanotube surfaces. Such a large decrease in T_g has not been observed with nanocomposites reinforced by organoclay nanoplatelets. The strong reduction of T_g with CNT may be because of the adsorption of epoxy molecules on the CNT, which has a much larger surface area than any other nano-inclusions. According to the preparation procedure, the sonicated CNT were first mixed with epoxy before addition of curing agent. As a result, the surface of CNT was coated by epoxy, which did not react with anhydride curing agent any more, producing a non-stoichiometric mixture, and this strongly decreased the T_g.

Some researchers reported on a constant or slightly decreased T_g in epoxy/clay nanocomposites [49, 50]. A slight decrease in T_g is found also in epoxy/silica nanocomposites, which is ascribed to the presence of a limited amount of unreacted epoxy resin around the silica-organosol particles, which can have some plasticising effect [43].

In contrast, increased T_g values were reported in some cases of intercalated nanocomposite systems [11, 13, 15, 45, 47, 48]. Brown and co-workers [11] reported on the increase of T_g of both intercalated and exfoliated morphologies of epoxy/organoclay nanocomposites with diamine as a curing agent. Hsueh and co-workers [45] prepared exfoliated nanocomposites by mixing amino laurate modified layered double hydroxides and epoxy resin, after thermal curing with amine. The T_g values of these exfoliated nanocomposites were increased, in comparison of the T_g of unfilled epoxy resin. The effect of T_g increase is attributed to the adhesion between the modified nanolayers and the epoxy molecules, reducing the mobility of the main chain of the epoxy molecules as the temperature increases.

3.2.1 Smectite/Epoxy Nanocomposites

The study of the thermal transition showed that the T_g of smectite/epoxy nanocomposites depends strongly on the degree of exfoliation [36]. A significant difference was found in the T_g values of nanocomposites by varying the processing conditions and the type of organoclay intercalant. **Figure 3.5** shows DSC thermograms of an STN/epoxy nanocomposites with 4, 6 and 10 vol% smectite content, prepared by the direct processing technique and cured with diethylenetriamine under the following thermal conditions: 4 h at 80 °C and post-cured for 1 hour at 140 °C. The amine hardener is added in stoichiometric proportions according to the epoxy resin (15/100), thus reducing the excess of hardener produced by the reactive organoclay.

The DSC temperature scans of the post-cured samples were taken using a Perkin-Elmer DSC-7. Samples of about 1 mg were sealed in aluminium pans and heated from 0 to 300 °C at scanning rates of 10 °C/min under a nitrogen atmosphere. The T_g (midpoint) was determined from the curves using the data of the second run.

The T_g of the intercalated STN/epoxy nanocomposites is found to decrease slightly, with $\Delta T_g \sim 6$–10 °C for increased smectite content of 4–10 vol%. This effect could be associated with that observed by IR spectroscopy study of the reactivity between the

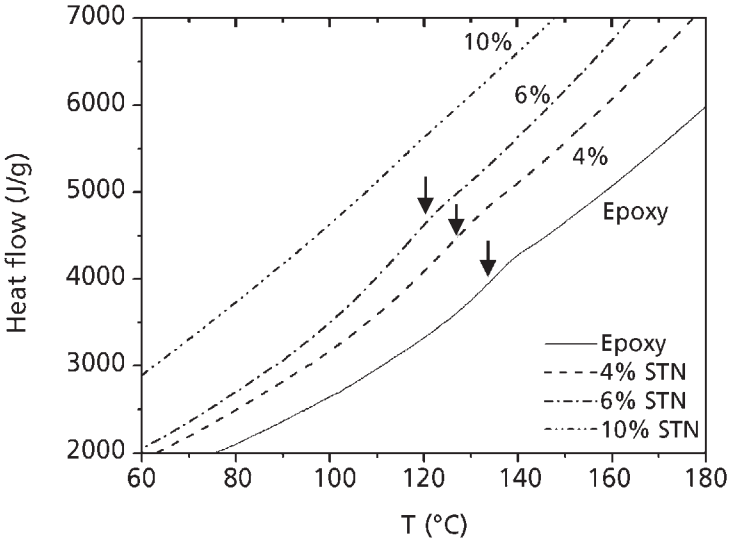

Figure 3.5 DSC thermograms of epoxy resin and STN/epoxy nanocomposites prepared by the direct processing technique and cured with diethylenetriamine; the volume fraction of smectite varies from 4 to 10%. The scanning rate is 10 °C/min. Arrows point to T_g (midpoint).

Data from [36]

epoxy resin and the organic intercalant (**Figure 3.4a**). The organic ions at the silicate surface obviously catalyse homopolymerisation of the absorbed epoxy molecules, leading to a cured interface layer of low crosslink density. Thus, homopolymerisation results in a decrease of the T_g of nanocomposites by increasing the smectite content.

Similar results are shown in **Figure 3.6**, which compares the plots of T_g versus volume content of STN and SAN smectite/epoxy nanocomposites produced by direct processing and cured with DETA. The DSC measurements are carried out using a Mettler-Toledo DSC with heating in the temperature range 25–180 °C, and scanning rates of 20 °C/min under a nitrogen atmosphere. The T_g (midpoint) values determined from the second run are presented. The decrease of the T_g of the 5 vol% smectite/epoxy nanocomposites is about $\Delta T_g \sim 5$–6 °C, and the effect of the organoclay modifier on the decreasing of T_g is relatively low.

In conclusion, the intercalated epoxy/smectite nanocomposites produced by direct processing and cured by diethylenetriamine show a slight reduction of T_g, compared to that of the unfilled resin. This could be related to the bonded interface layer having a low crosslink density.

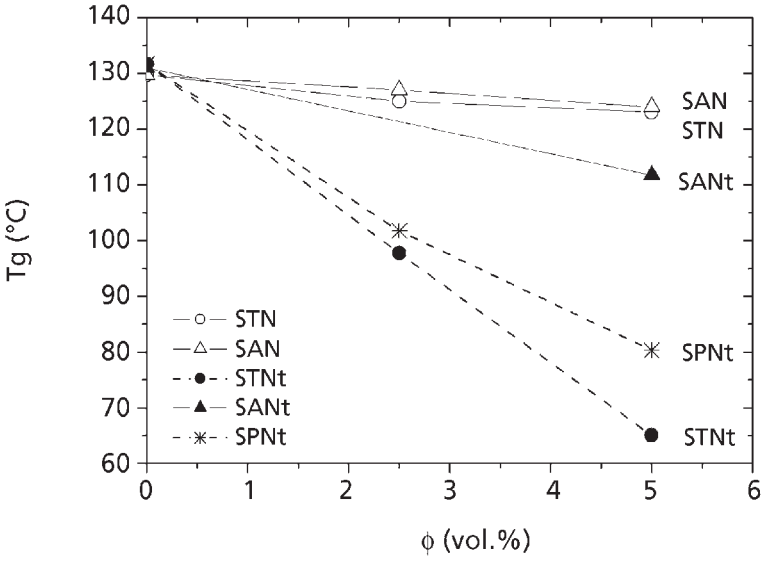

Figure 3.6 Glass transition temperature T_g versus volume fraction of smectite, ϕ, for SAN and STN/epoxy nanocomposites produced by direct processing, as well as SANt, STNt and SPNt/epoxy nanocomposites produced by solvent (toluene) processing. Diethylenetriamine is used as the curing agent; the scanning rate is 20 °C/min.

Data from [36]

However, dramatic changes in T_g are observed for SAN, SPN and STN smectite/epoxy nanocomposites prepared by solvent processing techniques. **Figure 3.6** compares the T_g *versus* volume content using toluene as a solvent for preliminary dispersion of the smectites. The systems investigated contained 0, 2.5 and 5 vol% of SAN, SPN and STN smectites, and the curing agent is DETA. It can be seen that the T_g of the solvent-processed systems decreases significantly, compared to that of the pure epoxy resin. For example, at 5% smectite content, the decrease in T_g is ΔT_g = 18 °C in SANt/epoxy, ΔT_g = 50°C in SPNt/epoxy, and ΔT_g = 65°C in STNt/epoxy nanocomposites. This could be associated with the strong plasticising effect produced by the organic modifier and the residual molecules of the high-boiling toluene in the systems.

The solvent processing technique ensures that the smectites are dispersed first in the solvent, and then the epoxy resin is added, followed by degassing and blending with the hardener. Hence, extraction of the organic modifier from the intra-gallery spacing into the extra-gallery volume produced by the solvent is possible, which increases the plasticising effect of the organic modifier on the curing of the epoxy resin. Obviously, the exfoliated nanocomposites produced with assistance from the solvent are accompanied by the strong plasticising effects of both organic modifier and possibly the rest of the solvent molecules. As found before (**Figure 3.4b**), the plasticising effects in solvent-assisted processing seem to suppress chemical bonding at the interfaces, thus reducing the strength of the polymer–surface interactions.

3.2.2 Graphite- and Diamond-Containing Epoxy Nanocomposites

The materials studied here are hybrids of Araldite LY556 epoxy resin filled with nanosized graphite/diamond (GD) and diamond (D) particles, with a specific surface area of S = 590 m^2/g and 300 m^2/g, respectively. The characteristics of the ingredients have been presented in **Tables 2.3** and **2.5**. As shown in **Table 2.5**, the graphite/diamond nanofiller consists of a mixture of 67% finely dispersed graphite and 33% nanoscale diamond. The nanoscale diamond was obtained from the graphite/diamond mixture by chemical purification and further thermal treatment, which activates the diamond surfaces [52]. Both nanofillers are dried for 24 hours at 100 °C before blending with the resin, but they are not treated additionally with an organic modifier.

Dispersions of nanoparticles in epoxy resin are prepared by sonication of nanofiller in epoxy resin, followed by mixing with diethylenetriamine as a hardener, added in stoichiometric proportions according to the epoxy resin. The curing process is followed in two stages: 1 h at room temperature, followed by post-curing of 3 h at 140 °C.

Figure 3.7 compares the DSC thermograms of the cured epoxy resin and carbon/epoxy nanocomposites with varying graphite/diamond contents [53]. As can be seen, the DSC curve of the unfilled epoxy resin shows a T_g (midpoint) at approximately of 98 °C. The

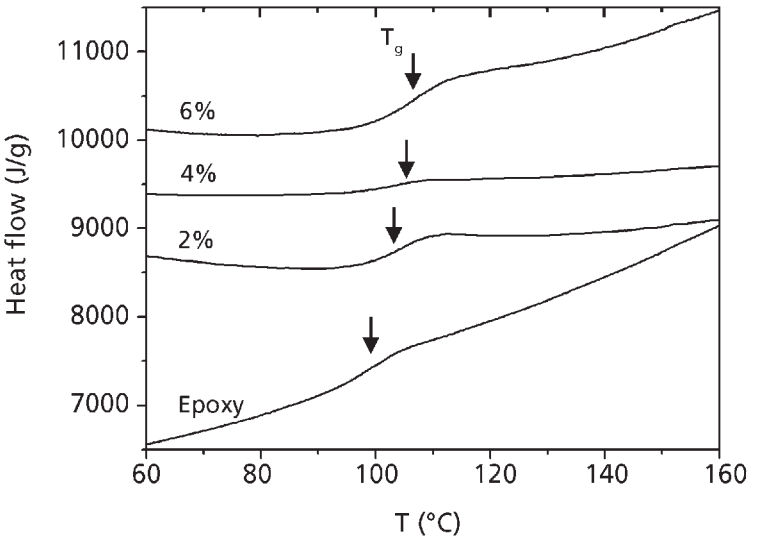

Figure 3.7 DSC thermograms of epoxy resin and carbon/epoxy (carbon as graphite/diamond) nanocomposites with varying volume fraction of filler in the range 2–6%. Arrows point to T_g (midpoint).

Reproduced with permission from [53]. ©Wiley Periodicals, 2005

addition of carbon nanofiller of 2–6 vol% increases the T_g by about ΔT_g = 5–10 °C, as compared to the T_g of the epoxy resin. This confirms the assumption drawn from the rheological data (see **Figure 2.9** and **Table 2.2**) that the polymer chains in dispersions must be under constraint because of the attraction of epoxy molecules at the graphite/diamond surface. Such increase in T_g has been discussed by other authors [54, 55] in terms of an absorbed (bonded) layer around the filler particles due to chains being tied down by the inorganic surface.

Figure 3.8 compares the relative glass transition temperature, $T_{g,comp}/T_{g,resin}$, versus volume content, ϕ, of (graphite/diamond)/epoxy and diamond/epoxy composites. These results clarify that the T_g increase becomes significant above the percolation threshold, ϕ^*, wherein the greatest amount of the polymer is immobilised at the nanofiller surface and the interfacial effects dominate the bulk properties of the material. Moreover, the T_g increase is much higher in diamond/epoxy composites than in (graphite/diamond)/epoxy composites. For example, at 6 vol% nanofiller content, the T_g increases by 35% in epoxy composites with diamond and by only 7% in graphite/diamond systems. This effect could be a result of adhesion between the nanofiller surface and the epoxy resin molecules, which obviously is much stronger in diamond/epoxy systems than in the graphite/diamond one. Based on the difference in T_g of diamond/epoxy and (graphite/diamond)/epoxy systems, it could be proposed that the diamond nanofiller surface is much more active for the

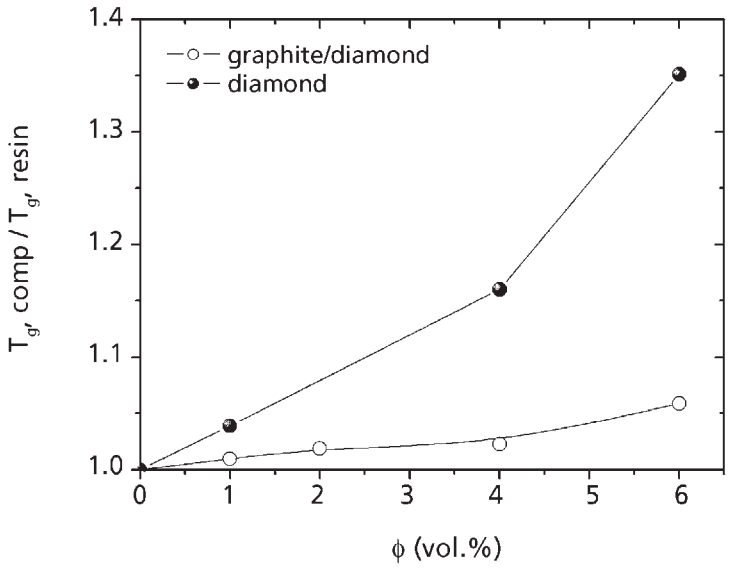

Figure 3.8 Relative glass transition temperature, $T_{g,comp}/T_{g,resin}$, versus volume fraction of nanofiller, ϕ, of (graphite/diamond)/epoxy and diamond/epoxy composites.

Data from [36]

attraction of epoxy molecules than the graphite/diamond surface, and thus is probably related to the chemical purification and thermal treatment [52].

Both adhesion between the two phases, resin and nanofiller, and cluster–cluster aggregates (flocs) formed by the nanofiller and the attracted polymer above the percolation threshold, ϕ*, lead to the restrained mobility of epoxy resin molecules upon heating. Taken in the context of the increased T_g of epoxy nanocomposites with diamond and graphite/diamond, the results appear to indicate that the cooperative motion decreases steeply due to the large and active surfaces of nanoparticles, which absorb and bond the resin molecules. However, it is an open question whether the curing reaction of epoxy resin is affected by the presence of nanoparticles. It is assumed here that the curing conditions of systems containing non-modified graphite/diamond filler allow the epoxy resin to achieve the full degree of curing.

3.3 Conclusions

The results of this study confirm the well-reported mechanism of clay/thermoset nanocomposite formation. Additionally, it was observed that the chemical structure of nanocomposites is controlled by the organic modifier, but the solvent assists in

exfoliation morphology of the clay/epoxy systems. A balance between the miscibility and the reactivity of the components is required, in order for them to become exfoliated nanocomposites.

The extent of curing of the nanocomposites was found to be roughly equivalent with that of the unfilled epoxy resin. The chemical structure of nanocomposites is controlled by the organic modifier, but the solvent assists in exfoliated morphology of the smectite/epoxy systems.

The organic modifiers ensure miscibility as well as surface reactivity of silicates, leading to intercalation and the formation of the bonded polymer layer. The solvent compatibilises the mixture as well as increasing the mass transport of reagents from the medium into the interlayer by decreasing the viscosity, leading to a rapid layer separation before gelation, as well as to the formation of exfoliated nanostructures. However, the solvent-assisted processing seems to influence the chemical bonding at the interfaces, due to the plasticising effects of the organic modifier and a residual amount of toluene molecules, resulting in a reduction of T_g.

In the graphite/diamond-containing hybrids in thermoset matrices, adhesion between the two phases, resin and nanofiller, and cluster–cluster aggregates (flocs or network) formed by the nanofiller and the attracted polymer above the percolation threshold lead to restrained mobility of resin molecules upon heating. This produces an increased T_g of carbon/epoxy nanocomposites, indicating a steeply decreased cooperative motion.

Acknowledgements

The authors would like to thank D. Duraccio and M. Raimo for carrying out the DSC experiments.

References

1. Y. Nakamura, M. Yamaguchi, A. Tanaka and M. Okubo, *Polymer*, 1993, **34**, 15, 3220.

2. S-W. Koh, J-K. Kim and Y-W. Mai, *Polymer*, 1993, **34**, 16, 3446.

3. M. Alexandre and P. Dubois, *Materials Science and Engineering Reports*, 2000, **28**, 1-2, 1.

4. T. Lan and T.J. Pinnavaia, *Chemistry of Materials*, 1994, **6**, 12, 2216.

5. Z. Wang, T. Lan and T.J. Pinnavaia, *Chemistry of Materials*, 1996, **8**, 9, 2200.

6. T. Lan, P.D. Kaviratna and T.J. Pinnavaia, *Chemistry of Materials*, 1995, **7**, 11, 2144.

7. C. Zilg, R. Mülhaupt and J. Finter, *Macromolecular Chemistry and Physics*, 1999, **200**, 3, 661.

8. Z. Wang and T.J. Pinnavaia, *Chemistry of Materials*, 1998, **10**, 12, 3769.

9. M.S. Wang and T.J. Pinnavaia, *Chemistry of Materials*, 1994, **6**, 4, 468.

10. O. Becker, R.J. Varley and G.P. Simon, *Polymer*, 2002, **43**, 16, 4365.

11. J.M. Brown, D. Curliss and R.A. Vaia, *Chemistry of Materials*, 2000, **12**, 11, 3376.

12. P.B. Messersmith and E.P. Giannelis, *Journal of Polymer Science: Polymer Chemistry*, 1995, **33**, 7, 1047.

13. P.B. Messersmith and E.P. Giannelis, *Chemistry of Materials*, 1994, **6**, 10, 1719.

14. T. Lan, P.D. Kaviratna and T.J. Pinnavaia, *Chemistry of Materials*, 1994, **6**, 5, 573.

15. Y. Ni, S. Zheng and K. Nie, *Polymer*, 2004, **45**, 16, 5557.

16. J.W. Gilman, *Applied Clay Science*, 1999, **15**, 1–2, 31.

17. R.A. Vaia, G. Price, P.N. Ruth, H.T. Nguyen and J. Lichtenhan, *Applied Clay Science*, 1999, **15**, 1–2, 67.

18. Z. Wang and T.J. Pinnavaia, *Chemistry of Materials*, 1998, **10**, 7, 1820.

19. X. Kornmann, H. Lindberg and L.A. Berglund, *Polymer*, 2001, **42**, 4, 1303.

20. J. Park and S.C. Jana, *Macromolecules*, 2003, **36**, 22, 8391.

21. J. Park and S.C. Jana, *Polymer*, 2004, **45**, 22, 7673.

22. L. Jiankun, K. Yucai, Q. Zongneng and Y. Xiao-Su, *Journal of Polymer Science: Polymer Physics*, 2001, **39**, 1, 115.

23. T.J. Pinnavaia, T. Lan, Z. Wang, H. Shi and P.D. Kaviratna, in *Nanotechnology – Molecularly Designed Materials*, Eds., G-M. Chow and K.E. Gonsalves, ACS Symposium Series, No. 622, American Chemical Society, Washington, DC, 1996, Chapter 17, p. 250.

24. A. Usuki, T. Mizutani, Y. Fukushima, M. Fujimoto, K. Fukumori, Y. Kojima, N. Sato, T. Kurauchi and O. Kamigaito, inventors; Kabushiki Kaisha Toyoto Chuo Kenkyusho, assignee; US Patent 4,889,885, 1989.

25. T. Lan, Z. Wang, H. Shi and T.J. Pinnavaia, *Proceedings of the ACS Division of Polymer Material Science Engineering*, 1994, **71**, 297.

26. T. Lan, P.D. Kaviratna and T.J. Pinnavaia, *Proceedings of the ACS Division of Polymer Material Science Engineering*, 1994, **71**, 527.

27. H. Shi, T. Lan and T.J. Pinnavaia, *Chemistry of Materials*, 1996, **8**, 8, 1584.

28. A. Zerda and J.A. Lesser, in *Filled and Nanocomposite Polymer Materials*, Eds., A.I. Nakatani, R.P. Hjelm, M. Gerspacher and R. Krishnamoorti, MRS Symposium, Vol. 661, Materials Research Society, Pittsburgh, 2001, KK7.2.1–KK7.2.6.

29. R.A. Vaia, H. Ishii and E.P. Giannelis, *Chemistry of Materials*, 1993, **5**, 12, 1694.

30. X. Kornmann, L.A. Berglund, J. Sterte and E.P. Giannelis, *Polymer Engineering and Science*, 1998, **38**, 8, 1351.

31. D.J. Suh, Y.T. Lim and O.O. Park, *Polymer*, 2000, **41**, 24, 8557.

32. R.K. Bharadwaj, A.R. Mehrabi, C. Hamilton, C. Trujillo, M. Murga, R. Fan, A. Chavira and A.K. Thompson, *Polymer*, 2002, **43**, 13, 3699.

33. W. Xu, S. Bao, S. Shen, W. Wang, G. Hang and P. He, *Journal of Polymer Science B: Polymer Physics*, 2003, **41**, 4, 378.

34. H. Xie, B. Liu, Z. Yuan, Y. Shen and R. Cheng, *Journal of Polymer Science B: Polymer Physics*, 2004, **42**, 20, 3701.

35. R. Kotsilkova, *Journal of Applied Polymer Science*, 2005, **97**, 6, 2499.

36. R. Kotsilkova, *Relationship Between Technology, Structure and Properties of Thermoset Nanocomposites*, Sofia, 2005 [D.Sc. Thesis, in Bulgarian].

37. H. Miyagawa and L.T. Drzal, *Polymer*, 2004, **45**, 15, 5163.

38. M.O. Abdalla, D. Dean and S. Campbell, *Polymer*, 2002, **43**, 22, 5887.

39. R. Krishnamoorti and A.S. Silva, in *Polymer–Clay Nanocomposites*, Eds., T.J. Pinnavaia and G.W. Beall, John Wiley & Sons, New York, NY, USA, 2001, p.315.

40. R. Krishnamoorti, R.A. Vaia and E.P. Giannelis, *Chemistry of Materials*, 1996, **8**, 8, 1728.

41. J.L. Keddie, R.A.L. Jones and R.A. Cory, *Europhysics Letters*, 1994, **27**, 59.

42. J.L. Keddie, R.A.L. Jones and R.A. Cory, *Faraday Discussions*, 1994, **98**, 219.

43. G. Ragosta, M. Abbate, P. Musto, G. Scarinzi and L. Mascia, *Polymer*, 2005, **46**, 23, 10506.

44. C.S. Triantafillidis, P.C. LeBaron and T.J. Pinnavaia, *Chemistry of Materials*, 2002, **14**, 10, 4088.

45. H-B. Hsueh and C-Y. Chen, *Polymer*, 2003, **44**, 18, 5275.

46. C. Zilg, R. Thomann, J. Finter and R. Mülhaupt, *Macromolecular Materials and Engineering*, 2000, **280/281**, 1, 41.

47. D.C. Lee and L.W. Jang, *Journal of Applied Polymer Science*, 1998, **68**, 12, 1997.

48. P. Kelly, A. Akelah, S. Qutubuddin and A.J. Moet, *Journal of Materials Science*, 1994, **29**, 9, 2274.

49. J. Massam and T.J. Pinnavaia, in *Material Research Society Symposium Proceedings*, 1998, **520**, 223.

50. P. Bajaj, N.K. Jha and R.A. Kumer, *Journal of Applied Polymer Science*, 1990, **40**, 1–2, 203.

51. K.T. Gam and H-J. Sue in *Proceedings of the ACS Polymeric Materials: Science and Engineering, Spring Meeting*, San Francisco, CA, USA, 2000, Volume 82, p.288.

52. S. Stavrev, R. Kotsilkova, J. Karadjov and Z. Karagyozova, in *Nanoscience and Nanotechnology*, Volume 1, Eds., E. Balabanova and I. Dragieva, Heron Press, Sofia, Bulgaria, 2001, p.154.

53. R. Kotsilkova, D. Fragiadakis and P. Pissis, *Journal of Polymer Science: Polymer Physics*, 2005, **43**, 5, 522.

54. *Proceedings of the 3rd International Conference on Composite Interfaces – Controlled Interphases in Composite Materials*, Ed., H. Ishida, Elsevier, New York, NY, USA, 1990.

55. H. Ishida and G. Kumar, *Molecular Characterization of Composite Interfaces*, Plenum Press, Seattle, WA, USA, 1983.

4 Structure and Morphology of Epoxy Nanocomposites With Clay, Carbon and Diamond

C. Silvestre, S. Cimmino, D. Duraccio and R. Kotsilkova

4.1 Introduction

Generally speaking, a polymer nanocomposite consists of a polymer filled with particles that have at least one dimension less than 100 nm. There are, therefore, three kinds of nanocomposites that are categorised by whether the filler particles have one, two or three dimensions in the nanometre range [1, 2].

- In type 3 nanocomposites the nanoparticles are generally isodimensional, such as spherical silica nanoparticles, diamond nanoparticles, etc. [1–5].
- In type 2 nanocomposites the nanoparticles have two dimensions in the nanometre range, such as carbon nanotubes and cellulose whiskers.
- In type 1 nanocomposites the nanoparticles have only one dimension in the nanometre range, and usually exist in the form of sheets 1–3 nm thick with the other dimensions being two or more orders of magnitude larger. Nanocomposites that contain these structures are generally obtained by using an intercalating agent.

In this last category, epoxy/clay nanocomposites are a large class of new materials where the inclusion of clays in epoxy matrices has enhanced the tensile and compressive properties of the matrix. The fillers also cause an increase in chemical resistance, barrier properties and dimensional stability [6–9].

The purpose of this chapter is to provide a brief overview of the current state of the art for the morphology and structure of epoxy/clay nanocomposites.

The chapter covers recent progress in the area of polymer/clay nanocomposites. An innovative use of epoxy/clay nanocomposites is illustrated: epoxy/clay nanocomposites were further filled with carbon or diamond particles, successfully produced semi-industrially by the Bulgarian Academy of Sciences [10], to form hybrid nanocomposites and finally mixed with isotactic polypropylene (iPP). Nanoscale diamond and carbon particles are expected to be promising fillers with respect to their tribotechnical properties, adhesion and corrosion resistance. All these performance benefits could be

available without increasing the density or reducing the light transmission properties of the base polymer. In particular, an iPP suitable for fibre production is used, with the final aim to obtain a polypropylene nanocomposite material with improved flammability for textiles. The study of the interactions between the fillers together with the results of flammability tests are also reported.

In principle, iPP is not considered a well-suited polymer for clay nanocomposite development. Isotactic polypropylene/clay nanocomposites are relatively difficult to obtain, because iPP does not contain any polar group in its backbone and it is not compatible with clay. On the other hand, polypropylene is one of the most important commodity polymers, with a broad range of applications [11, 12]. Numerous studies are still in progress to increase the use of iPP in fields where this polymer presents some limitations (due, for example, to high flammability, low stiffness at high temperature or insufficient barrier properties): one route is to modify iPP by adding appropriate fillers. The majority of the results were summarised in the extensive reviews by Pinnavaia and Beall [8] and Ray and Okamoto [9].

4.2 General Outline

Entropic and enthalpic factors determine the outcome of whether organically modified clay will be dispersed, intercalated or exfoliated in a polymer [13–15]. Dispersion of clay in a polymer requires sufficiently favourable enthalpic factors, which is achieved when the polymer–clay interactions are favourable. For most polar polymers the use of alkyl-ammonium surfactants is adequate to offer sufficient excess enthalpy and to promote contributions favouring nanocomposite formation. According to Kornmann and co-workers [16] the driving force for initial resin diffusion into the galleries is the high surface energy of the clay, which attracts the polar resin molecules. Research efforts into nanocomposites indicate that the surface modifier has a dominant influence on the exfoliation behaviour and could act as an intra-gallery catalyst for amine–epoxy polymerisation.

Three polymer/layered silicate morphologies are thermodynamically achievable: intercalated nanocomposites, exfoliated nanocomposites, and flocculated nanocomposites that present an intermediate morphology (**Figure 4.1**) [17]. Their appearance is dependent on the strength of interfacial interactions between the matrix and the filler.

As reported by Ray and Okamoto [9], in intercalated nanocomposites, the insertion of a polymer matrix into the layered silicate structure occurs in a crystallographically regular fashion, regardless of the clay-to-polymer ratio. Intercalated nanocomposites are normally interlayered by a few molecular layers of the polymer. In some cases silicate layers are flocculated due to the hydroxylated edge–edge interaction of the silicate layers. The exfoliated nanocomposites consist of individual nanometre-thick layers suspended

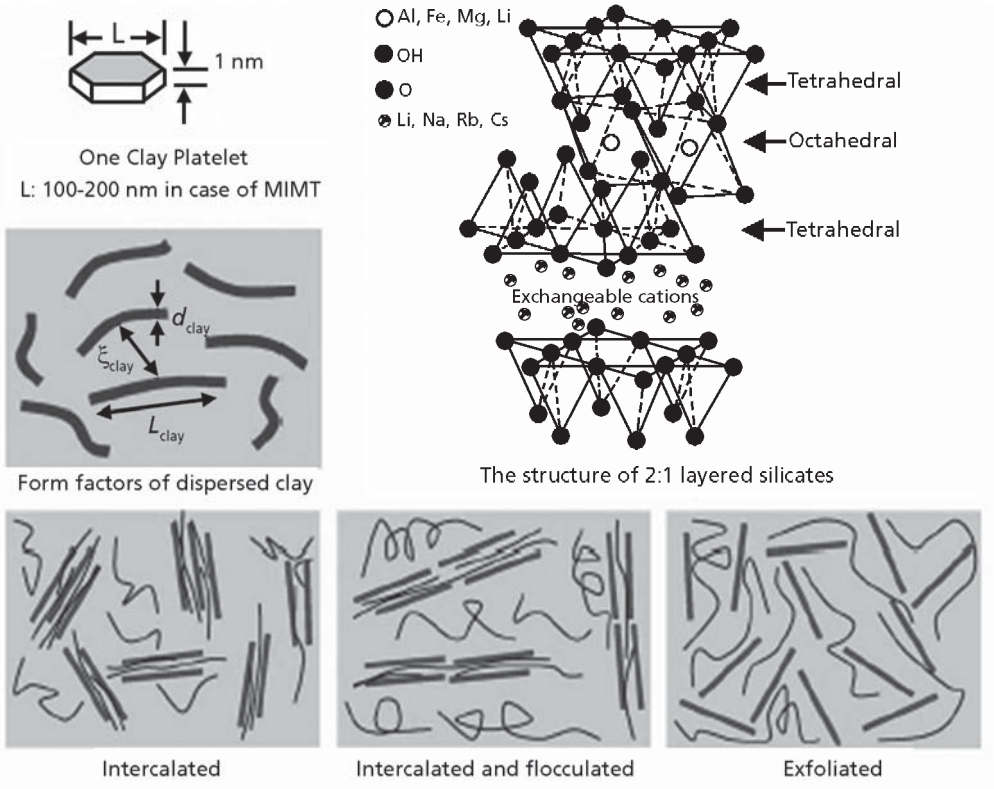

Figure 4.1 Schematic illustration of three different types of thermodynamically achievable polymer/layered silicate nanocomposites.

Reproduced with permission from [17]. ©ACS, USA, 2003

in a polymer matrix and are a result of extensive penetration of the polymer into the silicate layers. The *d*-spacing between the layers is significantly expanded, up to 10 nm or more. Exfoliation has been the ultimate goal of most researchers in this area because this morphology is expected to lead to dramatic improvements of the properties with a reduced loading of fillers compared to traditional composites. The methodology to achieve an exfoliated clay nanocomposite structure in an epoxy matrix has been extensively described in several papers, where the reader can find full and detailed descriptions [1, 3, 6, 8].

The overall morphology in nanocomposites is very complex and the classification given above for discerning the degree of intercalation and exfoliation is too simplified. In the range of exfoliated structures, an additional classification (into ordered, partially ordered and disordered structures) was introduced to adequately describe nanoscale morphologies and to avoid confusion in the structure–properties relationship of nanocomposites.

Vaia [18] proposed an expanded classification scheme where the intercalated and exfoliated structure can be listed into ordered or disordered structures (**Figure 4.2**), depending on the change of spacing and orientation of nanoparticles. An intermediate morphology between intercalation and exfoliation, called partial exfoliation, can also be present. In the case of ordered exfoliation, the ordered and parallel arrangement of nanolayers is preserved and a homogeneous morphology is observed. In the case of disordered exfoliation, individual nanolayers are randomly distributed in the matrix.

The overall morphology in clay nanocomposites is still more complex, as changes in the structure and morphology of the matrix can also occur due to the presence of the filler. Consequently, the characterisation of structures, for both the polymer matrix and the layer structure dispersion on nano- and microscales, is essential to establish relationships among preparation, structure, morphology processing and properties.

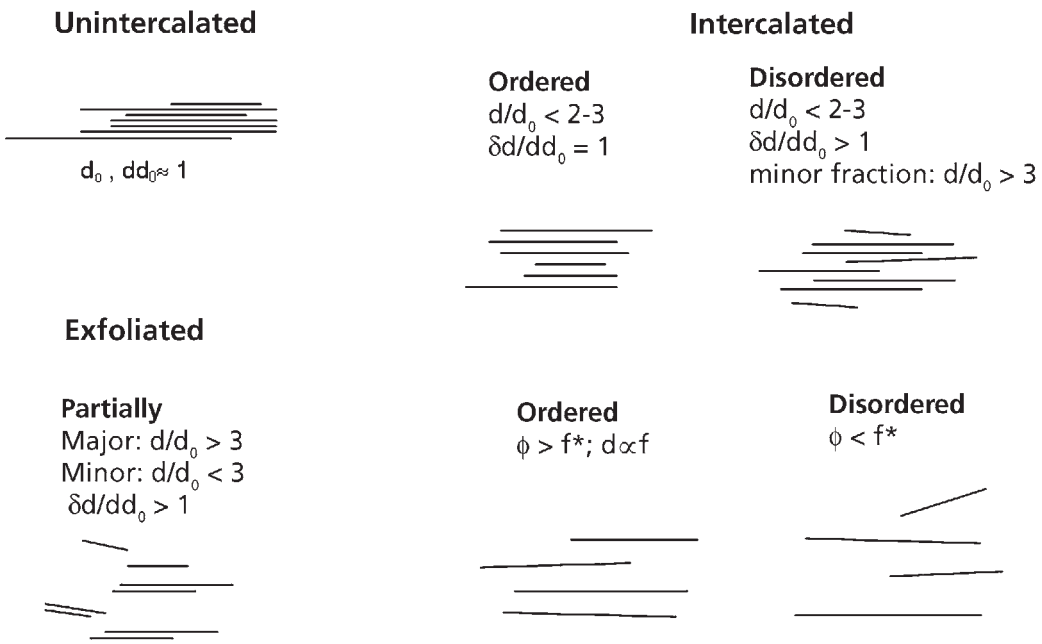

Figure 4.2 Classification scheme for unintercalated, intercalated and exfoliated structures.

Reproduced with permission from [18]. ©ACS, USA, 1995

4.3 Epoxy Nanocomposites with Clay, Carbon and Diamond

Wide-angle X-ray diffraction (WAXD) and transmission electron microscopy (TEM) are the most common techniques used in order to establish the morphology of polymer layered composite structure. Through WAXD it is possible to monitor the position, shape and intensity of the basal reflections from the silicate layers and therefore to identify the nanocomposite structures. In the exfoliated nanocomposites, the extensive layer separation results in the disappearance of any diffraction peak from the layers. Conversely, for intercalated nanocomposites, the increase of the distance between layers provides a peak at lower angles. TEM analysis is complementary to WAXD and can give insights into the spatial distribution of the layers. Moreover direct images can be obtained and studied. Also atomic force microscopy (AFM) has been used to obtain more details on the morphology.

Many researchers claim to have obtained epoxy/clay nanocomposites with exfoliated structures based on X-ray and TEM results. Several examples of X-ray diffraction (XRD) patterns of epoxy/clay nanocomposites formed from different organoclays are shown in **Figure 4.3(a)**. All these patterns are characterised by the absence of the 00*l* diffraction peaks, providing strong evidence that the clay nanolayers have been exfoliated in the thermosetting curing process. The exfoliated state is confirmed by TEM analysis shown in **Figure 4.3(b)**.

Recently solid-state nuclear magnetic resonance (NMR) [19] has been used as a tool for gaining information about the structure and surface chemistry. To describe the structure of nanocomposites, some authors have also used Fourier transform infrared (FTIR) and Raman spectroscopy [20].

In this chapter the following systems will be described:

1. Epoxy/clay nanocomposites (ECN);

2. Epoxy/clay/carbon nanocomposites (ECCN) and epoxy/clay/diamond nanocomposites (ECDN);

3. iPP/ECN blends (iPP/hybrid clay), iPP/ECCN blends (iPP/hybrid carbon) and iPP/ECDN blends (iPP/hybrid diamond).

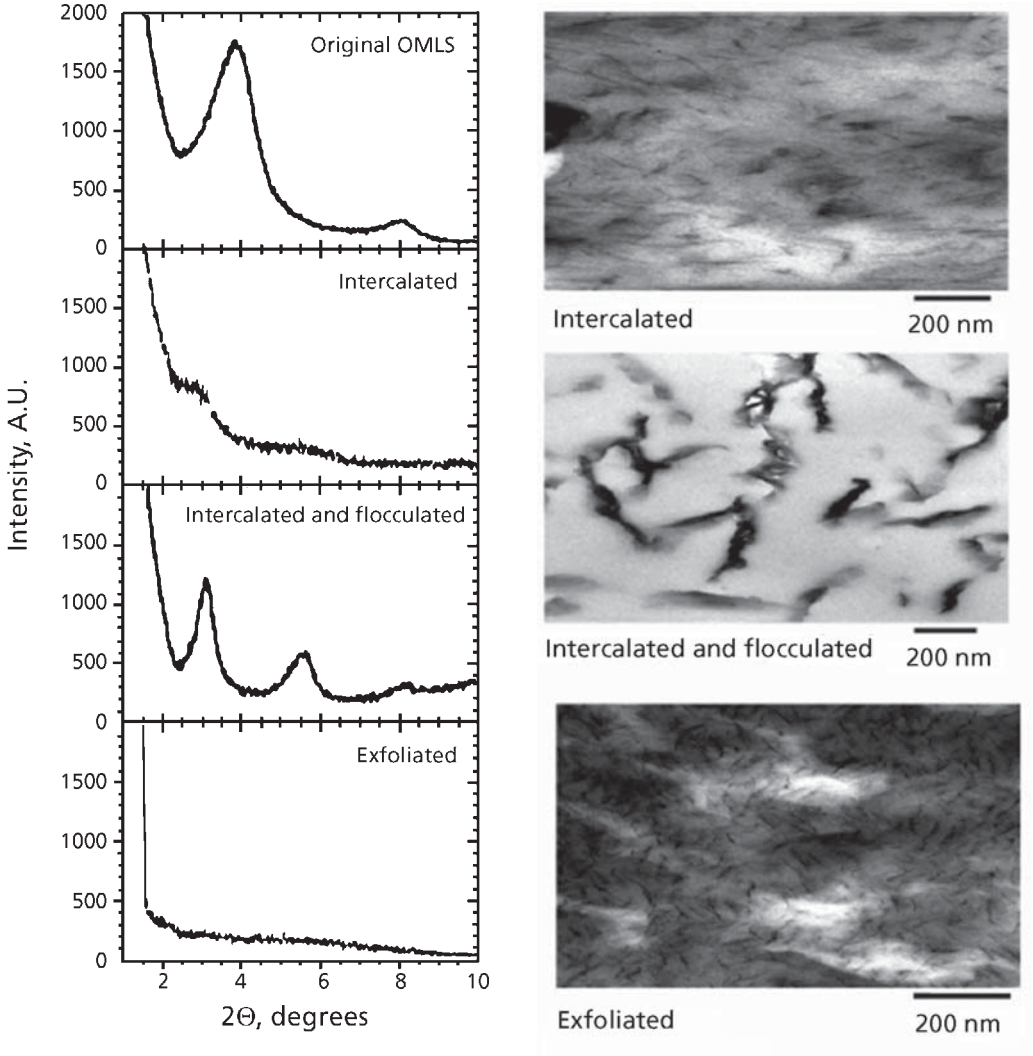

Figure 4.3 (a) WAXD patterns and (b) TEM images of three different types of nanocomposites.

Reproduced with permission from [9]. ©Elsevier, The Netherlands, 2003

4.4 Materials

The clay samples under study were lyophilised smectite (COOP Chemical), obtained from hydrophilic smectite intercalated with Na^+ ions by substituting them with three types of quaternised ammonium (QA) salts, denoted here as SAN, STN and SPN. The type of QA used and the characteristics of the smectites are reported earlier in **Table 2.4**.

A low-viscosity (15 Pa at 25 °C) epoxy resin (Araldite LY556, CIBA) was used as the basic matrix for the smectite suspensions, and diethylenetriamine was added as a curing agent for synthesising solid composites. Toluene was chosen as a very good solvent for the organically modified smectites in the study. The carbon nanofiller with a specific surface area S = 590 m^2/g and diameter d = 3 nm as well as diamond with S = 230 m^2/g and d = 10 nm were supplied by the Bulgarian Academy of Sciences. Diamond and carbon nanoparticles were obtained by decomposition of appropriate explosives as a result of a detonation process (shock-wave technology) [10].

The polypropylene used in this work is a commercial product, Moplen S30S (kindly provided by Basell, Ferrara, Italy), suitable to be extruded in the form of fibres with a melt flow index of 1.8 g/10 min.

4.5 Procedures and Techniques

4.5.1 Structural and Morphological Analysis

Wide-angle X-ray diffraction was carried out using a Philips diffractometer (PW 1050) operating with Cu Kα radiation. Measurements of diffracted intensity were made in the angular range of 3–45° (2Θ), at room temperature.

Optical analysis and measurements were made with an Axioskop polarising microscope (Zeiss, Thornwood, NY) equipped with a THMS 600 hot stage (Linkam Scientific Instruments Ltd, UK) and a TMS91 temperature control unit (Linkam). Samples for optical microscopy were prepared by squeezing a small quantity of the material onto a glass cover slip.

Scanning electron microscopy (SEM) analysis was performed with a Philips 501 SEM (Philips, The Netherlands) after vacuum metallisation of the samples by means of a Polaron sputtering apparatus with Au–Pd alloy. Samples for SEM analyses were prepared by fracturing the compression moulded samples in liquid nitrogen.

Atomic force microscopy (AFM) analysis is used to study the morphology of the film surfaces. The AFM micrographs were obtained by operating in non-contact mode. The surface analyses were performed by using an AFM TMX 2100 Explorer microscope.

4.5.2 Thermal Analysis

The thermal stability of samples was measured using a TC10 Mettler instrument, equipped with an M3 analytical thermobalance (Mettler-Toledo Inc., Columbus, OH). Each sample was heated from 313 to 473 K at a scan rate of 0.083 K/s in air. Analysis of calorimetric properties and non-isothermal overall crystallisation were obtained by differential scanning calorimetry (DSC) using a Mettler TA-3000.

4.5.3 Analysis of Flammability Properties

Preliminary tests for studying the flammability properties were performed on compression-moulded specimens (27 × 4 × 1 mm) of iPP/hybrid nanocomposite systems. These tests do not follow the standard tests for flammability of plastic materials for parts in devices and appliances (UL94), but are intended to serve as a preliminary indication of the flammability of the samples.

The samples were suspended horizontally and set on fire for 5 s. All the samples started soon to burn. The time from ignition to the flaming drip phenomenon was measured as a function of the hybrid nanocomposite used.

4.6 Epoxy/Clay Nanocomposites (ECN)

4.6.1 Preparation

The synthesis methods include two processing techniques for epoxy–smectite dispersions, denoted as *direct processing* and *solvent processing*. In direct processing, an appropriate amount of smectites was added directly to the resin. In solvent processing, the smectite was added to toluene and the resulting dispersion was mixed with the epoxy resin. For the preparation of clay/epoxy nanocomposites, diethylenetriamine was added to the smectite–epoxy suspension as a hardener. Preparation details are reported in [21, 22].

4.6.2 Results

The effect of various factors, such as the organic modifier, volume fraction of smectite clay and processing conditions, on the morphology is investigated by infrared (IR) spectroscopy, WAXD, TEM and SEM analyses. The IR spectroscopy results of post-cured systems of epoxy resin and 2.5 vol% SAN, STN and SPN nanocomposites prepared by direct processing and solvent processing techniques are reported in Chapter 3. These results indicate that the epoxy groups have completely reacted and that direct attachment of the epoxy matrix to the silicate layers exists, maximising the interfacial adhesion between the two phases.

Figure 4.4 compares the TEM micrographs of a typical 5% SAN nanocomposite obtained with the two different methods. The micrographs indicate that the direct processing technique produces intercalated structures whereas the solvent processing technique presumably leads to an exfoliated structure. The nanocomposite prepared by direct processing is characterised by thick stack-like smectite aggregates that are mostly oriented in one direction, which appear in the micrographs as dark lines 100–150 nm long and thickness varying from a few nanometres to 100 nm, whereas the nanocomposite prepared by solvent processing results in the formation of thinner stacks of fibrils.

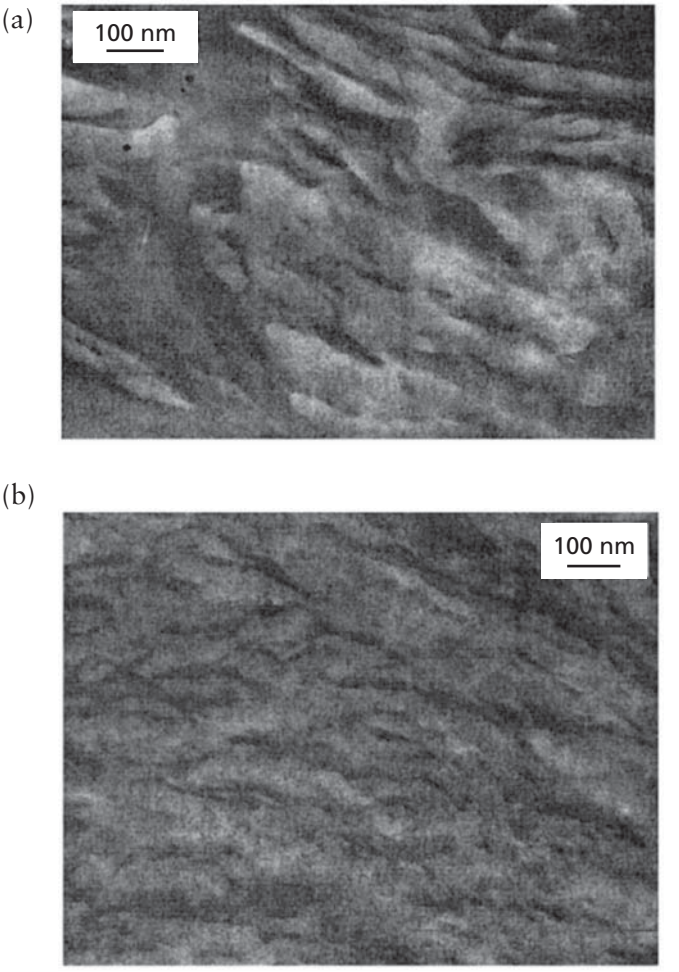

Figure 4.4 (a) TEM micrographs of 5% SAN nanocomposites prepared by (a) direct processing and (b) solvent processing.

Reproduced with permission from [22]. ©Wiley Periodicals, 2005

It was proposed by Kotsilkova [22] that the large-scale heterogeneity of the structure produced by direct processing is replaced by small-scale heterogeneity in the solvent-processed nanocomposites.

The WAXD patterns of the post-cured systems of these samples (shown in **Figures 3.2(c)** and **3.3** of Chapter 3) indicate that the structure of the pure epoxy resin does not change when it is prepared by direct or solvent processing techniques. However, the XRD spectra of SAN, STN and SPN nanocomposites prepared by solvent processing show the absence of the basal reflection, which differs from the spectra for direct processing, where it can be deduced that both SAN and STN nanocomposites form intercalated structures whereas the SPN nanocomposite is presumably exfoliated.

Kotsilkova [22] stated that in exfoliated-type nanocomposites obtained by the solvent processing technique the role of the organic modifier is insufficient for structure formation. In contrast, when the direct processing technique is used, the type of organic modifier controls the structure of nanocomposites during curing, resulting in either intercalated or exfoliated structures.

AFM and SEM micrographs of the surfaces of epoxy resin and epoxy/clay nanocomposites are reported in **Figures 4.5**, **4.6** and **4.7**.

The epoxy resins show a surface characteristic of a brittle glass material (**Figure 4.5**). The morphology is completely different if clay is added to the resin. Moreover, the morphology is also dependent on the kind of clay used.

For the STN nanocomposites (**Figure 4.6(a)**) two different regions can be observed, presenting different morphology. The darker regions (**Figure 4.6(b)**) are characterised by a relatively smoother surface, with the presence of round domains with a broad distribution of dimensions. For the lighter regions (**Figure 4.6(c)**) the surface is very rough.

SAN and SPN nanocomposites (**Figure 4.7**) do not present different morphological regions. The fracture surface of the SPN nanocomposite samples is homogeneous with few domains dispersed in the matrix and very well connected to it.

4.7 Hybrid Epoxy/Clay/Carbon or Diamond Nanosystems

4.7.1 Preparation

Two hybrid systems were prepared:

1. Epoxy hybrid containing a mixture of 48 wt% smectite clay (SAN) and 2 wt% nanoparticles of diamond (this system will be called hybrid diamond);

(a)

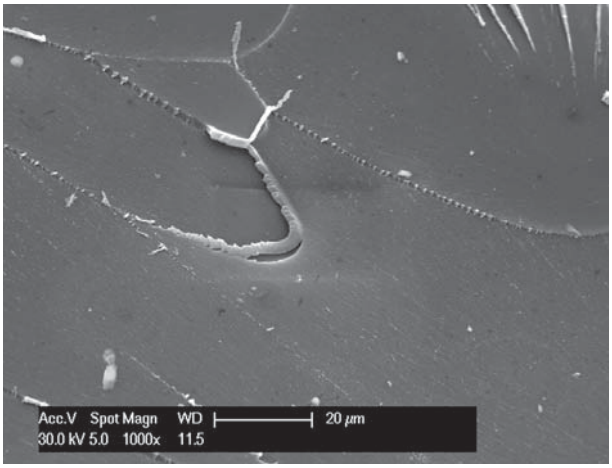

(b)

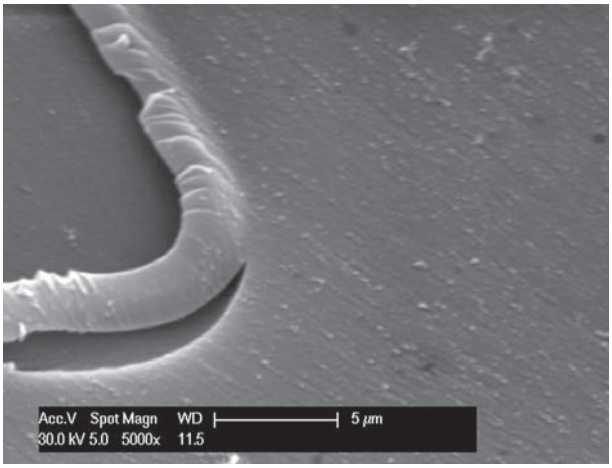

Figure 4.5 SEM micrographs of the fractured surfaces of epoxy resin obtained by solvent techniques

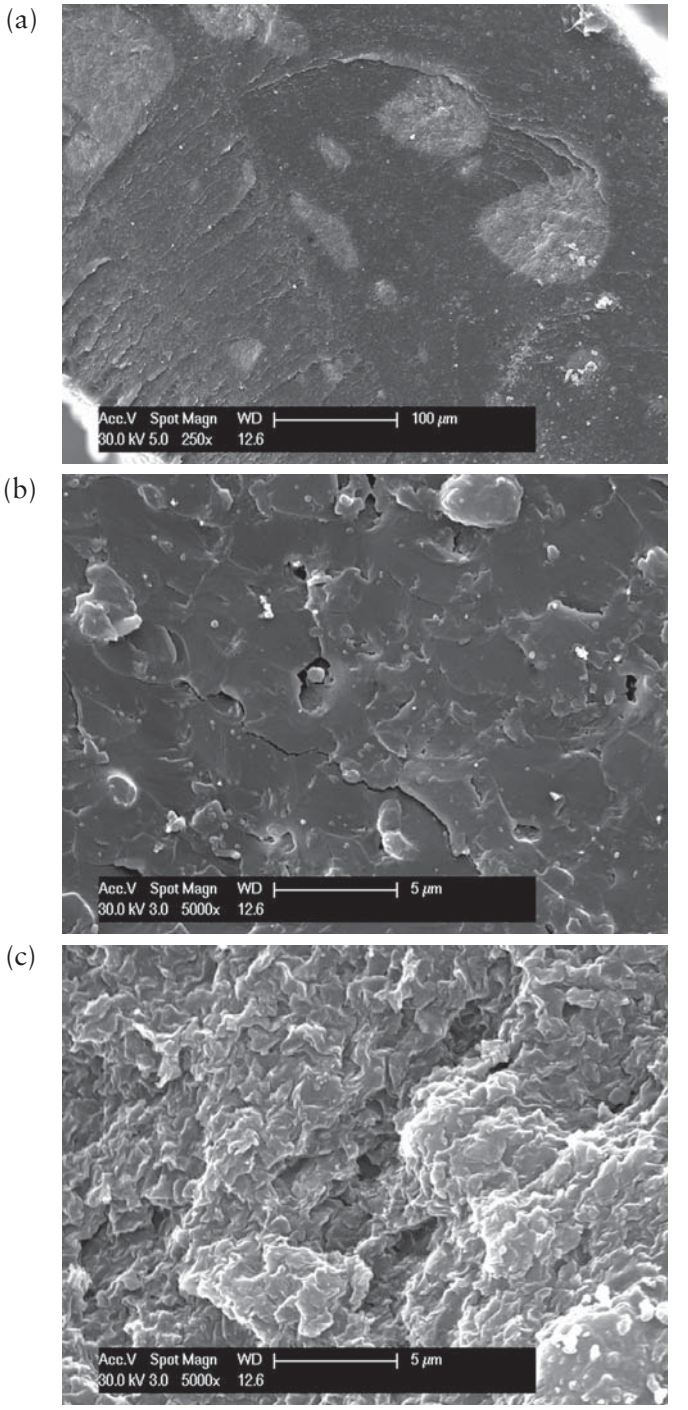

Figure 4.6 SEM micrographs of fractured surfaces of STN, for samples obtained by direct techniques

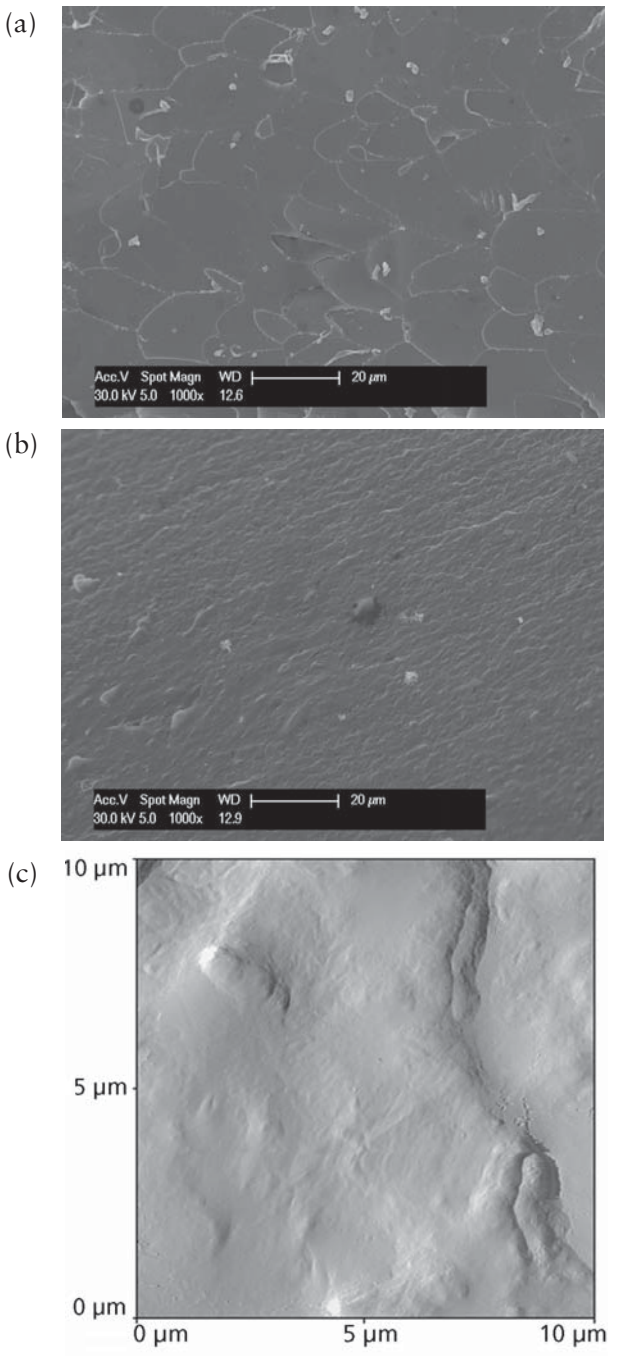

Figure 4.7 SEM and AFM micrographs of surfaces for SAN and SPN samples obtained by solvent techniques: (a) SEM micrograph of fractured surface of SAN; (b) SEM micrograph of fractured surface of SPN; and (c) AFM micrograph of surface of compression-moulded SAN sample

2. Epoxy hybrid containing a mixture of 48 wt% smectite clay (SAN) and 2 wt% nanoparticles of carbon (this system will be called hybrid carbon).

The liquid nanocomposite systems containing smectite clay were prepared by intercalation of epoxy matrix (bisphenol A epoxy resin) within the clay galleries. Details of the preparation are reported in [21, 23, 24].

4.7.2 Results

The WAXD patterns of the carbon hybrid and diamond hybrid systems are reported in **Figure 4.8**, where the pattern of epoxy/clay is also reported for comparison. For the hybrid system a basal reflection at $2\Theta = 5°$ appears together with a reflection at 8°. The basal reflection at lower angle indicates an intercalating phenomenon; probably part of the clay layers seem to be expanded.

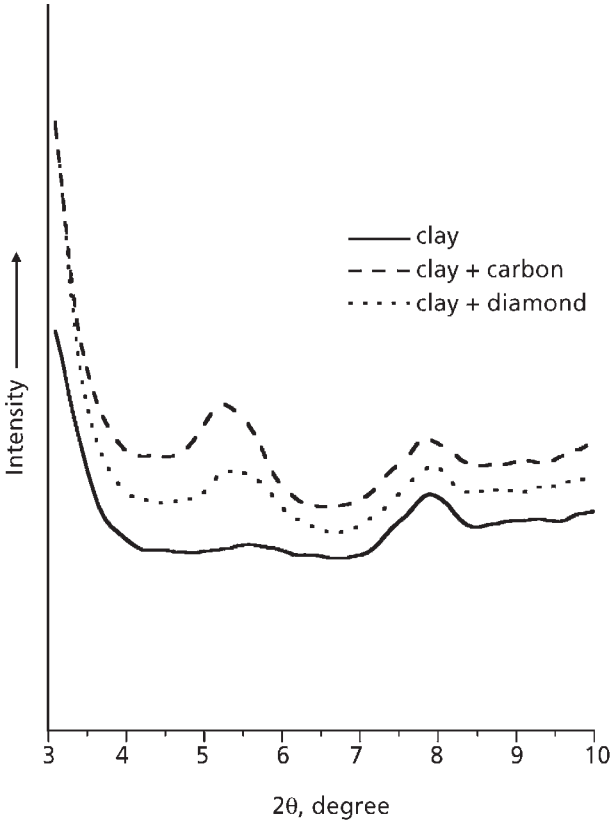

Figure 4.8 X-ray profiles for carbon hybrid and diamond hybrid systems

Fractured surfaces of carbon hybrid and diamond hybrid systems were analysed by SEM (**Figure 4.9** and **4.10**). The surfaces of the two samples are different. For the carbon hybrid, the surfaces are very similar to that of the epoxy SAN sample. Also in this case an almost homogeneous surface can be observed with the presence of small domains and few holes due probably to air bubble. For the diamond hybrid, on the contrary, the fractured surface is characterised by domains segregated in the matrix. The adhesion of these domains to the matrix is not strong.

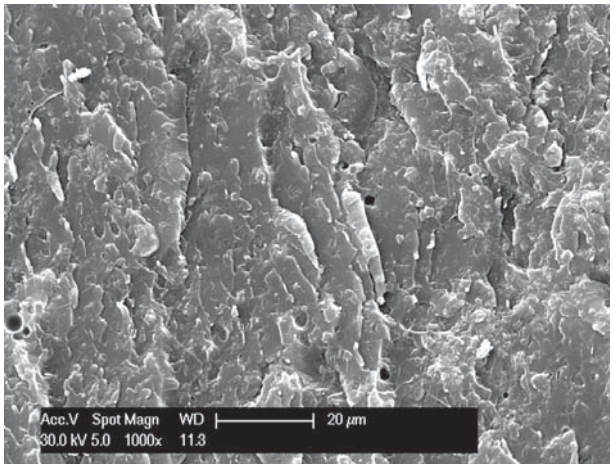

Figure 4.9 SEM micrograph of fractured surface of carbon hybrid

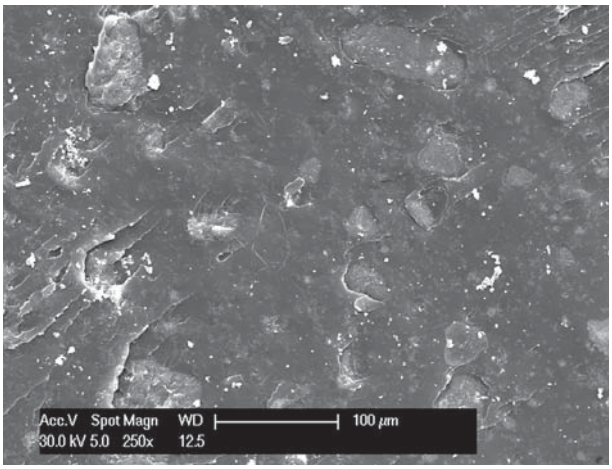

Figure 4.10 SEM micrograph of fractured surface of diamond hybrid

4.8 Nanocomposite Blends Based on iPP

4.8.1 Preparation

In order to improve the compatibility of iPP with clay and diamond or carbon nanoparticles, hybrid systems were first prepared by nano-level dispersing of filler in an epoxy resin matrix, and then introduced as a swelling agent into iPP.

The blends of iPP containing 5 wt% of epoxy nanocomposite systems were prepared by melt mixing in a Brabender-like apparatus at 483 K and 32 rpm for 600 s. Thus, the final polypropylene composite blends contain about 2.5 wt% smectite clay and 0.1 wt% diamond or carbon, respectively.

The materials were compression moulded in a press at 473 K for 300 s to allow complete melting without pressure. Then a pressure of 5 MPa was applied for 300 s. The samples were cooled to room temperature with a water cooling serpentine system present inside the plates of the press. Finally the pressure was released and the mould containing the 0.12 × 6 × 12 cm sheet was removed from the press. Dumbbell-shaped specimens for tensile tests were cut from the sheets and used for mechanical tensile measurements according to ASTM D256 [25] standard.

4.8.2 Structure and Morphology

Isotactic polypropylene (iPP) is a material with several crystal modifications [26–29]. The different polymorphs are distinct for the different chain packing geometries of the helices. The appearance of these structures is critically dependent upon the crystallisation conditions and pressure.

The WAXD profiles of all the samples obtained by compression moulding are reported in **Figure 4.11** [30]. The pure iPP and the iPP/hybrid clay system present the characteristic profile of the α form. For the iPP/carbon hybrid and iPP/diamond hybrid systems, a mixture of α and β crystals of polypropylene is generated. In fact the characteristic peaks of the two forms (between 18° and 19°, corresponding to the (130) plane of the α phase; and between 15.5° and 16.5°, corresponding to the (200) plane of the β phase) are present. An approximate β/α ratio could be calculated as the ratio between the heights of the two peaks: this approximate procedure gives a value of 35% and 45% β phase for the iPP/diamond hybrid and the iPP/carbon hybrid sample, respectively.

This result indicates that nanoparticles of diamond and carbon favour nucleation of the β form of iPP crystal, acting as nucleating agents, whereas clay nanolayers do not have any influence on the crystal structure of iPP. Moreover, it seems that the β

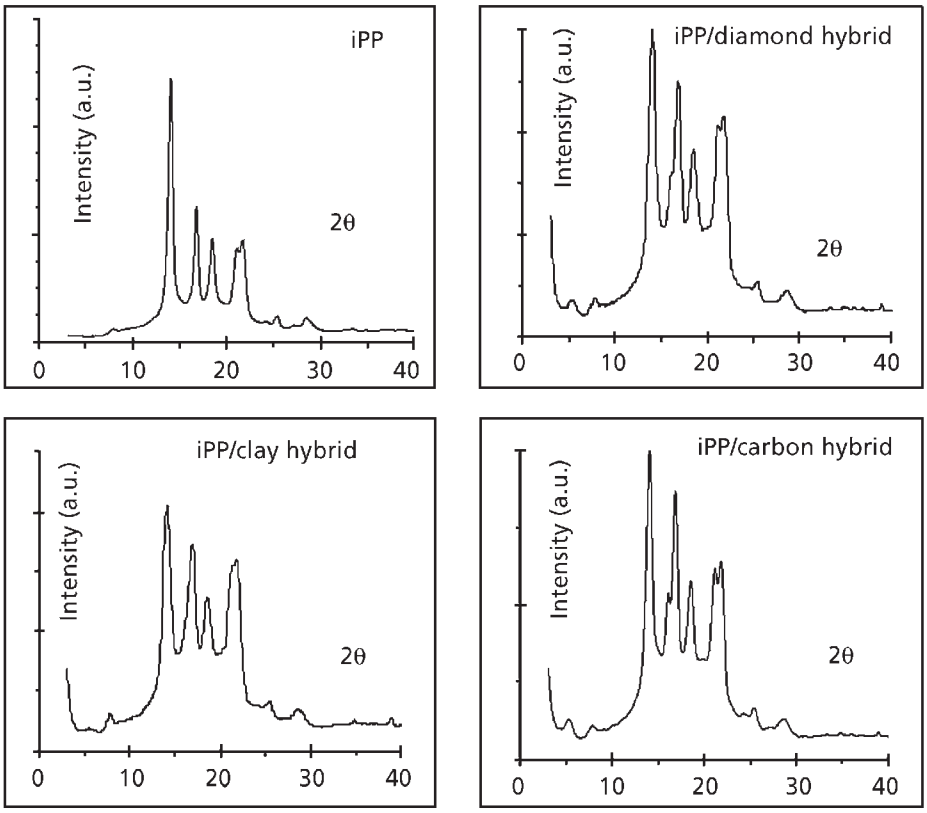

Figure 4.11 X-ray profiles for iPP and iPP/nanoparticle systems. The intensity is in arbitrary units (au).

Reproduced with permission from [30]. ©Wiley-VCH, Germany, 2005

nucleation effect is more marked when carbon nanoparticles are present. The WAXD patterns also offer a way to determine the interlayer spacing of the silicate layers in the nanocomposites. The appearance of the basal reflection at $2\Theta = 5°$ could indicate the expansion of the clay layers associated with intercalation, as already reported. Surfaces of compression-moulded samples were analysed by SEM and AFM (**Figure 4.12**). The micrographs of iPP and iPP/hybrid clay show homogeneous surfaces. The surfaces of iPP/diamond hybrid and iPP/carbon hybrid present instead small homogeneously distributed domains. For both samples the distribution of the domain size is very narrow. The sizes of the domains depend on the type of nanoparticles. For the iPP/diamond hybrid samples the dimension of the domains is about 50 nm, whereas it is about 100 nm for the iPP/carbon hybrid sample. The morphology during isothermal and non-isothermal crystallisation from the melt at the selected cooling rate is always spherulitic.

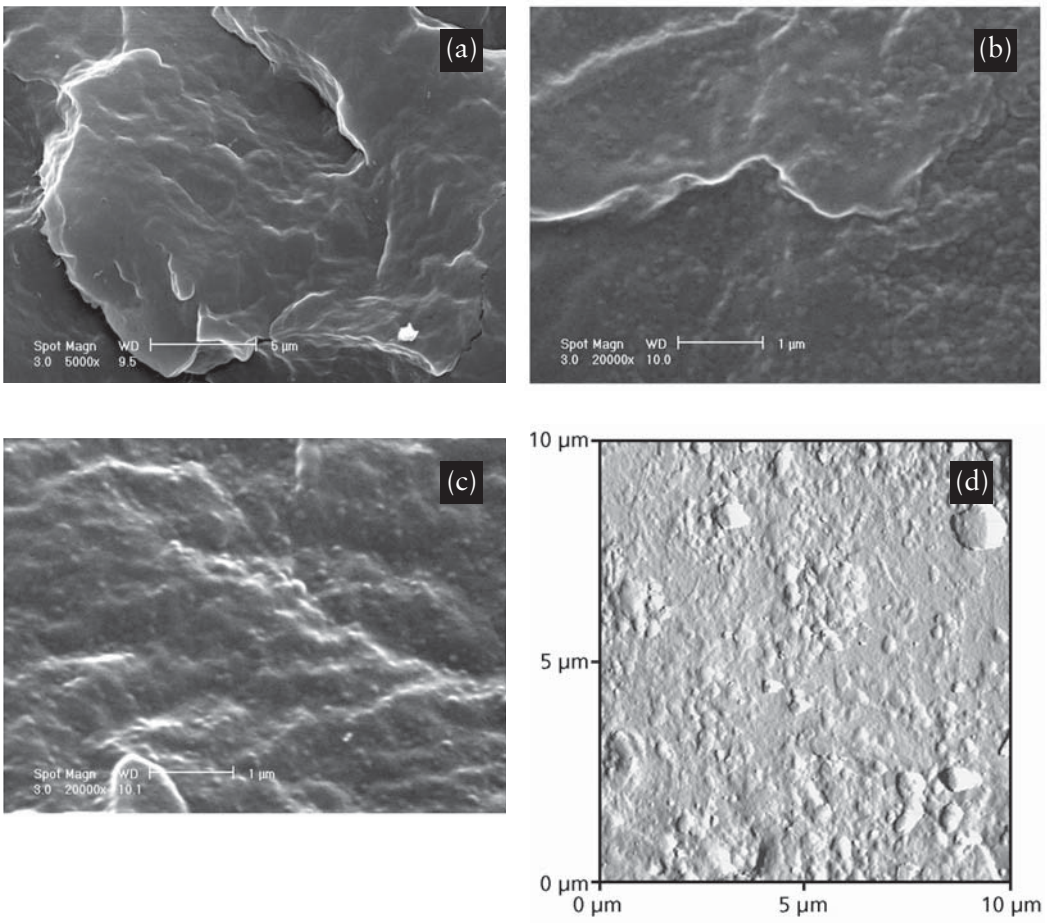

Figure 4.12 SEM and AFM micrographs of the surfaces of hybrid samples obtained by compression moulding: (a) SEM micrograph of iPP/clay hybrid; (b) SEM micrograph of iPP/diamond hybrid; (c) SEM micrograph of iPP/carbon hybrid; and (d) AFM micrograph of iPP/carbon hybrid.

Parts (a)–(c) reproduced with permission from [30]. ©Wiley-VCH, Germany, 2005

For pure iPP and the iPP/clay hybrid, the spherulites present generally weak birefringence. A few negative highly birefringent spherulites (β-spherulites) are very sporadically detected. For the iPP/diamond hybrid and iPP/carbon hybrid systems, β-spherulites are frequently detected, in agreement with the X-ray results. At the end of the crystallisation process, for all the nanocomposite systems under investigation, larger spherulites than those observed for pure iPP are obtained, for a given crystallisation procedure, as shown in **Figure 4.13**.

(a)

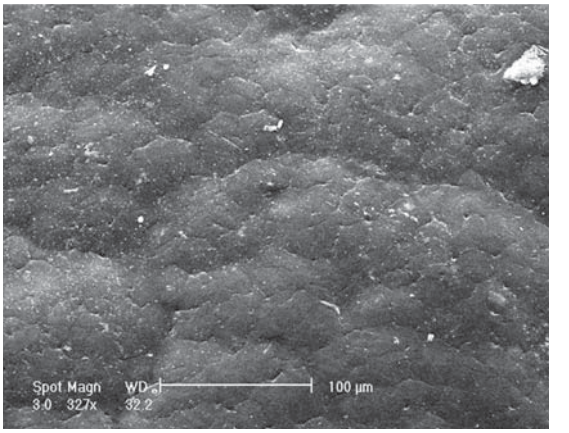

(b)

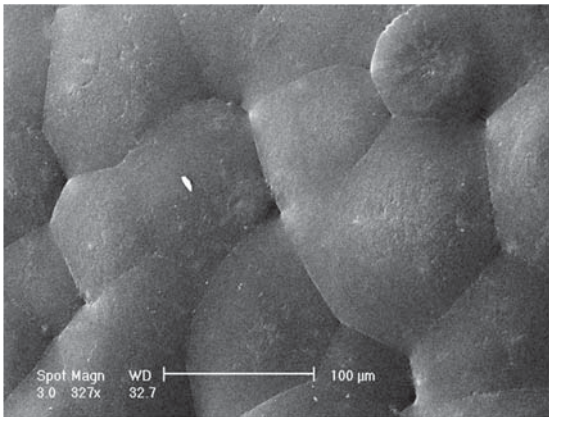

(c)

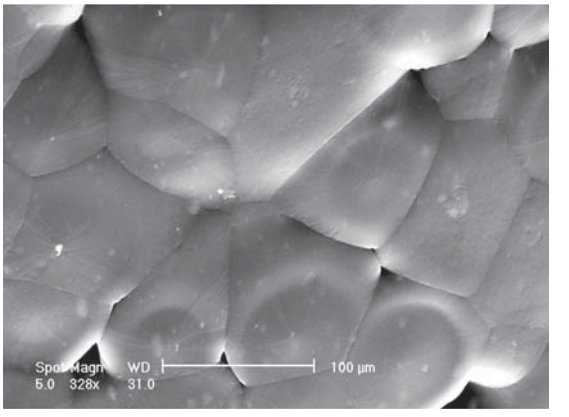

Figure 4.13 SEM micrographs of samples crystallised by cooling from the melt: (a) iPP; (b) iPP/clay hybrid; and (c) iPP/diamond hybrid.

Reproduced with permission from [30]. ©Wiley-VCH, Germany, 2005

4.8.3 Thermal Analysis

The thermal stability of iPP/diamond hybrid and iPP/carbon hybrid in air is improved with respect to the stability of neat polypropylene, whereas no influence on thermal stability is detected when only clay is added to iPP (see **Figure 4.14**).

Indeed, the iPP/diamond hybrid and iPP/carbon hybrid nanocomposites start to lose weight at almost the same temperature as iPP, but the subsequent loss of weight is slowed down and occurs at temperatures tens of degrees higher than that of polypropylene. In **Table 4.1** the temperature corresponding to the inflection point of the curves is reported. As the thermogravimetric analysis shows that the decomposition temperature of iPP/clay

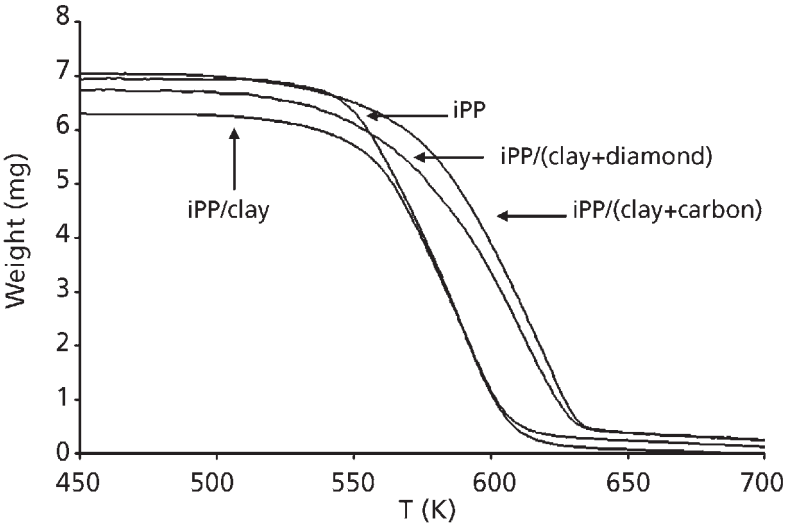

Figure 4.14 Weight as a function of temperature for nanocomposites.
Reproduced with permission from [30]. ©Wiley-VCH, Germany, 2005

Table 4.1 Inflection points of thermogravimetric curves of samples	
Sample	**Inflection temperature (K)**
iPP	589
iPP/hybrid clay	592
iPP/hybrid diamond	611
iPP/hybrid carbon	618
Reproduced with permission from [30]. ©Wiley-VCH, Germany, 2005	

is slightly affected by the presence of the clay, the higher stability of iPP/diamond hybrid and iPP/carbon hybrid has to be due to the presence of nanoparticles of diamond and carbon, respectively.

This increased thermal stability could be attributed to a slower diffusion of volatile decomposition products within the nanocomposites containing diamond and carbon, suggesting also the hypothesis that these systems could present higher barrier properties, as observed for other polymer nanocomposites [9, 23, 31].

4.8.4 Analysis of Flammability and Tensile Properties

In **Table 4.2** is reported the time between the start of ignition and the flaming drips phenomenon. The system that shows the best resistance to fire is the carbon hybrid. The resistance could also be improved by changing the amount of the nanocomposite.

Table 4.2 Time required by the sample to start the flaming drip phenomenon from ignition

Sample	Time (s)
iPP	6
iPP/hybrid clay	10
iPP/hybrid diamond	10
iPP/hybrid carbon	15

Nominal stress–strain curves of the samples of iPP/nanoparticle blends tested at room temperature are presented in **Figure 4.15**. The neat iPP exhibits a yield point followed by necking, full cold drawing and fibre rupture, the classic behaviour of semicrystalline polymers at room temperature. The behaviours of the blends are dependent on the kind of nanocomposite system added.

The iPP/carbon hybrid blend shows ductile behaviour, yielding and cold drawing phenomena, and the formation of a fibre. The other systems show brittle behaviour with failure before necking. These results can be related with the very high percentage of β phase present in the iPP/carbon hybrid samples. It was in fact reported that in iPP the presence of β form within the crystalline portion is beneficial to the toughness and ductility of the polymer [32, 33].

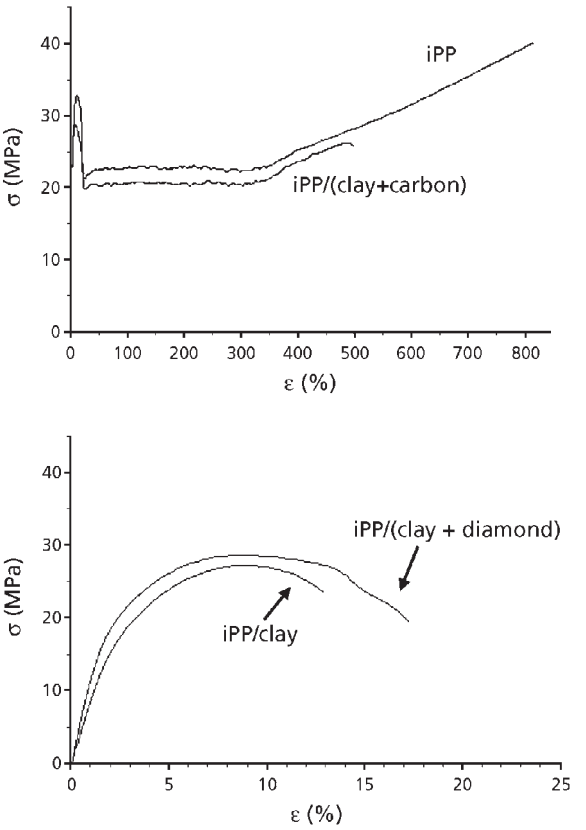

Figure 4.15 Stress–strain curves for various samples.
Reproduced with permission from [30]. ©Wiley-VCH, Germany, 2005

4.9 Conclusion

This chapter has provided a brief overview of the current state of the art for the morphology and structure of epoxy/clay nanocomposites. It was underlined that the overall morphology in nanocomposites is very complex. The classification usually given, which only accounts for the degree of intercalation and exfoliation, is too simplified, as changes in the structure and morphology of the matrix can also occur due to the presence of the filler. Consequently, characterisation of the structures of both the polymer matrix and the layer structure dispersion at nano- and microscales is essential to establish relationships among preparation, structure, morphology, processing and properties.

This chapter has also covered recent progress in the area of polymer/clay nanocomposites. In particular, an innovative use of the epoxy/clay nanocomposites was illustrated: the

epoxy/clay nanocomposites were further filled with carbon or diamond particles to form hybrid nanocomposites and finally mixed with isotactic polypropylene.

The results have shown that the addition of two combined fillers, smectite clay plus diamond and smectite clay plus carbon nanoparticles, to iPP causes drastic modifications in the structure, morphology, tensile and thermal properties of iPP. In particular, it was found that diamond and carbon hybrids favour the nucleation of β form of iPP crystal, whereas clay nanolayers do not have any influence on the crystal structure of iPP.

Acknowledgements

This work is supported by a project under the program for scientific cooperation between CNR (Italy) and BAS (Bulgaria).

References

1. J. Liu, W.J. Boo, A. Clearfield and H-J. Sue, *Materials and Manufacturing Processes*, 2006, **21**, 2, 143.

2. N. Herron and D.L. Thorn, *Advanced Materials*, 1998, **10**, 15, 1173.

3. J.E. Mark, *Polymer Engineering and Science*, 1996, **36**, 24, 2905.

4. E. Reynaud, C. Gauthier and J. Perez, *Revue de Métallurgie/Cahier d'Information Technique,* 1999, **96**, 2, 169.

5. T. Van Werne and T.E. Patten, *Journal of the American Chemical Society*, 1999, **121**, 32, 7409.

6. E. Giannelis, *Advanced Materials*, 1996, **8**, 1, 29.

7. R. Krishnamoorti and E. Giannelis, *Macromolecules*, 1997, **30**, 14, 4097.

8. *Polymer–Clay Nanocomposites*, Eds., T.J. Pinnavaia and G.W. Beall, John Wiley & Sons, Chichester, UK, 2000.

9. S. Sinha Ray and M. Okamoto, *Progress in Polymer Science*, 2003, **28**, 11, 1539.

10. S.Y. Stavrev, S.B. Lazarov, K.L. Stoev, L.G. Markov and V.I. Ivanov, inventors; no assignee; US 5353708, 1994.

11. *Macplast*, 1998, **5**, 7, 75.

12. *Polypropylene to 2004 – Market Size, Market Share, Demand Forecast and Sales*, Freedonia Group, Cleveland, OH, USA, 2000.

13. R.A. Vaia and E.P. Giannelis, *Macromolecules*, 1997, **30**, 25, 7990.

14. R.A. Vaia and E.P. Giannelis, *Macromolecules*, 1997, **30**, 25, 8000.

15. A.C. Balazs, C. Singh and E. Zhulina, *Macromolecules*, 1998, **31**, 23, 8370.

16. X. Kornmann, H. Lingberg and L. Berglund, *Polymer*, 2001, **42**, 4, 1303.

17. S. Sinha Ray, K. Okamoto and M. Okamoto, *Macromolecules*, 2003, **36**, 7, 2355.

18. R. Vaia, K. Jandt, E. Kramer and E. Giannelis, *Macromolecules*, 1995, **28**, 24, 8080.

19. D.L. VanderHart, A. Asano and J.W. Gilman, *Macromolecules*, 2001, **34**, 12, 3819.

20. L.S. Loo and K.K. Gleason, *Macromolecules*, 2003, **36**, 8, 2587.

21. R. Kotsilkova, *Mechanics of Time Dependent Materials*, Volume 6, Kluwer Academic, Dordrecht, The Netherlands, 2002, p.283.

22. R. Kotsilkova, *Journal of Applied Polymer Science*, 2005, **97**, 6, 2499.

23. R. Kotsilkova, V. Petkova and J. Pelovski, *Journal of Thermal Analysis and Calorimetry*, 2001, **64**, 591.

24. A. Kanapitsas, P. Pissis and R. Kotsilkova, *Journal of Non-Crystalline Solids*, 2002, **305**, 1-3, 204.

25. ASTM D256-06a, *Standard Test Methods for Determining the Izod Pendulum Impact Resistance of Plastics*, 2006.

26. S. Bruckner, S.V. Meille, V. Petraccone and B. Pirozzi, *Progress in Polymer Science*, 1991, **16**, 2, 361.

27. J. Varga, *Polypropylene Structure: Blends and Composites*, *Volume 1: Structure and Morphology*, Ed., J. Karger-Kocsis, Chapman and Hall, London, UK, 1995.

28. C. Silvestre, S. Cimmino and E. Di Pace, *Handbook of Polyolefins*, 2nd Edition, Revised and expanded, Ed., C. Vasile, Marcel Dekker, New York, NY, USA, 2000, Chapter 7, p.175–205.

29. A. Phillips and M.D. Wolkowicz in *Polypropylene Handbook*, Ed., E.P. Moore, Jr., Hanser, Munich, Germany, 1996.

30. C. Silvestre, S. Cimmino, M. Raimo, C. Carfagna, V. Capuano and R. Kotsilkova, *Macromolecular Symposia*, 2005, **228**, 99.

31. S.J. Ahmadi, Y.D. Huang and W. Li, *Journal of Materials Science*, 2004, **39**, 6, 1919.

32. J. Karger-Kocsis, J. Varga and G.W. Ehrenstein, *Journal of Applied Polymer Science*, 1997, **64**, 11, 2057.

33. J. Kotex, M. Raab, J. Baldrian and W. Grellmann, *Journal of Applied Polymer Science*, 2002, **85**, 6, 1174.

5 Molecular Dynamics of Thermoset Nanocomposites

P. Pissis

5.1 Introduction

Polymer nanocomposites, i.e., composite materials with a polymeric matrix and (typically) inorganic fillers with characteristic size in the range 1–100 nm, have attracted much interest in recent years [1–3]. The main reason for this is the significant improvement of their properties, in particular mechanical properties, thermal stability and barrier properties, even at very low filler contents, much lower than those required to achieve the same level of improvement with conventional macroscale or microscale composites [1].

There is as yet no satisfactory theoretical explanation for the origin of the improvement of the properties of polymer nanocomposites. It is generally accepted, however, that the large surface-to-volume ratio of the nanoscale inclusions plays a significant role. Results obtained by various techniques indicate the presence of an interfacial polymer layer around the filler, with structure/morphology and chain dynamics modified with respect to those of the bulk polymer matrix [4–8]. The existence of such an interfacial layer was postulated for conventional composites long ago, and various experiments provided support for that view [9–11]. Questions related to the existence of such an interfacial layer, its thickness and the variation of polymer properties within the layer with respect to the bulk properties become crucial for nanocomposites. The reason for this is that, due to the small particle size, resulting in a large surface area presented to the polymer by the nanoparticles, the interfacial layer can represent a significant volume fraction of the polymer in nanocomposites.

The investigation of structure–property relationships, i.e., of the relationships between composition, processing, structure/morphology, molecular dynamics and final properties, is a fundamental issue in materials science. The profound understanding of these relationships provides a basis for the optimisation of composition and synthesis and/or processing conditions for designing new materials with predictable properties tailored to specific applications. This is particularly true for polymer nanocomposites for at least two reasons. The first, common to multicomponent systems, is related to the large number of combinations of two or more components in the nanocomposite. The second, specific to nanocomposites, refers to the pronounced dependence of properties, for the

same composition, on morphology, which, in its turn, can be modified and tailored over wide ranges by the synthesis and processing conditions [1–3].

Molecular dynamic studies form an essential part of the investigation of structure–property relationships in polymer nanocomposites. In addition to that application, molecular dynamics studies in polymer nanocomposites have attracted much interest from the point of view of basic research, as they may provide answers to fundamental questions, such as the question about the modification of chain dynamics by the presence of and interactions with the nanoparticles. That modification is closely related to the morphology of the nanocomposite, in particular the distribution of nanoparticles. A central topic in the field of polymer nanocomposites is the investigation of the distribution of nanoparticles in the matrix, and a real challenge for today's research is how to control that distribution. Morphological characterisation techniques are typically employed to investigate the distribution of nanoparticles, which is, however, not an easy task [12]. In that respect it is essential that molecular dynamics studies may provide, even if indirectly, significant information on morphology, in particular the distribution of nanoparticles in polymer nanocomposites [13].

Several experimental techniques have been employed to investigate molecular dynamics in polymer nanocomposites. These include mainly differential scanning calorimetry (DSC) to follow the glass transition [14], dynamic mechanical analysis (DMA) [15], dielectric techniques [16] and nuclear magnetic resonance (NMR) [17]. Each of these techniques is characterised by special features rendering it attractive for specific applications. This is because each technique probes molecular mobility in a different way. Thus, the combination of two or more techniques is essential, as in that case several aspects of molecular dynamics can be studied [18]. The polymer nanocomposites investigated include systems based on thermoplastic, thermosetting and rubber matrices, with a variety of inclusions, such as silica, clays and carbon nanotubes (CNTs). The results are often discussed in terms of two contradictory effects of nanoparticles on chain dynamics: (i) immobilisation and/or reduction of mobility of a fraction of the chains at the interfaces, due to chemical or physical bonds with the particles; and (ii) loosened molecular packing of the chains, due to tethering and geometrical confinement, resulting in an increase of free volume [19]. Computer simulations have attracted much interest in recent years as a promising tool for investigating chain dynamics in polymer nanocomposites [20, 21].

This chapter deals with the investigation of polymer dynamics in thermoset nanocomposites. We focus mostly on results obtained by our research team in Athens, which are, however, discussed in relation to results obtained by others. Results obtained with thermoplastic and rubber matrices are also presented for comparison and to emphasise special aspects of polymer dynamics. Dielectric techniques are the main techniques employed in our studies. They have been proved to be a powerful tool for the investigation of the molecular dynamics of polymers and composites [16, 22–25]. Dielectric techniques are often employed in the framework of the investigation of structure–property relationships in polymeric systems, which provide a basis for the

optimisation of composition and synthesis and/or processing conditions for designing new materials with predicted properties. The main advantage of dielectric techniques, as compared to other similar techniques for studying molecular dynamics, is the broad frequency range, which can be relatively easily covered (10^{-4}–10^{9} Hz in the present work). This broad frequency range allows one to measure, on the same sample, processes with very different characteristic (relaxation) times and, correspondingly, different characteristic length scales. These include the following: fast secondary (local) relaxations of the polymer matrix at high frequencies with characteristic length scales of below 1 nm; cooperative relaxations like the glass transition of the polymer matrix at intermediate frequencies, with characteristic length scales of a few nanometres (cooperativity length of the glass transition); and dc conductivity and conductivity effects (like the interfacial Maxwell–Wagner–Sillars relaxation) at lower frequencies, with characteristic length scales in the nanometre to micrometre range. As a consequence, dielectric techniques often provide significant information for structural and/or morphological characterisation of polymers and composites [26].

The organisation of this chapter is as follows. Dielectric techniques, the main techniques employed in our studies, are briefly introduced in the next section. Section 5.3 is then devoted to the overall dielectric response of thermoset nanocomposites, whereas in the following three sections we discuss in some detail the results obtained for the effects of the nanoparticles on the local, secondary relaxations in the thermoset nanocomposites (Section 5.4), the cooperative, primary (segmental) α relaxation and the glass transition (Section 5.5), and electrical conductivity and conductivity effects (Section 5.6). Final conclusions are drawn in Section 5.7.

5.2 Dielectric Techniques for Molecular Dynamics Studies

Dielectric techniques are a powerful tool for studying molecular dynamics in various materials, including polymers and composites. The main advantage of dielectric techniques over other techniques for measuring molecular dynamics is the extremely broad frequency range covered, which extends from about 10^{-5} to about 10^{11} Hz [27–29]. Obviously, this broad frequency range cannot be covered by a single technique.

5.2.1 Broadband Dielectric Spectroscopy

In most cases, measurements are carried out isothermally in the frequency domain, and the term (broadband) dielectric spectroscopy (DS) or (broadband) dielectric relaxation spectroscopy (DRS) is then used. Other names frequently used for DRS are impedance spectroscopy and admittance spectroscopy. Impedance spectroscopy (*cf.* Section 5.2.3) is usually used in connection with electrical conductivity, electrolytes and electrochemical studies, whereas admittance spectroscopy often refers to semiconductors and devices.

Isothermal measurements in the time domain are often used, either as a convenient tool for extending the range of measurements to low frequencies (slow time-domain spectroscopy, dc transient current method, isothermal charging–discharging current measurements) or for fast measurements corresponding to the frequency range of about 10 MHz–10 GHz (time-domain spectroscopy or time-domain reflectometry). Finally, thermally stimulated depolarisation currents (TSDC) is a special dielectric technique in the temperature domain, which will be discussed in Section 5.2.2.

For measurements in the frequency domain, capacitance bridges, impedance analysers, frequency response analysers, radio-frequency reflectometers and network analysers are typically employed. In **Figure 5.1** we show schematically the frequency range of dielectric measurements covered by different techniques and equipment [24]. The principle of these measurements is as follows. The sample under investigation is placed in a capacitor with empty capacitance C_0, which becomes part of an electric circuit. A sinusoidal voltage with angular frequency ω is applied to the circuit and the complex impedance $Z(\omega)$ of the sample is measured. The complex dielectric permittivity $\varepsilon(\omega) = \varepsilon'(\omega) - i\varepsilon''(\omega)$, defined by:

$$\varepsilon(\omega) = \frac{C}{C_0} \tag{5.1}$$

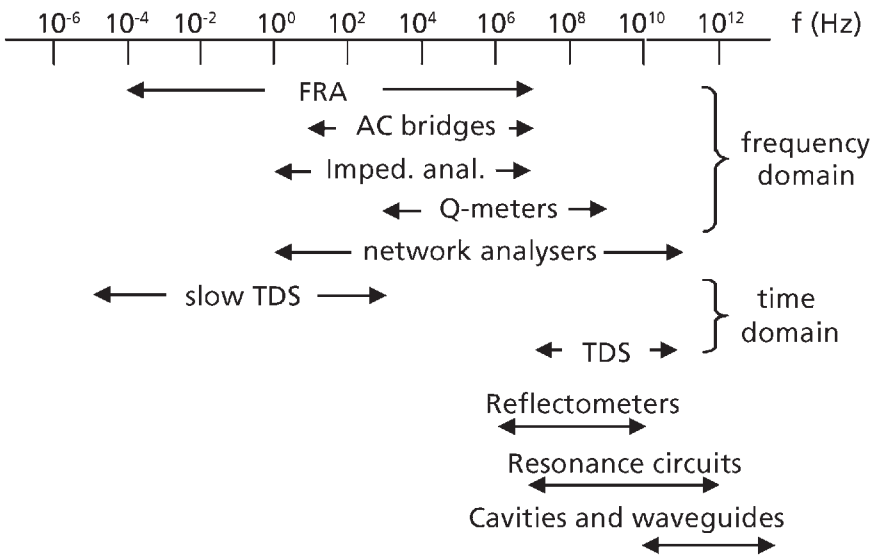

Figure 5.1 Techniques and equipment for dielectric measurements. FRA means frequency response analyser; TDS is time-domain spectroscopy.

where C is the capacitance of the filled capacitor, is then obtained from:

$$\varepsilon(\omega) = \frac{1}{i\omega Z(\omega) C_0} \tag{5.2}$$

In slow time-domain spectroscopy, a voltage step V_p is applied to the sample and the polarisation or depolarisation current $I(t)$ is measured as a function of time. The time-dependent dielectric permittivity $\varepsilon(t)$ is then given by:

$$\varepsilon(t) = \frac{C(t)}{C_0} \quad \text{and} \quad \frac{d\varepsilon}{dt} = \frac{I(t)}{C_0 V_p} \tag{5.3}$$

Usually the depolarisation current is measured to avoid the dc conductivity contribution. The dielectric relaxation spectrum is then obtained by Fourier transform or approximate formulae, e.g., the Hamon approximation [27]. By carefully controlling the sample temperature and accurately measuring the depolarisation current, precision measurements of dielectric permittivity down to 10^{-6} Hz are possible [30]. In fast time-domain spectroscopy or reflectometry, a step-like pulse propagates through a coaxial line and is reflected from the sample section placed at the end of the line. The difference between the reflected and the incident pulses recorded in the time domain contains information on the dielectric properties of the sample [31, 32].

In addition to dielectric permittivity ε, which is the most physically meaningful dielectric function to describe the material response, under the condition that in the experiments the electric field is the independent variable and the charge is the dependent one (i.e., ε is a compliance), the electric modulus M is often employed to analyse relaxation phenomena in ionic conductors [33]:

$$M = \frac{1}{\varepsilon} = M' + iM'' = \frac{\varepsilon'}{\varepsilon'^2 + \varepsilon''^2} + i\frac{\varepsilon''}{\varepsilon'^2 + \varepsilon''^2} \tag{5.4}$$

The formalisms $\varepsilon(\omega)$ and $M(\omega)$ are equivalent. Transformation from one to the other may emphasise, and therefore help to resolve, particular aspects of the relaxation process (as demonstrated later in this chapter), but no new information can be extracted.

Independently of the specific dielectric technique used, the results of dielectric measurements are usually analysed in the form of complex dielectric permittivity $\varepsilon(\omega) = \varepsilon'(\omega) - i\varepsilon''(\omega)$ at constant temperature by fitting empirical relaxation functions to $\varepsilon(\omega)$. In the examples to be given later in this chapter, often the two-shape-parameters Havriliak–Negami (HN) expression [34]:

$$\varepsilon(\omega) - \varepsilon_\infty = \frac{\Delta\varepsilon}{[1 + (i\omega\tau)^{1-\alpha}]^\beta} \tag{5.5}$$

is fitted to the experimental data for a relaxation mechanism. In this equation $\Delta\varepsilon$ is the dielectric strength, $\Delta\varepsilon = \varepsilon_s - \varepsilon_\infty$, where ε_s and ε_∞ are the low- and high-frequency limits of ε', respectively, τ is the relaxation time, $\tau = 1/2\pi f_{HN}$, where f_{HN} is a characteristic frequency closely related to the loss peak frequency f_{max}, and α, β are the shape parameters describing the shape of the $\varepsilon''(\omega)$ curve below and above the frequency of the peak, respectively, $0 < \alpha \leq 1$ and $0 < \beta \leq 1$. This expression becomes the single Debye form for $\alpha = 0$, $\beta = 1$, the symmetric Cole–Cole form for $\alpha \neq 0$, $\beta = 1$, and the asymmetric Cole–Davidson form for $\alpha = 0$, $\beta \neq 1$ [34, 35]. A proper sum of HN expressions is fitted to $\varepsilon(\omega)$ in the case of more than one overlapping mechanism plus a term for the contribution of the conductivity, if the latter makes a contribution at the temperature of the measurements. For each relaxation mechanism there are then three sources of information: the timescale of the response (τ or f_{max}), the dielectric strength ($\Delta\varepsilon$) and the shape of the response (α, β). By measuring $\varepsilon(\omega)$ at several temperatures, the timescale of the response is analysed in terms of the Arrhenius equation for secondary relaxations and the Vogel–Tammann–Fulcher (VTF) equation for the primary α relaxation, and valuable information on the activation parameters is obtained [24, 25]. Examples will be given later in this chapter.

The dielectric permittivity $\varepsilon(\omega)$ describes the material response to the application of an alternating electric field $E(\omega)$. For small electric field strengths a linear relationship holds between E and the polarisation P:

$$P(\omega) = [\varepsilon(\omega) - 1]\varepsilon_0 E(\omega) \tag{5.6}$$

where ε_0 is the permittivity in vacuum [27]. By the theory of dielectric relaxation $\varepsilon(\omega)$ is related to the correlation function $\phi(t)$ of the polarisation fluctuations [24, 25]:

$$\frac{\varepsilon(\omega) - \varepsilon_\infty}{\varepsilon_s - \varepsilon_\infty} = \int_0^\infty \left[-\frac{\mathrm{d}\Phi(t)}{\mathrm{d}t} \right] \exp(-\mathrm{i}\omega t)\, \mathrm{d}t \tag{5.7}$$

and

$$\Phi(t) = \frac{\langle \Delta P(t)\, \Delta P(0) \rangle}{\langle \Delta P(0)^2 \rangle} \tag{5.8}$$

where ΔP denotes a fluctuation of the polarisation around its equilibrium value and the angular brackets denote the averaging over an ensemble or time t.

Next to DS, several other experimental techniques, such as mechanical spectroscopy, nuclear magnetic resonance, neutron scattering, dynamic light scattering, Raman spectroscopy, are often employed to investigate molecular dynamics in polymeric systems. When comparing the results obtained with the same material and different techniques, one should take into account the difference in timescale and the difference in local

(spatial) scale. The first is obvious: e.g., the main-chain relaxation (α relaxation) related to the glass transition is measured at higher temperatures in high-frequency DRS than in low-frequency dynamic mechanical analysis. The latter deserves closer examination and is the object of intense investigation: different spectroscopies look at different species and thus probe mobility at different spatial scales. Discrepancies at first glance among the results of different spectroscopies on the same material turn out to be very informative in identifying the molecular units whose mobility is being probed [36].

5.2.2 Thermally Stimulated Depolarisation Currents Techniques

The thermally stimulated depolarisation currents (TSDC) method is a dielectric method in the temperature domain, which allows for a rapid characterisation of the dielectric response of the material under investigation. The method consists of measuring the thermally activated release of stored dielectric polarisation. It corresponds to measuring dielectric losses against temperature at constant low frequencies of 10^{-2}–10^{-4} Hz [37, 38]. The low equivalent frequency is a characteristic feature of the TSDC method, which is often used to extend the range of dielectric measurements down to low frequencies. In this method, the sample is inserted between the plates of a capacitor and polarised by the application of an electric field E_p at temperature T_p for time t_p, which is large in comparison with the relaxation time at T_p of the dielectric dispersion under investigation. With the electric field still applied, the sample is cooled to temperature T_0 (which is sufficiently low to prevent depolarisation by thermal excitation) and then is short-circuited and reheated at a constant rate b. A discharge current is generated as a function of temperature, which is measured with a sensitive electrometer. The resultant TSDC spectrum often consists of several peaks whose shape, magnitude and location provide information on the timescale and the dielectric strength of the various relaxation mechanisms present in the sample [37]. In contrast to DS (isothermal measurements in the frequency domain), the stages of polarisation and depolarisation (stimulus and response) are separated in the TSDC method. This is beneficial with respect to conductivity effects in ionically conducting polymers, where dipolar processes (typically the α relaxation associated with the glass transition) are often masked by ionic conductivity in DS measurements, but not however in TSDC measurements [39]. The method is characterised by high sensitivity and, owing to its low equivalent frequency [37], by high resolving power. In addition, it provides special variants to experimentally analyse complex relaxation mechanisms into approximately single responses [37–39]. Examples will be given later in this chapter.

5.2.3 Impedance Spectroscopy and Ionic Conductivity Measurements

For ionic conductivity measurements, the same equipment may be used as for dielectric measurements described in Section 5.2.1. The term ‘impedance spectroscopy’ is used

preferably in that case instead of DS, the latter being reserved mostly for dipolar dielectric materials. In addition to characterising the bulk electrical properties of materials, impedance spectroscopy includes also the investigation of effects at the interfaces between the sample and the electronically conducting electrodes [29]. In recent years the frequency range of ionic conductivity measurements has been significantly extended to higher frequencies, spanning more than 17 decades and ranging from less than 10^{-3} Hz to more than 10^{14} Hz. For that broad frequency range, 'conductivity spectroscopy' is a better term [40]. This includes, in addition to the traditional impedance regime, which is below a few MHz, the radio regime, which ranges from a few MHz to a few GHz, the microwave regime, which ranges from a few GHz to about 150 GHz, and the far-infrared regime, which is above 150 GHz. Electrodes are used only in the first regime, whereas guided and unguided electromagnetic waves are employed in the second and third regimes and in the fourth regime, respectively [40]. Results to be presented and discussed later in this chapter refer exclusively to the impedance regime.

In the basic impedance spectroscopy experiment, an electrical stimulus (a known voltage or current) is applied to the electrodes and the response (the resulting current or voltage) is measured [29]. Similar to dielectric measurements (Section 5.2.1), in most cases measurements are performed in the frequency domain by applying a single-frequency voltage to the sample under investigation and measuring the phase shift and amplitude, or real and imaginary parts, of the resulting current at that frequency. Information obtained from impedance measurements refers either to the bulk material (conductivity, mobilities of charges, generation–recombination rates, etc.) or to the material–electrode interface (capacitance of the interfacial region, adsorption–reaction rate constants, etc.). Our interest in this chapter is focused on the investigation of bulk material properties. Special methodologies of measurements and data analysis allow one to separate bulk from interfacial effects [29].

The results of impedance spectroscopy measurements are often presented in a (complex) impedance plot. Referring again to the basic experiment of applying a sinusoidal voltage $V(t) = V_0 \sin(\omega t)$ to the sample (Section 5.2.1), we now record the resulting steady-state current $I(t) = I_0 \sin(\omega t + \varphi)$ and define the impedance $Z(\omega) \equiv V(t)/I(t)$ with magnitude $|Z(\omega)| = V_0/I_0(\omega)$ and phase angle $\varphi(\omega)$:

$$
\begin{aligned}
&Z(\omega) = Z' + iZ'' = |Z| \exp(i\varphi) \\
&Z' = \mathrm{Re}(Z) = |Z| \cos\varphi \\
&Z'' = \mathrm{Im}(Z) = |Z| \sin\varphi \\
&\varphi = \tan^{-1}\left(\frac{Z''}{Z'}\right) \\
&|Z| = \left[(Z')^2 + (Z'')^2\right]^{1/2}
\end{aligned}
\qquad (5.9)
$$

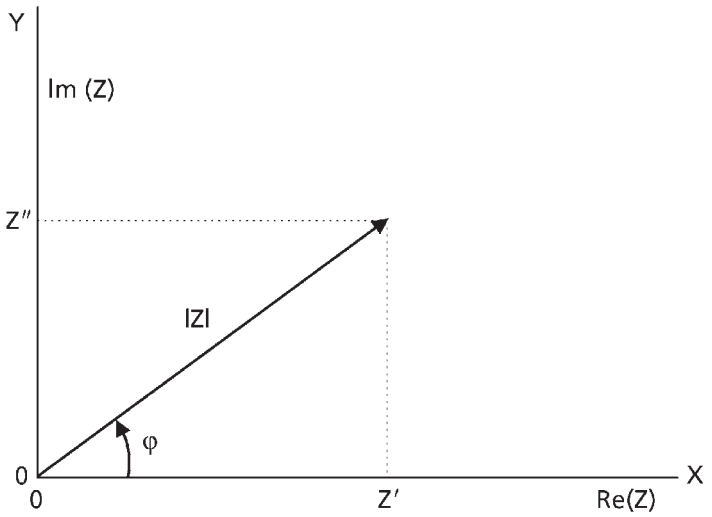

Figure 5.2 Representation of the impedance, *Z*, using rectangular and polar coordinates.

The impedance is plotted in the complex plane (Argand diagram) as a planar vector using rectangular and polar coordinates (**Figure 5.2**).

In conventional impedance spectroscopy, *Z* is measured (nowadays mostly automatically) as a function of frequency over a wide frequency range in the linear regime (small voltage signal for linear response). Plots of $Z(\omega)$ against ω then provide information on the electrical properties of the material under investigation. Very popular and comprehensive are plots of $-\mathrm{Im}(Z)$ (or $\mathrm{Im}(Z)$, if we write $Z(\omega) = Z' - iZ''$ instead of Equation (5.9)) against $\mathrm{Re}(Z)$ with the frequency ω as parameter (complex impedance plots), which provide (often by extrapolation) directly the value of resistance and, by knowing the geometrical characteristics of the sample, the value of the dc conductivity σ_{dc} at the temperature of the measurements. Examples will be given later in this chapter.

When the emphasis is put on the bulk electrical properties of the material under investigation in comparison with the predictions of theoretical models, ac conductivity plots, i.e., plot of ac conductivity σ_{ac} against frequency ω at constant temperature, are well suited for presenting and discussing the results of ionic conductivity measurements [29, 40]. The data are recorded isothermally with variation of the frequency ω and $\sigma_{ac}(\omega)$ is calculated from these data (in fact, the real part σ'_{ac} of the complex conductivity), e.g., in the admittance presentation (Equation (5.2)):

$$\sigma_{ac}(\omega) = \omega\varepsilon_0\varepsilon''(\omega) \tag{5.10}$$

Jonscher suggested the following power-law dependence (universal dynamic or dielectric response) [35]:

$$\sigma_{ac}(\omega) = \sigma_{dc} + A\omega^{s}, \qquad 0.5 < s < 0.7 \tag{5.11}$$

where A and s are temperature-dependent parameters. Equation (5.11) and its modifications are frequently used for fitting to experimental data. Examples will be given later in this chapter.

5.3 Overall Behaviour

The discussion of the overall molecular dynamics in polymer nanocomposites will be based on results obtained with three systems of thermoset nanocomposites. Common to these systems is that epoxy resin is used as the matrix. The inclusions are layered silicates (clays) in the first system, diamond and magnetic nanoparticles in the second, and conductive carbon nanoparticles in the third. For comparison, a fourth system will be discussed based on polyimide reinforced with sol–gel derived organosilicon nanophase.

5.3.1 Epoxy Resin/Layered Silicate Nanocomposites

These nanocomposites have been prepared by dispersing an organically modified smectic clay in a low-viscosity epoxy resin (ER) – Araldite LY556 (CIBA) [41, 42]. The clay (COOP Chemical Co. Ltd, Japan) consists of an octahedral Al_2O_3 sheet sandwiched between two SiO_2 tetrahedral layers (of ~1 nm thickness and ~50 nm length) with the charges being adjusted by substituting Al^{3+} or Si^{4+} by Mg^{2+} and/or Fe^{2+}. The depressed charges were neutralised with alkaline cations intercalated into the interlayer spaces, leading to a laminate structure of several hundred layers. The following type of alkaline cations were used: SAN (hexadecyl-octadecyl-ammonium) $[C_{16}H_{33})_x(C_{18}H_{37})_yN^+(CH_3)_2]$ ($x = 0.5$, $y = 1.5$); STN (trioctyl-methyl-ammonium) $[(C_8H_{17})_3(CH_3)N^+]$; and SPN (oligo(oxypropylene)-diethyl-methyl-ammonium) $[(C_2H_5)_2(CH_3)N^+(O\text{-}iPr)_{25}]$. The samples investigated were nanocomposites of 5 vol% (SAN, STN) and 10 vol% (SPN) smectite in epoxy resin (ER), corresponding to about 5 wt% smectic clay in the composite. The synthesis method includes mechanical mixing and ultrasonic treatment of the epoxy–clay dispersions. The compositions were then moulded and cured by a two-stage curing process (2 h at 75 °C and an additional 2 h at 130 °C) in the presence of amine curing agent. Transmission electron microscopy (TEM) studies showed that exfoliated structures had been prepared [42].

Figure 5.3 shows comparative TSDC plots for the ER/layered silicate nanocomposites. In terms of the more familiar DS, this plot corresponds to a plot of dielectric losses against temperature at a fixed, low frequency in the range 10^{-2}–10^{-4} Hz [37, 38]. This means that faster relaxations will be recorded at lower temperatures and slower relaxations at higher temperatures. In the temperature range of the measurements, the samples are in

the glassy state, as revealed by DS measurements to be reported later, so in the TSDC thermogram we expect to follow the local (secondary, sub-glass) relaxations. The weak peak at about –100 °C in ER contains contributions from the γ and the β relaxations. The former is attributed to local motion of unreacted epoxide rings, ether and amine groups, the latter to motion of hydroxyl groups [43]. In the 10 vol% SPN and the 5 vol% SAN nanocomposites, dielectric losses at low temperatures increase with respect to the epoxy resin matrix (as indicated by increased depolarisation currents), whereas the opposite is observed in the 5 vol% STN. It is not clear at this stage whether the peaks at about –95 °C in the 10 vol% SPN and at –80 °C in the 5 vol% STN are due to the γ and β relaxations (which would mean increasing in magnitude and becoming slower) or due to new relaxations. Note that new relaxations (not present in the pure matrix) may appear in the nanocomposites, in particular when nanofillers have been chemically treated, this point often being ignored in the literature. The temperature position of these TSDC peaks allows one to bring them into correspondence with loss peaks measured by DS at higher temperatures (to be shown later).

The peaks at temperatures higher than about –50 °C in **Figure 5.3** and their DS counterparts measured at higher temperatures are in the region where in ER ω relaxations have been observed and analysed [43]. Interfacial effects due to heterogeneity of the samples are also expected to occur in this temperature or frequency region. The results in **Figure 5.3** show that at temperatures between –50 and 20 °C dielectric losses increase in the composites with respect to ER and are highest in the 10 vol% SPN hybrid. This might be related to the higher clay content of this sample.

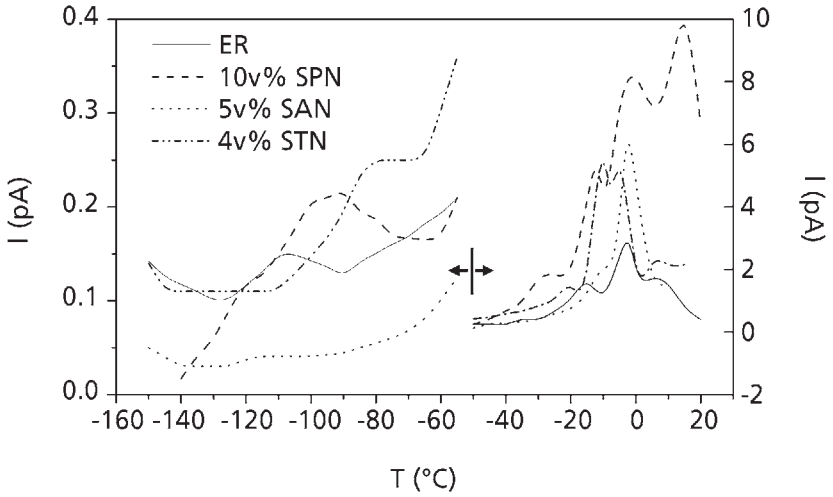

Figure 5.3 TSDC thermograms obtained with the samples indicated on the plot. Note the change of vertical scale at –50 °C.

Figures 5.4 and **5.5** show results for the frequency dependence of the real and imaginary parts of the dielectric permittivity, ε′ and ε″, respectively, in the pure ER matrix over a wide range of temperature, 30–140 °C, covering also the glass transition temperature T_g (about 60–80 °C, see below). Thus, the DS measurements are expected to provide information on the primary (segmental) α relaxation, associated with the glass transition (dynamic glass transition [44]), and on conductivity effects, being, in that respect, complementary to the TSDC measurements. An overall increase of ε′ with temperature at low frequencies and a structure (step) at 10^1–10^3 Hz are observed. At higher frequencies, ε′ increases with temperature up to about 60–70 °C and then decreases, suggesting that T_g is around 60–70 °C [41]. In **Figure 5.5** ε″(f) shows a structure (shoulder) corresponding to the ε′ step in **Figure 5.4**. The step in ε′(f) and the corresponding shoulder in ε″(f) are indicative of the so-called conductivity current relaxation (CCR) [45], to be discussed later in Section 5.6. At lower frequencies and higher temperatures, the slope of ε″(f) in **Figure 5.5** is –1, which is typical for dc conductivity. This is confirmed by the corresponding ac conductivity plots, $\sigma_{ac}(f)$, to be discussed later, which exhibit a dc conductivity plateau at low frequencies and/or high temperatures. At low frequencies and high temperatures ε′ exhibits high values, which do not reflect the bulk properties, but are rather related with conductivity, space charge polarisation and electrode polarisation, to be discussed in Section 5.6. No loss peak corresponding to the α relaxation is observed in **Figure 5.5**. This is because the α loss peak is masked by conductivity, this situation often being encountered in polymers [46]. Special representations and/or other formalisms for treating the experimental data can then be used to make the α loss peak visible (see below).

Figures 5.6 and **5.7** show for the SPN composite plots similar to those of **Figures 5.4** and **5.5**, respectively, for the polymer matrix, extended now to 170 °C. At first glance, the overall behaviour is similar to that of the pure ER matrix. However, there are distinct differences in the spectra, reflecting differences in molecular dynamics. The plots of the SAN and STN nanocomposites (not shown here) exhibit many similarities to those of the SPN nanocomposites in **Figures 5.6** and **5.7**. It should be noted that, as the results in **Figures 5.6** and **5.7** and the following figures are discussed in terms of molecular mobility of the polymer matrix, the dielectric response of the pure clay and the organic modifiers should, in principle, be subtracted from that of the composite. This was, however, not necessary here, at least with respect to the dielectric loss of clay, because the overall values of ε″ of the clay were smaller than 0.05 and the amount of clay in the composites only about 5%.

The main result obtained by comparing the ε′(f) and the ε″(f) plots in the pure ER matrix and the nanocomposites is that molecular mobility decreases in the nanocomposites. This is an interesting observation with respect to understanding the improvement of final properties in layered silicate nanocomposites, such as mechanical properties, thermal stability and barrier properties [1, 47, 48], at the molecular level. The reduction of molecular mobility in the nanocomposites is best discussed in terms of the real part

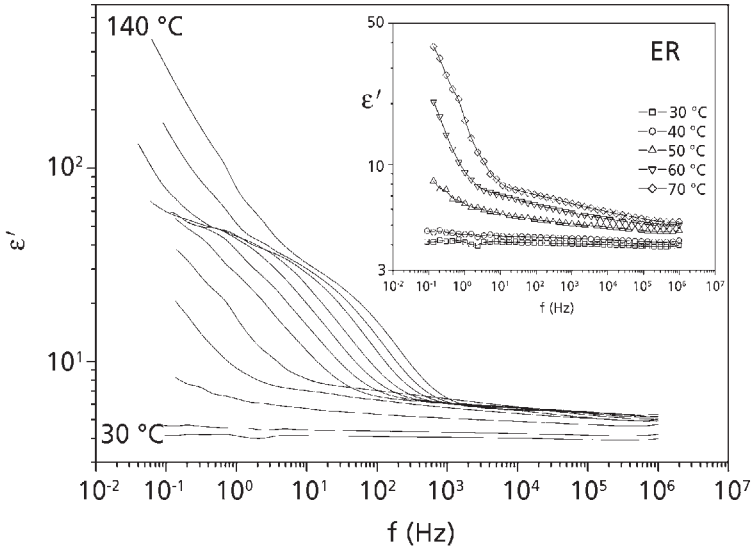

Figure 5.4 Real part of the dielectric permittivity ε′ against frequency *f* of the epoxy resin matrix at temperatures between 30 and 140 °C in steps of 10 °C. The inset shows a magnification at temperatures between 30 and 70 °C.

Reproduced with permission from [41]. ©Elsevier Science, 2002

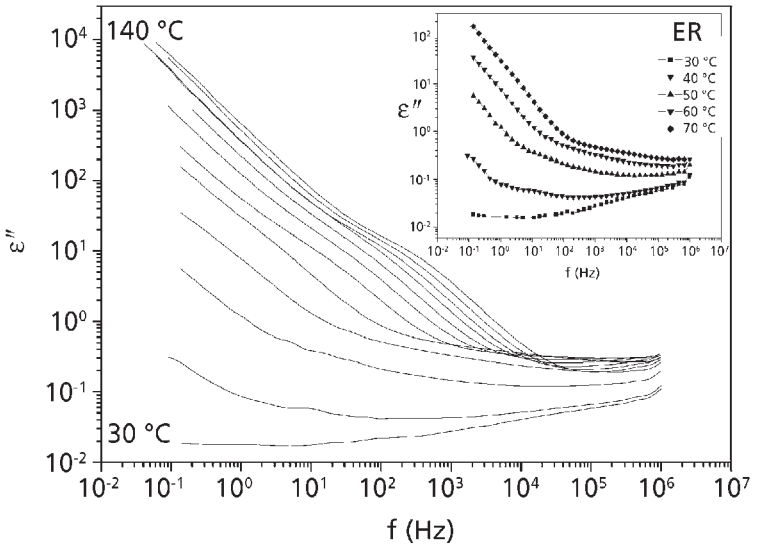

Figure 5.5 Dielectric loss ε″ against frequency *f* of the epoxy resin matrix at temperatures between 30 and 140 °C in steps of 10 °C. The inset shows a magnification at temperatures between 30 and 70 °C.

Reproduced with permission from [41]. ©Elsevier Science, 2002

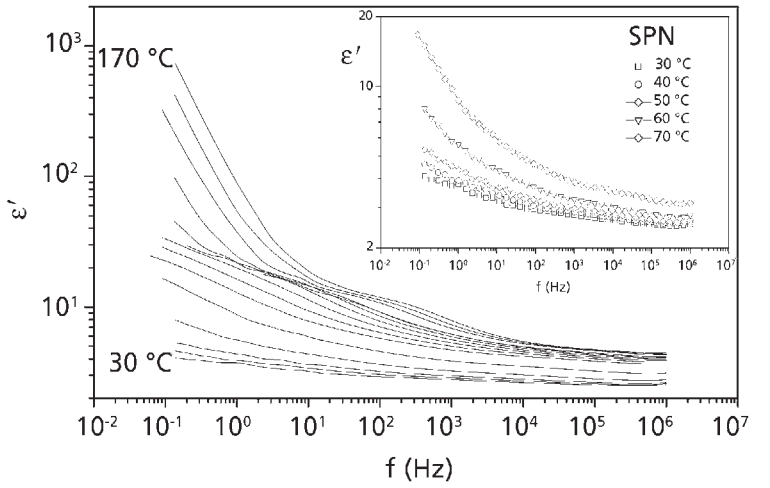

Figure 5.6 Real part of the dielectric permittivity ε′ against frequency *f* of the SPN nanocomposite at temperatures between 30 and 170 °C in steps of 10 °C. The inset shows a magnification at temperatures between 30 and 70 °C.

Reproduced with permission from [41]. ©Elsevier Science, 2002

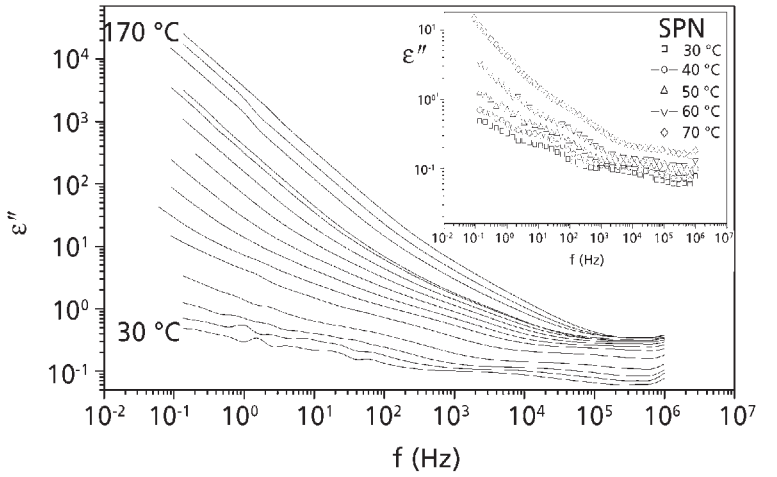

Figure 5.7 Dielectric loss ε″ against frequency *f* of SPN nanocomposite at temperatures between 30 and 170 °C in steps of 10 °C. The inset shows a magnification at temperatures between 30 and 70 °C.

Reproduced with permission from [41]. ©Elsevier Science, 2002

of the dielectric permittivity ε′, as ε′ is a measure of polarisability [49]. By comparing **Figures 5.4** and **5.6** with each other, we observe that at each temperature ε′(f) is lower in the nanocomposite. To demonstrate this point better, we show in **Figure 5.8** a comparative plot of ε′ against temperature T for ER and the three nanocomposites at a fixed frequency of 10^5 Hz. The data shown in **Figure 5.8** have been recorded isothermally (compare **Figures 5.4** and **5.6**) and have been replotted. A high frequency, 10^5 Hz, has been selected for that plot to get rid of conductivity effects, which dominate the behaviour at lower frequencies. The step in ε′(T) in **Figure 5.8**, around 60 °C in pure ER and at higher temperatures in the nanocomposites, corresponds to the dynamic glass transition to be discussed in Section 5.5. Note that, at temperatures higher than T_g, ε′(T) becomes approximately constant in the pure ER matrix, whereas in the nanocomposites it continues to increase with increasing temperature, although the rate of increase decreases at temperatures higher than about 80–100 °C. We think that this behaviour is typical for polymeric systems, where additional constraints to molecular mobility are imposed, such as nanocomposites, semicrystalline polymers and networks. We observe in **Figure 5.8** that, at each temperature, both below and above T_g, ε′ is lower in the nanocomposites as compared to the pure ER matrix. Moreover, systematic differences are observed between the nanocomposites, which will not be discussed further here.

A second interesting result obtained by comparing the ε′(f) and the ε″(f) plots in the pure ER matrix and the nanocomposites is that the structure in ε′(f) and ε″(f) at 10^1–10^3 Hz in **Figures 5.4** and **5.5**, respectively, weakens or disappears in the SPN nanocomposite (**Figures 5.6** and **5.7**). With respect to that point, the SAN and the STN nanocomposites

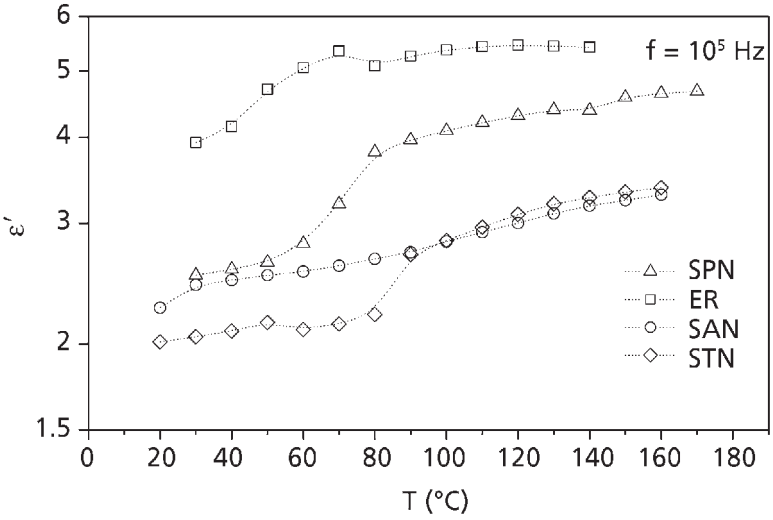

Figure 5.8 Real part of the dielectric permittivity ε′ against temperature T of the samples indicated on the plot at 10^5 Hz.

show intermediate behaviour between those of the ER matrix and the SPN composite and closer to the latter. The implications of these results on morphology will be discussed later in Section 5.6. In that respect, interesting results are observed at temperatures lower than and close to T_g (compare the insets to **Figures 5.4–5.7**). Two loss peaks are observed in the SPN composite, at about 10 Hz and 10^3–10^4 Hz at 30 °C (inset to **Figure 5.7**), both of them shifting to higher frequencies with increasing temperature. As the peaks are absent in the pure polymer matrix, they are ascribed to effects related to the presence of clay, probably to interfacial polarisation effects [45].

Figure 5.9 shows a comparative plot of the frequency dependence of dielectric loss, ε″, at 30 °C in the pure ER matrix and the three nanocomposites. We recall that at this temperature the systems are in the glassy state. We observe that in the frequency range of the measurements ε″ increases in the nanocomposites, as compared to the polymer matrix, in the order SAN, STN, SPN. Interestingly, rheological measurements in smectite–epoxy dispersions at 25 °C show an overall increase of both the storage and loss moduli, following the same order as observed here for the cured solid samples [50]. Note that, in contrast to the results for ε″ in **Figure 5.9**, ε′ decreases in the nanocomposites, as compared to the pure ER matrix. An interesting result is also that, in contrast to what is observed in **Figure 5.9** at 30 °C, at higher temperatures, in particular at intermediate ones, ε″ decreases in the nanocomposite, as compared to the matrix (compare **Figures 5.5** and **5.7**).

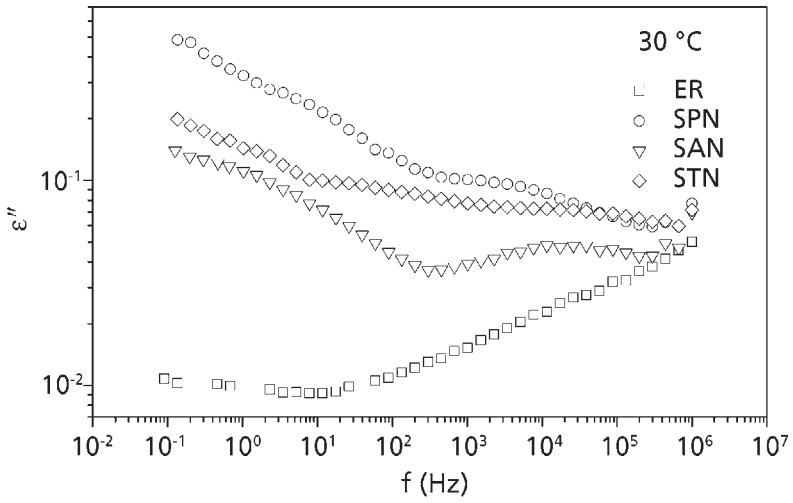

Figure 5.9 Comparative log–log plot of dielectric loss ε″ against frequency *f* of the samples indicated on the plot at 30 °C.

Reproduced with permission from [41]. ©Elsevier Science, 2002

5.3.2 Epoxy Resin Reinforced With Diamond and Magnetic Nanoparticles

The materials for which results are presented in this section consist of epoxy resin (ER), the same matrix as used for preparing the epoxy resin/layered silicate nanocomposites of Section 5.3.1, containing nanosized diamond or magnetic particles [51]. The diamond particles were synthesised by a shock-wave method [52] and have a diameter of about 6 nm. The magnetic inclusions are nanoparticles of $BaFe_{12}O_{19}(CoTi)_{0.45}$, i.e., barium hexaferrite (BHF) $BaFe_{12}O_{19}$ where magnetic ions are substituted with Co and Ti, and which will subsequently be called simply BHF. They have a diameter of approximately 100 nm. To prepare the ER matrix and the nanocomposites, procedures similar to those described in Section 5.3.1 were followed. The filler concentrations used are shown in **Table 5.1**, along with a very rough estimation of the interparticle distance, calculated by assuming spherical particles on a hexagonal lattice. We use this value for the interparticle distance only as an order-of-magnitude estimate, keeping in mind that any agglomeration of the particles will considerably increase the interparticle distance.

Table 5.1 Volume fraction, mean particle size and interparticle distance for the nanocomposites studied. The interparticle distance is a rough approximation, calculated for spherical particles on a hexagonal lattice

Sample	Filler volume fraction (%)	Filler size (nm)	Interparticle distance (nm)
Pure ER	0	–	–
ER + 0.5% diamond	0.5	6	18
ER + 1.2% diamond	1.2	6	13
ER + 0.7% BHF	0.7	100	373
ER + 6% BHF	6	100	131

Figure 5.10 shows results for the frequency dependence of dielectric permittivity $\varepsilon = \varepsilon' - i\varepsilon''$ for the nanocomposite with 1.2 vol% diamond at temperatures between 30 and 160 °C. At selected temperatures, the frequency range of measurements has now been extended to 10^9 Hz by using a Hewlett-Packard impedance/material analyser 4291A integrated with a Tabai Espec temperature chamber SU-240-Y. For direct comparison, the insets show the corresponding plots for the ER matrix, results shown already in **Figures 5.4** and **5.5**. Similar to the results shown in Section 5.3.1, ε' in **Figure 5.10(a)** generally increases with increasing temperature due to increasing molecular mobility. The structure (step) seen at low frequencies in the pure ER is much less pronounced in the nanocomposite. There is a large increase of ε' for the pure ER between 40 and 50 °C, which suggests an increase in the molecular mobility in this temperature range. This indicates that the glass transition of the epoxy resin takes place between 40 and 50 °C.

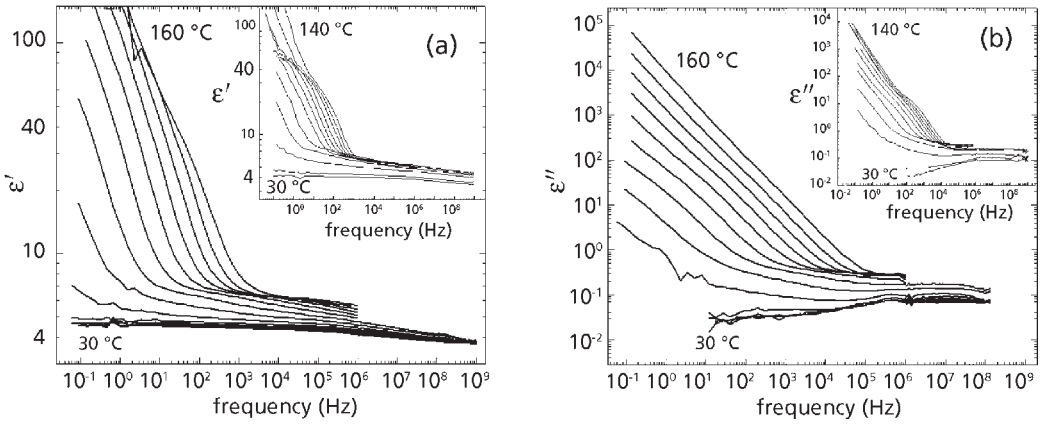

Figure 5.10 Log–log plot of (a) the real part and (b) the imaginary part of the dielectric permittivity for the 1.2% ER/diamond nanocomposites at various temperatures, in steps of 10 °C. The insets show the corresponding plots for the ER matrix.

This increase is observed in the nanocomposite at higher temperatures, 70–100 °C, and is much more gradual.

Figure 5.10(b) shows the corresponding plot of dielectric loss $\varepsilon''(f)$. At low frequencies and high temperatures we observe an increase with a slope of approximately –1, characteristic of dc conductivity. In the pure ER a shoulder appears corresponding to the step in $\varepsilon'(f)$. The peak due to the α relaxation of the polymer, associated with the glass transition, is also in the frequency range of this measurement and is obscured by the conductivity; however, it is resolved by further analysis. An exception is the sample with 6% BHF, which exhibits a broad and very strong peak due to the conductivity of the filler, which completely obscures the α relaxation. This peak was not studied further.

Figure 5.11 shows comparative isochronal (constant frequency) $\varepsilon'(T)$ plots at 10^5 Hz for the two diamond nanocomposites of **Table 5.1** and the pure ER matrix, for the latter as the continuous line. The data have been recorded isothermally and replotted here as a function of temperature. A step is observed in $\varepsilon'(T)$ around 50–60 °C in pure ER and is interpreted as a manifestation of the dynamic glass transition. The step is shifted to higher temperatures and is more gradual in the nanocomposites. This point will be discussed in more detail in Section 5.5 on the basis of the corresponding $\varepsilon''(T)$ plot. The main point of interest here is that the nanocomposites exhibit lower values of $\varepsilon'(T)$, as compared to pure ER, at temperatures lower than about 120 °C, which are interpreted in terms of reduced molecular mobility in the nanocomposites. The reduction is larger in the nanocomposite with the higher filler fraction. It is interesting

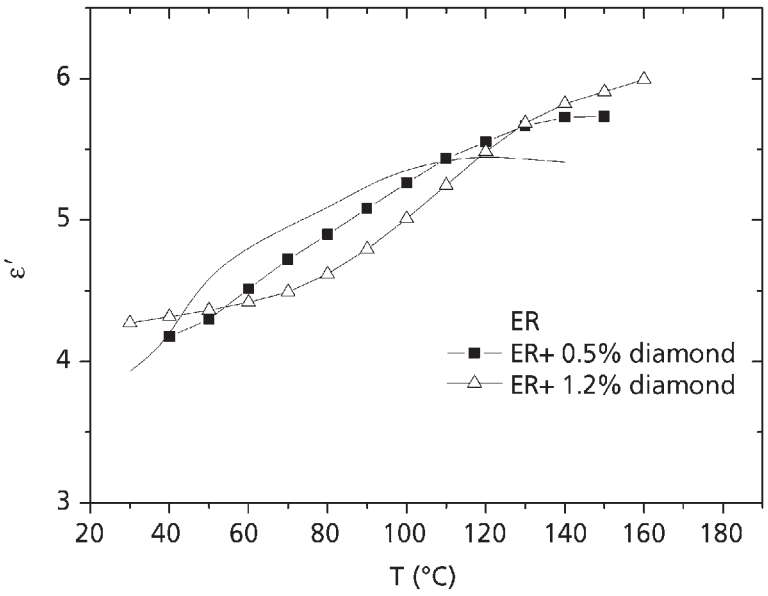

Figure 5.11 Real part of the dielectric permittivity ε′ against temperature *T* of the ER/diamond samples indicated on the plot at 10^5 Hz.

to note that the reduction of molecular mobility is less pronounced and in a restricted temperature range in the diamond nanocomposites, as compared to the layered silicate nanocomposites of Section 5.3.1. However, note the lower filler fraction of the diamond nanocomposites. The corresponding ε′(*T*) plot for the BHF nanocomposites is shown in **Figure 5.12**. Now ε′(*T*) increases, in general, in the nanocomposites, as compared to pure ER, and the increase is higher at higher filler fraction. This result should not be interpreted in terms of increased molecular mobility in the nanocomposites, as at the same time the step (and the corresponding peak in ε″(*T*)) are shifted to higher temperatures. The higher dielectric response in the nanocomposites arises from the contribution of the magnetic inclusions, as often observed in magnetic nanocomposites [53]. This point requires attention when dielectric results obtained with polymer composites and nanocomposites are discussed in terms of the molecular dynamics of the polymer matrix, as, in principle, the dielectric response of the filler has to be subtracted from the measured effective response. This is often a difficult task. Even in that case, however, information on the modification of polymer dynamics by the presence of and/or interactions with the filler can be obtained by following the dielectric relaxations of the polymer matrix in the composite. For the BHF nanocomposites, this will be done on the basis of DS and TSDC results for the secondary sub-glass and the primary α relaxation in Sections 5.4 and 5.5, respectively.

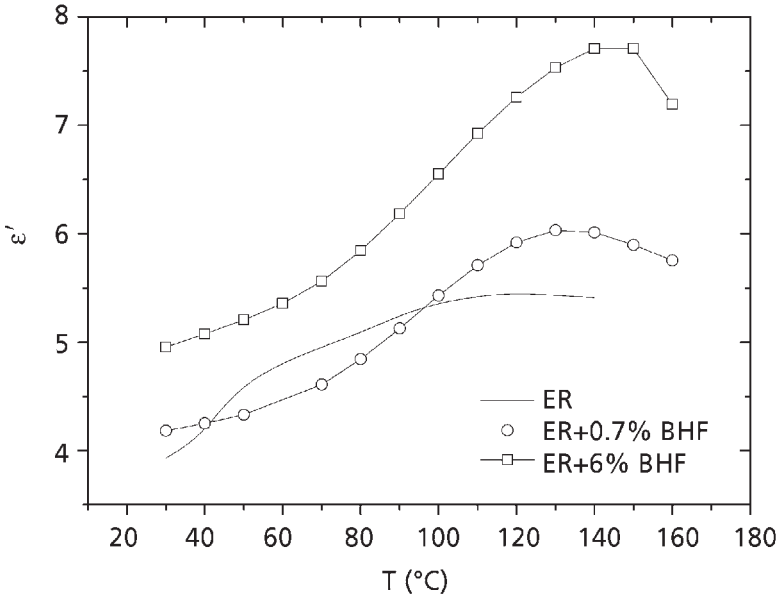

Figure 5.12 Real part of the dielectric permittivity ε′ against temperature *T* of the ER/BHF samples indicated on the plot at 10^5 Hz.

5.3.3 Epoxy Resin/Carbon Nanocomposites

This is a system of particular interest, as the filler is conductive and the results of dielectric studies of molecular mobility can be discussed in terms of percolation and thus provide additional information on morphology. The nanosized carbon particles (NCP) were prepared by a shock-wave propagation method [52]. Semidilute and concentrated dispersions of 1–10 vol% NCP were prepared by dispersing the proper amount of filler in the ER matrix by using a high-power ultrasonic disperser. Samples of solid composites were prepared by adding diethylenetriamine in stoichiometric proportions as a hardener and curing for 1 h at room temperature, followed by post-curing for 3 h at 140 °C. Details of the preparation and morphological characterisation of the nanocomposites have been given elsewhere [54].

Molecular dynamics in the nanocomposites were studied by broadband DS in wide ranges of temperatures. **Figure 5.13** shows results for the temperature dependence of ε′ and ε″ in the ER/NCP composites at a constant frequency of 80,805 Hz. The data have been recorded isothermally by scanning the frequency and have been replotted here. A relatively high frequency has been chosen for the presentation, in order to eliminate conductivity effects present at lower frequencies. An overall increase of molecular mobility is observed in **Figure 5.13**, in agreement with TSDC data to be reported in

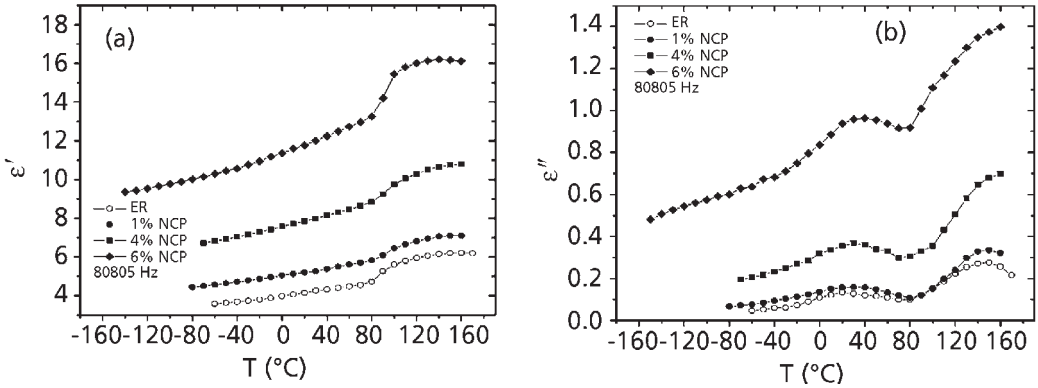

Figure 5.13 Temperature dependence of (a) the real part ε′ and (b) the imaginary part (dielectric loss) ε″ of the dielectric permittivity of the ER/NCP samples indicated on the plot at 80,805 Hz.

Section 5.4 in relation to effects on secondary relaxations, in the sense that, at each temperature, ε′ and ε″ increase with increasing filler content. This is to a large extent related to the formation of a percolation structure of the nanoparticles.

To further follow this point, we show in **Figure 5.14** comparative frequency scans of ε′ at a low temperature of –50 °C to get rid of the relaxations (loss peaks) observed in **Figure 5.13**. We observe a systematic increase of ε′(*f*) with increasing filler content. The inset to **Figure 5.14** shows the dependence of ε′ at a frequency of 1 Hz on volume concentration ϕ of NCP. The well-known equation for the dependence of ε′ on ϕ from percolation theory [55–57]:

$$\varepsilon'(\phi) = \varepsilon'_m + A|\phi - \phi_c|^{-t} \qquad (5.12)$$

where ε'_m is the dielectric constant of the matrix, ϕ_c the percolation threshold and *t* a critical exponent, has been fitted to the data, and the values of ϕ_c and *t* determined to be 7.4% and 0.69, respectively. It is interesting to note that the percolation threshold ϕ_c determined by DS on solid composites is close to that determined by rheological measurements in the carbon–epoxy dispersions [54].

Two relaxations, a secondary β relaxation at lower temperatures and the primary α relaxation at higher temperatures, associated with the glass transition of the ER matrix, are observed in **Figure 5.13**. They will be discussed in Sections 5.4 and 5.5, respectively, in relation also to TSDC results.

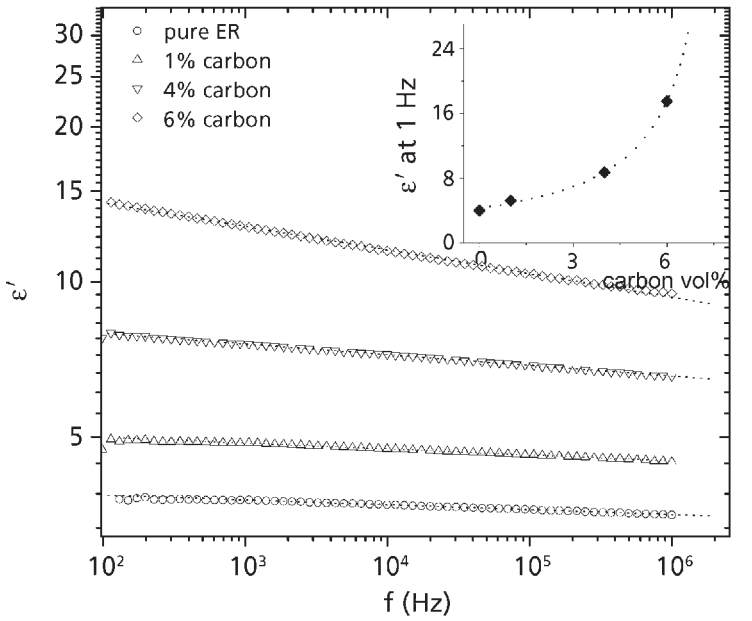

Figure 5.14 Real part of the dielectric permittivity ε′ against frequency (at –50 °C). The inset shows ε′ against volume concentration of NPC. The line is a fit of Equation (5.12) to the data.

5.3.4 Polyimide/Silica Nanocomposites

There is an increasing demand in microelectronics for materials with low values of the real part of the dielectric permittivity ε′ (better known as low-*k* materials) to be used as intermetallic and interlayer dielectrics. Candidate materials should combine low ε′ values (below 3.0, possibly even below 2.5) with several other good properties, including good thermal stability, high thermal conductivity, chemical resistance, low water absorption and good processability [58]. Polymers and polymer-based materials, in particular polyimides (PI), have attracted much interest in recent years for such applications. However, ε′ of the starting polymer (typically in the range 3.0 to 3.5 for polyimides) should be further reduced. The introduction of porosity into the polymer (ε′ of air being practically 1.0) [58] and reinforcement by inorganic nanoparticles, resulting in overall decrease of molecular mobility [59–61], are possible routes for ε′ reduction. The second route seems more effective, as the other properties are also improved at the same time.

We reported recently the preparation of PI/silica nanocomposites by the *in situ* generation of crosslinked organosilicon nanophase (ON) through the sol–gel process (PI/ON hybrids) and their characterisation by various techniques [62, 63]. DS measurements

showed a non-additive decrease of ε′ in the nanocomposites, which was treated in terms of effective medium theories (EMT) and attributed to a loose inner structure of the spatial aggregates of ON, in agreement with the results of density measurements [62]. On the other hand, these nanocomposites are characterised by the presence of chemical bonds between the ON and the PI matrix, which may affect the dynamics of the PI chains. Thus, it appears interesting from the fundamental point of view to investigate molecular dynamics in the PI/ON hybrids. DS measurements are performed in broad frequency and temperature ranges and the results are discussed in terms of effects on molecular mobility arising from both porosity and chemical bonds between the components.

The PI/ON hybrids were prepared from polyamic acid of molar mass 5,000 or 10,000 or 15,000 (series 5, 10, 15, respectively), with ethoxysilane end-groups (PAAS) and methyl triethoxysilane (MTS). The PAAS/MTS mass ratio was systematically varied from 100/0 to 100/120, corresponding to PI/ON mass ratio varying from 100/0 to 64.4/35.6. Details of preparation have been given elsewhere [62, 63]. Samples are coded by the PAAS/MTS ratio followed by the series number 5, 10 or 15, e.g., 100/70-15.

Figure 5.15 shows results for the frequency dependence of ε′ of the hybrids of series 10 at 20 °C. We observe an overall decrease of ε′ with increasing ON content. Similar results have been obtained for the hybrids of the other two series. At first glance the results look surprising in terms of EMT, as ε′ of compact silica is in the range of 3.8–4.0. Two effects may contribute to the reduction of ε′ in the nanocomposites: porosity of the ON [62]; and decrease of ε′ of the PI matrix as a result of reduced molecular mobility due

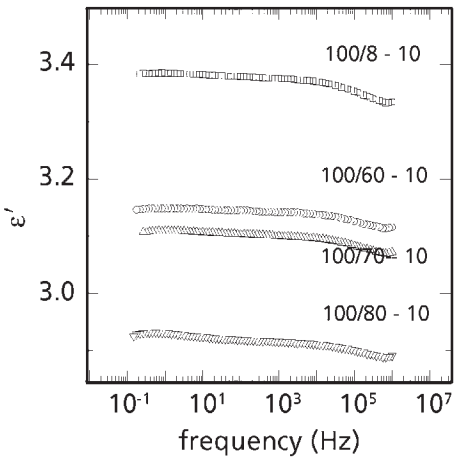

Figure 5.15 Dielectric permittivity ε′ versus frequency *f* at room temperature for the PI/ON nanocomposites of series 10.

Reprinted with permission from [63]. ©IOP Publishing, 2005

to the formation of chemical bonds with the ON [19]. In that respect it is interesting to note that the drop of $\varepsilon'(f)$ at higher frequencies in **Figure 5.15** is due to the γ relaxation of the PI matrix. Detailed investigation of the effects of the ON content and molecular mass of PI on the magnitude of the relaxation in Section 5.4 will provide further insight into the origin of $\varepsilon'(f)$ reduction in **Figure 5.15**.

5.4 Secondary (Local) Relaxations

Much less attention has been paid in the literature to the investigation of the effects of nanoparticles on local (secondary) relaxations, as compared to effects on the primary α relaxation associated with the glass transition. Such effects may be expected, however, by considering the possibility that free volume may change as a result of changes in molecular packing of polymeric chains in the nanocomposites [19]. The discussion of the effects of the presence of and interactions with nanoparticles on secondary relaxations of the polymer matrix in this section will be based on results obtained with thermoset nanocomposites (epoxy resins reinforced with diamond, magnetic nanoparticles and carbon nanoparticles) and, for comparison, with polyimide reinforced with sol–gel derived organosilicon nanophase.

5.4.1 Epoxy Resin Reinforced With Diamond and Magnetic Nanoparticles

Brief information on the preparation of these samples has been given in Section 5.3.2 and the samples investigated are listed in **Table 5.1**. The secondary relaxations in these nanocomposites were investigated by TSDC measurements in the temperature range from –150 to 10 °C. At these temperatures the materials are in the glassy state and only the secondary relaxations of the epoxy resin can be studied. **Figure 5.16(a)** shows TSDC thermograms for the pure epoxy resin and nanocomposites with 0.5% and 1.2% diamond. The peak at around –100 °C corresponds to the β relaxation of the epoxy resin matrix, associated with the motion of hydroxyl groups, while the small shoulder on the low-temperature side of the peak corresponds to the γ relaxation, associated with amine and ether groups [43, 64]. An additional relaxation is observed in the ER matrix at higher temperatures, at around –40 to –20 °C, the so-called ω relaxation, which has been less intensively studied. The ω relaxation has been found to be strongly affected by the heterogeneity of the material, and it may be attributed to the main relaxation in less dense regions [43].

The strength of the β relaxation is seen to increase significantly in the ER/diamond nanocomposites as compared to the matrix, while there is no appreciable shift in its temperature position (i.e., in the timescale of the relaxation). A similar increase in local chain mobility due to the incorporation of nanoparticles has been found in other nanocomposites (e.g., polyimide/silica systems [19]). A possible explanation for this

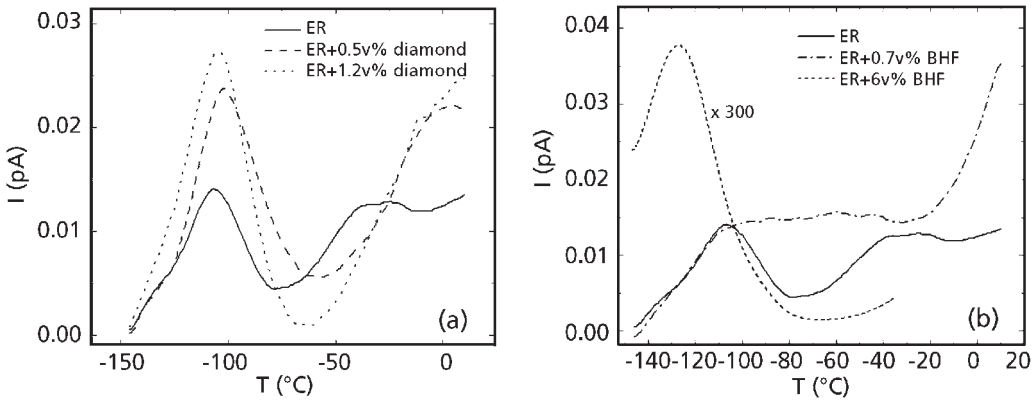

Figure 5.16 TSDC thermograms for the ER matrix and the (a) diamond and (b) BHF nanocomposites. Note the change of the scale for the ER + 6 vol% BHF sample.

increase in local mobility is that confinement of the polymer in nanoscale spaces between the nanoparticles and strong polymer–particle interactions cause loosened molecular packing of polymeric chains and increased free volume in the composites with respect to the pure matrix. This explanation is supported by the fact that no such effect on the β relaxation is observed for the 0.7% BHF nanocomposite (**Figure 5.16b**), where the interparticle distance is much larger due to the larger particle size (compare **Table 5.1**). Instead, the β relaxation there remains unchanged and an additional peak appears centred at around –60 °C. Finally, in the composite with 6% BHF, a very large peak is observed around –130 °C, which completely obscures the β relaxation. The values of the relaxation strength of this peak are three orders of magnitude larger than those of the relaxations of the polymer in this region, and therefore this peak cannot be dipolar in origin. Moreover, at these temperatures the dc ionic conductivity of the matrix is negligible. Thus, this peak must be related to charge movements through the network of filler particles that is formed in this sample. Finally, the ω relaxation is suppressed in the diamond nanocomposites and appears to be shifted to higher temperatures, which may support the conclusion that the heterogeneity of the ER matrix is reduced by the incorporation of the diamond nanoparticles, as indicated by the results shown in **Figure 5.10** and to be discussed in Section 5.6.

It is interesting to compare the results for molecular mobility obtained on the basis of secondary relaxations in this section with those obtained on the basis of the overall dielectric behaviour in the previous section. At first glance there is a contradiction between the conclusion about decreased molecular mobility in the diamond nanocomposites, with respect to the pure matrix polymer, on the basis of the $\varepsilon'(T)$ plots in **Figure 5.11**, and the conclusion about increased mobility based on the TSDC results for the β relaxation in **Figure 5.16**. However, note the different range of measurements. In fact, the conclusion

on increased molecular mobility in the nanocomposites on the basis of the TSDC results for the β relaxation refers to the low temperature of –100 °C and are complementary to the conclusion on decreased mobility in the temperature range of approximately 40–120 °C on the basis of the ε′(*T*) plots in **Figure 5.11**.

5.4.2 Epoxy Resin/Carbon Nanocomposites

Brief information on the preparation of these samples has been given in Section 5.3.3. Effects of NCP on the secondary relaxations were studied by broadband DS and TSDC measurements [54]. In **Figure 5.13** we showed results for the temperature dependence of ε′ and ε″ in the nanocomposites at a constant frequency of 80,805 Hz. Two relaxations, a secondary β relaxation at lower temperatures and the primary α relaxation at higher temperatures, associated with the glass transition of the ER matrix, are observed. For both relaxations the strength (i.e., the magnitude of the peak in ε″(*T*) and the corresponding step in ε′(*T*)) increases in the nanocomposites, in particular for the sample with the highest ϕ value. The timescale (temperature position) of the response shows, however, a different behaviour for the two relaxations. For the local β relaxation it does not change with composition. Thus, the results of DS provide a basis for discussing molecular mobility in terms of the relaxation strength and the timescale of the response. A third source of information, the shape of the loss peak [24, 25], can hardly be evaluated here. The increase of relaxation strength for the β relaxation with increasing filler content in **Figure 5.13** can be understood in terms of increased free volume, in agreement with results obtained with the epoxy resin/diamond nanocomposites in Section 5.4.1, as well as with other nanocomposites [19].

The dynamics of the β relaxation can be further studied on the basis of the Arrhenius plot (activation diagram) shown in **Figure 5.17**. The Arrhenius equation [22–25]:

$$f_{\max} = f_0 \exp\left(-\frac{E_{\text{act}}}{kT}\right) \tag{5.13}$$

where E_{act} is the apparent activation energy, f_0 the pre-exponential frequency factor and k Boltzmann's constant, was fitted to the data, and E_{act} and f_0 determined for each composition. The results show that, although the timescale of the response does not change with the composition, the dynamics does change: E_{act} decreases in the nanocomposites (0.69 eV in ER, compared to 0.51, 0.59 and 0.63 eV in the nanocomposites with 1, 4 and 6% NCP, respectively), the same as the corresponding frequency factor f_0.

Figure 5.18 shows results of TSDC measurements in the pure ER matrix and the three ER/NCP nanocomposites. With respect to **Figure 5.13**, the temperature range of measurements has now been extended to 150 °C to follow the α relaxation and conductivity effects, which will be discussed in Sections 5.5 and 5.6, respectively.

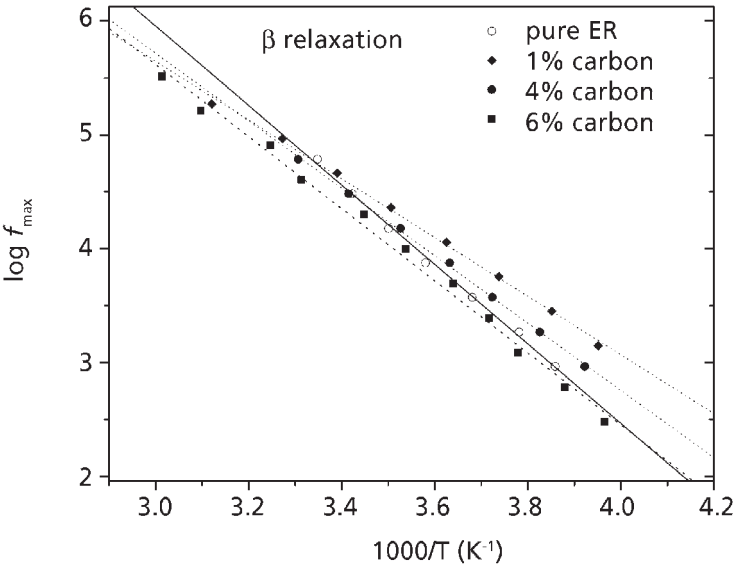

Figure 5.17 Arrhenius plot for the β relaxation in the carbon/epoxy nanocomposites.

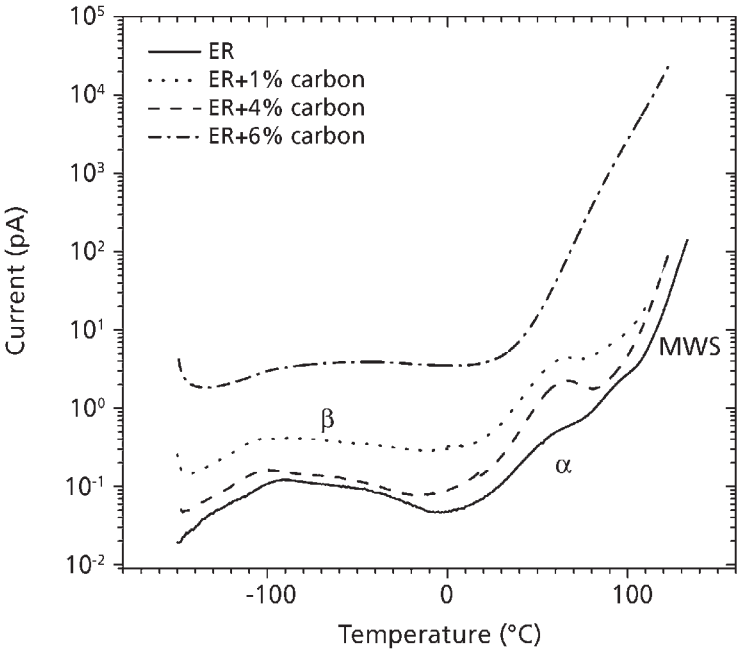

Figure 5.18 TSDC thermograms for the ER/NCP samples indicated on the plot.

For the β relaxation we observe, in agreement with the DS results of **Figure 5.13**, a significant increase of the magnitude of the relaxation, without any systematic change of the temperature position of the peak. Note the logarithmic current scale, as well as the fact that the β relaxation is superimposed on a background, which also increases significantly with increasing filler content and is attributed to interfacial polarisation within the clusters formed by association of the carbon particles. The origin of the background will be discussed in more detail in Section 5.6.

5.4.3 Polyimide/Silica Nanocomposites

Brief information on the preparation of these samples has been given in Section 5.3.4. The dynamics of the secondary γ relaxation in the hybrid nanocomposites was studied in detail by broadband DS and TSDC measurements [62, 63].

Figure 5.19 shows TSDC thermograms recorded on samples of series 5 (molecular mass of PI 5000) in the temperature region of the γ relaxation. The γ relaxation has been assigned to small-scale, local oscillations of imide cycles. With respect to efforts to reduce the dielectric permittivity ε′ of PI for microelectronics applications [58], the investigation of the γ relaxation is of particular importance, as this relaxation is

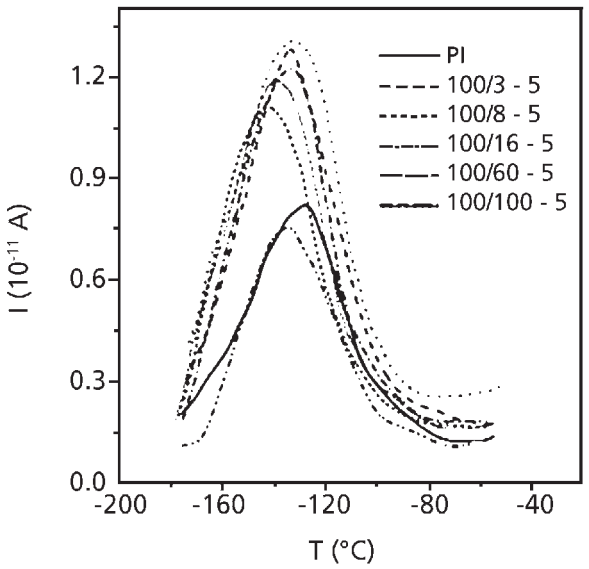

Figure 5.19 TSDC thermograms in the region of the γ relaxation obtained with the samples indicated on the plot.

Reprinted with permission from [63]. ©IOP Publishing, 2005

in the temperature and/or frequency region typical for microelectronics applications. We observed in **Figure 5.15** that this relaxation is in the frequency region of several hundred hertz at room temperature. We observe in **Figure 5.19** a significant increase of the magnitude (relaxation strength $\Delta\varepsilon$) of the relaxation in the nanocomposites and a slight shift to lower temperatures. Similar results were obtained also with DS. They can be explained in terms of loosened packing of PI chain fragments in the nanocomposites due to tethering on the ON particles, resulting in increase of free volume. This effect is more pronounced in the case of short and rigid polymer chains, like PI in the present study, and obviously overcompensates the reduction of molecular mobility imposed by the presence of the ON particles.

Figure 5.20 shows DS results for selected nanocomposites of series 10 (molecular mass of PI 10,000): $\varepsilon''(f)$ plots in the region of the γ relaxation at three temperatures. With respect to comparing these results with those shown in **Figure 5.19**, we recall that the TSDC measurements correspond to measuring dielectric loss ε'' as a function of temperature at a fixed low frequency in the range 10^{-2}–10^{-4} Hz [37, 38]. The main result in **Figure 5.20** is the significant reduction of the magnitude of the relaxation with increasing amount of ON and with respect to pristine PI (not shown in the figure) by far more than the presence of ON, which makes no contribution to the γ relaxation, and additivity would suggest. Our explanation for this behaviour is that, with the

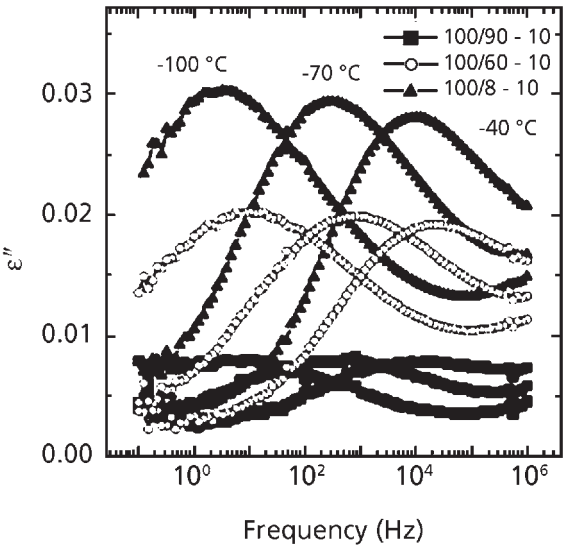

Figure 5.20 Dielectric loss ε'' against frequency in the region of the γ relaxation for the samples and the temperatures indicated on the plot.

Reprinted with permission from [63]. ©IOP Publishing, 2005

longer PI chains of series 10, the increase of free volume due to loosened molecular packing of the chains is overcompensated by the decrease of molecular mobility due to constraints imposed by the presence of the ON particles [62, 63].

The results shown in **Figures 5.19** and **5.20** can be quantified in terms of timescale, magnitude and shape of the response, following methodologies for data treatment described very briefly in Section 5.2.1 and in detail elsewhere [24, 25]. **Figure 5.21** shows the Arrhenius plot for the γ relaxation of the PI/ON hybrids of series 5 [62]. In addition to the DS data (at high frequencies), the TSDC data of **Figure 5.19** have also been included in the plot at the equivalent frequency of 1.6×10^{-3} Hz, corresponding to a relaxation time of 100 s [37, 28, 46]. The Arrhenius equation (5.13), characteristic of relaxation processes thermally activated over a barrier, has been fitted to the data. Both the apparent activation energy E_{act} and the frequency factor f_0 showed a tendency to decrease with increasing ON content [62]. Interestingly, a decrease of the apparent activation energy E_{act} without any significant change of the timescale of the response (temperature and/or frequency position of the loss peak) was observed also for the secondary β relaxation in epoxy resin/carbon nanocomposites (**Figure 5.17**).

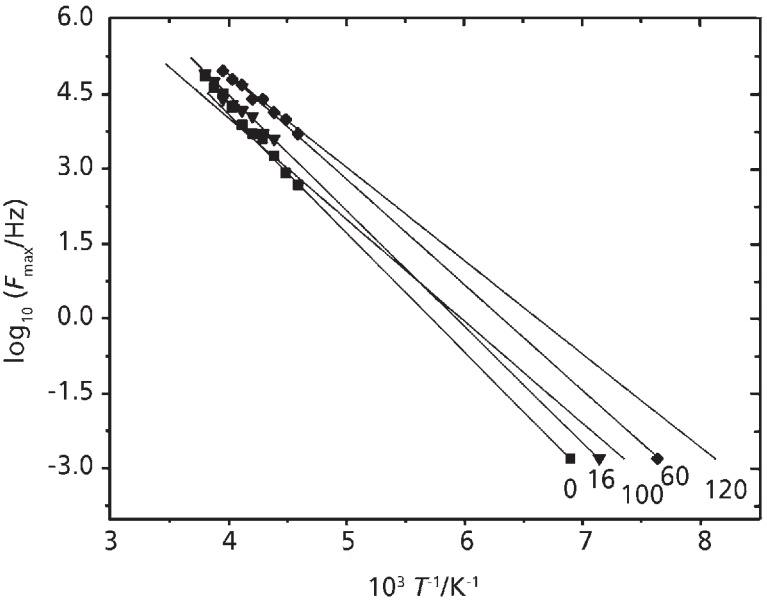

Figure 5.21 Arrhenius plot for the γ relaxation in the PI/ON hybrids. The numbers refer to the MTS content.

Reprinted with permission from [62]. ©John Wiley & Sons, Inc., 2004

Similar results to those shown in **Figure 5.19** were obtained, by both broadband DS and TSDC measurements, with a different series of PI/silica nanocomposites, synthesised from *p*-aminophenyltrimethoxysilane-terminated polyamic acids as PI precursors and tetramethoxysilane as silica precursor via a sol–gel process [19]. Also in that case the chains were covalently bound on the silica nanoparticles, the dimensions of the latter being in the range of about 100 nm, as revealed by electron microscopy. Three series of samples with molecular mass of PI 5,000, 7,500 and 10,000 were investigated. The magnitude of the γ relaxation was found to increase in the nanocomposites, whereas the timescale of the response remained practically unchanged. To further follow the hypothesis that increase of free volume due to loosened molecular packing of the chains was at the origin of the enhancement of the relaxation, water sorption of the nanocomposites from the vapour phase was measured and found to increase with increasing silica content and with respect to pristine PI [19]. This result is consistent with increase of free volume in the nanocomposites. At the same time, the hypothesis of reduction of chain mobility due to tethering on the silica nanoparticles was confirmed by following the glass transition in the nanocomposites by differential scanning calorimetry (DSC) and degradation of PI by thermogravimetric analysis (TGA). Both techniques provided evidence that segmental mobility and large-scale motion of the PI chains are reduced in the nanocomposites.

Thus, the picture emerging from these studies with the hybrid organic–inorganic nanocomposites is that of contradictory effects of the presence of and interactions with the inorganic nanoparticles on chain mobility: increase of free volume due to loosened molecular packing of the chains and, at the same time, constraints to the motion imposed by the inorganic nanoparticles. For small-scale, local motions (secondary relaxations) increase of free volume dominates, however only at low molecular masses of the polymer matrix (short chains). For large-scale, segmental motions (glass transition and degradation), on the other hand, the constraints imposed by the rigid nanoparticles dominate the behaviour, in particular for shorter chains. Note that secondary relaxations and primary α relaxation are active in different temperature regions, and information on molecular mobility provided by these relaxations refers to the temperature region where they are studied. We will come back to this latter point in the next section.

5.5 Primary α Relaxation and Glass Transition

In contrast to the effects of nanoparticles on small-scale, secondary relaxations of the polymer matrix, discussed in Section 5.4, much attention has been devoted in the literature to the investigation of effects on large-scale, segmental dynamics and the glass transition. The main reason for this is that it is generally agreed upon that modification of large-scale, segmental dynamics by the presence of and interactions with the filler surface is at the origin of the significant improvement of the properties of nanocomposites, in particular mechanical and thermal properties, as compared to conventional micro- and

macroscale composites and the pure matrix [19]. Due to the large surface-to-volume ratio of the nanoparticles, the polymer close to the interface constitutes a significant fraction of the material, and its behaviour significantly affects or even dominates the properties of the nanocomposites. However, experimental results on segmental dynamics and glass transition in nanocomposites are not conclusive concerning the mechanism and the details of this modification [8].

Several studies on polymer nanocomposites show a single glass transition temperature T_g, indicating single dynamics of the entire volume of the polymer. Very often T_g increases, as compared to the pure matrix, suggesting that the mobility of the entire volume of the polymer is restricted by the presence of the nanoparticles [65–67]. However, reduction of T_g has also been reported [18, 68, 69] in the case of weak interactions between filler and polymer, whereas in many cases the addition of nanoparticles causes no significant change to the glass transition of the polymer, presumably because effects causing increase and decrease of polymer mobility are present simultaneously and effectively cancel out [8, 19].

There are, however, many experimental results suggesting that the restriction of chain mobility caused by the nanoparticles does not extend throughout the material, but affects only the chains within a few nanometres of the filler surface, in relation to the presence of an interfacial polymer layer around the filler, with structure, morphology and chain dynamics modified with respect to the bulk polymer matrix, as mentioned in the introduction to this chapter. The existence of such an interfacial layer seems relatively well established in the case of silica-filled elastomers, as will be discussed in more detail in Section 5.5.4. However, its exact nature is not well understood: experimental results have been described in terms of one or two distinct interfacial layers or a gradual change in dynamics with changing distance from the particle. Thus, Tsagaropoulos and Eisenberg [4, 70] interpreted their observation of a second loss peak in dynamic mechanical measurements in several polymers filled with silica nanoparticles, located at 50–100 °C above the glass transition of the polymer matrix, in terms of a model, where there are three types of polymer: a strongly bound, immobile layer immediately surrounding the particle, which does not participate in the glass transition; a second, loosely bound interfacial layer, which is responsible for the second glass transition (at higher temperatures); and quasi-bulk polymer unaffected by the particle. This model is able to account for the observed reduction of the intensity of the second glass transition with increasing silica content. NMR measurements also support the existence of three types of polymer in silica nanocomposites [17]. On the other hand, results obtained with silica nanocomposites by both neutron scattering [71] and dynamic mechanical measurements [6, 72] are well described by a two-layer (interfacial and bulk) model. Finally, other studies provide evidence for a continuous distribution of glass transition temperatures or polymer mobilities as a function of the distance from the particle surface [5], in agreement also with results of molecular dynamics simulations [73].

In the following, the discussion of the effects of the presence of and interactions with nanoparticles on the primary α relaxation associated with the glass transition of the

polymer matrix will be based on results obtained with thermoset nanocomposites (epoxy resins reinforced with layered silicates, diamond, magnetic nanoparticles and carbon nanoparticles) and, for comparison, with polydimethylsiloxane reinforced with sol–gel derived silica nanoparticles.

5.5.1 Epoxy Resin/Layered Silicate Nanocomposites

Brief information on the preparation of these samples has been given in Section 5.3.1. The results of dielectric studies in **Figures 5.4-5.7** are not very conclusive with respect to the segmental α relaxation, corresponding to the glass transition (dynamic glass transition). The main reason for this is that the corresponding loss peak in **Figures 5.5** and **5.7** is masked by conductivity. However, indications for the temperature region of the glass transition are provided by the rate of variation of $\varepsilon'(f)$ with temperature in **Figures 5.4** and **5.6**, as briefly discussed in Section 5.1. **Figure 5.8** showed results for the temperature dependence of ε′ in ER matrix and the three nanocomposites at a fixed high frequency of 10^5 Hz. The step in $\varepsilon'(T)$ at around 60 °C in pure ER and at higher temperatures in the nanocomposites corresponds to the dynamic glass transition. This interpretation is based on the well-established fact that molecular dipoles that are frozen in the glassy state and thus do not contribute to ε′ become mobile and contribute to ε′ in the rubbery state. **Figure 5.22** shows the corresponding $\varepsilon''(T)$ plot. Conductivity effects at the high frequency of presentation of 10^5 Hz are, to a significant extent, suppressed and the α loss peak becomes visible. This peak is at about 90 °C in pure ER and is shifted, by about 20–40 °C, to higher temperatures in the nanocomposites, whereas at the same time it becomes less clear. Obviously, the glass transition temperature T_g is located at a lower temperature than the α loss peak in **Figure 5.22**, bearing in mind the convention that T_g may be determined from dielectric measurements as the temperature where the relaxation time of the α relaxation becomes equal to 100 s, corresponding to a peak frequency of 1.6×10^{-3} Hz [38, 44].

Thus, the results of dielectric studies in the ER/clay nanocomposites clearly indicate restriction of segmental dynamics in the nanocomposites, as compared to the pure matrix. The quality of dielectric data, in particular the large contribution of conductivity and of space charge polarisation to ε′ and ε″, precludes the discussion of the data in terms of a model. It is interesting to note, however, that the results in **Figures 5.8** and **5.22** appear incompatible with any model, where a significant part of the polymer in the nanocomposites has segmental dynamics similar to that of the pure matrix.

5.5.2 Epoxy Resin Reinforced With Diamond and Magnetic Nanoparticles

Brief information on the preparation of these samples has been given in Section 5.3.2 and the samples investigated are listed in **Table 5.1**. Similar to the results for the epoxy

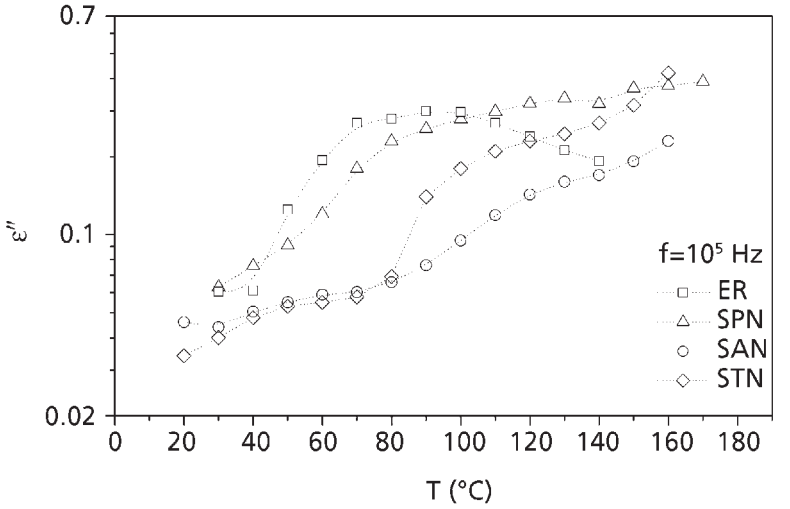

Figure 5.22 Dielectric loss ε″ against temperature *T* of the samples indicated on the plot at 10^5 Hz.

Reprinted with permission from [41]. ©Elsevier Science, 2002

resin/layered silicate nanocomposites discussed in Section 5.5.1, the α relaxation in the epoxy resin nanocomposites with diamond and magnetic inclusions is masked by conductivity and space charge polarisation (**Figure 5.10**). However, the isochronal ε′(*T*) for the diamond nanocomposites in **Figure 5.11** and the magnetic BHF nanocomposites in **Figure 5.12** provide evidence, on the same arguments as for the clay nanocomposites in Section 5.5.1, that in the nanocomposites the α relaxation, and thus the glass transition, is shifted to higher temperatures, as compared to the pure epoxy resin matrix.

For the diamond nanocomposites the shift of the α relaxation and of the glass transition to higher temperatures with respect to the pure epoxy resin matrix is more clearly observed in the isochronal ε″(*f*) plot of **Figure 5.23**. The α loss peak (the dynamic glass transition) at the frequency of representation of 10^5 Hz in **Figure 5.23** is shifted from about 90 °C in the pure ER matrix to about 130 °C in the two diamond nanocomposites. In addition to that clear shift, two more comments are in order with respect to **Figure 5.23**. The first is that the whole α loss peak is shifted to higher temperatures in the nanocomposites and there is no indication of a second loss peak located at the temperature of the α loss peak in the pure matrix. Thus, with respect to the ongoing discussion in the literature about the effects of the nanoparticles on segmental dynamics and the glass transition of the polymer matrix, the results in **Figure 5.23** indicate that in the diamond nanocomposites these effects are not limited to a surface layer around the nanoparticles. On the contrary, the molecular mobility of the whole matrix is (severely)

restricted in the nanocomposites. The second comment with respect to **Figure 5.23** refers to the observation that the shift to higher temperatures and the shape of the α loss peak is the same for the two nanocomposites, despite the different content of nanoparticles (0.5% against 1.2%) and the different mean distance between the particles (**Table 5.1**). We will come back to this point later in this section.

Despite the strong contribution of conductivity and space charge polarisation to the $\varepsilon'(f)$ and $\varepsilon''(f)$ data in **Figure 5.10**, the dynamics of the α relaxation could be analysed. It is possible, under certain conditions, for a relaxation, where the $\varepsilon''(f)$ loss peak is completely masked by dc conductivity, to eliminate the conductivity contribution by calculating $\varepsilon''(f)$ by a derivative method from the measured $\varepsilon'(f)$, where dc conductivity makes no contribution [74]. We followed that method and for the ER matrix and the nanocomposites at selected temperatures, where the contribution of the dc conductivity to $\varepsilon'(f)$ appeared negligible, calculated $\varepsilon''(f)$ by [74]:

$$\varepsilon''_{der} = -\frac{\pi}{2}\frac{\partial\varepsilon'(\omega)}{\partial\ln(\omega)} \approx \varepsilon''_{rel} \tag{5.14}$$

where $\omega = 2\pi f$. The frequency of the maximum of the dielectric loss f_{max} for the α relaxation was obtained from the calculated spectra at each temperature and is plotted in

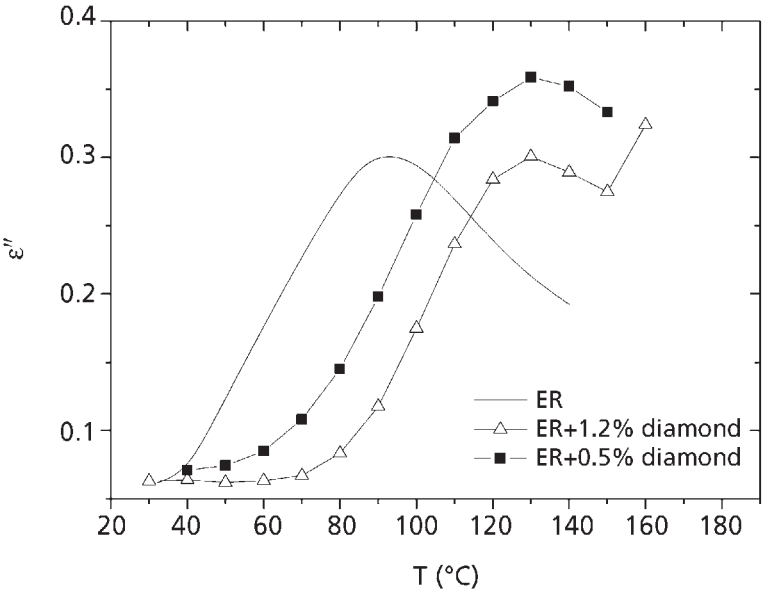

Figure 5.23 Dielectric losses ε'' against temperature for the samples indicated on the plot (at 10^5 Hz).

the Arrhenius diagram (activation diagram) of **Figure 5.24**. The temperature dependence of f_{max} is well described by the Vogel–Tammann–Fulcher (VTF) equation [44]:

$$f_{max} = A\exp\left[-\left(\frac{B}{T-T_0}\right)\right] \tag{5.15}$$

where A, B and T_0 (Vogel temperature) are temperature-independent empirical constants. The α relaxation is significantly slower in all the nanocomposites as compared to the matrix; note, however, that doubling the volume fraction of the filler from 0.5% to 1.2% or increasing the particle size (100 nm for the BHF inclusions as compared to the 6 nm diamond) seems to affect the α relaxation dynamics only slightly. The glass transition temperatures indicated by DRS measurements, calculated by extrapolating the data in **Figure 5.24** to a relaxation time of 100 s (equivalent frequency of 1.6×10^{-3} Hz) [38, 44], are 47 °C for the pure ER and about 80 °C for the nanocomposites.

Thus, both the isochronal $\varepsilon''(T)$ results in **Figure 5.23** and the results shown in the Arrhenius plot, obtained independently from each other (in the sense that the former were obtained from the measured $\varepsilon''(f)$, whereas the latter were from the $\varepsilon'(f)$ data), show a significant restriction of segmental dynamics and a significant reduction of glass transition temperature T_g in the nanocomposites, as compared to the pure matrix. It is

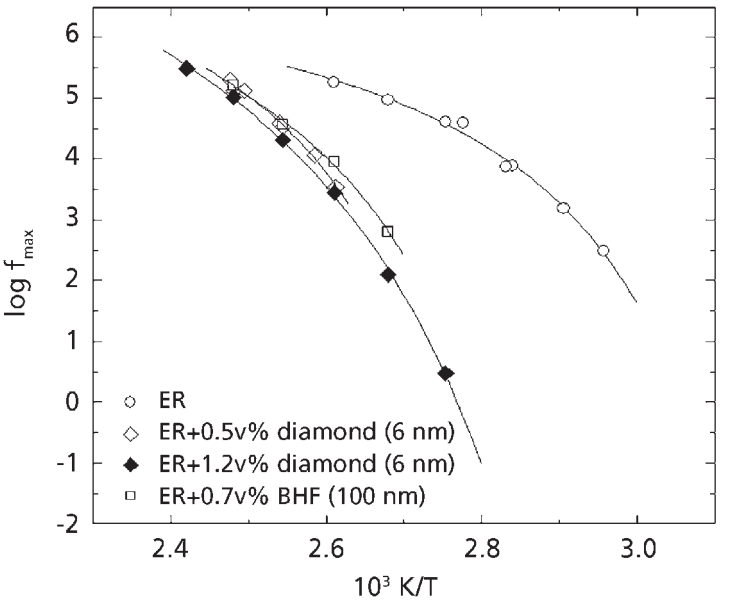

Figure 5.24 Arrhenius plot for the α relaxation of the ER matrix and the nanocomposites indicated on the plot. The lines are fits of Equation (5.15).

interesting to note that a severe restriction of segmental dynamics and a significant shift of T_g to higher temperatures, as compared to the pure ER matrix, was observed also in the layered silicate nanocomposites of the same matrix in Section 5.5.1. As mentioned in the introduction to Section 5.5, such changes in T_g are usually discussed in terms of a layer of polymer with reduced mobility (bound polymer) around the filler particles, with a thickness of the order of a few nanometres. When the interparticle distance becomes comparable to the thickness of this interfacial layer, it will constitute a large volume fraction of the overall material and its properties will dominate the bulk properties of the material. Note, however, that for the 0.7% BHF sample the interparticle distance (**Table 5.1**) is much larger than typical values obtained for the thickness of the interfacial layer found in the literature (a few nanometres), even assuming that the particles have been completely dispersed in the matrix. It cannot be excluded, however, that curing of the polymer in the presence of the nanoparticles (the method of preparation followed here) has a direct influence on the structure and the properties of the matrix. It is interesting to note in this connection that the degree of dispersion of silica nanoparticles generated *in situ* by the sol–gel process was found to be significantly different when the sol–gel processing was conducted before or after the crosslinking reaction [75].

5.5.3 Epoxy Resin/Carbon Nanocomposites

Brief information on the preparation of these samples has been given in Section 5.3.3. The α relaxation, associated with the glass transition, was followed in the TSDC thermograms of **Figure 5.18** and the isochronal $\varepsilon'(T)$ and $\varepsilon''(T)$ plots of **Figure 5.13**. In the TSDC thermograms the α peak appears at about 60–70 °C. Bearing in mind that TSDC and DSC are characterised by comparable timescales (equivalent frequencies) [37, 38, 44] and the well-established fact that the temperature position of the TSDC α peak is a good measure of the calorimetric T_g [26, 38], we may conclude that T_g of ER and the nanocomposites is in the range 60–70 °C. The TSDC results are not very conclusive with respect to changes in the temperature position (timescale) and the magnitude (relaxation strength) of the α relaxation in the nanocomposites, as compared to the pure matrix, as the α peak overlaps with, and at higher filler content is masked by, conductivity (**Figure 5.18**, note the logarithmic current scale). More information about these issues can be extracted from the isochronal $\varepsilon'(T)$ and $\varepsilon''(T)$ plots of **Figure 5.13** (and similar plots at other frequencies, selected high enough to suppress conductivity).

Two relaxations, a secondary β relaxation at lower temperatures and the primary α relaxation at higher temperatures, associated with the glass transition of the ER matrix, are observed in **Figure 5.13** [54]. The β relaxation has been discussed in Section 5.4.2. For both relaxations the strength (i.e., the magnitude of the peak in $\varepsilon''(T)$ and the corresponding step in $\varepsilon'(T)$) increases in the nanocomposites, in particular for the sample above the percolation threshold. The timescale (temperature position) of the response shows, however, a different behaviour. Whereas for the local β relaxation

it does not change with the composition, for the cooperative α relaxation the peak temperature increases slightly in the nanocomposites, in particular at higher filler contents, where it shifts out of the temperature range of **Figure 5.13**. It should be mentioned here that measurements at higher temperatures and/or lower frequencies are less conclusive for the higher-content nanocomposites, as the results are masked by conductivity effects. Thus, the results of DRS allow molecular mobility to be discussed in terms of the relaxation strength and the timescale of the response. The increase of relaxation strength for the α relaxation, as well as for the β relaxation, can be understood in terms of increased free volume, in agreement with results obtained with other nanocomposites [19]. The slowing down of the cooperative α relaxation (dynamic glass transition) provides additional evidence for immobilisation of polymer chains in the interface layer around the particles (formation of bound polymer).

The dynamics of both dielectric relaxations was further studied on the basis of the Arrhenius plot (activation diagram) shown in **Figure 5.25**. Results in this figure refer only to dipolar relaxations. Conductivity effects have been eliminated by fitting an appropriate expression to the dielectric data, following common practice in the analysis of dielectric measurements [8, 26]. For the β relaxation the DS results have already been shown in **Figure 5.17** and discussed in Section 5.4.2. In the Arrhenius

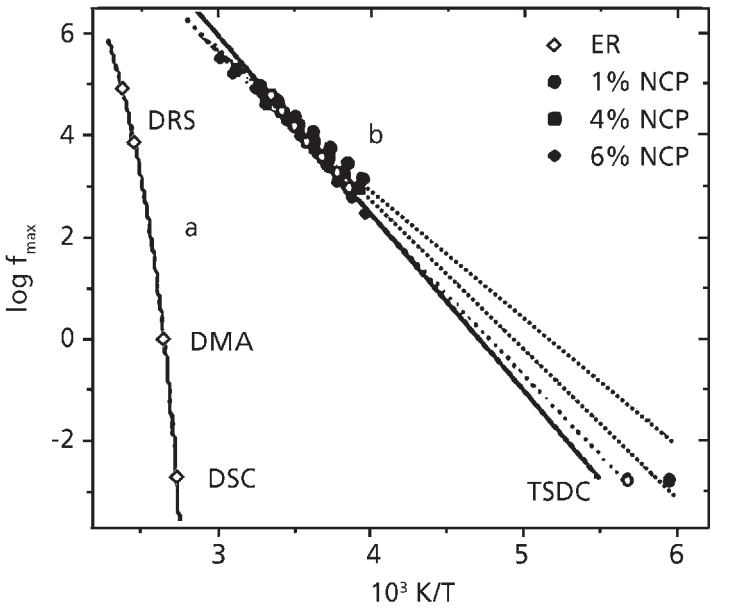

Figure 5.25 Arrhenius plot of (a) α and (b) β relaxations. The lines are fits of the VTF and Arrhenius equations, respectively, to the experimental data.

Reprinted with permission from [54]. ©John Wiley & Sons, Inc., 2005

plot of **Figure 5.25** we have included also TSDC data, given by the peak temperature of the TSDC α peak at the equivalent frequency of 1.6×10^{-3} Hz [38, 44]. The TSDC data, although at a single frequency, provide the possibility to significantly extend the frequency and/or temperature range of the plot and further support for the accuracy of activation energy determination. Besides, they are in rather good agreement with the DS data recorded at frequencies 5–8 orders of magnitude higher. For the α relaxation, where less dielectric data are available with the required accuracy, because of conductivity contributions, we show only the plot for the pure ER matrix with two DS points, as well as two points determined by DSC and DMA [54]. The DSC point is at the equivalent frequency of about 10^{-3} Hz, determined by the cooling rate of the DSC measurements and the mean temperature fluctuation [36, 76, 77], whereas the DMA data were recorded at 1 Hz [54]. The VTF equation (5.15) has been fitted to the data. The fit is good (note the broad frequency range covered) with reasonable values of the fitting parameters, providing support for the consistency of the three techniques involved [36].

5.5.4 Polydimethylsiloxane/Silica Nanocomposites

Polydimethylsiloxane (PDMS)/silica nanocomposites have proved to be an ideal system for investigating the effects of nanoparticles on polymer dynamics, in particular segmental dynamics, by dielectric techniques, as dc conductivity and conductivity effects are negligible [8]. Details of the preparation of the unfilled, crosslinked PDMS and of the nanocomposites, by a sol–gel process in the presence of the crosslinked PDMS, have been given elsewhere [8, 78]. Scanning electron microscope (SEM) images indicated good dispersion of silica in the PDMS matrix, with the diameter of the silica nanoparticles of about 10 nm [78]. The amount of filler incorporated into the network, calculated from the weights of the films (of about 1 mm thickness) before and after the generation of the filler, is listed in **Table 5.2**.

Table 5.2 Silica content by weight and volume, degree of crystallinity x_c, volume fraction of interfacial polymer x_{int}, and estimated thickness d of the interfacial layer around the filler particles

Sample	wt%	vol%	x_c	x_{int}	d (nm)
PDMS	0	0	0.61		
PDMS + 9.7% silica	9.7	6.1	0.44	0.13	2.3
PDMS + 14.1% silica	14.1	9.1	0.37	0.21	2.4
PDMS + 15.3% silica	15.3	9.9	0.40	0.22	2.3
PDMS + 23.5% silica	23.5	15.7	0.34	0.29	2.1

Figure 5.26 shows TSDC thermograms obtained for pure PDMS and the PDMS/silica nanocomposites in the temperature region of the glass transition. For the pure PDMS a single α peak is observed at –123 °C, in very good agreement with DSC measurements on the same sample [8]. For the nanocomposites the α relaxation is observed at the same temperature but with higher intensity due to decrease in crystallinity, resulting from constraints to crystallisation imposed by the presence of the nanoparticles and studied by DSC [8]. In addition, a shoulder appears on the high-temperature side of the main peak extending up to approximately 30 °C, its intensity increasing with increasing silica content. The shoulder in the TSDC thermograms of the nanocomposites is assigned to the α relaxation of PDMS chains in an interfacial layer close to the silica particles, where chain mobility is constrained due to interaction with the surface of the particles. The main relaxation at –123 °C in the composites is then assigned to the α relaxation of the PDMS chains that are sufficiently far from the filler surface as to exhibit quasi-bulk behaviour [8].

The thermal sampling (TS) technique, a special TSDC technique for experimentally analysing complex relaxations into approximately single responses [37, 38], was used to determine experimentally whether the TSDC signal corresponds to two distinct glass

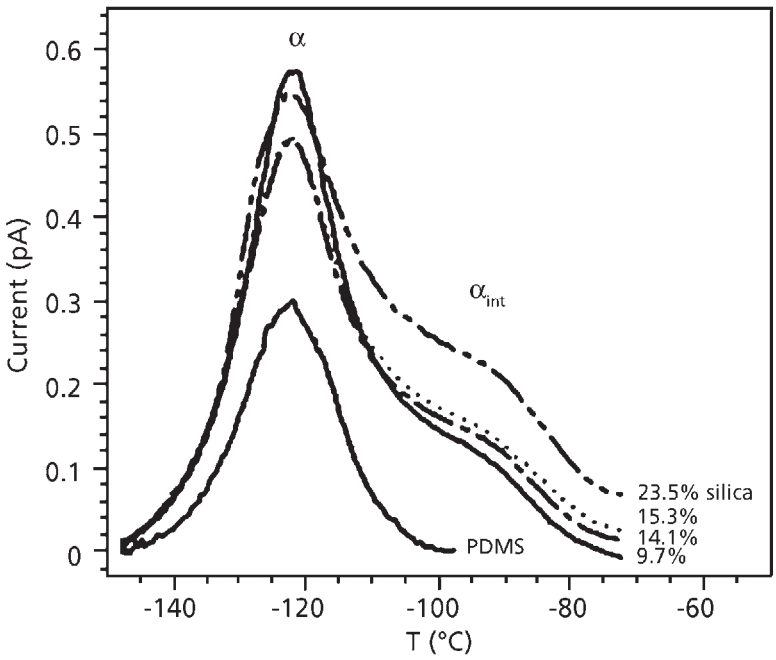

Figure 5.26 TSDC thermograms for PDMS and PDMS/silica nanocomposites in the region of the glass transition.

Reprinted with permission from [8]. ©Elsevier Science, 2005

transitions or to a continuous distribution of T_g values. In the TS results in **Figure 5.27** no sign of a double peak is observed in any of the TS responses. Moreover, the maximum current *versus* polarisation temperature shows a maximum, at the position of the bulk α relaxation, and decreases gradually at higher temperatures without showing a second maximum. These results indicate that the interfacial layer exhibits a continuous distribution of glass transition temperatures between the T_g of bulk PDMS (–123 °C) and approximately –90 °C. The inset to **Figure 5.27** shows the corresponding apparent activation energies obtained from the initial rise portion of each peak [37, 38]. The apparent activation energy in the temperature region of the shoulder is found to be smaller than the value in the region of the bulk α relaxation [8].

The fraction of PDMS with slower segmental dynamics, as compared to the bulk PDMS, was determined from the relative area of the main relaxation and the shoulder, and is listed in **Table 5.2**. From these values the thickness *d* of the interfacial layer around the nanoparticles was determined to 2.0–2.5 nm (**Table 5.2**), by considering the interfacial region as a spherical shell around each particle, neglecting the overlap of regions belonging to neighbouring particles. The values found for *d* are within the range of

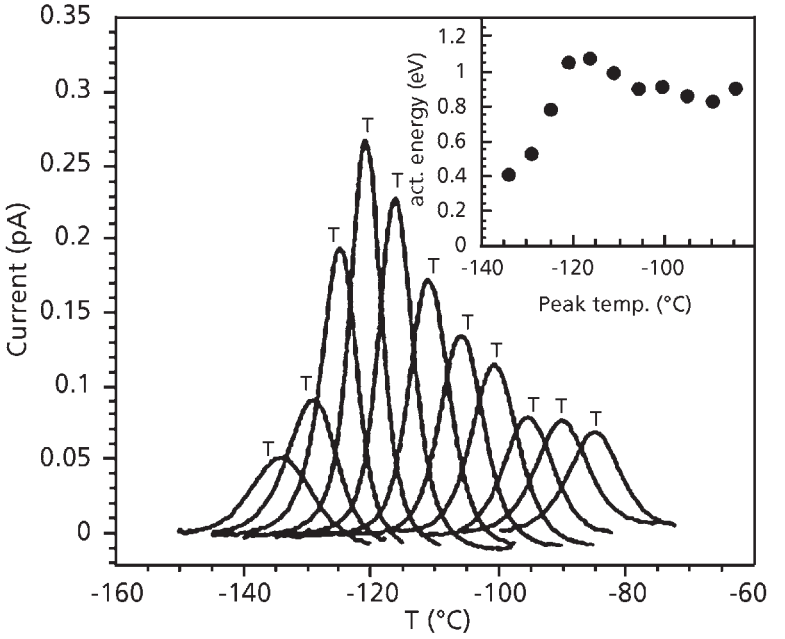

Figure 5.27 Thermal sampling curves for PDMS + 23.5% silica and apparent activation energy calculated from them (inset). The arrows show the polarisation temperature corresponding to each curve.

Reprinted with permission from [8]. ©Elsevier Science, 2005

values determined for PDMS/silica systems by various techniques [8]. Also, the TSDC results are better described by a simple two-layer model (interfacial and bulk) than by a three-layer model (bound, interfacial and bulk) [8].

Broadband DS was used to investigate the molecular dynamics in the bulk and interfacial layers by following the temperature dependence of the corresponding dielectric relaxations. **Figure 5.28** shows a representative dielectric spectrum for a PDMS/silica nanocomposite in the temperature region of the α relaxation [8]. Two loss peaks are visible at each temperature, assigned, in order of increasing frequency, to the α relaxation of the interfacial layer and of the bulk PDMS. However, a sum of three relaxations was necessary to reproduce the shape of the spectra, the third, weak relaxation being assigned to conductivity on the surface of the silica particles due to adsorbed water molecules [8]. The spectra for the other composites are similar to those in **Figure 5.28**, differing only in the relative magnitudes of the three relaxations.

Figure 5.29 shows the Arrhenius plot of the three relaxations, with TSDC data at the equivalent frequency of 1.6×10^{-3} Hz, corresponding to a relaxation time of

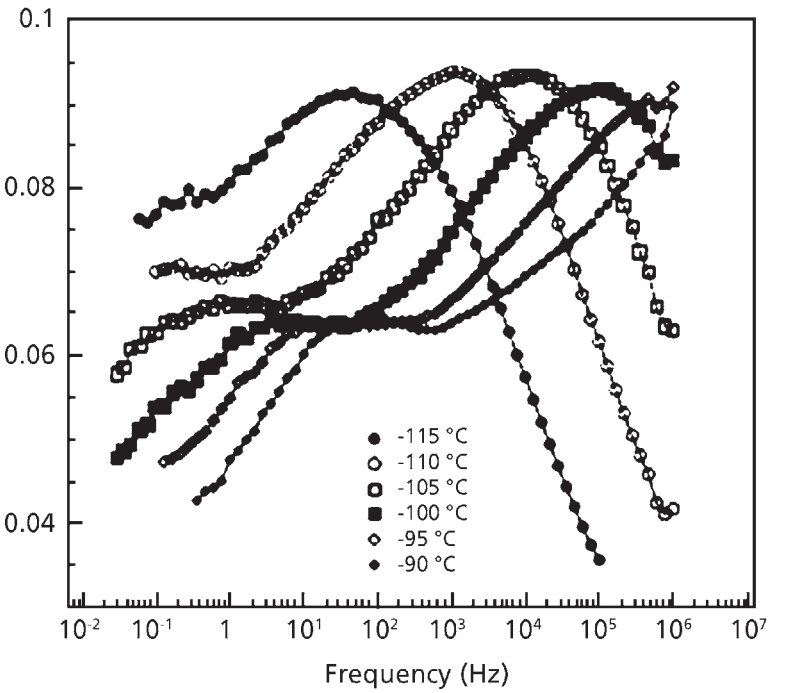

Figure 5.28 Dielectric loss ε″ versus frequency *f* for PDMS + 15.3% silica for the temperatures shown on the plot.

Reprinted with permission from [8]. ©Elsevier Science, 2005

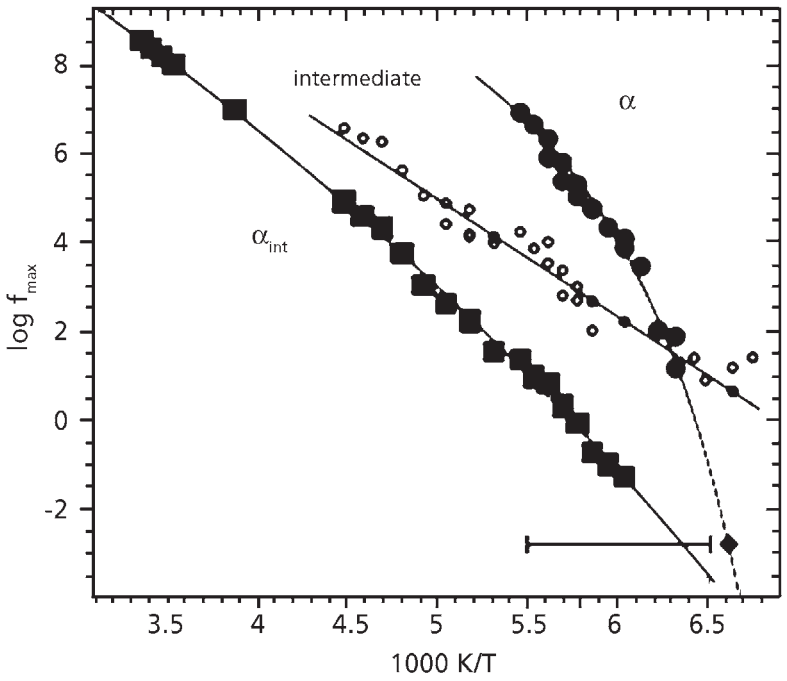

Figure 5.29 Arrhenius plot for the sample PDMS + 15.3% silica. The filled diamond (bottom right) corresponds to the temperature of the main peak in the TSDC thermogram and the horizontal bar to the TSDC shoulder; both have been placed at an equivalent frequency of 1.6 mHz. The lines are fits of Equation (5.15) for the two α relaxations and of Equation (5.13) for the intermediate relaxation.

Reprinted with permission from [8]. ©Elsevier Science, 2005

100 s, being included. The relaxation at high frequencies is in very good agreement with the quasi-bulk α relaxation in the TSDC data, whereas the low-frequency relaxation, α_{int}, corresponds to the TSDC shoulder. The weak intermediate relaxation has an Arrhenius temperature dependence (Equation (5.13)), whereas the other two relaxations are described by the VTF equation (Equation (5.15)). At high temperatures the α and α_{int} relaxations are well separated, their relaxation times differing by 3–4 decades. However, the interfacial relaxation has a weaker temperature dependence than the bulk α relaxation and a smaller curvature, having an almost Arrhenius behaviour. Thus, at lower temperatures and lower frequencies, approaching the glass transition, the α_{int} relaxation tends to converge with the bulk α. This behaviour is in agreement with the TSDC results, which correspond to lower frequencies (10^{-3} Hz) than those accessible with DS, and where the α_{int} relaxation appears as a shoulder on the α peak.

At first glance, there is an apparent inconsistency between the TSDC results, where there is no well-defined second T_g but a continuous distribution, and the DS results, where a distinct second α relaxation several decades slower is observed. This behaviour can be explained in terms of the interplay between the cooperativity length of the glass transition ξ [44] and the thickness *d* of the interfacial layer. At the glass transition these two characteristic lengths are comparable; however, with increasing temperature, *d* is found to be relatively constant but ξ decreases significantly, allowing the appearance of a second distinct relaxation.

5.6 Conductivity and Conductivity Effects

Electrical conductivity and conductivity effects, such as space charge polarisation and electrode polarisation, are usually considered as sources of problems in dielectric measurements, as they give rise to large values of stored polarisation and of losses, which may mask the bulk response of the dielectric material under investigation. When DS in the frequency domain, the most familiar dielectric technique, is employed to investigate polymer dynamics, conductivity, arising from intrinsic charge carriers and/or impurities, may give rise to high values of ε′ and ε″, in particular at low frequencies and high temperatures, which often mask the α relaxation. Examples of that behaviour were shown earlier in this chapter (**Figures 5.4–5.7**). On the other hand, the investigation of dc conductivity and conductivity effects may provide essential information on dynamics, often also on morphology, of the material under investigation. This is particularly true for polymeric systems, where ionic conductivity at temperatures higher than T_g is typically governed by the motion of the polymeric chains, so that its investigation may reveal significant aspects of chain dynamics, in particular segmental dynamics [22–24, 79, 80]. In addition, the investigation of conductivity and conductivity effects may reveal significant information on morphology, as the moving ions probe local morphology. Examples of that use of DS in thermoset nanocomposites will be given in this section on the basis of results obtained with an ER matrix reinforced with layered silicates and diamond, magnetic and carbon nanoparticles.

5.6.1 Epoxy Resin/Layered Silicate Nanocomposites

Brief information on the preparation of these samples has been given in Section 5.3.1. The $\varepsilon'(f)$ and $\varepsilon''(f)$ data at several temperatures in **Figures 5.4** and **5.5** for the pure ER matrix and in **Figures 5.6** and **5.7** for the SPN nanocomposite, as well as similar results obtained with the SAN and STN nanocomposites, indicated large effects of conductivity, giving rise to very high values of both ε′ and ε″, in particular at low frequencies and high temperatures. At low frequencies and high temperatures, the slope of $\varepsilon''(f)$ is –1, which is characteristic for dc conductivity, as follows from Equation (5.10). These results are confirmed by the corresponding ac conductivity plots (actually the real part of the

complex ac conductivity), $\sigma_{ac}(f)$, shown in **Figure 5.30** for the ER matrix and the SPN nanocomposite [41]. The plots exhibit, for both samples, a dc conductivity plateau at low frequencies and/or high temperatures and a step at 10^1–10^3 Hz.

We discuss first the absolute values of dc conductivity, σ_{dc}, in **Figure 5.30.** The temperature dependence of σ_{dc} will be studied later on the basis of Arrhenius plots. Our interest here is related to molecular mobility. In Section 5.3.1 we made use of $\varepsilon'(T)$ (**Figure 5.8**) to show that molecular mobility decreases in the nanocomposites, as compared to the pure matrix. The reduction of molecular mobility in the nanocomposites can be quantified by means of other measures too, in addition to $\varepsilon'(T)$, each measure stressing a different aspect of that reduction. Here we make use of dc conductivity (actually, for that we take σ_{ac} at 10^{-1} Hz, representative for σ_{dc}). We observe that, for the same temperature, σ_{dc} is lower in the nanocomposite, this effect being more pronounced at intermediate temperatures, e.g., σ_{dc} is about 5×10^{-11} S/cm at 100 °C in ER and only 1×10^{-11} S/cm in SPN at the same temperature. Although dc conductivity is determined not only by the mobility of charge carriers, but also by their concentration, and the latter may change with the composition of the samples, we consider that there is an analogy between the decrease of conductivity in the clay nanocomposites and their improved barrier properties to small molecules [1, 3].

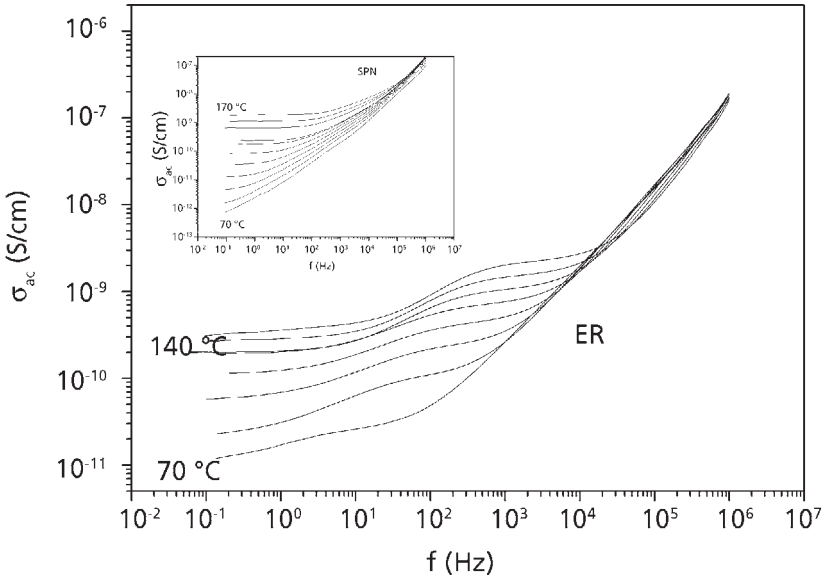

Figure 5.30 Real part of the ac conductivity σ_{ac} against frequency f for the ER matrix at temperatures between 70 and 140 °C in steps of 10 °C. The inset shows a similar plot for the SPN nanocomposite in the range 70–170 °C.

Reprinted with permission from [41]. ©Elsevier Science, 2002

The second point we would like to discuss with respect to **Figure 5.30** and the corresponding $\varepsilon'(f)$ and $\varepsilon''(f)$ plots in **Figures 5.4–5.7** is the structure observed in the frequency region 10^1–10^3 Hz, in the form of a shoulder in $\varepsilon''(f)$ and in $\sigma_{ac}(f)$ and of a step in $\varepsilon'(f)$. The step and the shoulder are indicative of the so-called conductivity current relaxation (CCR) [41, 45]. A model has been proposed in the literature, which accounts for the features of the effects observed here, in particular for the temperature independence of the height of the $\varepsilon'(f)$ step [81]. According to this model, the polarisation mechanism is assigned to the accumulation of charges at the interfaces between regions of different conductivity under conditions of dc conductivity for the sample as a whole. The model has been successfully used to correlate dielectric relaxations with morphological characteristics in various heterogeneous systems, including hydrogels and ionomers [46, 82]. The presence of CCR in the spectra of ER suggests a large-scale heterogeneity of the structure of the pure ER matrix, in agreement with results obtained by other techniques, including water sorption and/or diffusion [83].

The data for the CCR process were further analysed by fitting the sum of a Havriliak–Negami (HN) expression of the type in Equation (5.5) for the CCR process and a conductivity term to the experimental $\varepsilon''(f)$ data of **Figure 5.5** [41]:

$$\varepsilon''(f) = \frac{\sigma_{dc}}{\varepsilon_0 2\pi f} - \mathrm{Im}\left\{\frac{\Delta\varepsilon}{[(1+\mathrm{i}f/f_0)^{1-a}]^{\beta}}\right\} \qquad (5.16)$$

In Equation (5.16) σ_{dc} is the dc conductivity and ε_0 is the vacuum permittivity, whereas the parameters of the HN term have been introduced in Section 5.2.1. At first glance, it may look surprising that no term for the α relaxation at frequencies higher than those of the CCR process was added to Equation (5.16). Note, however, the low values of ε'' in the region of the α relaxation (**Figure 5.22**), as compared to the large ε'' values in the region of the CCR process.

The results of the analysis show that at each temperature between 100 and 140 °C the CCR process is described by a Debye loss peak ($\alpha = 0$, $\beta = 1$). A similar analysis was performed also for the SPN data in **Figure 5.7** at temperatures between 100 and 170 °C. The results of the analysis show that the CCR process in the nanocomposites, which is much weaker than that in the pure ER matrix, is described by an asymmetric loss peak of Cole–Davidson type, with $\alpha = 0$ and β in the range 0.35–0.45, increasing in general with increasing temperature. In addition, the fitting procedure provided data for the dc conductivity σ_{dc}, which are, in general, in good agreement with σ_{dc} directly determined as plateau values in **Figure 5.30**.

The timescale of CCR, obtained from the fits of Equation (5.16) to the $\varepsilon''(f)$ data in **Figures 5.5** and **5.7**, was further analysed with respect to its temperature dependence. **Figure 5.31** shows the Arrhenius plot for the frequency f_0 of the CCR loss peak, as well as for the dc conductivity σ_{dc}, both obtained by the analysis described above, for the ER matrix and the SPN nanocomposite. Included in the plot are also σ_{dc} values directly

determined as plateau values in **Figure 5.30**. The VTF equation (Equation (5.15)) was fitted to the CCR data. A similar equation for conductivity [46, 82]:

$$\sigma_{dc}(T) = \sigma_0 \exp\left[-\left(\frac{B}{T - T_0}\right)\right] \qquad (5.17)$$

was fitted to the σ_{dc} data. The fits are satisfactory, despite the limited temperature range of analysis, the fitting parameters being listed in **Table 5.3** [41].

The results in **Figure 5.31** and **Table 5.3** suggest that, in each of the two systems analysed, the CCR process and the dc conductivity are related to each other, as expected from the model [81]. For both processes the temperature dependence of the timescale of the response is described by the VTF equation, suggesting a connection of conductivity and CCR with the dynamic glass transition (α relaxation). It follows that the charge carrier transport is governed by the motion of the polymeric chains. From the methodological point of view, this is a significant result, as it implies that the investigation of dc conductivity and of conductivity effects, such as the CCR process, may provide information on chain dynamics [46, 79].

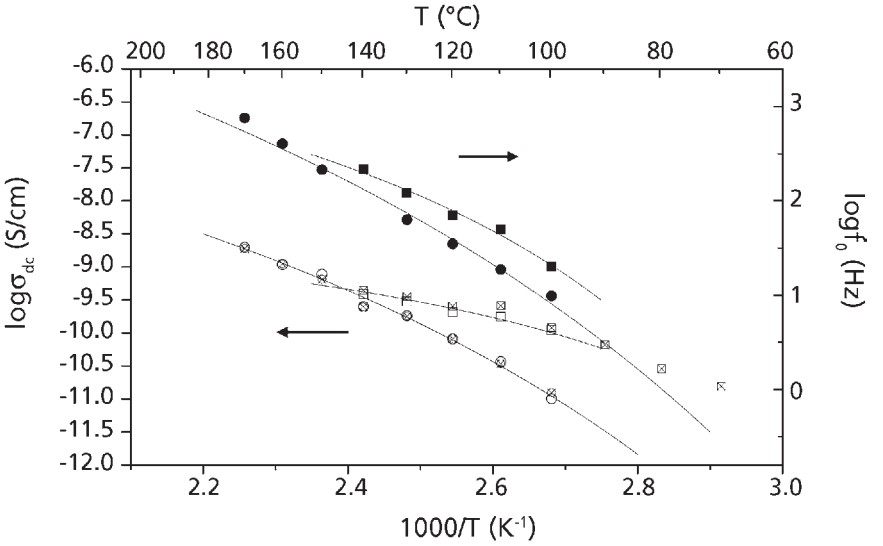

Figure 5.31 Arrhenius plot of the frequency f_0 of the CCR process (filled symbols) and of the dc conductivity σ_{dc} obtained from Equation (5.16) (open symbols) and from the $\sigma_{ac}(f)$ plots in **Figure 5.30** (open crossed symbols) for the ER matrix (squares) and the SPN nanocomposite (circles).

Table 5.3 Fitting parameters of the VTF analysis of the dc conductivity σ_{dc} and of the CCR process of the ER matrix and of the SPN nanocomposite

Sample	dc conductivity			CCR relaxation		
	$\log \sigma_0$ (S/cm)	B (K)	T_0 (K)	$\log A$ (Hz)	B (K)	T_0 (K)
ER	–8.0	406	285	4.5	660	283
SPN	–4.6	1925	242	6.4	1800	239

At temperatures lower than about 140 °C, σ_{dc} is smaller in the nanocomposites than in ER, as discussed above on the basis of **Figure 5.30**, and the CCR process is slower. In addition, the CCR process is much weaker in the nanocomposites (compare **Figures 5.4** and **5.5** with **Figures 5.6** and **5.7**, respectively), suggesting that the corresponding heterogeneity becomes less pronounced. The final morphology of the nanocomposites is determined by the specific method of preparation, where several processes may compete. The reduced large-scale heterogeneity in the nanocomposites indicates that clays act as a barrier to the process of formation of that heterogeneity. On the other hand, two relaxation mechanisms are observed in the nanocomposites at intermediate temperatures (compare **Figure 5.7**, inset), not present in pure ER. They are tentatively attributed to interfacial polarisation effects, suggesting increased small-scale heterogeneity in the nanocomposites, connected with the presence of the silicate layers.

Conductivity effects in the ER/clay nanocomposites were further studied by using the modulus formalism [33], introduced in Section 5.2.1, Equation (5.4). By using that formalism we can suppress the large contribution of dc conductivity and of conductivity effects to the $\varepsilon'(f)$ and $\varepsilon''(f)$ in **Figures 5.4–5.7**. The $M''(f)$ spectra show peaks that are related to the ionic conductivity, and their peak frequencies show the same temperature dependence as the dc conductivity. The results of the analysis are analogous to those of the mechanical modulus in solids [84].

Figure 5.32 shows the $\varepsilon''(f)$ data of **Figure 5.5** in the modulus presentation: imaginary part of the complex modulus as a function of frequency, $M''(f)$, at several temperatures. At temperatures higher than 60 °C a peak appears at low frequencies and shifts to higher frequencies with increasing temperature. This peak corresponds to the CCR process, which appears as a step in the $\varepsilon'(f)$ plots of **Figure 5.4** and as a shoulder in the $\varepsilon''(f)$ spectra of **Figure 5.5** at high temperatures. At temperatures higher than 120 °C a new relaxation has entered the frequency window of our measurements and appears as a shoulder on the low-frequency side of the CCR peak. This relaxation corresponds to the contribution of the conductivity in the $\varepsilon''(f)$ plots in **Figure 5.5** at low frequencies and high temperatures. The shift of the frequency of maximum $M''(f)$ of that relaxation with temperature corresponds to the conductivity relaxation (CR) [45, 46, 82]. At

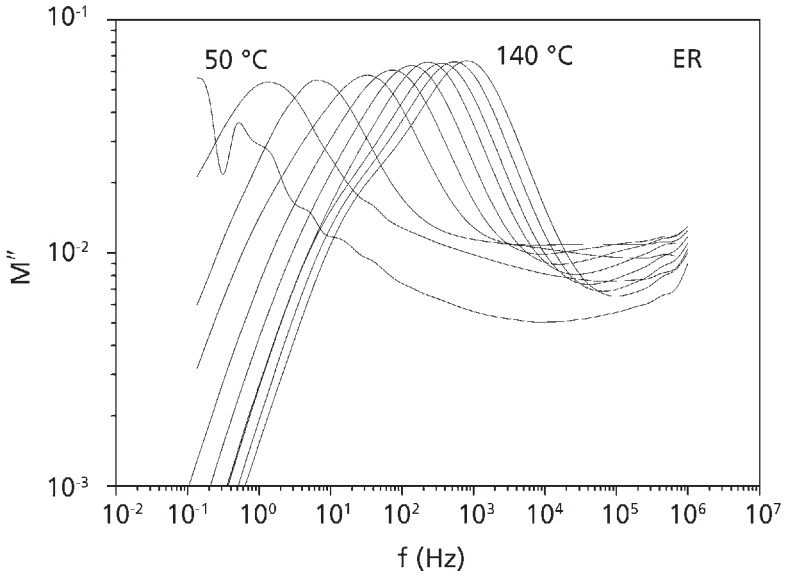

Figure 5.32 Imaginary part of modulus M'' against frequency f for the epoxy resin matrix at several temperatures between 50 and 140 °C in steps of 10 °C.

each temperature the region to the left of the CR peak is where the charge carriers are mobile over long distances, whereas the region to the right is where the charge carriers are spatially confined to their potential wells. Thus, in the peak region the transition from long-range to short-range mobility occurs.

Figure 5.32 is to be compared with **Figure 5.30**. In the latter we observe that, at temperatures higher than about 90 °C, $\sigma_{ac}(f)$ becomes independent of f at low frequencies, the plateau values being equal to the dc conductivity σ_{dc} at the respective temperature. As typically found in ionic conductors, the frequency region of constant conductivity (σ_{dc}) extends to higher frequencies with increasing temperature. The transition from the frequency-independent to the frequency-dependent region signals the onset of conductivity relaxation phenomena, corresponding to the CR peak in **Figure 5.32** [35]. Jonscher made use of a different possibility to define a peak frequency, f_p, characteristic for the CR process, by [35]:

$$\sigma_{ac}(f_p) = 2\sigma_{dc} \tag{5.18}$$

It is well established that the frequency f_p is very close to the frequency f_{max} of $M''(f)$ for the CR process.

Figure 5.33 shows a comparative plot of $M''(f)$ for the ER matrix and the three nanocomposites at T = 140 °C. For ER two relaxations are observed, located at about 10^2

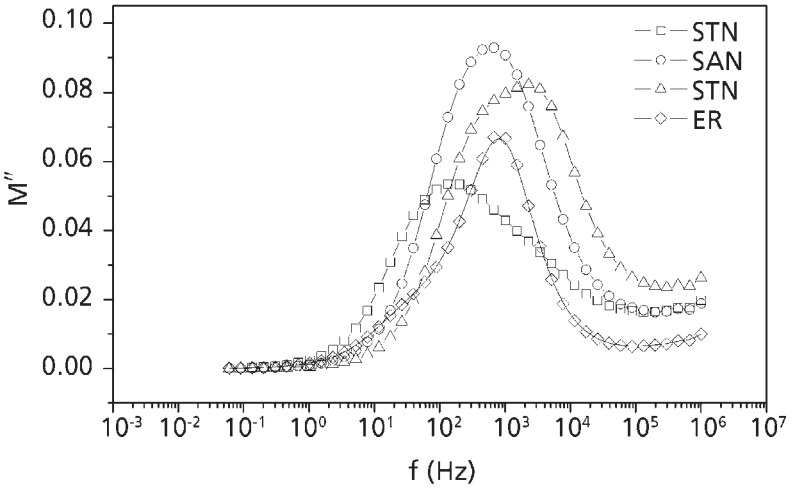

Figure 5.33 Plot of M'' versus frequency f for the ER matrix and the nanocomposites at T = 140 °C.

and 10^3 Hz, respectively. The low-frequency peak is due to the CR and is located in the frequency region of the transition from frequency-independent to frequency-dependent conductivity (**Figure 5.30**). The higher-frequency peak is attributed to the CCR process. In contrast to the ER matrix, in the nanocomposites the spectra are dominated by the CR peak: the CCR peak is overlapped by the CR peak. We have already commented on the weakening of the CCR process in the nanocomposites (**Figure 5.7**), indicating that the corresponding heterogeneity becomes of smaller length scale than in the ER matrix. The frequency position of $M''(f)$ CR peaks reflects the dc conductivity values of the samples. So, the SAN and STN nanocomposites seem to be more conductive, at T = 140 °C, than the STN nanocomposite and the ER matrix.

A second presentation of dielectric data providing values of dc conductivity σ_{dc}, next to $\sigma_{ac}(f)$ plots, is based on the use of the complex impedance formalism, introduced in Section 5.2.3. In the complex impedance formalism $Z(f) = Z'(f) - iZ''(f)$, $Z'(f)$ and $Z''(f)$ were obtained by transformation of $\varepsilon(f)$ data: $Z(\omega) = 1/i\omega\varepsilon(\omega)C_0$, where $\omega = 2\pi f$ and C_0 is the equivalent capacitance of free space [35]. Several graphical representations of impedance data are commonly used to discuss them in terms of equivalent circuits and models to obtain the bulk conductance G_{dc}, such as plots of imaginary versus real impedance (Nyquist plots). $Z''(Z')$ plots allow the best separation of bulk from electrode phenomena. Values of σ_{dc} are then obtained from the measured G_{dc} values and the geometry of the samples [35]. As an example of the use of the Z formalism, we show in **Figure 5.34** a linear $Z''(Z')$ plot for the ER matrix at 140 °C. In this plot the frequency of measurements is a parameter increasing from the right (high values of

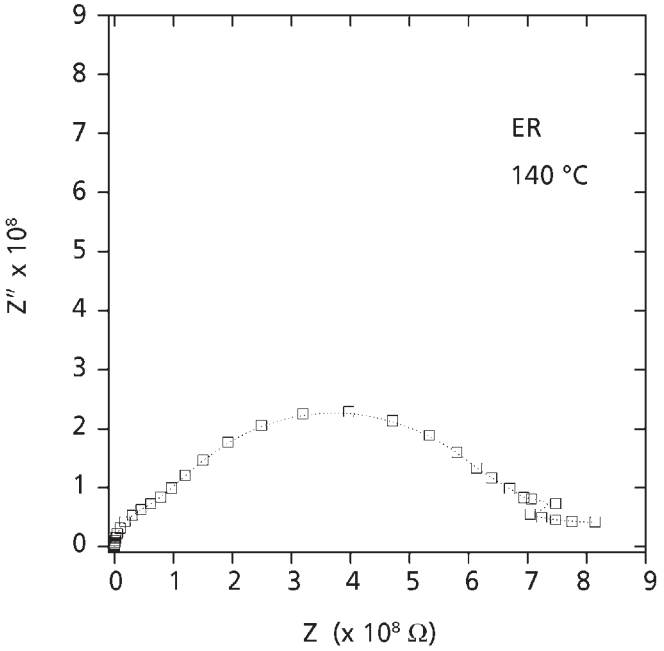

Figure 5.34 Linear Z plot for ER at 140 °C.

the resistance Z') to the left. The intercept on the real (Z') axis of the data extrapolated to lower frequencies gives R_{dc} (= $1/G_{dc}$). At frequencies lower than those of the Z'' minimum the response is dominated by electrode effects. In addition to that, we observe in **Figure 5.34** that the bulk response of the sample is described by the combination of two processes. The CR polarisation mechanism discussed above gives rise to the first semicircle in the Nyquist plot of **Figure 5.34**, whereas the second semicircle (in order of increasing frequency) corresponds to the CCR mechanism. The value obtained for σ_{dc} from the intercept of $Z''(Z')$ on the Z' axis, $\sigma_{dc} = 3.5 \times 10^{-8}$ S/m (**Figure 5.34**), is, within experimental errors, about the same as that determined from the $\sigma_{ac}(f)$ plot of **Figure 5.30** at low frequencies, $\sigma_{ac}(f = 10^{-2}\,\text{Hz}) = 3.6 \times 10^{-8}$ S/m).

The Arrhenius plot of σ_{dc} for the ER matrix is shown in **Figure 5.35**. It is interesting to compare this plot with that of **Figure 5.31**, showing results obtained within the permittivity formalism [41]. In the plot of Figure 5.35 we have also included σ_{ac} plateau values, which correspond to the CCR process (structure at about 10^3 Hz in **Figure 5.30**) and the frequencies of the CCR peaks from the $M''(f)$ spectra of **Figure 5.32**. The lines in **Figure 5.35** are fits of the VTF equations (5.15) and (5.17) to the data for f_{max} and σ_{dc}, respectively. The behaviour of σ_{dc}, well described by the VTF equation, suggests that the conductivity mechanism at temperatures higher than T_g is governed by the cooperative motion of the ER polymer chain segments. The apparent activation energy

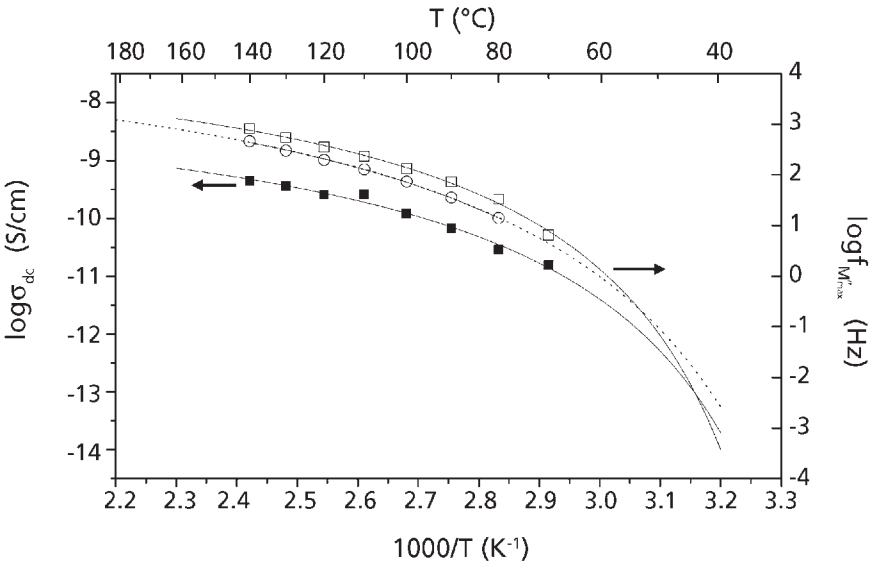

Figure 5.35 Arrhenius plot for σ_{dc} (filled squares) and for CCR in the conductivity formalism σ_{ac} (open circles) and in the modulus formalism (open squares) for the epoxy resin matrix. The lines are fits of the corresponding VTF equation to the experimental data.

Table 5.4 Fitting parameters of the VTF equations (5.15) and (5.17) to the data in **Figure 5.35**

	log *A*	*B* (K)	T_0 (K)
$f_{max,M''}$ (CCR)	4.5	457	287
σ_{ac} (CCR)	–7	531	276
σ_{dc}	–8	405	282

for the dc conductivity process, indicated by *B* values in **Table 5.4**, is close to that of the CCR process presented in the modulus formalism, reflecting the common origin of these processes. Strong evidence for this fact is provided also by the observed convergence of the VTF lines at low temperatures (for $T < T_g$) in **Figure 5.35**.

5.6.2 Epoxy Resin Reinforced With Diamond and Magnetic Nanoparticles

Brief information on the preparation of these samples has been given in Section 5.3.2, and the samples investigated are listed in **Table 5.1**. The strong contribution of dc

conductivity and of conductivity effects to the dielectric response of these materials is observed in the $\varepsilon'(f)$ and the $\varepsilon''(f)$ spectra of **Figure 5.10** [51]. In particular, at low frequencies and high temperatures, $\varepsilon''(f)$ increases with a slope of –1, characteristic of dc conductivity (Equation (5.10)). A structure (step) is observed in $\varepsilon'(f)$ at low frequencies and a shoulder in $\varepsilon''(f)$ in the same frequency range, both of them more pronounced in the pure ER matrix than in the nanocomposite. Similar results in the ER/clay nanocomposites were discussed in Section 5.6.1 in terms of the so-called conductivity current relaxation (CCR). The same discussion applies, in general, also for the results obtained with the materials under investigation here; further comments will be added later.

Figure 5.36 shows Arrhenius plots for the dc conductivity of the ER matrix and the nanocomposites containing diamond and BHF [51]. The conductivity of the matrix is well described by the VTF equation (5.17), suggesting a connection with the α relaxation, namely that charge carrier transport in the ER is governed by the segmental motion of the polymeric chains. In the 0.5% diamond nanocomposite, the temperature dependence of the conductivity is again given by the VTF equation, and is shifted to higher temperatures with respect to the matrix, in accordance with the higher glass transition temperature indicated by **Figure 5.10**, as discussed in Section 5.3.2. In the 1.2% diamond nanocomposite, however, the temperature dependence of σ_{dc} is markedly different and approaches Arrhenius behaviour described by the equation:

$$\sigma_{dc}(T) = \sigma_0 \exp\left[-\left(\frac{E_{act}}{kT}\right)\right] \qquad (5.19)$$

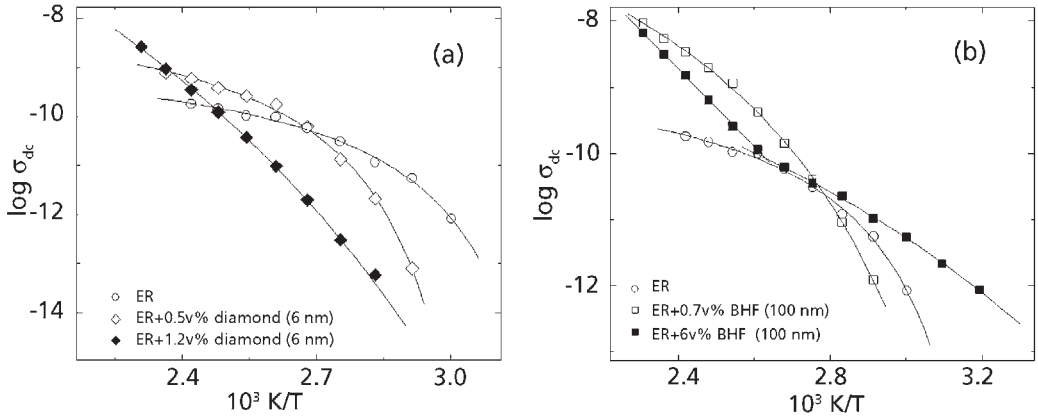

Figure 5.36 Arrhenius plot for the dc conductivity of the ER matrix and the (a) diamond and (b) BHF nanocomposites. The lines are fits of the VTF equation (5.17) or the Arrhenius equation (5.19) – see text.

where E_{act} is the apparent activation energy of dc conductivity σ_{dc}, σ_0 a pre-exponential factor and k Boltzmann's constant. This change of behaviour may indicate that in this composite a different mechanism, such as charge carrier diffusion, dominates dc conductivity [51]. Note also that at high temperatures dc conductivity is larger in the nanocomposites than in the ER matrix, probably due to larger charge carrier concentration. Regarding the BHF composites, the sample with 0.7% BHF shows VTF behaviour, while the 6% BHF composite shows two distinct regions: at low temperatures the behaviour is VTF and similar to the matrix, while at high temperatures it shifts to an Arrhenius dependence. This may be explained as follows: In the 6% composite, unlike the others, the concentration is high enough for the filler to form a continuous network through which electrons can move. This mechanism of conductivity, which has an Arrhenius temperature dependence, dominates at high temperatures, while at low temperatures the ionic conductivity through the polymer matrix, which has a VTF temperature dependence, is higher.

In the CCR process, observed in **Figure 5.10**, the polarisation mechanism consists of accumulation of charges at the interfaces between regions of different conductivity under conditions of dc conductivity for the sample as a whole [41, 45, 82]. The relaxation is characterised by high values of $\Delta\varepsilon$ (around 30 in the ER matrix), thus excluding a dipolar origin, and approximately independent of temperature. The shape of the relaxation is symmetrical (it is satisfactorily fitted by a Cole–Cole equation [23–25]), and the corresponding distribution of relaxation times is rather narrow (the Cole–Cole shape parameter is ~0.8, with 1 corresponding to a Debye peak). Moreover, the data for the relaxation time of this relaxation (Arrhenius plot in **Figure 5.37**) suggest that the CCR process is related to the dc conductivity as expected from the model [41, 45, 82]. The presence of the CCR suggests a large-scale heterogeneity in the structure of the ER matrix, in agreement with results obtained for similar epoxy resins by other techniques [43, 83]. The CCR process appears much weaker in the two diamond nanocomposites, suggesting that the corresponding heterogeneity becomes less pronounced [41, 51]. In the 0.7% BHF nanocomposites, on the other hand, the CCR process is comparable to that of the pure matrix. This suggests that the diamond nanoparticles, with their smaller size and interparticle distance and large surface area, suppress the heterogeneity of the ER matrix while the larger BHF nanoparticles at a similar volume fraction leave it unchanged [51].

5.6.3 Epoxy Resin/Carbon Nanocomposites

Brief information on the preparation of these samples has been given in Section 5.3.3. **Figure 5.38** shows frequency plots of ac conductivity, $\sigma_{ac}(f)$, at 140 °C for the pure ER matrix and three nanocomposites. For all the samples, dc conductivity, determined by the frequency-independent (plateau) values at low frequencies, is rather low (below 10^{-8} S/cm), indicating that all the filler concentrations are below the percolation threshold

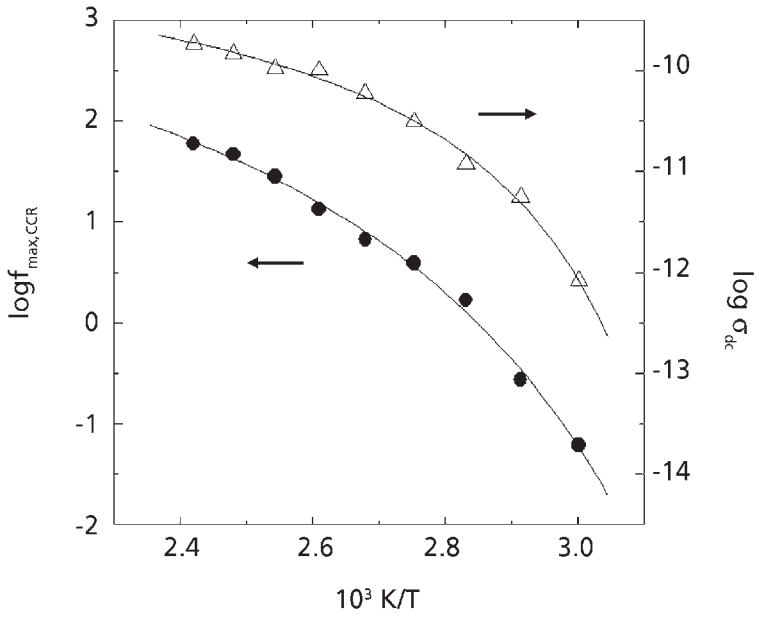

Figure 5.37 Arrhenius plot for the CCR relaxation and the dc conductivity of the ER matrix. The lines are fits of the VTF equations (5.15) and (5.17) to the CCR and the σ_{dc} data, respectively.

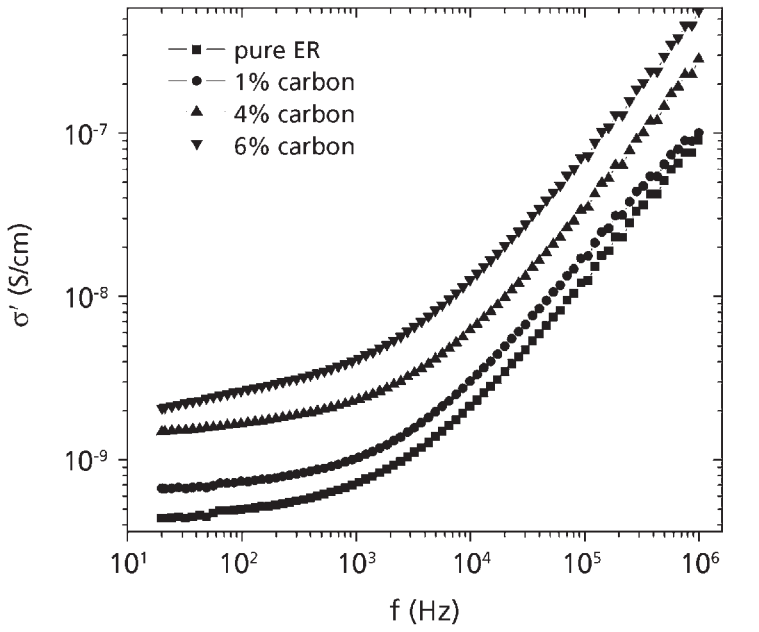

Figure 5.38 Real part of the ac conductivity against frequency (at 140 °C) for the samples indicated on the plot.

[54]. This dc conductivity, observed at temperatures higher than T_g, is attributed to ionic conductivity of the matrix polymer, as discussed in the previous two sections. We observe that both dc conductivity and ac conductivity at each frequency increase systematically with increasing filler content of the nanocomposites. Obviously, this increase reflects the higher concentration of conductive filler in the nanocomposites.

The Arrhenius plot for the dc conductivity relaxation time is presented in **Figure 5.39**. The modulus formalism has been used here to quantify dc conductivity relaxation times in terms of the peak frequency of the $M''(f)$ peak of conductivity relaxation (CR), as discussed in detail in Section 5.6.1. In the pure polymer the Arrhenius plot has a VTF dependence, described by Equation (5.17) with reasonable values of the fitting parameters, which indicates that charge carrier transport is governed by the cooperative motion of polymer chains (compare the discussion about that point in Section 5.6.1). In contrast, the dc conductivity relaxation time in the nanocomposites with filler content 4 and 6 vol% has an Arrhenius-type temperature dependence, described by Equation (5.19), at least in the limited temperature range of measurements of **Figure 5.39**, whereas an intermediate behaviour is observed for the nanocomposite with the lowest filler content of 1 vol%. The activation energy obtained in the two cases of Arrhenius temperature dependence reflects the activation energy of dc conductivity and is, in both cases, 1.0 eV.

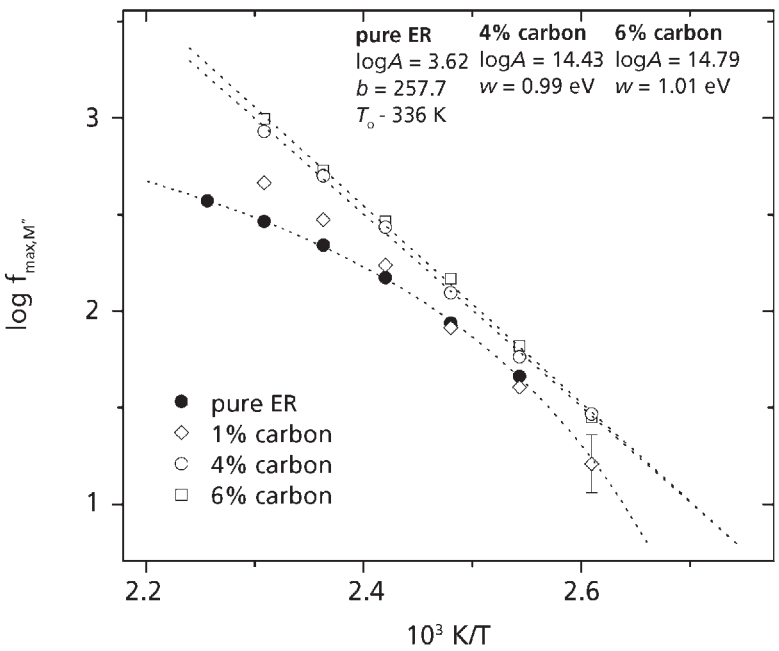

Figure 5.39 Arrhenius plot for the peak frequency of $M''(f)$ corresponding to the CR process in the samples indicated on the plot.

In the 6% sample, and to a lesser extent in the 4% sample, there is a contribution of a polarisation mechanism, which extends over extremely broad temperature and frequency ranges. This polarisation mechanism is reflected in both the TSDC and the DS measurements. In the TSDC thermograms of **Figure 5.18** the mechanism gives rise to an extremely wide peak centred at about –70 °C; note the logarithmic current scale. In the $\varepsilon'(f)$ and $\varepsilon''(f)$ plots of **Figure 5.13** the polarisation mechanism is observed as a large overall increase of both ε' and ε'' and as a power-law dependence:

$$\varepsilon''(f) \sim f^{-x} \qquad \varepsilon'(f) \sim f^{-y} \tag{5.20}$$

over large temperature and frequency ranges (**Figure 5.14**). These effects are attributed to interfacial polarisation within the clusters formed by the carbon particles. The wide frequency and temperature ranges correspond to morphology within these clusters that extends over a large range of spatial scales. As the carbon content increases and approaches the percolation threshold, such clusters are indeed expected to have a complex (self-similar) structure, reflected in the power-law frequency dependence of both ε' and ε'' [85].

5.7 Conclusions

Molecular dynamics studies form an essential part of investigations in polymer nanocomposites towards optimisation of composition and processing conditions, for at least two reasons. The first is related to the investigation of structure–property relationships, where molecular dynamics is, next to composition, processing, morphology and final properties, one of the building blocks of these relationships. In particular, molecular dynamics provides a link between morphology and final properties. A better understanding of molecular dynamics enables one to discuss the improvement of final properties in a nanocomposite at the molecular level, as demonstrated in this chapter on the example of improvement of mechanical properties and of thermal stability in epoxy resin/layered silicate nanocomposites, discussed in terms of reduction of chain mobility. The second reason for molecular dynamics studies in polymer nanocomposites is that these provide, even if indirectly, significant information on morphology, in particular on distribution of nanoparticles and degree of agglomeration. This is obvious in the case of conductive inclusions, where the results are discussed in terms of percolation. It is, however, true also for non-conductive inclusions, as demonstrated in several examples in this chapter.

Dielectric studies, in particular broadband dielectric spectroscopy, are especially suited for molecular dynamics studies in polymer nanocomposites. Effects of nanoparticles on chain dynamics by using these techniques are reflected in the real part of the dielectric permittivity as a function of frequency and temperature, the dc conductivity and the various relaxation mechanisms of the matrix polymer. In the case of relaxation mechanisms, the timescale and the magnitude (dielectric strength) of the response form

the two main sources of information, as demonstrated in several examples in this chapter. We also showed that not only the investigation of the primary α relaxation associated with the glass transition, but also that of the local, secondary relaxations, may reveal important aspects of effects of nanoparticles on chain dynamics.

Effects of nanoparticles on matrix polymer dynamics may depend sensitively on temperature, as demonstrated at several places in this chapter. The broad temperature range accessible to dielectric measurements then allows one to study in detail this temperature dependence. In addition, the extremely broad frequency range of dielectric measurements enables one to record, at the same temperature, several relaxation processes (secondary relaxations, primary α relaxation, conductivity relaxation and conductivity effects, in order of decreasing frequency), which correspond to different spatial scales (characteristic lengths). Thus, information on the effects of nanoparticles on matrix polymer dynamics at different length scales, ranging from microscopic (tenths of a nanometre) to macroscopic (nanometre to micrometre range) can be extracted from broadband dielectric spectroscopy.

Acknowledgements

The author wishes to thank his colleagues L. Bokobza, D. Fragiadakis, A. Kanapitsas, R. Kotsilkova and E. Logakis for providing data and/or for valuable discussions.

References

1. M. Alexandre and P. Dubois, *Materials Science and Engineering Reports*, 2000, **28**, 1-2, 1.

2. C. Sanchez, G.J. de A.A. Soler-Illia, F. Ribot, T. Lalot, C.R. Mayer and V. Cabuil, *Chemistry of Materials*, 2001, **13**, 10, 3061.

3. S.S. Ray and M. Okamoto, *Progress in Polymer Science*, 2003, **28**, 11, 1539.

4. G. Tsagaropoulos and A. Eisenberg, *Macromolecules*, 1995, **28**, 18, 6067.

5. J. Berriot, H. Montes, F. Lequeux, D. Long and P. Sotta, *Macromolecules*, 2002, **35**, 26, 9756.

6. V. Arrighi, I.J. McEwen, H. Qian and M.B. Serrano Prieto, *Polymer*, 2003, **44**, 20, 6259.

7. V.M. Litvinov, H. Barthel and J. Weis, *Macromolecules*, 2002, **35**, 11, 4356.

8. D. Fragiadakis, P. Pissis and L. Bokobza, *Polymer*, 2005, **46**, 16, 6001.

9. G.C. Papanicolaou, S.A. Paipetis and P.S. Theocaris, *Colloid and Polymer Science*, 1978, **256**, 7, 625.

10. G.C. Papanicolaou, M.V. Michalopoulou and N.K. Anifantis, *Composites Science and Technology*, 2002, **62**, 14, 1881.

11. C.S. Chouchaoui and M.L. Benzeggah, *Composites Science and Technology*, 1997, **57**, 6, 617.

12. L. Matejka, A. Strachota, J. Plestil, P. Whelan, M. Steinhardt and M. Slouf, *Macromolecules*, 2004, **37**, 25, 9449.

13. R. Pelster and U. Simon, *Colloid and Polymer Science*, 1999, **277**, 1, 2.

14. S. Vyazovkin and I. Dranca, *Journal of Physical Chemistry B*, 2004, **108**, 32, 11981.

15. A. Strachota, I. Kroutilova, J. Kovarova and L. Matejka, *Macromolecules*, 2004, **37**, 25, 9457.

16. P. Pötschke, M. Abdel-Goad, I. Alig, S. Dudkin and D. Lellinger, *Polymer*, 2004, **45**, 26, 8863.

17. V.M. Litvinov and H.W. Spiess, *Makromolekulare Chemie*, 1991, **192**, 12, 3005.

18. B.J. Ash, R.W. Stiegel and L.S. Schadler, *Macromolecules*, 2004, **37**, 4, 1358.

19. V.A. Bershtein, L.M. Egorova, P.N. Yakushev, P. Pissis, P. Sysel and L. Brozova, *Journal of Polymer Science: Polymer Physics Edition*, 2002, **40**, 10, 1056.

20. G.D. Smith, D. Bedrov, L. Li and O. Byuther, *Journal of Chemical Physics*, 2002, **117**, 20, 9478.

21. A.C. Balazs, *Current Opinion in Solid State and Materials Science*, 2003, **7**, 1, 27.

22. N.G. McCrum, B.E. Read and G. Williams, *Anelastic and Dielectric Effects in Polymeric Solids*, John Wiley & Sons, New York, NY, USA, 1967.

23. P. Hedvig, *Dielectric Spectroscopy of Polymers*, Adam Hilger, Bristol, UK, 1977.

24. *Dielectric Spectroscopy of Polymeric Materials*, Eds., J.P. Runt and J.J. Fitzgerald, American Chemical Society, Washington, DC, USA, 1997.

25. *Broadband Dielectric Spectroscopy*, Eds., F. Kremer and A. Schoenhals, Springer, Berlin, Germany, 2003.

26. S. Kripotou, P. Pissis, P. Sysel, V. Sindelar and V.A. Bershtein, *Polymer*, 2006, **47**, 1, 357.

27. V.N. Daniel, *Dielectric Relaxation*, Academic Press, London, UK, 1967.

28. N.E. Hill, W. Vaughan, A.H. Price and M. Davies, *Dielectric Properties and Molecular Behaviour*, Van Nostrand, London, UK, 1969.

29. *Impedance Spectroscopy*, Ed., J.R. Macdonald, John Wiley & Sons, New York, NY, USA, 1987.

30. S. Takeishi and S. Mashimo, *Review of Scientific Instruments*, 1992, **53**, 8, 1155.

31. R. Nozaki and T.K. Bose, *IEEE Transactions on Instrumentation and Measurement*, 1990, **39**, 6, 945.

32. Y. Feldman, A. Andrianov, E. Polygalov, I. Ermolina, G. Romanychev, Y. Zuev and B. Milgotin, *Review of Scientific Instruments*, 1996, **67**, 9, 3208.

33. C.T. Moynihan, L.P. Boesch and N.L. Laberge, *Physics and Chemistry of Glasses*, 1973, **14**, 122.

34. S. Havriliak, Jr., and S.J. Havriliak, *Dielectric and Mechanical Relaxation in Materials*, Hanser, Munich, Germany, 1997.

35. A.K. Jonscher, *Dielectric Relaxation in Solids*, Chelsea Dielectrics, London, UK, 1983.

36. A.S. Vatalis, A. Kanapitsas, C.G. Delides and P. Pissis, *Thermochimica Acta*, 2001, **372**, 1-2, 33.

37. J. Van Turnhout in *Electrets*, Ed., G. M. Sessler, Topics in Applied Physics, Volume 33, Springer, Berlin, Germany, 1980, p.81.

38. P. Pissis, A. Anagnostopoulou-Konsta, L. Apekis, D. Daoukaki-Diamanti and C. Christodoulides, *Journal of Non-Crystalline Solids*, 1991, **131–133**, Part 2, 1174.

39. A. Kyritsis, P. Pissis, J.L. Gomez Ribelles and M. Monleon Pradas, *Journal of Polymer Science B: Polymer Physics*, 1994, **32**, 6, 1001.

40. K. Funke and C. Cramer, *Current Opinion in Solid State and Materials Science*, 1997, **2**, 4, 483.

41. A. Kanapitsas, P. Pissis and R. Kotsilkova, *Journal of Non-Crystalline Solids*, 2002, **305**, 1-3, 204.

42. R. Kotsilkova, *Journal of Applied Polymer Science*, 2005, **97**, 6, 2499.

43. C. Maggana and P. Pissis, *Journal of Macromolecular Science B*, 1997, **36**, 6, 9.

44. *The Glass Transition: Relaxation Dynamics in Liquids and Disordered Materials*, Ed., E. Donth, Springer Series in Materials Science, Volume 48, Springer, Berlin, Germany, 2001.

45. G. Georgoussis, A. Kanapitsas, P. Pissis, Yu.V. Savelyev, V.Y. Veselov and E.G. Privalko, *European Polymer Journal*, 2000, **36**, 6, 1113.

46. A. Kyritsis, P. Pissis and J. Grammatikakis, *Journal of Polymer Science: Polymer Physics Edition*, 1995, **33**, 12, 1737.

47. O. Becker, K. Dusek and G.P. Simon, *Inorganic Polymeric Nanocomposites and Membranes, Advances in Polymer Science Series*, 2005, **179**, 29.

48. A. Usuki, N. Hasegawa, M. Kato and S. Kobayashi, *Inorganic Polymeric Nanocomposites and Membranes, Advances in Polymer Science*, 2005, **179**, 135.

49. G. Maier, *Progress in Polymer Science*, 2001, **26**, 1, 3.

50. R. Kotsilkova, P. Pissis, A. Kanapitsas and S. Rousseva in *Proceedings of the Workshop on Nanoscience and Nanotechnology 2000*, 2000, Sofia, Bulgaria, p.57.

51. D. Fragiadakis, P. Pissis, C. Ellie, A. Kanapitsas, R. Kotsilkova, S. Stavrev and I. Nedkov in *Proceedings of 10th International Conference on Mechanics and Technology of Composite Materials*, 2003, Sofia, Bulgaria, p.45.

52. S.Y. Stavrev, S.B. Lazarov, K.L. Stoev, L.G. Markov and V.I. Ivanov, inventors; no assignee; US Patent 5,353,708, 1994.

53. R. Pelster, A. Spanoudaki and T. Kruse, *Journal of Physics D: Applied Physics*, 2004, **37**, 3, 307.

54. R. Kotsilkova, D. Fragiadakis and P. Pissis, *Journal of Polymer Science: Polymer Physics Edition*, 2005, **43**, 5, 522.

55. Z-M. Dang, C-W. Nan, D. Xie, Y-H. Zhang and S.C. Tjong, *Applied Physics Letters*, 2004, **85**, 1, 97.

56. D. Stauffer and A. Aharony, *Introduction to Percolation Theory*, Taylor & Francis, London, UK, 1992.

57. R. Zallen, *The Physics of Amorphous Solids*, John Wiley & Sons, New York, NY, USA, 1983.

58. G. Maier, *Progress in Polymer Science*, 2001, **26**, 1, 3.

59. C-M. Leu, Y-T. Chang and K-H. Wei, *Chemistry of Materials*, 2003, **15**, 19, 3721.

60. M. Vasilopoulou, S. Tsevas, A.M. Douvas, P. Argitis, D. Davazoglou and D. Kouvatsos, *Journal of Physics: Conference Series*, 2005, **10**, 218.

61. Y-H. Zhang, S-G. Lu, Y-Q. Li, Z-M. Dang, J.H. Xin, S-Y. Fu, G-T. Li, R-R. Guo and L-F. Li, *Advanced Materials*, 2005, **17**, 8, 1056.

62. V.Y. Kramarenko, T.A. Shantalil, I.L. Karpova, K.S. Dragan, E.G. Privalko, V.P. Privalko, D. Fragiadakis and P. Pissis, *Polymers for Advanced Technologies*, 2004, **15**, 3, 144.

63. D. Fragiadakis, E. Logakis, P. Pissis, V.Y. Kramarenko, T.A. Shantalii, I.L. Karpova, K.S. Dragan, E.G. Privalko, A.A. Usenko and V.P. Privalko, *Journal of Physics: Conference Series*, 2005, **10**, 139.

64. J. Mijovic and H. Zhang, *Macromolecules*, 2003, **36**, 4, 1279.

65. H. Miyagawa, M.J. Rich and L.T. Drzal, *Journal of Polymer Science B: Polymer Physics*, 2004, **42**, 23, 4391.

66. K. Chen and S. Yang, *Journal of Applied Polymer Science*, 2002, **86**, 2, 414.

67. X. Liu and Q. Wu, *Polymer*, 2001, **42**, 25, 10013.

68. Y. Sun, Z. Zhang, K-S. Moon and C.P. Wong, *Journal of Polymer Science B: Polymer Physics*, 2004, **42**, 21, 3849.

69. B. Ash, L. Schadler and R. Siegel, *Materials Letters*, 2002, **55**, 1, 83.

70. G. Tsagaropoulos and A. Eisenberg, *Macromolecules*, 1995, **28**, 1, 396.

71. V. Arrighi, J. Higgins, A. Burgers and G. Floudas, *Polymer*, 1998, **39**, 25, 6369.

72. L. Matejka, O. Dukh and J. Kolarik, *Polymer*, 2000, **41**, 4, 1449.

73. F. Starr, T. Scroeder and S. Glotzer, *Macromolecules*, 2002, **35**, 11, 4481.

74. J. van Turnhout and M. Wuebbenhorst, *Journal of Non-Crystalline Solids*, 2002, **305**, 1-3, 50.

75. L. Bokobza and J-P. Chauvin, *Polymer*, 2005, **46**, 12, 4144.

76. E. Donth, *Relaxation and Thermodynamics in Polymers: Glass Transition*, Akademie Verlag, Berlin, Germany, 1992.

77. A. Hensel, J. Dobbertin, E.K. Schawe, A. Boller and C. Schick, *Thermal Analysis*, 1996, **46**, 3-4, 935.

78. L. Dewimille, B. Bresson and L. Bokobza, *Polymer*, 2005, **46**, 12, 4135.

79. F. Stickel, E.W. Fischer and R. Richert, *Journal of Chemical Physics*, 1996, **104**, 5, 2043.

80. G. Polizos, V.V. Shilov and P. Pissis, *Journal of Non-Crystalline Solids*, 2002, **305**, 1-3, 212.

81. K. Yamamoto and H. Namikawa, *Japanese Journal of Applied Physics*, 1988, **27**, 10, 1845.

82. P. Pissis, A. Kyritsis and V.V. Shilov, *Solid State Ionics*, 1999, **125**, 1-4, 203.

83. C. Maggana and P. Pissis, *Journal of Polymer Science B: Polymer Physics*, 1999, **37**, 11, 1165.

84. C.A. Angell, *Materials Chemistry and Physics*, 1989, **23**, 1-2, 143.

85. D.S. McLachlan, C. Chiteme, C. Park, K.E. Wise, S.E. Lowther, P.T. Lillehei, E.J. Siochi and J.S. Harrison, *Journal of Polymer Science B: Polymer Physics*, 2005, **43**, 22, 3273.

6 Performance of Thermoset Nanocomposites

R. Kotsilkova

6.1 Mechanical Properties

Thermoset nanocomposites are novel composite materials, which are resins reinforced with particles or platelets on the nanometre scale. Due to the nanosized particles obtained by chemical and physical dispersion processes, the nanocomposites exhibit markedly improved properties compared with the pure polymer or conventional microscale composites [1–15].

Fillers with high surface area-to-volume ratio have generally been found to give the best balance of properties; thus, the dimensional stability, conductivity, mechanical, thermal and other properties may be modified due to the incorporation of fine filler particles within the thermoset resins. However, the improvements in properties observed with conventionally prepared composites are modest when compared to those that have been established for polymer nanocomposites, especially if compared at equal volume filler content [1]. The addition of nanoscale fillers to polymers can have a dramatic effect on the mechanical properties [1–6] compared to micrometre scale fillers. This may be in large part due to the small size and the large surface area of nanoscale fillers. The development of effective nanocomposites is directly linked to the availability and the properties of the nano-reinforcements, which should be able to be dispersed in a polymeric matrix at a nanoscale level.

In more recent years, considerable emphasis has been placed on studies of nanofillers, particularly organoclays [2–15]. Because of their high surface area-to-volume ratio, nanofillers are found to have a high reinforcing efficiency even at very low concentrations. For example, a large array of improved thermomechanical properties have been attained at very low organoclay content (5 wt% or less) [4, 5]. Many works have proved that a complete exfoliation of silicate layers is the key to achieving polymer/clay nanocomposites that perform well [6–16]. Of the many types of polymer matrix composites, the enhanced modulus, decreased shrinkage and potential rigid-phase toughening of thermoset/layered silicate nanocomposites offer multiple opportunities. Undoubtedly, the unique combination of their key properties and potentially low production costs is a very good basis for a much broader range of applications. Furthermore, the quite low filler level required to display sizeable enhancement of properties makes nanocomposites competitive with other materials.

Nevertheless, there has to be a much better understanding of the actual structure–property relationships in some important areas such as physico-mechanical properties of thermoset silicate nanocomposites. A great need still exists for the development of thermoset nanocomposites that can be mixed, applied in various forms (e.g., as adhesive films, coatings, or castings), and cured by conventional means [5]. The substantial improvements in mechanical and physical properties brought by polymer nanocomposites are likely to widen the use of polymers in industry. For example, their improved mechanical and thermal properties might extend the use of thermoset polymers for applications in the automotive, aircraft and space industries. Moreover, their excellent barrier properties combined with good transparency make them ideal for coating applications.

6.1.1 Viscoelastic Properties – Dynamic Mechanical Thermal Analysis

The effects of molecular dispersion of nanofiller particles on the viscoelastic properties of the crosslinked polymeric matrix are usually investigated using dynamic mechanical thermal analysis (DMTA). This experiment involves applying an oscillatory strain to a sample and measuring the resultant stress, which consists of in-phase and out-of-phase components [17]. The resultant stress can be used to calculate the complex modulus and its two components, the storage modulus E' and the loss modulus E''. Then $\tan \delta = E''/E'$ is a measure of the ratio of energy lost to energy stored per cycle of deformation. In general, the storage modulus E' reflects the elastic properties of the materials, and the loss modulus E'' is related to the energy loss due to the friction associated with the motion of the polymer chains. The loss factor $\tan \delta$ is sensitive to the structural transformation of the material produced on increasing the temperature. The temperature dependence of $\tan \delta$ in a wide temperature range typically goes through a maximum and provides a very sensitive means of analysing the α and β relaxations, for example. The α transition is related to the Brownian motion of the main chains at the transition from the glassy to the rubbery state and the relaxation of dipoles associated with it. The β transition occurs at a lower temperature and, for example, is related to the rotation of the hydroxyl ether segments of the epoxy networks in the glassy state. At T_α (α transition) there is a sharp decrease in both moduli, with a peak in $\tan \delta$, indicating viscous damping due to segmental motion in the polymer, which is associated with the glass transition, T_α ($\sim T_g$). For crosslinked polymers, both $\tan \delta$ and E' generally increase with increasing crosslink density [5].

It is likely that in nanocomposites the segmental motions of polymer associated with α and β relaxation can be affected by the nano-reinforcements, being influenced by the large inorganic surfaces. Indeed, Beall [16] claimed that, for a concentration of 5% exfoliated clay, about 50% of the polymer chains are attracted by the silicate surface. Hence, such large surface–polymer interactions are expected to affect the viscoelastic and other mechanical properties of crosslinked nanocomposites.

6.1.1.1 DMTA of Clay-Containing Thermoset Nanocomposites

Different thermomechanical behaviour is reported for thermoset/layered silicate nanocomposites, which was found to depend significantly on the degree of exfoliation, the matrix–filler interactions, and the type of crosslinked resin (epoxy, polyester, polyimide, etc.).

A marked improvement of the storage modulus of nanocomposites was observed by several authors [3, 13, 18–28] especially above the glass transition temperature of the matrix resin, along with an increase in the glass transition temperature, T_α (~T_g), when only a small amount of silicate is added. The enhanced viscoelastic properties are mostly related with the clay exfoliation. Messersmith and Giannelis [5] prepared exfoliated nanocomposites of 4 vol% smectite clay (mica-type) pre-intercalated with bis(2-hydroxyethyl)methyl tallow ammonium, dispersed in bifunctional epoxy resin, such as diglycidyl ether of bisphenol A (DGEBA, e.g., DER332 or Epon). Three exfoliating curing agents were investigated: nadic methyl anhydride, benzyldimethylamine and boron trifluoride monoethylamine. The organic modifier of the clay had functional groups capable of reacting with the epoxy resin matrix. Dynamic mechanical analyses of the diamine-crosslinked epoxy nanocomposites showed about 58% improvement of the tensile storage modulus in the glassy region ($T < T_g$) and 450% higher modulus in the rubbery plateau region ($T > T_g$), compared to the unmodified epoxy. Such markedly improved properties were associated with the large aspect ratio of nanofiller and the strong interfacial adhesion between the epoxy matrix and the silicate platelets. For comparison, about 10% increase of the dynamic storage modulus is typical for conventional microcomposites at much higher filler content.

Brown and co-workers [29] observed that the dominant effect of organoclay addition to DGEBA-type resin appears in the modulus and distribution of relaxation (tan δ) around and above T_g. They synthesised exfoliated nanocomposites based on bis(2-hydroxyethyl) methyl tallow ammonium montmorillonite (S30A), as well as intercalated nanocomposites based on dimethyl ditallow ammonium montmorillonite (B34) and dimethyl tallow benzyl-ammonium montmorillonite (B24), dispersed in DGEBA-type resin (Epon 828). Polyoxypropylene diamine (Jeffamine D-series) was used as a hardener. Intercalated morphologies resulted in a small enhancement in shear modulus, G' around T_g; however steep decay, similar to the unfilled resin, is observed above T_g. In contrast, more substantial effects are observed in exfoliated morphologies (containing 10–15% S30A), wherein a significant enhancement of the shear elastic modulus is observed in a wide temperature range, around and above T_g.

A number of investigations of diamine-cured Epon 828/organoclay nanocomposites showed that different characterisation regimes and the global orientation of the layered silicate reinforcement in the test specimens make qualitative comparison of the dynamic modulus results difficult [13, 30, 31]. In general, the modulus of the unfilled resin is approximately 1–3 GPa below T_g and 1–3 MPa above T_g. Researchers from

Pinnavaia's group [14, 18-21] reported a 4–5 fold increase in rubbery modulus with the addition of 10% montmorillonite. Comparable increases in the rubbery region have been observed also for other DGEBA diamine-cured nanocomposites [5, 29, 23–26]. Modulus enhancement in the glassy region ($T < T_g$) is generally much less, only 1.25–2fold for 5–10 wt% loading. In general, the nanocomposites exhibit dynamic modulus reinforcement greater than conventionally filled epoxies with comparable filler loadings, and may lead to improved, lightweight epoxy composites.

Hsueh and Chen [26] prepared exfoliated nanocomposites based on DGEBA epoxy resin (Epon 828 cured with Jeffamine D400) and amino laurate-modified layered double hydroxides. Owing to the reaction between the amine groups of the intercalant and the epoxy groups, the adhesion between the double hydroxide nanolayers and epoxy molecules produced a significant enhancement of the thermomechanical properties of nanocomposites compared to the pristine epoxy. The elastic storage modulus was found to increase significantly if the filler content increased from 1 to 7 wt%. The height of the tan δ peak decreased with increasing nanofiller content because the stiffness of these exfoliated nanocomposites is enhanced by the exfoliated rigid nanolayers. It is proposed that, upon heating, the mobility of the main chains of the epoxy resins is restricted by the nanolayers because of the adhesion between the two phases; hence the polymer undergoes a high-temperature relaxation, α transition, causing the glass transition of these nanocomposites to increase about 33 °C with nanofiller content of 7 wt%.

In summary, the elastic storage modulus appears to be substantially enhanced at temperatures above T_g for the exfoliated DGEBA diamine-cured nanocomposites incorporating layered silicates with high aspect ratio. This effect is associated with a good interfacial adhesion between the epoxy matrix and silicate particles, as well as with the restriction of molecular mobility of polymeric segments near the silicate surface [26, 29]. A possible explanation for such an improvement could also be the creation of a three-dimensional network of interconnected long silicate layers, strengthening the material through mechanical percolation [4, 27, 28, 32, 33].

Similar results to those of the organoclay/DGEBA epoxy nanocomposites are reported also for the organoclay/polyimide nanocomposites, where a marked increase of the storage modulus and the glass transition temperature is observed on increasing the clay content [27, 28]. For example, Abdalla and co-workers [27] synthesised high-temperature thermoset polyimide/clay nanocomposites based on polyimide precursor solutions (PMR-15) with both unmodified and modified montmorillonite (pre-intercalated with dodecylamine and 11-amino-undecanoic acid). DMTA analysis showed significant increase in the thermomechanical properties (E' and E'') of 2.5 wt% clay-loaded nanocomposites in comparison with the neat polyimide. The effect of clay on the relaxation behaviour (i.e., T_α enhancement and broadening of β relaxation) is indicative of polymer–clay interactions at the segmental level. This trend was not observed for the 5 wt% nanocomposites, which was attributed to the potential variations in the interface caused by the degradation of modifier during thermal

imidisation. Tyan and co-workers [28, 32] obtained a marked 2.5 fold increase in the storage modulus of clay/polyimide nanocomposites in the glassy region at 7% clay content, as compared to that of the pure polyimide, while the glass transition temperature, measured by the tan δ peak, slightly increased by about 6 °C. The improved morphology of nanocomposites was related to the strong chemical bond between the swelling-agent-modified montmorillonite and the polymer molecules, thus resulting in dramatically enhanced thermal and mechanical properties.

An opposite thermomechanical behaviour related with a reduction of both the glass transition temperature and the viscoelastic response is reported for organoclay-containing nanocomposites based on either high-functionality epoxy resin or polyester resin [34-38]. Becker and co-workers [34] prepared nanocomposites of commercially available octadecyl-ammonium ion-modified montmorillonite (Nanomer 1.30E) dispersed within three different epoxy resins: a bifunctional resin (DGEBA, e.g., DER 331), trifunctional triglycidyl *p*-aminophenol (TGAP, e.g., Araldite MY0510), and tetrafunctional tetraglycidyldiaminodiphenylmethane (TGDDM, e.g., Araldite MY720). The curing agent used was diethyltoluenediamine. Wide-angle X-ray scattering (WAXS) and atomic force microscopy (AFM) analyses confirmed the exfoliated morphologies of the nanocomposites based on the bifunctional resin (DGEBA) and the intercalated morphologies of nanocomposites based on higher functionality resins (TGAP and TGDDM). A steady reduction of the glass transition temperature was found with increasing organoclay concentration, as determined from the tan δ peak of DMTA measurements. The reduction in T_α (~T_g) was found to be of the order of 15 °C for the DGEBA- and TGAP-based systems and 20 °C for the TGDDM-based systems at 10% organoclay, which indicated that it is not an absorbed layer effect. Moreover, a general trend of increasing tan δ peak broadness was observed in nanocomposites with increasing clay content. It was assumed that molecules that are located close to or even tethered to the silicate surface show a different mobility than those molecules in the volume, and that the amount of epoxy molecules associated with the clay layers is quite high. Since these systems are rather complicated, it was assumed that the α transition associated with the glass transition was reduced due to a combination of factors. The clay may change the chemistry of the reaction and indeed the organic ions may catalyse homopolymerisation [8]; hence, a lower crosslink density of the epoxy–amine reaction at the interfaces could be expected. In summary, the plasticising effect of the organic modifier, the presence of unreacted resin or the general lower crosslink density around the silicate surface are reasons why there could be a decrease in T_g. Additionally, Zax and co-workers [35] interpreted such a decrease in the glass transition temperature of intercalated polymers as due to the lack of surrounding entanglement.

Kornmann and co-workers [36-38] observed a reduction of T_α (~T_g) and an increase in both dynamic moduli in organoclay/TGDDM and DGEBA epoxy nanocomposites. This was attributed to interactions between the hydroxyl groups of the exfoliating agent used for the treatment of the organoclay and the resin components. The exfoliation was found to be very dependent on the clay modifier, curing agent and mixing. The diffusion

rate of the reactive species into the interlayers compared to the reaction rate outside the interlayer was proposed to be the controlling factor [39].

Bharadwaj and co-workers [40, 41] prepared crosslinked polyester/clay nanocomposites by dispersing methyl tallow bis(2-hydroxyethyl) quaternary ammonium-modified montmorillonite (Cloisite 30B) in pre-promoted polyester resin. This organoclay was chosen due to the presence of the polar hydroxyl group that presumably provides a good wetting surface for the unsaturated polyester. Clay concentration in nanocomposites was varied from 1 to 10 wt%. Crosslinking was initiated by adding methyl ethyl ketone peroxide (MEKP) catalyst to the resin–clay mixture at room temperature. Although the formation of nanocomposite structure was confirmed by transmission electron microscopy (TEM) and wide-angle X-ray diffraction (WAXD) measurements, the shear storage and loss moduli exhibited a progressively decreasing trend with increasing clay concentration, whereas the exact opposite is expected for a nanoscopically reinforced polymer [42]. This trend was explained on the basis of a progressive decrease in the degree of crosslinking with increasing clay concentration.

Suh and co-workers [43, 44] studied unsaturated polyester resin/styrene-based nanocomposites with montmorillonite, modified with octadecylamine and quaternary ammonium ions. Two mixing procedures of the components –resin, styrene and organoclay – were discussed: simultaneous mixing, leading to intercalated morphologies; and sequential mixing, resulting in exfoliated structures. DMTA analyses showed that the intercalated systems prepared by simultaneous mixing demonstrated about 10 °C lower T_α (~T_g) than that of the pristine unsaturated polyester resin, which was explained by the low crosslink density of these nanocomposites. In contrast, if the same compositions were prepared by sequential mixing, the resulting exfoliated nanocomposites displayed T_α (~T_g) about 50 °C higher and storage modulus G' about 50% bigger than that of the pristine resin. The authors concluded that the mechanism of exfoliation ruled by the manufacturing process of these nanocomposites has to be considered when the viscoelastic properties are studied.

Karger-Kocsis and Wu [45] surveyed the recent achievements with thermoset rubber/layered silicate nanocomposites, and showed that the properties of the 'nano-reinforced' rubbers depend strongly on the dispersion state of the silicate. Increasing reinforcement is accompanied by unexpectedly high elongation. The overall deformability of rubber nanocomposites was found to correspond to that of a less crosslinked rubber. A strong reduction of the α relaxation peak was observed in these nanocomposites, which is interpreted as a reliable indicator for improved intercalation and/or exfoliation, as well as being related to the reduced mobility of the rubber molecules owing to intercalation and strong bonding to the exfoliated clay platelets.

In our recent study [46, 47], the solvent-assisted processing technique was used as a controlling factor of the extent of exfoliation and the interfacial bonding, leading to different viscoelastic properties of smectite/epoxy nanocomposites. The DMTA results of

crosslinked *intercalated* and *exfoliated* nanocomposites based on Araldite LY556 resin and organo-smectite, modified with trioctyl-methyl-ammonium chloride (STN) were compared. The systems were cured with diethylenetriamine (DETA) by heating for 4 h at 80 °C and post-cured for 1 h at 140 °C. Dynamic mechanical thermal characteristics of the post-cured nanocomposites, storage E' and loss E'' moduli and tan δ, were determined on a Rheometric Scientific DMTA IV at strain amplitude of 0.2%, which was found to be the linear viscoelastic range for the systems studied. The samples were characterised in the bending mode at a frequency of 1 Hz and the heating rate was controlled at 2 °C/min. The measurement temperature ranged from 23 to 300 °C.

For preparation of *intercalated* STN/epoxy nanocomposites, the direct processing technique was used, where the organoclay was dispersed directly in the epoxy resin following by *in situ* polymerisation. The *exfoliated* nanocomposites were prepared by solvent-assisted processing, where the organoclay was premixed with toluene and then the epoxy resin added, following by vacuum evaporation and curing (see **Figure 2.10** in Chapter 2). Moreover, based on the infrared (IR) spectra results (Chapter 3), a strong chemical bonding at the filler–polymer interfaces is proposed for the intercalated smectite/epoxy nanocomposites prepared by direct processing. In contrast, the polymer–surface interactions are influenced by the plasticising effect of the clay intercalant and the solvent in the exfoliated nanocomposites, if prepared by solvent processing.

Our DMTA results [46, 47] demonstrated that the relation between the structure and the viscoelastic properties of smectite/epoxy nanocomposites depends significantly on the processing conditions.

As an example, **Figure 6.1** plots the dynamic storage modulus E' and tan δ *versus* temperature for the *intercalated* STN/epoxy nanocomposites prepared by *direct processing*, compared with the crosslinked epoxy resin. The STN smectite content is 2, 4 and 6 wt%. The α relaxation T_α is determined by the peak of tan δ. **Table 6.1** presents the characteristics of tan δ in the temperature region of the α relaxation – the values of T_α, the height and the broadness of the tan δ peak. It can be seen that the presence of smectite produces an overall increase of the storage modulus E' of intercalated nanocomposites compared to that of the pure epoxy resin. A slight increase of E' is observed in the glassy region ($T < T_g$), indicating reinforcement by the presence of rigid inorganic tactoids intercalated by the epoxy resin. The increase of E' in the rubbery region ($T > T_g$) is generally related with an increased crosslink density produced by the polymer–filler interactions. The position of the T_α peak of intercalated nanocomposites is increased by only ~2 °C on increasing the smectite content up to 6%. The height of the peak is decreased, and the broadness slightly increased by the smectite nanofiller, which is interpreted as a reliable indicator for intercalation.

Figure 6.2 presents dynamic storage modulus E' and tan δ *versus* temperature for the *exfoliated* STN/epoxy nanocomposites prepared by *solvent processing* with the assistance of toluene. The exfoliated nanocomposites show different viscoelastic behaviour from

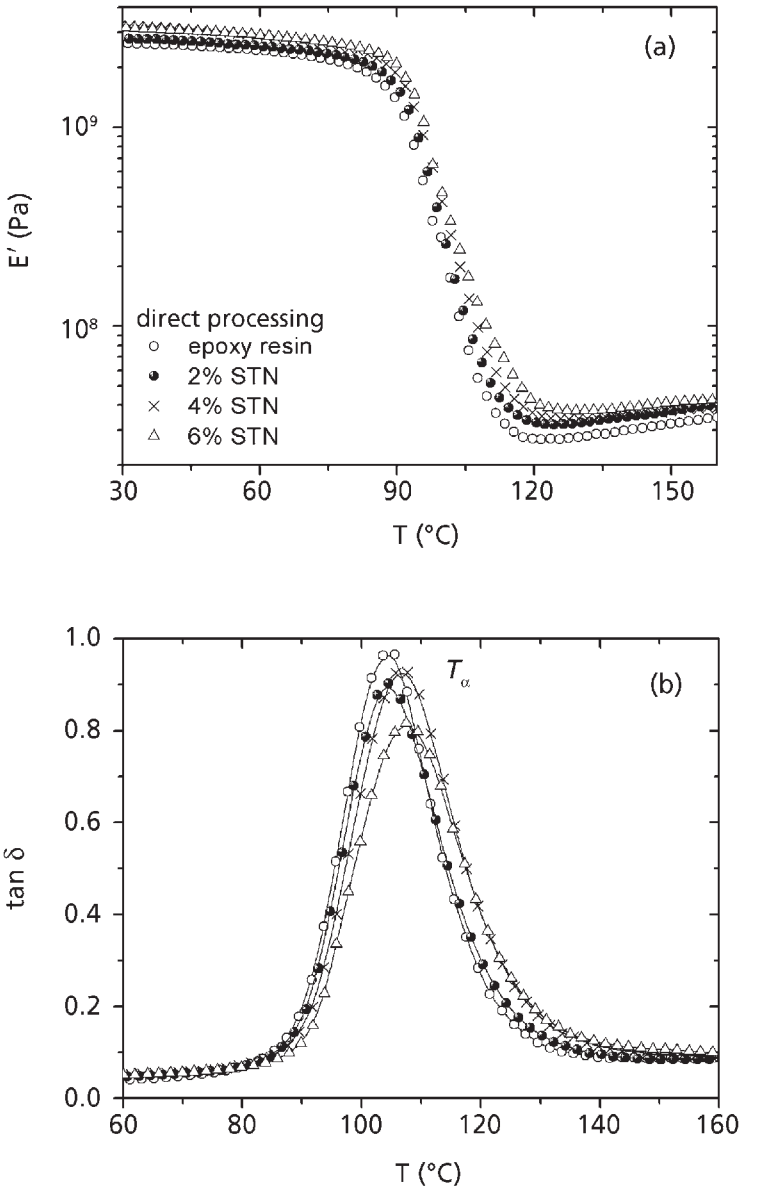

Figure 6.1 Dynamic mechanical thermal characteristics: (a) storage modulus *E′* and (b) tan δ *versus* temperature for intercalated STN/epoxy nanocomposites with 0, 2, 4 and 6 wt% smectite, prepared by direct processing and cured with DETA; T_α is presented by the peak of the tan δ curves.

Data from [47]

Table 6.1 Characteristics of tan δ peak of intercalated and exfoliated STN/epoxy nanocomposites produced by direct and solvent processing techniques, respectively

Sample code	Peak T_α (°C)		Height of tan δ peak		Broadness of tan δ peak (°C)	
	Intercalated, Direct process	Exfoliated, Solvent process	Intercalated, Direct process	Exfoliated, Solvent process	Intercalated, Direct process	Exfoliated, Solvent process
Epoxy	103.6	113.5	1.06	1.02	18	21
2% STN	104.6	110.7	0.90	0.89	22	23.5
4% STN	105.7	106.7	0.93	0.78	22.8	24
6% STN	107.5	102.1	0.82	0.72	23.5	22.5

Data from [46, 47].

that described above for the intercalated nanocomposites prepared by the same STN smectite and epoxy resin using direct processing.

As shown in **Figure 6.2(a)**, the storage modulus E' of exfoliated nanocomposites increases more pronouncedly with increasing smectite content in the glassy region ($T < T_g$), indicative of well-exfoliated and homogeneously dispersed smectite nanolayers. However, above the glass transition ($T > T_g$), the E' and the position of the T_α peak of tan δ decreased with increasing filler content. **Figure 6.2(b)** and **Table 6.1** show that T_α decreased by about 11 °C at 6% smectite. Such behaviour indicates facilitation of the chain mobility of the crosslinked epoxy resin in nanocomposites, compared to the pristine epoxy. The height of the tan δ peak decreased pronouncedly and the broadness slightly increased with increasing nanofiller content, which is indicative of the exfoliation of smectites.

As shown before by IR spectra results (**Figure 3.4**), the extent of curing of the STN/epoxy nanocomposites is roughly equivalent to that of the unfilled epoxy resin. Therefore, the increased chain mobility in exfoliated nanocomposites produced by solvent processing cannot be associated with the presence of incompletely reacted epoxy groups at the silicate surfaces. The observed increase in the elastic storage modulus in the glassy region confirms that the polymer–filler interfacial bonding is correspondingly good. Obviously, the plasticising effect produced by the organoclay pre-intercalated with quaternary alkyl-ammonium ions, as well as a residual amount of solvent, such as toluene, with high boiling temperature, are the reason for the increased chain mobility in the exfoliated nanocomposites investigated here.

Additionally, **Figure 6.3** compares the values of the storage modulus E' at 30 °C (the glassy region) and **Figure 6.4** presents E' at T_g + 30 °C (the rubbery region) for both intercalated and exfoliated STN/epoxy nanocomposites *versus* the smectite content.

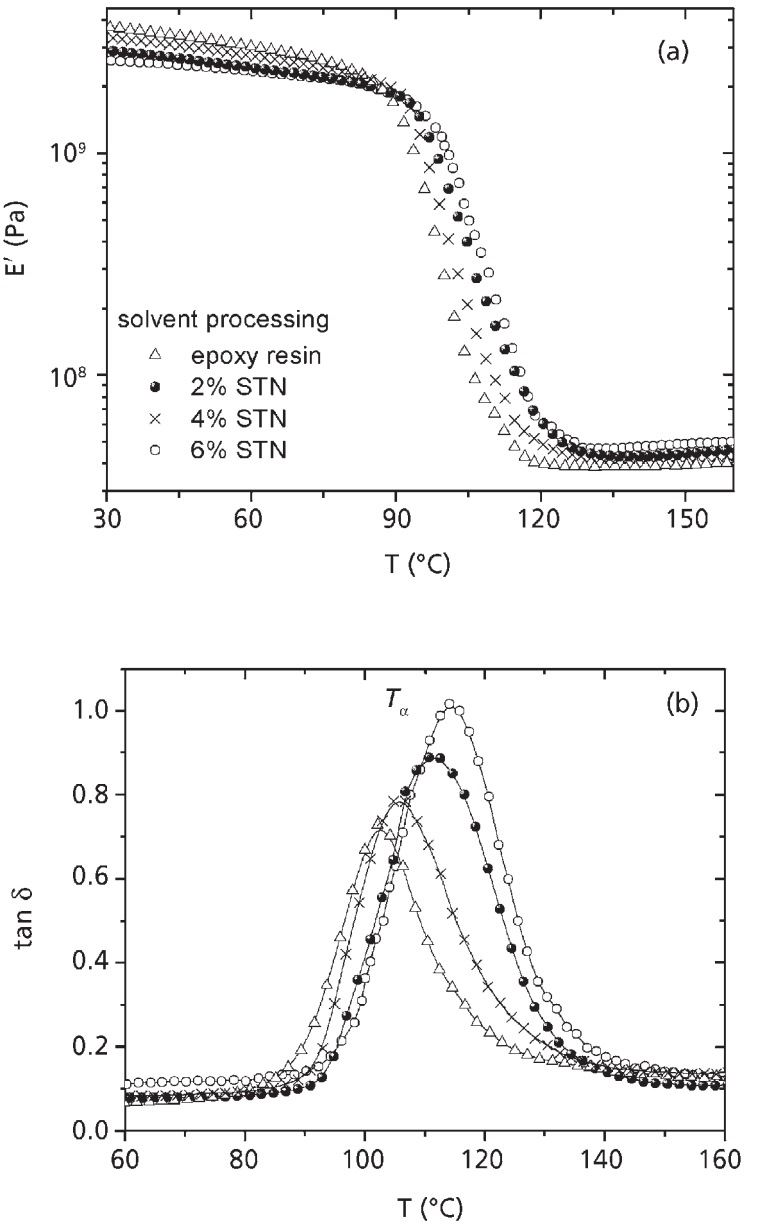

Figure 6.2 Dynamic mechanical thermal results: (a) storage E' and loss E'' moduli and (b) tan δ *versus* temperature for exfoliated STN/epoxy nanocomposites with smectite content of 0, 2, 4 and 6 wt%, prepared by solvent processing and cured with DETA.

Data from [47]

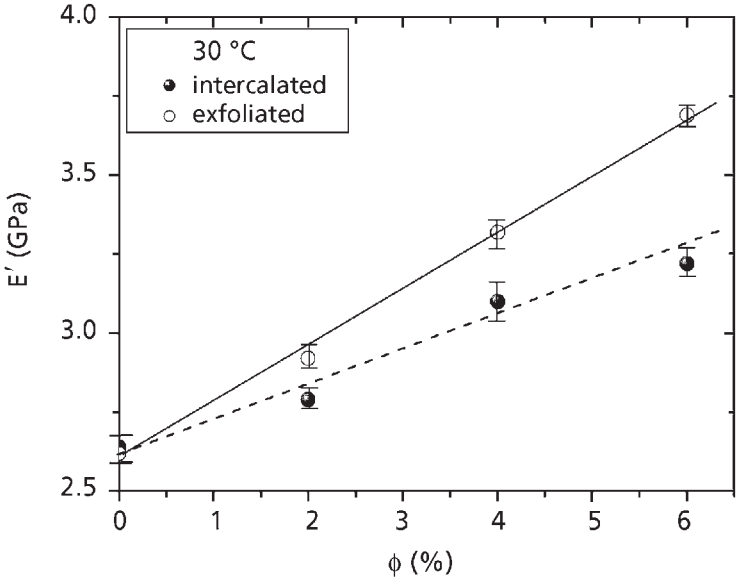

Figure 6.3 Storage modulus at 30 °C for direct and solvent-processed STN/epoxy nanocomposites *versus* smectite content.

Data from [47]

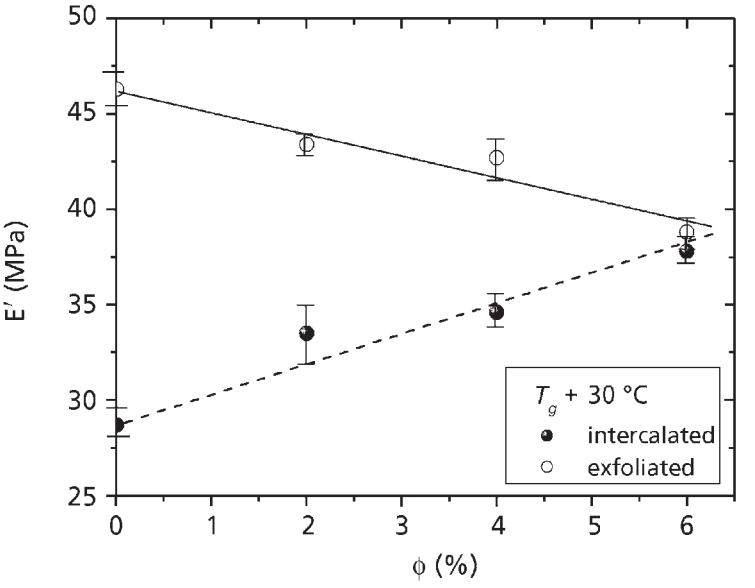

Figure 6.4 Storage modulus at T_g + 30 °C for direct and solvent-processed STN/epoxy nanocomposites *versus* smectite content.

Data from [47]

It is evident that at 30 °C the exfoliated systems prepared by solvent processing showed a larger improvement of the storage modulus than did the intercalated systems prepared by direct processing. For example, the 6% smectite content leads to 1.4 fold improvement, compared to 1.3 fold for the intercalated nanocomposites. In the rubbery region (T_g + 30 °C) the intercalated nanocomposites demonstrate reinforcement, but the exfoliated nanocomposites show decreased values of the storage modulus with increasing smectite content. The reinforcement effect in intercalated nanocomposites might be related to the increased crosslink density of the epoxy matrix, produced by bonding of epoxy molecules at the reactive silicate surfaces, leading to a reduced mobility of the main chain of the epoxy molecules as the temperature increases. In contrast, the decrease of the storage modulus in the rubbery region of exfoliated nanocomposites, prepared with the assistance of toluene, is related to the plasticising effect of the organic modifier and the remains of the toluene, resulting in increased chain mobility.

The results presented above lead to the conclusion that the nanolayer reinforcement in intercalated STN/epoxy nanocomposites may improve the stiffness, while in exfoliated nanocomposites both the stiffness and toughness of the epoxy resin may be improved. On this basis, therefore, the use of nanofillers in network polymers constitutes a more effective way of reinforcing and improving the thermal mechanical properties over direct modification of their molecular composition. This effect is not necessarily related to the increase in the crosslink density of network polymers, even if often this leads to an increase in strength and modulus.

6.1.1.2 DMTA of Thermosets With Nanoparticles

The reinforcement effects of particulate nanofillers on the viscoelastic properties of the epoxy resin have been reported at temperatures associated with the glassy region, $T < T_g$ [48-51]. Ragosta and co-workers [48] reported DMTA results for epoxy/silica nanoparticle composites produced by dispersing silica-organosol particles in high-functionality TGDDM epoxy resin, and further curing with 4,4′-diaminodiphenyl-sulphone hardener. The authors observed that the presence of the silica nanofillers slightly decreased the T_α (~T_g) value by about 7 °C, but had no effect on the position of the β relaxation peak. This was related to the presence of a limited amount of unreacted epoxy resin, which can have some plasticisation effect. However, the height of both peaks is decreased to an appreciable extent with the addition of the filler, which was ascribed to the non-dissipative nature of the filler, which reduces the viscoelastic response of the composite. Importantly, an overall increase of the storage elastic modulus in the glassy region was observed, which implies that the matrix–filler interfacial bonding is correspondingly good.

Miyagawa and Drzal [49] investigated the viscoelastic properties of DGEBA epoxy nanocomposites reinforced with fluorinated single-walled carbon nanotubes. The storage modulus of nanocomposites at 30 °C was found to increase substantially by 1.1 GPa

with the addition of only 0.3 wt% of carbon nanotubes, representing approximate 33% improvement. This was related with well-separated and homogeneously dispersed nanotubes because of pre-fluorination. However, the peak maximum of tan δ, T_α (~T_g), linearly decreased with increasing filler content. Thus, after adding only 0.2 wt% (0.14 vol%) carbon nanotubes, the glass transition temperature decreased by approximately 30 °C. Such a large decrease in the α transition has not been observed with nanocomposites reinforced with layered silicates by the addition of such a small amount of filler. A decrease of the storage modulus associated with a lower crosslink density of the epoxy matrix of the nanocomposites was found within the rubbery region ($T >> T_g$). This effect was explained in terms of a non-stoichiometric mixture produced by the adsorbed layer of epoxy molecules at the large nanotube surface, which no longer reacted with the methyltetrahydrophthalic anhydride hardener. After careful adjustment of the anhydride curing agent to achieve stoichiometry, the processed nanocomposites with extremely small amount of nanotubes still showed a large improvement of the storage modulus at room temperature.

Vassileva and Friedrich [50] studied the influence of the addition of alumina nanoparticles on the dynamic mechanical spectra of an amino-cured epoxy resin. Suppression of the small-scale cooperative motions related to the relaxation and an increase in the activation energy for the relaxation of the epoxy matrix were observed as the alumina content increased. This is explained in terms of an antiplasticisation effect of the alumina nanoparticles on the epoxy resin.

We have investigated the reinforcement effect on the viscoelastic properties of crosslinked epoxy hybrids incorporating nanosized carbon (graphite or diamond) particles in our previous study [51]. The carbon used is a mixture of finely dispersed graphite and diamond in a proportion 67/33, as shown earlier in **Table 2.5**. The epoxy resin Araldite LY556 (bisphenol A, CIBA) with viscosity η = 25 Pa s is used as a matrix polymer (see **Table 2.3**). Carbon/epoxy hybrids of 2, 4 and 6 vol% filler content are prepared as the desired amount of graphite or diamond nanoparticles is dispersed in the epoxy resin matrix using high-speed mixing at 7000 rpm for 15 min, followed by sonication for 5 min. The aggregates of carbon nanoparticles are dispersed into small clusters, which lead to a stable dispersion. The systems are cured with diethylenetriamine in stoichiometric proportions for 1 h at room temperature, followed by post-curing for 3 h at 140 °C. Dynamic mechanical characteristics of the post-cured samples were measured in bending mode at a strain amplitude of 0.2% and a frequency of 1 Hz. The measurement temperature ranged from 23 to 300 °C and the heating rate was controlled at 2 °C/min. The effect of nanofiller on the viscoelastic properties of the crosslinked epoxy matrix composites was probed using values of storage and loss moduli and loss tangent. When a polymer goes through the α transition, tan δ shows a maximum, at a temperature T_α; in addition, substantial drops in E' and E'' appear, indicating viscous damping due to segmental motion in the polymer. For crosslinked polymers, both E' and T_α generally increase with increasing crosslink density [52, 53].

Figure 6.5 shows the storage E' and loss E'' moduli and the loss tan δ *versus* temperature for the epoxy resin matrix and the carbon/epoxy composites with 2, 4 and 6 vol% graphite or diamond content [51]. The presence of carbon nanofiller enhances the values of E' modulus, and this effect appears with different magnitudes in the glassy and rubbery regions. The storage modulus E' is slightly improved by the nanofiller in the glassy region, $T < T_g$; however, above T_g the mechanical reinforcement by carbon nanoparticles in the epoxy resin becomes prominent. The α transition T_α associated with the glass transition increases significantly with increasing filler concentration. Moreover, a significant increase of E' modulus of hybrids, compared with that of the epoxy resin, is observed in the rubbery region. These results are indicative of an interface layer effect due to chains being tied down by the surface of carbon, which leads to increased crosslink density of carbon/epoxy hybrids. The tan δ peak decreases and becomes broader on increasing the filler content, which confirms the restricted chain mobility of the crosslinked epoxy by the presence of the carbon nanofiller.

In order to compare the effect of nanofiller in the three regions, glassy, α transition and rubbery states, **Figure 6.6** presents the normalised storage modulus E'_r calculated as a ratio of the storage modulus of nanocomposites E'_{NC} to that of the pure resin E'_{resin} *versus* the volume filler content ϕ. Three temperatures are compared 80, 106 and 150 °C, corresponding to the three regions, respectively. As seen, E'_r increases slightly in the glassy region at 80 °C. However, the reinforcement effect of nanofiller becomes significant at 106 and 150 °C. For example, at 6% carbon content the enhancement of E' is ~1.2 fold at 80 °C, ~5.1 fold at 106 °C, and ~2.3 fold at 150 °C, if compared to the storage modulus of the pure resin. The increase of E'_r at 106 °C is very large, from 1 to 5.1, as at this temperature the neat epoxy is in the rubbery state while the nanocomposites are still in the glassy state.

Notably, the reinforcement depends significantly on the amount of nanofiller, and thus E'_r increases strongly due to percolation (see Section 2.5.2). Obviously, the structure of fractal flocs formed by graphite/diamond nanofiller in epoxy resin around the first rheological threshold, $\phi^* \sim 5\%$, gives rise to a better modulus reinforcement [47, 51]. Typically, the conventionally prepared epoxy composites containing micrometre or larger size filler particles do not exhibit substantial changes in E' at filler volume contents up to 10–15 vol%.

It could be concluded that the characteristics of the superstructure of hybrids caused a remarkable effect on the reinforcement of thermosets with particulate nanofillers. The formation of fractal flocs of nanofiller particles incorporating matrix resin, at filler concentrations above the first rheological threshold, plays a critical role in the mechanical deformation processes. During the deformation, the flocs probably act as elastic barriers, which suppress the propagation of the microvoids. The interface (bond) polymer layer surrounding the nanoparticles, together with the flocculated structure formed by cluster–cluster aggregation, cause the changes in the morphology of the polymer matrix, which leads to the reinforcement.

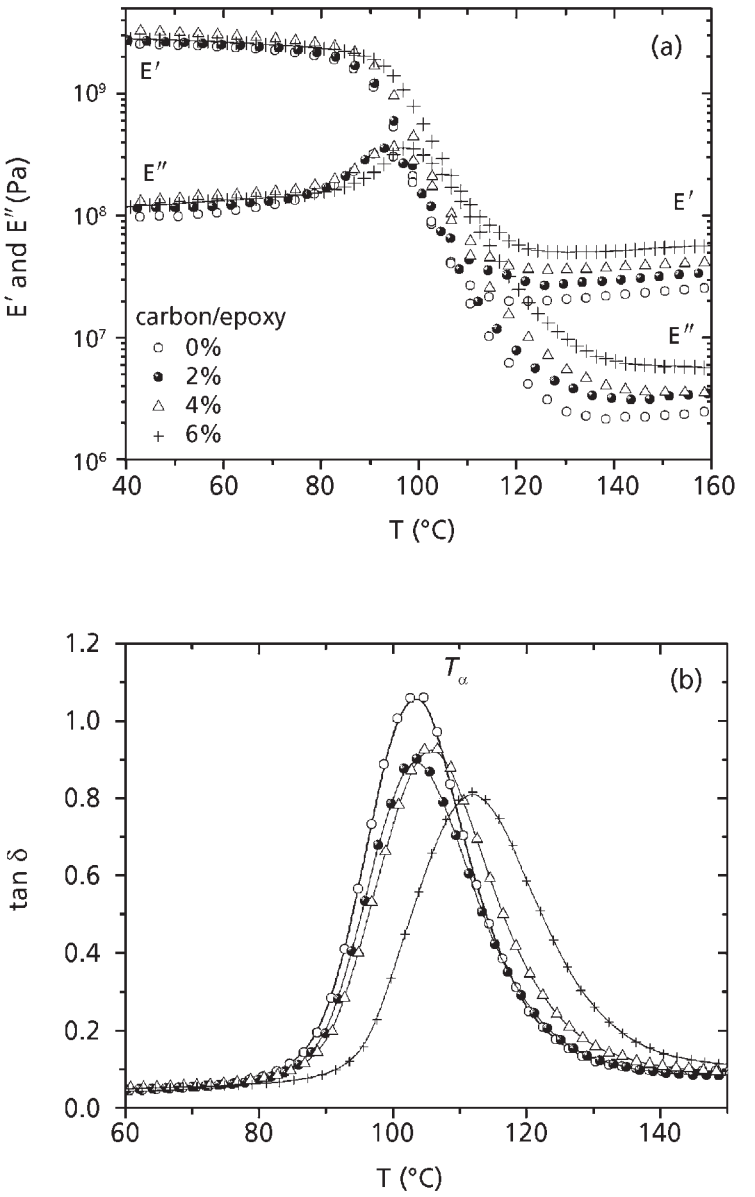

Figure 6.5 Dynamic mechanical characteristics: (a) storage and loss moduli, *E′* and *E″*, and (b) tan δ *versus* temperature for (graphite/diamond)/epoxy hybrids (GD) on varying the filler content of 0, 2, 4 and 6 vol%. The value of T_α is determined from the peak of the tan δ curves.

Reproduced with permission from [51]. ©Wiley Periodicals, 2005

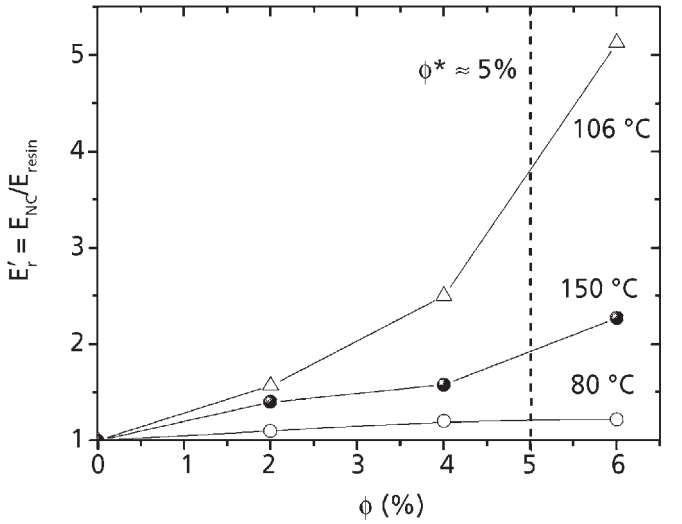

Figure 6.6 Normalised storage modulus $E'_r = E'_{NC}/E'_{resin}$ *versus* graphite or diamond volume fraction in crosslinked epoxy-based hybrids at three temperatures, 80, 106 and 150 °C, corresponding to the glassy, glass transition and rubbery regions. The dashed line shows the rheologically determined first percolation threshold, $\phi^* \sim 5\%$.

Data from [47, 51]. Reproduced with permission from [51]. ©Wiley Periodicals, 2005

6.1.2 Stiffness, Toughness and Elasticity

In general, the addition of inorganic filler particles to a polymer matrix produces an increase in stiffness, but sacrifices toughness, whereas rubber particles are added to increase toughness, but they reduce the stiffness [51, 52]. Recently, the introduction into a polymer matrix of inorganic nanofiller particles at a concentration of only a few weight per cent has resulted in a remarkable combination of high stiffness and toughness [53-62]. This synergy of properties is caused by changes in the morphology of the polymer matrix due to the combination of inorganic and organic components on a nanometre level. The enhanced modulus and potential rigid-phase toughening afford thermoset/layered silicate nanocomposites opportunities in applications of polymer matrix composites. Thus, one of the most important features of polymeric nanocomposite materials is the possibility of controlling their macroscopic properties by tailored manipulation of their structures at the level of different length scales [4, 53].

Polymer/clay nanocomposites form a nanostructured network of finely dispersed and uniformly oriented silicate layers with a strongly bonded polymer at the silicate surface. There, the nanofiller particles have a dual function during the deformation process [53]. Due to the well-organised structure they function as microvoid initiation sites, which are

necessary for high toughness. The silicate layers, bonded at the fringes of microvoids, prevent their further growth and, as a consequence, the stiffness of the nanocomposite is improved. Moreover, silicate nanolayers have high modulus and act as a rigid modifier, which is also responsible for high stiffness and modulus.

Although it is often found that improvement in modulus sacrifices toughness of the material, both toughness and stiffness could be improved by incorporation of organoclay in thermoset resins [14, 55]. The improved stiffness (modulus), toughness (stress at break) and elasticity (strain at break) make the nanocomposite strategy an attractive alternative to the commonly used micrometre-sized fillers. The enhanced modulus, elasticity and potential rigid-phase toughening afford thermoset/layered silicate nanocomposites opportunities as polymer matrix composites, as well as with regards to using epoxy nanocomposites as a matrix in conventional fibre-reinforced composites [29]. It is interesting to note that, for random orientation in three dimensions, isotropic platelets are three times as effective as fibres in providing stiffness reinforcement [63].

6.1.3 Tensile Properties

Epoxy resins find many applications as adhesives, construction materials, composites, laminates, coatings, and in the aircraft and spacecraft industries owing to their high strength, low viscosity and low shrinkage during cure, low creep and good adhesion to many substrates. However, epoxy resins are usually brittle materials in their cured state and exhibit poor resistance to crack growth. Thus, they are usually combined with a wide range of modifiers to attain greater flexibility. Recently, epoxy/clay nanocomposites have also been studied in order to improve the properties of the epoxy resin for many applications [14, 31, 36-39, 57].

Many authors have reported that epoxy resin-based nanocomposites display a totally different mechanical behaviour depending on whether their glass transition temperature is located below or above room temperature [12–15, 20, 21, 55–58]. Highly flexible and low glass transition elastomeric epoxy resins are shown to achieve better improvement in mechanical properties in comparison to rigid, highly crosslinked resins. Dramatic improvement in the tensile strength and modulus of organoclay/epoxy nanocomposites was observed when the epoxy resin matrix exhibits a sub-ambient glass transition temperature [12, 14, 30, 57, 58]. Pinnavaia and co-workers [57] found that the mechanical reinforcement provided by exfoliated clay layers is much more significant for a rubbery matrix than for a glassy matrix. For a rubbery matrix (e.g., elastomeric epoxy resin), the reinforcement provided by the silicate layers at 15 wt% loading was manifested by a more than 10 fold improvement in tensile properties. The improved stiffness is directly ascribed to the reinforcement of the exfoliated high-aspect-ratio platelets. Moreover, increasing the degree of clay exfoliation substantially increased both the tensile strength and the modulus in the rubbery matrix [12, 13, 30].

However, the strain at break of nanocomposites was found to be essentially the same as for the pristine matrix, suggesting that the exfoliated clay platelets did not disrupt the matrix continuity. The rubbery state of the matrix may allow alignment of the exfoliated clay layers upon applying strain, which contributes to the reinforcement. A large increase in the tensile modulus was observed for elastomeric thermoset matrices, related to the increasing length of the alkyl-ammonium cation of the organoclay modifier [14, 15]. While the clay modified by alkyl chains with low carbon number (up to 8) gives an intercalated structure with a low tensile modulus, the organoclays with carbon numbers 8, 12 and 16 produced exfoliated structures and consequently give much higher modulus values [15].

Pinnavaia and Lan have published several patents and publications [60–62] for the manufacture of elastic epoxy/clay nanocomposites with intercalated or exfoliated clay to be used for thin-layer applications, for example, as protective and decorative coatings and encapsulation, filament-wound tanks, etc. The nanocomposites are found to demonstrate superior tensile strength and chemical resistance in comparison with the conventional composites with clay or with the unfilled crosslinked epoxy resin. However, the authors claimed that the alkyl-ammonium ions prevent interactions between the epoxy matrix and the clay surfaces. Furthermore, the alkyl-ammonium ions are expensive and toxic. Therefore, in [62] the use of ammonium intercalant is eliminated and the clay is acidified. Moreover, the oligomer contains basic groups for reaction with the protons of the clay. The results show that the absence of ammonium intercalant increased the effectiveness of the clay reinforcement, producing total exfoliation in the clay/epoxy nanocomposites at high filler content from 5 to 15 wt%.

In contrast, in high-T_g epoxy thermosets [15, 34, 55], neither intercalated nor exfoliated nanostructures lead to a significant improvement of the tensile strength. Silicate nanolayers make the thermoset resins more brittle. Becker and co-workers [34] reported that the epoxy resin systems with a high glass transition temperature, such as bi-, tri- and tetrafunctional epoxy resins (DGEBA, TGDDM and TGAP, respectively), cured with diethyltoluenediamine, gain a quite modest improvement of mechanical performance. The increase in flexural modulus was in the range of 20% for organoclay content of 10 wt%. In these nanocomposites, the improvement in stiffness of the high-functionality epoxy resins (TGDDM and TGAP) is comparable with those achieved for the bifunctional (DGEBA) resin system [34, 55]. The fracture toughness, as quantified by the stress intensity factor K_{IC} determined by the compact tension test, indicated that the toughness of the glassy epoxy resin is improved through the incorporation of organoclay. The DGEBA and TGDDM epoxy resins show a linear increase of the normalised stress intensity factor K_{IC} by approximately 20% at an organoclay concentration of 10 wt%, whilst improvement in the high-functionality TGAP systems is significantly lower. The overall structure of the nanocomposites, responsible for the above-mentioned properties, was found to be a blend of intercalated and exfoliated organoclay layers.

The effect of nanocomposite formation on elasticity has been widely investigated. In general, the nanofiller reduced the elongation at break in thermoplastics. In contrast, the intercalated and particularly the exfoliated nanocomposites in crosslinked matrices display a large increase of the elongation at break, as reported for elastomeric epoxy [20] and polyol polyurethane [21] matrix nanocomposites. The improved elasticity is attributed to both the plasticising effect of the organic modifier of pre-intercalated organoclay and the conformational effects at the clay–matrix interface.

Hsueh and Chen [26] studied layered double hydroxides (LDH)/epoxy nanocomposites prepared on the basis of amine-cured Epon 828 resin. The elongation at break gradually increases with the filler content from 0 to 3 wt% in the exfoliated nanocomposites. The authors proposed that the increase in the elongation at break has two causes.

1. The adhesion between the inorganic and organic phases is enhanced by a reaction between the intercalant and the epoxy resin, which makes these nanocomposites less easy to break during extension.
2. The long alkyl chains of the intercalant plasticise the exfoliated nanocomposites.

Accordingly, exfoliated nanocomposites with excellent compatibility exhibit enhanced tensile properties, including tensile strength, Young's modulus and elongation at break.

Basic correlations between polymer morphology, clay superstructures, stiffness and toughness of the epoxy/clay nanocomposites were investigated by several authors. Zilg and co-workers [55, 56] proposed that intercalated clay promoted toughness whereas exfoliated clay platelets mainly improved the stiffness of the polymer matrix, due to energy-absorbing shearing of intercalated clay layers. These materials do have a lateral dimension in the micrometre scale and it is possible for such morphology to encourage crack stopping. However, the rather weak stiffness improvement is observed in the case of anhydride-cured epoxy nanocomposites, when true exfoliation structures were obtained [55]. Hence, it is proposed that the real key to matrix stiffness improvement resides in the formation of supramolecular assemblies, obtained by the presence of dispersed anisotropic laminated nanoparticles.

The improvement in mechanical properties of glassy and rubbery epoxy nanocomposites may elucidate the reinforcing mechanism, as proposed by Pinnavaia and co-workers [57]. Based on the increased elasticity of the rubbery epoxy matrix, it was assumed [14, 55-59] that reinforcement through clay exfoliation at temperatures above T_g is due to shear deformation and stress transfer to the platelet particles. In addition, the platelet alignment under stress may also contribute to the improved performance of exfoliated nanocomposites with a rubbery matrix as compared to a glassy matrix. Propagation of fracture across the polymer matrix containing aligned silicate layers is energy-consuming, and thus the tensile strength and modulus are reinforced. In a glassy matrix, clay alignment upon applied stress is minimal and blocking of the fracture by exfoliated clay is less efficient.

Interesting results are found for the fracture behaviour of epoxy nanocomposites containing silica nanoparticles [48]. The fracture of specimens of pure epoxy resin and nanocomposites always occurs in a brittle fashion. For the case of pure epoxy resin, the load–displacement curve is linear, and a sudden drop appears when a crack begins to propagate in catastrophic fashion. However, a series of crack stopping steps are identified in the load–displacement curves of nanocomposites, when the loading conditions for crack propagation are reached. Moreover, the maximum load leading to fracture was found to be higher when the silica content is increased. Such results give evidence for the mechanism of nano-reinforcement.

Unsaturated polyester is a typical resin applied in coating and composite technologies. Glass-fibre-reinforced composites based on unsaturated polyester resins have been widely used in many industrial applications, including automotive, marine and infrastructure applications, because of their outstanding combination of processability, excellent chemical resistance and low cost. However, the lack of good mechanical properties, volume shrinkage and severe surface quality require finding new methods of enhancing polymer properties, based on the nanocomposite concept.

Structure–property relationships in crosslinked polyester/clay nanocomposites were studied by Bharadwaj and co-workers [40, 41]. They prepared nanocomposites by dispersing methyl tallow bis(2-hydroxyethyl) quaternary ammonium chloride-modified montmorillonite in pre-promoted polyester resin and subsequently crosslinking at room temperature. The most important finding was that, although there is firm evidence showing the formation of a nanocomposite structure, the tensile modulus and the dynamic moduli progressively decreased with increasing clay content. A combination of the morphology and extent of crosslinking in the polyester/clay nanocomposites was used to understand this phenomenon. The overall decrease in the dynamic moduli and the tensile modulus of the polyester nanocomposites with increasing clay content led to the hypothesis that the intercalation and exfoliation of the clay in the polyester resin served to effectively decrease the number of crosslinks, and thus the degree of crosslinking was reduced. Interestingly, a greater drop in properties of the 2.5 wt% nanocomposite was found in comparison with the higher clay content, which was traced to the morphology. Thus, the 2.5 wt% sample showed exfoliation on a more global scale compared to the 10 wt% sample. Hence, the crosslink density was proposed to be proportional to the degree of exfoliation and macroscopic dispersion. Here, the effects of the clay–modifier–polymer interface, as well as the chemical effects of the organic modifier on the polyester resin, do not account for this property reduction. However, the establishment of a morphological hierarchy in polyester/clay nanocomposites was demonstrated to be the key factor in developing an understanding of structure–property relationships in these systems.

A significant improvement in the fracture toughness of clay/polyester nanocomposites was observed. Kornmann and co-workers [64, 65] reported on improvement in mechanical properties and fracture toughness of nanocomposites based on montmorillonite and

unsaturated polyester resin. This example is the first one to present an alternative method of modifying layered silicates by silane coupling reaction rather than interlayer ion exchange to form a nanocomposite. A significant increase was observed in Young's modulus and fracture toughness with increasing clay content up to 5 vol%. The increase in modulus is ~32%. In contrast, glass bead epoxy resins show an increase in modulus at a reinforcement content that is twice as high [66]. Favourable toughness improvement of this brittle unsaturated resin is gained with the addition of a small amount of clay. At 5 vol% the fracture toughness parameter K_Q is doubled and G_Q has increased three times as compared with the pure resin values. Moreover, the tensile strength (stress at break) of nanocomposites was virtually unchanged but it decreased at clay content of 3–4 vol%. The authors claimed that interfacial debonding is an important mechanism in reducing the tensile strength, and thus the lack of a reinforcement–matrix interface at the nanoscale could be a desirable feature of these nanocomposites.

Karger-Kocsis and co-workers [67] prepared nanocomposites of 5–15 wt% organoclay with a matrix composed of unsaturated ester and epoxy (ratio 1:1). After curing, the system was phase separated as an interpenetrating polymer network with organoclay being enrobed by the epoxy. They also found that the organoclay strongly increased the apparent fracture energy of this crosslinked resin, which is doubled at 5% filler content, and led to a dramatic difference in the fracture surface.

6.1.4 Flexural Properties of Clay-Containing Thermoset Nanocomposites

An improvement in flexural properties was found in our studies [46, 47] for the smectite/epoxy nanocomposites, and it was related to the exfoliation morphology. The nanocomposites were prepared by organo-smectites, pre-intercalated with hexadecyl-octadecyl-ammonium (SAN), trioctyl-methyl-ammonium (STN) and oligo(oxypropylene)-diethyl-methyl-ammonium (SPN) ions (see **Table 2.4**), finely dispersed in epoxy resin Araldite LY556. Samples were cured with DETA by heating for 4 h at 80 °C and post-cured for 1 h at 140 °C. As mentioned before, the direct processing technique led to the formation of intercalated nanocomposites with SAN and STN smectites and to exfoliated nanocomposites with SPN smectites (see **Figures 3.2** and **3.3**). In contrast, solvent processing assisted by toluene resulted in the formation of exfoliated nanostructures with the three organoclays SAN, STN and SPN in the epoxy matrix.

For example, **Figure 6.7** compares the bending stress–strain curves of the crosslinked glassy epoxy resin (T_g ~ 130 °C) and the intercalated and exfoliated SAN, STN and SPN/epoxy nanocomposites (SAN_{NC}, STN_{NC} and SPN_{NC}) of 5 vol% organoclay content, produced by the direct and solvent processing techniques. **Table 6.2** summarises the flexural characteristics, such as the modulus, the stress at break (flexural strength), the strain at break, and the reinforcement factors (normalised modulus, E_{NC}/E_{resin}, and normalised stress at break, $\sigma_{NC}/\sigma_{resin}$) of the investigated systems.

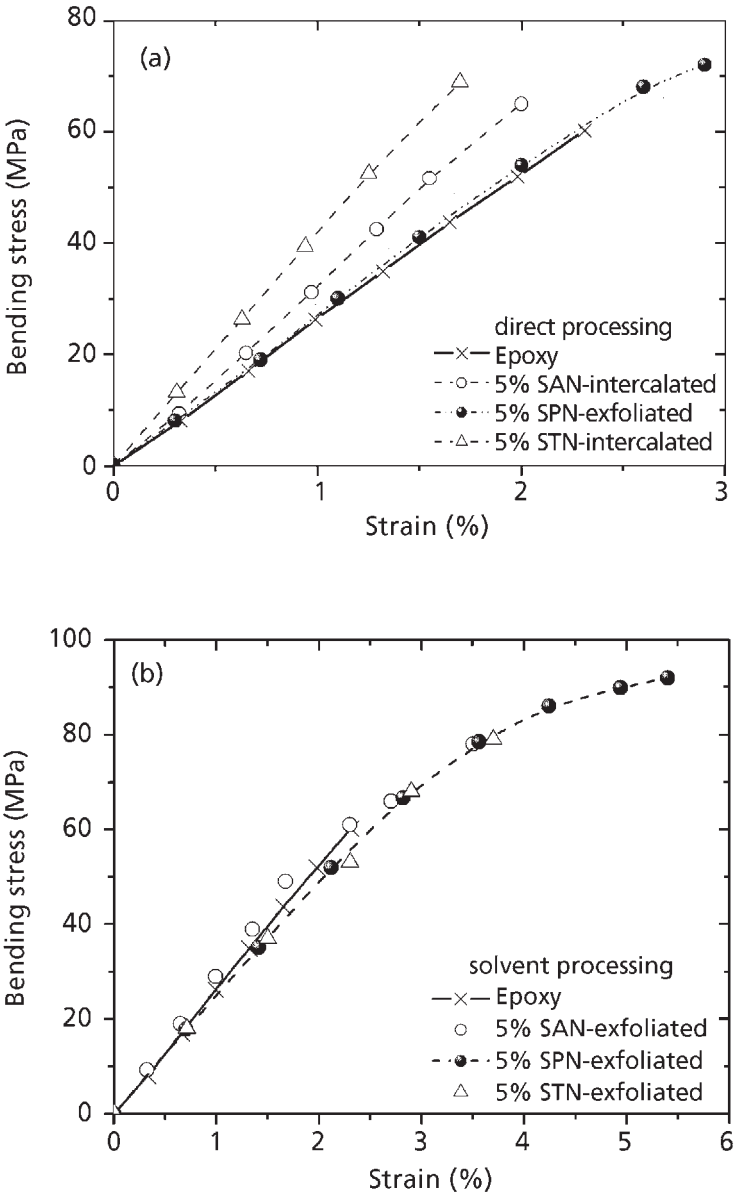

Figure 6.7 Bending stress–strain curves of glassy epoxy resin Araldite LY556 and 5 vol% smectite/epoxy nanocomposites, cured with DETA: (a) intercalated SAN and STN and exfoliated SPN nanocomposites produced by direct processing; and (b) exfoliated SAN, STN and SPN nanocomposites produced by solvent processing.

Data from [46-47]. Reproduced with permission from [46]. ©Wiley Periodicals, 2005

Table 6.2 Flexural characteristics of intercalated and exfoliated nanocomposites based on the glassy epoxy resin Araldite LY556 and 5 vol% SAN, STN and SPN organo-smectites produced by direct and solvent processing techniques

Sample code	Processing/ nano-structure	Flexural modulus, E (GPa)	Reinforce-ment factor, E_{NC}/E_{resin}	Stress at break, σ (MPa)	Reinforce-ment factor, $\sigma_{NC}/\sigma_{resin}$	Strain at break, (%)
Epoxy	–	2.65	1	60	1	2.3
5 vol% SAN	Direct/ intercalated	3.78	1.43	67	1.12	2.0
5 vol% STN	Direct/ intercalated	4.18	1.58	69	1.15	1.7
5 vol% SPN	Direct/ exfoliated	2.64	1	72	1.2	2.9
5 vol% SAN	Solvent/ exfoliated	2.70	1.02	78	1.3	3.5
5 vol% STN	Solvent/ exfoliated	2.45	0.92	79	1.32	3.7
5 vol% SPN	Solvent/ exfoliated	2.44	0.92	92	1.53	5.4

Data from [46, 47]. Reproduced with permission from [46]. ©Lulea University of Technology, Sweden, 2001

As can be seen in **Figure 6.7(a)** and **Table 6.2**, the intercalated nanocomposites, SAN_{NC} and STN_{NC}, produced by the direct processing technique display about 3–6% increase of bending strength (stress at break) in comparison with the unfilled epoxy resin. The flexural modulus (the slope of the linear initial part of the bending stress–strain curves) of the nanocomposites increases significantly depending on the organic modifier; however, the strain at break decreases by 13–26%. The reinforcement factor, determined by the normalised modulus, calculated as the ratio of the values for the nanocomposite to the values of the pure epoxy matrix, E_{NC}/E_{resin}, was found to be 1.43 (SAN_{NC}) and 1.58 (STN_{NC}).

In summary, the intercalated nanocomposites display an improved stiffness (flexural modulus) and toughness (stress at break), but the material is more brittle, with lower elasticity, in comparison to the unfilled epoxy. This effect may be associated with the intercalated nanostructures and the strong interfacial adhesion between the clay and the epoxy, observed as a result of the direct processing (**Figure 3.4a**).

In contrast, the exfoliated nanocomposites, SAN_{NC}, STN_{NC} and SPN_{NC}, produced by the solvent processing technique (**Figure 6.7b**), as well as the exfoliated SPN_{NC} produced by

the direct processing technique (**Figure 6.7a**), demonstrate significant improvement in toughness and elasticity, but the stiffness remains similar to that of the epoxy matrix. As shown in **Table 6.2**, a significant enhancement of bending strength, accompanied by a strong increase of the strain at break in the range of 26–135%, is observed for exfoliated nanocomposites. The reinforcement factor, determined by the normalised strength (stress at break), calculated as the ratio of the values for the nanocomposite to the values of the pure epoxy matrix, $\sigma_{NC}/\sigma_{resin}$ were found to be 1.3 (SAN), 1.32 (STN) and 1.53 (SPN). However, the flexural modulus is not changed substantially and shows values similar to that of the epoxy matrix. Much stronger enhancement of bending characteristics was found for the SPN_{NC} in comparison with SAN_{NC} and STN_{NC}, due to the higher exfoliation and plasticising effects of the paraffin-like SPN modifier. Moreover, the exfoliated SPN nanocomposites produced by the solvent processing technique display much larger improvement in flexural properties, about 28% in strength and 86% in elasticity (strain at break), in comparison with the same SPN nanocomposites produced by direct processing. These results confirm the positive role of solvent processing for the total exfoliation of organo-smectites in the epoxy matrix.

In summary, a large improvement in toughness (stress at break) and elasticity (strain at break) is observed in 5 vol% exfoliated nanocomposites, which can be attributed to the total exfoliation produced by solvent-assisted processing, as well as to the plasticising effect of the organic modifier and the residual amount of toluene. Such enhancement in mechanical properties could also be related to the small-scale heterogeneity associated with the exfoliated nanocomposite structures.

It could be concluded from the results above that the improvements in the flexural properties of the nanocomposites based on glassy epoxy resin and organoclay are strongly related to the structure and morphology (structure–property relationship). The direct processing technique produces mostly intercalated nanocomposites of a large-scale heterogeneity and strong interfacial bonding, which result in an increased stiffness, but higher brittleness. In contrast, solvent processing leads to exfoliated nanocomposites with a small-scale heterogeneity and altered interfacial interactions, which result in a significant enhancement in toughness and elasticity.

Improvement in the flexural properties of other thermoset/clay nanocomposites has been reported by several authors [68–75]. Nanocomposites based on clay and cyanate ester thermosetting polymers have received strong attention over the past few years. These polymers have excellent adhesive, thermal and mechanical properties useful for electronic encapsulation, structural materials for aerospace, and adhesives. Recently, layered silicates have been investigated as attractive additives for cyanate esters [68–72]. Most of the work on cyanate ester/layered silicate nanocomposites reported on the formation of intercalated nanostructures [69-71], which produced significant improvement of crack resistance [69, 70], mechanical properties [69, 70], thermal expansion and thermal stability [69, 71, 72].

Wooster and co-workers [68] prepared nanocomposites based on bisphenol E dicyanate ester and montmorillonite exchanged with various quaternary ammonium cations. Depending on the type of organoclay, nanocomposites were found to reside from the intercalated to the exfoliated end of the structure spectrum. The most dramatic increase in mechanical properties of the cyanate ester resin occurred in the crack resistance, wherein about 80% increase appeared at 3–4 wt% organoclay content. This increase is much more than would be expected with similar silica filler content [73]; however, it is comparable to other montmorillonite/epoxy systems [34, 55]. The large increase was explained by the large surface area of montmorillonite (~760 m^2/g), as opposed to ~0.8 m^2/g for silica particulate filler, available for interaction with the progressing crack front. The flexural properties of the cyanate ester were also affected by the addition of organoclay. At best, a 33% increase in flexural modulus was observed, similar in magnitude to those obtained in epoxy networks [34, 55], and a moderate decrease in strength (~23%) was found for the nanocomposites. The authors related these results to the high interfacial adhesion between the montmorillonite platelets and the cyanate ester resin, based on charge transfer interactions.

Polyimides produced by polymerisation of monomer reactants (PMR type) are thermosetting polymers, which combine excellent processing, mechanical properties and thermal oxidative stability. These materials are attractive for use in aerospace components where durability and reliability are critical concerns. There has been a significant amount of research aimed at increasing the thermal oxidative stability of the PMR-15 based polyimides. An alternative to modification of the polymer, in order to improve thermal properties, is the dispersion of layered silicate in the polymer matrix [27, 74]. Abdalla and co-workers [27] used a thermoset PMR-15 type polyimide and Na^+ montmorillonite (Nanocor) to synthesise a class of high-temperature nanocomposites. Both pure clay and modified organoclay with dodecylamine and amino-undecanoic acid were used. Nanocomposites were prepared by blending 2.5 and 5 wt% montmorillonite in a methanol solution of PMR-15 precursor. With the incorporation of 2.5% clay, the flexural modulus exhibited a 23% increase, while the nanocomposites loaded with 2.5% organoclay showed from 31% to 63% increase, compared to the neat PMR-15. The increase in flexural modulus was accompanied by 14% to 49% increase in flexural strength and a small increase in elongation at break. The properties were enhanced significantly for the acid-modified organoclay followed by unmodified clay, due to the more favourable interaction between the polymer and the carboxylic acid functional groups of the modifier or the silicates. Interestingly, this trend was not observed for the 5% nanocomposites. In fact, a decrease was observed on doubling the clay loading percentage. This variation in the trend was attributed to the morphological heterogeneity of the intercalated structures of the 5% nanocomposites. It is suggested that a more homogeneous exfoliated morphology of the low clay content nanocomposite would exhibit even better properties [75].

6.1.5 Flexural Properties of Thermosets Incorporating Nanoparticles

Particulate fillers are used in thermosetting resins primarily to increase the mechanical properties, hardness and abrasion resistance for coating applications, as well as to reduce the thermal shrinkage and the coefficient of thermal expansion in the manufacture of castings or moulded products. Fine particulate fillers used in polymers normally have particle size of 5–100 μm in diameter and the amount is limited around 15–30 vol% in order to obtain good processing characteristics and fracture toughness. The importance of particle size has been examined, and generally the mechanical properties are improved with decreasing particle diameter of filler [1-3, 76]. For example, work on the effectiveness of particle size of natural zeolite filler in epoxy resins has shown that better mechanical properties are achieved with the use of smaller particles [77].

In more recent years, considerable emphasis has been placed on studies of nanofillers because their high surface area-to-volume ratio is found to have a high reinforcing efficiency even at very low concentrations. Schadler and Siegel [78] prepared epoxy-based nanocomposites containing *in situ* generated TiO_2 nanoparticles and reported a beneficial effect on mechanical properties. Ragosta and co-workers [48] found a conspicuous increase of flexural modulus and yield by increasing the silica content in the nanocomposites with TGDDM epoxy resin and an isopropanol emulsion of silica nanoparticles. The reinforcement factors, determined by the normalised modulus and the normalised yield strength, calculated as the ratio of the values for the nanocomposite to the values of the pure epoxy matrix, were found to be constant over a wide temperature range (25–180 °C). Both reinforcement factors were increased linearly with increasing filler content, reaching a value of about 1.5 for the modulus and 1.3 for the yield strength at a silica content of 10 wt%. The addition of silica nanoparticles up to 10 wt% produced a considerable increase in fracture toughness and an increase in critical crack length for the onset of brittle fracture. These results were considered to arise from the restrictions on segmental motion produced by the reaction between the epoxy groups and the silanol groups on the surface of the silica nanoparticles. The reaction contributed to enhance the interfacial strength. The enhancement in toughness of epoxy/silica nanocomposites was found to be larger than that achieved up to now with macro-sized particles.

Improved flexural properties of thermoset nanocomposites based on epoxy and polyester resins incorporating particulate nanofillers are observed in our studies [47, 79]. With the aim of characterising the properties of these nanocomposites for potential protective coating applications, we developed nano-reinforced thermosets from a variety of nanofiller and resin formulations. Nanocomposites are prepared with nanoscale diamond and alumina, Al_2O_3-untreated (D40) and treated by organic modifiers (OS1 and OS2). The characteristics of nanofillers were summarised in **Table 2.5**. Epoxy resin (AP1) plasticised with dibutylphthalate, as well as unsaturated polyester resin (Viapal VUP 4627) containing styrene, are used as basic matrices; diethylenetriamine and MEKP, respectively, being the curing agents (**Table 2.3**). Systems are cured at ambient conditions and post-cured over the course of 6 h at 80 °C. Epoxy and polyester resin-based hybrids

with 1.3 vol% (3 wt%) alumina and epoxy-based hybrids with 0.7 and 2.1 vol% (2 and 6 wt%) diamond are prepared for investigation of mechanical properties.

The resins are characterised by a low glass transition temperature of T_g ~ 40 °C for AP1 and T_g ~ 51 °C for Viapal, which is an indicator of flexibility. As shown in **Table 6.3**, the composite systems with 1.3 vol% alumina in the epoxy and polyester resins display negligible changes in the glass transition temperature. However, a significant increase of the glass transition is observed in the epoxy-based hybrids with diamond (e.g., ~3 °C and 14 °C at 0.7 and 2.1 vol% diamond respectively), compared to the glass transition of the pure epoxy resin, indicating strong interfacial interactions.

Representative data for the flexural properties of the reinforced compositions with 1.3% alumina nanofillers are shown in **Table 6.3** [47, 79]. In spite of the small filler content, the modulus values and the flexural strength (stress at break) show a significant improvement, depending on the type of composition. The reinforcement factors, determined by the normalised modulus, E_{NC}/E_{resin}, and normalised flexural strength, $\sigma_{NC}/\sigma_{resin}$, were found to be the best for the D40 and OS2 alumina in the epoxy and the polyester resins, reaching maximum values of 1.27 for D40 and of 1.16 for OS2.

Table 6.3 Flexural properties of nanocomposites based on unsaturated Viapal polyester resin and AP1 epoxy resin with diamond and alumina nanoparticles – untreated (D40) and organically treated (OS1 and OS2)

Sample code	Nanofiller content		T_g (°C)	Flexural modulus, E (MPa)	Reinforcement factor, E_{NC}/E_{resin}	Stress at break, (MPa)	Reinforcement factor, $\sigma_{NC}/\sigma_{resin}$
	(vol%)	(wt%)					
Polyester resin Viapal	0	0	51.5	911	1	82	1
Viapal/D40	1.3	3	49.1	1119	1.23	104	1.27
Viapal/OS1	1.3	3	47.4	896	0.98	57	0.7
Viapal/OS2	1.3	3	47.8	1003	1.1	86	1.05
Epoxy resin AP1	0	0	40.6	589	1	71	1
AP1/D40	1.3	3	37.7	639	1.08	79	1.11
AP1/OS1	1.3	3	40.7	503	0.85	73	1.03
AP1/OS2	1.3	3	39.4	686	1.16	75	1.06
0.7% AP1/ diamond	0.7	2	43.5	690	1.17	95	1.34
2.1% AP1/ diamond	2.1	6	54.8	897	1.4	134	1.89
Data from [47]							

The reinforcement effect could be related to the absorption of the resin molecules at the large and active nanofiller surface. In contrast, the compositions with OS1 alumina show lower flexural characteristics compared to that of the unfilled resins, which can be related to the lower swelling of these aluminas by the polyester resin, observed previously from the rheological experiments. Moreover, higher reinforcement effect is observed for the alumina nanofillers in polyester resin, compared to the reinforcement in epoxy resin, which may be related to the better dispersivity of alumina/polyester systems, determined rheologically in Section 2.4.4.1.

If diamond nanoparticles are incorporated in epoxy resin AP1, the flexural properties of the resin are improved significantly with increasing filler content from 0.7 to 2.1 vol% [47]. **Table 6.3** shows that at 2.1 vol% diamond the reinforcement factor is 1.4, determined by normalised modulus, and 1.89, determined by normalised strength. If we compare the reinforcement effect by normalised strength of diamond to that of alumina at similar volume content, it can be seen that 0.7 vol% diamond produces larger reinforcement (1.34 fold) than that produced by 1.3% alumina nanofiller (1.06). However, the effect of both nanofillers is similar if we compare the reinforcement determined by normalised modulus.

These results indicate that there is a stronger interfacial adhesion between the diamond and the epoxy resin molecules than that produced by unmodified alumina, which is probably based on charge transfer interactions. The surface of the shock wave synthesised diamond is oxidised and polar, and is covered with carboxyl, carbonyl and hydroxyl groups [79]. This may lead to the formation of strong hydrogen bonds of the resin molecules at the diamond nanofiller surfaces, resulting in increased glass transition temperature and reinforcement.

Moreover, the reinforcement effect of the alumina nanofiller is strongly related to the degree of dispersion in the resin matrix. Thus, the improvement in flexural characteristics of the crosslinked polyester systems incorporating D40 and OS2 alumina could be related to the better dispersability of these nanofillers in the polyester resin, compared to OS1 alumina. Owing to the low swelling of the OS1 alumina by the polyester resin, the interfacial adhesion is probably suppressed, which leads to the decrease of the flexural properties compared to that of the pure resin.

6.1.6 Impact Properties

In general, stiffness/strength and impact strength work against each other in conventional polymer composites. For example, the anhydride-cured epoxy microcomposites resulted in a rigid epoxy material, and thus the values of the impact strength are relatively low.

The Izod impact strength of epoxy resin was maintained by Miyagawa and Drzal [49] with the addition of a small amount (0.1–0.2 vol%) of fluorinated single-walled

carbon nanotube reinforcement. A larger amount of carbon nanotubes resulted in a decrease of the impact strength. Therefore, the maintenance of the impact strength with carbon nanotubes is a benefit of epoxy/carbon nanotube nanocomposites that show an excellent reinforcing effect on the elastic modulus without sacrificing the impact strength. In summary, the amount of nano-inclusions should be optimised to maximise the improvement of the elastic modulus and minimise the reduction of Izod impact strength. The best balance in the Izod impact strength and the elastic properties is found to occur at approximately 0.21 vol% (0.3 wt%) carbon nanotubes. In another study of epoxy/silica nanocomposites [80], the impact strength is found to decrease after adding 5 wt% silica, and the viscosity of the diglycidyl ether of bisphenol F (DGEBF) epoxy resin, Epon 862, radically increased after adding this relatively large amount of nanofiller. The authors inferred that the decrease in Izod impact strength is caused by adding a large amount of nano-inclusions after the mixture has become extremely viscous.

The impact properties of epoxy resins might be significantly improved by the addition of a small amount of organoclay [5, 81]. Isik and co-workers [81] synthesised impact-modified epoxy/polyether polyol/montmorillonite nanocomposites. The DGEBA epoxy resin modified with polyether polyol is used as a matrix polymer with triethylenetetramine as curing agent. The organoclay used in this study is montmorillonite, modified by methyl tallow bis(2-hydroxyethyl) quaternary ammonium chloride. In samples with both clay and polyether polyol, the impact strength was increased approximately 130% in the material containing 1 wt% organoclay and 1 wt% polyether polyol in comparison to the values of the neat epoxy resin. Beyond this optimum of clay and polyether polyol, a reduction in impact strength is observed. The binary systems containing epoxy resin and organoclay displayed approximately 60% increase of impact strength, but a reduction is observed with increasing clay content. Especially at high clay contents, it is proposed that clay particles agglomerate and act as stress concentrators, decreasing the impact strength.

The effects of the organoclay content and the degree of exfoliation on the impact properties of epoxy nanocomposites were demonstrated in our previous study [47]. The nanocomposites investigated are based on STN organoclay and glassy epoxy resin Araldite LY556, cured with DETA. **Figure 6.8** compares exfoliated STN/epoxy nanocomposites produced by solvent processing and intercalated STN/epoxy nanocomposites produced by direct processing. The results show that the impact strength is improved by the addition of a small amount of organoclay, with maximum values at about 2–3 vol%. This optimal filler content is close to the first rheological percolation threshold, which was determined to be $\phi^* \sim 2.5$ and 3 vol% for the exfoliated and the intercalated nanocomposites, respectively (see Section 2.3.3.1.4). A decrease in impact strength is observed on adding a larger amount of organoclay beyond the first percolation threshold, $\phi > \phi^*$. Obviously, the superstructure of flocs formed by the clay platelets acts as stress concentrators, which results in decreased impact strength. The maximum reinforcement determined by the normalised impact strength, calculated as the ratio of the values for the nanocomposite to the values of the pure epoxy matrix, is found to be a factor of

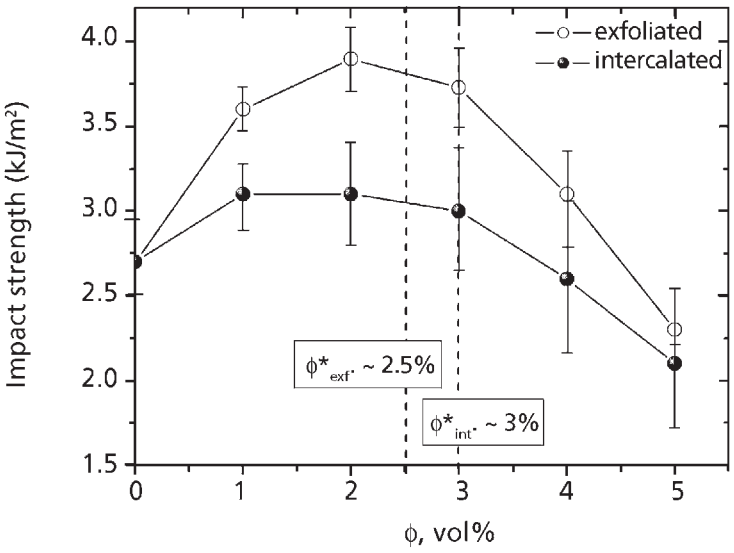

Figure 6.8 Impact strength of diethylenetriamine-cured epoxy nanocomposites based on epoxy resin Araldite LY556 and STN organo-smectite *versus* volume content. Exfoliated (open symbols) and intercalated (full symbols) nanocomposites are produced by solvent and direct processing techniques, respectively. Dashed lines indicate the first rheological percolation thresholds of intercalated and exfoliated systems.

Data from [47]

1.44 for the exfoliated systems and 1.12 for the intercalated systems. Therefore, the exfoliated clay nanolayers improve the impact properties of systems much more than the intercalated nanostructures.

Similar to the epoxy resin, the addition of a small amount of organoclay was found to decrease the brittleness and improve the impact characteristics of the polyester resins [39, 64-66]. Suh and co-workers [43, 44] demonstrated that the resulting properties of polyester/clay nanocomposites were greatly dependent on the preparation procedure with regards to the order of mixing and the curing conditions. The morphological hierarchy at a nanolevel is proposed as a key factor for the structure–property relationship in polyester-based clay nanocomposites [40].

In summary, the relatively good resistance to impact, together with the high modulus and good flexural characteristics, are attractive properties of the clay-containing epoxy and polyester nanocomposites, which have allowed them to partially or fully replace fibres in regards to using these nanocomposites as a matrix in conventional fibre-reinforced composites.

6.1.7 Reinforcement in Relation to Percolation Mechanism

Some researchers have reported that the improvement in mechanical properties of nanocomposites depends significantly on the filler content [34, 57, 82], which is associated with the structural transition of percolation [68, 83]. Becker and co-workers [34] reported a monotonic increase in modulus of high-functionality epoxy resins with increasing organoclay concentration up to 10%. Pinnavaia and co-workers [57] found that the flexural strength of intercalated and exfoliated clay/epoxy nanocomposites displays similar values at low clay loading. At high clay loading (>5 wt%), the exfoliated nanocomposites exhibited much greater reinforcing effect.

Wooster and co-workers [68] observed a dramatic increase in the crack resistance of bisphenol E dicyanate ester nanocomposites with increasing montmorillonite content. However, there is a decrease after the rheologically determined percolation limit (~4 wt%). Moreover, the addition of organoclay caused a systematic increase in flexural modulus, but a decrease was observed from 4 to 5 wt%. This decrease reflected the difficulties in clay dispersion above the percolation limit. Hsieh and co-workers [83] also observed a relation between mechanical response and rheological properties of polycarbonate/layered silicate nanocomposites above and near the percolation threshold.

The mechanical properties of concentrated nanocomposites, incorporating nanofillers well above the percolation limit, have hardly been reported. A highly filled epoxy/montmorillonite (MMT) nanocomposite was prepared by Salahuddin and co-workers [33], with silicate content up to 70 wt%. The organically (dimethyl-benzyl hydrogenated tallow ammonium chloride) modified MMT and the trifunctional low-viscosity epoxy type (Araldite XVMY 0505) cured by aromatic hardener (HY5200) were used as ingredients. The hybrid had a special structure, determined by TEM studies, in which MMT was dispersed homogeneously and oriented parallel to the surface. Silicate lamellae intercalated with epoxy resin were found assembled into a cluster of about 50–120 nm thickness, and these clusters were further assembled into superclusters with an average thickness of 300 nm. Exfoliated composites with a clay content up to 70 wt% exhibit unusual transparency, which is related to the spatial distribution and the molecular level dispersion of the mineral nanodomains. Studies by the Vickers hardness test of an epoxy/MMT nanocomposite containing 60 wt% MMT indicated that the diamond pyramid hardness was 10–29 kg/mm^2.

In Section 2.5 we proposed a rheological approach to a prognostic design of the properties of polymer nanocomposites based on the rheologically determined first and second percolation thresholds, ϕ^* and ϕ^{**} (**Figure 2.20**). Further, various examples are shown in order to confirm the applicability of the two rheological percolation thresholds to prognosticate the optimal range of nanofiller content wherein maximal improvement of the mechanical properties might be expected.

Figure 6.9 displays the flexural strength of crosslinked SPN clay/epoxy nanocomposites *versus* volume content of the organoclay [47]. Epoxy resin Araldite LY556 and organo-

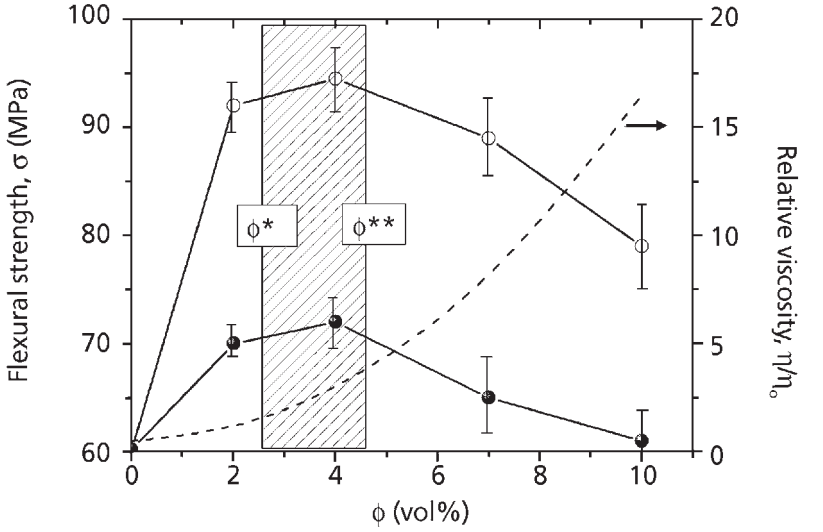

Figure 6.9 Flexural strength of crosslinked nanocomposites *versus* volume content ϕ of SPN/epoxy systems. Exfoliated nanocomposites prepared by solvent processing (open symbols) and direct processing (full symbols) are compared. The dashed line plots the relative viscosity of precursor dispersions, η/η_0 *versus* ϕ. The hatched region determines the 'prognostic window' limited by the first and second rheological percolation thresholds, $\phi^* \sim 2.5\%$ and $\phi^{**} \sim 4.5\%$.

Data from [47]

smectite, modified with oligo(oxypropylene)-diethyl-methyl-ammonium chloride (SPN), are used with DETA as a hardener. The nanocomposite ingredients are characterised in **Tables 2.3** and **2.4**. Samples are prepared by two types of processing techniques, solvent processing and direct processing. As shown before (**Figures 3.2c** and **3.3**), solvent processing produces better exfoliation of the SPN organoclay in epoxy resin compared to direct processing. Therefore, the stronger improvement in flexural strength of the solvent-processed nanocomposites than that of directly processed nanocomposites is obviously caused by the better exfoliation.

In **Figure 6.9**, the bending property of crosslinked nanocomposites *versus* volume content of organoclay (points and full line) is compared with the viscosity of precursor dispersions (dashed line). As can be seen, at an organoclay content below the first percolation threshold ϕ*, the flexural strength of nanocomposites increases strongly with increasing organoclay content, corresponding to a slight increase in the viscosity of dispersions. However, a decrease is observed in strength at a filler content above the second percolation threshold ϕ**, which corresponds to a strong increase of the viscosity. The hatched region determines the 'prognostic window' limited by

the two rheological percolation thresholds, $\phi^* \sim 2.5$ vol% and $\phi^{**} \sim 4.5$ vol% (for the solvent-processed precursors). The two rheological transitions are determined by using rheology method II, described in Section 2.3.3. Importantly, the optimal improvement of the flexural strength is found for clay contents within the prognostic window of $\phi^* < \phi < \phi^{**}$. At best, a 58% increase in flexural strength is observed for the solvent-processed and a 20% increase for the directly processed exfoliated SPN/epoxy nanocomposites at about 4 vol% SPN, compared to the values of the pure epoxy resin.

Figure 6.10 compares the reinforcement effect of the graphite/diamond mixture and the nanoscale diamond in AP1 epoxy-based nanocomposites cured with DETA, as plotted *versus* filler content [47]. The reinforcement is determined by the normalised impact strength, calculated as the ratio of the values for the nanocomposite to the values of the pure epoxy matrix. It can be seen that the reinforcement effect increases in the range of low nanofiller contents of 1–3 vol%, which is below the first rheological percolation $\phi^* \sim 5$ vol%. Near and above the first percolation threshold, $\phi \leq \phi^*$, the normalised impact strength decreases rapidly. This could be associated with the strong cluster–cluster aggregation of carbon nanoparticles.

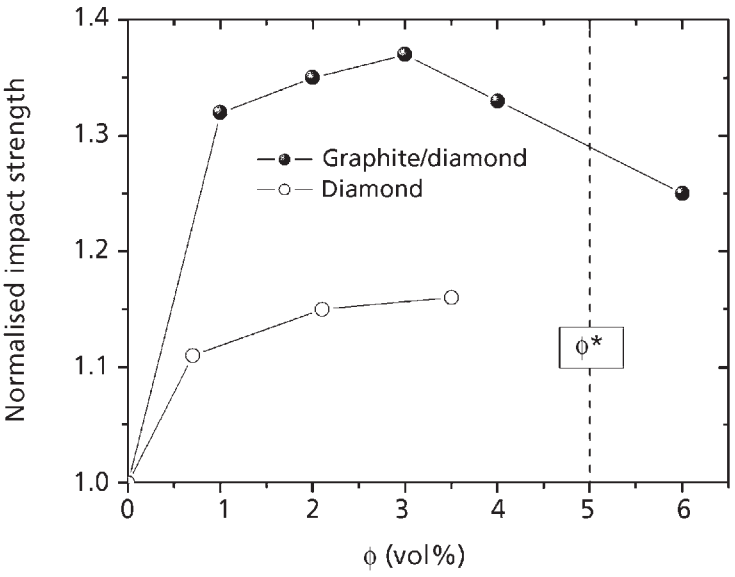

Figure 6.10 Normalised impact strength *versus* volume content of crosslinked AP1 epoxy-based hybrids with nanoscale graphite/diamond (full symbols) and diamond (open symbols), cured by DETA. The dashed line marks the rheological percolation threshold, ϕ^*.

Data from [47]

Similar results from **Figure 6.8** have been already discussed, for the impact properties of organoclay/epoxy nanocomposites. Here, the impact strengths of the intercalated and the exfoliated clay/epoxy nanocomposites are shown to increase and pass through a maximum value at about 2 vol% SPN organoclay, which is prior to the percolation threshold, $\phi^* \sim 2.5$ and 3 vol% for the solvent- and direct-processed nanocomposites, respectively. Above the first percolation threshold, $\phi > \phi^*$, a strong decrease in the impact strength is observed.

Further, **Figure 6.6** showed the role of the rheological percolation threshold for the improvement of the dynamic storage modulus of (graphite/diamond)/epoxy hybrids. The normalised storage modulus, $E'_r = E'_{NC}/E'_{resin}$ *versus* volume content was presented for the carbon/epoxy hybrids at three temperatures, corresponding to the glassy, the glass transition and the rubbery regions, respectively. At the high temperatures of 106 °C (glass transition) and 150 °C (rubbery region), a strong increase of the relative storage modulus was observed around the first rheological percolation threshold, $\phi^* \sim 5$ vol%, which is an indicator of the increased crosslink density [47, 51].

In summary, the importance of double rheological transitions, the first and the second percolation thresholds, ϕ^* and ϕ^{**}, for improvement of the mechanical properties of crosslinked nanocomposites is undoubted. Both thresholds have a structural origin. The prognostic window of the optimal nanofiller concentrations, $\phi^* < \phi < \phi^{**}$, is associated with the formation of a network structure of fractal flocs, which filled the volume and comprised a large amount of the matrix resin bonded at the nanofiller surfaces. Such superstructure is proposed to play a determining role for the reinforcement of thermoset nanocomposites [46, 47, 51], which allows them to undergo the deformation process easily and to improve the mechanical properties (stiffness and toughness) of the nanocomposites significantly. Deformation probably started inside the flocs and the crack propagation into the polymer matrix is prevented by the nano-inclusions, as well as by the strong bonding between the fillers and the matrix. This resulted in an improvement of the flexural properties. However, the fractal flocs formed by nanofiller near to the percolation threshold, ϕ^*, and polymer obviously act as stress concentrators, which decreased the impact properties at high nanofiller contents, $\phi \geq \phi^*$.

All these results confirm the applicability of the two rheological thresholds, ϕ^* and ϕ^{**}, for the design prognostic window of the filler concentrations where optimal enhancement of mechanical properties might be expected. Obviously, the improvement of mechanical properties is sensitive to the interconnectivity of the nanofiller particles, as well as to the polymer–filler interactions, and thus it may be related somehow to the critical concentrations of percolation. We propose that the first percolation threshold ϕ^* (related to the formation of individual fractal floss) is the filler concentration needed to realise a brittle–tough transition. Whilst the second percolation threshold ϕ^{**} indicates the effect of network superstructure of continuous flocs on the mechanical properties. A high filler content above the second percolation threshold $\phi > \phi^{**}$ reflects the dificulties in nanofiller dispersion above the saturation limit of filler content, indicating the inhomogeneity, which resulted in a significant decrease of the overall mechanical properties.

Therefore, prior identification of the prognostic window of two percolation thresholds ($\phi^* < \phi < \phi^{**}$) by rheological investigations might be a very useful practical tool for the design of crosslinked nanocomposites with optimally enhanced mechanical properties.

6.2 Thermal Properties

The performance of polymer nanocomposites containing layered silicates is interesting in another way, which concerns the strong improvement in their thermal properties. Most of the reported studies on thermal properties have referred to thermoplastic polymer/clay nanocomposites [4, 28, 32, 33, 84–86]. Investigations of the thermal properties of thermoset-based nanocomposites containing layered silicates are rarely reported [29, 86, 87]. Gilman [85] published a detailed review on the effect of clay on the thermal stability and flammability of diverse thermoplastic polymers, and concluded that the best results are observed for exfoliated nanocomposites, but intercalated systems also demonstrated significant improvement. The existence of a common mechanism of flammability reduction originates in char formation on the burning surface, which insulates the underlying material and acts as a barrier for the mass transport of decomposition products. Therefore, the combustion process is found to be similar for the different polymers, but the type of organoclay and the degree of dispersion could influence the effectiveness of the improvement in thermal properties [86].

6.2.1 Enhanced Thermal Stability

A thermogravimetric analytical method (TGA), including thermogravimetry (TG), differential thermogravimetry (DTG) and differential thermal analysis (DTA), is applied to study the thermal decomposition process of polymeric nanocomposites. In order to estimate the thermal stability of the samples, various degradation stages, temperature peaks and mass losses are determined. For engineering uses, the TGA results are usually presented in terms of several parameters. The thermal stability is characterised by the temperature of the onset of TG curve at 5% weight loss, $T_{5\%}$ (°C). The thermal degradation (decomposition) is presented either by the temperature $T_{50\%}$ (°C), representing the 50% weight loss, or by T_{peak}, displaying the peak of the DTG curve corresponding to the TG inflection. The total weight loss, W (wt%), and the char content, 100 – W (wt%), characterise the degradation level and the flammability resistance.

One of the most important property enhancements expected upon formulation of a polymer nanocomposite is the retardation of the thermal degradation [87–91]. The thermal stability and degradation were found to be strongly affected by the amount of organoclay and its exfoliation in the polymer matrix, as well as by the thermal stability of the organoclay intercalant [87, 88].

Thermal analysis of several different polymer/layered silicate nanocomposites, including thermoset nanocomposites, showed the intriguing result that intercalated nanocomposites are more thermally stable than exfoliated nanocomposites; thus, the most pronounced thermal stabilisation of the polymer occurred when the inorganic layers are separated by 3 nm, which is typical for an intercalated structure [92–95]. However, Hsueh and Chen [26] observed that dispersion of exfoliated layered double hydroxides in an epoxy nanocomposite, based on amine-cured Epon 828 resin, effectively enhanced the thermal stability of the resin. The thermal stability is evaluated by the weight loss due to volatilisation of degraded products as a function of temperature. The results indicated that 7 wt% loaded nanocomposite is degraded at a temperature 23 °C above the degradation temperature of the pristine epoxy resins. Two factors are responsible for these nanocomposites possessing better thermal stability than that of the epoxy resin: the chemical structure of the nanocomposites is different from that of the pristine epoxy; and the thermal motion of the epoxy molecules is restricted by the inorganic nanolayers. Additionally, the enhanced thermal stability was also attributable to the fact that out-diffusion of the volatile gas from the thermal decomposition products was prevented because the exfoliated and well-dispersed nanolayers act as a gas barrier, reducing the permeability of the volatile products.

It is important to mention that not all reported results on thermoset/clay nanocomposites demonstrate enhanced thermal properties. Slight changes of the structure may produce contradictory results on thermal stability, as reported by Gilman and co-workers [86, 92, 96]. In the *Flammability of Polymer Clay Nanocomposite Consortium: Year One Annual Report* [86], the thermal and mechanical properties of tethered and non-tethered nanocomposites, based on Epon 828 and alkyl-ammonium montmorillonite, cured by aromatic amine and anhydride, are discussed. One of the samples has an intercalated structure but the other two epoxy nanocomposites have apparently larger *d*-spacings and even some delaminated layers. The authors found that, although there is an improvement in the shear modulus, the thermal properties (TGA, T_g) of the nanocomposites were not improved. The T_g values are 10–15 °C lower than those for the neat epoxies, and the thermal stabilities are 10–20 °C lower. The studied nanocomposite samples became disordered upon curing, i.e., partially exfoliated. These results were lower compared to the results published previously [85, 92] for the highly improved thermal stability of the intercalated DGEBA epoxy-based clay nanocomposites. The difference in the structure formed in the nanocomposites was proposed as a reason for such contradictory results.

The chemistry and thermal stability of clay organic modifier may have an adverse effect on the thermal stability of thermoset nanocomposites. Wang and Pinnavaia [97] evaluated synthetic layered silicic acids as alternatives to smectic clays for the preparation of epoxy-based nanocomposites. The objective was to avoid the purification processing required by clays and the use of relatively expensive compatibilisers, which may also function as undesirable plasticisers and adversely affect the thermal stability of the matrix.

Recently, oligomeric molecules have been used as organoclay intercalant, which reduce flammability, but this is also found to reduce the thermal stability [89]. Bharadwaj and co-workers [40, 41] reported the TGA results of crosslinked polyester nanocomposites. The authors prepared intercalated and exfoliated crosslinked polyester/clay nanocomposites by dispersing organically modified montmorillonite in pre-promoted polyester resin and subsequently crosslinking at room temperature. The onset of degradation was slightly but progressively hastened upon addition of clay to the nanocomposites as compared to the pure polymer. The nanocomposites degraded at a faster rate compared to the pure polymer. The monotonic increase in the rate of degradation in these nanocomposites was related to the presence of an increasing amount of hydroxyl groups in the organic modifier, which provides a supply of oxygen.

The thermal stability and degradation of intercalated and exfoliated epoxy/smectite nanocomposites has been examined in our laboratory and a strong improvement in thermal properties was observed [47, 98]. For preparation of nanocomposites, organo-smectites pre-intercalated with quaternised ammonium salts, SAN, STN and SPN, are used (**Table 2.4**), which are dispersed in glassy epoxy resin, Araldite LY556. The hardener was anhydride HY917 and the accelerator was DY070 (CIBA), blended in proportions 100/90/2 (resin/anhydride/accelerator). The X-ray diffraction (XRD) data showed that the crosslinked epoxy/anhydride/STN and SAN nanocomposites are intercalated, but the SPN/epoxy nanocomposites formed disordered (exfoliated) structure. Samples contain 2.5, 5 and 10 vol% organo-smectites in the epoxy resin (i.e., from 0.4 to 3.5 wt% inorganic clay in crosslinked nanocomposites). The direct processing technique is used for nanocomposite preparation, which includes ultrasonic dispersing of the smectites in the epoxy resin, following by blending with the anhydride hardener and accelerator. The thermosetting process is followed in two stages: curing for 2 h at 75 °C and post-curing for 2 h at 130 °C. The TGA analysis is applied to study the thermal decomposition process of the post-cured systems. The heating curves are recorded in the temperature range 293–1073 K, at heating rate of 5 K/min. The composite degradation is investigated in air atmosphere without induced circulation.

Figure 6.11(a) compares the thermal stability of the organoclay fillers, on varying the organic modifier used as pre-intercalant, SPN, SAN and STN. Significant differences are observed in the thermal characteristics of organo-smectites, which can be attributed to the different kinetics of degradation of the alkyl-ammonium ions, having different chain lengths of C_{37}, C_{25} and C_5, for SAN, STN and SPN, respectively. The lowest carbon number onium ion C_5 (SPN) produces low thermal stability with $T_{5\%}$ ~ 400 K, whilst the high carbon number onium ions C_{37} (SAN) and C_{25} (STN) are much more stable, with $T_{5\%}$ ~ 573 K (SAN) and 473 K (STN), respectively. Total weight losses of 31 wt% (STN), 54.5 wt% (SAN) and 64.5 wt% (SPN) are calculated for organo-smectites, which give evidence about the proportion of alkyl-ammonium salt to inorganic silicate in organo-smectite. Moreover, the decomposition processes of the three organo-smectites have different mechanisms. The SPN clay decomposes in two stages with a high mass

loss within the low-temperature stage, but in contrast the kinetics of mass loss of SAN and STN clays proceeds in three stages.

Figure 6.11(b) compares the TG, DTG and DTA curves of 10 vol% organoclay/epoxy nanocomposites (SPN_{NC}, SAN_{NC} and STN_{NC}), representing the organoclay amount in the epoxy resin matrix before addition of anhydride hardener. While, the inorganic silicate content in the crosslinked epoxy/anhydride systems is calculated as 1.8 wt% (SPN), 2.6 wt% (SAN) and 3.5 wt% (STN), respectively. Note that the inorganic silicate content of organo-smectites is determined from the TGA results representing the fraction of

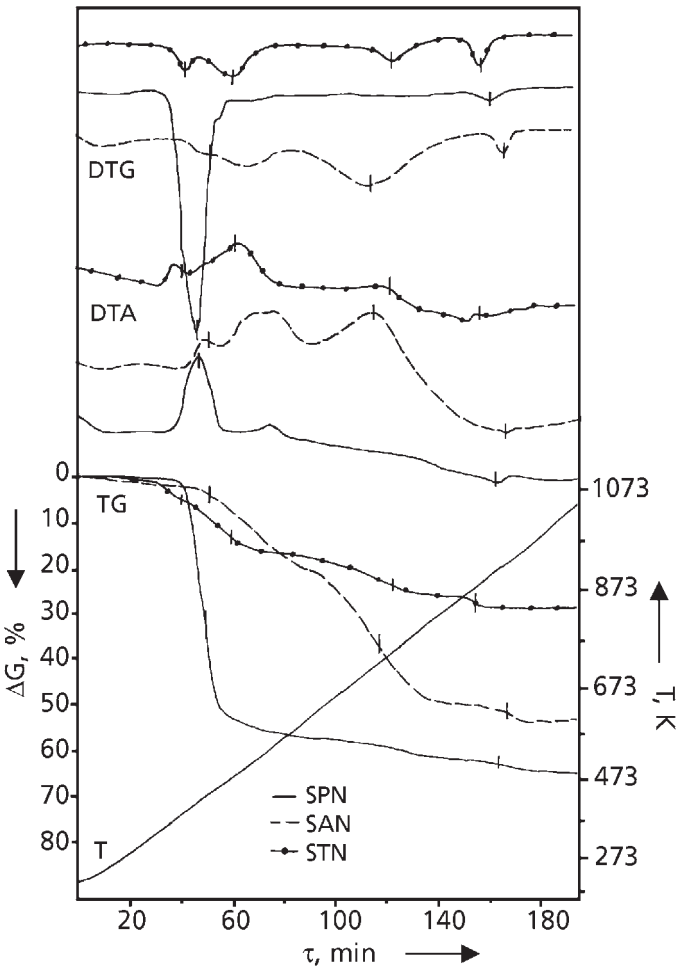

Figure 6.11a Comparison of the thermal DTA, DTG and TG curves *versus* time and temperature for organo-smectites, SPN, SAN and STN.

Reproduced with permission from [98]. ©Springer US, 2001

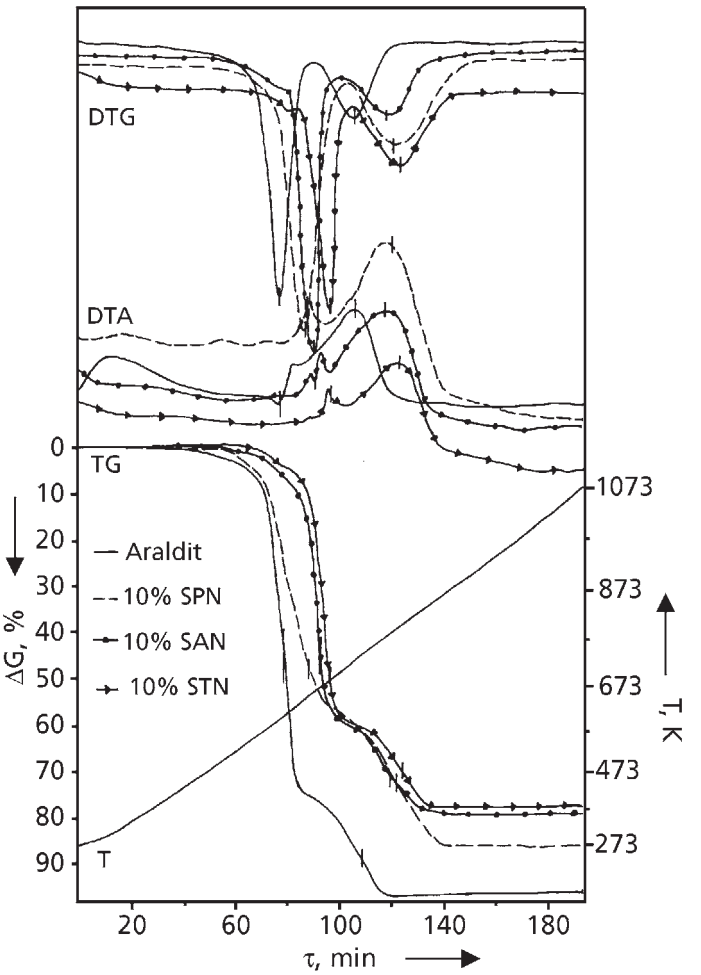

Figure 6.11b Comparison of the thermal DTA, DTG and TG curves *versus* time and temperature for Araldite epoxy resin and 10% smectite containing epoxy nanocomposites, cured by anhydride.

Reproduced with permission from [98]. ©Springer US, 2001

silicate material that remains at 800 °C, as follows: 35.5 wt% (SPN), 45.5 wt% (SAN) and 69 wt% (STN) (see **Table 2.4** and **Figure 6.11a**).

As can be seen, the curves of the nanocomposites represent a mix of the corresponding curves of the epoxy resin and the smectite clay. Generally, the thermal stability of the nanocomposites is much higher than that of the unfilled epoxy resin, and the decomposition proceeds in two stages, similar to that of the neat epoxy. Two peaks of

DTG curves, corresponding to the relevant TG inflections, are observed. In stage I of degradation (e.g., weight loss of 0–50 wt%), the improvement in the thermal properties of the nanocomposites is influenced by both the thermal stability of the organic modifier used as pre-intercalant and the degree of exfoliation. Stage II of degradation (e.g., weight loss beyond 50 wt%) is associated with the decomposition of the bulk epoxy resin, affected by the presence of inorganic silicates. Thus, because of the insufficient thermal stability of SPN organoclay, the SPN_{NC} system shows much lower thermal stability in stage I as compared to SAN_{NC} and STN_{NC}. If we consider the first DTG peak as a characteristic of degradation, it appears at 603 K for the unfilled epoxy/anhydride crosslinked system, but at 643 K for SPN_{NC}, at 683 K for SAN_{NC} and at 713 K for STN_{NC}, respectively. Obviously, the highest silicate content, together with the high thermal stability of the STN onium ion, are the reason for the best improvement in thermal properties of the STN/epoxy/anhydride nanocomposites.

In order to verify the effects of the nanocomposite structure, we compare the thermal characteristics of the three nanocomposite systems, SAN_{NC}, STN_{NC} and SPN_{NC}, *versus* the inorganic silicate content. **Figure 6.12** displays (a) the thermal stability, determined by the onset of degradation at 5% weight loss, $T_{5\%}$, and (b) the thermal degradation, determined by the decomposition temperature at 50% weight loss, $T_{50\%}$, *versus* the inorganic silicate content, $\phi_{silicate}$ [47]. The $\phi_{silicate}$ value is calculated based on the inorganic content of organo-smectite fillers, assigned to the epoxy/anhydride matrix.

It can be seen that the overall thermal stability of nanocomposites increases significantly with increasing silicate content. Moreover, the STN_{NC} and SAN_{NC} display very high improvement of the thermal stability and the values are similar for both organoclays. In contrast, this effect is much lower for the SPN_{NC}. Such observations might be related to the effects of nanostructure, intercalated in STN_{NC} and SAN_{NC}, and exfoliated in SPN_{NC}. For example, if we consider the onset of degradation, $T_{5\%}$, at a relatively low silicate content $\phi_{silicate}$ = 1.5 wt%, the intercalated STN_{NC} and SAN_{NC} display an increase of $\Delta T_{5\%} \sim 40$ °C; however, a decrease is observed for the exfoliated SPN_{NC}. A similar effect is observed for the decomposition temperature, $\Delta T_{50\%}$, which increases by $\Delta T_{50\%} \sim 55$ °C for the intercalated STN_{NC} and SAN_{NC}, and by $\Delta T_{50\%} \sim 35$ °C for the exfoliated SPN_{NC}. A much larger improvement of the thermal stability is obtained if high silicate content is added; thus, ~100 °C improvement of the thermal stability is observed for STN systems at $\phi_{silicate}$ = 3.5 wt%, e.g., the $T_{5\%}$ increases from 270 °C for the epoxy resin to 370 °C for the nanocomposites. A similar increase is found for $T_{50\%}$, from 330 °C for the epoxy resin to 440 °C for the nanocomposites.

Figure 6.13 displays the char content *versus* the inorganic silicate content $\phi_{silicate}$ in smectite/epoxy/anhydride nanocomposites, on varying the type of organo-smectite (SAN, STN and SPN). The char content, 100 – *W* (wt%), where *W* is the total weight loss, represents the fraction of nanocomposite material that remains after burning at 600 °C. As can be seen, the char content increases significantly with increasing silicate content in the nanocomposites. Thus, at $\phi_{silicate}$ = 3.5 wt% the char content increase

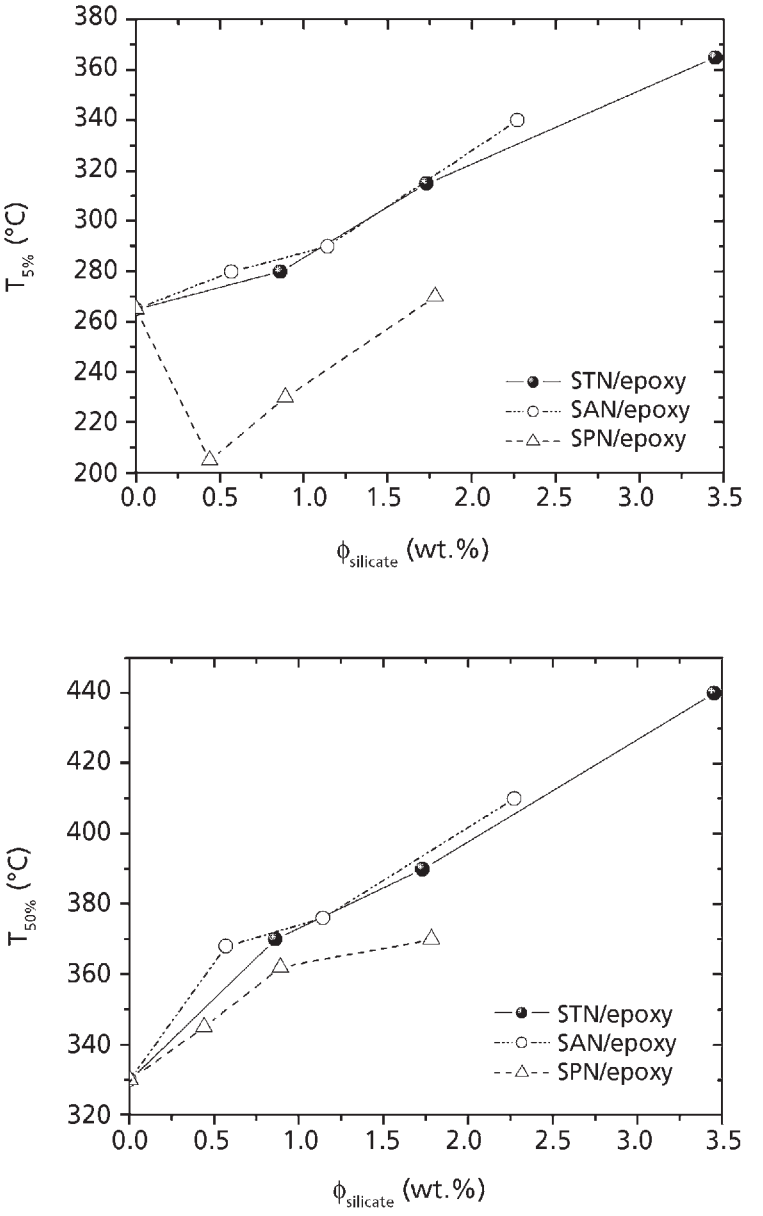

Figure 6.12 (a) Thermal stability, $T_{5\%}$, and (b) thermal degradation, $T_{50\%}$, of organo-smectite/epoxy nanocomposites *versus* volume content of inorganic silicate, on varying the type of alkyl-ammonium pre-intercalant, SAN, STN and SPN.

Data from [47]

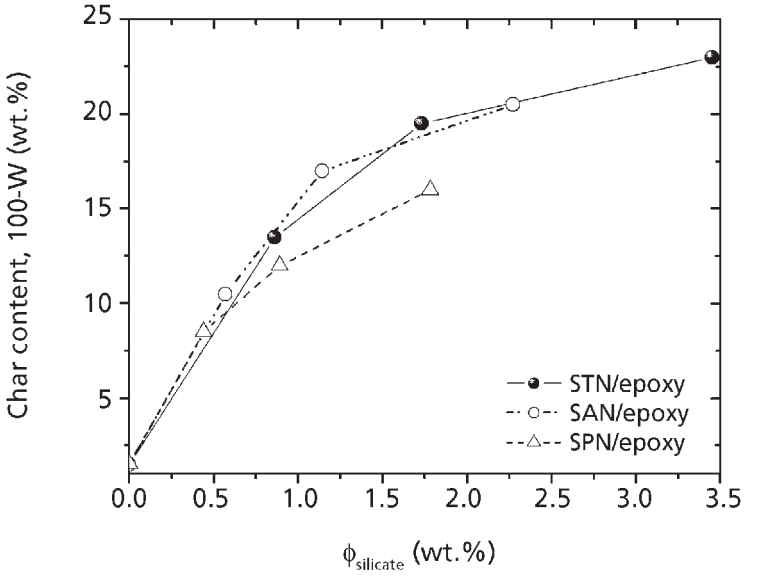

Figure 6.13 The char content (100 – *W*), where *W* is the total weight loss of organo-smectite/epoxy nanocomposites after burning at 600 °C, *versus* the weight fraction of inorganic silicate in nanocomposites.

Data from [47]

from 1.5 wt% for unfilled epoxy/anhydride matrix to 23% for nanocomposites. Here, again, the STN_{NC} and SAN_{NC} show similar values, which are higher than that of the SPN_{NC}. Interestingly, the rate of char increase appears much stronger at low silicate concentrations, up to ~1.5 wt%, and the rate of char increase becomes lower at high silicate concentrations, beyond 1.5 wt%. Thus, the 1.5 wt% silicate leads to about 11.7 fold increase, but the 3.5 wt% silicate produces 15.3 fold increase of char content after burning nanocomposites at 600 °C.

In summary, the results above demonstrate that the thermal stability of thermoset nanocomposites might be successfully controlled by varying the silicate content and the chain length of the intercalant. Thus, the onset of degradation, $T_{5\%}$, depends strongly on the thermal stability of the organoclay modifier. However, the thermal decomposition, $T_{50\%}$, is mostly affected by the silicate content and the type of nanocomposite structure. The dramatic improvement of thermal stability by the addition of such a small amount of silicates could be attributed to the presence of high-surface silicate nanolayers, as well as to the morphological hierarchy in smectite/epoxy nanocomposites. Intercalated clay/epoxy nanocomposites, which contain silicate/polymer multilayers, produce a larger improvement of thermal stability than

that produced by exfoliated nanocomposites, which contain randomly dispersed single nanolayers. These results confirm the results obtained from other authors [92–95] for thermoplastic and epoxy nanocomposites.

Intercalated nanocomposites are generally characterised by confined polymer molecules within the silicate galleries, with bonding or tethering at the silicate surfaces. Obviously, after burning the interfaces, such an ordered superstructure strongly prevents diffusion processes by the so-called 'tortuous path' mechanism, which explains the exclusive thermal stability. It is also assumed that the retention of a larger fraction of carbonaceous char in the condensed phase plays an important role for the mechanism of the reduced thermal degradation of the smectite/epoxy/anhydride nanocomposites [92–95]. Our results show that the silicate content in nanocomposites needs to be larger than 1.5 wt% to ensure optimal char content. The carbonaceous silicate sheets act as barrier for heat transfer towards the inside of the composite, and suppress mass transport of the volatile products generated as the matrix polymer and the alkyl-ammonium salts decompose. This is indicative of flame retardancy.

The thermal stability improvement in nanocomposites is found to be similar at fixed inorganic silicate content; however, the degree of order and the thermal stability of the organoclay might influence the effectiveness. Based on such structural peculiarity, the large improvement in thermal properties of smectite/epoxy nanocomposites may open great possibilities for the application of these new materials in fibre-reinforced composites for automotive, air- and spacecraft, and building industries.

6.2.2 Flammability Resistance

Conventional polymers have excellent physical properties, but almost all of them are highly flammable. For example, epoxy resin is a widely used commercial thermoset polymer for composites, fibre-reinforced plastics, coatings and adhesives [99]. A reduction in flammability of this inherently highly flammable material should increase its use. Therefore, flame-retardant additives are commonly used in the end application when good fire performance is required. Recently, a new scientific approach based on new flame-retardant principles has been proposed by using clay-containing nanocomposites. Researchers have reported that the incorporation of layered silicate into the epoxy may result in enhanced flammability resistance [85, 92–98] and enhanced ablation resistance [95]. Evaluations of flammability properties were achieved using a cone calorimeter [100].

Gilman and co-workers [92, 96] studied nanocomposites prepared with DGEBA epoxy (DER 332, Dow Chemical) and dimethyl ditallow ammonium montmorillonite, Cloisite-15A. Methylenedianiline (MDA) and benzyldimethylamine (BDMA) were used as curing agents. Intercalated-type nanocomposites were prepared. About 40% reduction of the peak of heat release rate (HRR) was observed for 6 wt% clay/DGEBA/MDA nanocomposites, compared to the unfilled resin. Moreover, other physical and mechanical

properties are greatly improved by the silicate and the materials are easily recycled. Furthermore, this system did not increase the carbon monoxide or soot produced during combustion. The authors suggested that the source of the improved flammability properties of these materials is due to a difference in condensed-phase decomposition processes and not to a gas-phase effect.

Importantly, only a little improvement in the char yields was observed by Gilman and co-workers [92, 96] for the thermoset nanocomposites. This result contradicted other studies [101] of thermal reactions in layered organic silicate systems, at 400 °C, which reported the formation of carbonaceous silicate residues and other reaction products. Interestingly, a multilayered silicate structure of intercalated nanocomposites still remains after combustion, with carbonaceous silicate sheets forming a large array of fairly even layers. In contrast, the delaminated hybrid structure of exfoliated nanocomposites appears to collapse during combustion. Therefore, the multilayered structure of the char obviously enhances the performance of the char layers, which act as an isolator and mass transport barrier for the volatile products generated during polymer degradation. Moreover, the interlayer spacing of the char, determined by XRD analysis was the same, 1.3 nm, independent of the chemical structure of the polymer (thermoplastic or thermoset) or nanostructure (exfoliated or intercalated) of the nanocomposite. The conclusion is drawn that, although the mechanism of flame retardancy may be very similar for each of the nanocomposites studied, it is not via retention of a large fraction of carbonaceous char in the condensed phase.

Rossetti [102] reported results on flammability and thermal degradation of epoxy-based nanocomposites, prepared by DGEBA and organoclays, with anhydride hardener. Primary ammonium ions, $C_nH_{2n+1}NH_3^+Cl^-$, with n = 4, 8, 12 and 18 were used as intercalants of the organoclays. The author observed that low carbon number organoclay did not change the flammability of the epoxy resin sufficiently; however, about 40% reduction of the mass loss rate is produced by organoclay with n = 18. Additionally, a reduction of the maximum temperature of degradation by about 25 °C was observed.

Brown and co-workers [29] examined the role of various quaternary ammonium-modified montmorillonites in DGEBA epoxy/diamine nanocomposite formulations, leading to different flammability effects. Intercalated and partially exfoliated clay nanocomposites in Epon 828/D2000 were produced with enhanced heat-distortion temperature and increased flammability resistance. It was found that unfilled Epon 828/D2000 burns using an open flame, leaving an oily, tacky residue. In contrast, resin containing intercalated clay also burns, but produces a rigid graphitic char. However, increased exfoliation of the clay layers resulted in a self-extinguishing behaviour upon removal of the flame. The resulting char exhibited a highly uniform microcellular microstructure, which is retention of the original hierarchical structure of the layered silicate. The authors proposed that graphitisation of exfoliated layered silicate polymer nanocomposite may yield new routes to structured ceramic foams.

Importantly, Gilman and co-workers [86] observed that the flammability of DGEBA epoxy/clay nanocomposites might not be improved upon slight changes in the structure. In their recent focus for their consortium's *Year One Annual Report*, they compared tethered and non-tethered epoxy nanocomposites and evaluated the effect of the type of clay on the flammability properties. An aromatic amine-cured epoxy nanocomposite was prepared using Epon 828 (Shell) and Curative W, in proportions 100/26.5 parts, and organic treated montmorillonite from Southern Clay Products (SCPX 2003, a bis(2-hydroxyethyl) alkyl-ammonium MMT). An anhydride-cured epoxy nanocomposite was also prepared using Epon 828, cured with hexahydro-4-methylphthalic anhydride and benzyldimethylamine, in proportions of 100/68/1 parts, and organic treated montmorillonite (SCPX 2165, a non-reactive, quaternary alkyl-ammonium MMT). Clay addition was adjusted to a mass fraction of 5% inorganic in the samples. Samples were cured for 1 h at 100 °C, 1 h at 150 °C and 1 h at 175 °C. Here, the epoxy/anhydride/MMT (tethered) nanocomposite formed an intercalated structure, but the two other epoxy nanocomposites, which are non-tethered, produced a disordered structure of apparently larger *d*-spacings and even some delaminated layers, indicating partially exfoliated systems.

Gilman and co-workers [86] observed that, although the nanodispersion appears very good for nanocomposites, the HRR peak for the epoxy/MMT was the same as (tethered systems) or up to 20% lower than (non-tethered systems) the control peak of the unfilled resin. The HRR early in the burn was significantly higher. Here, the lower thermal stability seen in the TGA data was proposed as being responsible for the overall loss of effectiveness in the epoxies. These results were lower compared to the results published previously [92, 96] for the DGEBA epoxy-based clay nanocomposites, but cured with methylenedianiline, where a 40% reduction in HRR was observed for an epoxy nanocomposite. The previous DGEBA clay-containing nanocomposites remained ordered, i.e., had an XRD peak, and were therefore intercalated nanocomposites. In contrast, the latest nanocomposite samples became disordered upon cure, i.e., partially exfoliated, which might be the reason for such contradictory results.

6.2.3 Shrinkage Control and Formability

Particulate fillers are used in thermosetting resins primarily to reduce thermal shrinkage in the manufacture of castings or moulded products and to lower the coefficient of thermal expansion of finished products [103–110]. The use of nanofillers in thermoset polymers constitutes a more effective way of improving the overall mechanical properties and formability compared to direct modifications of their molecular composition [48].

For example, the free-radical copolymerisation of unsaturated polyester resin (UP) and styrene (St) leads to a high degree of polymerisation shrinkage, about 7–10%, which causes low surface quality and dimension control problems during manufacturing. An efficient way to reduce the shrinkage is to add a small amount of thermoplastic

material as a low-profile additive (LPA). This approach was found to be effective in high-temperature curing processes, because the proposed mechanism for thermal expansion during heating and microvoid formation during cooling contributes to shrinkage control [104]. However, most low-profile additives do not work well in low-temperature curing processes, because of the lack of strong temperature changes during moulding. The authors agree that in the UP/St/LPA system phase separation occurs during curing, resulting in UP-rich and LPA-rich phases. If microvoids can form in the LPA-rich phase or at the interface between the two phases, polymerisation shrinkage can be strongly reduced without any thermal effect. The local cracking leads to volume expansion of the curing system, thus compensating for some of polymerisation shrinkage.

Lee and Xu [105-108] reported that the presence of organoclay greatly enhanced the polymerisation rate of UP/St systems. Based on these results, the authors made an attempt to combine the effects of both the clay and the LPA in order to improve the shrinkage control. A small clay content of 1–3% in the UP/St/LPA was found to provide superior volume shrinkage control. Thus, the final shrinkage of the cured samples was ~1.44% for the systems with 3% organoclay, compared to ~7% final shrinkage of the UP/St/LPA system without nanoclay. The TEM observation of the cured samples showed that all of the clay platelets resided in the LPA-rich phase, which increased the reaction rate in it. This resulted in earlier microvoid formation and volume expansion, leading to better shrinkage control of the filled UP/St/LPA system cured at room temperature, as well as to great improvement in composite surface quality.

Haque and Armeniades [109] prepared zero-shrinkage and expanding polyester polymer concrete formulations with concomitant enhancement in strength. This was achieved by dispersing a small amount (~0.2%) of natural montmorillonite into the resin. The authors claimed that, during the curing of the system, the resin interacted with the hydrated mineral; thus, at temperatures above 100 °C, some of the hydration water is released, creating expansion forces, which counteracted resin shrinkage.

Additionally, the linear coefficient of thermal expansion (CTE) of high-temperature thermoset polyimides PMR-15 was successfully controlled by adding montmorillonite. Abdalla and co-workers [27] prepared nanocomposites of PMR-15 precursor solution and 2.5–5 wt% montmorillonite, both unmodified and organically modified with dodecylamine and amino-undecanoic acid. The solution was further imidised in two heating stages and pressed under high temperature to form samples. The authors found that the CTE decreased if unmodified clay was used for nanocomposite preparation, while it increased for the organically modified clay/polyimide nanocomposites. This effect was attributed to the potential variations in the interface, caused by modifier thermal degradation, and the heterogeneous morphology, which could possibly lead to the increase in the CTE of nanocomposites [110].

6.2.4 Thermal Conductivity

The evaluation and study of the thermal conductivity of materials is of interest primarily for engineering purposes, where it is essential to define the heat flow, or to ensure uniform heating of the material. For example, low thermal conductivity is required of materials used for heat/thermal insulation. In contrast, construction parts subjected to friction require materials with a high thermal conductivity. The variations of thermal conductivity also give insights into structural and molecular changes of the polymeric material. No theory exists to accurately predict the thermal conductivity of polymers. The conductivity properties become more complicated with addition of fillers to polymers [111]. The effects of nano-reinforcements on the thermal conductivity of polymer nanocomposites have still not been investigated.

Most expressions for the thermal conductivity of polymers are based on the Debye theory of heat transport [112], which leads to the equation:

$$K = \Delta C_p \rho u L \tag{6.1}$$

where K is the thermal conductivity, C_p is the heat capacity, ρ is the density, u is the velocity of elastic waves (sound velocity), L is the average free path length, and Δ is a constant of the order of magnitude of unity. Consideration of Equation (6.1) indicates that crystalline materials will have a higher thermal conductivity than their corresponding amorphous state due to the overwhelming effect of higher values of ρ and u.

Various methods and techniques are used for measuring the thermal conductivity of materials, most of them being limited by high cost and large sample size requirements [113, 114]. So far, a number of studies have shown that modification of differential scanning calorimetry (DSC) gives reasonably good K data. The DSC-based methods have the advantage of requiring small and easily prepared samples, but the techniques are sensitive to sample thickness variations relative to the standard.

Khanna and co-workers [114] introduced a new concept based on DSC, which enabled a rapid estimation of the thermal conductivity of materials, requiring no instrument modification. They used a Perkin-Elmer model DSC-2C differential scanning calorimeter. An empty sample pan is used as the reference. The sample is cut from a uniform flat sheet of the material into the shape of a disc, which just fits into a sample pan. A melting point standard, such as indium, is placed on top of the sample. The DSC is then heated at a constant rate to a temperature above the melting point of the standard. The melting of the standard, as observed through the sample, is influenced by the thermal conductivity of the sample, and it is used for the K data calculations.

Based on the DSC method described above, the thermal conductivity of six thermoset nanocomposite materials were measured in our study [47]. The samples are prepared with epoxy resin matrix and various nanofillers at a fixed volume fraction of 3 vol% [47, 114]. The aim of the study was to determine the effect of a small amount of nanofiller

on the thermal conductivity of the epoxy resin matrix. Nanocomposites are prepared with Araldite LY556 epoxy resin (**Table 2.3**) with various nanofillers, such as SAN, STN and SPN organo-smectites (**Table 2.4**), graphite/diamond and diamond (**Table 2.5**). Anhydride HY917 is used as a hardener. The direct processing technique is applied for nanocomposite preparation, including ultrasonic mixing of epoxy resin and nanofillers, following by degassing and thermal curing at 80 °C for 4 h and post-curing at 140 °C for 1 h (see Chapter 2). The DSC samples with a uniform disc shape of the material and thickness of ~1 mm, which just fits into a sample pan, are tested. The indium standard (mp 156.6 °C) and a heating rate of 5 °C/min are used in the measurements. The thermal conductivity results are presented in **Table 6.4**.

Our first results on using this DSC method for estimation of the thermal conductivity of thermoset nanocomposites showed that the thermal conductivity is strongly influenced by the type of nano-reinforcement. In general, the addition of organoclay reduced the thermal conductivity of the epoxy resin, which is associated with a low coefficient of thermal conductivity for the clay. For example, only ~2 vol% of inorganic silicate in STN_{NC} reduced the thermal conductivity of the epoxy resin from 0.15 to 0.084 W/m K (~44%). However, at low silicate content of about 1–1.3 vol%, the effect of nano-

Table 6.4 Thermal conductivity of unfilled epoxy resin and epoxy-based nanocomposites and nanofillers of various materials, measured by a standard DSC unit [47] using an indium standard (at 156.6 °C)

Sample	Content of organofiller (vol%)	Inorganic content (vol%)	K (W/m K)	$\Delta K = K_{NC}/K_{resin}$
Epoxy resin	0	0	0.15	0
3% STN/epoxy nanocomposite	3	2	0.084	0.56 / 44%
3% SAN/epoxy nanocomposite	3	1, 3	0.145	0.97 / 3%
3% SPN/epoxy nanocomposite	3	1	0.13	0.87 / 13%
3% Graphite/diamond/ epoxy hybrid	3	3	0.17	1.13 / 13%
3% Diamond/epoxy hybrid	3	3	0.44	2.93 / 193%
Natural diamond*	–	100	2000	–
Nanoscale diamond powder (compacts), d = 6 nm, S = 360–400 g/cm^3	–	100	1260	–
Graphite†	–	100	105.5	–
Natural clay†	–	100	0.75	–

*Results determined from other methods, published in: *: [111], and*
† The Handbook for Chemists, Khimiya, Moscow, 1963, Volume 1

reinforcement on the thermal conductivity is found to be insufficient, e.g., in the range of accuracy of ±20% considered in the literature for thermal conductivity evaluation.

In contrast, the addition of graphite/diamond mixture and diamond improved the thermal conductivity of the epoxy resin, which is related to the high thermal conductivity of the carbon nanofiller inclusions and particularly the diamond. A dramatic enhancement, ~193%, of the thermal conductivity is observed for a small amount (3 vol%) of diamond nano-reinforced epoxy hybrids, while only ~13% enhancement was found if graphite/diamond is added to the epoxy resin, compared to that of the pristine epoxy.

In summary, our preliminary results show that, by varying the type of inorganic nanofiller (in an amount of only 2–3 vol%), it was possible to change the thermal conductivity of the epoxy resin in a wide range, from 0.084 to 0.44 W/mK. Thus, the clay/thermoset nanocomposites with $K \sim 0.084$ W/mK may be proposed as prospective heat/thermal insulation materials for buildings, constructions and other engineering applications. In addition, diamond nano-reinforced epoxy hybrids with $K \sim 0.44$ W/mK might be classified as novel materials with high thermal conductivity, applicable for tribology, electronics, etc. Further investigations are required to prove in detail the effects of increasing filler content of various nano-reinforcements on the thermal conductivity of the matrix polymer.

6.3 High Protective and Barrier Properties

6.3.1 Wear Resistance

There is a growing demand for abrasion-resistant polymer systems for coating applications in sensors, optics, textiles and numerous consumer goods. The use of conventional polymer coatings in some applications, however, is limited due to low wear and chemical resistance, poor mechanical characteristics and high permeability. An innovation used to overcome these limitations is the incorporation of nanosized fillers in the polymer matrix. Despite widespread and growing use of polymers in applications where abrasion is present, wear of these materials is ill-understood. The need for scratch and abrasion resistance is well established in various coating applications, but many scientific aspects have to be studied to gain a fundamental understanding of the wear mechanisms in filled polymers [115-119].

The advantages of nano-reinforcement over traditional filling materials open new frontiers of polymer nanocomposites in an ever-growing range of applications, including surface protection [120–125]. Recently, nanosized particles were found to enable coating surfaces to be protected more uniformly and more completely in terms of abrasion resistance compared with conventional coating additives. Moreover, the incorporation of nanofillers in surface coatings can provide long-term abrasion resistance without significantly affecting optical clarity, colour, gloss, or physical properties [45, 120–126].

A few studies have shown that wear resistance can be increased in polymer composites by incorporation of hard particles, while at the same time the wear of the counterbody decreases and the sliding coefficient of friction decreases [117–119]. This type of tribological behaviour will have an impact in polymeric bearings and coatings. In order to design composites with the optimum properties and predict performance, several authors [117–122] have discussed the limitations that must be overcome. Tripathy and Furey [117] summarise the results of a fundamental study of the tribological behaviour of graphite-reinforced epoxy composites. In addition to friction and wear, surface temperatures generated by friction and their possible effects on friction and wear were examined. The authors concluded that the maximum temperature reached during sliding of polymer composites appears to be controlled by the glass transition temperature of the matrix material. Moreover, based on SEM observations, the authors claimed that the revealed adhesion and fatigue are the dominant wear mechanism of the composite material.

A relationship was observed between surface temperature and wear. Kishore and co-workers [118] studied the wear characteristics of glass fibre/epoxy composite, filled with either rubber or oxide particles. The selection of these fillers was based on studying the influence of the presence of an elastomeric substance for improving the stretchability, as well as an oxide known for its non-deforming nature and ability to sustain load and temperature increase due to friction during wear. The results showed differing trends for reducing wear with load for the two types of fillers.

Luo [119] investigated phenolic resin-bonded diamond composites containing copper, carbon black and silicon carbide fillers, prepared by compression moulding, which are widely used for manufacturing various abrasive tools. The author found that a small amount of carbon black filler added to the diamond/phenolic composite with 20–30 vol% Cu filler has a positive effect on diamond retention and wear loss. However, the diamond composite containing a higher proportion of carbon black exhibited a large amount of diamond pull-out in the wear scar. This caused the wear loss of the composite to increase rapidly. The average particle size was in the micrometre range and varied between 15 and 45 μm.

In general, the understanding of the mechanisms contributing to wear performance in filled polymers is poor. This requires detailed study of the role of the filler–matrix interface and the effect of particle size, as well as developing appropriate models that consider the interface or size of the filler. The mechanism that lowers the coefficient of friction is unclear for non-lubricious nanoparticles. Moreover, nanoparticle-filled polymers have not been comprehensively explored for wear applications despite strong evidence suggesting a large improvement of wear resistance.

The ability to tailor the surfaces of nanosized particles to improve the electronic, optical and chemical performance of polymer-based materials will enable new functional, abrasion-resistant coatings to be developed in the future [121–125]. Nano-alumina, Al_2O_3, is especially well-suited for incorporation into coating systems, greatly enhancing

abrasion resistance with minimal effects on the clarity, gloss and physical properties of the coatings. Recently, nano-additives marketed under the trade names NANOBYK-3600 and NANOBYK-3601 have been produced by BYK-Chemie and Nanophase Technology Corp. USA as a dispersion of nanocrystalline Al_2O_3 (45 m^2/g) in various solvents [121]. These products were developed to improve the scratch and wear resistance of coatings that can also be applied to plastics.

A carbon filament-wound epoxy composite sensor coating that is subjected to severe in-use wear is processed by continuous dip-coating of the carbon fibre reinforcement prior to filament winding. Conventional epoxy materials generally do not provide enough wear resistance. To solve these problems, a polymer dispersion incorporating nanocrystalline alumina was developed [122, 123]. For the carbon filament-wound epoxy composites, a nanocrystalline Al_2O_3 powder (57 m^2/g) was rendered compatible with the composite polymer matrix, Shell 862, by coating and chemically modifying the powder to enable covalent incorporation into the Shell 862 resin. The relative wear resistance of the Al_2O_3/Shell 862 composite was compared with that of other material systems, such as elastomer-extended epoxy filled with ceramic particles, amorphous silica, calcium silicate and TiO_2. Laboratory wear testing demonstrated that nanocrystalline polymer coated Al_2O_3 covalently incorporated into an epoxy formulation at 45 wt% provides nearly 4 times and 19 times more wear resistance compared to two other commercial materials, 80–83 wt% filled epoxy and 46.5 wt% filled elastomer-modified epoxy, respectively. The nanocrystalline polymer coated Al_2O_3/epoxy dispersion is also the only material that can be processed by filament winding techniques.

There are strong indications that polymers filled with hard nanoparticles will exhibit significant improvements in tribological performance as compared to traditional filled polymers. Hard filler particles are frequently added to improve the wear resistance, but they increase both the abrasive wear to the counterface and the sliding coefficient of friction. The ideal filler for polymers would be inert, non-abrasive, reinforcing and reduce the coefficient of friction; thus, hard nanoparticles are proposed to be the ideal candidates. Recent studies have shown that the wear resistance can increase in various thermoplastic polymer composites filled with hard nanoparticles (e.g., Al_2O_3), while at the same time the wear of the counterbody decreases and the sliding coefficient of friction decreases [124–126]. This type of tribological behaviour will have an impact in polymeric bearings, covering the spectrum from industrial applications needing dry sliding bearings, to orthopaedic implant materials, to self-lubricating bearings for space environments.

The tribotechnical properties of composites based on polytetrafluoroethylene (PTFE) with ultradispersed diamond powder and natural technical diamond powder have been investigated by Adrianova and co-workers [127]. It was established that using the natural diamond powders as abrasive material in diamond tools gives essential improvement in the abrasive abilities of the materials. The investigation of friction against steel and different minerals has shown that the use of natural diamond powders in formulations is very good for polishing different stones, metals, etc.

Recently, a new class of materials, polymer/quasicrystal composites, with useful properties for beneficial exploitation in applications such as dry bearings and composite gears, has been reported [128]. Preliminary results indicate that the new composites enhance the properties of certain polymers while providing a new means of processing quasicrystals. The Al–Cu–Fe quasicrystal materials significantly improved wear resistance to volume loss in polymer-based composites. Some results indicated that the quasicrystal-filled polymers were between 5 and 10 times better in resisting wear than any other polymer or polymer composite that was tested.

Epoxy and unsaturated polyester resins are widely used for coatings, gel coats, protection of natural stone, etc. Improvement of the wear resistance without significantly affecting the optical clarity and processability of these resins are important challenges for such applications. We have studied [129] the effect of various nanofiller particles, such as diamond, alumina and graphite/diamond, on the improvement of the wear resistance of epoxy and polyester resins. Nanocomposites are prepared from a variety of nanofiller and resin formulations. The diamond and graphite/diamond nanofillers are produced by the Space Research Institute, Bulgarian Academy of Sciences, using shock-wave technology (see Section 2.4.1). The nanoscale alumina, Al_2O_3, both untreated (D40) and treated with organic modifiers (OS1 – *p*-toluenesulfonic acid; OS2 – benzenesulfonic acid), is supplied by the SASOL company, Germany. **Tables 2.3** and **2.5** earlier presented the characteristics of the resins and the nanoparticles, respectively. The direct processing technique is used, where nanofillers are dispersed in polymer matrices of epoxy resin (AP1) and unsaturated polyester resin (Viapal) by sonication. Samples are cured under ambient conditions and post-cured for 6 h at 80 °C, using diethylenetriamine and methyl ethyl ketone peroxide as the curing agents for the epoxy resin and the polyester resin, respectively. The wear resistance experiments are performed in agreement with ISO 4649:2002 [130] (ASTM D5963-04 [132]) using a rotating cylindrical drum device with a corundum abrasive surface. Cylindrical specimens of size d = 6 mm and h = 20 mm were tested at a sliding distance of 18 m, load of 10 N and velocity of 0.3 m/s. The wear resistance was represented by the weight loss (grams), $\Delta G = (G_0 - G)$, where G_0 is the weight of the sample before the test (g), and G is the weight of the sample after the wear test (g). The improvement in wear resistance, $\Delta G_{resin}/\Delta G_{NC}$ was calculated as a ratio of the weight loss of the pure resin, ΔG_{resin}, to that of the nanocomposite, ΔG_{NC}.

A significant improvement of the wear resistance was found for nanocomposites, which is strongly dependent on the hardness of the nanoparticles and the degree of dispersivity. Laboratory experiments demonstrated that the incorporation of a small amount of nanoscale diamond (0.5–5 vol%) in the polyester resin formulations resulted in a significant decrease of the wear mass loss, compared to that of the pure resin, indicating a strong improvement of the wear resistance [47, 115, 129]. **Figure 6.14** compares the concentration dependence of both the wear weight loss, ΔG, of crosslinked hybrids and the relative viscosity, η/η_0, of precursor dispersions.

At volume contents ranging from 0.5 to 5 vol%, the diamond nanofiller significantly improves the wear resistance of the matrix polyester resin by 11–35%. This effect might be related to the physical properties of diamond – extreme hardness and high thermal conductivity. In contrast, the graphite/diamond (66/32) mixture, as a soft filler, has an insignificant effect on the wear properties of the polyester resin. Moreover, the viscosity of dispersions is slightly increased in this filler concentration region, indicating good processability of the systems.

The effect of diamond concentration on both characteristics, wear resistance and viscosity, is rather similar but exhibits certain specific features with respect to growth dynamics. The effect of nanofiller on the improvement of the wear resistance appears at very low filler content of 0.5 vol% and tends to saturation above 4 vol%. It is important to note that the improvement in wear resistance of crosslinked systems with increasing diamond filler content is somehow related to the viscosity of the precursor dispersions. Wear mass loss decreases rapidly within the range of slower augmentation of viscosity at filler contents $\phi < \phi^{**}$, and then its values tend to a plateau, while the viscosity increases sharply. Obviously, this is due to the type of superstructure formed by nanoparticles in

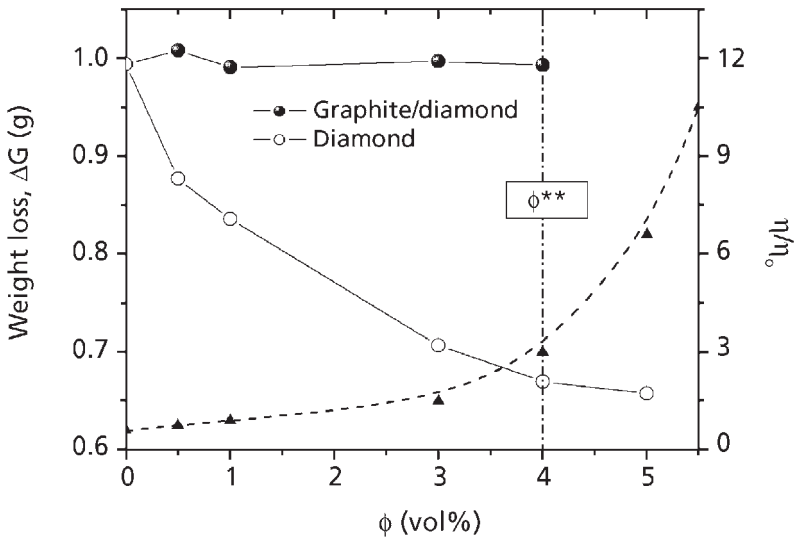

Figure 6.14 Wear mass loss, ΔG, *versus* nanofiller volume concentration, ϕ, of crosslinked polyester hybrids (full lines). Results for diamond and graphite/diamond (67/33) are compared. The dashed line plots the relative viscosity, η/η_0, *versus* ϕ of the precursor diamond/resin dispersions. The second percolation threshold $\phi^{**} \sim 4\%$ is indicated by the vertical line.

Reproduced with permission from [115].

the polymer matrix. At volume fractions below the second rheological threshold, $\phi < \phi^{**}$, the diamond particles form fractal flocs consisting of cluster-cluster aggregates and a matrix polymer enclosure within (so-called interphase). At higher volume fractions, $\phi \geq \phi^{**}$, a dense three-dimensional network of floccules is formed. The second rheological transition, $\phi^{**} \sim 4$ vol%, is somehow related with the saturation of the wear resistance improvement. Obviously, the formation of a network superstructure of nanofiller in the polymer matrix at ϕ^{**} enables nanocomposite surfaces to be more uniformly and completely abrasion resistant compared with unfilled polyester resin. Thus, the wear resistance improvement at 4–5 vol% (~ϕ^{**}) diamond/polyester nanocomoposite is ~51%, compared to that of the pure resin.

The strong improvement of the wear resistance of diamond-containing nanocomposites may be assigned also to the enhanced thermal conductivity of the resin by incorporation of diamond nanofiller. Most of the conventional composites containing micrometre size fillers have low thermal conductivity and high hardness, which produces very high surface friction temperature. The surface friction temperature is a critical parameter for the tribological behaviour of polymeric materials [117, 132]. In contrast, nanoscale diamond-containing hybrids showed good tribological characteristics, based on the high hardness and high thermal conductivity, leading to a decrease of the surface friction temperature.

Figure 6.15 compares the wear resistance improvement, $\Delta G_{resin}/\Delta G_{NC}$, of polyester- and epoxy-based hybrids containing 1.3 vol% (3 wt%) alumina, Al_2O_3 (untreated – D40, and treated – OS1 and OS2) [129]. Evidently, the treatment of the alumina by targeted organic modifiers contributes to the improvement in wear resistance of polyester and epoxy resin matrices. For example, the wear resistance improvement of the epoxy resin filled with 1.3 vol% D40 and OS2 alumina is ~30%, while an insignificant effect was observed for the OS1/epoxy composite system.

Importantly, the wear resistance of the polyester resin systems is not significantly affected, or even worsened, at this low filler content. It is interesting to relate these results with the degree of nanofiller dispersivity in the resin matrix. The rheological results of the precursor dispersions, shown before in **Figures 2.18** and **2.19**, demonstrated that the dispersability of alumina in epoxy resin is found much lower that that in polyester resin. It seems that the alumina aggregates are dispersed to the level of single nanoscale particles of few nanometres size in polyester resin matrix. In contrast, alumina aggregates with larger size are present in the epoxy-based dispersions. Similarly, **Figure 2.18** shows that epoxy systems with D40 and OS2 aluminas have lower degree of dispersion, compared to OS1.

Based on the rheological results, it can be assumed that a full dispersion of alumina aggregates to nanoscale particles of a few nanometres has a negative effect, leading to a decrease of the wear resistance, compared to that of the pure polymer. Based on morphological observations with SEM and AFM [47], it was claimed that, in order to obtain high wear resistance improvement by nanofiller particles, it is important for the nano-reinforcements to have larger aggregate size, ~50–100 nm.

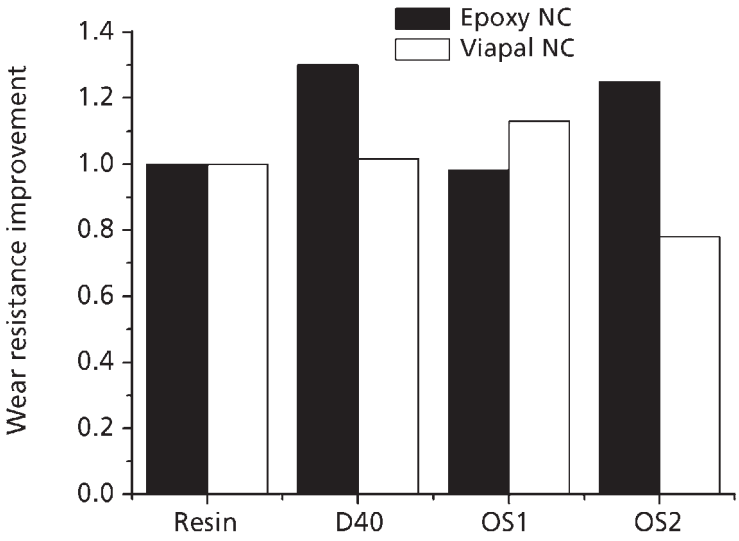

Figure 6.15 Wear resistance improvement, $\Delta G_{resin}/\Delta G_{NC}$, of crosslinked nanocomposites based on epoxy resin AP1 (full bars) and polyester resin Viapal (empty bars) filled with 1.3 vol% alumina (untreated – D40, and organically treated – OS1 and OS2).

Reproduced with permission from [129]. ©Heron Press, Bulgaria, 2006

It is interesting to compare the wear resistance improvement produced by diamond (**Figure 6.14**) and alumina (**Figure 6.15**) nanofillers in the polyester resin matrix. The results taken at a fixed low volume fraction (e.g., 1.3 vol%) show that the wear resistance improvement of the diamond/polyester systems (17%) is higher than the best results obtained for the OS1 alumina/polyester systems (13%). In the context of the discussions above, a lower degree of dispersivity of the aggregates of diamond compared to the alumina in the polyester resin matrix can be assumed.

6.3.2 Permeability Control

Conventional polymer coatings and materials for packaging in many applications are limited because of high permeability. An innovation proposed to overcome these limitations is the incorporation of a small amount of nanosized fillers for producing protective coatings with controlled permeability. Along with mechanical properties and flame retardancy, barrier properties constitute one of the principal advantages of polymer nanocomposites, especially for packaging applications.

The substantial decrease of permeability brought by nanocomposite structure is a major advantage of polymer/clay nanocomposite. The incorporation of plate-like fillers with a

high aspect ratio is found to improve the barrier properties of composite films towards low-molecular-weight compounds (e.g., oxygen, carbon dioxide, water vapour) [18, 23]. This effect can be easily understood in a qualitative way, since diffusion through the crystalline filler particles is much smaller than through the polymer matrix. Therefore the incorporation of fillers forces the diffusing molecules to take a longer diffusion path through the composites [116].

It was first reported by the Toyota researchers [133] that polyamide-6/clay hybrid had a rate of water absorption reduced by 40% as compared to the unfilled polymer. Messersmith and Giannelis [23] observed a dramatic decrease of water permeability, up to 80%, with only 5 vol% of clay, with poly(ε-caprolactone) layered silicate nanocomposites. The gas barrier properties are shown to improve dramatically upon exfoliation of clay platelets in a number of polymeric matrices [18, 23, 134–136]. The gas permeability in a rubber/clay hybrid was reduced by 30% with 4 vol% of delaminated clay [134].

The mechanism for improvement is attributed to the increase in the tortuosity of the diffusive path for a penetrant molecule [137–141]. By incorporating impermeable plate-like nanoparticles in the polymer matrix, the permeating molecules are forced to wiggle around them in a random walk, diffusing through a tortuous pathway. The decrease of the transmission rate of the small molecules is found to be dependent on the aspect ratio, volume fraction and orientation of the inclusions. A simple tortuosity-based model is proposed by Bharadwaj [40, 41], which was found to reproduce the experimental results satisfactorily [135–137]. The reduction of permeability is given by the tortuosity factor $\tau = 1 + \phi p/2$, and the permeability ratio is given by:

$$P_{NC}/P_0 = (1 - \phi)/(1 + \phi p/2) \tag{6.2}$$

where P_{NC} is the permeability through the nanocomposite, P_0 is that through the pure polymer, ϕ is the volume fraction, $p = L/W$ is the aspect ratio of nano-inclusions, L is the length and W is the width of the sheets.

This expression assumes that the sheets are oriented orthogonally to the diffusive pathway. Recently, modified expressions have been proposed by the same author in order to include orientational order and the state of dispersion of the sheets in addition to the concentration. The first modification of Equation (6.2) introduced an orientation factor, $S = \langle 3\cos^2\theta - 1\rangle/2$, where θ is the angle between the average plate orientation and the flux direction. The following values of S can be calculated depending on the angle of orientation: for random orientation $S = 1/4$, for perpendicular orientation $S = -1/2$, and for parallel orientation $S = 1$.

Based on the orientation parameter, Equation (6.2) was modified in the following way:

$$P_{NC}/P_0 = (1 - \phi)/[1 + F(S)\phi p/2] \tag{6.3}$$

In order to predict the effect of the degree of dispersion, Bharadwaj [40, 41] suggested that the aspect ratio should be modified considering not individual clay platelets, but rather their short stacks. Their length remains unchanged, but the stack thickness depends on the number of layers and the intra-gallery spacings. Thus, $p = L/nW$, where n represents the number of layers within the stack. Hence, the relative permeability is expected to depend strongly on the extent of dispersion.

However, many factors cannot be accounted for by using this modified expression, Equation (6.3), such as: the possibility of lateral displacement of clay layers because of polymer intercalation; the confinement and solidification of polymer on the silicate surface, which reduces the molecular mobility and increases the barrier properties; and other complex factors. Nevertheless, these models help in understanding the mechanism controlling permeability through nanolayer reinforcement.

Furthermore, the effective length and width of nanostructure species in nanocomposites are found to change rapidly through aggregation. The floccules, formed by cluster–cluster aggregation, are proposed to be essentially impermeable. The impressive decrease of permeability was recently attributed to the large aspect ratio of the clay layers, which was confirmed by measurements of the permeability of polyimide/clay hybrids using clays with different aspect ratios [136]. However, some recent investigations [137, 141] contradicted this idea, showing a reduction of water permeability of polymer/clay nanocomposites as compared with the pristine polymer. The results led to the conclusion that the constraint brought about by nanocomposite structure to the polymer chains may be the essential factor contributing to the decrease of permeability.

The permeation properties of thermoset nanocomposites are rarely reported [40, 41, 142]. Bharadwaj and co-workers [40, 41] studied the permeability of O_2 in crosslinked clay/polyester nanocomposite films prepared by dispersing organically modified montmorillonite in pre-promoted polyester resin and subsequently crosslinking at room temperature. Oxygen permeability was found to be progressively reduced with increasing clay concentration, implying that the degree of aggregation is increased with the clay concentration. The improvement in permeability for the nanocomposite containing 2.5 wt% clay over the pure crosslinked polymer is found to be approximately a factor of 2.7. The barrier properties of nanocomposites are found to correlate well with the observed exfoliated morphology.

Osman and co-workers [142] prepared epoxy/organo-montmorillonite nanocomposites and studied their oxygen and vapour permeation with the perspective to using them in laminate production or in coating polyolefin foils to improve their barrier performance. The DGEBA epoxy resin was cured with amine hardener. Organo-montmorillonites were prepared by treating unmodified clay with various alkyl-ammonium ions. The chemical structure of the organic monolayer ionically bonded to the clay surface was varied and its influence on the swelling, intercalation and exfoliation behaviour of the organoclay was studied. It was proposed that the exfoliated layers built a barrier for the

permeating gas molecules, while the polymer intercalated tactoids did not contribute much to the permeation barrier performance. At 5% organoclay loading the relative vapour transmission rate was reduced to half and the permeability coefficient of the epoxy matrix reduced to one-quarter. The reduction was attributed to the tortuous pathway the gas molecules have to cover during their random walk to penetrate the composite. The transmission rate of the water vapour through the composite was found to be influenced more by the interfacial interactions than by the oxygen transmission, and hence the hydrophobicity of the inclusions might play an important role for the permeability reduction.

6.3.3 Water, Solvent and Corrosion Resistance

Water, acid rain, smog and pollution all corrode unprotected steel and other construction surfaces. Therefore, a great need exists for new coatings that have better surface resistance than standard coatings. The extraordinary barrier properties of polymer/layered silicate nanocomposites open new frontiers for their application as surface protection materials [3, 137, 141]. Epoxy and unsaturated polyester resins are widely used for coatings, adhesives, laminates and other applications, and recently a few investigations have been reported on new approaches for improving the water, solvent and corrosion resistance of resins by incorporating nanofillers, without significant changes of their optical properties and processability [129, 143–145].

We have studied [129] the effect of nanocrystalline alumina particles on improving the water resistance of epoxy and polyester resins by investigating the water absorption. Nanocomposites have been prepared by the direct processing method described above in Section 6.3.1. The nanoscale alumina, Al_2O_3 – untreated (D40) and treated by organic modifiers (OS1 – *p*-toluenesulfonic acid; OS2 – benzenesulfonic acid) – are incorporated in a small amount of 1.3 vol% (3 wt%) in the epoxy resin (AP1) and the unsaturated polyester resin (Viapal).

Water absorption experiments are performed in compliance with standard ISO 62:1999 [146] (ASTM D570 [147]). This test method covers the determination of the relative rate of absorption of water by plastics when immersed for 24 h or more at 40 °C. Our tests were performed for 168 h water treatment. Bulk post-cured specimens with a diameter of 6 mm and length of 30 mm were exposed to natural water at 40 °C and the weight of the samples was recorded every 24 h for a total duration of 168 h. The water absorption was calculated as the percentage increase in the weight of the water-treated sample (G) in comparison with the initial dry sample (G_0): $\Delta G/G_0$ (%) = $[(G - G_0)/G_0] \times 100$. The rate of water absorption, $\Delta G/G_0$, is studied within 0–168 h water treatment [129].

Figure 6.16 presents the results of water absorption, $\Delta G/G_0$ (%), *versus* time, t (h), for nanocomposites based on (a) Viapal polyester resin and (b) AP1 epoxy resin mixed with 1,3 vol% (3 wt%) alumina. Figure 6.16(a) shows that up to 96 h water treatment,

the polyester resin nanocomposites with D40 and OS2 alumina demonstrate values of water absorption similar to that of the pristine resin; while the OS1 compositions show higher water absorption and therefore low water resistance. However, after 96 h treatment the water absorption of the pure polyester resin increases sharply and finally decreases with increasing time to 168 h, which is associated with a degradation of the polymer. In contrast, the absorption curves of nanocomposites tend to plateau after 96 h treatment having lower values of ~0.5% (particularly for D40 and OS2 systems), than that of the pristine resin (0.73%). Therefore, the alumina nanofiller significantly improves the water resistance of the polyester resin after a long water treatment, and at a very low filler content (3 wt%).

Obviously, the water resistance of the Viapal polyester resin /alumina nanocomposites is much higher than that of the AP1 epoxy/alumina systems. **Figure 6.16(b)** demonstrates that the water absorption of the epoxy resin AP1 and the epoxy/alumina nanocomposites is twice higher, if compared to that of the polyester systems. The values of water absorption are similar for the OS2 and D40 nanocomposites (1.15-1.4%) and the pristine polyester resin (1.2%), while mostly pronounced water absorption is observed for the OS1 systems (2.1%) at 96 h treatment. Importantly, the water treatment above 96 h produces a decrease of the absorption curves for the pure epoxy resin AP1 and nanocomposites, which is indicative of molecular damage and mass extraction caused by the large amount of absorbed water.

These results confirm the possibility for improving and controlling the water absorption of thermoset resins by addition of particulate hard nanofillers, such as alumina. Obviously, the alumina inclusions actually exhibit some barrier effects, because of their large surface area and the impermeability of inorganic nanoparticles. However, the absence of strong interfacial interactions, such as for composites with OS1 alumina, leads to a significant decrease of water resistance. Further investigations of the water resistance of nanocomposites are planned to evaluate the effect of nanofiller concentration. A large amount of nanofiller, beyond the first rheological threshold ϕ^*, is expected to produce a greater improvement in the water resistance, due to the flocculated structure, which is proposed to be essentially impermeable.

The difference in the water resistance of the epoxy and polyester resins might be explained by the effect of the plasticiser, dibutylphthalate, which amounts to 20% of the epoxy resin AP1. In contrast, the unsaturated polyester resin Viapal contains styrene, which participates actively in the crosslinking proces. The low crosslink density in one of the two phases may be proposed as a reason for the higher water absorption and the faster degradation of the AP1 epoxy resin, compared to the polyester resin. Additionally, the effect of OS1 nanofiller, which strongly differs from that of the other alumina, needs further structural investigations.

Similar results were reported by Maganna and Pissis [143], showing that the presence of plasticiser THIOCOL (0–40%) in the DGEBA epoxy resin, cured by triethylenetetramine,

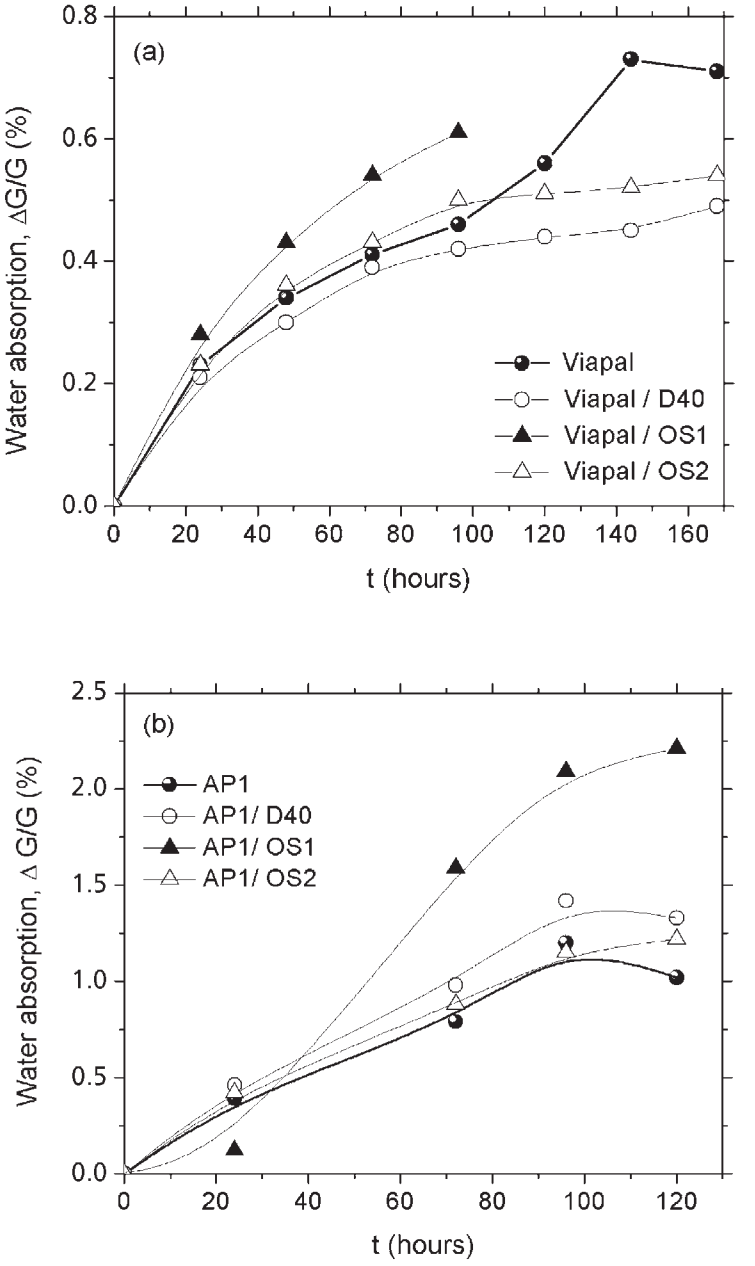

Figure 6.16 Water absorption of nanocomposites based on (a) Viapal polyester resin and (b) AP1 epoxy resin at 40 °C *versus* time. The nanofiller used is 1.3 vol% (3 wt%) alumina (untreated – D40; and treated – OS1 and OS2).

Data from [47, 115, 129].

permitted the formation of products with different crosslink densities and hydrophilic characters. The authors used dynamic water absorption experiments to investigate the characteristics of sorption and diffusion of water in epoxide systems. A new model was proposed, which considered the epoxide product as a two-phase system, consisting of a master phase (where the major part of the water is absorbed) that is homogeneous and non-polar, and a second phase with different density and hydrophilic character. The diffusion coefficients were measured to be different for the two phases, because of the different crosslink densities.

Improved barrier properties of nanocomposites were found to enhance also the solvent and corrosion resistance. A recent study of Harcup and Yee [144] performed on epoxy/clay nanocomposites demonstrated that nanocomposites offer a better resistance to organic solvents (alcohols, toluene and chloroform), particularly when the solvent molecules are small enough to penetrate into the polymer network and large enough so that, once they are absorbed, they cause molecular damage to the epoxy matrix, as with propanol or toluene. The increase in solvent resistance was attributed to the high barrier properties of polymer/clay nanocomposites.

Kouloumbi and co-workers [145] reported on the new iron oxide-filled epoxy coating, which demonstrated better corrosion resistance than standard epoxy coatings. The iron oxide was only a small portion of the mixture (15% by weight), well dispersed in bisphenol-A-based epoxy resin, and cured by high-viscosity polyaminoamide. Crosslinked specimens with a dry film coating were then exposed to a 3.5% NaCl solution to study the corrosion resistance. The anticorrosive and dielectric characteristics were monitored. In the early stages of the experiment, steel substrates treated with the iron oxide-filled epoxy showed no significant damage. Samples of the iron oxide-filled epoxy coatings performed better than the ordinary epoxy-coated sample. The corrosive properties were enhanced and the coatings containing iron oxide exhibited some capacitive behaviour. After 30 days, there was still no visible blistering or rust, but some green-coloured spots did appear, which could have been caused by chloride ions attacking the iron oxide or by the corrosion of the steel substrate. During the formation of iron oxide in a chloride environment, green complexes are precipitated as intermediate products. These bulky corrosion products were proposed to exhibit some barrier effects.

Acknowledgements

The DMTA experiments were possible thanks to Dr. T. Takahashi from VBL, Yamagata University, Yonezawa, Japan. Dr. M. Raimo from ICTP-CNR, Italy, is acknowledged for the innovative thermal conductivity experiments.

References

1. Y. Nakamura, M. Yamaguchi, M. Okubo and T. Matsumoto, *Polymer*, 1991, **32**, 16, 2976.

2. H. Lee and K. Neville, *Epoxy Resins, Their Application and Technology*, McGraw-Hill, New York, NY, USA, 1975.

3. L. Nielsen and R. Landel, *Mechanical Properties of Polymers and Composites*, 2nd Edition, Marcel Dekker, New York, NY, USA, 1994.

4. M. Alexandre and P. Dubois, *Material Science and Engineering Reports*, 2000, **28**, 1-2, 1.

5. P.B. Messersmith and E.P. Giannelis, *Chemistry of Materials*, 1994, **6**, 10, 1719.

6. E.P. Giannelis and P.B. Messersmith, inventors; Cornell Research Foundation Inc., assignee; US 5,554,670, 1996.

7. Usuki, T. Mizutami, Y. Fukushima, M. Fujimoto, K. Fukumon, Y. Kojima, N. Sato, T. Kurauchi and O. Kamigaito, inventors; Kabushiki Kaisha Toyota Chuo Kenkyusho, assignee; US 4,889,885, 1989.

8. M.S. Wang and T.J. Pinnavaia, *Chemistry of Materials*, 1994, **6**, 4, 468.

9. T.J. Pinnavaia, T. Lan, P.D. Kaviratna, Z. Wang and H. Shi, *Proceedings of the ACS Division of Polymeric Materials: Science and Engineering (PMSE)*, 1994, **73**, 117.

10. T. Lan, P.D. Kaviratna and T.J. Pinnavaia, *Proceedings of the ACS Division of Polymeric Materials: Science and Engineering (PMSE)*, 1994, **71**, 527.

11. T. Lan, Z. Wang, H. Shi and T.J. Pinnavaia, *Proceedings of the ACS Division of Polymeric Materials: Science and Engineering (PMSE)*, 1995, **73**, 296.

12. W.L. Ijdo, T. Lee and T.J. Pinnavaia, *Advanced Materials*, 1995, **8**, 1, 79.

13. H. Shi, T. Lan and T.J. Pinnavaia, *Chemistry of Materials*, 1996, **8**, 8, 1584.

14. T. Lan and T.J. Pinnavaia, *Chemistry of Materials*, 1994, **6**, 12, 2216.

15. T. Lan, P.D. Kaviratna and T.J. Pinnavaia, *Chemistry of Materials*, 1995, **7**, 11, 2144.

16. G.W. Beall in *Polymer Clay Nanocomposites*, Eds., T.J. Pinnavaia and G.W. Beall, John Wiley & Sons, Chichester, UK, 2000, p.267.

17. J-D. Ferry, *Viscoelastic Properties of Polymers*, John Wiley & Sons, New York, NY, USA, 1980.

18. T. Lan, P.D. Kaviratna and T.J. Pinnavaia, *Chemistry of Materials*, 1994, **6**, 5, 573.

19. T. Lan, P.D. Kaviratna and T.J. Pinnavaia, *Journal of Physics and Chemistry of Solids*, 1996, **57**, 6-8, 1005.

20. Z. Wang, and T.J. Pinnavaia, *Chemistry of Materials*, 1998, **10**, 7, 1820.

21. Z. Wang and T.J. Pinnavaia, *Chemistry of Materials*, 1998, **10**, 12, 3769.

22. Y. Tanaka and R.S. Bauer in *Epoxy Resin Chemistry and Technology*, Ed., C.A. May, Marcel Dekker, New York, NY, USA, 1988, p.285.

23. P.B. Messersmith and E.P. Giannelis, *Journal of Polymer Science A: Polymer Chemistry*, 1995, **33**, 7, 1047.

24. J. Massam and T.J. Pinnavaia, in *MRS Symposia Proceedings*, Volume 520, Materials Research Society, Pittsburgh, 1998, p. 223.

25. J. Massam, Z. Wang, T.J. Pinnavaia, T. Lan and G. Beall, *Proceedings, ACS Division of Polymeric Materials: Science and Engineering (PMSE)*, 1998, **78**, 274.

26. H-B. Hsueh and Ch-Y. Chen, *Polymer*, 2003, **44**, 18, 5275.

27. M.O. Abdalla, D. Dean and S. Campbell, *Polymer*, 2002, **43**, 2, 5887.

28. H-L. Tyan, Y-Ch. Liu and K-H. Wei, *Chemistry of Materials*, 1999, **11**, 7, 1942.

29. J.M. Brown, D. Curliss and R.A. Vaia, *Chemistry of Materials*, 2000, **12**, 11, 3376.

30. M.S. Wang, T. Lan and T.J. Pinnavaia, *Chemistry of Materials*, 1996, **8**, 9, 2200.

31. P. Kelly, A. Akelah, S. Qutubuddin and A.J. Moet, *Journal of Materials Science*, 1994, **29**, 9, 2274.

32. H-L. Tyan, C-M. Leu and K-H. Wei, *Chemistry of Materials*, 2001, **13**, 1, 222.

33. N. Salahuddin, A. Moet, A. Hiltner and E. Baer, *European Polymer Journal*, 2002, **38**, 7, 1477.

34. O. Becker, R.J. Varley and G.P. Simon, *Polymer*, 2002, **43**, 16, 4365.

35. D. Zax, D. Yang, R. Santos, H. Hegemann, E. P. Giannelis and E. Manias, *Journal of Chemistry and Physics*, 2000, **112**, 6, 1951.

36. X. Kornmann, R. Thoman, R. Mulhaupt, J. Finter and L.A. Berglund, *Polymer Engineering and Science*, 2002, **42**, 9, 1815.

37. X. Kornmann, H. Lindberg and L.A. Berglund, *Polymer*, 2001, **42**, 4, 4493.

38. X. Kornmann, H. Lindberg and L.A. Berglund, *Polymer*, 2001, **42**, 4, 1303.

39. X. Kornmann, *Synthesis and Characterization of Thermoset-Layered Silicate Nanocomposites*, Luleå University of Technology, Sweden, 2001 [Ph.D. Thesis].

40. R.K. Bharadwaj, A.R. Mehrabi, C. Hamilton, C. Trujillo, M. Murga, R. Fan, A. Chavira and A.K. Thompson, *Polymer*, 2002, **43**, 13, 3699.

41. R.K. Bharadwaj, *Macromolecules*, 2001, **34**, 26, 9189.

42. R. Krishnamoorti, R.A. Vaia and E.P. Giannelis, *Chemistry of Materials*, 1996, **8**, 8, 1728.

43. D.J. Suh, Y.T. Lim and O.O. Park, *Polymer*, 2000, **41**, 24, 8557.

44. D.J. Suh and O.O. Park, *Journal of Applied Polymer Science*, 2002, **83**, 10, 2143.

45. J. Karger-Kocsis and C-M. Wu, *Polymer Engineering and Science*, 2004, **44**, 6, 1083.

46. R. Kotsilkova, *Journal of Applied Polymer Science*, 2005, **97**, 6, 2499.

47. R. Kotsilkova, *Relationship Between Technology, Structure and Properties of Thermoset Nanocomposites*, Sofia, Bulgaria, 2005 [D.Sc. Thesis, in Bulgarian].

48. G. Ragosta, M. Abbate, P. Musto, G. Scarinzi and L. Mascia, *Polymer*, 2005, **46**, 23, 10506.

49. H. Miyagawa and L.T. Drzal, *Polymer,* 2004, **45**, 15, 5163.

50. E. Vassileva and K. Friedrich, *Journal of Applied Polymer Science*, 2003, **89**, 14, 3774.

51. R. Kotsilkova, D. Fragiadakis and P. Pissis, *Journal of Polymer Science B: Polymer Physics*, 2005, **43**, 5, 522.

52. N.S. Enikolopyan, M.L. Fridman, I.O. Stalnova and V.L. Popov, *Filled Polymers in Science and Technology*, *Advances Polymer Sciences Series*, 1990, **96**, 1.

53. G.M. Kim, D.H. Lee, B. Hoffmann, J. Kressler and G. Stöppelmann, *Polymer*, 2001, **42**, 3, 1095.

54. E. Reynaud, T. Jouen, C. Gauthier, G. Vigie and J. Varlet, *Polymer*, 2001, **42**, 21, 8759.

55. C. Zilg, R. Mülhaupt and J. Finter, *Macromolecular Chemistry and Physics*, 1999, **200**, 3, 661.

56. C. Zilg, R. Thomann, J. Finter and R. Mülhaupt, *Macromolecular Materials Engineering*, 2000, **280/281**, 1, 41.

57. T.J. Pinnavaia, T. Lan, Z. Wang, H. Shi and P.D. Kaviratna in *Nanotechnology: Molecularly Designed Materials*, Eds., G.M. Chow and K.E. Gonsalves, ACS Symposium Series No.622, American Chemical Society, Washington, DC, USA, 1996, Chapter 17, p.250.

58. Z. Wang, J. Massam and T.J. Pinnavaia in *Polymer-Clay Nanocomposites*, Eds., T.J. Pinnavaia and G.W. Beall, John Wiley & Sons, Chichester, UK, 2000, p.127.

59. S. Sarasaran, *Journal of Applied Polymer Science*, 1990, **39**, 8, 1635.

60. T.J. Pinnavaia and T. Lan, inventors; Board of Trustees, Michigan State University, assignee; US 5,760,106, 1998.

61. T.J. Pinnavaia and T. Lan, inventors; Board of Trustees, Michigan State University, assignee; US 5,801,216, 1998.

62. T.J. Pinnavaia and T. Lan, inventors; Claytec Inc., assignee; US 5,853,886, 1998.

63. R.M. Christensen, *Mechanics of Composite Materials*, Krieger, Malabar, FL, USA, 1991, p.144.

64. X. Kornmann, L.A. Berglund, J. Sterte and E.P. Giannelis, *Polymer Engineering and Science*, 1998, **38**, 8, 1351.

65. X. Kornmann, R. Thomann, R. Muelhaupt, J. Finter and L. Berglund, *Journal of Applied Polymer Science*, 2002, **86**, 10, 2643.

66. H. Zhang and L.A. Berglund, *Polymer Engineering and Science*, 1993, **33**, 2, 100.

67. J. Karger-Kocsis, O. Gryshchuk, J. Fröhlich and R. Mülhaupt, *Composite Science and Technology*, 2003, **63**, 14, 2045.

68. T.J. Wooster, S. Abrol and D.R. MacFarlane, *Polymer*, 2005, **46**, 19, 8011.

69. S. Ganguli, D. Dean, K. Jordan, G. Price and R. Vaia, *Polymer*, 2003, **44**, 4, 1315.

70. S. Ganguli, D. Dean, K. Jordan, G. Price and R. Vaia, *Polymer*, 2003, **44**, 22, 6901.

71. D.S. Kim and K.M. Lee, *Journal of Applied Polymer Science*, 2003, **90**, 10, 2629.

72. A.B. Morgan and J.W. Gilman, *Journal of Applied Polymer Science*, 2003, **87**, 8, 1329.

73. T.J. Wooster, S. Abrol, J. Hey and D.M. Macfarlane, *Composites A: Applied Science Manufacturing*, 2004, **35A**, 1, 75.

74. H.B. Hsueh and C.Y. Chen, *Polymer*, 2003, **44**, 4, 1151.

75. P. Le Baron, Z. Wang and T. Pinnavaia, *Applied Clay Science*, 1999, **15**, 1, 11.

76. Y. Nakamura, M. Yamaguchi, M. Okubo and T. Matsumoto, *Journal of Applied Polymer Science*, 1992, **45**, 7, 1281.

77. J.Y. Lee, M.J. Shim and S.W. Kim, *Polymer Engineering and Science*, 1999, **39**, 10, 1993.

78. L.S. Schadler, C.B.Ng and R.W. Siegel, *Nanostructured Materials*, 1999, **12**, 1-4, 507.

79. S. Stavrev, R. Kotsilkova, J. Karadjov and Z. Karagyozova, in *Nanoscience and Nanotechnology*, Eds., E. Balabanova and I. Dragieva, Heron Press, Sofia, Bulfgaria, 2001, Volume 1, p.154.

80. H. Miyagawa M.J. Rich and L.T. Drzal in the *Proceedings of the 31st Annual Conference of the North American Thermal Analysis Society (NATAS)*, Albuquerque, NM, 2003, CD-ROM #109.

81. Isik, U. Yilmazer and G. Bayram, *Polymer*, 2003, **44**, 20, 6371.

82. P. Jawahar and M. Balasubramanian, *Journal of Nanomaterials*, 2006, **1**, 1.

83. Hsieh, P. Moy, F. Beyer, Ph. Madison, E. Napadensky, J. Ren and R. Krishnamoorti, *Polymer Engineering and Science*, 2004, **44**, 5, 825.

84. L.A. Utracki, *Clay-Containing Polymeric Nanocomposites*, Rapra Technology, Shawbury, Shrewsbury, UK, 2004.

85. J.W. Gilman, *Applied Clay Science*, 1999, **15**, 1, 31.

86. J.W. Gilman, T. Kashiwagi, A.B. Morgan, R.H. Harris Jr., L. Brassel, M. Vanlandingham and C.L. Jackson, *Flammability of Polymer Clay Nanocomposite Consortium: Year One Annual Report*, US Department of Commerce, National Institute of Standards and Technology, Report NISTIR#6531, Gaithersburg, MD, USA, 2000.

87. E. Manias, A. Touny, L. Wu, B. Lu, K. Strawhecker, J.W. Gilman and T.C. Chung, *Proceedings of the ACS Division of Polymeric Materials: Science and Engineering (PMSE)*, 2000, **82**, 282.

88. J. Zhu, F.M. Uhl, A.B. Morgan and C.A. Wilkie, *Chemistry of Materials*, 2001, **13**, 12, 4649.

89. S. Su, D.D. Jiang and C.A. Wilkie, *Polymer Degradation and Stability*, 2004, **83**, 2, 333.

90. G.S. Sur, H.L. Sun, S.G. Lyu and J.E. Mark, *Polymer*, 2001, **42**, 24, 9783.

91. S. Bandyopadhyay, E.P. Giannelis and A.J. Hsieh, *Proceedings of the ACS Division of Polymeric Materials: Science and Engineering (PMSE)*, 2000, **82**, 208.

92. J.W. Gilman, T. Kashiwagi, S. Lomakin, E.P. Giannelis, E. Manias, J.D. Lichtenhan and P. Jones in *Fire Retardancy of Polymers: the Use of Intumescence*, Eds., G. Camino, M. Le Bras, S. Bourbigot and R. DeLobel, Royal Society of Chemistry, Cambridge, UK, 1998, p.203.

93. J. Lee, T. Takekoshi and E. Giannelis in *Nanophase and Nanocomposite Materials II*, Volume 457, Eds., S. Komarneni, J.C. Parker and H.J. Wollenberger, MRS Symposia Proceedings, Materials Research Society, Pittsburgh, PA, USA, 1998, p.513;

94. J. Lee and E. Giannelis, *Polymer Preprints*, 1997, **38**, 2, 688.

95. R.A. Vaia, G. Price, P.N. Ruth, H.T. Nguyen and J. Lichtenhan, *Applied Clay Science*, 1999, **15**, 1, 67.

96. J.W. Gilman, T. Kashiwagi, N. Nyden, J.E.T. Brown, C.L. Jackson, S. Lomakin, E.P. Giannelis and E. Manias in *Chemistry and Technology of Polymer Additives*, Eds., M.A. Malden, S. Ak-Malaika, A. Golovoy and C.A. Wilkie, Blackwell Science, Oxford, UK, 1999, Chapter 14, p.249.

97. Z. Wang and T.J. Pinnavaia, *Journal of Materials Chemistry*, 2003, **13**, 9, 2127.

98. R. Kotsilkova, V. Petkova and Y. Pelovski, *Journal of Thermal Analysis and Calorimetry*, 2001, **64**, 2, 591.

99. *Epoxy Resin Chemistry II*, Ed., R.S. Bauer, ACS Symposium Series, No.221, American Chemical Society, Washington, DC, USA, 1983.

100. V. Babrauskas and R. Peacock, *Fire Safety Journal*, 1992, **18**, 3, 255.

101. J.M. Thomas, *Intercalation Chemistry*, Academic Press, London, UK, 1982, Chapter 3, p.55.

102. F. Rossetti, *Meccanismi di Degradazione Termica e di Ritardo all Fiamma di Nanocomposite Polimerici*, University of Torino, Italy, 1999/2000 [Thesis].

103. L. Mascia, *The Role of Additives in Plastics*, Edward Arnold, London, UK, 1974, p. 87.

104. K.E. Atkins, J.V. Koleske, P.L. Smith, E.R. Walter and V.E. Matthews, in *Proceedings of the Society of the Plastics Industry 31st Annual Conference of Reinforced Plastics/Composites Institute – Reinforced Plastics – The Revolution of '76*, Washington, DC, USA, 1976, Section 2-E, p.1.

105. W. Li and L.J. Lee, *Polymer*, 2000, **41**, 2, 685.

106. W. Li and L.J. Lee, *Polymer*, 2000, **41**, 2, 697.

107. W. Li, K.H.Hsu and L.J. Lee, *Polymer*, 2000, **41**, 2, 711.

108. L. Xu and L. Lee, *Polymer*, 2004, **45**, 21, 7325.

109. E. Haque and C.D. Armeniades, *Polymer Engineering and Science*, 1986, **26**, 21, 1524.

110. Y. Kojima, A. Usuki, M. Kawasumi, A. Okada, Y. Fukushima, T. Kurauchi and O. Kamigaito, *Journal of Materials Research*, 1993, **8**, 5, 1185.

111. S. Stavrev, L. Markov, J. Karadjov and A. Petrova in *Nanoscience and Nanotechnology*, Eds., E. Balabanova and I. Dragieva, Heron Press, Sofia, Bulgaria, 2001, p.155.

112. D.W. Van Krevelen and P.J. Hoftyzer, *Properties of Polymers*, Elsevier, Amsterdam, The Netherlands, 1976, Chapter 17, p.395.

113. A.W. Pratt in *Thermal Conductivity*, Ed., R.P. Type, Academic Press, New York, NY, USA, 1969, Volume 2, p. 301.

114. Y.P. Khanna, T.J. Taylor and G. Chomyn, *Polymer Engineering and Science*, 1988, **28**, 16, 1034.

115. E. Ivanov, *Rheological Behavior and Properties of Thermosetting Resins Incorporating Nanoscale Carbon Particles*, Sofia, Bulgaria, 2006 [Ph.D. Thesis, in Bulgarian].

116. T. Davidson in *Conductive and Magnetic Fillers in Functional Fillers for Plastics*, Ed., M. Xanthos, Wiley-VCH, Weinheim, Germany, 2005.

117. B.S. Tripathy and M.J. Furey in *Proceedings of the ASM 1993 Materials Congress, Materials Week '93*, Pittsburgh, PA, USA, 1993, p.131.

118. B. Kishore, P. Sampathkumaran, S. Seetharamu, S. Vynathea, A. Murali and R.K. Kumar, *Wear*, 2000, **237**, 1, 20.

119. S.Y. Luo, *Wear*, 1999, **236**, 1, 339.

120. Y. Fukushima and S. Inagaki, *Journal of Inclusion Phenomena*, 1987, **5**, 4, 473.

121. Nanophase Technologies (NANX), *http://www.nanophase.com*

122. R.W. Brotzman, and J.H. Aikens, inventors; Nanophase Technologies Corporation, assignee; US 5,993,967, 1999.

123. R.W. Brotzman, and J.H. Aikens, inventors; Nanophase Technologies Corporation, assignee; US 6,033,781, 2000.

124. D. Burris and W.G. Sawyer, *Tribology Transactions*, 2005, **48**, 2, 147.

125. P. Bhimaraj, D.L. Burris, J. Action, W.G. Sawyer, C.G. Toney, R.W. Siegel and L.S. Schadler, *Wear*, 2005, **258**, 9, 1437.

126. W.G. Sawyer, D.K.D. Freudenberg, P. Bhimaraj and L.S. Schadler, *Wear*, 2003, **254**, 5, 573.

127. O.A. Adrianova, S.N. Popov and E.Yu. Shitz, *Journal of Friction and Wear*, 1998, **19**, 1, 71.

128. P.D. Bloom, K.G. Baikerikar, J.U. Otaigbe and V.V. Sheares, *Materials Science and Engineering A*, 2000, **294–296**, 156.

129. R. Kotsilkova, E. Ivanov, E. Krusteva, B. Milosheva, A. Topliyska, C. Silvestre, S. Cimmino and M. Raimo in *Nanoscience and Nanotechnology*, Ed., E. Balabanova and I. Dragieva, Heron Press, Sofia, Bulgaria, 2006, p.141.

130. ISO 4649, Rubber, vulcanised or thermoplastic - Determination of abrasion resistance using a rotating cylindrical drum device, 2002.

131. ASTM D5963, Test method for Rubber Property - Abrasion Resistance (Rotary Drum Abrader), 2005.

132. R.W. Siegel and J.A. Eastman in *Multicomponent Ultrafine Microstructures*, Eds., L.E. McCandlish, B.H. Kear, D.E. Polk and R.W. Siegel, MRS Symposia Proceedings, Volume 132, Materials Research Society, Pittsburgh, PA, USA, 1989, p.3.

133. A. Okada, M. Kawasumi, A. Usuki, Y. Kojima, T. Kurauchi and O. Kamigaito in Polymer Based Molecular Composites, Eds., D.W. Schaefer and J.E. Mark, *MRS Symposia Proceedings*, Volume 171, Materials Research Society, Pittsburgh, PA, USA, 1990, p.45.

134. Y. Kojima, K. Fukumori, A. Usuki, A. Okada and T. Kurauchi, *Journal of Materials Science Letters*, 1993, **12**, 12, 889.

135. K. Yano, A. Usuki, A. Okada, T. Kurauchi and O. Kamigaito, *Journal of Polymer Science A*: *Polymer Chemistry,* 1993, **31**, 10, 2493.

136. K. Yano, A. Usuki and A. Okada, *Journal of Polymer Science A*: *Polymer Chemistry*, 1997, **35**, 11, 2289.

137. J.C. Matayabas and S.R. Turner in *Polymer–Clay Nanocomposites*, Eds., T.J. Pinnavaia and G.W. Beall, John Wiley & Sons, New York, NY, USA, 2001, p.207.

138. A.A. Gusev and H.R. Lusti, *Advanced Materials*, 2001, **13**, 21, 1641.

139. D.M. Eitzman, R.R. Melkote and E.L. Cussler, *AIChE Journal*, 1999, **42**, 1, 2.

140. G.H. Fredrickson and J. Bicerano, *Journal of Chemical Physics*, 1999, **110**, 4, 2181.

141. L.E. Nielsen, *Journal of Macromolecular Science, Part A: Chemistry*, 1967, **1**, 5, 929.

142. M.A. Osman, V. Mittal, M. Morbidelli and U.W. Suter, *Macromolecules*, 2004, **37**, 19, 7250.

143. C. Maggana and P. Pissis, *Journal of Polymer Science B: Polymer Physics*, 1999, **37**, 11, 1165.

144. J.P. Harcup, A.F. Yee and M.K. Akkapeddi in the *Proceedings of the SPE ANTEC '99 Conference*, New York, NY, USA, 1999, Volume 3, p.3396.

145. N. Kouloumbi, G.M. Tsangaris, S.T. Kyvelidis and G.C. Psarras, *British Corrosion Journal*, 1999, **34**, 3, 267.

146. ISO 62, Plastics - Determination of Water Absorption, 1999.

147. ASTM D570, Test Method for Water Absorption of Plastics, 2005.

7 Design Physical Properties of Thermoset Nanocomposites

R. Kotsilkova

7.1 Introduction

Nanostructured materials have unusual physical and chemical properties as a result of their extremely small size and large specific area, and this has encouraged the search for new fields of applications for these functional materials. The combination of inorganic and organic components in a nanosized single particle has made an immense area of new functional materials accessible – the next generation of semi-structural and electronic materials, sensors, catalysers, etc. [1–7]. In the past few years, conducting and semiconducting particles of nanometre size have become the objects of rapidly growing interest. The unique surface and electronic properties of nanoparticles combined with the properties of matrix polymers are used to tailor novel physical properties of nanocomposites [3, 4, 7]. Special attention has been paid to the *in situ* synthesis of nanocomposites, their chemical interactions, and the size and distribution of the nanoparticles in the polymer matrix [5, 6].

Pelster and Simon [5] reported that the degree of order depends on the distribution of particle size and interparticle spacings, and this is reflected in the dielectric response of the composites. In their recent book, Pomagailo and Kestelman [6] described the action of numerous metallopolymer nanocomposites with regards to their ability to modify polymers, leading to novel magnetic, electrical and optical properties. Yang and co-workers [8] reported the development of a novel nanostructured polymer/ceramic composite based on an epoxy formula with high dielectric constant, approximately 110. Two epoxy resin-based polymers were used, i.e., a cycloaliphatic epoxy and bisphenol A. The high dielectric constant was obtained by increasing the dielectric constant of the epoxy matrix by doping with cobalt acetylacetonate, and by using a combination of lead magnesium niobate, lead titanate and barium titanate as the ceramic nanofiller. The new nanocomposite was proposed for application as integral capacitors in printed circuit boards.

Generally, polymers exhibit good insulating properties. However, they become relatively good conducting materials when incorporating appropriate fillers, e.g., metal or carbon particles [7-11]. The electrical properties of carbon black-filled polymer composites have been studied extensively with both fundamental and applied purposes in mind

[12–20]. Organic materials possessing both conducting and ferromagnetic functions are extremely useful due to their unique properties and potential application as batteries, electrochemical display devices, sensors, and other electronic materials. Recently, polymer composites incorporating nanosized metal or carbon particles have become very important due to their promising capabilities of electromagnetic shielding, microwave absorption, conductivity and prevention of electric charging [5-7, 11].

The conductivity of polymer composites filled with carbon black has been widely studied and is found to depend strongly on the filler content and agglomeration processes [13, 14]. At the critical filler content of percolation, a sharp increase of the conductivity by several orders of magnitude occurs. This phenomenon is mostly explained in terms of the percolation theory, and it is related with the agglomeration of particles and the formation of an infinite cluster [18–23]. For most polymer systems the critical volume fraction for percolation is determined to be between 5 and 20 vol%, which is in agreement with the geometrical models [21, 22]. Recently, a lower percolation threshold has been observed for carbon black-filled epoxy resins [13–15], not obeying the predictions of the standard percolation model, which is suitable for randomly dispersed but not interacting fillers.

Colloid theory is applied to describe interactions among particles and agglomeration processes in relation to composite conductivity [1, 2, 24]. Scientists generally agree, for example, that, for a given weight of carbon black, finer agglomerates enable one to achieve smaller interparticle distances and, therefore, electrons can be transferred from particle to particle throughout the matrix [25–30]. Several authors [25–27] have noticed that the electrical and structural properties must be affected by the preparation conditions of the material, namely by the occurrence of a colloidal phase. The preparation of well-defined systems for such specific applications requires the control of dispersion processes and structure [1, 2, 5, 11, 13, 14]. In recent reviews on the electrical conductivity of binary mixtures, Carmona [25] and Lux [26] assumed that the mixing process may induce electrical charging of carbon particles and thus might stimulate interactions between the particles and the polymeric host. Such effects have not been well investigated with respect to the relation between rheology, electrical and microwave properties of thermoset nanocomposites.

In our studies [31–37] we focused on the relation between rheology, conductivity and microwave properties of thermoset nanocomposites containing nanoparticles of carbon and metal oxides. Various modes were used to gain control over interactions among particles and agglomeration processes; thus, the most important variables were volume content, additives and processing technology. The rheological characteristics were correlated with conductivity and microwave properties in a wide concentration range of the filler. The results of this study were proposed as a very useful way to assess the optimal compounding conditions of nanoparticles in a given polymeric system in order to maintain certain physical properties.

7.2 Carbon/Thermoset Nanocomposites

7.2.1 Experimental

The filler component used was a finely dispersed graphite/diamond (GD) mixture, called carbon, which was synthesised by a patented method of shock-wave propagation from the free carbon of the explosive [38] and was supplied by the Space Research Institute at the Bulgarian Academy of Sciences (BAS). By using optimal synthesis conditions (pressure, time and temperature), this shock-wave technology allowed the 'raw' graphite/diamond mixture with a controlled content and particle size to be obtained. The mixture of 67% disordered graphite and 33% diamond was used for the preparation of nanocomposites, having an average particle diameter of about 6 nm, a density of 1.86 g/cm^3, and a specific surface of 590 m^2/g (by the Brunauer–Emmett–Teller (BET) method for the analysis of gas sorption surface area) [31-37] (see **Table 2.5**). **Figure 7.1** presents the X-ray diffraction (XRD) spectra obtained for the carbon mixture with a basal peak at d = 0.331 nm for graphite and a peak at d = 0.208 nm for diamond [31].

Acrylic resin (AR, polymethylacrylate), polyurethane (PU, polyol isocyanate) and epoxy resin (ER, Araldite LY556, CIBA) were used as matrix polymers (see **Table 2.3**). Dispersions of graphite/diamond nanoparticles (0–15 vol% GD) in the matrix resins were prepared by two steps of processing. The first step (I) was 15 min mixing with

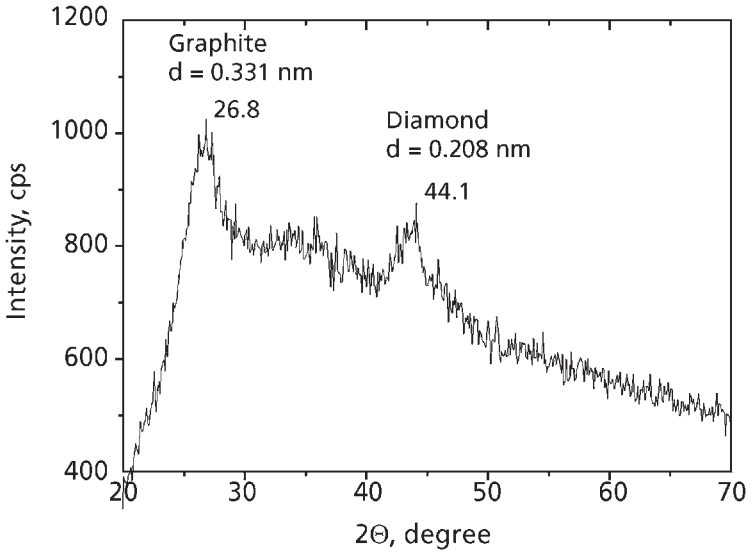

Figure 7.1 XRD spectra of nanoscale graphite/diamond mixture.

Reproduced with permission from [31]. ©Wiley Periodicals, 2004

a high-speed disintegrator at 7000 rpm, and the second step (II) was 1 h mixing by a laboratory magnetic stirrer. The two steps of processing induced good dispersion of carbon particles within the polymer matrix and reduced the size of particle agglomerates. Solid nanocomposite films of the acrylic- and the polyurethane-based systems were prepared by solvent evaporation and polymerisation of the dispersions at room temperature followed by 4 h post-curing at 60 °C. The epoxy-based systems were cured by amine hardener (EH-629, Vianova) in the ratio of 100:30 in the course of 1 h at room temperature, followed by post-curing for 3 h at 140 °C [31–36].

The rheological measurements of carbon/acrylic dispersions were performed with a Rheotron Brabender viscometer using cone-and-plate geometry. Steady-state viscosity was measured within the shear rate region from 0.1 to 100 s^{-1}. Oscillatory shear mode with frequency sweeps between 0.1 and 75 s^{-1} at low strain amplitude was used to measure the dynamic moduli within the linear elastic range [31, 33, 34].

The volume dc conductivity of the solid composites was measured at room temperature with a Keithley 610C electrometer. The experiments were carried out at the Institute of Solid State Physics of the BAS. Thin sections were cut from films with dimensions of approximately 10 mm length, 1 mm width and a thickness of 0.01 mm. Planar electrical contacts (~1 mm spaced and 10 mm long) made of silver paint were made on both long sides of the samples. Various applied voltages were used on different samples, depending on the level of conductivity of the specimens; thus the voltage of 100 V was applied for the matrix polymer and the composites below 5 vol% of carbon, and 1 V for the composites above 5 vol% of carbon. A minimum of three samples were used to determine the electrical properties for each composition [31, 32].

The microwave absorption characteristics were measured using a Network Analyzer hp 8720 ES, with wide-band SOLT (short–open–load–'thru') calibration within the frequency range 2.5–15 GHz. These experiments were done in the Institute of Electronics of BAS. Samples with up to three layers (sandwich type) were studied for increasing the microwave-absorbing effect. The size of the single layer was ~0.002 mm. Additionally, the method was followed in a fixed frequency domain at 9.4 GHz for determination of microwave absorption (a, %), reflection (r, %) and transmission (t, %). The measuring device used in this method consisted of a reflectometer circuit in free space with two opposite directed horns – transmitter and receiver. A deposition of metal sheet (short-circuit) at a definite distance from the horns was used to avoid problems connected with the positioning of samples in the near zone to the horns. Sample films were subsequently positioned at the place of the short-circuit.

7.2.2 Rheological Optimisation of Dispersions

Besides single-particle characteristics, the structure of nanodispersions is of great importance for achieving good physical properties. Applications such as electromagnetic

absorbers and electrical conductivity need paths of agglomerating particles for energy dissipation [5, 13, 14]. Generally, it is expected that finely dispersed carbon particles would enable smaller interparticle distances to be achieved. Interactions between particles cannot be neglected, and thus charge transport via hopping may occur, which depends strongly on the distribution of interparticle spacings [5].

Therefore, the preparation of well-defined systems requires good control of the dispersion processes. In our study on the carbon/resin systems, three factors are varied for rheological optimisation of the dispersions: mixing conditions, filler content and polar additives [31-35]. These factors are used to control the cluster–cluster aggregation processes that can dramatically change the structure of the nanoparticle dispersions. Thus, by controlling the structure, it is expected to gain control over the physical properties of the final crosslinked nanocomposites. A rheological experiment is used for monitoring the rheological properties of dispersions. The rheological methods I and II, proposed in Chapter 2, are applied here for analysis of the dispersivity and the structure of the dispersions. Moreover, the impact of the preparation conditions on the rheology of dispersions and, consequently, on the composite conductivity and microwave-absorbing properties are further correlated [31-33].

7.2.2.1 Effect of Shearing During Processing

Figure 7.2 compares the viscosity curves of (graphite/diamond)/acrylic (GD/AR) dispersions, as measured after the first step (I) of high-speed mixing, and after the second step (II) of magnetic stirring. The volume fraction of carbon mixture varies in the range 1–10%. Importantly, the viscosity of the dispersions after long-duration mild mixing at step II is much lower than that measured after short-duration high-speed mixing at step I. This effect becomes significant at high filler concentrations (8–10%) and at low shear rates. For example, at $\dot{\gamma} = 0.5\ s^{-1}$, the dispersions after stirring 1 h in a magnetic field (step II) show ~4 times lower viscosity than those sheared for only 15 min at high speed (step I). However, insufficient difference in the viscosities of the dispersions after the two steps of mixing is observed at high shear rates of about $\dot{\gamma} > 50\ s^{-1}$.

We interpret these observations in terms of a decreased plasticity as a result of the shear-induced deflocculation. Step II of long, mild shearing in a magnetic field produces a more extensive dispersion of nanoparticles within the polymer matrix than that at step I, leading to the formation of floccules of a smaller size. Therefore, we can optimise the dispersion state and the size of floccules in the systems by changing the shearing conditions; the rheological characteristics can also be used as a tool for a control of the dispersions. Dispersions of GD in polyurethane and epoxy resin show qualitatively similar rheological behaviour to that of the acrylic resin-based systems.

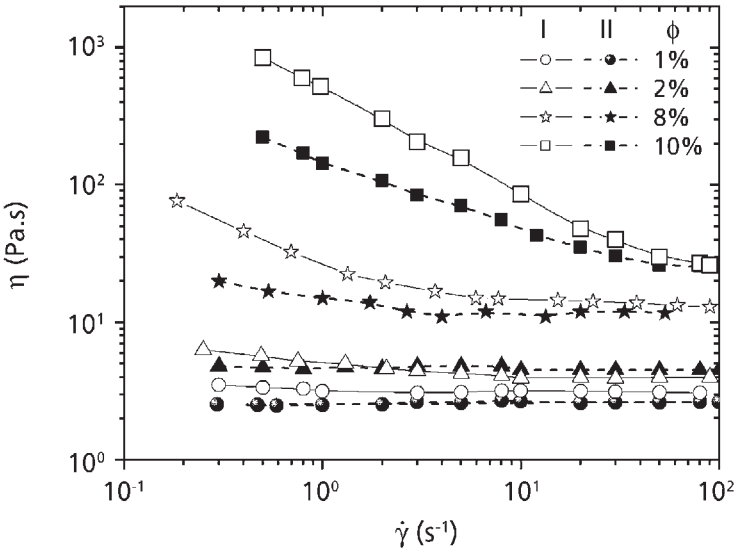

Figure 7.2 Viscosity *versus* shear rate of 1, 2, 8 and 10 vol% GD/acrylic dispersions, as influenced by the shearing during processing: step I – high-speed mixing; and step II – magnetic stirring.

Reproduced with permission from [31]. ©Wiley Periodicals, 2004

7.2.2.2 Effect of Filler Content – Rheological Percolation Thresholds

Small variations of the carbon filler content in the resin matrix can change the degree of order of the nanoparticles, leading to structural transitions in the nanodispersions, namely first and second percolation thresholds. The two structural thresholds were determined rheologically by using rheology methods I and II, as in Chapter 2. The first and second percolation thresholds, having values of $\phi^* \sim 4$ vol% and $\phi^{**} \sim 8$ vol%, respectively, were determined from the rheological study of GD/acrylic dispersions by plotting both dynamic moduli G_0' and G_0'' (at $\omega = 0.1\ s^{-1}$) *versus* the volume content of the filler (Section 2.4.3.2, **Figure 2.16**).

Here, **Figure 7.3** presents the experimental data of the viscosity at high shear rate, $\dot{\gamma} = 100\ s^{-1}$ *versus* filler volume fraction ϕ, for the GD/acrylic dispersions. The viscosity changes in the context of the two percolation transitions are discussed. Generally, the viscosity increases non-linearly with increasing nanoparticle content. At very low filler concentrations, before reaching the first percolation threshold, $\phi \leq \phi^*$, the viscosity increases linearly with a low slope and this hydrodynamic disturbance is theoretically described by the Einstein model (see Equation (2.9)) for particles with different shapes [39]. Further, at $\phi^* < \phi < \phi^{**}$, the function becomes non-linear, upon reaching the

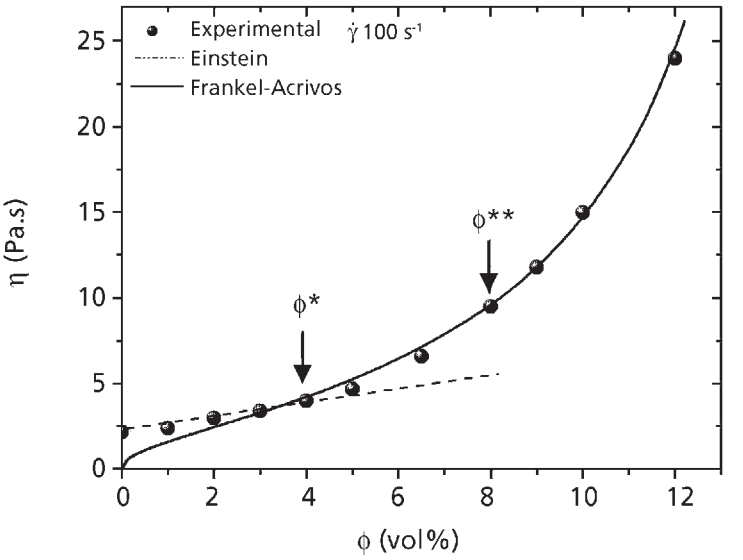

Figure 7.3 Viscosity *versus* volume fraction of GD in acrylic resin dispersions: points show experimental data at $\dot{\gamma}$ = 100 s^{-1}; lines show predictions by the Einstein model (Equation (2.9), dashed line) and the Frankel–Acrivos model (Equation (2.11), full line). The arrows point to the two rheological thresholds, ϕ^* = 4% and ϕ^{**} = 8%, determined in **Figure 2.16**.

Reproduced with permission from [31]. ©Wiley Periodicals, 2004

second percolation threshold, ϕ^{**}, which is associated with the agglomeration processes of nanoparticles and indicates the formation of an infinite cluster (network of fractal flocs). Above the second rheological threshold, $\phi > \phi^{**}$, the viscosity increases sharply with increasing filler content because of the formation of a dense network.

The Frankel–Acrivos model (Equation (2.11)) is used for colloidal dispersions to predict the rapid rise of viscosity at high concentrations, accounted for by the hydrodynamic interactions of neighbouring spheres [40]. The applicability of this model was proved in our study [31, 33] for modelling platelet nanodispersions, shown in Chapter 2. Here, the model is applied in **Figure 7.3**, to describe the viscosity data of nanoscale graphite/diamond dispersions in acrylic resin. It is seen that this equation fits well the experimental data in the concentration range above the first percolation threshold, $\phi > \phi^* > 4\%$, where the hydrodynamic interactions of nanoparticles become prominent. The model prediction of the concentration dependence of viscosity is proposed here as another method for calculation of the second percolation threshold. We examine the curvature K for the Frankel–Acrivos equation ($K = |y''|/(1 + y'^2)^{3/2}$) by finding its first and second derivatives. It is seen that an inflection point exists for $\phi \approx 8\%$, at which point the first derivative of the curvature function has a minimum. This is assumed as

the approximate limiting value (the second percolation), after which the rate of viscosity rise becomes higher.

The viscosity is a very sensitive characteristic, which represents the qualitative changes in the structure of nanoparticle dispersions due to particle network formation throughout the concentration range, particularly at the first, ϕ^*, and the second, ϕ^{**}, percolation transitions. The first percolation threshold is associated with the concentration wherein the viscosity starts to increase rapidly because of intensive cluster–cluster aggregation. This leads to the formation of a conductive pathway of contacting carbon particles through a thin polymer layer, which produces the sharp increase of the conductivity. Further increasing the viscosity indicates the formation and strengthening of the network superstructure, which produces a conductivity saturation above the second percolation threshold [31]. Thus, the viscosity to concentration dependence may be related to both structure of the dispersion and expected physical properties.

7.2.2.3 Effect of Additives

Electrostatic particle–particle interaction has to be taken into account when describing agglomeration processes of nanoparticles in polymers. Additives have been successfully used to decrease the potential barrier between particles [3, 4, 27, 41]. Generally, additives influence the particle–particle interactions by changing both the ionic strength and the viscosity of the matrix polymer. We have studied three types of additives, which differ in their chemical nature: a salt ($CuCl_2$), oleic acid (OA) and polyethyleneglycol dodecyl ether (polyol Brij 35, POE) [33, 35]. In order to obtain information about the agglomeration processes of carbon nanoparticles controlled by the additives, the rheological behaviour of hybrid dispersions in shear flow was investigated on varying the type of additives. Some of the results were shown in Section 2.4.3.3 (**Figure 2.17**).

Figure 7.4 compares the normalised viscosity, η_{ad}/η, of 8% graphite/diamond dispersions based on acrylic resin (AR) and polyurethane (PU), on varying the type of additives. The normalised viscosity, η_{ad}/η, is calculated as the ratio of the viscosity of the dispersion with the additive to that without the additive, where the viscosity values at $\dot{\gamma} = 100\ s^{-1}$ are taken into consideration.

It can be seen that, generally, the viscosity of dispersions is increased by the addition of a small amount (~0.01%) of polar additives. The effectiveness of the additives varies from 1.7- to 4.5-fold increase of the viscosity depending on the chemical nature of the additive and the matrix resin. This can be related to the compatibility between the ingredients, but the low viscosity of the matrix can also assist in the process. Thus, particle diffusion is easier within the low-viscosity polyurethane (η = 1.3 Pa-s) and acrylic resin (η = 2.1 Pa-s), than within the higher-viscosity epoxy resin (η = 25 Pa-s) (**Table 2.3**). The reduction of the potential barrier among the carbon nanoparticles due to polar additives allows the filler easily to form agglomerates with the support of Brownian motion. As a result, the density of the created 3D superstructure in 8% carbon

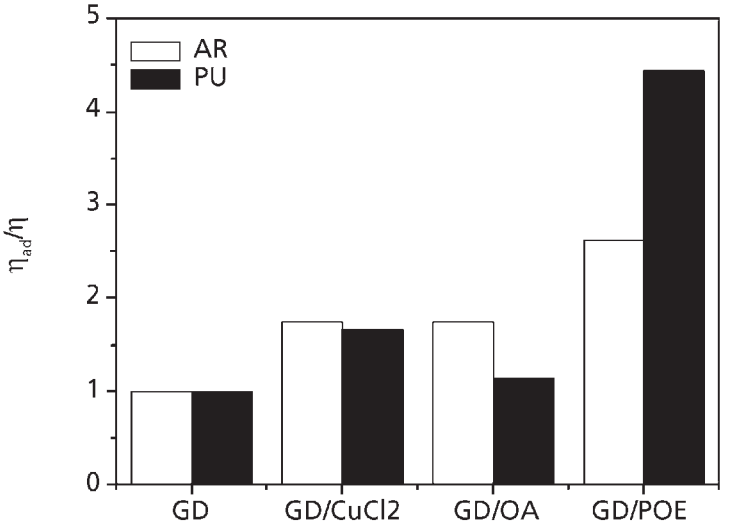

Figure 7.4 Normalised viscosity, η_{ad}/η, of 5% graphite/diamond (GD) dispersions in acrylic resin (AR) and polyurethane (PU) on varying the polar additives: $CuCl_2$, oleic acid (OA) and polyol (POE). The shear rate was $\dot{\gamma} = 100\ s^{-1}$.

Data from [33]

dispersions with additive becomes higher than that of the system without additive, thus leading to higher viscosity. Note that POE produces much stronger increase of the viscosity of the polyurethane and the epoxy systems, respectively, compared to that of the inorganic salt ($CuCl_2$) and OA. This could reduce the Brownian motion of nanoparticles and suppress the agglomeration processes, resulting in a reduction of the conductivity effect of crosslinked systems.

In summary, the various types of polar additives have a different level of effect on the viscosity of dispersions. This effect depends significantly on the chemical nature of the additives and the matrix resin; as well, the low viscosity of the matrix polymer plays a positive role. A small amount of polar additives can control the particle–particle and polymer–particle interactions of graphite/diamond dispersions in thermoset resins by increasing the ionic strength of the dispersions. Therefore, the polar additives are suitable for designing particle networks with the desired perfection. The mechanism of the process is related with the reduction of the potential barrier among the graphite/diamond nanoparticles, thus allowing the filler easily to form agglomerates with the support of Brownian motion. Therefore, the structural changes due to polar additives are expected to have a strong influence on the conductivity of crosslinked systems; thus, the additives can be used to design carbon/thermoset nanocomposites of different strength and functional properties.

Further, based on the structural origin, we relate the viscosity of nanodispersions with the alteration of the physical properties of crosslinked nanocomposites, such as conductivity and microwave absorption, but only to the extent where the solid film properties depend on the microstructure and hence on the initial structure formation, determining the viscosity too.

7.2.3 Electrical Conductivity of Crosslinked Nanocomposites

Generally, the electrical conductivity of polymer composites incorporating carbon particles depends strongly on the filler content. Conductive particles agglomerate in the composite as clusters at relatively low filler concentrations. As the size and number of clusters increase with increasing filler content, above a critical concentration, called the percolation threshold, the clusters started to agglomerate in floccules, which fill the whole volume and form a network structure, and thus the material becomes conductive. One of the main features of polymer composites filled with conductive particles is that the agglomerates of particles in the infinite cluster (network) are still separated by thin gaps of a polymer layer, which results in a variety of conduction mechanisms in such composites. Variations of the filler content, the size or shape of the particles, as well as the size of floccules help to reveal the mechanism governing the conductance within, for example, the carbon/polymer composites [29]. Because of this, the factors that influence agglomeration processes will play an important role in controlling the conduction mechanisms.

The factors that control the agglomeration processes in (graphite/diamond)/resin dispersions were discussed above by the study of the rheological properties of dispersions. The variables studied were the shearing (**Figure 7.2**), the volume content of nanofiller (**Figure 7.3**) and the polar additives (**Figure 7.4**), and their effects on the viscosity was discussed. It is interesting to compare the effects of these variables on the conductivity of crosslinked hybrids.

Figure 7.5 compares the dc conductivity *versus* volume fraction of nanoparticles in GD/acrylic nanocomposites. The factors varied are the shearing during processing, i.e., step I (high-speed mixing) and step II (magnetic stirring), as well as the addition of polar additive ($CuCl_2$). The first and second percolation thresholds, $\phi^* \sim 4\%$ and $\phi^{**} \sim 8\%$, are indicated, which are determined rheologically for the dispersions without additive [31, 33]. Optical micrographs visualise the structure of composites formed by cluster–cluster aggregation of graphite/diamond nanoparticles at the two critical concentrations, 4% (pathways of single flocs) and 8% (dense network).

It was found that the electrical conductivity of nanocomposites slightly increases with increasing graphite/diamond filler content below the first percolation threshold, $\phi < \phi^*$, if compared with that of the pure matrix resin. This is associated with the formation of cluster–cluster aggregates separated by thin polymer barriers, so that charge hopping

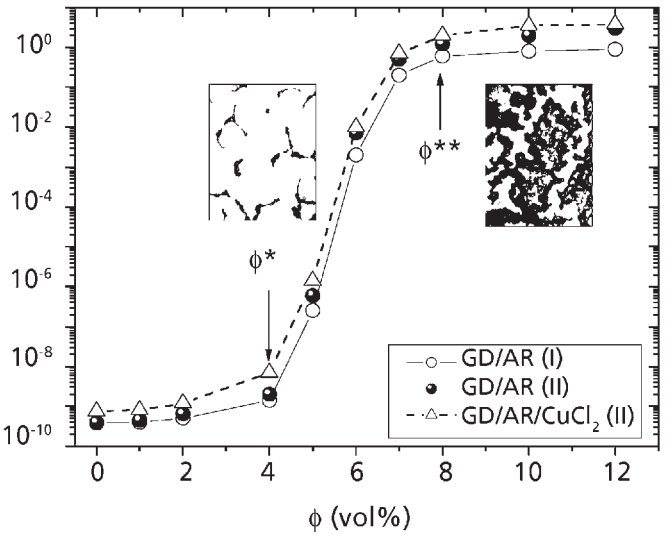

Figure 7.5 The dc conductivity *versus* volume fraction of GD in acrylic nanocomposites. The factors varied are: the shearing during processing (step I – high-speed mixing; step II – magnetic stirring), and the polar additive ($CuCl_2$). Optical micrographs of the structure at the thresholds, $\phi^* \sim 4\%$ and $\phi^{**} \sim 8\%$, are also presented.

Data from [31, 33]. Reproduced with permission from [31]. ©Wiley Periodicals, 2004

may occur on increasing the filler content [29]. Our further studies on the carrier transport mechanism of those composites around the percolation concentration are in progress. Above the first percolation threshold, the conductivity increases by 10 orders of magnitude and it is attributed to the formation of carrier paths of particle agglomerates (fractal flocs), as visualised by the optical micrographs. Further increase in the carbon content above the second percolation threshold, $\phi > \phi^{**}$, leads to a saturation plateau of the conductivity, which correlates with the dense network of particles, as shown in **Figure 7.5**.

If we compare the effect of shearing on the conductivity, the longer shearing allows about 1.5 fold (50%) increase of the dc conductivity of nanocomposites at the saturation plateau. Higher overall conductivity and a slight decrease of the percolation threshold are observed for the samples crosslinked after step II of magnetic stirring, in comparison with the samples crosslinked after step I of high-speed mixing. The comparison of the rheological results (**Figures 7.2** and **7.3**) with the conductivity results (**Figure 7.5**) leads to the suggestion that the reduction of the size of particle agglomerates and a possible charging during more intensive shearing may be the reasons for the overall improvement of the electrical conductivity of composites.

Moreover, the addition of a small amount of the salt $CuCl_2$ leads to better (~70%) improvement of the conductivity of nanocomposites than that produced by long-term magnetic stirring (50%). Obviously, the polar additives are very effective for the design of nanoparticle structure with desired perfection. As a result of the additive, a well-defined three-dimensional network and, accordingly, a higher conductivity are created at low filler content. The comparison of the results from **Figures 7.4** and **7.5** shows that the effect of additives on the viscosity of dispersions corresponds well to their effect on the conductivity of the crosslinked nanocomposites.

In conclusion, the conductivity percolation and saturation limits of the crosslinked nanocomposites coincide well with the two rheologically determined percolation thresholds, ϕ^* and ϕ^{**}, of the dispersions. Therefore, rheological results from the precursor dispersion could provide preliminary information about the effectiveness of different factors, such as shearing and additives, used for control of the conductivity of crosslinked nanocomposite [31-33].

It is interesting to verify the role of the matrix resin on the conductivity of nanocomposites. **Figure 7.6** compares the dc conductivity of the nanocomposite films prepared from three basic resins (acrylic, polyurethane and epoxy), incorporating 0–15 vol% graphite/diamond nanoparticles. The samples are cured after step II of magnetic stirring, without additives.

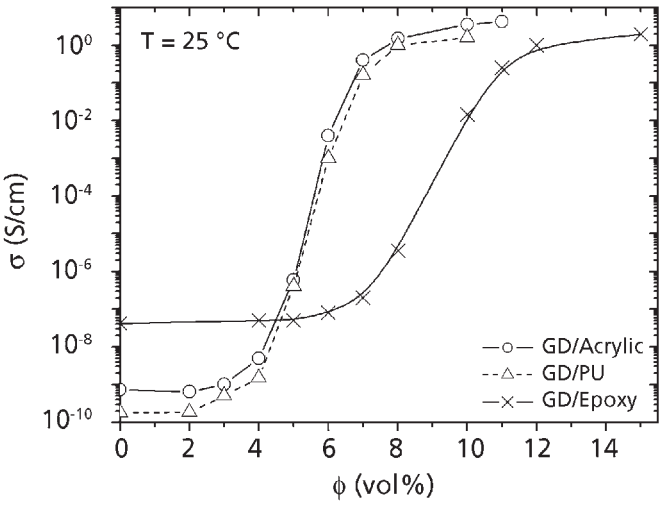

Figure 7.6 Conductivity *versus* volume fraction of GD nanoparticles in composites with acrylic, polyurethane and epoxy matrices at T = 25 °C, cured after step II of magnetic mixing.

Reproduced with permission from [31]. ©Wiley Periodicals, 2004

A strong difference was found in the conductivity of nanocomposites based on the low-viscosity polyurethane and acrylic resin, compared to that of the epoxy-based systems on varying the carbon volume content. This result can be attributed to the viscosity and the nature of the matrix polymer. The percolation threshold increases in the order: $\phi^* \sim 3\%$ (polyurethane nanocomposites), $\phi^* \sim 4\%$ (acrylic nanocomposites) and $\phi^* \sim 6\%$ (epoxy nanocomposites). The saturation threshold ϕ^{**} also depends on the nature of the polymer matrix, changing from 7% for polyurethane- to 8% for acrylic- and 10% for epoxy resin-based nanocomposites. The final conductivity values at the saturation plateau vary within $\sigma \sim 2$–8 S/cm depending on the matrix polymer.

Table 7.1 summarises the values of the dispersion viscosity and the composite conductivity of graphite/diamond nanocomposites with polyurethane, acrylic and epoxy resins, on

Table 7.1 Viscosity η (at $\dot{\gamma} = 100\ s^{-1}$), conductivity σ and microwave absorption *a* (at 9.4 GHz) of the matrix polymers and graphite/diamond (GD) system with polyurethane, acrylic and epoxy resins on varying the polar additives and nanofiller content

Matrix polymer	G/D ϕ (vol%)	η (Pa-s)	σ (S/cm)	a (%)
Polyurethane	0	1.3	1.79×10^{-10}	0
	3 (ϕ^*)	2.7	3.5×10^{-10}	0.6
	7 (ϕ^{**})	5	0.87	–
	8	6.3	1	–
	10	11	1.6	37.1
Polyurethane + $CuCl_2$	8	10.5	1.8	38
Polyurethane + OA	8	7.2	0.09	34
Polyurethane + POE	8	28	0.8	–
Acrylic resin	0	2.1	7.24×10^{-10}	0
	4 (ϕ^*)	4.5	1.2×10^{-9}	–
	8 (ϕ^{**})	8.2	3	30
	11	15	8.25	30.3
Acrylic resin + $CuCl_2$	8	14.6	8.55	40
Acrylic resin + OA	8	14	0.17	38
Acrylic resin + POE	8	21	0.72	29
Epoxy resin	0	25	4.20×10^{-8}	0
	6 (ϕ^*)	31	7.60×10^{-8}	0
	10 (ϕ^{**})	83	0.014	11.2
	15	103	1.96	11

Data from [33]

varying both the polar additives and nanofiller content. Data for the pure resins are also presented. The results confirm [15] that a low-viscosity matrix polymer is better for the formation of conductive paths in the filler/polymer systems than the high-viscosity matrix. Particle diffusion is much easier within the low-viscosity polyurethane and acrylic resin matrices, and thus the conductive pathways are formed at lower carbon content than within the high-viscosity epoxy resin. The additives produce changes in the ionic conductivity of the pure matrix. This obviously affects the percolation limits and the final dc conductivity of the nanocomposites at the saturation plateau. More detailed investigations need to be followed in order to get a clear assessment of these effects.

If the 8% GD/resin systems are considered, the salt additive ($CuCl_2$) produces the best improvement in the conductivity of the nanocomposites. The other polar additives, OA and POE, result in a decrease of the conductivity, compared with that of the filled system without additive. This result could be related with the dominant role of additives on cluster–cluster aggregation in polymer matrices.

7.2.4 Microwave Absorption

Polymeric nanocomposites possessing conducting, ferromagnetic or microwave-absorbing functions are extremely useful in many electronics applications. Therefore, not only the conductivity but also the microwave absorption properties of graphite/diamond thermosets have been investigated in our study [33, 37]. **Figure 7.7** shows the microwave (MW) absorption *a* and reflection *r versus* volume content of nanoparticles for GD/acrylic composite films. It is seen that at low filler content the microwave-absorbing effect of nanocomposites is low. However, above the first rheological percolation threshold, $\phi^* \sim 4\%$, the microwave characteristics sharply increase. At filler concentration above the second rheological percolation threshold, $\phi > \phi^{**}$, the MW absorption and reflection reach their maximal saturation values of $a \sim 30\%$ and $r \sim 8\%$, respectively [31].

When comparing **Figures 7.6** and **7.7**, one can see that a strong correlation exists in the concentration dependence of the conductivity and microwave absorption characteristics of nanocomposites. In general, the microwave characteristics at 9.4 GHz and the conductivity are significantly improved by increasing the carbon volume fraction. The percolation and the saturation limits appear at the same volume concentrations of GD nanofiller for the conductivity and the microwave absorption. Obviously, both characteristics depend in a similar way on the formation of the superstructure in nanocomposites, leading to the carrier paths and the infinite cluster (network).

Similar to conductivity, the microwave characteristics of nanocomposites at 9.4 GHz depend significantly on the type of the polymer matrix. **Table 7.1** presents the microwave absorption *a* of polyurethane, acrylic and epoxy nanocomposites containing graphite/diamond particles. Thus, the acrylic resin- and polyurethane-based

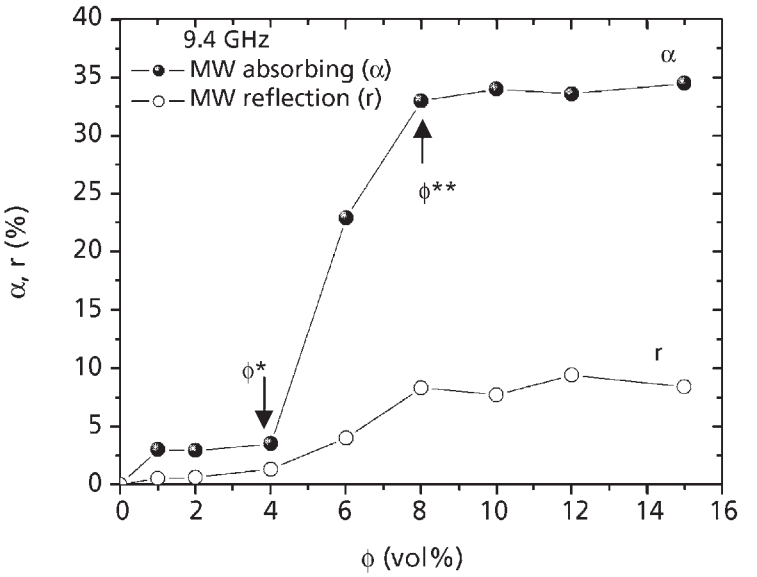

Figure 7.7 Microwave absorption and reflection characteristics *versus* volume fraction of GD/acrylic nanocomposites at 9.4 GHz.

Reproduced with permission from [31]. ©Wiley Periodicals, 2004

nanocomposites display the best absorbing ability. The MW absorbing characteristics of the epoxy resin-based nanocomposite are relatively low. The results clearly show that the low viscosity of the matrix polymer and the additives significantly improve the microwave properties of the composites.

The thickness of the protective film also plays an important role for the absorption ability of nanocomposites. **Figure 7.8** compares the microwave-absorbing properties of (a) one-layer, (b) two-layer and (c) three-layer samples of 8% GD/polyurethane nanocomposites, prepared with the addition of various additives. Here, the MW absorption is studied within the frequency range from 2.5 to 15 GHz. If we consider the one-layer sample with film thickness about 0.002 mm, a strong influence of the polar additives is observed, where the addition of the salt $CuCl_2$ produces a remarkable (~63–70% at 15 GHz) improvement of the microwave-absorbing properties, compared to the sample without the additive. The large effect of the salt additive on the microwave absorption is similar to that of the conductivity, indicative of the same structural origin associated with the cluster–cluster aggregation of nanoparticles and the formation of a homogeneous and dense network. The addition of polyol and OA produces similar improvement of the MW absorption, ~40% at 15 GHz, compared to the nanocomposite system without additive, but at the same carbon filler content.

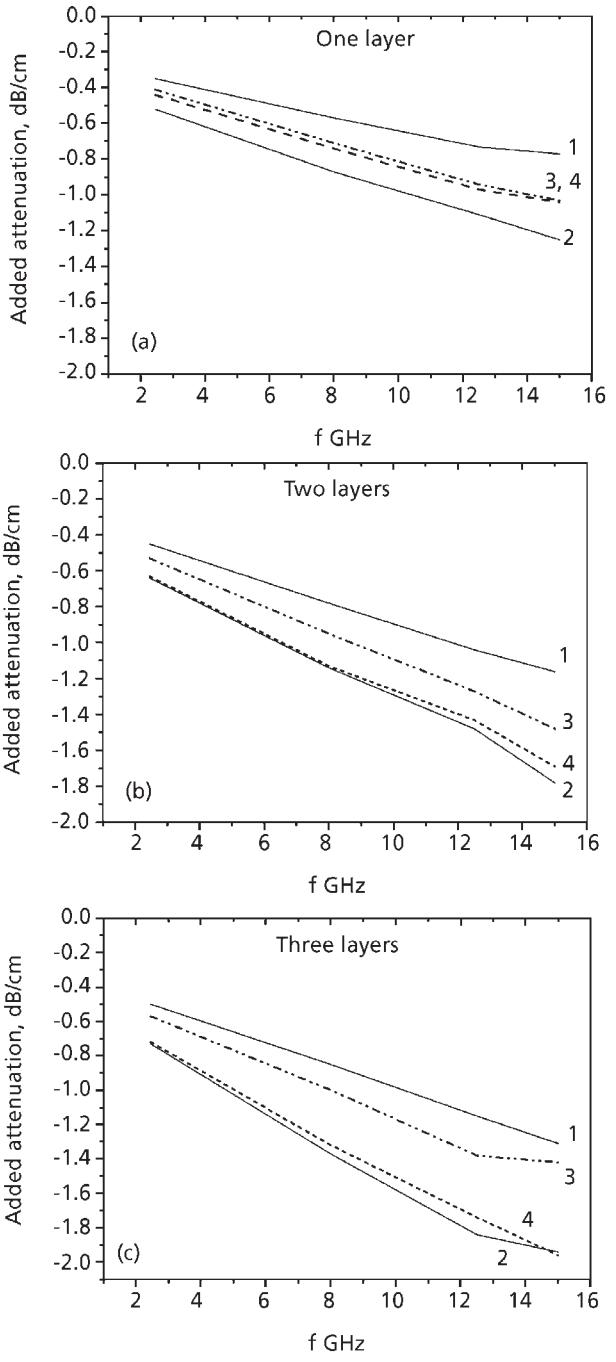

Figure 7.8 Attenuation for 8% GD/polyurethane layers *versus* functional frequency for (a) one-layer, (b) two-layer and (c) three-layer samples, on varying the polar additive: (1) GD/PU without additive; (2) GD/PU with $CuCl_2$; (3) GD/PU with OA; and (4) GD/PU with polyol. *Data from [33]*

Further, the study is focused on the possibilities to create a multilayered structure from the investigated composites. With increasing number of layers, the thickness of the absorbing film increases, which produces a significant increase of the MW absorbing effect. It is seen from **Figure 7.8** that for the two-layer sample (b) with a film thickness of about 0.004 mm, the microwave absorption is about 50% higher than that produced by the one-layer film (a). Here, the samples containing $CuCl_2$ and polyol show the best level of MW absorption. However, further increasing the number of layers to three (thickness ~0.006 mm) improves the microwave-absorbing properties insignificantly.

In summary, the microwave investigations of graphite/diamond nanocomposites with thermosetting polymers show that the polyurethane- and acrylic-based systems, where the carbon nanofiller is responsible for the dielectric losses, are promising for microwave applications. The nanocomposites developed could be used as paints, coatings or bulk materials for protective screens, showing significantly improved microwave absorption within the range 2.5–15 GHz, combined with enhanced mechanical properties.

7.2.5 Correlation of Rheological and Physical Characteristics

Based on the dominant role of the superstructure formed by nanofiller in polymer, we correlate the viscosity of the dispersions with the conductivity and microwave properties of crosslinked nanocomposites.

The concentration dependence of the viscosity, the dc conductivity and the microwave characteristics are discussed above in **Figures 7.3**, **7.5** and **7.7**, and the same critical concentrations ϕ^* and ϕ^{**} are determined for the three functions studied for a fixed matrix polymer (acrylic resin). We explain this relationship with structural transitions produced by cluster–cluster aggregation. A small increase of the nanoparticle content resulted in a strong decrease of the interparticle spacings, resulting in significant interactions between nanoparticles. The first rheological threshold ϕ^* can be attributed to the electrostatic interactions between nanoparticles, which appear if the mean distance between them is in the range of $2d$, with d being the nanoparticle diameter [1–5]. Such small spacing induces nanoparticle flocculation and charge hopping. Further increasing the nanofiller content, around second rheological threshold, ϕ^{**}, can be associated with the percolation of the flocs and the formation of a dense network, leading to the saturation of both conductivity and microwave absorption.

Based on this structural origin, **Figure 7.9(a)** presents the correlation between the viscosity and conductivity at a definite filler concentration, wherein the points correspond to 0, 1, 3, 5, 6, 8, 10 and 12 vol% filler, respectively. It is seen that the correlation between the viscosity and the conductivity is very good at all filler concentrations up to the second percolation threshold, $\phi \leq \phi^{**} \leq 8\%$. A correlation coefficient of 0.966, calculated by linear regression

analysis, and a relative mean square error of 6.3% are determined for the viscosity *versus* conductivity function in the concentration range 1–8%. Further increase of the filler concentrations, $\phi > \phi^{**}$, leads to a different effect of the filler on both characteristics. The viscosity sharply increases, while the conductivity tends to a saturation plateau, both related to the formation of a dense network of nanofiller-polymer floccules.

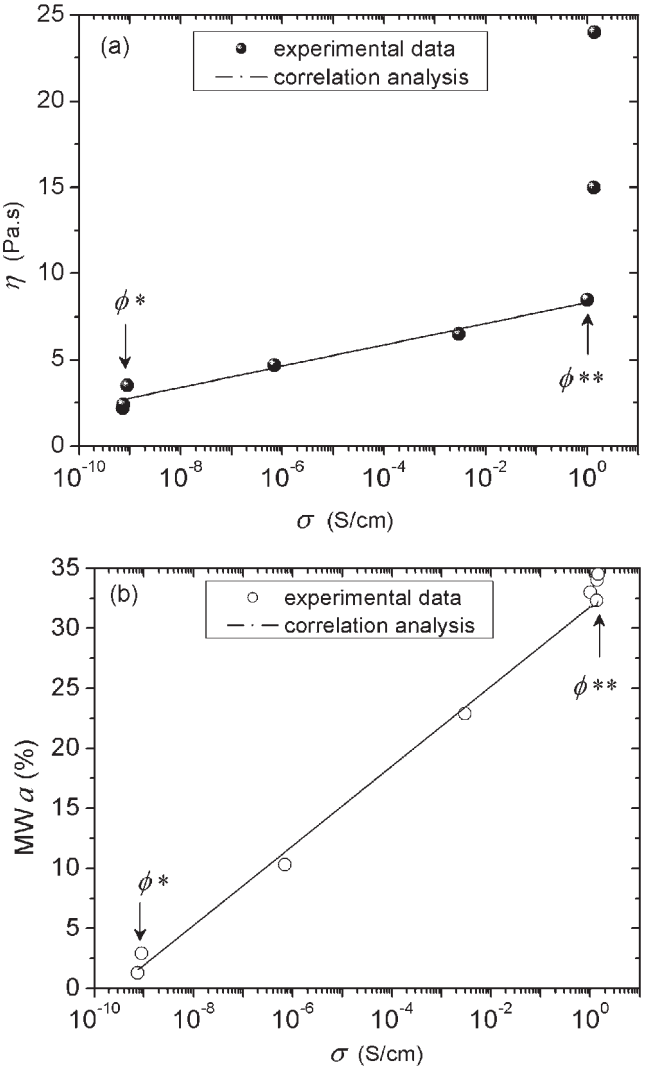

Figure 7.9 Correlation between (a) viscosity and conductivity and (b) microwave absorption and conductivity. The points present data for the filler concentrations of 0, 1, 3, 5, 6, 8, 10 and 12 vol% GD/acrylic nanocomposites.

Reproduced with permission from [31]. ©Wiley Periodicals, 2004

Figure 7.9(b) shows the correlation between the microwave absorption and the conductivity of the same systems as in **Figure 7.9(a)**. A correlation coefficient of 0.985 is determined and the error is 7.8%, which seems to be very good in the full concentration range of 1–12 vol% graphite/diamond. The present results confirm the above suggestion that the electrical conductivity and the microwave properties of composites have a similar behaviour with increasing volume content of carbon nanoparticles. This is associated with the structural origin of both characteristics, as well as with the nanoscale hopping mechanism, which could appear at very small interparticle distance, due to the electrostatic interactions between nanoparticles through a thin polymer layer.

The correlations presented in **Figure 7.9** show that the agglomeration processes affected the viscosity, conductivity and microwave-absorbing characteristics in similar ways. Such good correlation between the liquid dispersion and the crosslinked nanocomposites confirms the effectiveness of using the viscosity function and the two rheological percolation thresholds as a tool for predicting the percolation and saturation limits of physical characteristics, such as conductivity and microwave absorption of nanocomposites.

The samples produced in this study are examples of nanoparticle composites. The results obtained show that nanosized graphite/diamond particles produced by shock-wave technology may offer new opportunities to modify the electrical and microwave properties of insulating polymer matrices. The relation between rheology and physical properties can be applied to assess the optimal compounding conditions of carbon nanoparticles in a given polymeric system.

7.3 Nanoscale Binary Fillers of Carbon and Ferroxides in Thermosetting Polymers

Monomodal suspensions are useful in scientific investigations on model systems but they are rarely encountered in practice. Usually, particle type and size polydispersity are applied to achieve adequate materials reinforcement while still maintaining processability, e.g., maximise loading with minimum increase in viscosity. This can be accomplished by optimising the combination of particle size ratios and concentrations. The challenging case of bimodal suspensions of particles with identical shape but dissimilar size has been addressed for micrometre size particles [42–46]. The effect of the polydispersity of the binary fillers on the packing density of microcomposites has been rigorously studied by many authors and a number of models have been developed for application in various fields of technology (concrete, ceramics, powder metallurgy, packed beds). It is known that at high loading levels the viscosity can be reduced dramatically by applying binary or higher-modality fillers, i.e., the filling degree can be increased [42, 46].

Recently, the application of nanoscale fillers in polymer matrices has become a topic of growing interest in composite materials science. Nanocomposites exhibit a number

of advantages related to their improved microstructure and mechanical and physical behaviour, based on the specific filler properties. However, no publications are to be found on the effects of nanoscale binary fillers on either the processability or the properties of nanocomposites.

We have studied the polydispersity of filler components as a factor of major importance for structure formation in composite materials for the case of nanoscale graphite/diamond and coarser barium hexaferrite and magnetite particles dispersed in a polyurethane matrix [36]. Here the rheological properties of polyurethane-based binary dispersions are presented with the view of achieving the possibly most favourable physical properties of the composites at high loading levels when the systems are still processable. The study is aimed at revealing the specific effects of binary fillers of conducting and ferromagnetic nanoparticles, as well as investigating the influence of the filler volume fraction ratio on the rheology and the microwave-absorbing properties of nanocomposites.

7.3.1 Materials Characterisation

A binary particle suspension may in general be composed of two types of particles, a small one (S) and a large one (L), not necessarily of the same shape. Their respective participation in the composite fluid is represented by the total volume fraction of solids:

$$\phi = \phi_S + \phi_L.$$

In order to test the effect of polydispersity of nanoscale particles, bimodal dispersions were prepared of graphite/diamond and ferroxide particles in a polyurethane matrix. The small (S) component represents carbon (graphite/diamond) nanoparticles, synthesised by the shock-wave method [38]. As shown above (Section 7.2.1), the average particle diameter of the carbon mixture was about $d \sim 6$ nm (the polydispersity varies from 3 to 20 nm), density of 1.86 g/cm^3, and specific surface of 590 m^2/g (BET) [46]. Two types of coarser filler particles (L) were used: barium hexaferrite (BaH), aspect ratio $D/L \sim 800/1000$ nm and density 5.6 g/cm^3; and natural magnetite (M), diameter $D \sim 640$ nm and density 6.2 g/cm^3. Ferroxides were synthesised in the Institute of Electronics, BAS. The mean diameter of the prolate barium hexaferrite particles is $D_m = (1000 + 800 + 800)/3 \approx 870$ according to a formula used in hydraulics. The polymer matrix was polyurethane (polyol isocyanate solution) with a density of 1.1 g/cm^3 and viscosity of 1.3 Pa-s.

The filler volume fraction of the monomodal dispersions studied was within the range of 0–15 vol% for the small carbon nanofiller and 0–35 vol% for the coarser ferroxide filler. Bimodal dispersions were prepared having a total concentration of solids of 13 vol%, i.e., $\phi = \phi_S + \phi_L = 0.13$, while the individual species participation was varied, i.e., the fraction of the small species (the carbon particles) was 0.50, 0.60, 0.75 and 1.00. The dispersions were characterised by low-amplitude dynamic measurements. Oscillatory shear mode was applied for measuring the dynamic moduli within the range from 0.1 to 60 s^{-1} at low strain

amplitude. The microwave-absorbing characteristics of crosslinked nanocomposite films were measured within the frequency range 2.5–15 GHz, as described in Section 7.2.1.

7.3.2 Packing Density of Dispersions

In the case of monomodal filler components, the effective maximum packing density $\phi_{m,e}$ of the carbon (GD), barium hexaferrite (BaH) and magnetite (M) in the polyurethane matrix was determined experimentally [33, 36]. The effective maximum packing limit $\phi_{m,e}$ is determined by using a method proposed by Thomas [48] for plotting experimental rheological data of the relative viscosity, $[(\eta/\eta_0) - 1]^{-1}$, *versus* volume fraction ϕ and extrapolating to zero ordinate. Thus, values of $\phi_{m,e} = 0.16$, 0.35 and 0.4 were determined as the effective maximum packing density of the GD, M and BaH nanoparticles in the polyurethane resin, respectively. The determined values of $\phi_{m,e}$ are much lower than the theoretical maximum random packing limit, which varies in the range $\phi_m \sim 0.52–0.74$, calculated from geometrical considerations for hard spheres from simple cubic packing to rhombohedral packing. The possible implication of the relatively small values of the effective maximum packing limit of monomodal particles, $\phi_{m,e}$, compared to the theoretically predicted maximum volume fraction, ϕ_m, is associated with the high surface area of the nanoparticles, which attracts a large amount of the polymer matrix at the interfaces as a bound polymer layer around particles [1-4].

The maximum filling capacity of the bimodal dispersions under optimum loading conditions was calculated using the following modified equation [46, 49]:

$$\phi_m = \phi_{m,e,S} + \phi_{m,e,L} - f\phi_{m,e,S}\phi_{m,e,L} \tag{7.1}$$

where $\phi_{m,e,S}$ is the effective maximum packing density of monomodal small particles, $\phi_{m,e,L}$ is the effective maximum packing density of monomodal large particles, and f is a coefficient representing the mechanical interaction between particles.

This model is based on geometrical sphere packing concepts, taking into account the mechanical interaction between particles (i.e., without considering agglomeration and interparticle electrostatic, Van der Waals and other cohesive and repulsive interactions). However, we use it for the purposes of the present study because of its convenience, assuming that the above-mentioned interactions are implicitly reflected in the low maximum packing densities of the fillers due to the interparticle forces.

Using this model, we calculate the maximum packing densities ϕ_m of the filler combinations of GD, BaH and M in the polyurethane matrix. The values of $\phi_{m,e,S} = 0.16$ (for GD) and $\phi_{m,e,L} = 0.35$ and 0.4 (for M and BaH), calculated above, were taken as the effective maximal packing density of the monomodal small and large particles, respectively. Thus, the following values are calculated as maximum filling capacity of the binary dispersions studied: $\phi_m = 0.496$ for the GD/BaH dispersions and $\phi_m = 0.454$ for the GD/M dispersions.

7.3.3 Effect of Polydispersity on Rheology of Binary Dispersions

The bimodal nanodispersions of carbon/barium hexaferrite (GD/BaH) and carbon/magnetite (GD/M) in the polyurethane matrix are characterised by rheological methods [36]. The example dispersions contain 13 vol% total amount of filler, wherein the combinations of the small filler (GD) and the large filler (BaH or M) are varied in the range 50%, 60%, 75% and 100% (e.g., ϕ_{GD} = 0.50, 0.60, 0.75 and 1.00) of carbon content. The studied dispersions show a non-Newtonian rheological behaviour with a plastic-type response. The storage and loss moduli exhibit a plateau at low frequencies and the dynamic viscosity shows a yield stress. The rheological characteristics strongly depend on the combinations of the small GD and the large BaH fractions.

Figure 7.10 displays the dynamic viscosity of the binary dispersions *versus* the volume content of the small fraction (carbon) varying within ϕ = 0.5-0.8 and the large fraction (BaH and M) within ϕ = 0.5-0.2, respectively, at various frequencies. The total amount of the binary fillers (GD/BaH and GD/M) in the dispersions was 13 vol%. **Figure 7.10(a)** presents results for the carbon/barium hexaferrite dispersions in polyurethane, and **Figure 7.10(b)** shows results for the carbon/magnetite dispersions in polyurethane.

All the rheological data in **Figure 7.10** show a clearly expressed minimum for the binary dispersions at the filler combinations of 0.60/0.40 (GD/BaH) and 0.62/0.38 (GD/M) for the carbon systems containing barium hexaferrite and magnetite, respectively. The viscosity minimum is much more pronounced for low shear rates and characterises the optimal carbon/ferroxide combination in the binary filled dispersions. The minimum is shifted to the right for the magnetite filler due to its higher specific mass. The minimum in this case is also shallower and the viscosity values are a bit lower than those for the barium hexaferrite dispersions, which could be attributed to the anisometry of barium hexaferrite particles.

It was first suggested by Farris [42] that the suspension viscosity of a random mixture of particles of identical shape and diverse sizes can be discussed as the product of the relative viscosities of two hypothetical suspensions, each containing a single solid component and the dispersion medium. The viscosity of a binary system is represented as follows:

$$\eta = h_1(\phi_1)h_2(\phi_2)\eta_0 \tag{7.2}$$

where $h_1(\phi_1)$ and $h_2(\phi_2)$ are the viscosity functions of the two components in the case of binary fillers and η_0 is the viscosity of the medium.

This is equivalent to theorising that the suspension of small particles acts as the suspending medium for the large particles, and thus the small particles and the medium can reside in any free spaces in between their larger neighbours. Such an approach to representing the viscosity of systems with two or more filler fractions (regarding the dispersion medium with the finer fraction as the matrix for the coarser filler fraction)

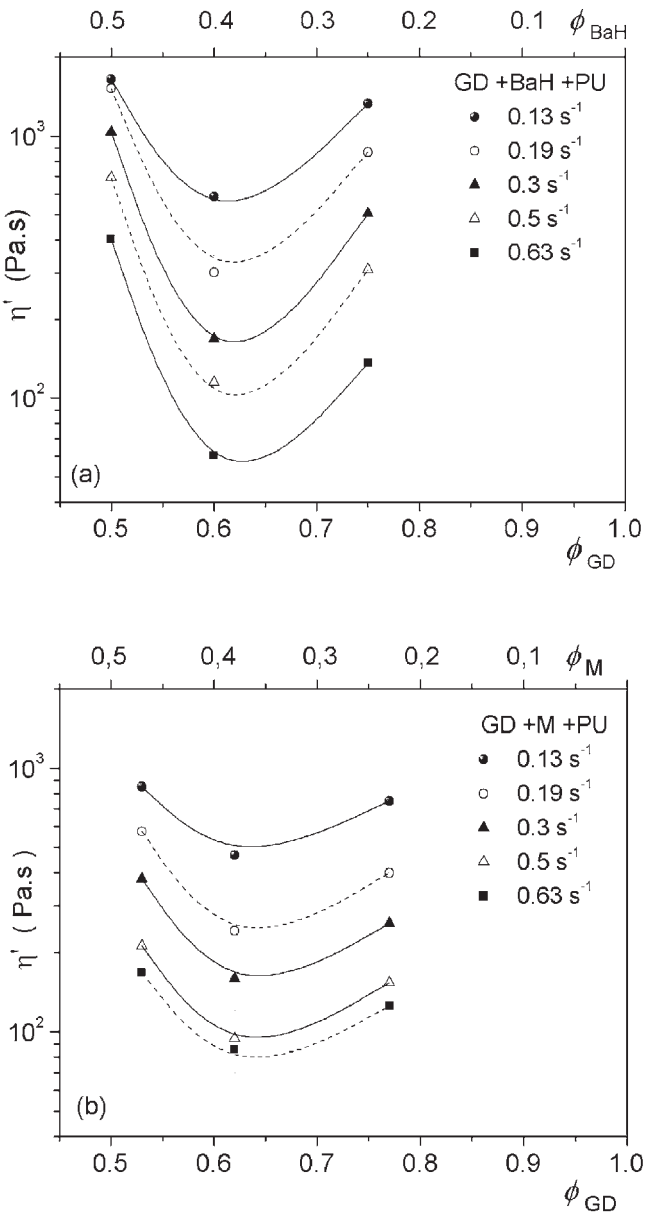

Figure 7.10 Dynamic viscosity minimum of 13 vol% bimodal dispersions as a function of the volume fraction of small (ϕ_{GD}) and large (ϕ_{BaH} and ϕ_M) particles at various frequencies: (a) carbon/barium hexaferrite in polyurethane; and (b) carbon/magnetite in polyurethane.

Reproduced with permission from [36]. ©Heron Press, Bulgaria, 2004

has proved to be very successful. According to this theory the condition for maximum packing density and hence that for viscosity reduction in polydisperse suspensions is that the coarse particles should be at least 10 times bigger than the fine ones.

In the present case of binary nanofiller dispersions, the ratio between the small and large particles is $\delta = d/D = 6/640 = 0.0094$ for carbon/magnetite and $\delta = 6/870 = 0.0069$ for carbon/barium hexaferrite. Therefore, the diameter of the coarse particles is ~100 (M) and ~150 (BaH) times larger than that of the fine ones (GD). This indicates that a viscosity minimum can be expected in binary mixtures of nanoscale particles with such diverse sizes. Note that the carbon/magnetite dispersions in polyurethane have an identical shape of particles. However, for the dispersions of carbon/barium hexaferrite a large particle shape variation is represented too. The prolate barium hexaferrite particles are anisometric, while magnetite and carbon have an isometric shape.

Farris's method is applied for calculation of the functions $h_1(\phi_1)$ and $h_2(\phi_2)$ in Equation (7.2) to represent the viscosity dependence as a function of the volume fraction of the small particles (carbon) and the large particles (BaH and M) at a fixed total solid content of 13%. Following the method of Farris we have used the Frankel–Acrivos equation [40] (see Chapter 2, Equation (2.11)) for the calculation of the functions $h_1(\phi_1)$ and $h_2(\phi_2)$, substituting for ϕ_m the values of 0.16, 0.35 and 0.40 for carbon, magnetite and barium hexaferrite, respectively. The viscosity minimum is observed in the region of the calculated maximum packing density; thus, for example, $\phi_m = 0.496$ for the GD/BaH dispersions and $\phi_m = 0.454$ for the GD/M dispersions at 13 vol% ($\phi = 0.13$) total filler volume content.

Figure 7.11 presents the relative shear viscosity of carbon/barium hexaferrite dispersions in polyurethane *versus* volume fraction of the small particles of carbon, ϕ_{GD}, predicted by the Farris model for the three total solid volume fractions, $\phi = 0.1$, 0.13 and 0.15 (dashed lines). The full points present the experimental values of the relative viscosity of the 13 vol% GD/BaH/PU bimodal dispersions at $\omega = 0.63\ s^{-1}$, containing 0.5, 0.6 and 0.75 volume parts of carbon particles (GD), as well as 0.5, 0.4 and 0.25 volume parts of BaH, respectively.

As seen from **Figures 7.10** and **7.11**, the experimentally determined minimum in the viscosity of bimodal dispersions is shifted to higher small particle contents, $\phi_{GD} = 0.60$–0.62 carbon, compared to the maximum packing density of the same bimodal dispersion, $\phi_m = 0.45$–0.50. A similar effect was found by Johansen and Andersen [45] for the viscosity of concrete mixtures. Those authors reported that the viscosity minimum is not necessarily observed at the maximum packing density – it is shifted to higher small particle contents, and this is important for processing at higher shear rates and using vibration.

The Frankel–Acrivos [40] equation (see Equation (2.11)) is chosen from the numerous relationships describing the viscosity dependence on the volume fraction of particulates

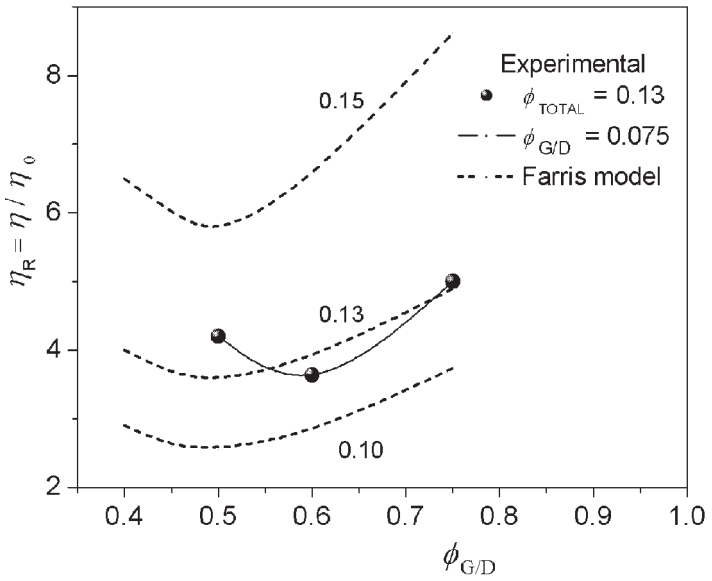

Figure 7.11 Relative shear viscosity of carbon/barium hexaferrite dispersions in polyurethane *versus* volume fraction of carbon, ϕ_{GD}, according to the Farris model for different total solid volume fractions (0.1, 0.13 and 0.15).

Reproduced with permission from [36]. ©Heron Press, Bulgaria, 2004

because its validity has already been proved for the investigated carbon-containing nanodispersions (see **Figure 7.3**). Here, the viscosity dependence on solid volume fraction ϕ is plotted in **Figure 7.12** for three monomodal dispersions of carbon (graphite/diamond), barium hexaferrite and magnetite in a polyurethane matrix, which differ in the size and shape of the nanoparticles. The Frankel–Acrivos equation is found to describe sufficiently well the relative viscosity dependence on volume fraction over a broad concentration range for monomodal dispersions of the three filler types. The arrows point to the second rheological percolation threshold, ϕ^{**}, which indicates the formation of a network superstructure, relevant to the dispersion. The ϕ^{**} values are determined by examining the curvature of the Frankel–Acrivos equation at the inflection point, where the first derivative of the curvature function has a minimum.

Evidently, the size and shape of the nanofiller particles play an important role for the concentration dependence of the viscosity. The second percolation threshold ϕ^{**} is shifted towards lower values on decreasing the particle size. Thus, the threshold values of ϕ^{**} = 7%, 16% and 24% are determined for the carbon (6 nm), magnetite (640 nm) and barium hexaferrite (~870 nm, prolate shape) dispersions, respectively.

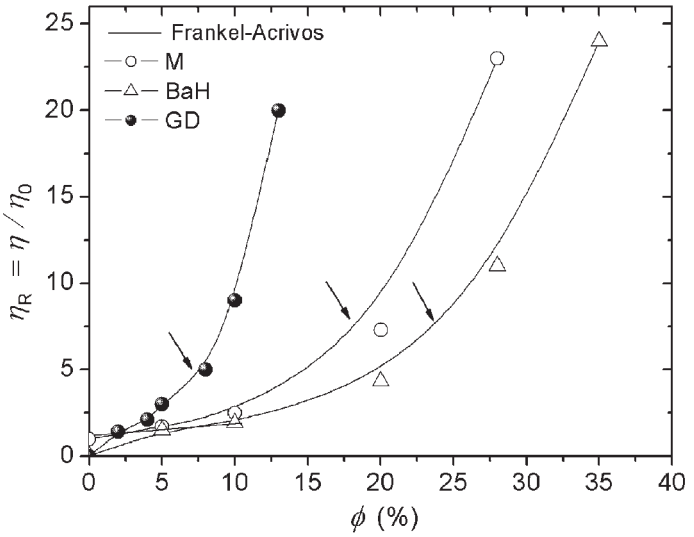

Figure 7.12 Relative viscosity η_R (at $\dot{\gamma}$ = 100 s^{-1}) of monomodal dispersions with GD, BaH and M particles in polyurethane corresponding to the different filling degrees. The arrows point to the second rheological percolation threshold, ϕ^{**}.

Data from [33]

The Frankel–Acrivos equation is proved here also for the binary compositions [33]. Importantly, when plotting the relative viscosity, $\eta_R = \eta/\eta_0$, as a function of the reduced volume fraction, ϕ/ϕ_m, all the data points for the studied systems fit on a single master curve (**Figure 7.13**). The reduced volume fraction, ϕ/ϕ_m, is obtained by dividing the current volume fraction, ϕ, by the corresponding maximum packing parameter, ϕ_m. Values of ϕ_m = 0.16, 0.35 and 0.40 were calculated above (Section 7.3.2) for the monomodal dispersions containing carbon, magnetite and barium hexaferrite particles, respectively, whereas ϕ_m = 0.496 and 0.454 were calculated for the bimodal GD/BaH and GD/M dispersions in the polyurethane resin matrix. The solid line in **Figure 7.13** represents the Frankel–Acrivos equation (2.11). A good fit was observed of the experimental viscosity data to the prediction of the model for a large number of monomodal and bimodal dispersions containing the three types of nanofiller particles. The contribution of the carbon/polyurethane matrix to the formation of the rheological properties of the bimodal dispersions is found to be of major importance.

In conclusion, this important result allows the assumption that the master curve, $\eta_R = f(\phi/\phi_m)$, described by the Frankel–Acrivos model might be used as a universal function to predict the relative viscosity of nanoscale dispersions. Moreover, the results confirm the significant effects of binary fillers on minimising the viscosity of nanoparticle dispersions by optimising the combinations of the small and the coarse filler. The rheological

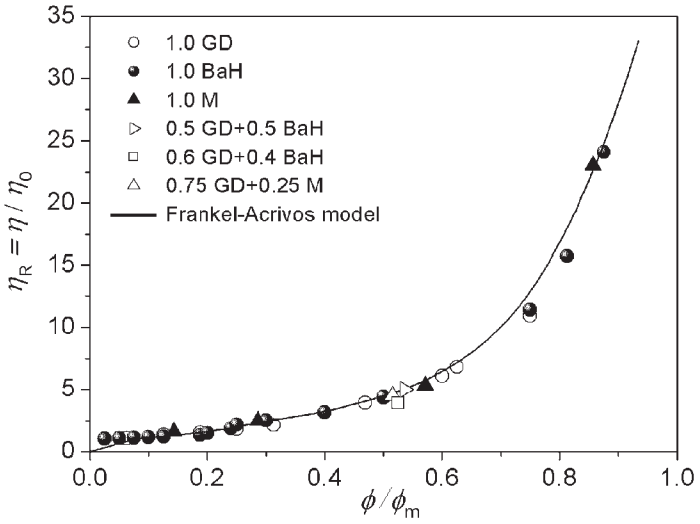

Figure 7.13 Relative viscosity of various monomodal dispersions of carbon (GD), barium hexaferrite (BaH) and magnetite (M) and bimodal dispersions of GD/BaH and GD/M in polyurethane matrix *versus* reduced volume fraction ϕ/ϕ_m (universal function).

Reproduced with permission from [36]. ©Heron Press, Bulgaria, 2004

approaches allow the determination of the percolation threshold and optimisation of the formulation in single and binary dispersions. In this way optimum filling degrees of the carbon and ferroxide particles can be achieved in binary dispersions with minimum values of the viscosity. Such optimised filler ordering is expected to result in a significant improvement of the physical properties of nanocomposites.

7.3.4 Effect of Ferromagnetic Fillers on Polymeric Structure

The binary carbon/ferroxide fillers in a thermosetting resin possess an important combination of conducting and magnetic filler properties with the dielectric properties of the polymer matrix. The strong magnetic field of the coarse ferroxide particles is expected to play an important role in the degree of ordering of the small carbon nanoparticles, as well as in producing strong polymer–filler interactions. The optimal combination by size and volume content of the small carbon nanoparticles and the coarser ferroxide particles produces a minimum of the viscosity of the bimodal dispersions, which indicates that an optimal particle ordering corresponding nearly to the maximum packing density has been achieved. Such optimal particle ordering is expected to produce a maximum effect of the magnetic field of coarser particles on the structure of the crosslinked composites.

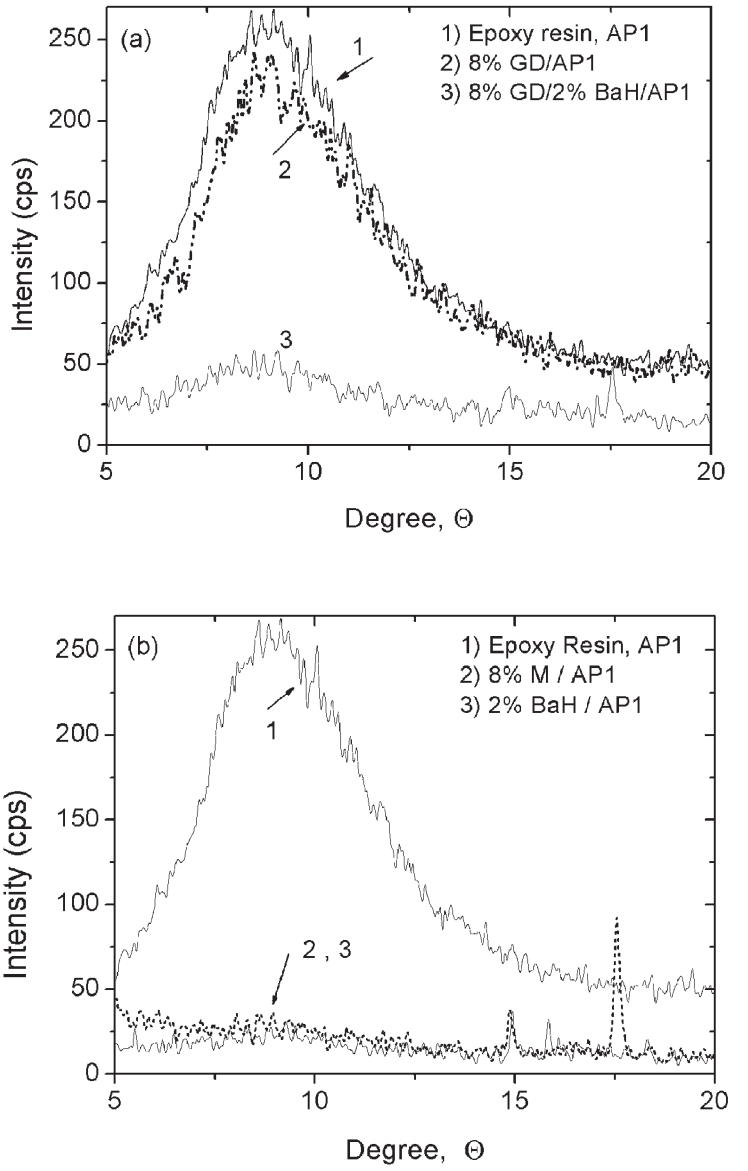

Figure 7.14 XRD spectra of (a) monomodal carbon/epoxy and bimodal carbon/barium hexaferrite/epoxy composites and (b) monomodal epoxy composites containing magnetite and barium hexaferrite.

Data from [33]

Proof of the above-mentioned suggestions for the effect of the magnetic field of inclusions is presented in **Figure 7.14** by comparing typical XRD spectra of crosslinked epoxy systems containing various nanofillers, such as graphite/diamond, barium hexaferrite and magnetite. **Figure 7.14(a)** compares the spectra of the pure epoxy resin with those of the monomodal carbon/epoxy and bimodal carbon/BaH/epoxy systems. In the last, the binary fillers combination is of 8% GD and 2% BaH. It is seen that in monomodal systems the addition of 8% graphite/diamond slightly decreases the intensity of the broad basal peak of the epoxy resin, indicative of a small effect of the carbon nanofiller on the resin structure. In contrast, for the binary fillers containing both coarse BaH and small carbon nanoparticles, the basal reflection disappears, indicating a dramatic effect of the ferroxide particles on the structure of the bimodal nanocomposites. This may be associated with a strong orientation of the resin molecules at the interfaces, produced by the magnetic field of the prolate BaH particles. Obviously the overall structure of the resin is totally changed by the presence of magnetic particles.

A similar effect is demonstrated in **Figure 7.14(b)**, where the spectra of the epoxy resin is compared with those of two monomodal ferroxide/epoxy composites containing 8% magnetite and 2% barium hexaferrite, respectively. In general, an alignment of the resin molecules in the magnetic field of the ferroxide particles might be proposed at these filler concentrations, which dominate the size of the epoxy domains formed in the crosslinked systems.

7.3.5 Synergy of Properties

The microwave absorption properties of the crosslinked bimodal carbon/ferroxide composites have been investigated and compared with those of the monomodal composites containing nanoscale carbon (e.g., graphite/diamond) in thermoset resins [33, 37]. A strong increase of the microwave-absorbing properties is observed for the bimodal systems within the frequency range 1–20 GHz, which depends significantly on the composite formulation. A synergy of binary nanofillers, both conducting and magnetic, is observed, resulting in wide-band absorbing properties of the bimodal composites, when the optimal formulation (minimal viscosity) is reached. Such effects are rarely discussed in the reported literature. Our preliminary investigations [33, 37] on the synergistic effect of conducting and magnetic nanofillers on the physical properties of nanocomposites showed interesting and promising results, which need further development.

Figure 7.15 compares the added attenuation *versus* frequency of one-layer samples (thickness 15–20 μm) of various compositions containing nanoscale carbon and binary carbon/magnetite filler in polyurethane and acrylic resins [33]. The bimodal composite systems are optimised by the rheological method for minimising the viscosity of binary filled systems with diverse sizes, shown above. The total filler content is chosen higher

than the second percolation limit, $\phi > \phi^{**}$, where saturation of physical properties is expected. The microwave absorption properties of the novel nanocomposites are compared with that measured for the conventional MW-absorbing paint Eccosorb EC269 (USA).

It can be seen that the bimodal system of carbon/ferroxide displays much higher absorbing characteristics than that of the monomodal system containing only carbon nanofiller. Importantly, the system with the optimal formulation (0.62:0.38) of small filler (carbon) and coarse filler (magnetite), determined by the minimum of the viscosity, demonstrates much higher microwave absorption properties than are measured for the other systems. Importantly, the optimal formulation of the binary type nanocomposites shows better microwave-absorption characteristics in the range 1–15 GHz than the conventional absorbing paints produced at present (e.g., Eccosorb EC269) [33, 37].

It may be assumed that the rheologically designed structure of bimodal dispersions, containing conducting and magnetic nanoparticles with diverse sizes, dominates the physical properties of solid nanocomposites. The presence of a network structure

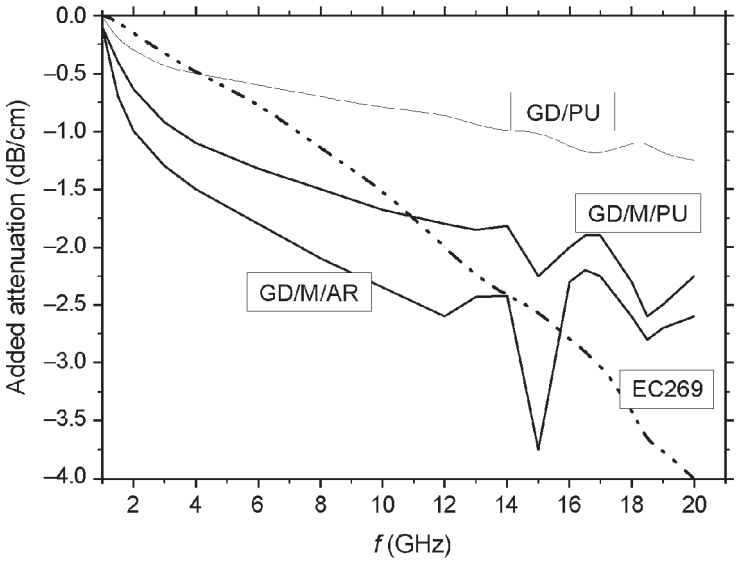

Figure 7.15 Added attenuation *versus* frequency of one-layer nanocomposite samples, compared with that of the microwave-absorbing paint Eccosorb EC269 (USA). The compositions are 8% monomodal GD/PU and 15% bimodal GD/M (0.05/0.95) in polyurethane, and GD/M (0.62/0.38) in acrylic resin.

Data from [33]

of binary fillers, having maximal packing density, plays an important role for the improved physical properties of crosslinked nanocomposites. The polymer molecules in such an environment are totally adsorbed at the particle surface and oriented in the magnetic field of the coarse particles. Such nanocomposite structure probably has the optimal degree of order and the best homogeneity, respectively. Such hybrid structure produces enhancement in physical properties, and thus, for example, the highest microwave absorption effect compared to other binary and monomodal systems.

The synergistic effect of the binary conducting and magnetic nanofillers with diverse sizes observed in the optimal nanocomposite formulations is expressed in widening of the microwave-absorbing spectra within the region of 1–20 GHz, as well as in decreasing of reflection losses. This is probably due to the maximal packing density of the small and coarse particles in the polymer matrix, which produces a better homogeneity and an orientation of the epoxy molecules in the magnetic field of the particles. Here, the important role of interfacial interactions, as well as the effect of the matrix polymer, needs to be further investigated. Preliminary results show excellent microwave-absorbing properties for the bimodal composites based on the low-viscosity polyurethane and acrylic resin. However, the epoxy-based systems, having about 10 fold higher matrix viscosity than the other resins, demonstrate lower microwave-absorbing properties. This result may be associated with the swelling ability and cluster–cluster aggregation processes, which are reduced in the epoxy matrix compared to the low-viscosity polyurethane and acrylic resins.

The microwave investigations of nanoscale carbon and natural ferroxide particles in acrylic resin and polyurethane matrices show that these polymer nanocomposites are promising functional materials. The carbon nanofiller is responsible for the dielectric losses, which is important for microwave applications of polymer nanocomposites. Moreover, the ferroxides are responsible for the magnetic losses, widening the field of nanocomposite applications as functional materials.

The thermoset nanocomposites containing binary fillers of nanoscale carbon and ferroxide, having diverse sizes, may be proposed for paint, coating and bulk materials applications. The novel bimodal nanocomposites are competitive materials, if compared to the conventional microwave absorbers produced at present, showing significant improvement of the absorbing ability within the microwave range 1–15 GHz. Such materials serve as wide-band absorbers ensuring dielectric losses up to 10 dB. Moreover, the absorbing properties could be successfully controlled and improved by the use of appropriate additives and by increasing the number of layers (see **Table 7.1** and **Figure 7.8**). Additionally, the graphite/diamond nanofiller produces a significant reinforcement, and enhancement of the thermal and mechanical properties of the films, as shown in Chapter 6. Hence, the bimodal-type nanocomposites may be proposed as promising microwave-absorbing materials for the protection of electronic equipment and biological objects, as well as for various electronic applications [33, 37].

Acknowledgements

All the microwave characterisations and the preparation of the ferroxide nanoparticles were performed at the Institute of Electronics of the Bulgarian Academy of Sciences. The dc conductivity experiments were carried out at the Institute of Solid State Physics of the Bulgarian Academy of Sciences. The author thanks Professors Ivan Nedkov and Diana Nesheva for fruitful collaboration.

References

1. G. Schmid, *Clusters and Colloids*, VCH, Weinheim, Germany, 1994.
2. G. Schmid, *Chemical Reviews*, 1992, **92**, 8, 1709.
3. G. Schön and U. Simon, *Colloid and Polymer Science*, 1995, **273**, 2, 101.
4. G. Schön and U. Simon, *Colloid and Polymer Science*, 1995, **273**, 3, 202.
5. R. Pelster and U. Simon, *Colloid and Polymer Science*, 1999, **277**, 1, 2.
6. A.D. Pomagailo and V.N. Kestelman, *Metallopolymer Nanocomposites*, Springer, Berlin, Germany, 2005.
7. T. Davidson in *Conductive and Magnetic Fillers in Functional Fillers for Plastics*, Ed., M. Xanthos, Wiley-VCH, Weinheim, Germany, 2005.
8. R. Yang, S. Ogitani, P. Kohl and C.P. Wong, *Journal of Applied Polymer Science*, 2002, **83**, 5, 1084.
9. J.S. Andrade, N. Ito and Y. Shibusa, *Physical Review B*, 1996, **54**, 6, 3910.
10. A.T. Ponomarenko, V.G. Schevchenko and N.S. Enikolopyan, *Filled Polymers I: Science and Technology Advances in Polymer Science*, 1990, **96**, 125.
11. P. Pötschke, T.D. Fornes and D.R. Paul, *Polymer*, 2002, **43**, 11, 3247.
12. N. Dishovsky and M. Grigorova, *Materials Research Bulletin*, 2000, **35**, 3, 403.
13. L. Flandin, T. Prasse, R. Schueler, K. Schulte, W. Bauhofer and Y.J. Cavaille, *Physical Review B*, 1999, **59**, 22, 14349.
14. T. Prasse, L. Flandin, K. Schulte and W. Bauhofer, *Applied Physics Letters*, 1998, **72**, 22, 2903.
15. S.P. Rwei, F.H. Ku and K.C. Cheng, *Colloid and Polymer Science*, 2002, **280**, 12, 1110.

16. J. Feng and C.M. Chan, *Polymer Engineering and Science*, 1998, **38**, 10, 1649.

17. Y. Luo, G. Wang, B. Zhang and Z. Zhang, *European Polymer Journal*, 1998, **34**, 8, 1221.

18. J.G. Mallette, A. Marquez, O. Manero and R. Castro-Rodriguez, *Polymer Engineering and Science*, 2000, **40**, 10, 2272.

19. M. Mucha and J. Marszal, *Polymer*, 2000, **41**, 11, 4137.

20. P. Ghosh and A. Chakrabarti, *European Polymer Journal*, 2000, **36**, *5*, 1043.

21. S. Kirkpatrick, *Review of Modern Physics*, 1973, **45**, 4, *574*.

22. R. Zallen, *The Physics of Amorphous Solids*, John Wiley & Sons, New York, NY, USA, 1983.

23. D. Stauffer and A. Aharony, *Introduction to Percolation Theory,* 2nd Edition, Taylor & Francis, London, UK, 1992.

24. P.C. Hiemenz, *Principles of Colloid and Surface Chemistry*, Marcel Dekker, New York, NY, USA, 1986, Chapter 4.

25. F. Carmona, *Physica A*, 1989, **157**, 1, 461.

26. F. Lux, *Journal of Materials Science*, 1993, **28**, 2, 285.

27. R. Schueler, J. Petermann, K. Schulte and H.P. Wentzel, *Journal of Applied Polymer Science*, 1997, **63**, 13, 1741.

28. J. Sandler, M.S.P. Shaffer, T. Prasse, W. Bauhofer, K. Schulte and A.H Windle, *Polymer*, 1999, **40**, 21, *5967*.

29. Y. Chekanov, R. Ohnogi, S. Asai and M. Sumita, *Journal of Materials Science*, 1999, **34**, 22, *5589*.

30. A.I. Medalia, *Rubber Chemistry and Technology*, 1986, **59**, 3, 432.

31. R. Kotsilkova, D. Nesheva, I. Nedkov, E. Krusteva and S. Stavrev, *Journal of Applied Polymer Science*, 2004, **92**, 4, 2220.

32. R. Kotsilkova, E. Krusteva, D. Nesheva, T. Djunova and S. Stavrev in *Nanosciences and Nanotechnology, Volume 3,* Eds., E. Balabanova and I. Dragieva, Heron Press, Sofia, Bulgaria, 2003, p.169.

33. R. Kotsilkova, *Relationship Between Technology, Structure and Properties of Thermoset Nanocomposites*, Sofia, Bulgaria, 2005 [D.Sc. Thesis, in Bulgarian].

34. R. Kotsilkova and E. Krusteva in *Proceedings of the 6th European Conference on Rheology, Eurheo '2002*, Eds., H. Münstedt, H. Kashta and J. Merten, 2002, p.99.

35. R. Kotsilkova and E.H. Ivanov in *Nanosciences and Nanotechnology, Volume 4,* Eds., E. Balabanova and I. Dragieva, Heron Press, Sofia, Bulgaria, 2004, p.123.

36. E. Krusteva and R. Kotsilkova in *Nanosciences and Nanotechnology, Volume 4,* Eds., E. Balabanova and I. Dragieva, Heron Press, Sofia, Bulgaria, 2004, p.127.

37. Nedkov, B. Vichev, S. Kolev, T. Merodijska, R. Kotsilkova and S. Stavrev in *Nanosciences and Nanotechnology, Volume 3,* Eds., E. Balabanova and I. Dragieva, Heron Press, Sofia, Bulgaria, 2003, p.118.

38. S.Y. Stavrev, S.B. Lazarov, K.L. Stoev, L.G. Markov and V.I. Ivanov, inventors; no assignee; US 5,353,708, 1994.

39. R. Simha, *Journal of Applied Physics*, 1952, **23**, 9, 1020.

40. N.A. Frankel and A.D. Acrivos, *Chemical Engineering Science*, 1967, **22**, 6, 847.

41. J.S. Bradley in *Clusters and Colloids*, Ed., G. Schmid, VCH, Weinheim, Germany, 1994, p.549.

42. R.J. Farris, *Transactions of the Society of Rheology*, 1968, **12**, 2, 281.

43. D.C-H. Cheng, A.P. Kruszewski, J.R. Senior and T.A Roberts, *Journal of Materials Science*, 1990, **25**, 1, 353.

44. J. Poslinski, M.E. Ryan, R.K. Gupta, S.G. Seshadri and F.J. Frechette, *Journal of Rheology*, 1988, **32**, 8, 751.

45. V. Johansen and P.J. Andersen in *Materials Science of Concrete*, Vol. II, Eds., J. Skalny and S. Mindess, American Ceramic Society, Westerville, OH, USA, 1991, p.111.

46. C. Tsenoglou and S. Yang, *Polymer Engineering and Science*, 1990, **30**, 21, 1407.

47. S. Stavrev, R. Kotsilkova, J. Karadjov and Z. Karagyozova in *Nanosciences and Nanotechnology, Volume 1*, Eds., E. Balabanova and I. Dragieva, Heron Press, Sofia, Bulgaria, 2001, p.154.

48. D.G. Thomas, *Journal of Colloid and Science*, 1965, **20**, 3, 267.

49. R. Ben Aim and P. Le Goff, *Powder Technology*, 1968, **1**, 5, 281.

Abbreviations

ac	Alternating current
AFM	Atomic force microscopy
AR	Acrylic resin
ASTM	American Society for Testing and Materials
au	Arbitrary units
BaH	Barium hexaferrite
BAS	Bulgarian Academy of Sciences
BDMA	Benzyldimethylamine
BET	Brunauer-emmett-teller
CCA	Cluster-cluster aggregation
CCR	Conductivity current relaxation
CNT	Carbon nanotubes
CR	Conductivity relaxation
CTE	Coefficient of thermal expansion
D	Diamond
dc	Direct current
DETA	Diethylenetriamine
DGEBA	Diglycidyl ether of bisphenol-A
DMA	Dynamic mechanical analysis
DMTA	Dynamic mechanical thermal analysis
DRS	Dielectric relaxation spectroscopy
DS	Dielectric spectroscopy
DSC	Differential scanning calorimetry
DTA	Differential thermal analysis

DTG	Differential thermogravimetry
ECCN	Epoxy-clay carbon nanocomposties
ECDN	Epoxy-clay diamond nonocomposites
ECN	Epoxy-clay nanocomposites
EMT	Effective medium theories
ER	Epoxy resin
FRA	Frequency response analyser
FTIR	Fourier transform infrared spectroscopy
GD	Graphite/diamond
GD/M	Graphite/diamond/magnetite
HN	Havriliak-Negami
HRR	Heart release rate
iPP	Isotactic polypropylene
IR	Infra red
ISO	International Organisation for Standardisation
K-BKZ	Kaye-bernstein, kearsley, zapas
LCP	Liquid crystal polymer
LDH	Layered double hydroxide(s)
LPA	Low profile additive
M	Magnetic
MDA	Methylenedianilamine
MEKP	Methyl ethyl ketone peroxide
MMT	Montmorillonite
MTS	Methyl triethoxysilane
MW	Microwave
NCP	Nanosized carbon particle(s)
NMR	Nuclear magnetic resonance
OA	Oleic acid
ON	Organosilicon nanophase
PAAS	Polyamic acid with ethyl silane end-groups

PDMS	Polydimethylsiloxane
PI	Polyimide(s)
PMMA	Polymethylmethacrylate
PMR	Polymerisation of monomer reactants
POE	Polyoxyethylene 23 lauryl ether(Brij 35)
PP	Polypropylene
PS	Polystyrene
PU	Polyurethane
QA	Quaternised ammonium
SAN	Hexadecyl-octadecyl ammonium chloride
SEM	Scanning electron microscopy
SOLT	Short-open-load-thru
SPN	Oligo(oxypropylene)-diethyl-methyl ammonium chloride
St	Styrene
STN	Trioctyl methyl ammonium chloride
TDS	Time-domain spectroscopy
TEM	Transmission electron microscopy
T_g	Glass transition temperature
TG	Thermogravimetry
TGA	Thermogravimetric analysis
TGAP	Trifunctional triglycidyl *p*-aminophenol
TGDDM	Tetraglycidyl diaminodiphenylmethane
TS	Thermal sampling
TSDC	Thermally stimulated depolarisation currents
UP	Unsaturated polyester resin
VTF	Vogel-tammann- fulcher
WAXD	Wide angle X-ray diffraction
WAXS	Wide angle X-ray scattering
XRD	X-ray diffraction

Index

E

F

G

H

I

P

R

U

V

W

Y

Z

ISBN: 978-84735-062-6

Smithers Rapra Technology

Smithers Rapra Technology is the leading independent international organisation with over 80 years of experience providing technology, information and consultancy on all aspects of rubbers and plastics.

The company has extensive processing, testing and analytical facilities. It provides testing to a range of national and international standards and offers UKAS accredited analytical services. Rapra also undertakes commercially focused innovative research projects through multi-client participation.

Rapra publishes books, technical journals, reports, technological and business surveys, conference proceedings and trade directories. These publishing activities are supported by an Information Centre which maintains and develops the world's most comprehensive database of commercial and technical information on

SMITHERS

Shawbury, Shrewsbury, Shropshire SY4 4NR, UK
Telephone: +44 (0)1939 250383
Fax: +44 (0)1939 251118
http://www.rapra.net